

**Dario Slejko**

# Seismic Hazard Assessment



**Pavia, September 2017**

First version released on October 2006  
Second version released on August 2011  
Third version released on August 2017

---



**CONTENTS**

1. EARTH AND EARTHQUAKES	1
1.1. The structure of the Earth	1
1.2. The moving Earth	1
1.2.1. Continental drift	3
1.2.2. Sea-floor spreading	6
1.2.3. Subduction	8
1.2.4. Hot spots	9
1.2.5. Plate tectonics	10
1.2.6. Mapping the ocean floor	
1.2.6.1. The continental margin	
1.2.6.1.1. The passive continental margin	16
1.2.6.1.2. The active continental margin	16
1.2.6.2. The deep-ocean basin	16
1.2.6.3. The oceanic ridge	17
1.3. Faults	19
1.3.1. Fault types	20
1.3.2. Dip-slip faults	20
1.3.3. Strike-slip faults	23
1.3.4. Oblique-slip faults	25
1.3.5. Fault characterization	25
1.4. Earthquakes	26
1.4.1. Earthquake myths	29
1.4.1. Tectonic earthquakes	30
1.4.2. Induced earthquakes	33
1.5. Effects of earthquakes	34
1.5.1. Landslides and liquefaction	34
1.5.2. Tsunamis	35
1.6. Stress and strain	39
1.7. Elastic-rebound theory	40
1.8. Theoretical models for earthquake occurrence	42
1.9. Coulomb stress failure	44
1.10. Faults generating earthquakes	45
2. NON-INSTRUMENTAL SEISMOLOGY	57
2.1. Macroseismic intensity	57
2.2. The macroseismic scales	57
2.2.1. The Rossi – Forel scale (1873)	59
2.2.2. The Mercalli-Cancani-Sieberg scale (1930)	60
2.2.2. The Modified Mercalli scale (1956)	61
2.2.3. The Medvedev–Sponheuer-Karnik scale (1964)	62
2.2.4. The European Macroseismic Scale	63
2.3. Isoleismals	66
2.4. Macroseismic parameters	69
2.5. Historical seismology	71
2.5.1. Value of historical seismicity	74
2.5.2. The family tree of the historical earthquakes	76
2.6. Palaeoseismology	77
2.6.1. Archaeoseismology	78
2.6.2. Destruction of buildings correlating with historical earthquakes	82
2.7. “ShakeMap”: a new technology to aid emergency response	82
2.8. The Community Internet Intensity Map	83
3. INSTRUMENTAL SEISMOLOGY	85

3.1. Elementary seismic waves	85
3.2. Dependent seismic waves	85
3.3. Travel-time tables	89
3.4. Seismic instruments	92
3.4.1. Theory of the seismograph	98
3.4.2. Characteristics of the seismographs	101
3.5. Interpretation of seismograms	103
3.5.1. Locating earthquakes	105
3.5.1.1. The graphical procedure	105
3.5.1.2. The automatic procedure	106
3.5.1.3. Software for earthquake location	107
3.6. Magnitude	107
3.7. Seismic moment	113
3.8. Energy	114
3.9. Focal mechanisms	115
3.9.1. Stress tensor inversion	120
3.10. Foreshocks and aftershocks	120
3.11. Earthquake statistics	123
3.11.1. The Gutenberg – Richter law	124
4. STRONG GROUND MOTION	129
4.1. Ground motion parameters	129
4.1.1. Amplitude parameters	129
4.1.2. Frequency content parameters	133
4.1.2.1. Ground motion spectra	133
4.1.3. Duration	139
4.1.4. Other ground motion parameters	139
4.2. Development of predictive relationships	141
4.2.1. Peak acceleration	146
5. SEISMIC HAZARD	151
5.1. Deterministic approach	152
5.2. Probabilistic approach	154
5.2.1. The historical probabilism	158
5.2.2. The seismotectonic probabilism	164
5.2.2.1. The original Cornell (1968) approach for PSHA	164
5.2.2.1.1. Line source	164
5.2.2.1.2. Peak ground motion results	171
5.2.2.1.3. General source results	172
5.2.3. The general probabilistic hazard model	176
5.2.3.1. Step 1: spatial identification of the earthquake sources	178
5.2.3.2. Step 2: seismic characterization of the earthquake sources	180
5.2.3.2.1. Gutenberg-Richter recurrence law	181
5.2.3.2.2. Bounded Gutenberg-Richter recurrence laws	183
5.2.3.2.3. Characteristic earthquake recurrence laws	187
5.2.3.3. Step 3: attenuation relationships	189
5.2.3.4. Step 4: the hazard curve	190
5.2.3.5. Step 5: time occurrence models	192
5.2.3.5.1. Poisson model	192
5.2.3.5.2. Other time occurrence models	193
5.2.3.6. Considerations on the hazard model parameters	197
5.2.3.7. Deaggregation	198
5.2.3.8. The treatment of uncertainties	199
5.2.3.8.1. The logic tree method	200
5.2.4. The smoothed seismicity approach	202

5.2.5. Earthquake prediction	203
5.2.5.1. Long-term forecast	204
5.2.5.1.1. Seismic gap method	204
5.2.5.1.2. Stress transfer	204
5.2.5.1.3. Seismicity patterns	205
5.2.5.2. Short-term forecast	205
5.2.5.2.1. Precursors and anomalous phenomena	205
5.2.5.2.2. The 1975 Haicheng earthquake prediction	207
5.2.5.2.3. The Parkfield experiment	207
5.3. Software for PSHA	210
5.4. Seismic hazard maps	211
5.5. Site effects in seismic hazard maps	216
5.5.1. The litho-stratigraphic site effects	218
5.5.2. The morphological site effects	223
5.5.2.1. Reliefs	223
5.5.2.2. Slopes	224
5.5.2.3. Canyons	224
5.5.2.4. Quantification of the morphological site effects	224
5.6. The SSHAC methodology in PSHA for strategic facilities	226
6. SEISMIC RISK	231
6.1. Risk and hazard	232
6.2. Examples of studies on seismic risk assessment	235
6.3. Global urbanization and increased seismic risk	243
6.4. Earthquake preparedness	244
7. BUILDING CODES	247
7.1. The Eurocode 8	250
7.1.1. Fundamental requirements	250
7.1.2. Ground conditions	252
7.1.3. Seismic zones	253
7.1.4. Seismic action	254
7.2. The U.S. building code	255
7.2.1. The NEHRP Provisions	257
References	263
Appendix A: Glossary of interest to earthquake and engineering seismologists	273
Appendix B: Definitions	281
Appendix C: Basics of statistics and probability concepts	285



## PREFACE

These notes collect the main material presented during the courses on basics of seismology and seismic hazard assessment, held at the Rose School of Pavia during several years. They are mainly a sort of travel through seismology and engineering seismology, where some aspects are deeply investigated, some others are highlighted, and some are only mentioned. It is not intention of this text to be exhaustive and complete: a much larger documentation would have been necessary and deeper experience needed.

It is assumed that the student following this course has little or no knowledge of the subjects related to seismology and seismic hazard assessment. Nevertheless, some topics are probably treated only superficially, without entering into specific details. This is mainly due to the fact that the subjects of quantitative seismology are not touched at all.

These notes are divided into seven chapters: the first three are related to seismology and the others to engineering seismology.

Entering into details, the first chapter describes the Earth, its composition and the theories supporting the earthquake genesis. The second chapter is dedicated to the non-instrumental seismology, the part of this discipline which aims at observations rather than measurements. The importance of this part of the Earth sciences is pointed out with description of the activity developed in the past and that presently conducted. The third chapter treats the instrumental seismology and introduces the seismic waves, the recording instruments, and the quantities related to earthquakes.

The second part of the notes are devoted to engineering seismology. The fourth chapter, in fact, treats the strong ground motion seismology: a border subject between seismology and engineering seismology. The main quantities describing the ground motion are introduced together with their related scaling laws. The fifth chapter is the bulk of these notes and introduces the concepts of seismic hazard, the ingredients needed for its assessment, and the methodologies used. A suite of examples is presented on the construction of seismic hazard maps, that have been developed during the time in the framework of some important research projects. The sixth chapter describes what seismic risk is and gives some examples of its calculation. The seventh, and last, chapter gives some pieces of information about some building codes, with reference to the parts linked to the ground motion.

**Acknowledgements.** Only some parts of these notes are completely original: most of the material presented here comes from the basic literature of Seismology and Earthquake Engineering. More precisely, some parts are simply taken from Richter (1958), Reiter (1990), and Kramer (1996). Two seminal scientific papers on probabilistic seismic hazard assessment are in large parts reported because they put the bases of this discipline; they are the Epstein and Lomnitz (1962) and Cornell (1968) works. Moreover, some sections are taken from the notes prepared by Julian Bommer and Fabio Sabetta for the courses that they had at the Rose School. Furthermore, some parts come from several documents available in the Internet, among which a special citation goes to the Wikipedia.

Several pictures of these notes are taken from several documents available in the Internet, among which a special citation goes to the material available at the USGS and NOAA web sites. The due credits are not always given to the material (texts and pictures) taken from the Internet: this deficiency is caused by the fact that the material in Internet appears and disappears and/or changes address, making difficult, sometimes, its search.



## 1. EARTH AND EARTHQUAKES

Earthquakes are the shaking, rolling or sudden shock of the Earth's surface. Earthquakes happen along "fault lines" in the Earth's crust. Earthquakes can be felt over large areas although they usually last less than one minute. Earthquakes cannot be predicted, although scientists are working on it!

Most of the time, you will notice an earthquake by the gentle shaking of the ground. You may notice hanging plants swaying or objects wobbling on shelves. Sometimes you may hear a low rumbling noise or feel a sharp jolt. A survivor of the 1906 earthquake in San Francisco said the sensation was like riding a bicycle down a long flight of stairs.

The intensity of an earthquake can be measured. One measurement is called the Richter scale. Earthquakes below 4.0 on the Richter scale usually do not cause damage, and earthquakes below 2.0 usually cannot be felt. Earthquakes over 5.0 on the scale can cause damage. A magnitude 6.0 earthquake is considered strong and a magnitude 7.0 is a major earthquake.

Earthquakes are sometimes called temblors, quakes, shakers or seismic activity. The most important thing to remember during an earthquake is to DROP, COVER and HOLD ON. So remember to DROP to the floor and get under something for COVER and HOLD ON during the shaking.

### 1.1. The structure of the Earth

The Earth can be considered as being approximately spherical, although it is actually of slightly larger radius at the equator. The Earth's radius is approximately 6370 km and the Earth is divided into three chemical layers: the core, the mantle and the crust (Fig. 1.1).

The core is composed of mostly iron and nickel and remains very hot, even after 4.5 billion years of cooling; its radius being about 0.55 that of the Earth. The core is divided into two layers: a solid inner core (1390 km thick) and a liquid outer core (3470 km thick).

The middle layer of the Earth, the mantle, is 2900 km thick and is made of minerals rich of iron, magnesium, silicon, and oxygen; its thickness is about 0.45 the Earth radius. The discontinuity between the crust and the mantle is known as the Mohorovicic discontinuity (after the Yugoslavian seismologist who first identified its presence from interpretation of seismograms) or simply Moho.

The crust is rich of oxygen and silicon with lesser amounts of aluminium, iron, magnesium, calcium, potassium, and sodium. There are two types of crust. Basalt is the most common rock on Earth. Oceanic crust is made of relatively dense rock called basalt. Continental crust is made of lower density rocks, such as andesite and granite. Its thickness varies from 25 to 40 km beneath the continents, with greater thickness occurring under some mountain chains, and from 7 to 12 km beneath parts of ocean basins. The discontinuity between the granites and the basalts is known as the Conrad discontinuity. The crust can be thought of as floating on the mantle and the variation of thickness with surface elevation (i.e., Archimedes' principle) is known as isostasy.

The outermost layers of the Earth can be divided by their physical properties into lithosphere and asthenosphere (Fig. 1.2).

The lithosphere (from the Greek *lithos*, stone) is the rigid outermost layer made of crust and uppermost mantle. The lithosphere is the "plate" of the plate tectonic theory.

The asthenosphere (from the Greek *asthenos*, devoid of force) is part of the mantle that flows, a characteristic called plastic behaviour. It might seem strange that a solid material can flow. A good example of a solid that flows, or of plastic behaviour, is the movement of toothpaste in a tube. The flow of the asthenosphere is part of mantle convection, which plays an important role in moving lithospheric plates.

### 1.2. The moving Earth

The theory of plate tectonics has done for geology what Charles Darwin's theory of evolution did for biology. It provides geology with a comprehensive theory that explains "how the Earth works." The theory was formulated in the 1960s and 1970s as new information was obtained about the nature

of the ocean floor, Earth's ancient magnetism, the distribution of volcanoes and earthquakes, the flow of heat from Earth's interior, and the worldwide distribution of plant and animal fossils.

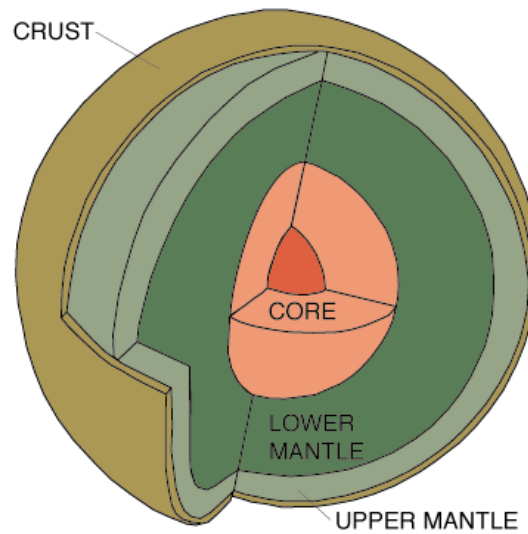


Fig. 1.1 - The parts of the Earth.

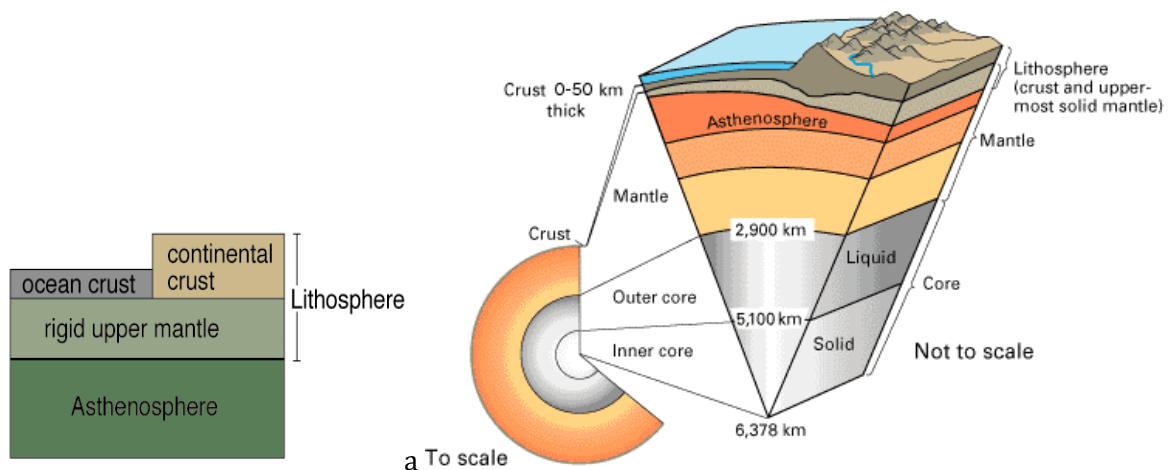


Fig. 1.2 - The Earth's outer layer is called the lithosphere: it is made of the rigid upper mantle and the crust, the lithosphere moves on the asthenosphere, part of the mantle that flows. Plates are made of crust and rigid upper mantle.

The theory states that Earth's outermost layer, the lithosphere, is broken into 7 large, rigid pieces called plates: the African, North American, South American, Eurasian, Australian, Antarctic, and Pacific plates. Several minor plates also exist, including the Arabian, Nazca, and Philippines plates.

The plates are all moving in different directions and at different speeds (from 2 cm to 10 cm per year, about the speed at which your fingernails grow) in relationship to each other. The plates are moving around like cars in a demolition derby, which means they sometimes crash together, pull apart, or sideswipe each other. The place where the two plates meet is called a plate boundary. Boundaries have different names depending on how the two plates are moving in relationship to each other

- crashing: convergent boundaries,
- pulling apart: divergent boundaries,
- or sideswiping: transform boundaries.

The edges of these plates, where they move against each other, are sites of intense geologic activity, such as earthquakes, volcanoes, and mountain building.



Plate tectonics is a combination of two earlier ideas, continental drift and sea-floor spreading. Continental drift is the movement of continents over the Earth's surface and in their change in position relative to each other. Sea-floor spreading is the creation of new oceanic crust at mid-ocean ridges and movement of the crust away from the mid-ocean ridges.

### 1.2.1. Continental drift

Continental drift was originally proposed by Alfred Wegener, a German meteorologist, in 1912. Wegener used the fit of the continents (mainly South America and Africa), the distribution of fossils, a similar sequence of rocks at numerous locations, ancient climates, and the apparent wandering of the Earth's polar regions to support his idea. Wegener used his observations to hypothesize that all of the present-day continents were once part of a single supercontinent called Pangaea (Fig. 1.3).

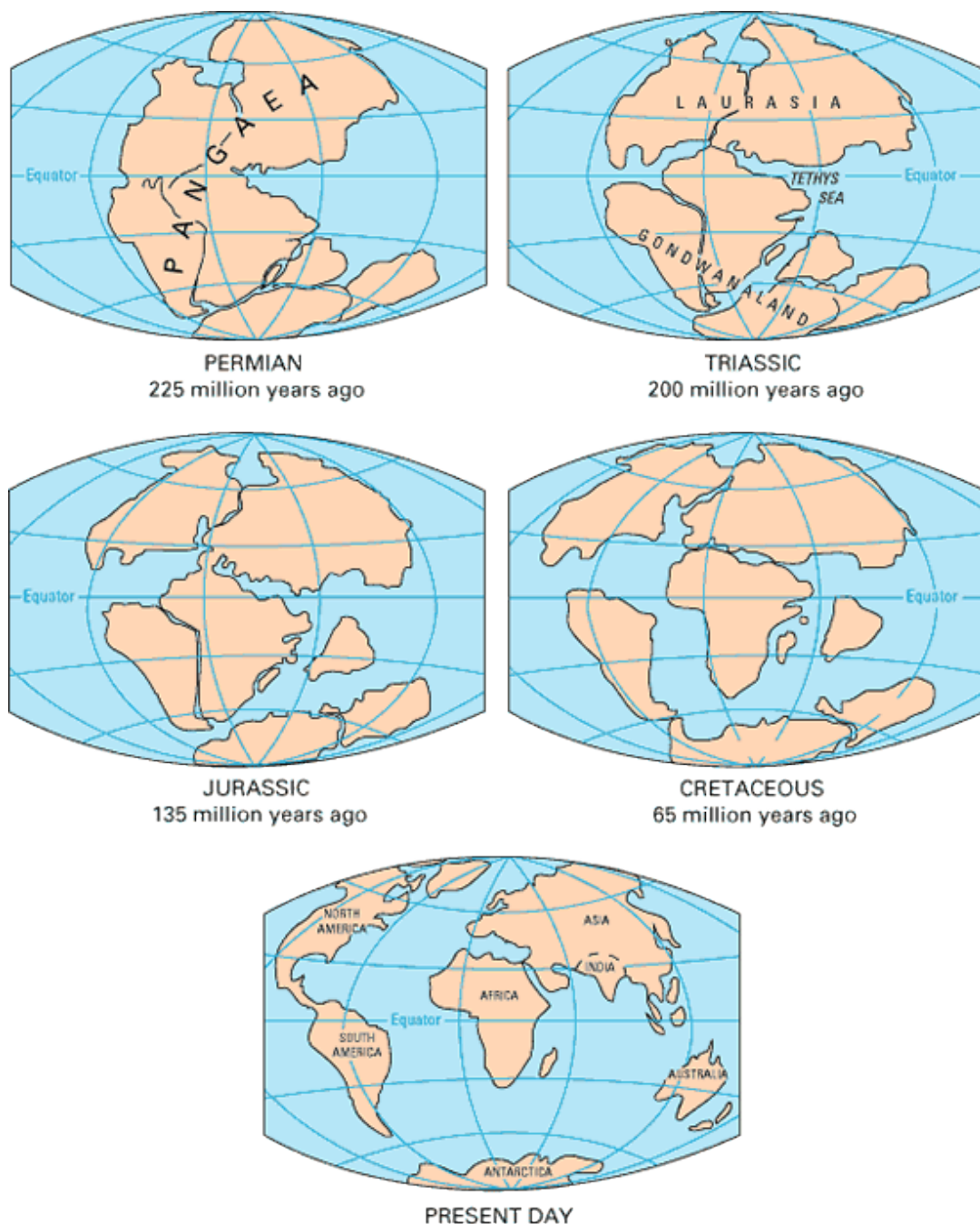


Fig. 1.3 - 225 million years ago all of the present-day continents combined to form a single supercontinent Pangaea, then the continental drift started.

Fossils of the same species were found on several different continents (Fig. 1.4). Wegener proposed that the species dispersed when the continents were connected and later carried to their present positions as the continents drifted. For example, *Glossopteris*, a fern, was found on the continents of South America, Africa, India, and Australia. If the continents are reassembled into Pangaea, the distribution of *Glossopteris* can be accounted for over a much smaller contiguous geographic area. The distribution of other species can also be accounted for by initially spreading across Pangaea, followed by the breakup of the supercontinent, and movement of the continents to their present positions.

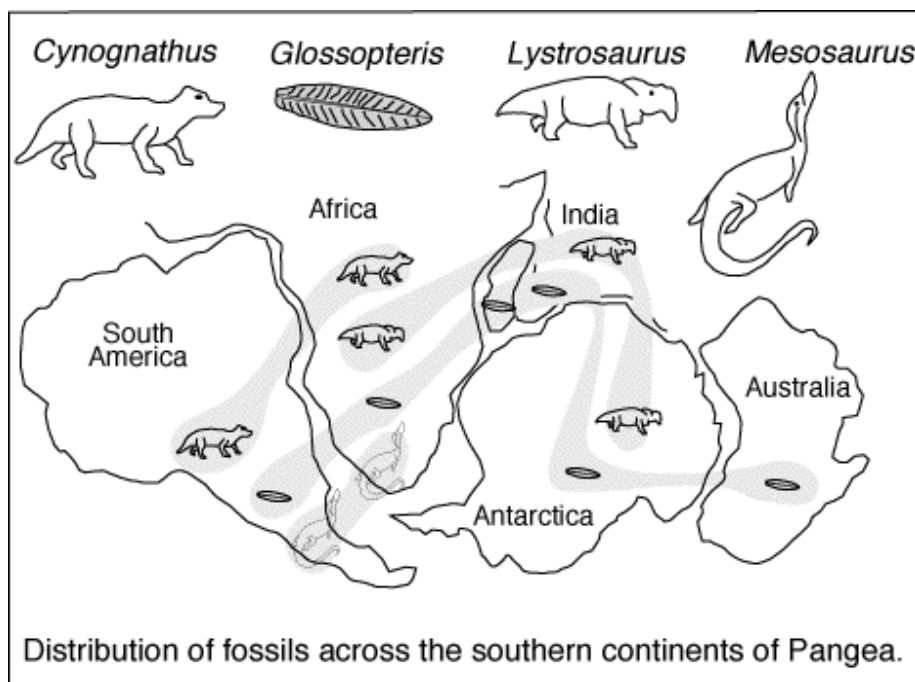


Fig. 1.4 - Fossils of the same species were found on several different continents.

Rock sequences in South America, Africa, India, Antarctica, and Australia show remarkable similarities. Wegener showed that the same three layers occur at each of these localities. The bottom (oldest) layer is called tillite and is thought to be a glacial deposit. The middle layer is composed of sandstone, shale, and coal beds. *Glossopteris* fossils are in the bottom and middle layers. The top (youngest) layer is lava flows. The same three layers are in the same order in areas now separated by great distances. Wegener proposed that the rock layers were made when all the continents were part of Pangaea. Thus, they formed in a smaller contiguous area that was later broken and drifted apart.

Glaciation in South America, Africa, India, and Australia is best explained if these continents were once connected. Glaciers covered all or part of each of these continents during the same time period in the geologic past. If the continents were in their present position, a major glaciation event that covered nearly all of the continents and extended north of the equator would be required. Geologists have found no evidence of glacial action in the northern hemisphere during this time period. In fact, during this time period, the climate in North America was warm. Wegener proposed that the continents were adjacent to each other during the glacial event. Therefore, glaciers spread over a much smaller area in the southern hemisphere and probably did not influence the climate of the northern hemisphere.

Wegener used the distribution of specific rock types to determine the distribution of climate zones in the geologic past. For example, glacial till and striations (scratches on the rock), sand dunes, and coral reefs, indicate polar, desert, and tropical climates, respectively. Note how the distribution of reefs, deserts, and glacial ice constrain the position of the rotational pole of the Earth. Using the distribution of rock types, Wegener reconstructed the distribution of climate zones at specific times in the geologic past. He found that, unlike the present distribution, in which zones are parallel to the equator (Fig. 1.5), the past zones occupied very different positions (Fig. 1.6). This implies that the rotational pole was in very different locations relative to today. Wegener proposed an alternative

interpretation. He believed that the climate zones remained stationary and the continents drifted to different locations. The drift of the continents caused the apparent movement of the climate zones.

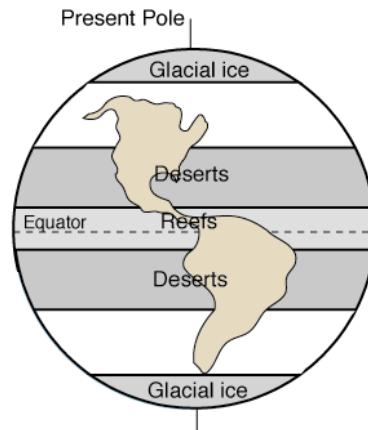


Fig. 1.5 – Present-day climate zones and associated geologic features define a pattern relative to the pole of rotation.

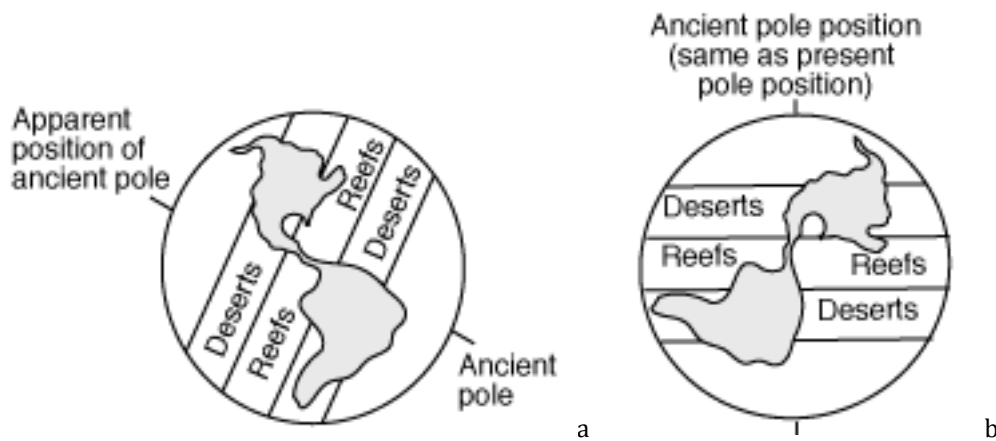


Fig. 1.6 – Two possible interpretations of the distribution of ancient climate zones: a) the continents remained fixed and the poles wander; b) the poles remained fixed and the continents wander.

Wegener used the distribution of climate zones to determine the location of the poles at different times in the geologic past. He found that the rotational pole appears to gradually change location, arriving at its present position only in the very recent geologic past. The apparent movement in the pole position over time is called polar wandering. Wegener offered an alternative explanation. He suggested that the poles remained stationary and that the continents changed their positions relative to the poles.

Wegener's model was not accepted by all geologists. Some thought that dispersion by winds or ocean currents could explain the distribution of fossil species. Other geologists thought the poles might wander and continents remain stationary. Many geologists thought Wegener's evidence was insufficient. The greatest shortcoming, at least in the eyes of American geologists, was the lack of an adequate mechanism for moving the continents. Wegener proposed that the Earth's spin caused the continents to move, plowing through the oceanic plate and producing mountains on their leading edges. Geologists at that time understood enough about the strength of rocks to know that this was highly unlikely. Wegener's work was largely unaccepted in the northern hemisphere. In the southern hemisphere, where geologists were familiar with the rocks that Wegener used to support his hypothesis, continental drift was generally accepted.

A mechanism to move continents was proposed by Arthur Holmes, Scottish geologist in 1928. He believed heat trapped in the Earth caused convection currents, areas where fluids beneath the Earth's crust rise, flow laterally, and then fall (Fig. 1.7). The currents would rise beneath continents, spread laterally, then plunge beneath the oceans (geologists now know that solid rock, not fluids, convect in

the mantle). Unfortunately, Wegener died in 1930 while exploring the Greenland ice cap. He never had the opportunity to adapt Holmes' ideas to his views of continental drift.

During the 1940s and 1950s, great advances were made in our knowledge of the sea floor and in the magnetic properties of rocks. Both of these fields of study provided new evidence to support continental drift.

Geologists have known for over a century that a ridge exists in the middle of the Atlantic Ocean. The Mid-Atlantic Ridge is 2,000 m above the adjacent sea floor, which is at a depth of about 6,000 m below sea level. In the 1950s, a seismologist showed that the global system of mid-ocean ridges was also an active seismic belt, or zone of earthquakes. An international group of geologists proposed that the seismic belt corresponded to a trough, or rift, system similar to the trough known at the crest of the Mid-Atlantic Ridge. The rifts are about 30 km wide and 2,000 m deep. In all, the oceanic ridges and their rifts extend for more than 60,000 km in all the world's oceans.

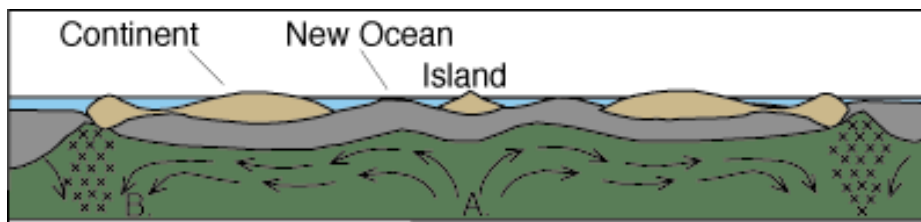


Fig. 1.7 – Holmes' model of convection currents: A = areas of upwelling; B = areas of downwelling and melting.

### 1.2.2. Sea-floor spreading

In 1960 but published in 1962, a geologist presented an explanation for the global rift system. Harry Hess proposed that new ocean floor is formed at the rift of mid-ocean ridges. The ocean floor, and the rock beneath it, are produced by magma that rises from deeper levels. Hess suggested that the ocean floor moved laterally away from the ridge and plunged into an oceanic trench along the continental margin (Fig. 1.8).

A trench is a steep-walled valley on the sea floor adjacent to a continental margin. For example, ocean crust formed at the East Pacific Rise, an oceanic ridge in the east Pacific, plunges into the trench adjacent to the Andes Mountains on the west side of the South American continent. In Hess' model, convection currents push the ocean floor from the mid-ocean ridge to the trench. The convection currents might also help move the continents, much like a conveyor belt.

As Hess formulated his hypothesis, Robert Dietz independently proposed in 1961 a similar model and called it sea floor spreading. Dietz's model had a significant addition. It assumed the sliding surface was at the base of the lithosphere, not at the base of the crust.

Hess and Dietz succeeded where Wegener had failed. Continents are no longer thought to plow through oceanic crust but are considered to be part of plates that move on the soft, plastic asthenosphere. A driving force, convection currents, moved the plates. Technological advances and detailed studies of the ocean floor, both unavailable during Wegener's time, allowed Hess and Dietz to generate the new hypotheses.

Before being widely accepted, a new hypothesis must be tested. One test for the sea-floor-spreading hypothesis involved magnetic patterns on the sea floor.

In the late 1950's, scientists mapped the present-day magnetic field generated by rocks on the floor of the Pacific Ocean. The volcanic rocks which make up the sea floor have magnetization because, as they cool, magnetic minerals within the rock align to the Earth's magnetic field. The intensity of the magnetic field they measured was very different from the intensity they had calculated. Thus, the scientists detected magnetic anomalies, or differences in the magnetic field from place to place. They found positive and negative magnetic anomalies. Positive magnetic anomalies are places where the magnetic field is stronger than expected. Positive magnetic anomalies are induced when the rock cools and solidifies with the Earth's north magnetic pole in the northern geographic hemisphere. The Earth's magnetic field is enhanced by the magnetic field of the rock. Negative magnetic anomalies are magnetic anomalies that are weaker than expected. Negative magnetic anomalies are induced when the rock cools and solidifies with the Earth's north magnetic pole in the southern geographic

hemisphere. The resultant magnetic field is less than expected because the Earth's magnetic field is reduced by the magnetic field of the rock.

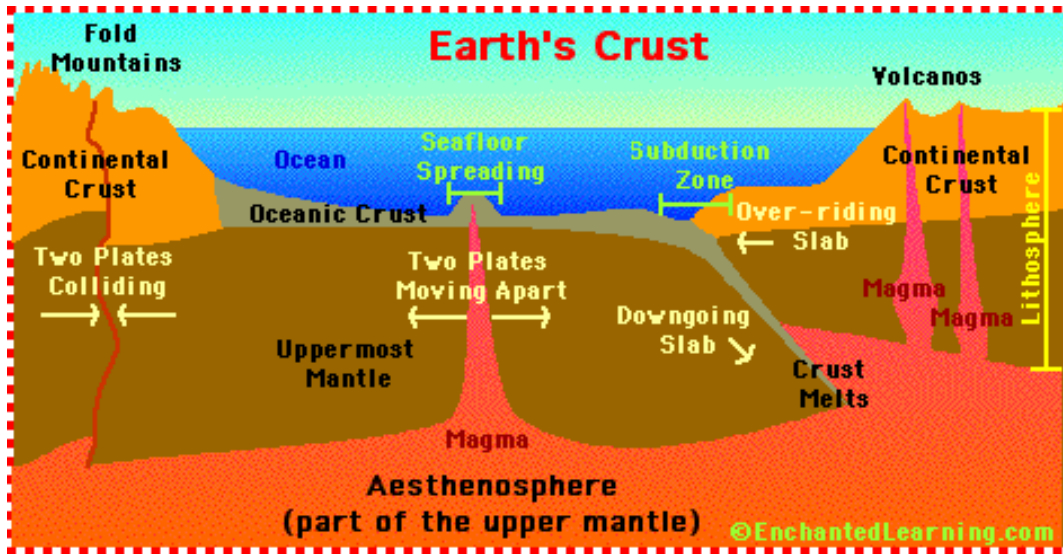


Fig. 1.8 – Sketch of the sea floor spreading.

When mapped, the anomalies produce a zebra-striped pattern of parallel positive and negative bands (Fig. 1.9). The pattern was centred along, and symmetrical to, the mid-ocean ridge. A hypothesis was presented in 1963 by Fred Vine and Drummond Matthews to explain this pattern. They proposed that lava, erupted at different times along the rift at the crest of the mid-ocean ridges, preserved different magnetic anomalies. For example, lava erupted in the geologic past, when the north magnetic pole was in the northern hemisphere, preserved a positive magnetic anomaly. In contrast, lava erupted in the geologic past, when the north magnetic pole was in the southern hemisphere, preserved a negative magnetic anomaly. Lava erupting at the present time would preserve a positive magnetic anomaly because the Earth's north magnetic pole is in the northern hemisphere (Fig. 1.10).

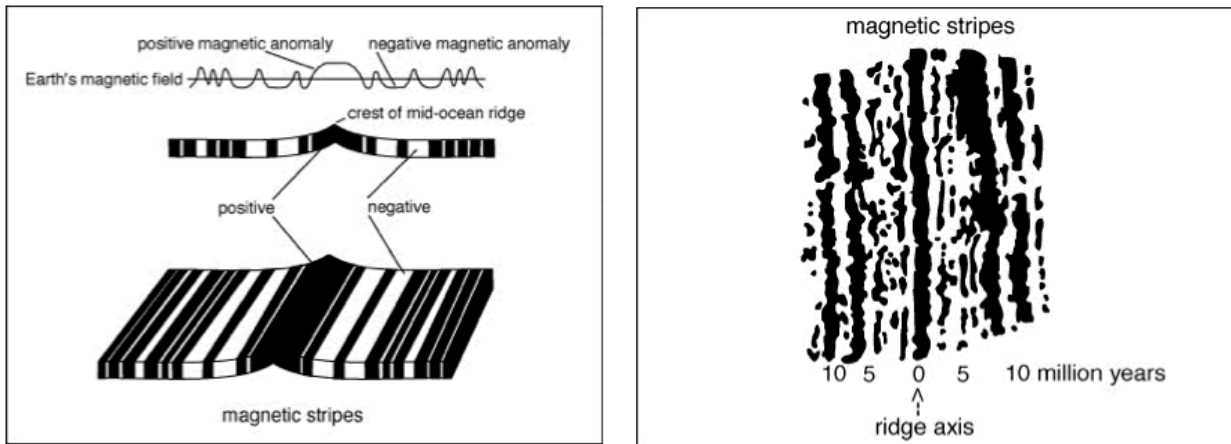


Fig. 1.9 – Pattern created by magnetic stripes along the Mid-Atlantic Ridge south of Iceland.

Vine and Matthews proposed that lava erupted on the sea floor on both sides of the rift, solidified, and moved away before more lava was erupted. If the Earth's magnetic field had reversed (changed from one geographic pole to the other) between the two eruptions, the lava flows would preserve a set of parallel bands with different magnetic properties. The ability of Vine and Matthews' hypothesis to explain the observed pattern of ocean floor magnetic anomalies provided strong support for sea floor spreading (Fig. 1.11).

The convection currents in the mantle are responsible for the continent movement and involve hot spots and subduction zones.



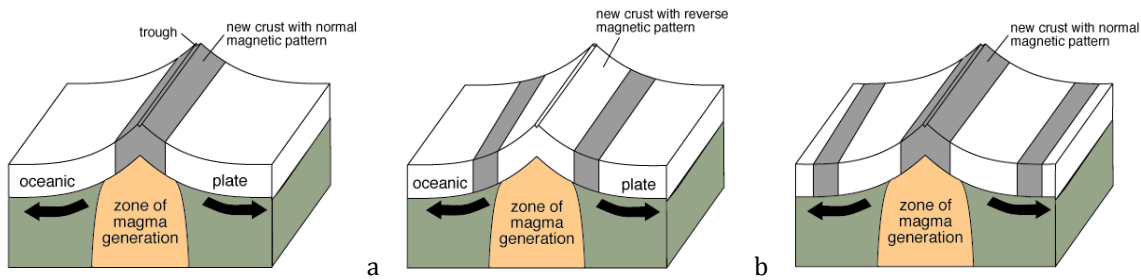


Fig. 1.10 – Formation of magnetic stripes: a) as magma solidifies along the edge of the oceanic plate, it preserves a magnetic record of the Earth's magnetic field at that time (in this case, the north magnetic pole is in the northern hemisphere; b) if the pole is in the southern hemisphere, the rocks record a reverse magnetic pattern; c) at the present time, rocks record a normal pattern because a north magnetic pole is in the northern hemisphere.

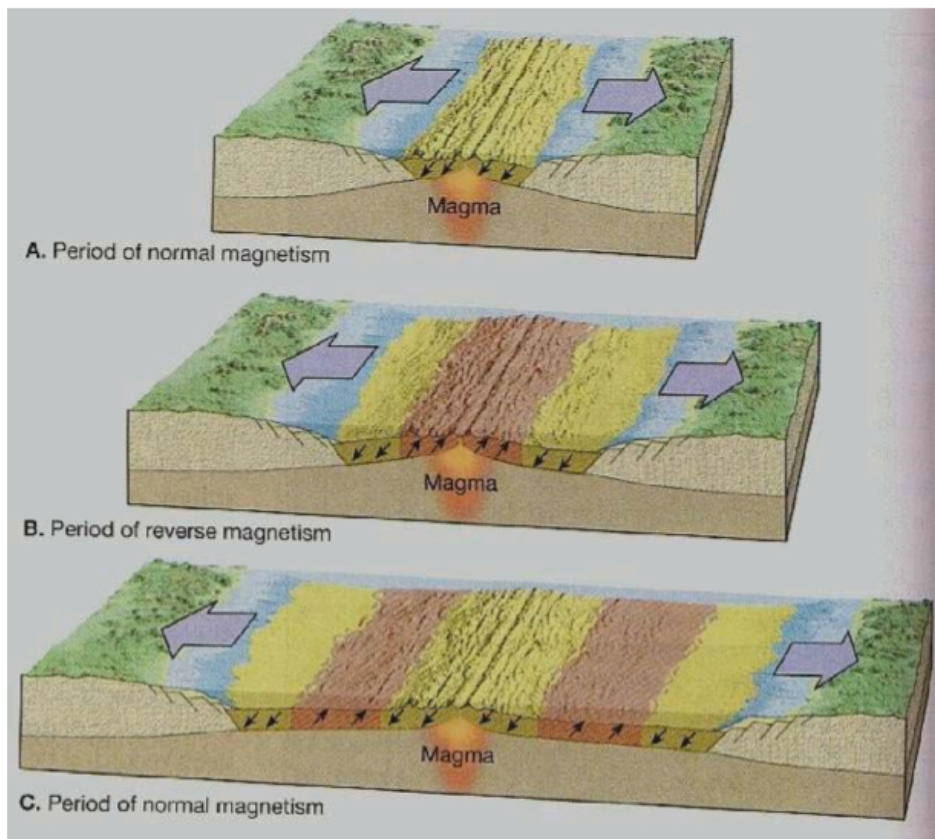


Fig. 1.11 – Formation of an oceanic rift.

### 1.2.3. Subduction

If new oceanic lithosphere is created at mid-ocean ridges, where does it go? Geologists had the answer to this question before Vine and Matthews presented their hypothesis. In 1935, K. Wadati, a Japanese seismologist, showed that earthquakes occurred at greater depths towards the interior of the Asian continent. Earthquakes beneath the Pacific Ocean occurred at shallow depths. Earthquakes beneath Siberia and China occurred at greater depths. After World War II, H. Benioff observed the same distribution of earthquakes but could not offer a plausible explanation.

The movement of oceanic lithosphere away from mid-ocean ridges provides an explanation. Convection cells in the mantle help carry the lithosphere away from the ridge. The lithosphere arrives at the edge of a continent, where it is subducted or sinks into the asthenosphere. Thus, oceanic lithosphere is created at mid-ocean ridges and consumed at subduction zones, areas where the lithosphere sinks into the asthenosphere (Fig. 1.12). Earthquakes are generated in the rigid plate as it is subducted into the mantle. The dip of the plate under the continent accounts for the distribution of

the earthquakes. Magma, generated along the top of the sinking slab, rises to the surface to form stratovolcanoes.

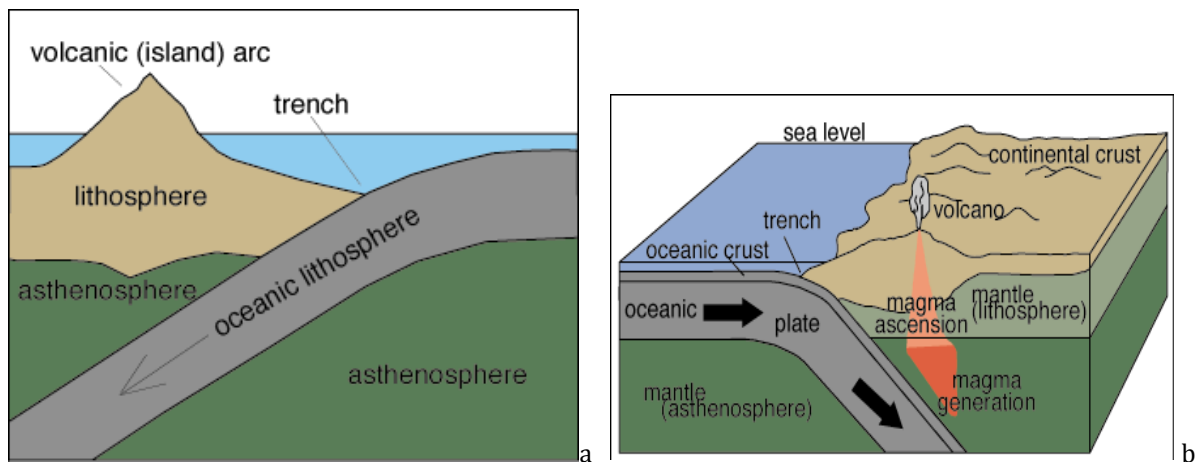


Fig. 1.12 – Subduction: a) the oceanic lithosphere is lighter than the continental one; b) magma is generated at subduction zones where dense oceanic plates are pushed under lighter continental plates.

#### 1.2.4. Hot spots

In 1963, J. Tuzo Wilson, the Canadian geophysicist who discovered transform faults, came up with an ingenious idea that became known as the "hot spot" theory. Wilson noted that in certain locations around the world, such as Hawaii, volcanism has been active for very long periods of time. This could only happen, he reasoned, if relatively small, long-lasting, and exceptionally hot regions, called hot spots, existed below the plates that would provide localized sources of high heat energy (thermal plumes) to sustain volcanism (Fig. 1.13). Specifically, Wilson hypothesized that the distinctive linear shape of the Hawaiian Island-Emperor Seamounts chain resulted from the Pacific Plate moving over a deep, stationary hot spot in the mantle, located beneath the present-day position of the Island of Hawaii. Heat from this hot spot produced a persistent source of magma by partly melting the overriding Pacific Plate. The magma, which is lighter than the surrounding solid rock, then rises through the mantle and crust to erupt onto the seafloor, forming an active seamount. Over time, countless eruptions cause the seamount to grow until it finally emerges above sea level to form an island volcano. Wilson suggested that continuing plate movement eventually carries the island beyond the hot spot, cutting it off from the magma source, and volcanism ceases. As one island volcano becomes extinct, another develops over the hot spot, and the cycle is repeated. This process of volcano growth and death, over many millions of years, has left a long trail of volcanic islands and seamounts across the Pacific Ocean floor.

According to Wilson's hot spot theory, the volcanoes of the Hawaiian chain should get progressively older and become more eroded the farther they travel beyond the hot spot. The oldest volcanic rocks on Kauai, the north-westernmost inhabited Hawaiian island, are about 5.5 million years old and are deeply eroded. By comparison, on the "Big Island" of Hawaii (south-easternmost in the chain and presumably still positioned over the hot spot) the oldest exposed rocks are less than 0.7 million years old and new volcanic rock is continually being formed.

The possibility that the Hawaiian Islands become younger to the SE was suspected by the ancient Hawaiians, long before any scientific studies were done. During their voyages, sea-faring Hawaiians noticed the differences in erosion, soil formation, and vegetation and recognized that the islands to the NW (Niihau and Kauai) were older than those to the SE (Maui and Hawaii). This idea was handed down from generation to generation in the legends of Pele, the fiery Goddess of Volcanoes. Pele originally lived on Kauai. When her older sister Namakaokahai, the Goddess of the Sea, attacked her, Pele fled to the Island of Oahu. When she was forced by Namakaokahai to flee again, Pele moved SE to Maui and finally to Hawaii, where she now lives in the Halemaumau Crater at the summit of Kilauea Volcano. The mythical flight of Pele from Kauai to Hawaii, which alludes to the eternal struggle between the growth of volcanic islands from eruptions and their later erosion by ocean waves, is

consistent with geologic evidence obtained centuries later that clearly shows the islands becoming younger from NW to SE.

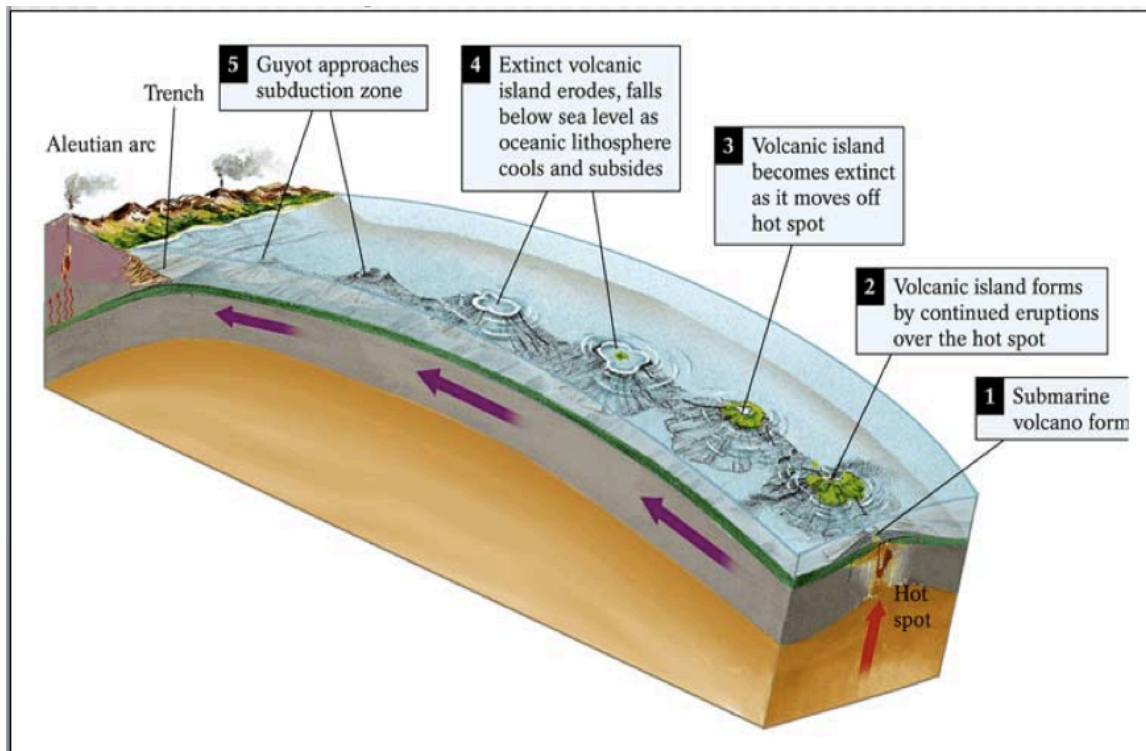


Fig. 1.13 – Scheme of a hot spot.

Although Hawaii is perhaps the best known hot spot, others are thought to exist beneath the oceans and continents. More than a hundred hot spots beneath the Earth's crust have been active during the past 10 million years. Most of these are located under plate interiors (for example, the African Plate), but some occur near diverging plate boundaries. Some are concentrated near the mid-oceanic ridge system, such as beneath Iceland, the Azores, and the Galapagos Islands (Fig. 1.14).

A few hot spots are thought to exist below the North American Plate. Perhaps the best known is the hot spot presumed to exist under the continental crust in the region of Yellowstone National Park in north-western Wyoming. Here are several *calderas* (large craters formed by the ground collapse accompanying explosive volcanism) that were produced by three gigantic eruptions during the past two million years, the most recent of which occurred about 600,000 years ago. Ash deposits from these powerful eruptions have been mapped as far away as Iowa, Missouri, Texas, and even northern Mexico. The thermal energy of the presumed Yellowstone hot spot fuels more than 10,000 hot pools and springs, geysers (like Old Faithful), and bubbling *mudpots* (pools of boiling mud). A large body of magma, capped by a *hydrothermal system* (a zone of pressurized steam and hot water), still exists beneath the caldera. Recent surveys demonstrate that parts of the Yellowstone region rise and fall by as much as 1 cm each year, indicating the area is still geologically restless. However, these measurable ground movements, which most likely reflect hydrothermal pressure changes, do not necessarily signal renewed volcanic activity in the area.

### 1.2.5. Plate tectonics

The new hypotheses of the early 1960s explained several puzzling sets of observations but a synthesis of these hypotheses was still missing.

The synthesis began in 1965 when Tuzo Wilson introduced the term plate for the broken pieces of the Earth's lithosphere. In 1967, Jason Morgan proposed that the Earth's surface consists of 12 rigid plates that move relative to each other because of deep mantle convection in which narrow plumes of deep material rise and spread out laterally in the asthenosphere (Fig. 1.15). Two months later, Xavier Le



Pichon published a synthesis showing the location and type of plate boundaries and their direction of movement (Fig. 1.16).

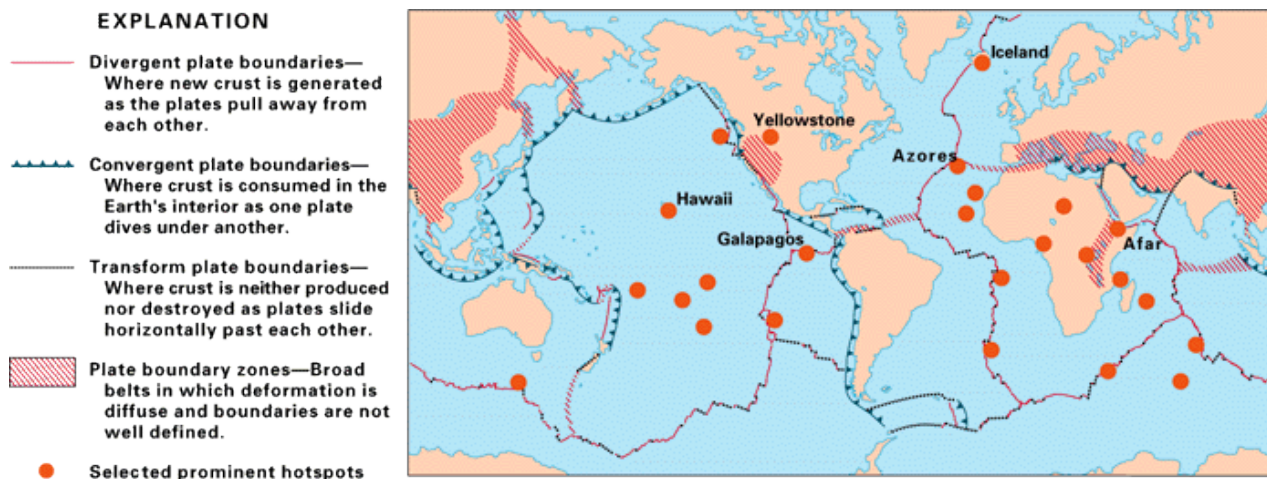


Fig. 1.14 – Location of the principal hot spots.

Since the mid-1960s, the plate tectonic model has been rigorously tested. Because the model has been successfully tested by numerous methods, it is now called the plate tectonic theory and is accepted by almost all geologists.

There is a debate within the geophysics community as to whether convection is likely to be 'layered' or 'whole'. This debate is linked to the controversy regarding whether intraplate volcanism is caused by shallow, upper-mantle processes (Fig. 1.17a) or by plumes from the lower mantle (Fig. 1.17b) or by a combination of the 2 hypotheses (Fig. 1.17c). Geochemists have argued that the lavas erupted in intraplate areas are different in composition from shallow-derived mid ocean ridge basalts. This has been interpreted as their originating from a different region, suggested to be the lower mantle. Others, however, have pointed out that the differences indicate the inclusion of a small component of near-surface material from the lithosphere. Seismologists are also divided, with some arguing that there is no evidence for whole-mantle convection, and others arguing that there is.

Earthquakes and volcanoes, evidence of unrest in the Earth, help locate the edges of plates (Fig. 1.18). Earthquakes are distributed in narrow, linear belts that circle the Earth. Some of these belts have only shallow (0-35 km) earthquakes, like the mid-Atlantic and east Pacific ridges. In contrast, earthquakes in other belts, like western South America and south-central Asia, are at shallow, intermediate (30-70 km), and deep (70-700 km) levels.

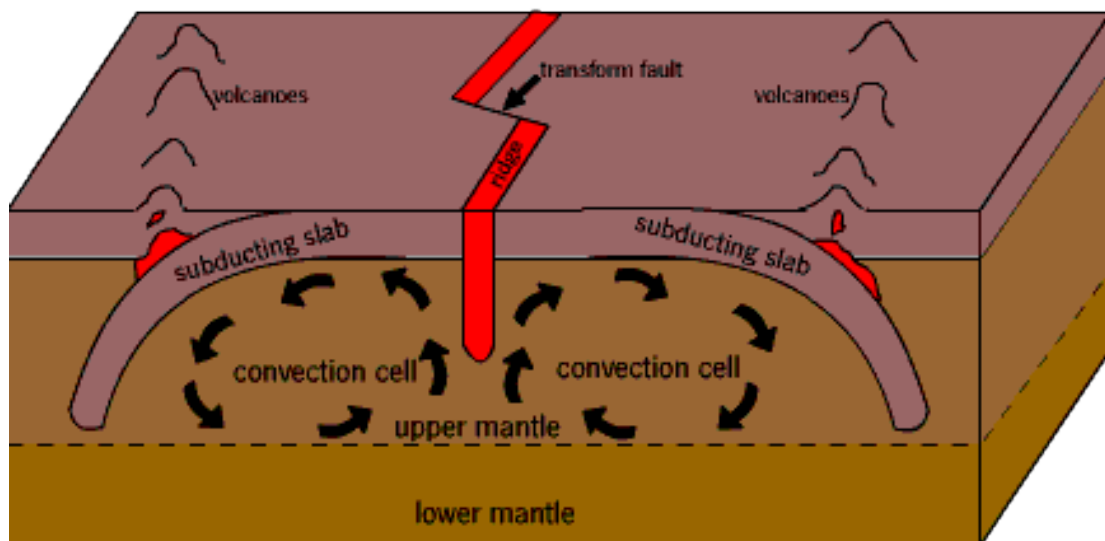


Fig. 1.15 – Heat convection within the Earth's mantle.

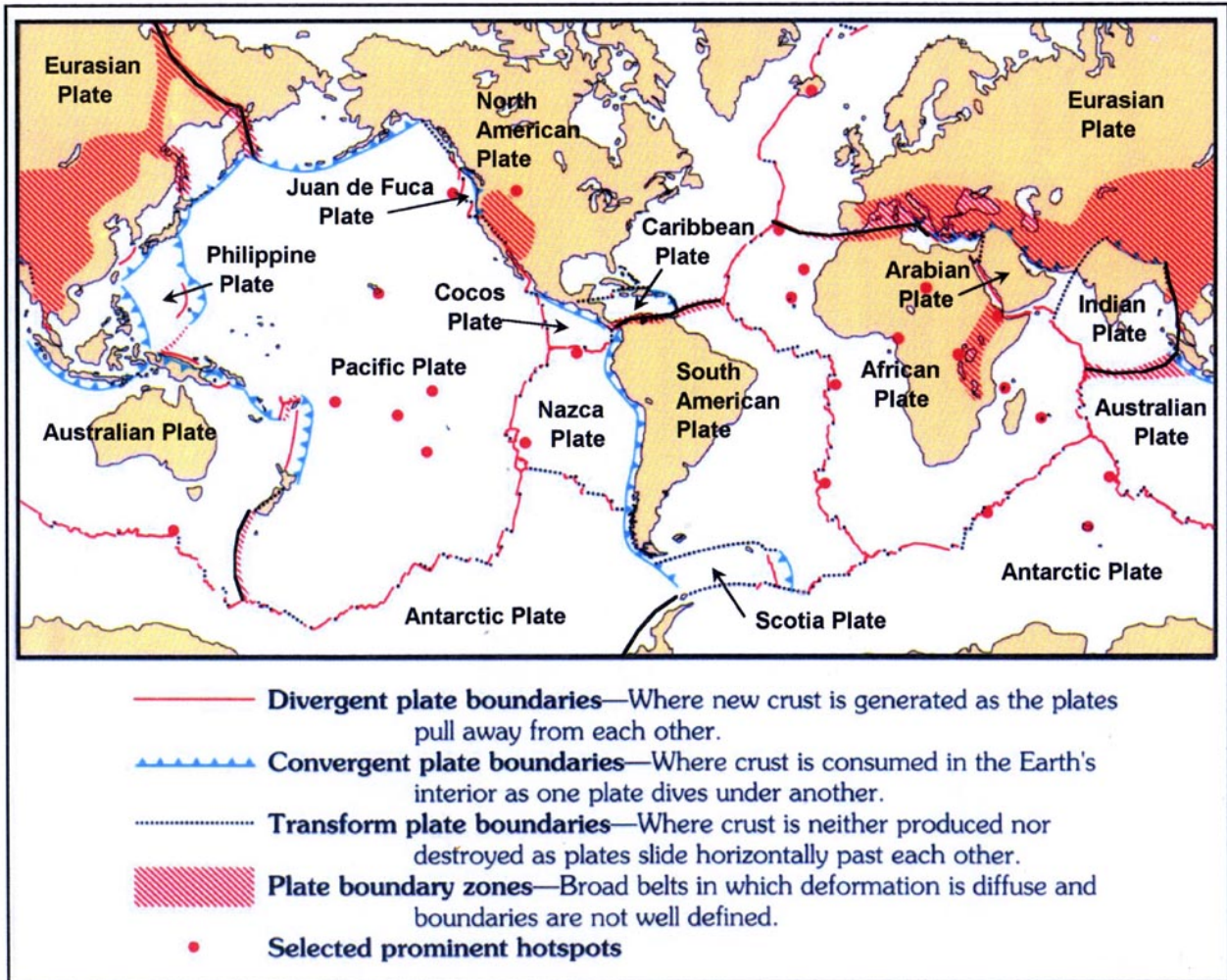


Fig. 1.16 - Major tectonic plates of the world.

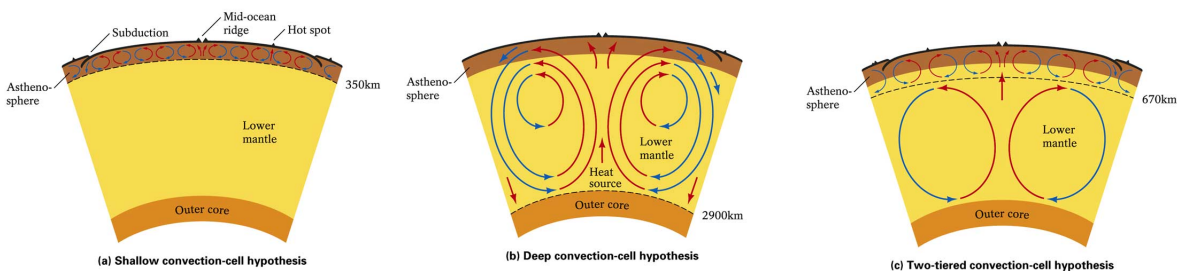
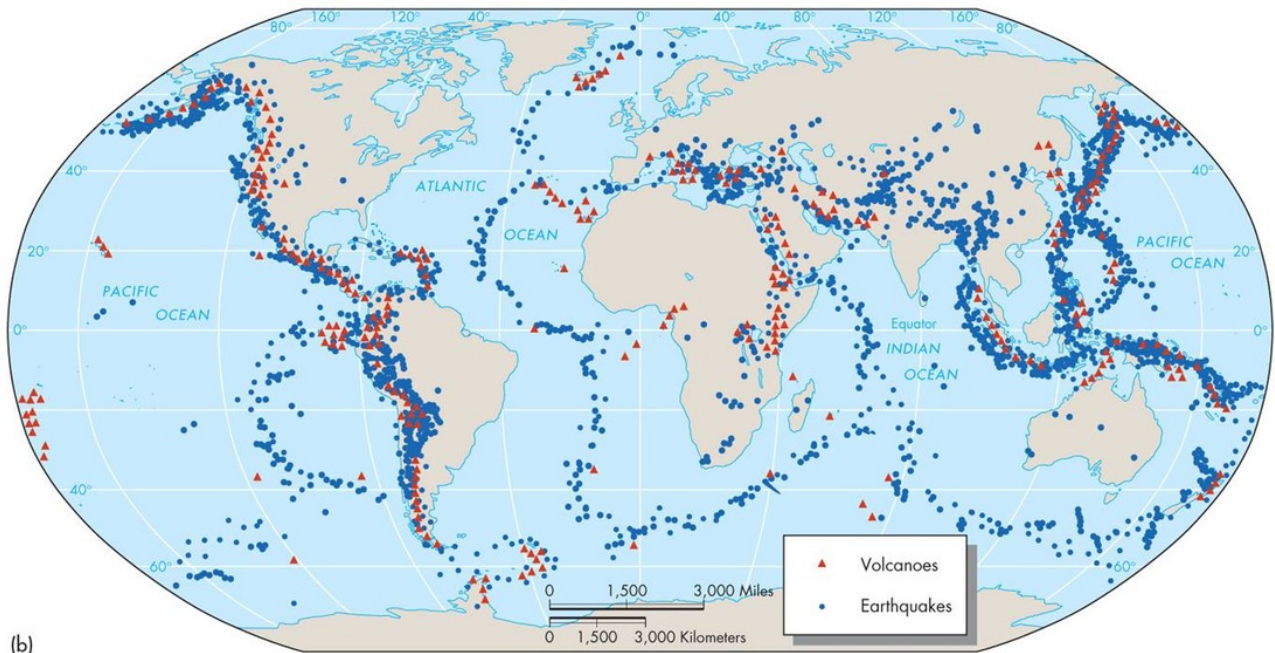


Fig. 1.17 - Three hypotheses of Earth convection: a) asthenosphere shallow convection model (most popular); b) deep mantle/core convection (Morgan) model, according which plumes cause mid-ocean ridges ; c) combination of the previous two models.

Volcanoes are also distributed in long belts that circle the Earth. A dramatic example is the line of volcanoes that circles most of the Pacific Ocean. This belt is known as the "Ring of Fire" (Fig. 1.19) because it is the site of frequent volcanic eruptions. The distribution of earthquakes and volcanoes coincides at most locations. The Ring of Fire is an excellent example. Geologists believe that areas of intense geologic activity, indicated by earthquakes, volcanoes, and/or mountain building, mark the boundaries between lithospheric plates. The distribution of earthquakes, volcanoes, and mountain ranges define 7 large plates and 20 smaller plates. The Nazca and Juan de Fuca Plates consist of only oceanic lithosphere. The Pacific Plate is mostly oceanic lithosphere only with a small slice of continental lithosphere in southern California and Baja Mexico. Most of the other plates consist of both oceanic and continental lithosphere.





(b)

Copyright © 2008 Pearson Prentice Hall, Inc.

Fig. 1.18 - Global distribution of volcanoes (red triangles) and earthquakes (blue dots).

The ways that plates interact depend on their relative motion and whether oceanic or continental crust is at the edge of the lithospheric plate. Plates move away from, toward, or slide past each other. Geologists call these divergent, convergent, and transform plate boundaries (Figs. 1.16 and 1.20).

Places where plates are coming apart are called divergent boundaries (Fig. 1.20a). As shown in the drawing above, when Earth's brittle surface layer (the lithosphere) is pulled apart, it typically breaks along parallel faults that tilt slightly outwards from each other. As the plates separate along the boundary, the block between the faults cracks and drops down into the soft, plastic interior (the asthenosphere). The sinking of the block forms a central valley called a rift. Magma (liquid rock) seeps upwards to fill the cracks. In this way, new crust is formed along the boundary. Earthquakes occur along the faults, and volcanoes form where the magma reaches the surface.

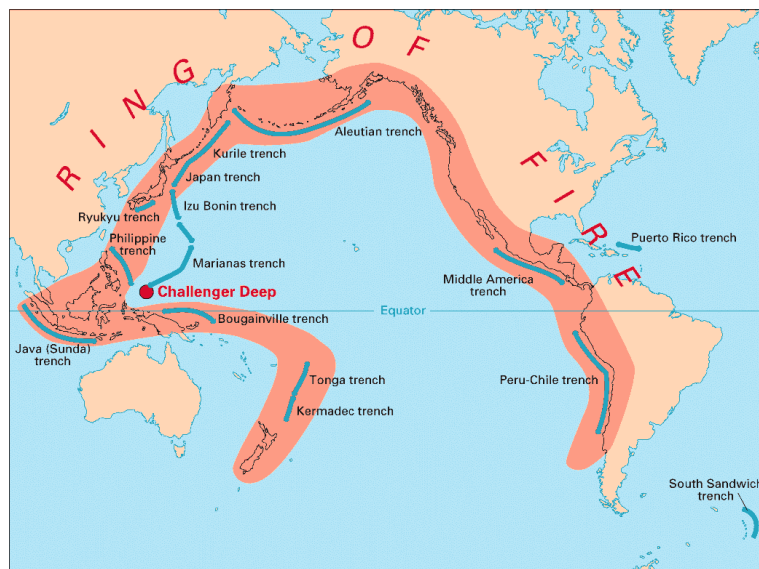


Fig. 1.19 - The Pacific Ring of Fire.

Where a divergent boundary crosses the land, the rift valleys which form are typically 30 to 50 km wide. Examples include the East Africa rift in Kenya and Ethiopia, and the Rio Grande rift in New

Mexico. Where a divergent boundary crosses the ocean floor, the rift valley is much narrower, only a kilometre or less across, and it runs along the top of a mid-oceanic ridge. Oceanic ridges rise a kilometre or so above the ocean floor and form a global network tens of thousands of kilometres long. Examples include the Mid-Atlantic ridge and the East Pacific Rise.

Plate separation is a slow process. For example, divergence along the Mid Atlantic ridge causes the Atlantic Ocean to widen at only about 2 cm per year.

Places where plates crash or crunch together are called convergent boundaries (Fig. 1.20b). Plates only move a few centimetres each year, so collisions are very slow and last millions of years. Even though plate collisions take a long time, lots of interesting things happen. For example, an oceanic plate has crashed into a continental plate and looking at two plates colliding is like looking at a single frame in a slow-motion movie of two cars crashing into each other. Just as the front ends of cars fold and bend in a collision, so do the "front ends" of colliding plates. The edge of the continental plate has folded into a huge mountain range, while the edge of the oceanic plate has bent downwards and dug deep into the Earth. A trench has formed at the bend. All that folding and bending makes rock in both plates break and slip, causing earthquakes. As the edge of the oceanic plate digs into Earth's hot interior, some of the rock in it melts. The melted rock rises up through the continental plate, causing more earthquakes on its way up, and forming volcanic eruptions where it finally reaches the surface. An example of this type of collision is found on the west coast of South America where the oceanic Nazca Plate is crashing into the continent of South America. The crash formed the Andes Mountains, the long string of volcanoes along the mountain crest, and the deep trench off the coast in the Pacific Ocean.

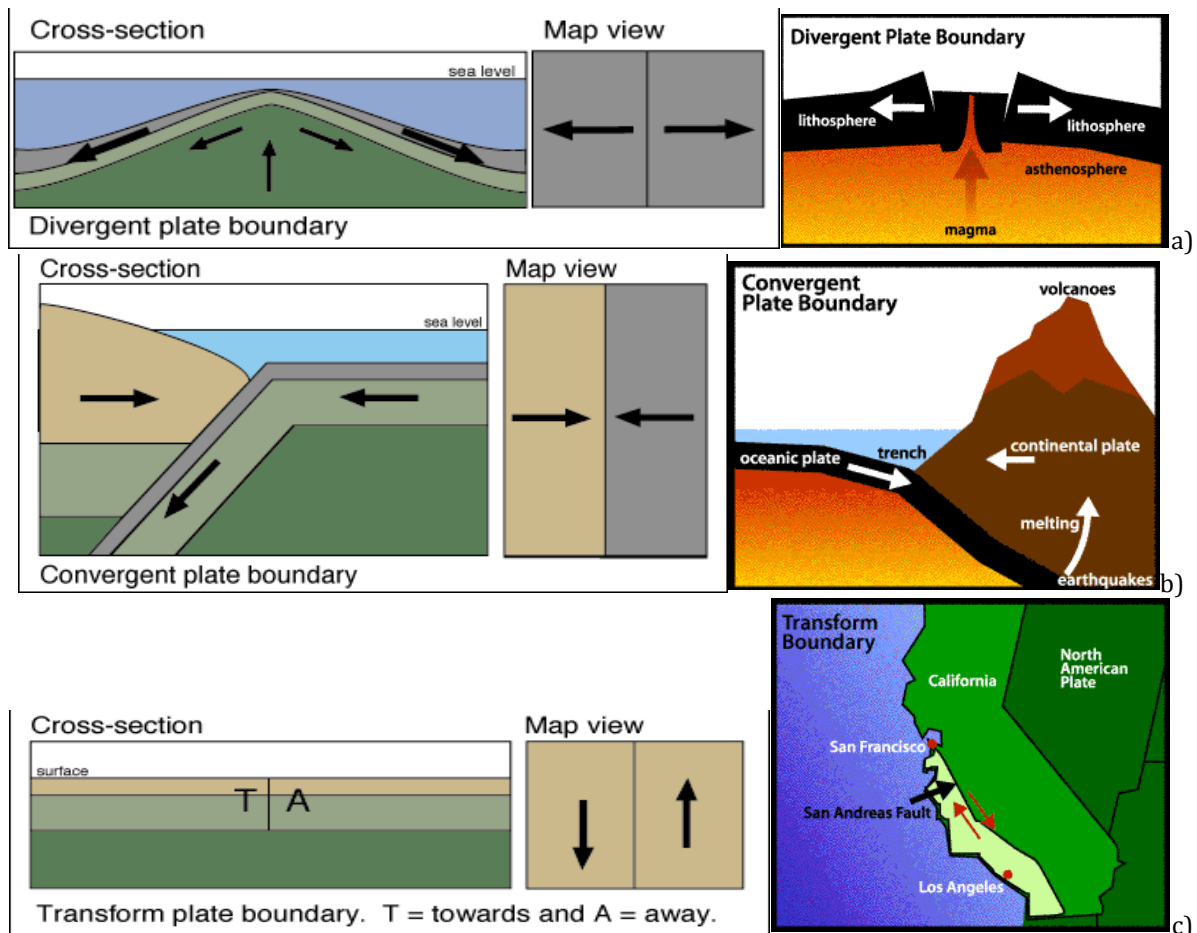


Fig. 1.20 - Plate boundaries: a) divergent; b) convergent; c) transform (T = towards, A = away).

Mountains, earthquakes, and volcanoes form where plates collide. Millions of people live in and visit the beautiful mountain ranges being built by plate collisions. For example, the Rocky Mountains in North America, the Alps in Europe, the Pontic Mountains in Turkey, the Zagros Mountains in Iran, and the Himalayas in central Asia were formed by plate collisions. Each year, thousands of people are

killed by earthquakes and volcanic eruptions in those mountains. Occasionally, big eruptions or earthquakes kill large numbers of people. In 1883 an eruption of Krakatau volcano in Indonesia killed 37,000 people. In 1983 an eruption-caused mudslide on Nevada del Ruiz in Columbia killed 25,000 people. In 1976, an earthquake in Tangshan, China killed an astounding 750,000 people. On the other hand, earthquakes and volcanoes occurring in areas where few people live harm no one. If we choose to live near convergent plate boundaries, we can build buildings that can resist earthquakes, and we can evacuate areas around volcanoes when they threaten to erupt. Convergent boundaries are dangerous places to live, but with preparation and watchfulness, the danger can be lessened somewhat.

Places where plates slide past each other are called transform boundaries (Fig. 1.20c). Since the plates on either side of a transform boundary are merely sliding past each other and not tearing or crunching each other, transform boundaries lack the spectacular features found at convergent and divergent boundaries. Instead, transform boundaries are marked in some places by linear valleys along the boundary where rock has been ground up by the sliding. In other places, transform boundaries are marked by features like stream beds that have been split in half and the two halves have moved in opposite directions.

Perhaps the most famous transform boundary in the world is the San Andreas fault (Fig. 1.21). The slice of California to the west of the fault is slowly moving north relative to the rest of California. Since motion along the fault is sideways and not vertical, Los Angeles will not crack off and fall into the ocean as popularly thought, but it will simply creep towards San Francisco at about 6 cm per year. In about ten million years, the two cities will be side by side!

Although transform boundaries are not marked by spectacular surface features, their sliding motion causes lots of earthquakes. The strongest and most famous earthquake along the San Andreas fault hit San Francisco in 1906. Many buildings were shaken to pieces by the quake, and much of the rest of the city was destroyed by the fires that followed. More than 600 people died as a result of the quake and fires. Recent large quakes along the San Andreas include the Imperial Valley quake in 1940 and the Loma Prieta quake in 1989.



Fig. 1.21 - An aerial view of the San Andreas fault in the Carrizo Plain, Central California.



In summary (Fig. 1.22), at a divergent plate boundary lithospheric plates move away from each other. The mid-Atlantic Ridge, a topographically high area near the middle of the Atlantic Ocean, is an example of a divergent plate boundary. At a convergent plate boundary, lithospheric plates move towards each other. The west margin of the South American continent, where the oceanic Nazca Plate is pushed towards and beneath the continental portion of the South American Plate, is an example of a convergent plate boundary. At a transform plate boundary, plates slide past each other. The San Andreas fault in California is an example of a transform plate boundary, where the Pacific Plate slides past the North American Plate.

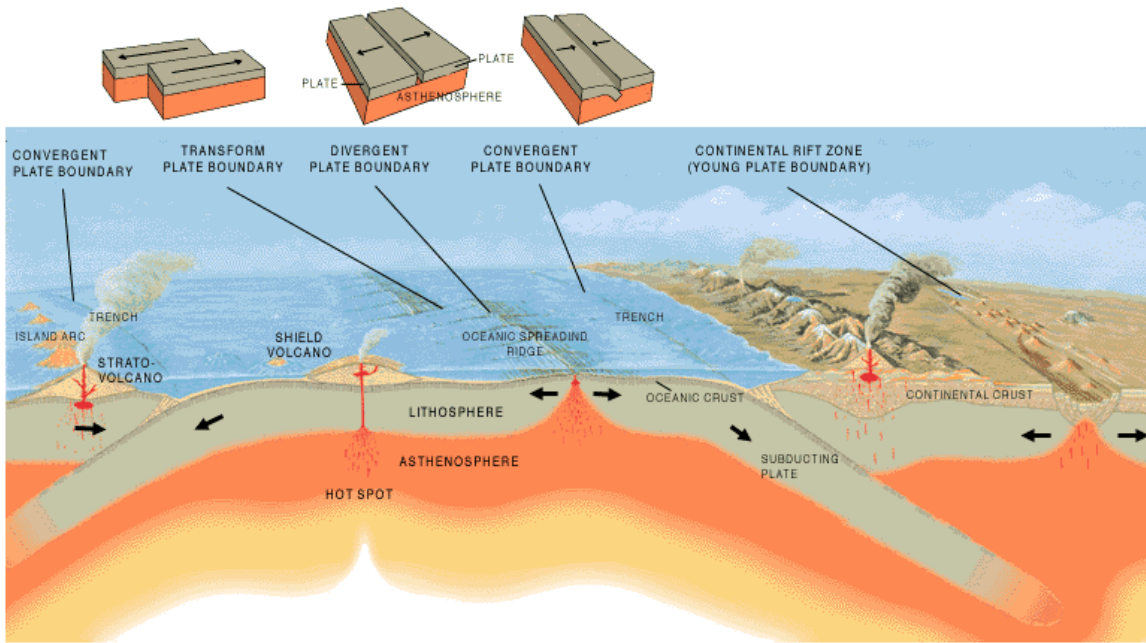


Fig. 1.22 - General scheme of the activity along the boundaries.

### 1.2.6. Mapping the ocean floor

The three major topographic units of the ocean floor are: the continental margin, the deep-ocean basins, and the oceanic ridges.

#### 1.2.6.1. The continental margin

A continental margin is the submarine edge of the continental crust distinguished by relatively light and isostatically high-floating material in comparison with the adjacent oceanic crust. It is the name for the collective area that encompasses the continental shelf, continental slope, and continental rise. The characteristics of the various continental margins are shaped by a number of factors. Chief among these are tectonics, fluctuations of sea level, the size of the rivers that empty onto a margin as determined by the amount of sediment they carry, and the energy conditions or strength of the ocean waves and currents along the margin.

The continental margins can be either passive or active.

##### 1.2.6.1.1. The passive continental margin

Passive continental margins (Fig. 1.23) are found along coastal areas that surround oceans, not near active plate boundaries. They show little volcanism and few earthquakes, an example is given by the eastern coast of the U.S.A. The main features of a passive continental margin are: the continental shelf, the continental slope, and the continental rise.

The continental shelf is a broad, relatively shallow submarine terrace of continental crust forming the edge of a continental landmass. The geology of continental shelves is often similar to that of the adjacent exposed portion of the continent, and most shelves have a gently rolling topography called ridge and swale. Continental shelves make up about 8% of the entire area covered by oceans.

The continental slope is the seaward border of the continental shelf. The world's combined continental slope has a total length of approximately 300,000 km and descends at an average angle in excess of  $4^\circ$  from the shelf break at the edge of the continental shelf to the beginning of the ocean basins at depths of 100 to 3,200 m.

The continental rise is a major depositional regime in oceans made up of thick sequences of continental material that accumulate between the continental slope and the abyssal plain. Continental rises form as a result of three sedimentary processes: mass wasting, the deposition from contour currents, and the vertical settling of clastic and biogenic particles.

#### 1.2.6.1.2. The active continental margin

The main characteristics of an active continental margin (Fig. 1.24) are that the continental slope descends abruptly into a deep-oceanic trench and that sediment and oceanic crust scraped off ocean crust to form accretionary wedges.

Active continental margins are located primarily around the Pacific Ocean.

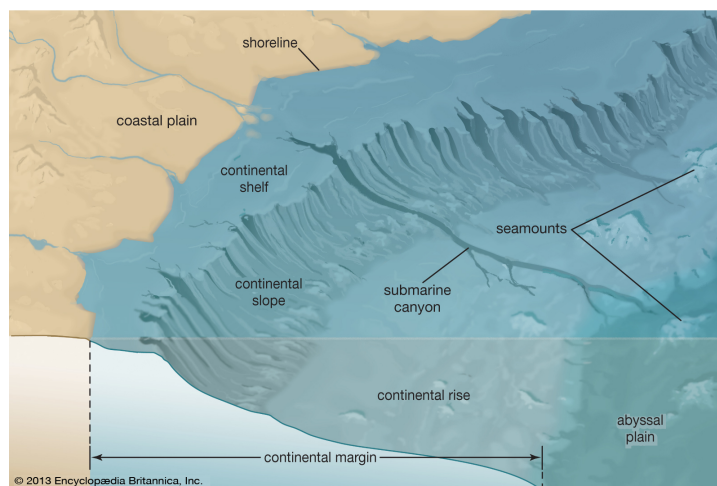


Fig. 1.23 – Cartoon showing the main features of a passive continental margin (from Encyclopædia Britannica, Inc.).

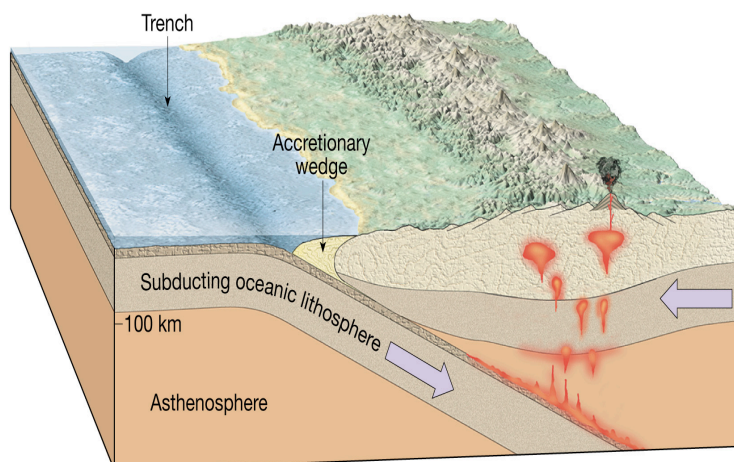


Fig. 1.24 – Cartoon showing the main features of an active continental margin (from Encyclopædia Britannica, Inc.).

Ocean basin, any of several vast submarine regions that collectively cover nearly three-quarters of Earth's surface. Together they contain the overwhelming majority of all water on the planet and have an average depth of almost 4 km. A number of major features of the basins depart from this average—for example, the mountainous ocean ridges, deep-sea trenches, and jagged, linear fracture zones. Other significant features of the ocean floor include aseismic ridges, abyssal hills, and seamounts and guyots. The basins also contain a variable amount of sedimentary fill that is thinnest on the ocean ridges and usually thickest near the continental margins.

#### 1.2.6.2. The deep-ocean basin

The main features of a deep-ocean basin are: the deep-ocean trench and the abyssal plain.

The deep-ocean trench is represented by any long, narrow, steep-sided depression in the ocean bottom in which occur the maximum oceanic depths, approximately 7,300 to more than 11,000 metres. They typically form in locations where one tectonic plate subducts under another and are associated with volcanic activity. Most of the deep-ocean basins are located in the Pacific Ocean. The deepest known depression of this kind is the Mariana Trench, which lies east of the Mariana Islands in the western North Pacific Ocean: it reaches 11,034 m at its deepest point.

The abyssal plain (Fig. 1.25) is a flat seafloor area at an abyssal depth (3,000 to 6,000 m), generally adjacent to a continent. These submarine surfaces vary in depth only from 10 to 100 cm per kilometre of horizontal distance. Irregular in outline but generally elongate along continental margins, the larger plains are hundreds of kilometres wide and thousands of kilometres long. In the North Atlantic the Sohm Plain alone has an area of approximately 900,000 km<sup>2</sup>. The plains are largest and most common in the Atlantic Ocean, less common in the Indian Ocean, and even rarer in the Pacific, where they occur mainly as the small, flat floors of marginal seas or as the narrow, elongate bottoms of trenches. The abyssal plains can be sites of thick accumulations of sediment and are studded by old cold seamounts and ridges.

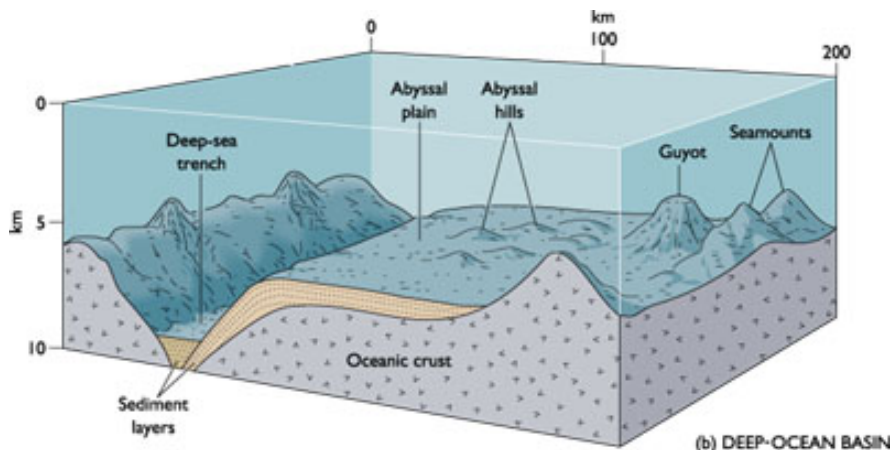


Fig. 1.25 – Cartoon showing the main features of an abyssal plain.

#### 1.2.6.3. The oceanic ridge

An oceanic ridge (Fig. 1.26) is a continuous submarine mountain chain extending approximately 80,000 km through all the world's oceans. Individually, ocean ridges are the largest features in ocean basins. Collectively, the oceanic ridge system is the most prominent feature on Earth's surface after the continents and the ocean basins themselves. In the past, these features were referred to as mid-ocean ridges, but, as will be seen, the largest oceanic ridge, the East Pacific Rise, is far from a mid-ocean location, and the nomenclature is thus inaccurate. Oceanic ridges are not to be confused with aseismic ridges, which have an entirely different origin.



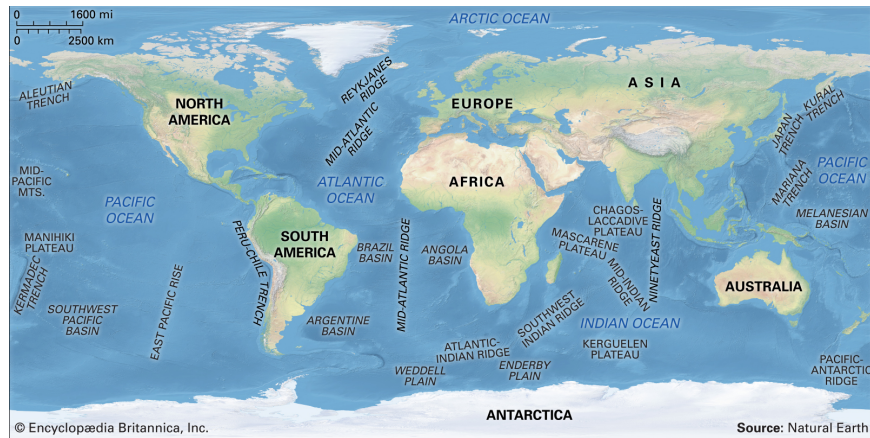


Fig. 1.26 – Trenches and ridges in the oceans (from Encyclopædia Britannica, Inc.).

### 1.3. Faults

Geologic faults or simply faults are planar rock fractures which show evidence of relative movement. Large faults within the Earth's crust are the result of shear motion and active fault zones are the causal locations of most earthquakes. Earthquakes are caused by energy release during rapid slippage along faults. The largest examples are at tectonic plate boundaries, but many faults occur far from active plate boundaries. Since faults usually do not consist of a single, clean fracture, the term fault zone is used when referring to the zone of complex deformation associated with the fault plane.

The two sides of a fault are called the hanging wall and footwall. By definition, the hanging wall occurs above the fault and the footwall occurs below the fault (Fig. 1.27).

The sense of slip is defined by the relative movements of geological features present on either side of the fault plane and is a vector. The sense of slip defines the type of fault. This is distinct from the throw of the fault, which is the vertical offset. Heave is the measured horizontal offset of the fault (Fig. 1.28).

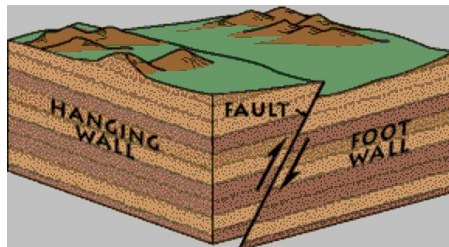


Fig. 1.27 – Hanging wall and footwall.

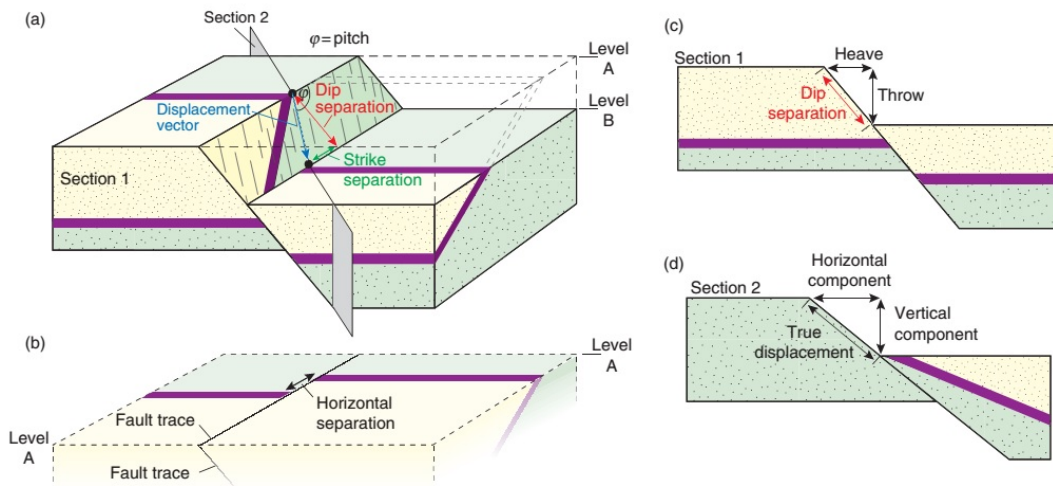


Fig. 1.28 – Definition of heave and throw.

### 1.3.1. Fault types

Faults can be categorized into three groups based on the sense of slip (Fig. 1.29). A fault where the main sense of movement (or slip) on the fault plane is vertical is known as a dip-slip fault. Where the main sense of slip is horizontal the fault is known as a transform (or strike-slip) fault. Oblique-slip faults have significant components of both strike and dip slip.

For all naming distinctions, it is the orientation of the net dip and sense of slip of the fault which must be considered, and not the present day orientation, which may have been altered by local or regional folding or tilting.

### 1.3.2. Dip-slip faults

Dip-slip faults include both normal and reverse. A normal fault occurs when the crust is in extension (Figs. 1.30 and 1.31). The hanging wall moves downwards relative to the footwall. The depressed ground between two parallel normal faults is called a graben (Fig. 1.32). An upthrown block between two parallel normal faults is called a horst. Low-angle normal faults with regional tectonic significance may be designated detachment faults.

A reverse fault is the opposite of a normal fault: the hanging wall moves up relative to the footwall. Reverse faults are indicative of shortening of the crust. The dip of a reverse fault is relatively steep, greater than  $45^\circ$ .

A thrust fault has the same sense of motion as a reverse fault, but with the dip of the fault plane at less than  $45^\circ$  (Figs. 1.33 to 1.35). Thrust faults typically form ramps, flats and fault-bend (hanging wall and foot wall) folds. Thrust faults are responsible for forming nappes and klippen in the large thrust belts.

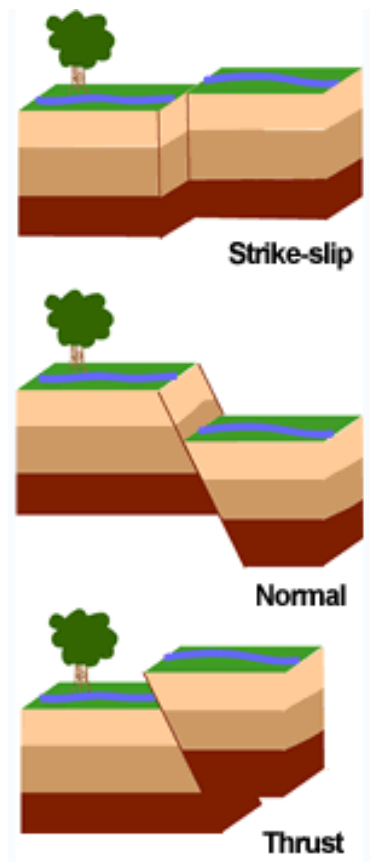


Fig. 1.29 - Types of faults.



Fig. 1.30 - Soft-linked normal faults in Carboniferous sandstones and shales from Saundersfoot, Pembrokeshire.



Fig. 1.31 - Sanech planar normal faults - domino block.



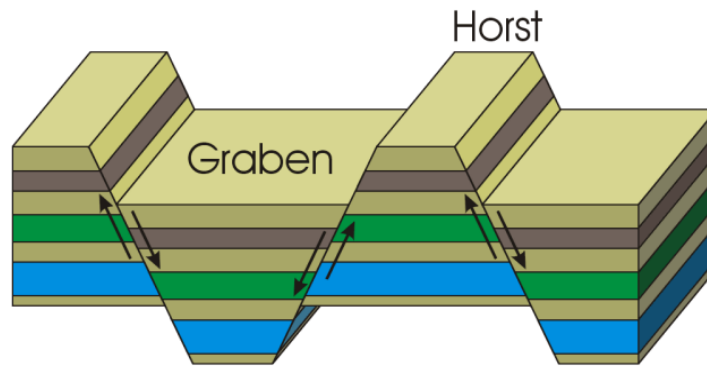


Fig. 1.32 – Sketch of a horst-graben system.



Fig. 1.33 - The Keystone thrust near Las Vegas, Nevada, is a spectacular example of a thrust fault. The dark-gray Cambrian limestone of the Bonanza King Formation is moved sideways and above the pink Aztec Sandstone, of Jurassic age. The thrust fault was most active about 70 million years ago, during the long Sevier orogeny (mountain-building episode). Compressive forces caused by tectonic plate interactions to the west pushed the upper crust eastwards. Movement on this thrust fault, which is part of the extensive Sevier fold-thrust belt, appears to have been nearly 100 kilometres.



Fig. 1.34 – Detail of a thrust fault.



Fig. 1.35 – Thrust fault: hanging wall deflection.

The fault plane is the plane that represents the fracture surface of a fault. Flat segments of thrust fault planes are known as flats, and inclined sections of the thrust are known as ramps. Typically thrust faults move within formations by forming flats, and climb up section with ramps.

Fault-bend folds are formed by faults from the pressure of the hanging wall and footwall moving against one another.

In Fig. 1.36, you see a normal fault at left. A reverse fault is the same, except the hanging wall moves up instead of down. At right, you see a thrust fault

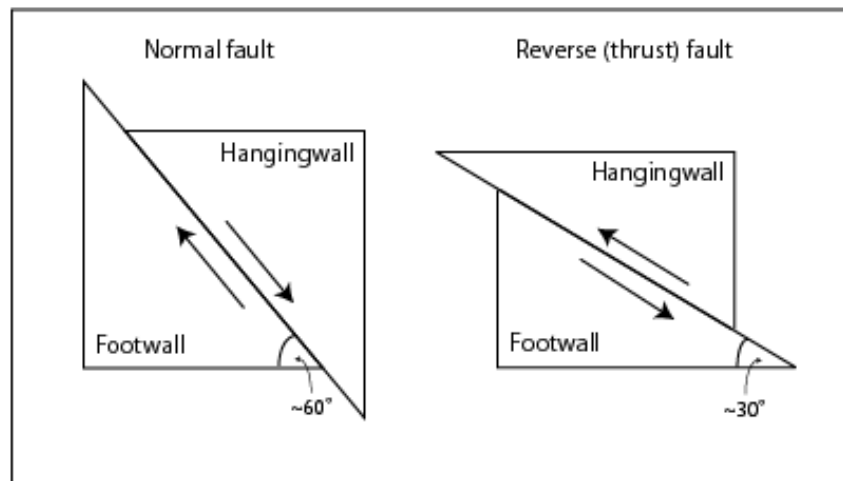


Fig. 1.36 - Schematic illustration of normal and reverse faults. Note that the view is a cross-section through the Earth, such that the up-direction on the page is away from the centre of the Earth.

### 1.3.3. Strike-slip faults

In the strike-slip faults, the fault surface is usually near vertical and the footwall moves either left or right or laterally with very small vertical motion (Fig. 1.37). Strike-slip faults with left-lateral motion are also known as sinistral faults. Those with right-lateral motion are also known as dextral faults. A special class of strike-slip faults is the transform faults which are a plate tectonics feature related to spreading centres such as mid-ocean ridges.

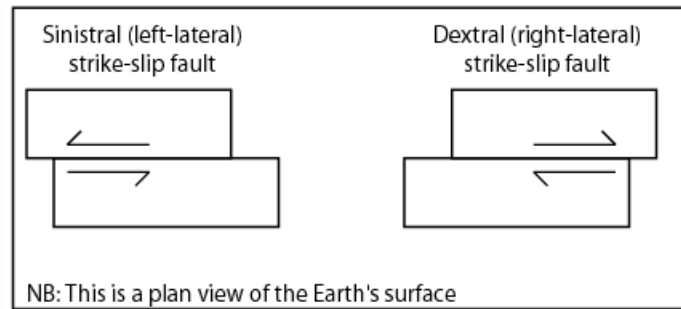


Fig. 1.37 - Schematic illustration of the two strike-slip fault types. The view is of the Earth's surface as from space.

The San Andreas fault is a remarkable example of a strike-slip fault. It marks the boundary between the North American and Pacific Plates in California (Fig. 1.38). These two tectonic plates are sliding horizontally past each other along the transform fault. Rock on the Pacific Plate is being carried NW and juxtaposed against different rock at the edge of the North American Plate.

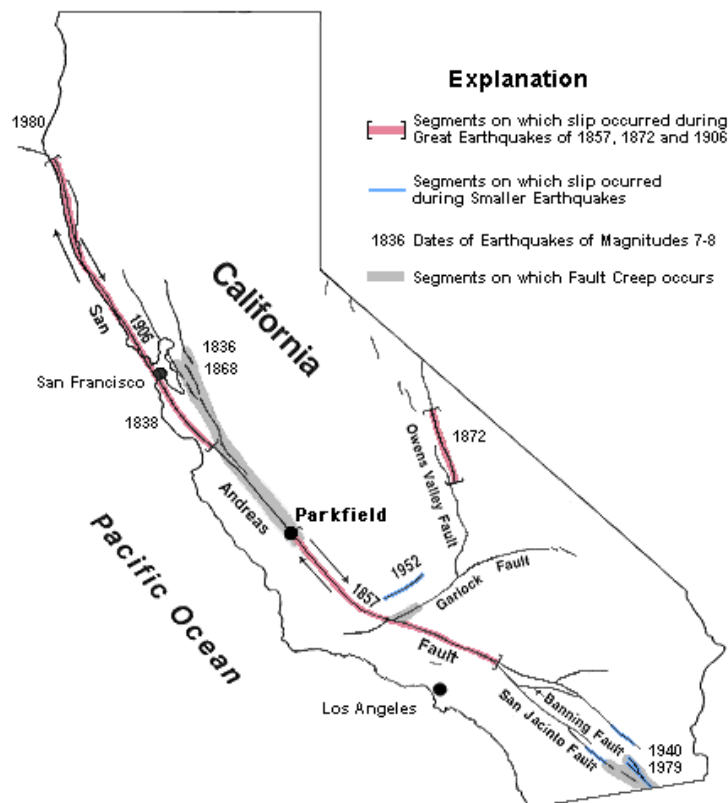


Fig. 1.38 – Main features of the San Andreas fault.

Normally, the interface is buried by Quaternary sediments or overgrown by vegetation. In Tejon Pass near the town of Gorman, however, the contact between the two plates is clearly evident (Fig. 1.39). The fault runs up a hillside and separates rocks of different composition and colour. To the SW is grey, metamorphic quartz monzonite and to the NE across the fault is rich brown sedimentary sandstone and siltstone. These two rocks could not have formed together and therefore must have been brought together by fault motion. Between the grey and tan is a black layer of fault gouge, rock that has been pulverized and cooked by frictional heating generated by earthquakes. The entire hillside is granulated and appears gouged due to the constant grinding of the plates. A diagonal colour discontinuity defines the surface rupture of the 1857 earthquake, which moved the rocks on one side of the fault about 9 m relative to other. This magnitude 8.0 temblor was the largest earthquake in California's recorded history. The San Andreas fault is about 1100 km long, stretching from Cape Mendocino to the Salton Sea. On average, the Pacific side is moving horizontally past the North



American side at a rate of 34 mm per year, about as fast as a fingernail grows. But the fault here is not moving every single minute: it only moves during large earthquakes, which happen once every few hundred years. At Wallace Creek, it moved 9 m on January 9, 1857.



Fig. 1.39 – The San Andreas fault in the Tejon Pass area.

#### 1.3.4. Oblique-slip faults

A fault which has a component of dip-slip and a component of strike-slip is termed an oblique-slip fault. Nearly all faults will have some component of both dip-slip and strike-slip, so defining a fault as oblique requires both dip and strike components to be measurable and significant. Most oblique faults occur within transtensional and transpressional regimes (Fig. 1.40).

#### 1.3.5. Fault characterization

A fault is characterized by its surface expression (if any), by its type (strike slip and dip slip), and by its geometry (length and area). In addition, if the fault is active, there are some parameters that characterize its activity: the slip rate, the slip per event, the earthquake size, and the recurrence interval.

The slip rate ( $SR$ ) is the average rate of deformation across the fault. It is given by:

$$SR = (\text{Accumulative Offset}) / (\text{Time of Offset}) \quad (1-1)$$

This formula assumes that strain is accumulated and released uniformly and that the tectonic environment is unchanged in time. Some example are given by the San Andreas Fault with an  $SR$  of 20-50 mm/yr and the Wasatch Fault (Utah) with an  $SR$  of 1-2 mm/yr.

The slip per event ( $SpE$ ) is the amount of slip released during an earthquake. Considering a specific fault, it is important to know the average, the maximum, and the minimum slip per event. Slip per event is an additional information to the slip rate because it is very different if a 50-mm

displacement per year occurs in one large event or in many small events. Considering a long fault, the amount of slip may vary in its different segments.

It is not easy to identify the size of the earthquake that a fault can generate. Some faults may have a characteristic magnitude (e.g., earthquakes of the same magnitude tend to repeat) others not and, in this case, it is important to estimate the maximum magnitude that a fault can express. The quantity related to the earthquake magnitude is the rupture length, that, if not known by surface evidence, is generally taken as 1/3 to 1/2 of the fault length. The “rule of thumb” associate an  $M=5$  to a 1-km rupture, an  $M=6$  to a 10-km rupture, and an  $M=7.5$  to a 100-km rupture. Better correlations refer to fault area vs. magnitude etc. (see chapter 1.12)

The recurrence interval ( $RI$ ) is the average time span for a given earthquake to occur. Considering a fault generating characteristic earthquakes (events of the same magnitude), it is possible to estimate the annual number of these characteristic earthquakes ( $N$ ) and their  $RI$  by:

$$N = SR/SpE \quad (1-2)$$

$$RI = 1/N \quad (1-3)$$

The recurrence law provides a definition of temporal distribution of earthquakes, i.e., it indicates how often earthquakes of different sizes occur. A recurrence law provides a link between slip rate and earthquake size giving a rate of occurrence for earthquakes of different magnitudes.

#### 1.4. Earthquakes

An earthquake is a vibration or oscillation of the surface of the Earth caused by a transient disturbance of the elastic or gravitational equilibrium of the rocks at or beneath the surface. Earthquakes are classified as natural or artificial according to the nature of the source. They are called artificial if the disturbance was caused by man with a blast: the quantity of explosive needed in this case, is very great if the shock is used for geophysical research and the movement of the Earth has to be recorded at different points. Natural earthquakes are caused by natural processes in the Earth and their nature can be volcanic or tectonic. Volcanic earthquakes are determined by a volcanic activity, they are placed in well known parts of the Earth and they constitute a small number of all the shocks that amount to about 1 million per year. In this type of earthquakes the direct cause is an induced effect of the geodynamic process. In tectonic earthquakes the direct cause is the geodynamic movement itself.

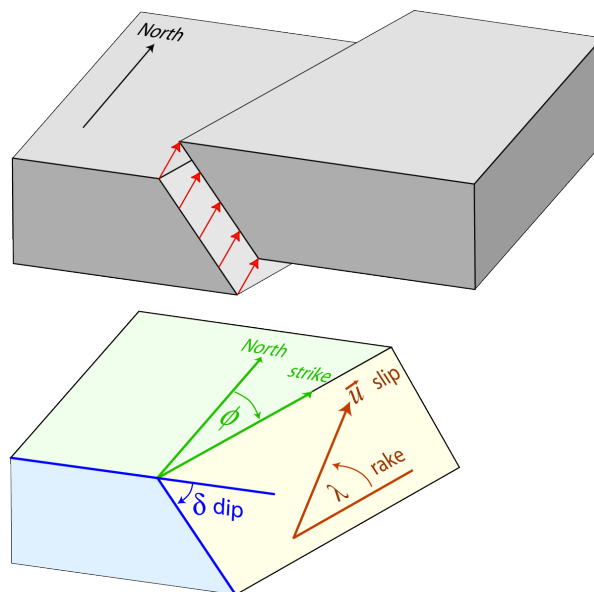


Fig. 1.40 – Definition of dip, strike, and rake of a fault rupture.



The stress at a point in the interior of a body is determined by the systems of forces acting in the vicinity of that point. The deformation of the body in the vicinity of a given point is termed strain. The concepts of stress and strain are fundamental to the theory of seismic waves and to understand the deformation of rocks. The stresses are set up beneath the sedimentary layers by the creeping or flowing of great masses of rock in a complex kind of pattern. If the structure is sufficiently plastic to adjust itself to the changing stresses and can gradually revert to a condition of no strain there will be no earthquakes; but if the structure is rigid enough to resist this slow deformation, the stresses will accumulate until the elastic limit of the rock is reached and then the structure will snap somewhere. This is a simple description of the mechanism of an earthquake.

The hypocentre or focus is the point inside the Earth where the crack begins (Fig. 1.41). For very strong shocks the concept of hypocentre is generally substituted by that of focal volume. The epicentre is the projection of the hypocentre on the surface of the Earth and it is generally the place where the most severe damages occur.

Earthquakes can be divided into three categories according to the depth of the focus:

- shallow, with hypocentre in the crust with a maximum depth of 60 km;
- intermediate, with a depth varying from 60 to 300 km;
- deep, with a depth varying from 300 to 650 km.

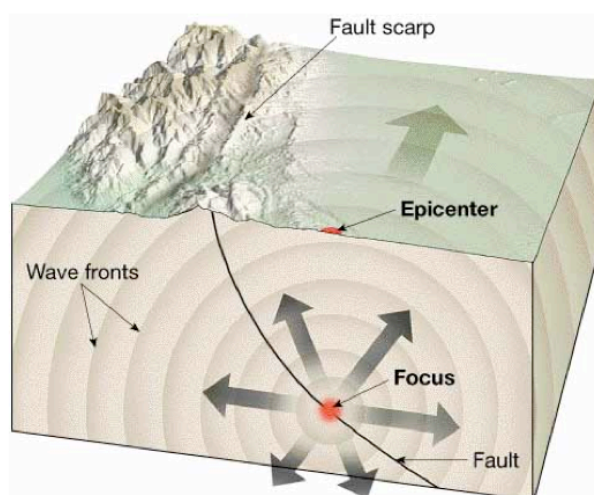


Fig. 1.41 – Hypocentre and epicentre locations.

If the hypocentre is very deep the major damage is not concentrated at a single point on the Earth's surface but there is an epicentral area corresponding to the base of a cone having its vertex in the focus. When an earthquake occurs a very great energy is released under different forms. A very important quantity of energy is transmitted as seismic energy: the Earth reacts as an elastic solid and seismic waves are propagated to all parts of the Earth following paths through the body of the Earth itself and around its surface.

The main dates of the history of seismology are described in the following.

Ca 132 BC: First seismoscope, showing the direction of incoming earthquake waves, is developed in China.

1875: The first seismometer is invented by Filippo Cecchi in Italy.

1889: A distant earthquake is recorded instrumentally for the first time. The recording is made in Potsdam, Germany of a Japanese earthquake (Fig. 1.42).

1892: John Milne develops a seismometer, which is installed at ca. 40 observatories around the world. This is the beginning of global earthquake monitoring.

1906: Richard Oldham discovers Earth's core by studying seismic waves.

1909: Andrija Mohorovicic discovers the Moho discontinuity, which is the boundary between Earth's crust and mantle.

1935: Charles Richter develops the magnitude scale (the so-called "Richter's magnitude scale"), which is used for determining the size of earthquakes as applied in southern California.

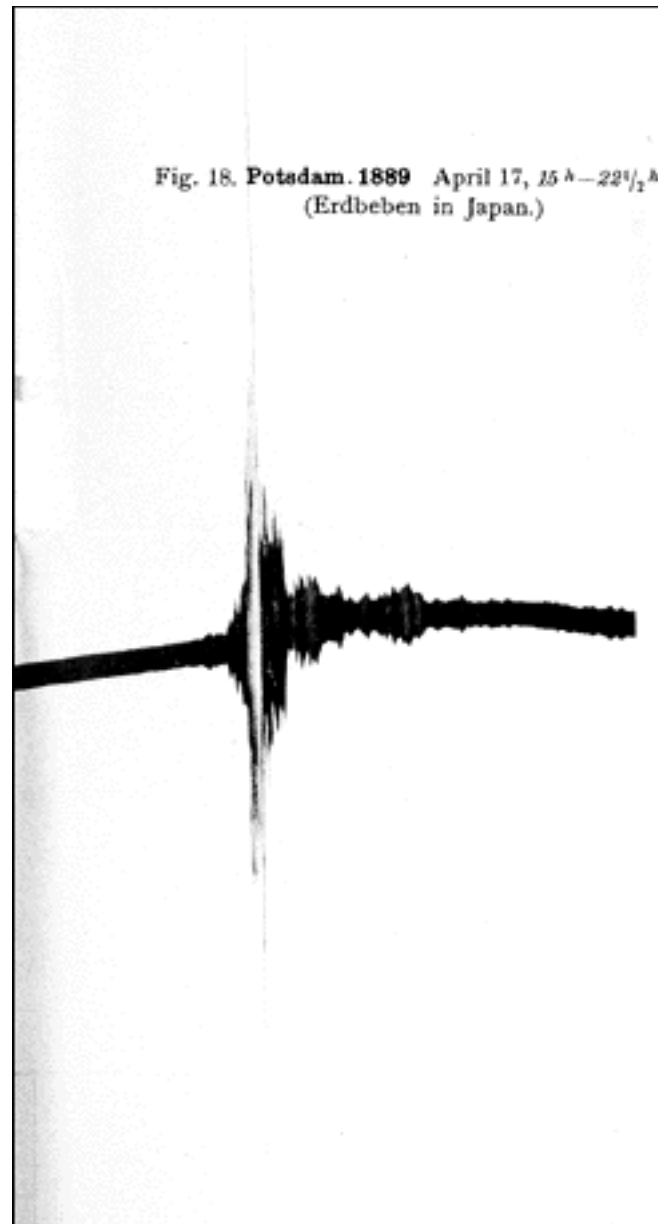


Fig. 1.42 – Japan earthquake of April 17, 1889 recorded in Potsdam.

1936: Inge Lehmann from Denmark discovers the Earth's inner core.

1946: A nuclear explosion is recorded by a seismograph for the first time.

1960: The largest recorded earthquake occurs in Chile, with a magnitude 9.5.

1961: The World-Wide Standardized Seismic Network (WWSSN) is established for monitoring both earthquakes and nuclear testing. WWSSN has played a central role in supplying data supporting the theory of continental drift and plate tectonics, which helps understanding the fundamental deformational processes of the Earth. WWSSN is later taken over by IRIS (Incorporated Research Institutions for Seismology) and now continues as the Global Seismic Network (GSN).

1966: Keiiti Aki defines seismic moment, which is a physical measure of the magnitude of an earthquake.

1969-72: Apollo astronauts place a seismometer on the Moon, and the first "moonquakes" are registered.

1977: Hiroo Kanamori establishes the moment magnitude scale, which is a measure of earthquake magnitude based on seismic moment. The moment magnitude scale is used by most seismologists today.

1996: The Comprehensive Nuclear-Test-Ban Treaty (CTBT) is established. As of 2005, the treaty is signed by 174 countries. At the same time, the International Data Center is established in Vienna,

coordinating the monitoring in connection to the treaty. Seismic monitoring is done through the International Monitoring System (IMS). Fig. 1.43 shows the global network of stations that are part of GSN and IMS.

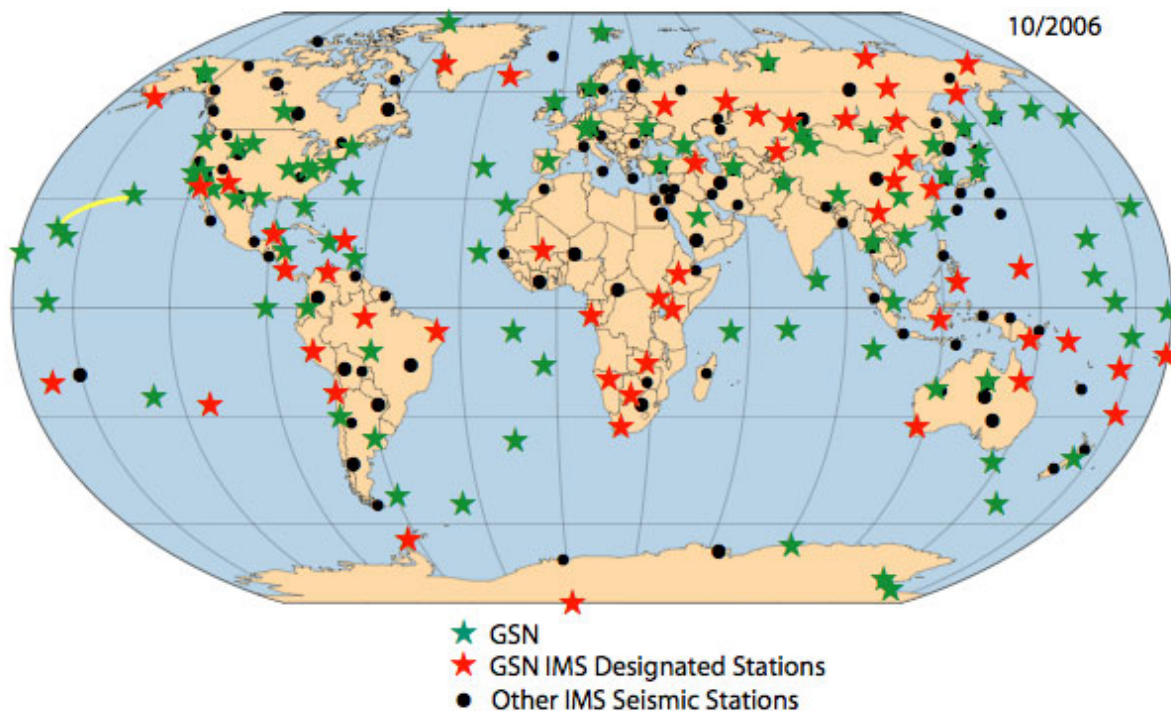


Fig. 1.43 – GSN and IMS networks as in October 2006 (from the IRIS web page).

#### 1.4.1. Earthquake myths

Far back in history, people have tried to explain why earthquakes occur. Ancient cultural explanations of earthquakes were often along the lines of the mythical Japanese Namazu: a giant catfish with the islands of Japan on his back. A demigod holds a heavy stone over his head to keep him from moving. Once in a while the demigod is distracted so Namazu moves and the Earth trembles. Moreover, different cultures around the world have attempted to explain earthquakes in different ways. Here are some legends about what makes the ground shake.

- 1) **India:** The Earth is held up by four elephants that stand on the back of a turtle. The turtle is balanced on top of a cobra. When any of these animals move, the Earth trembles and shakes.
- 2) **Assam (Between Bangladesh and China):** There is a race of people living inside the Earth. From time to time, they shake the ground to find out if anyone is still living on the surface. When children feel a quake, they should shout "Alive, Alive!" so the people inside the Earth will know they are there and stop shaking.
- 3) **Mexico:** El Diablo, the devil, makes giant rips in the Earth from the inside. He and his devilish friends use the cracks when they want to come and stir up trouble on Earth.
- 4) **Siberia:** The Earth rests on a sled driven by a god named Tuli. The dogs who pull the sled have fleas. When they stop to scratch, the Earth shakes.
- 5) **Japan:** A great catfish, or namazu, lies curled up under the sea, with the islands of Japan resting on his back. A demigod, or daimyojin, holds a heavy stone over his head to keep him from moving. Once in a while, though, the daimyojin is distracted, the namazu moves, and the Earth trembles.
- 6) **Mozambique:** The Earth is a living creature, and it has the same kinds of problems people have. Sometimes, it gets sick with fever and chills and we can feel its shaking.
- 7) **Greece:** According to Aristotle, and also to William Shakespeare in a play called Henry IV, strong, wild winds are trapped and held in caverns under the ground. They struggle to escape, and

earthquakes are the result of their struggle.

- 8) Belgium:** When people on Earth are very, very sinful, God sends an angry angel to strike the air that surrounds our planet. The blows produce a musical tone that is felt on the Earth as a series of shocks.
- 9) Native American:** Once a Chickasaw chief was in love with a Choctaw princess. He was young and handsome, but he had a twisted foot, so his people called him Reelfoot. When the princess' father refused to give Reelfoot his daughter's hand, the chief and his friends kidnapped her and began to celebrate their marriage. The Great Spirit was angry and stomped his foot. The shock caused the Mississippi River to overflow its banks and drown the entire wedding party. (Reelfoot Lake, on the Tennessee side of the Mississippi River, was formed as a result of the New Madrid earthquake of 1812).
- 10) West Africa:** The Earth is a flat disk, held up on one side by an enormous mountain and on the other by a giant. The giant's wife holds up the sky. The Earth trembles when he stops to hug her.
- 11) India:** Seven serpents share the task of guarding the seven sections of the lowest heaven. The seven of them also take turns holding up the Earth. When one finishes its turn and another moves into place, people on the Earth may feel a jolt.
- 12) Latvia:** A god named Drebkuhls carries the Earth in his arms as he walks through the heavens. When he's having a bad day, he might handle his burden a little roughly. Then the Earth will feel the shaking.
- 13) Colombia:** When the Earth was first made, it rested firmly on three large beams of wood. But one day the god Chibchacum decided that it would be fun to see the plain of Bogota underwater. He flooded the land, and for his punishment he is forced to carry the world on his shoulders. Sometimes he's angry and stomps, shaking the Earth.
- 14) Scandinavia:** The god Loki is being punished for the murder of his brother, Baldur. He is tied to a rock in an underground cave. Above his face there is a serpent dripping poison, which Loki's sister catches in a bowl. From time to time, she has to go away to empty the bowl. Then the poison falls on Loki's face. He twists and wiggles to avoid it, and the ground shakes up above him.
- 15) New Zealand:** Mother Earth has a child within her womb, the young god Ru. When he stretches and kicks as babies do, he causes earthquakes.
- 16) East Africa:** A giant fish carries a stone on his back. A cow stands on a stone, balancing the Earth on one of her horns. From time to time, her neck begins to ache, and she tosses the globe from one horn to the other.
- 17) Central America:** The square Earth is held up at its four corners by four gods. When they decide the Earth is becoming overpopulated, they tip it to get rid of surplus people.
- 18) Romania:** The world rests on the divine pillars of faith, hope and charity. When the deeds of human beings make one of the pillars weak, the Earth shakes.
- 19) West Africa:** A giant carries the Earth on his head. All the plants that grow on the Earth are his hair, and people and animals are the insects that crawl through his hair. He usually sits and faces the east, but once in a while he turns to the west and then back to the east, with a jolt that is felt as an earthquake.

#### *1.4.2. Tectonic earthquakes*

Most naturally occurring earthquakes are related to the tectonic nature of the Earth. Such earthquakes are called tectonic earthquakes. The majority of tectonic earthquakes originate at depths not exceeding a few tens of kilometres. Earthquakes occurring at boundaries of tectonic plates are called interplate earthquakes, while the less frequent events that occur in the interior of the lithospheric plates are called intraplate earthquakes.

Where the crust is thicker and colder, earthquakes occur at greater depths of hundreds of kilometres along subduction zones where plates descend into the Earth's mantle. These types of earthquakes are called deep focus earthquakes. They are possibly generated when subducted lithospheric material catastrophically undergoes a phase transition (e.g., olivine to spinel), releasing

stored energy-such as elastic strain, chemical energy or gravitational energy-that cannot be supported at the pressures and temperatures present at such depths.

Earthquakes may also occur in volcanic regions and are caused by the movement of magma in volcanoes. Such quakes can be an early warning of volcanic eruptions.

A recently proposed theory suggests that some earthquakes may occur in a sort of earthquake storm, where one earthquake will trigger a series of earthquakes each triggered by the previous shifts on the fault lines, similar to aftershocks, but occurring years later, and with some of the later earthquakes as damaging as the early ones. Such a pattern was observed in the sequence of about a dozen earthquakes that struck the Anatolian Fault in Turkey in the 20th century, the half dozen large earthquakes in New Madrid in 1811-1812, and has been inferred for older anomalous clusters of large earthquakes in the Middle East and in the Mojave Desert.

Small earthquakes occur every day all around the world, and often multiple times a day in places like California and Alaska in the United States, as well as Indonesia and Japan on the other side of the Pacific. Large earthquakes occur less frequently, the relationship being exponential; namely, roughly ten times as many earthquakes larger than magnitude 4 occur in a particular time period than earthquakes larger than magnitude 5. Strong earthquakes can cause severe damage and a large number of fatalities when they occur in proximity of populated regions. Sometimes, secondary effects (tsunamis, landslides, fires, etc.) can increase the number of victims caused by the ground shaking and, it is not evident any improvement in seismic risk reduction passing the time (Table 1.1). Fortunately, several strong earthquakes occurs far away from populated areas and, consequently, do not cause a large number of deaths.

The largest magnitude recorded (observations started at the beginning of the 20th century with the deployment of seismic instruments) refers to the Chile earthquake of 1960, with a magnitude around 9.5 (Fig. 1.44). If the occurrence of a strong earthquake produces a remarkable information, the huge number of small events passes unknown as they are generally not felt by population (Fig. 1.45).

Table 1.1. – Earthquakes with the largest number of victims.

<b>N.</b>	<b>Deaths</b>	<b>Earthquake</b>	<b>Location</b>	<b>Date</b>
1	820,000-830,000	1556 Shaanxi	China	January 23, 1556
2	280,000	2004 Indian Ocean	Indonesia	December 26, 2004
3	242,769-700,000	1976 Tangshan	China	July 28, 1976
4	273,400	1920 Haiyuan	Ningxia, China	December 16, 1920
5	250,000-300,000	526 Antioch	Byzantine Empire (now Turkey)	May 526
6	260,000	115 Antioch	Roman Empire (now Turkey)	December 13, 115
7	230,000	1138 Aleppo	Zengid dynasty (now Syria)	October 11, 1138
8	200,000	1303 Hongdong	Mongol Empire (now China)	September 17, 1303
8	200,000	856 Damghan	Abbasid Caliphate (now Iran)	December 22, 856
8	200,000	1780 Tabriz	Iran	January 8, 1780
9	170,000	896 Udaipur	India	896
10	160,000	2010 Haiti	Haiti	January 12, 2010

The number of earthquake reporting stations increased from about 350 in 1931 to about 4,000 today. As a result, many more earthquakes are reported than in the past, currently, about 35 per day worldwide. This does not necessarily mean that the number of earthquakes has increased, however. The U.S. Geological Survey (USGS) estimates that, since 1900, there have been an average of 18 major earthquakes (magnitude 7.0-7.9) and one great earthquake (magnitude 8.0 or greater) per year, and that this average has been relatively stable. In fact, in the last decades of the 20<sup>th</sup> century, the number of major earthquakes per year has actually decreased (Fig. 1.44). More detailed statistics on the size and frequency of earthquakes is available from the USGS web site.

Most of the world's earthquakes (90%, and 81% of the largest) take place in the 40,000 km-long, horseshoe-shaped zone called the circum-Pacific seismic belt, also known as the Pacific Ring of Fire, which for the most part bounds the Pacific Plate. Massive earthquakes tend to occur along other plate boundaries, too, such as along the Himalaya Mountains.



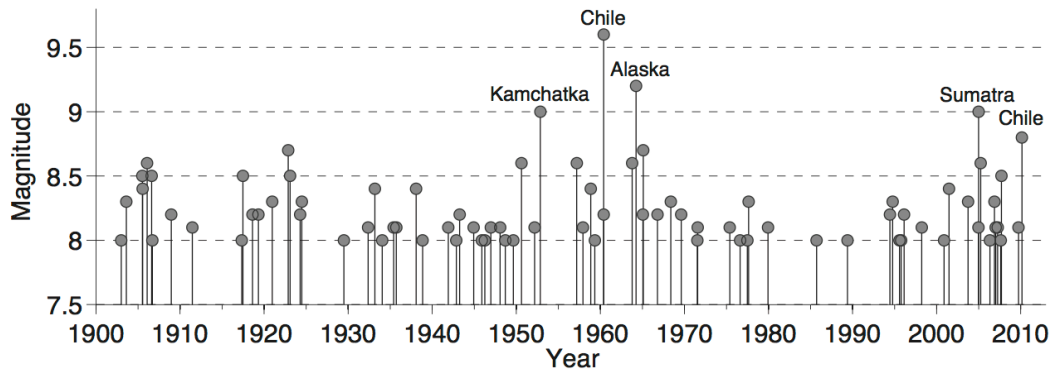


Fig. 1.44 – Great (magnitude 8 and over) earthquakes from 1900 to 2010. The lack of strong events from 1970 to 2000 is evident.

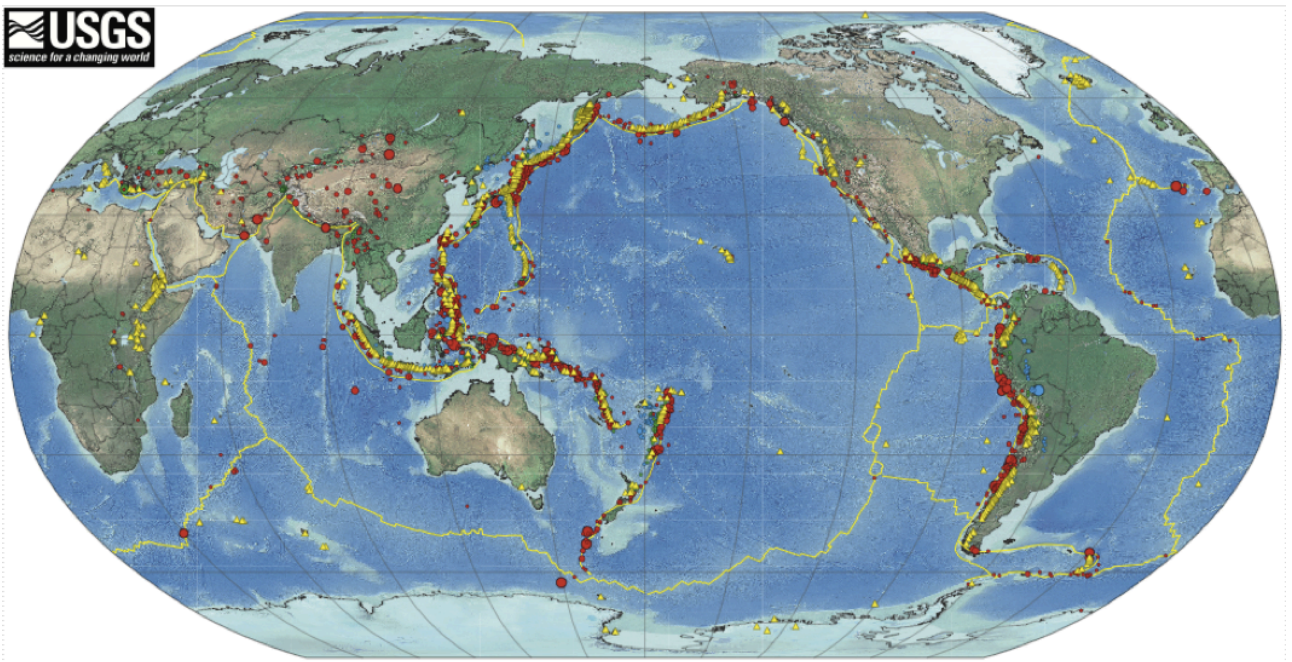


Fig. 1.45 - One year of earthquakes across the world (image courtesy the USGS).

Fig. 1.46 illustrates how most earthquakes are located at the boundaries of tectonic plates. Such earthquakes are associated directly with the forces generated by the interaction of the tectonic plates. Zones of earthquake activity at depth in the subducted slab are generally referred to as Wadati-Benioff zones after the seismologists who independently and simultaneously identified them. Earthquakes in these zones can occur at depths of as much as 700 km.

Comparison of Figs. 1.16 and 1.46 immediately show how the dense bands of seismicity around the world coincide with the boundaries between tectonic plates. Earthquakes occurring on the boundaries between plates are generally referred to as interplate events. There are earthquakes, however, that occur far from the boundaries of tectonic plates and which do not appear therefore to be directly related to the interaction between tectonic plates. Such events are generally referred to as intraplate earthquakes but here a finer distinction is needed. Some intraplate earthquakes occur within areas where there is apparently very little or no deformation of the crust taking place and hence it is unlikely that these events are triggered by increases in crustal stresses driven by plate interactions as is the case at the plate margins (Bommer, 2004). These areas, which include Australia, eastern North America, Brazil, peninsular India, and north-western Europe, are known as stable continental regions. A number of different causes have been put forward as possible explanations for the generation of earthquakes in stable continental regions including the stress concentrations around pre-existing zones of weakness and plutonic intrusions, release of crustal stresses due to deglaciation, or reduction of the mechanical strength of crustal rocks due to the action of fluids or of heat.

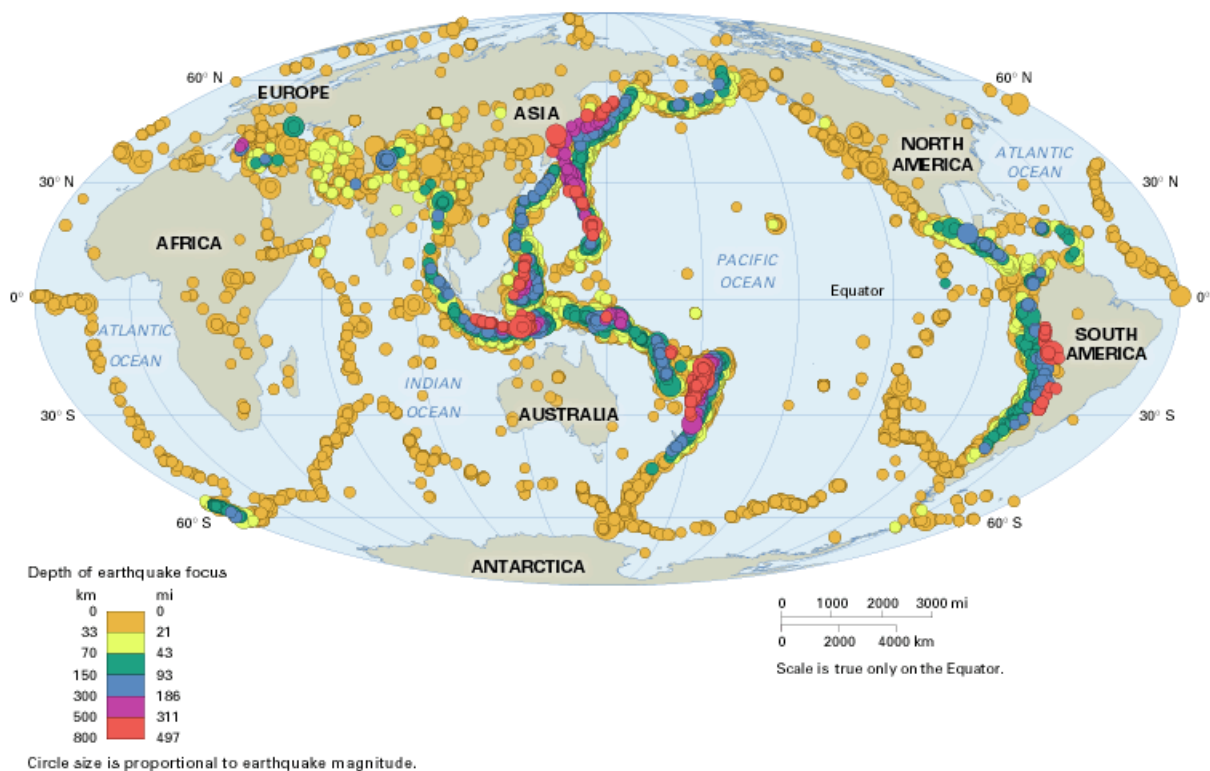


Fig. 1.46 – Earthquakes with magnitude larger than, or equal to, 5.5 recorded in the period 1975 – 1999: 75% of the seismicity occurs along the circum-Pacific belt, 23% along the trans-Asian/Alpine belt.

There are also intraplate earthquakes, however, which occur at locations that appear to be remote from plate boundaries but nonetheless are due to crustal deformations.

Most large earthquakes are accompanied by other, smaller ones that can occur either before or after the main shock; these are called foreshocks and aftershocks, respectively (Fig. 1.47). While almost all earthquakes have aftershocks, foreshocks occur in only about 10% of events (see more in chapter 3.10).

Sometimes the seismic episode is not formed by the standard foreshock/mainshock/aftershock sequence but a long series of events occur with a few of similar largest magnitude: this episode is called a seismic swarm.

### 1.4.3. Induced earthquakes

Some earthquakes have anthropogenic sources, such as extraction of minerals and fossil fuel from the Earth's crust, the removal or injection of fluids into the crust, reservoir-induced seismicity, massive explosions, and collapse of large buildings. Seismic events caused by human activity are referred to by the term induced seismicity. They however are not strictly earthquakes and usually show a different seismogram than earthquakes that occur naturally.

A rare few earthquakes have been associated with the build-up of large masses of water behind dams, such as the Kariba Dam in Zambia, Africa, and with the injection or extraction of fluids into the Earth's crust (e.g., at certain geothermal power plants and at the Rocky Mountain Arsenal). Such earthquakes occur because the strength of the Earth's crust can be modified by fluid pressure. Earthquakes have also been known to be caused by the removal of natural gas from subsurface deposits, for instance in the northern Netherlands. The world's largest reservoir-induced earthquake occurred on December 10, 1967 in the Koyna region of western Maharashtra in India. It had a magnitude of 6.3 on the Richter scale; however, the USGS reported the magnitude of 6.8.

The detonation of powerful explosives, such as nuclear explosions, can cause low-magnitude ground shaking. Thus, the 50-megaton nuclear bomb code-named Ivan detonated by the Soviet Union in 1961 created a seismic event comparable to a magnitude 7 earthquake, producing the seismic shock so powerful that it was measurable even on its third passage around the Earth. In an effort to promote



nuclear non-proliferation, the International Atomic Energy Agency uses the tools of seismology to detect illicit activities such as nuclear weapons tests. The nuclear nations routinely monitor each other's activities through networks of interconnected seismometers, which allow to precisely locate the source of an explosion.

In the geothermal world, induced seismicity has been documented in a number of operating geothermal fields. Induced seismicity has been observed for over thirty years in a variety of sites all over the world. The events are predominantly microearthquakes that are not felt by people, but also include earthquakes of magnitudes up to magnitude 4. There are several different mechanisms that have been hypothesized to explain these occurrences of induced seismicity in geothermal settings: pore-pressure increase, temperature changes, volume change due to fluid withdrawal/injection, and chemical alteration of fracture surfaces. Between December 2 and 8, 2006 approximately 11,500 m<sup>3</sup> of water was injected into a 5-km-deep well at high pressures in the city of Basel. A six-sensor borehole array, was installed at depths between 300 and 2700 m around the well to monitor the induced seismicity. The network recorded approximately 11,200 events during the injection phase, more than 3500 of which were located. The water injection was reduced after an  $M_L$  2.7 event and then stopped after another  $M_L$  2.5 event. A few hours later, an earthquake with  $M_L$  3.4 was felt within the city and caused the stop of the experiment.

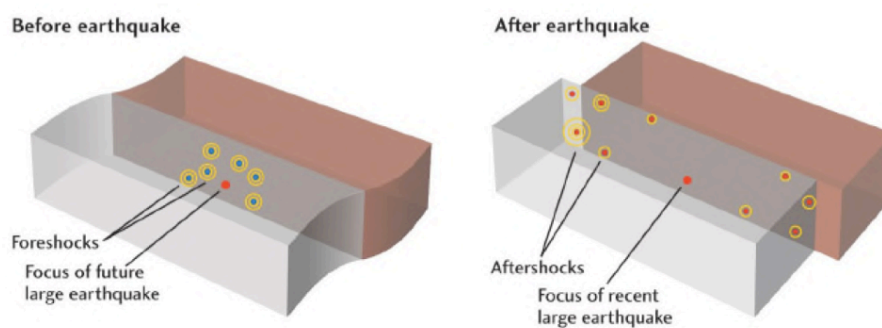


Fig. 1.47– Scheme of a seismic sequence made up by foreshocks, main shock, and aftershocks.

## 1.5. Effects of earthquakes

It is well known how seismic waves vibrate the ground which can lead directly to the collapse of structures. There are other, secondary effects that are caused by earthquakes, most often a result of strong shaking. A simple example common in many earthquakes are landslides. The shaking causes regions of the rock and soil to slide downhill. The same material would eventually fail with increased time, but earthquakes trigger many slides that produce large damage.

### 1.5.1. Landslides

Buildings are not the only thing to fail under the stresses of seismic waves. Often unstable regions of hillsides or mountains fail. In addition to the obvious hazard posed by large landslides, even non lethal slides can cause problems when they block highways causing problems for emergency and rescue operations.

Occasionally large landslides can be triggered by earthquakes. In 1970 an earthquake off the coast of Peru produced a landslide that began 130 km away from the earthquake epicentre. The slide was large (witnesses estimated it's height at about 30 m), travelled at more than 160 km/h and plowed through part of one village and annihilated another, killing more than 18,000 people.

Earthquake-triggered landslides can be generated by either an increase in shear stress due to horizontal acceleration, or a decrease in soil strength. The latter could be the result of a decrease in interparticle bonding, or an increase in pore pressure induced by cyclic loading. Investigation of earthquake-triggered landslides has been conducted since the 18th century. Keefer and Wilson (1989) proposed a relationship between earthquake magnitude and area affected by landslide:

$$\text{Log}A = M - 3.46 \quad (+/-0.47) \quad (1-4)$$

where  $A$  is the area in  $\text{km}^2$  and  $M$  is the magnitude of the earthquake.

### 1.5.2. Soil liquefaction

In some cases, when the surface is underlain by a saturated, sand rich layer of soil, prolonged shaking can cause the expulsion of fluid from the sand layer resulting in large "sand blows" that erupt through the overlying strata.

In the 1811-12 earthquakes the sand blows were enormous and covered large regions of the Missouri bootheel. Liquefaction can cause other problems as the soil loses its ability to resist shear and flows much like quick sand. Anything relying on the substrata for support can shift, tilt, rupture, or collapse.

Liquefaction takes place when loosely packed, water-logged sediments at or near the ground surface lose their strength in response to strong cyclic ground shaking (transformation of a granular deposit from a solid state into a liquefied state). Liquefaction features may vary from place to place in geometry, type, and dimension, due to the anomalous propagation and amplification of the seismic waves at the surface and to the differing site conditions (grain size and density of deposits, position of the ground-water level). The most common and conclusive surficial features induced by liquefaction are sand blows that occur both isolated (sand volcanoes) or along fissures. Other clear liquefaction-induced phenomena are the lateral spreads of huge masses of soil overlying a liquefied layer or the geometrical settlement of surficial deposits (i.e., craters). A typical effect on anthropic structures is the differential settlement and tilting of buildings, bridges and quays, the swelling of pavement of the ground-floors of buildings or swimming-pools, and the apparent extrusion of pillars or wells above the ground surface, due to the sinking of the surrounding soil. Liquefaction occurring beneath buildings and other structures can cause major damage during earthquakes. For example, the 1964 Niigata earthquake caused widespread liquefaction in Niigata, Japan, which destroyed many buildings (Fig. 1.48). Also, during the 1989 Loma Prieta, California earthquake, liquefaction of the soils and debris used to fill in a lagoon caused major subsidence, fracturing, and horizontal sliding of the ground surface in the Marina district in San Francisco.

The bounding equation of distance from the epicentre of sites interested by phenomena of liquefaction ( $R$ ) and magnitude ( $M_s$ ) suggested by Galli (2000) calibrated on 61 earthquakes which occurred from 1900 to 1990 is:

$$M_s = 1.5 + 3.1 \times \log R \quad (1.5)$$

### 1.5.3. Tsunamis

A sometimes dramatic byproduct of certain types of earthquakes are tsunamis. Tsunami is a Japanese term that means "harbour wave". Tsunamis are frequently confused with tidal waves, but they have nothing to do with the tides, they are the result of a sudden vertical offset in the ocean floor caused by earthquakes, submarine landslides, and volcanic deformation. In 1883 the volcanic eruption of Krakatoa resulted in the collapse of a caldera that initiated a tsunami which killed 36,000 people on nearby islands. On June 25, 1896 an earthquake off the Japanese coast generated a tsunami that hit the shore with wave heights ranging from 3 to 30 m. As the fishing fleets returned to shore following an overnight trip they found their villages destroyed and 22,000 people dead. In the last century more than 50,000 people have died as a result of tsunamis.

A sudden offset changes the elevation of the ocean and initiates a water wave that travels outwards from the region of sea-floor disruption. Tsunamis can travel all the way across the ocean and large earthquakes in Alaska and Chile have generated waves that caused damage and deaths in regions as far away as California, Hawaii and Japan.



Fig. 1.48 – Effects of liquefaction during the 1964 Niigata earthquake.

Tsunamis are initiated by a sudden displacement of the ocean, commonly caused by vertical deformation of the ocean floor during earthquakes. Other causes such as deformation by landslides and volcanic processes also generate tsunamis (Fig. 1.49).

The physics beneath the tsunami generation is quite simple:

$$v = \sqrt{g \times h} \quad (1-6)$$

where  $v$  is the wave velocity (900 km/h in deep seas),  $g$  is the gravity acceleration, and  $h$  is the depth of the sea bottom.

Considering that the energy of the sea wave  $E$  is:

$$E \sim v \times a^2 \quad (1-7)$$

where  $a$  is the wave height, for the principle of energy conservation (Green law):

$$E_1 = E_2 \quad (1-8)$$

we obtain:

$$v_1 \times a_1^2 = v_2 \times a_2^2 \quad (1-9)$$

and

$$\frac{a_2}{a_1} = \sqrt{\frac{v_1}{v_2}} \sim \sqrt[4]{\frac{h_1}{h_2}} \quad (1-10)$$

Consequently, when  $h$  decreases the wave length increases.

The speed of this wave depends on the ocean depth and is typically about as fast as a commercial passenger jet (about 0.2 km/s or 712 km/hr). This is relatively slow compared to seismic waves, so we are often alerted to the dangers of the tsunami by the shaking before the wave arrives. The trouble is that the time to react is not very long in regions close to the earthquake that caused the tsunami.

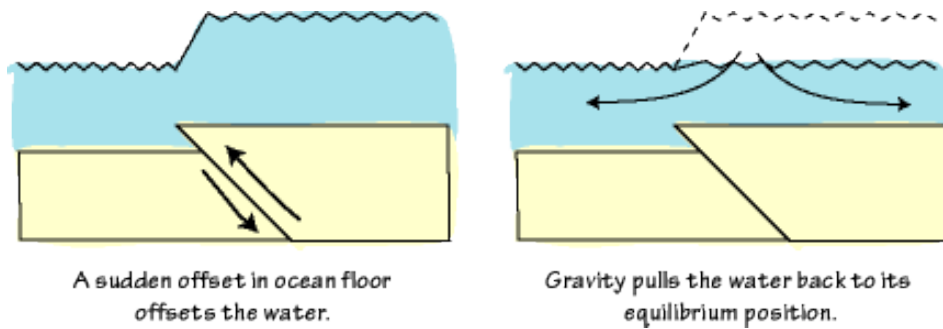


Fig. 1.49 – Genesis of a tsunami.

In deep water tsunamis are not large and pose no danger. They are very broad with horizontal wavelengths of hundreds of kilometres and surface heights much smaller, about 1 m (Fig. 1.50).

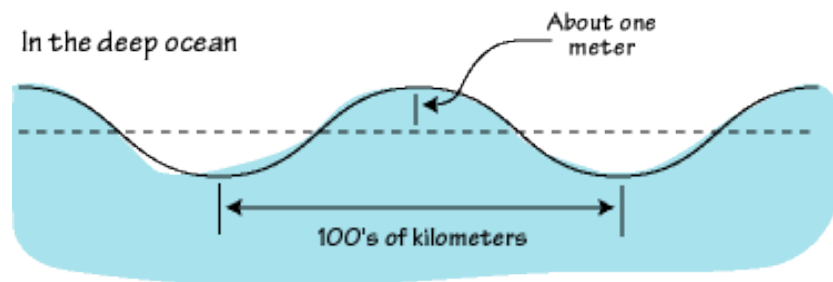


Fig. 1.50 – Tsunami initiation.

Tsunamis pose no threat in the deep ocean because they are only 1 m or so high in deep water. But as the wave approaches the shore and the water shallows, all the energy that was distributed throughout the ocean depth becomes concentrated in the shallow water and the wave height increases (Fig. 1.51).

When a tsunami approaches the shore, the water depth decreases, the front of the wave slows down, the wave grows dramatically, and surges on land.

Typical heights for large tsunamis are on the order of tens of metres and a few have approached 90 m. These waves are typically more devastating to the coastal region than the shaking of the earthquake that caused the tsunami. Even the more common tsunamis of about 10-20 m can "wipe clean" coastal communities.

Deadly tsunamis occur about every one to two years and they have at times killed thousands of people. In 1992-1993 three large tsunamis occurred: one in Japan, Indonesia, and Nicaragua. All struck at night and devastated the local communities.

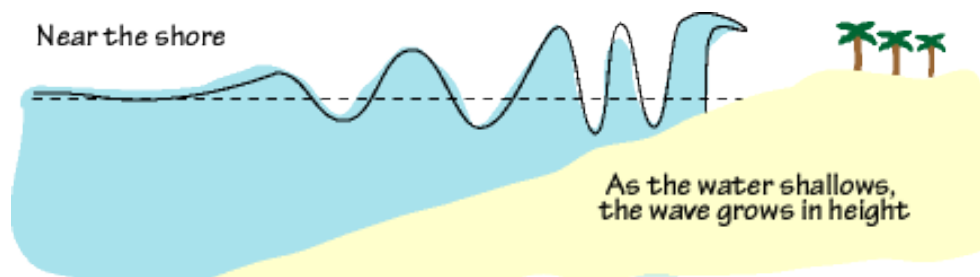


Fig. 1.51 – Tsunami end.

Four violent earthquakes have occurred recently offshore, causing strong tsunamis that increased the level of fatalities and damage: they are the 2004 Sumatra, the 2010 Haiti, the February 2011 Chile, and the March 2011 Japan events.

The magnitude 9.1 Sumatra-Andaman earthquake of December 26, 2004, was one of the largest earthquakes ever recorded. This enormous quake generated the most deadly and damaging tsunami in recorded history (Fig. 1.52). The tsunami travelled from the Bay of Bengal through the Indian Ocean,



leaving victims and destruction from Sumatra to as far away as Africa (Fig. 1.53). Over 200,000 people died. Tsunami created giant waves as high as 10-12 m; in several instances, objects were found on top of the trees after the tsunami. In the islands of Great Nicobar, Car Nicobar and Little Andaman, buildings constructed on the coast were washed away by the great waves, while those located on high grounds survived. When a number of rows of buildings existed on the coast, buildings in the first row from the sea suffered extensive damage, those in the rear rows did better due to the shielding provided by the front row. In general, constructions circular in plan (e.g., circular water tanks, light house) did better under the onslaught of tsunamis as the water could easily flow around such objects.



Fig. 1.52 – The 2004 Sumatra tsunami.

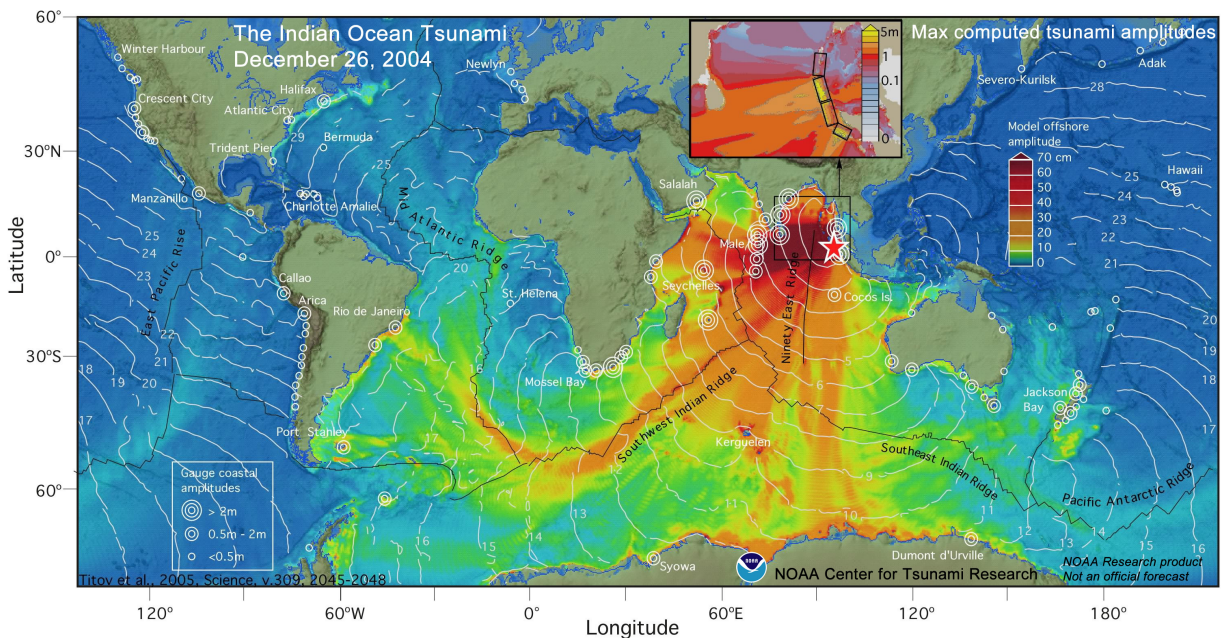


Fig. 1.53 - Maximum computed tsunami amplitudes (from the web site of the NOAA center for tsunami research).

The devastating 2010 earthquake in Haiti also set off a swarm of unusual tsunamis (Fig. 1.54), which killed three people and destroyed several homes. The waves, which averaged about 3 m high, slammed shores along the Bay of Port-au-Prince and the southern coast of the island of Hispaniola, which is shared by Haiti and the Dominican Republic. At least one wave hit the shore as far as 100 km away from the earthquake's epicentre, near Port-au-Prince, Haiti.

A magnitude 8.8 underwater earthquake occurred off Chile on February 27, 2011. This was the largest earthquake in the Pacific for 50 years, since the 1960 Chilean earthquake. The earthquake

triggered a tsunami which devastated several coastal towns in south-central Chile (Fig. 1.55) and damaged the port at Talcahuano. Tsunami warnings were issued in 53 countries, and the wave caused minor damage in the San Diego area of California and in the Tohoku region of Japan, where damage to the fisheries business was estimated 66.7 million US\$. A tsunami of 4.7 m (measured from trough to crest) was recorded off the coast of Chile. In Queensland, a maximum tsunami wave of 0.4 m (measured from trough to crest) was recorded at the Gold Coast on Sunday afternoon 28 February 2010.

On March 11, 2011 a 9.0 magnitude earthquake occurred 130 km off the east coast of Sendai, Honshu, Japan, triggering a massive tsunami (Fig. 1.56). Forecasted wave heights in Japan were up to 20 m and there were many reports of tsunami waves three stories high in parts of Japan. Across the Pacific Ocean, many countries issued evacuations along the coasts because of the predicted tsunami waves. In addition to the forecasted wave heights, the model also shows over 40 m of runup, which is the highest topographic elevation that the tsunami reaches. Observations have confirmed the runup height in parts of Japan. As the tsunami radiated out from Japan, it encountered the complex topography and bathymetry of sea floor, causing the wave to scatter and reflect. After 8 hours, the tsunami hit Hawaii and after 9.5 hours, the tsunami made landfall on the west coast of the United States. After 16 hours, the tsunami wave entered the Indian Ocean and after 22 hours, the wave had propagated throughout the entire Pacific Ocean and was an incredibly complex wave due to the varied topography and bathymetry of the sea floor.



Fig. 1.54 - The 2010 Haiti tsunami.

### 1.6. Stress and strain

Stress is a force per unit area or a force that acts on a surface. The forces associated with the different styles of faulting are stresses (the force per unit area on the fault). Friction is a stress which resists motion and acts in all natural systems. For earthquake studies, friction on faults and the orientation and relative magnitudes of the "regional" stresses that determine the style of faulting are of primary interest and importance.

Strain is a measure of material deformation such as the amount of compression when you squeeze or the amount of elongation when you stretch something. In elastic deformation the amount of elongation is linearly proportional to the applied stress, and an elastic material returns to its original shape after the stress is relieved. Additionally, a strained, elastic material stores the energy used to deform it, and that energy is recoverable.





Fig. 1.55 – The 2011 Chile tsunami.



Fig. 1.56 – The 2011 Japan tsunami.

### 1.7. Elastic-rebound theory

In geology, the elastic rebound theory was the first theory to satisfactorily explain earthquakes. Previously it was thought that ruptures of the surface were the result of strong ground shaking rather than the converse suggested by this theory.

Some regions repeatedly experience earthquakes and this suggests that perhaps earthquakes are part of a cycle. The effects of repeated earthquakes were first noted late in the 19<sup>th</sup> century by American geologist G.K. Gilbert. Gilbert observed a fresh fault scarp following the 1872 Owens Valley, California, earthquake and correlated the scarp and uplift from a single earthquake with the uplift of the Sierra Nevada mountains.

After the devastating 1906 San Francisco, California earthquake, a fault trace was discovered that could be followed along the ground in a more or less straight line for 430 km (Fig. 1.57). It was found that the Earth on one side of the fault had slipped compared to the Earth on the other side of the fault by up to 7 m. This fault trace drew the curiosity of a number of scientists, especially since nobody had yet been able to explain what was happening within the Earth to cause earthquakes. Up until this earthquake, it had generally been assumed that the forces leading to the occurrence of earthquakes must be close to the locations of the earthquakes themselves.



Fig. 1.57 - San Francisco earthquake April 18, 1906. Main fault between Point Reyes Station and Olema. View is southeast. The ground at the right of the fault has moved towards the observer; the ground at the left has moved from the observer (from the USGS website).

Harry Fielding Reid, after studying the fault trace of the 1906 earthquake, postulated that the forces causing earthquakes were not close to the earthquake source but very distant. Reid's idea was that these distant forces cause a gradual build up of stress in the Earth over tens or hundreds or thousands of years, slowly distorting the Earth underneath our feet. Eventually, a pre-existing weakness in the Earth, called a fault or a fault zone, cannot resist the strain any longer and fails catastrophically. This is something like pulling a rubber band gradually until the band snaps. This theory is known as the "elastic rebound theory."

The key to Reid's (1910) success was the availability of "before" and "after" observations for the earthquake which allowed him to see strain build in the crust before the event, and, then, to see strain released during the earthquake.

The seismic cycle is illustrated in Fig. 1.58, where we have two blocks of rock separated by a fault. As the two blocks move in opposite directions, friction acting on the fault resists movement and keeps the two sides from sliding. The rock strains as elastic energy is added, eventually, the strain loads the fault too much and overcomes the frictional "strength" of the fault. The rocks on either side of the fault jerk past each other in an earthquake. The earthquake releases the stored elastic strain energy mainly mechanically (e.g., rock displacement) and the remaining energy as heat along the fault and as seismic vibrations.

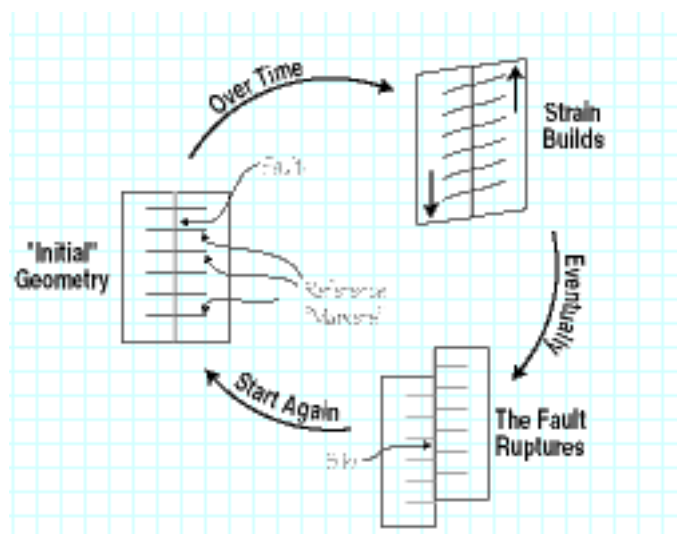


Fig. 1.48 – Scheme of the ideal seismic cycle.



The earthquake is, then, the result of the elastic rebound of previously stored elastic strain energy in the rocks on either side of the fault. In an interseismic period the Earth's plates move relative to each other except at most plate boundaries where they are locked. Thus if a road is built across the fault, as in panel Time 1 of Fig. 1.59, it is perpendicular to the fault trace at the point E where the fault is locked. The far field plate motions (large arrows) cause the rocks in the region of the locked fault to accrue elastic deformation (figure panel Time 2). The deformation builds at the rate of a few cm per year, over a time period of many years. When the accumulated strain is great enough to overcome the strength of the rocks an earthquake occurs. During the earthquake the portions of the rock around the fault, that were locked and had not moved, 'spring' back, relieving the displacement in a few seconds that the plates moved over the entire interseismic period (D1 and D2 in Time 3). The time period between Time 1 and Time 2 could be months to hundreds of years, while the change from Time 2 to Time 3 is seconds. Like an elastic band the more the rocks are strained the more elastic energy is stored and the greater potential for the event. Modern measurements using GPS largely support Reid's theory as the basis of seismic movement, though actual events are often more complicated

For an ideal elastic-rebound fault, the stress on the fault periodically cycles between a minimum and maximum value and if the two blocks continue to move at a constant rate, the recurrence time (the time between earthquakes) is also uniform (Fig. 1.60). Unfortunately, actual faults are more complex, and the recurrence time is not periodic (which is one reason why earthquake prediction is so difficult). We have few observations of complete earthquake cycles because earthquakes take so long to recur.

Fig. 1.61 shows the observations from the Nankaido region of Japan (the grey region, the older values are estimated from earthquake histories), one of the few regions where observations on strain throughout several earthquake cycles exist. You can see that neither the time nor the slip is uniform from earthquake-to-earthquake.

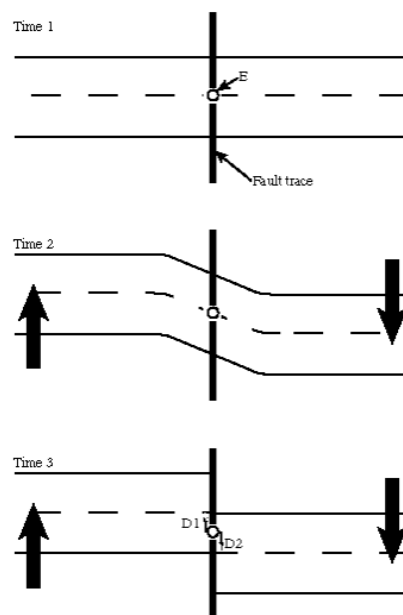


Fig. 1.59 - Elastic rebound scheme.

### 1.10. Theoretical models for earthquake occurrence

Reid's elastic rebound theory combined with our knowledge of plate tectonics gives hope that we might someday be able to predict earthquakes. The observation that some faults fail with quasi-periodic behaviour is fundamental for earthquake prediction and hazard mitigation. Theoretically, if plate motions are steady, strain accumulation will increase steadily and slip will occur at regular time intervals; the amount of time between slip episodes is called a **recurrence interval**. There are three

basic models for earthquake prediction (Fig. 1.62): 1) the characteristic earthquake, 2) the time-predictable earthquake, and 3) the slip-predictable earthquake (Lay and Wallace, 1995). Each model is based on the history of stress accumulation and relaxation during an earthquake cycle. In the characteristic earthquake model, shear stress builds on a fault to the level of the fault strength,  $\tau_1$ . When the shear stress reaches  $\tau_1$ , the fault ruptures and the shear stress is reduced to a level equal to the friction on the fault,  $\tau_2$ . The amount of slip on the fault is the same for each earthquake and the recurrence interval is constant over time. Unfortunately, characteristic earthquake behaviour is not commonly observed in nature because the model assumes that plate motions are steady and fault friction and fault strength are constant. However, a section of the San Andreas fault near Parkfield, California may be one example of a fault that follows the characteristic earthquake model. This fault segment has had at least five  $M > 6$  earthquakes with a mean recurrence interval of 22 years since 1857. There is some variability in the recurrence interval, but studying this characteristic behaviour may be the first step towards understanding fault behaviour.

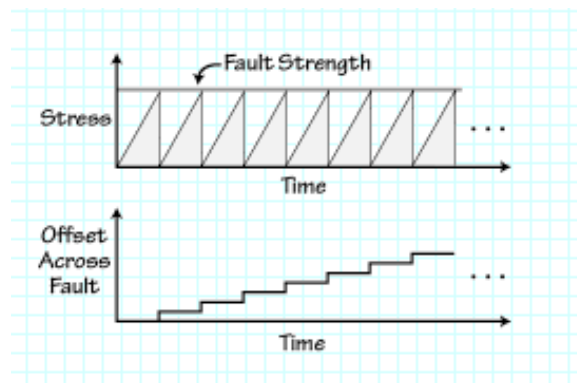


Fig. 1.60 – Stress drop in the ideal earthquake cycle.

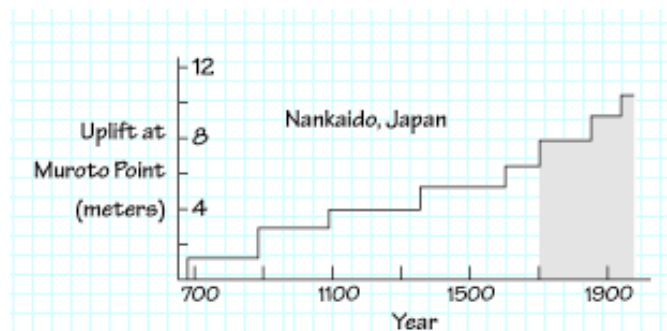


Fig. 1.61 – Uplift in the Nankaido region (Japan).

The time-predictable model assumes that fault strength is constant and that the fault will always rupture when the shear stress reaches the level of  $\tau_1$ . However, slip on the fault can vary with each rupture. This model assumes that a large slip on the fault will reduce the level of shear stress more than a small slip. Thus, after a large slip it will take longer for the shear stress to build to the level of  $\tau_1$ , assuming steady plate motions. Knowing the amount of slip during the past earthquake, the time-predictable model allows prediction of the time of the next earthquake. The Calaveras fault near San Francisco Bay, California appears to have time-predictable behaviour over at least the short time window of observation from 1962–1977. The cumulative amount of slip is linear over time even though the amount of slip during any one earthquake varies.

In the slip-predictable model, the fault does not rupture at the same shear stress,  $\tau_1$ , each time. Rather, an earthquake always reduces the shear stress on the fault to  $\tau_2$ , the level of the fault friction. This model cannot be used to predict when rupture will occur, but it can be used to predict the magnitude of the earthquake that would occur at any given time. After an earthquake, stress on the fault will increase at a constant rate from  $\tau_2$ . The potential fault slip at any time is proportional to the shear stress on the fault. Thus, if the time of the last rupture is known, the shear stress on the fault and the potential displacement can be determined at any particular time.

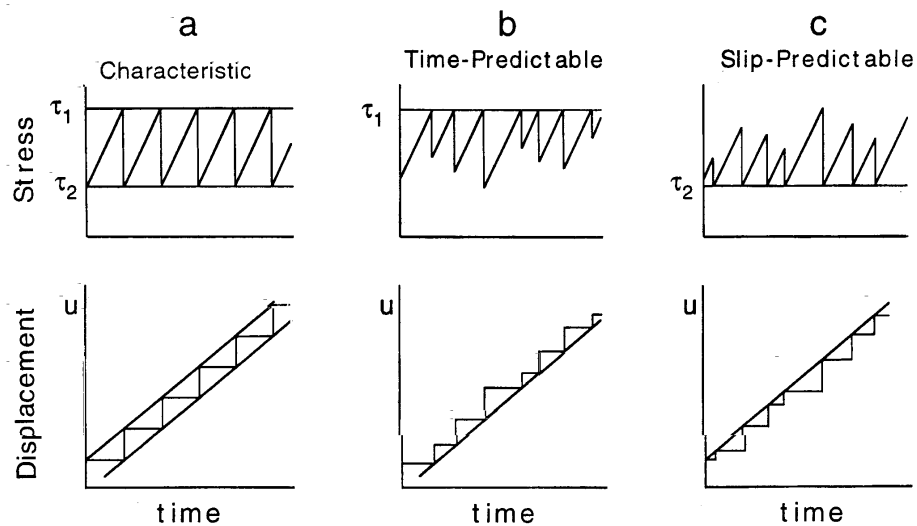


Fig. 1.62 – Models for earthquake prediction based on changes in fault stress for a constant loading rate. The upper box shows the stress history on the fault for the different predictive models:  $\tau_1$  is the shear stress at initiation of slip and reflects fault strength,  $\tau_2$  is the shear stress at which slip ceases and reflects fault friction. In the lower box,  $u$  is the slip or displacement on the fault that corresponds with the stress history. a) Characteristic model of stick-slip faulting. Each earthquake is identical in stress history, recurrence interval and slip. b) Time-predictable model. This model assumes the fault strength is constant and that slip initiates when the stress on the fault reaches  $\tau_1$ . If slip is proportional to stress drop, and plate motions are steady, we can predict the time of the next earthquake based on the amount of slip during the previous earthquake. c) Slip-predictable model. This model assumes the stress on the fault is always reduced to  $\tau_2$  by an earthquake. Knowing the time of the last earthquake and assuming a steady plate motion, we can predict the size of an earthquake expected at a particular time (modified from Shimazaki and Nakata, 1980).

### 1.11. Coulomb stress failure

Coulomb stress transfer is an interaction criterion that promises a deeper understanding of earthquake occurrence, and a better description of probabilistic hazard.

An earthquake reduces the average value of the shear stress on the fault that slipped, shear stress rises at sites in addition to the fault tips. This discovery lay in waiting for 20 years, when lobes of off-fault aftershocks were seen to correspond to small calculated increases in shear or Coulomb stress.

In its simplest form, the Coulomb failure stress change,  $\Delta sf$  (also written  $\Delta CFS$  or  $\Delta CFF$ ) is:

$$\Delta sf = \Delta t + m \times (\Delta P + \Delta sn) \quad (1-11)$$

where  $\Delta t$  is the shear stress change on a fault (reckoned positive in the direction of fault slip),  $\Delta sn$  is the normal stress change (positive if the fault is unclamped),  $\Delta P$  is the pore pressure change in the fault zone (positive in compression), and  $m$  is the friction coefficient (with range 0-1). Failure is encouraged if  $\Delta sf$  is positive and discouraged if negative; both increased shear and unclamping of faults promote failure. The tendency of  $\Delta P$  to counteract  $\Delta sn$  is often incorporated into the above equation by a reduced 'effective' friction coefficient,  $m$ .

The calculated off-fault stress increases are rarely more than a few bars (1 bar = 0.1 MPa circa equivalent to the atmospheric pressure at sea level), or just a few percent of the mean earthquake stress drop. In addition, the proximity to failure at any site is presumably variable and, in any event, unknown. It is unclear why aftershocks concentrate at the site of such small stress increases. Studies by United States and international teams find a surprisingly strong influence of stress change on seismicity, explaining it in terms of rupture nucleation phenomena observed in the laboratory.

Over the past years, it has become generally accepted that small co-seismic stress perturbations can influence the location and timing of future events (Fig. 1.63). Stress changes in the crust due to an earthquake can hasten the failure of neighbouring faults and induce earthquake sequences

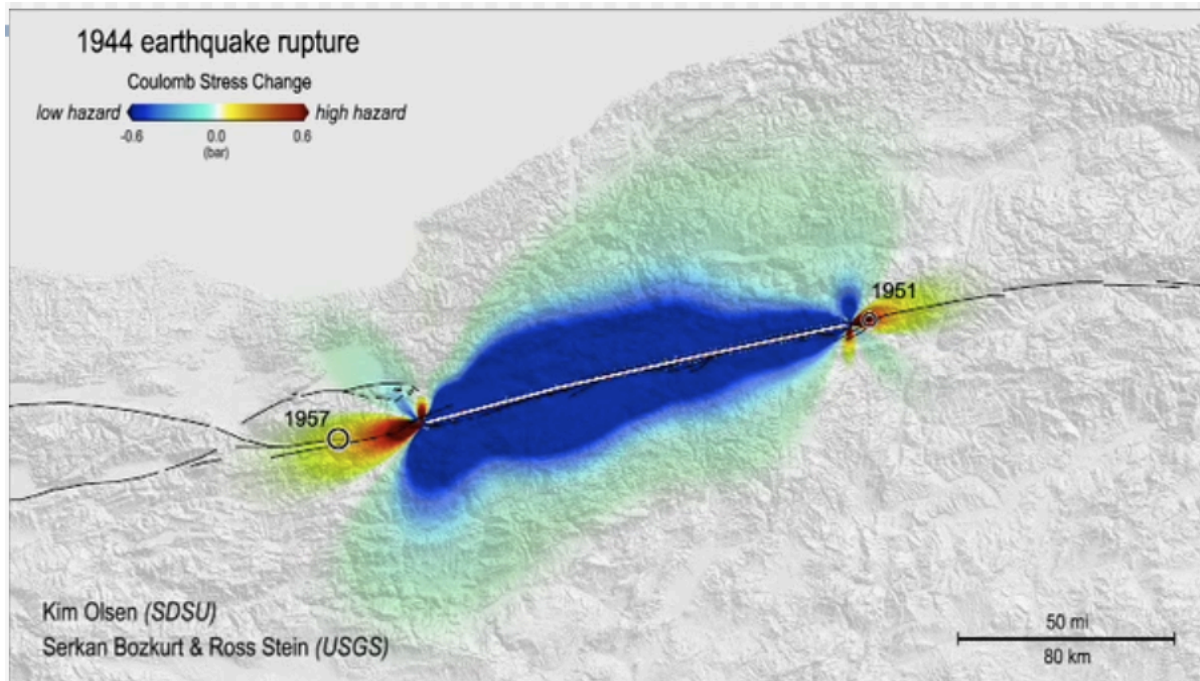


Fig. 1.63 – Coulomb stress change along the North Anatolian Fault caused by the 1944 Bolu-Gerede earthquake of 7.2 magnitude, triggering the 1951 and 1957 quakes.

### 1.12. Faults generating earthquakes

The basic measures of the size of an earthquake are magnitude and seismic moment. As the size of an earthquake increases, so does the size of the fault rupture area, as indicated in Fig. 1.64. For earthquakes of magnitude 6, this figure suggests that the average area of the fault rupture will be of the order of  $75 \text{ km}^2$ , which would correspond to circle of about 5 km radius. The ruptures of events of this size and smaller may be approximately circular or elliptical in shape, but once the dimensions of the rupture are comparable to the thickness of the seismogenic layer of the crust the rupture will tend to become rectangular with increasing magnitude (Bommer, 2004).

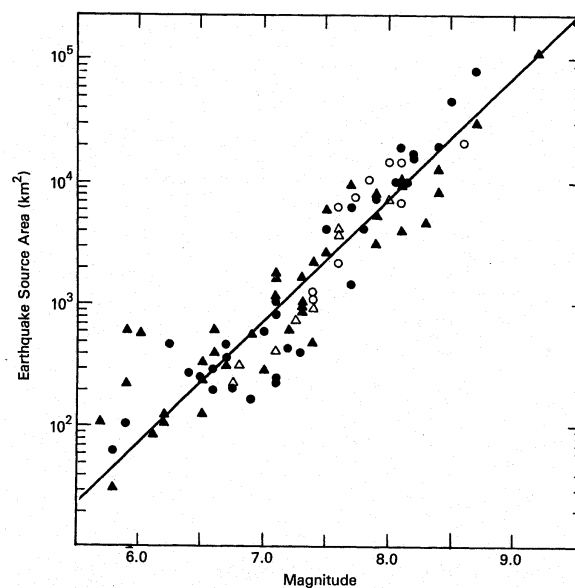


Fig. 1.64 – Earthquake rupture area and magnitude (from Wyss, 1979).



Empirical correlations between the dimensions of fault ruptures, their slip and earthquake magnitude are very useful for performing seismic hazard assessment. The equations are derived in each case using all of the available data and also grouping the data according to rupture mechanism.

Two rules of thumb are also worth committing to memory. The first is that on average the maximum slip observed on faults is about twice the average slip. The second is that in continental regions the average slip is usually in the range of  $5\text{--}10 \times 10^{-5}$  times the fault rupture length.

Approximately rectangular fault ruptures can be characterised by their length,  $L$ , and their width,  $W$ , the former measured along the strike, the latter down the dip of the fault plane. Many studies have produced empirical regressions between dimensions of the fault rupture, or the slip, and the earthquake magnitude (Fig. 1.65), most notably the study of Wells and Coppersmith (1994). Such empirical equations are obtained by performing regression of rupture dimensions or slip on magnitude or vice versa, producing different results in each case, as illustrated in Fig. 1.66; the equations should only be used to obtain estimates of the value on the left-hand side from known values on the right-hand side of the equation.

Figs. 1.67 to 1.84 illustrates the faults that generated some of the major earthquakes.

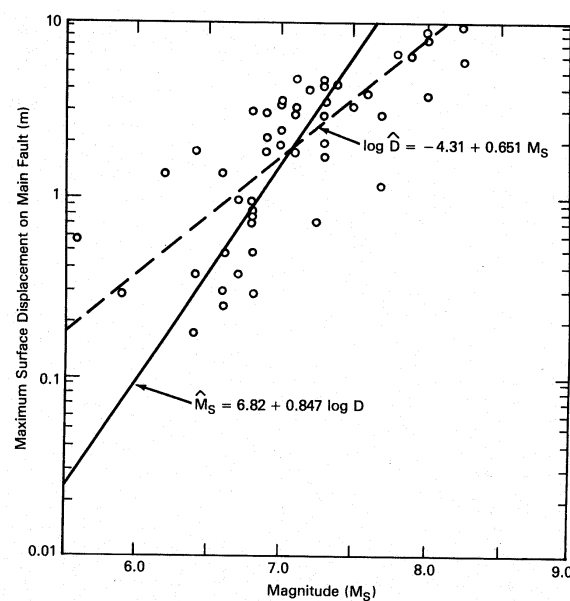


Fig. 1.65 – Regression relationships between earthquake magnitude ( $M_S$ ) and maximum surface displacement based on worldwide data (from Slemmons, 1982).

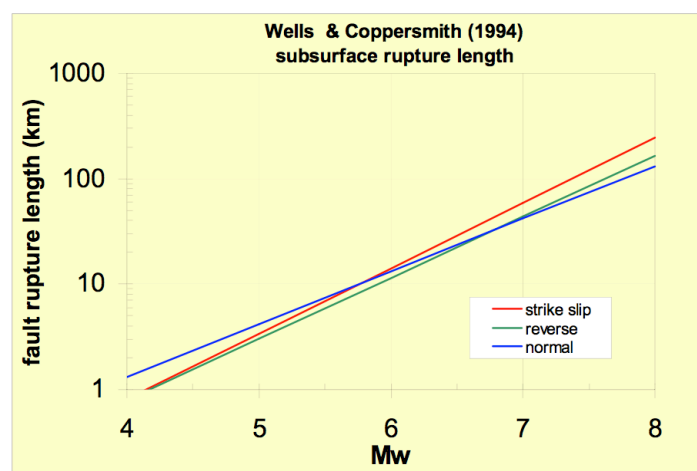


Fig. 1.66 – Relations for fault rupture length vs. magnitude  $M_W$  by Wells and Coppersmith (1984) for different fault styles.



Fig. 1.67 - San Francisco earthquake April 18, 1906. Fault trace 2 miles north of the Skinner Ranch at Olema. View is north (from the USGS website).



Fig. 1.68 - Fence offset by the causative fault of the San Francisco earthquake of April 18, 1906, on ranch of E.R. Strain, 1 1/2 miles north of Bolinas Lagoon, looking NE. The sheer offset is 8 1/2 feet; the total displacement, shown partly by crooking of fence, is 11 feet (from the USGS website).



Fig. 1.69 - Nevada earthquake December 16, 1954. Fault scarp near Fairview Park resulting from the earthquake.



Fig. 1.70 - Alaska earthquake of March 27, 1964. Hanning Bay fault scarp on Montague Island, looking NW. Vertical displacement in the foreground, in rock, is about 12 feet. The maximum measured displacement of 14 feet is at the beach ridge near the trees in the background.





Fig. 1.71 - Alaska earthquake of March 27, 1964. Hanning Bay fault on Montague Island, looking SW from the bay. The fault trace on the ridge is marked by active landslides.



Fig. 1.72 - San Fernando earthquake of February 9, 1971. Trace of the main reverse fault where it crosses Little Tujunga Road. By the time this photograph was taken a dirt ramp at right had been built up the scarp. The scarp indicates more than 1-m reverse dip-slip movement. The fence indicates little strike-slip displacement at this place, which is near the last end of the line of surface rupture.



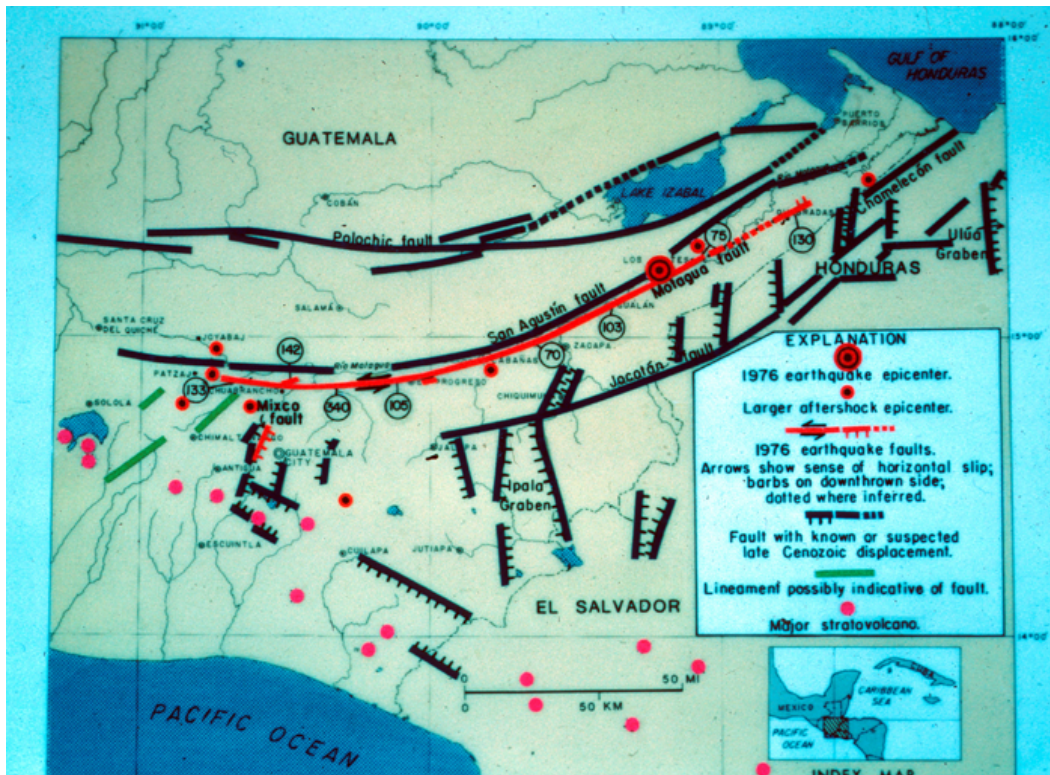


Fig. 1.73 - Guatemala earthquake 1976. Map showing the relation of segments of the Motagua and Mixco faults that moved during the earthquake of February 4, 1976, (in red) to the main shock epicentre, the larger aftershock epicentres, and major structural and volcanic features in northern Central America. Circled numbers along the Motagua fault indicate selected measured sinistral displacements in centimetres. The green lines in the western part of the map area are lineaments, some of which may have undergone minor fault displacement during the earthquake.



Fig. 1.74 - Guatemala earthquake 1976. Typical appearance of the Motagua fault rupture that caused the destructive earthquake.



Fig. 1.75 - Guatemala earthquake of 1976. Westwards, along the Motagua fault trace in the area of maximum displacement 33 km NE of Guatemala City. The fault trace is marked by a zone less than 3 m wide of en echelon linear cracks with connecting short pressure ridges. There is an en echelon offset of several metres where the fault crosses the creek in the upper part of the slide. The meandering creek does not follow the trace of the fault, which suggests that the fault rupture is geologically young at this locality.



Fig. 1.76 - Imperial Valley, California, earthquake of October 15, 1979. Imperial Fault trace 1 km south of County Highway S-80 (11.3 kilometres northwest of the southeast end of the fault). Echelon fissures (vertically oriented) trend N. 20-50 degrees W. The fault trace trends between N. 30-40 degrees W. Compression features (dark horizontal bands) join the ends of the separate echelon fractures. The distance between the manmade berms (wide dark diagonal bands) is about 9.1 metres. The maximum width of the obviously deformed zone is about 0.6 m. View is south.





Fig. 1.77 - Idaho earthquake of October 28, 1983. Willow Creek at Double Spring Pass Road. Fault scarps that outline the trough (graben) produced during the earthquake. This block is, in effect, a miniature "rift valley". At least three previous displacements, accompanied by earthquakes of similar magnitude as that of October 1983, have occurred along this part of the fault within the past several thousand years.



Fig. 1.78 - Izmit earthquake of 1999. This picture shows an offset 3m and is in a large field with a well expressed moletrack that is also seen in "moletrack and sag in field". A moletrack is a descriptive term for how strike slip faults often look when seen at the surface.

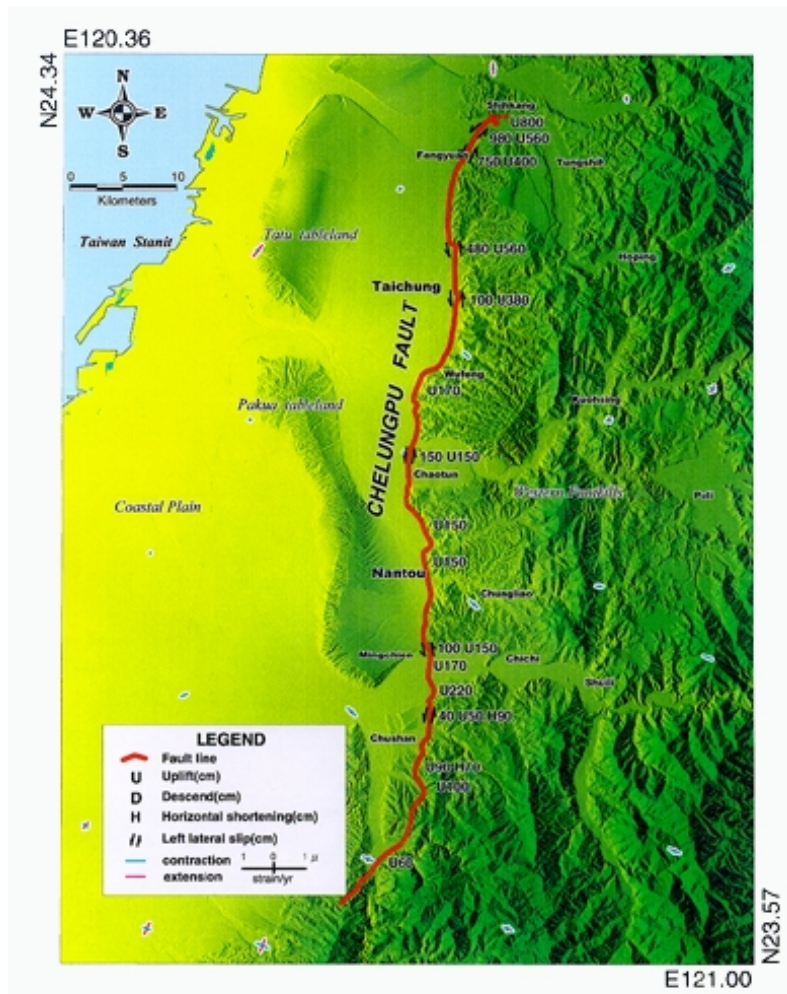


Fig. 1.79 – Displacements along Chelungpu fault of Chichi 1999 earthquake.



Fig. 1.80 - Chichi (Taiwan) earthquake of 1999. The fault tore up the adjacent road and levee in a narrow and relatively uncomplicated pattern.





Fig. 1.81 - Chichi (Taiwan) earthquake of 1999. Behind the building complex (upper left), the fault offset the originally level ground and railroad tracks by about 3 m vertically.



Fig. 1.82 - Chichi (Taiwan) earthquake of 1999. The fault cuts diagonally across the picture. Almost all movement was thrust, with less than 1 m left lateral slip.





Fig. 1.83 - Hector Mine earthquake of 1999.

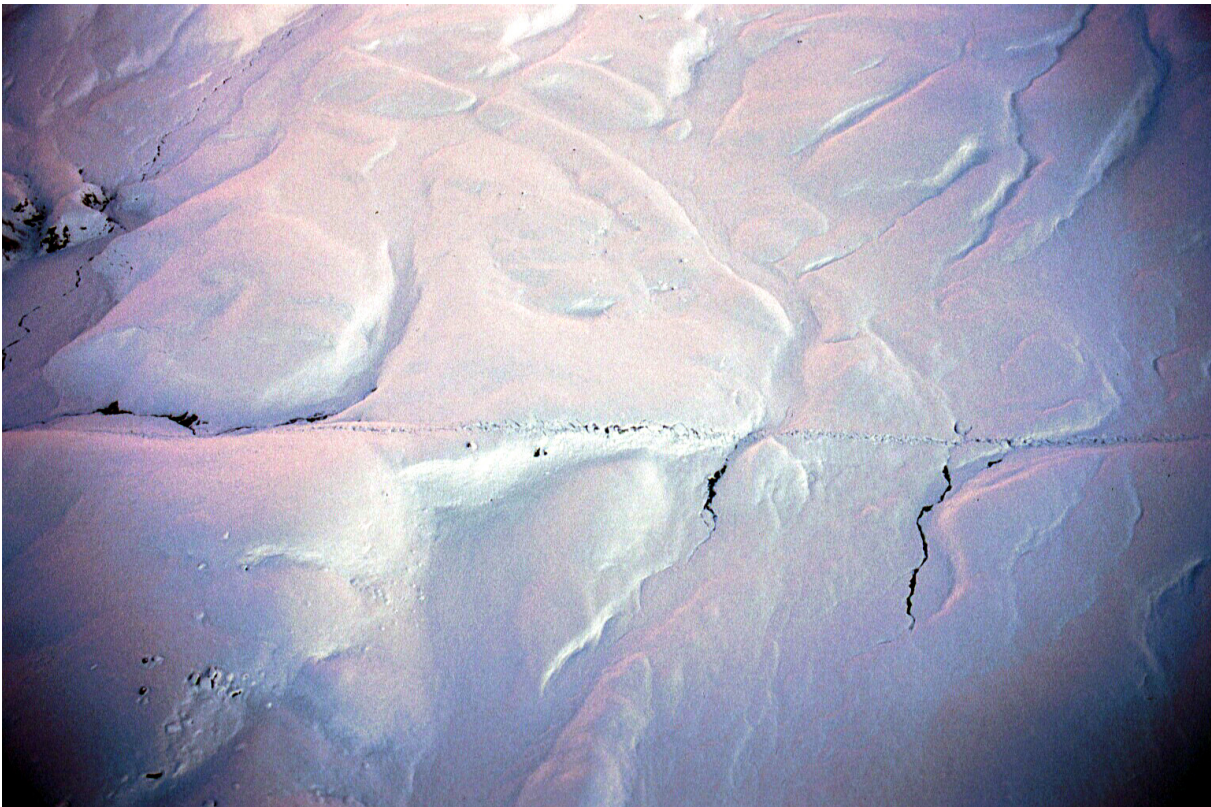


Fig. 1.84 - Denali M7.9 earthquake of November 3, 2002. Aerial view of fault trace in snow in the fault trench between Gakona and Chistochina glaciers. Topography and stream drainages reflect previous offsets.



## 2. NON-INSTRUMENTAL SEISMOLOGY

In several countries the earthquake history is well documented and the data coming from the pre-instrumental era (beginning of the 20<sup>th</sup> century) represents the bulk of information for seismic hazard assessment. The non-instrumental data are in general qualitative and, for this reason, they were considered, sometimes in the past, not suitable for a scientific study of the seismicity. In the recent years the importance of the macroseismic data has been greatly re-evaluated and they represent now a large part of the seismological information available.

Macroseismic data do not refer only to the pre-instrumental events but are still collected because 1) they give information which is additional to the instrumental one and 2) they are frequently associated to building vulnerability and, consequently, useful in seismic risk assessment. Moreover, techniques have been developed for deriving some hypocentral parameters (coordinates, magnitude, etc.) from the macroseismic data.

### 2.1. Macroseismic intensity

The first evaluation of the importance of an earthquake is given by information about damage caused by the shock and about how it was felt also at great distance from the epicentre.

Intensity is an index that reflects the strength of ground shaking at a particular location during an earthquake. Therefore, it is not really a measure of the size of the earthquake, in the same way as moment or magnitude, but rather a measure of ground motion. In order to make clear the index nature of intensity it is usually represented by Roman numerals and in fact it is meaningless to write a value of intensity as a decimal value because it is not a continuous variable. Intensity VIII indicates a level of shaking that may cause damage in engineered structures; stronger shaking that does not quite qualify as intensity IX may legitimately be represented as VIII-IX, VIII+ or IX-, but to write 8.5 is incorrect (Bommer, 2004).

### 2.2. The macroseismic scales

The intensity scale differs from the Richter magnitude scale in that the effects of anyone earthquake vary greatly from place to place, so there may be many intensity values (e.g.: IV, VII) referring to one earthquake. Each earthquake, on the other hand, should have just one magnitude, although the several methods of estimating it will yield slightly different values (e.g.: 6.1, 6.3). Rating the intensities produced by an earthquake does not require any instrumental measurements. Thus, seismologists can use newspaper accounts, diaries, and other historical records to make intensity ratings of past earthquakes, for which there are no instrumental recordings. Such research helps promote our understanding of the earthquake history of a region, and estimate future hazards.

The lower levels of intensity are defined primarily by how people feel the shaking but as values increase human perception of the movement becomes progressively less important as damage to buildings becomes more prominent. Firstly, intensity III is generally considered as the threshold of perceptibility, below which the ground shaking is not felt by most people. Intensity VI limits the area where damage (minimal for intensity VI) is observed. Intensity VII can be thought of as the threshold of appreciable building damage, although this might be intensity VIII for engineered structures. Intensity XII is very rarely, if ever, encountered in reality and therefore XI can be treated as the upper bound. In practice, X appears to be an effective upper bound.

One final point must be made: the intensity scales are neither continuous nor linear. The variation from degree to degree is not gradual, each increase in one degree representing a jump in the level of shaking. Furthermore, the jumps between different degrees are not equal: the increase in the level of ground shaking from IV to V is not the same and the increase from VII to VIII.

Intensity is evaluated either by direct field observations or by questionnaires sent to the affected areas, although the latter is really only suitable for lower intensity values.

The definition of the degrees of intensity assumes a sample of observations from which to make the observations. Within a small area, say a village, the observations that would be attached to each



individual house may indicate a variation of two or three degrees of intensity, possibly more. This will reflect that some houses are older and poorly maintained, others are relatively newer and stronger. Since the objective is to infer from the building damage the level of ground shaking, it is important not to allow the assigned intensity value to be unduly influenced by the local variations in the earthquake resistance of the affected houses.

In principle, when several observations are available, say from a number of streets or blocks in a town or village, a single value may be assigned. This should not be the maximum observation, since this will probably reflect a very localised amplification effect or else a particular vulnerable group of buildings. To take the arithmetic mean value of the observations is meaningless, because of the non-linear and discrete nature of the intensity scales. The value assigned must be the modal observation (Bommer, 2004). Although this is clear and logical and has often been stated, in practice it is not always followed.

The ancient Greek already tried to measure the earthquakes. Jacopo Gastaldi, a mapmaker from Piedmont, worked out the most formerly intensity scale in 1564. He did it to measure the big earthquake of Nizza's vicinity in 1594. In the 17th-18th centuries, the scales generally had four grades, but in the 20th century, the geologists described the destructive power of the earthquakes with ten grades. The first known isoseismal map was produced for the 1810 earthquake in Mór, Hungary, and published by Kitaibel and Tomtsányi in 1814. The earliest recognisable use of intensity, as we know it today, was by Egen in dealing with a Belgian earthquake in 1828, although simple quantifications of damage had been made in the previous century by Schiantarelli in Italy in 1783 (Fig. 2.1) after the Calabrian earthquake of that year (Musson, 2006). However, Egen's innovation did not really catch on at first.

The most popular intensity scales are the Rossi-Forel, the Mercalli and its improvements, the Medvedev-Sponheuer-Karnik, and the European Macroseismic ones. The only important intensity scale that does not have twelve degrees (now the Rossi-Forel Scale is no longer in use) is the seven-degree Japanese Meteorological Agency Scale (JMA Scale): it is based on the work of Omori, and it is the scale generally used in Japan (but nowhere else).

Fig. 2.2 compares the different scales.



Fig. 2.1 - Detail of Schiantarelli's map of the the 1783 Calabrian earthquake: different symbols are used for villages according to the amount of damage (from Musson, 2006).



### 2.2.1. The Rossi – Forel scale (1873)

It was only in the last quarter of the 19<sup>th</sup> century that the use of intensity became widespread. Credit for this goes jointly to an Italian, Michele Stefano Conte de Rossi, and a Swiss, François-Alphonse Forel, who published quite similar intensity scales independently in 1874 and 1881, respectively. The two of them then combined their efforts and produced a joint scale, the Rossi-Forel Scale, with ten degrees of intensity in 1883. This was the first scale to be widely used internationally. It was used for about two decades until the introduction of the Mercalli intensity scale in 1902 but the description of the effects on construction seems to be specifically European.

- I: Microseismic shock.** Recorded by a single seismograph or by seismographs of the same model, but not by several seismographs of different kinds. The shock felt by an experienced observer.
- II: Extremely feeble shock.** Recorded by several seismographs of different kinds. Felt by a small number of persons at rest.
- III: Very feeble shock.** Felt by several persons at rest. Strong enough for the direction or duration to be appreciable.
- IV: Feeble shock.** Felt by persons in motion. Disturbance of movable objects, doors, windows, cracking of ceilings.
- V: Shock of moderate intensity.** Felt generally by everyone. Disturbance of furniture, ringing of some bells.
- VI: Fairly strong shock.** General awakening of those asleep. General ringing of bells. Oscillation of chandeliers, stopping of clocks, visible agitation of trees and shrubs. Some startled persons leaving their dwellings.
- VII: Strong shock.** Overthrow of movable objects, fall of plaster, ringing of church bells. General panic. No damage to buildings.
- VIII: Very strong shock.** Fall of chimneys, cracks in the walls of buildings.
- IX: Extremely strong shock.** Partial or total destruction of some buildings.
- X: Shock of extreme intensity.** Great disaster, ruins, disturbance of the strata, fissures in the ground, rock falls from mountains.

MODIFIED MERCALLI	ROSSI FOREL	JMA	MERCALLI CANCANI SIEBERG	MEDVEDEV SPONHEUER KARNIK
I	I		II	I
II	II	I	III	II
III	III		IV	III
IV	IV	II	V	IV
V	V	III	VI	V
VI	VI	IV	VII	VI
VII	VII	V	VIII	VII
VIII	VIII		IX	VIII
IX	IX	VI	X	IX
X	X		XI	X
XI		XII	XII	XI
XII		VII		XII

Fig. 2.2 – Comparison of different macrosesimic scales (from Richter, 1958).

### 2.2.2. The Mercalli-Cancani-Sieberg scale (1930)

The defects of the Rossi-Forel scale were removed by the Italian volcanologist Giuseppe Mercalli (Fig. 2.3), who in 1902 prepared an intensity scale at first with ten degrees (he had also published in 1883 an earlier scale of six degrees which was a modification of Rossi's first scale), later with twelve following a suggestion by the Italian physicist Adolfo Cancani. However, Cancani omitted to flesh out his twelve degrees with full descriptions, and restricted himself to titles for each degree (like "destructive") and estimated ground acceleration values. It was later completely re-written by the German geophysicist August Heinrich Sieberg who presented a twelve degree intensity scale with full descriptions of each degree; the first version was published by him in 1912 and subsequently revised twice. Sieberg's scale became the foundation of all modern twelve-degree scales (i.e., the majority of scales in use today). A version of this scale with slight modifications was published as the Mercalli-Cancani-Sieberg Scale, or MCS Scale, still in use in southern Europe today.

Besides the description of the occurrences (the effects on the buildings from the 6th grade) there are measurable acceleration-intervals, which are given in  $\text{mms}^{-2}$  assigned to each degree.



Fig. 2.3 – Giuseppe Mercalli (1850-1914).

- I: Not perceptible.** Only perceptible with devices.
- II: Very weak.** Only certain people notice in houses, mainly upstairs.
- III: Weak.** Smaller parts of those, who in the houses notice it. Generally, it is similar to the effect of a proceeding vehicle.
- IV: Moderated.** A lot of people notice it in houses and a few outdoors during the day. Some people awake at night. The plates, doors, windows give clanking sounds. The wall crackles. It has a similar effect to the building jolting of heavier vehicles. It swings the parking cars.
- V: Quite strong.** Almost everyone notice it. A lot of people awake. The windows break. Certain objects overturn, the objects hanging from the ceiling swing. The pendulum clock could stop. The trees could sway.

- VI: Strong.** Everyone notices it. Many people get frightened and run out of the houses. One or more weighty pieces of furniture move from their places. Several chimneys could collapse.
- VII: Very strong.** Everyone runs from the house in their alarm. Does small damage to well-built buildings, and does more serious damage in not-well-built houses. Many chimneys collapse. Drivers notice it while driving.
- VIII: Quite destructive.** The quarter of the buildings, suffer heavy losses. Some collapse, many become inhabitable. The chimneys of the dwellings fall down, factory chimneys fall apart, monuments, statues collapse, move on. Muddy water is impressed from the wet ground. Greatly prevents drivers from driving.
- IX: Destroying.** The half of the dwellings heavily damages. Relatively many collapse, the most become inhabitable. Clefts occur in the ground, the buried transmission lines break.
- X: Very destroying.** Heavy damages occur in the  $\frac{3}{4}$  part of the buildings. The most collapse. The well-built buildings suffer heavy damage, too. Considerable landslides happen, colossal clefts occur in the ground.
- XI: Catastrophic.** All stone building collapse, the bridges give away, the transmission lines get unusable, and the rails bend.
- XII: Totally catastrophic.** Every human structure gets deteriorate. The waves appear on the surface, certain objects are tossed into the air from the ground.

### *2.2.3. The Modified Mercalli scale (1956)*

In 1931 the Mercalli-Cancani-Sieberg scale was translated into English by Harry O. Wood and Frank Neumann who, for some reason, ignored Cancani and Sieberg, and published it under the name of the Modified Mercalli Scale (MM Scale). This was completely overhauled in 1956 by Charles F. Richter, who refrained from adding his name to the new version in case of further confusion with "Richter Scale" magnitudes. Richter's version became instead the "Modified Mercalli Scale of 1956" despite the fact that the link to Mercalli was now extremely remote. The terms Mercalli intensity scale or Mercalli scale should not be used unless one really means the original ten-degree scale of 1902.

To avoid ambiguity of language the quality of masonry is specified and it is classified in four categories as follows:

- masonry A: good workmanship, mortar and design; reinforced, especially laterally and bound together by using steel, concrete, etc.; designed to resist lateral forces;
- masonry B: good workmanship and mortar; reinforced, but non designed in detail to resist lateral forces;
- masonry C: ordinary workmanship and mortar; no extreme weaknesses like failing to tie in at corners, but-neither reinforced nor designed against horizontal forces;
- masonry D: weak materials, such as adobe; poor mortar; low standards of workmanship; weak horizontally.

The common form of the Modified Mercalli Scale used nowadays in the U.S.A. was abridged and rewritten by Richter in 1956 and is the following.

- I:** Not felt. Marginal and long-period effects of large earth quakes.
- II:** Felt by persons at rest, on upper floors, or favourably placed.
- III:** Felt indoors. Hanging objects swing. Vibration like passing of light trucks. Duration estimated. May not be recognized as an earthquake.
- IV:** Hanging objects swing. Vibration like passing of heavy trucks; or sensation of a jolt like a heavy ball striking the walls. Standing motor cars rock. Windows, dishes, doors rattle. Glasses clink. Crockery clashes. In the upper range of IV wooden walls and frame creak.
- V:** Felt outdoors; direction estimated. Sleepers wakened. Liquids disturbed, some spilled. Small unstable objects displaced or upset. Doors swing, close, open. Shutters, pictures move. Pendulum clocks stop, start, change rate.
- VI:** Felt by all. Many frightened and run outdoors. Persons walk unsteadily. Windows, dishes, glassware, broken. Knickknacks, books, etc., off shelves. Picture off walls. Furniture moved or

overturned. Weak plaster and masonry D cracked. Small bells ring (church, school). Trees, bushes shaken; visibly, or heard to rustle.

- VII:** Difficult to stand. Noticed by drivers of motor cars. Hanging objects quiver. Furniture broken. Damage to masonry D, including cracks. Weak chimneys broken at roof line. Fall of plaster, loose bricks, stones, files, cornices, unbraced parapets and architectural ornaments. Some cracks in masonry C. Waves on ponds; water turbid with mud. Small slides and caving in along sand or gravel banks. Large bells ring. Concrete irrigation ditches damaged.
- VIII:** Steering of motor cars affected. Damage to masonry C; partial collapse. Some damage to masonry B; none to masonry A. Fall of stucco and some masonry walls. Twisting, fall of chimneys, factory stacks, monuments, towers, elevated tanks. Frame houses moved on foundations if not bolted down; loose panel walls thrown out. Decayed piling broken off. Branches broken from trees. Changes in flow or temperature of springs and wells. Cracks in wet ground and on steep slopes.
- IX:** General panic. Masonry D destroyed; masonry C heavily damaged, sometimes with complete collapse; masonry B seriously damaged. General damage to foundations. Frame structures, if not bolted, shifted off foundations. Frames racked. Serious damage to reservoirs. Underground pipes broken. Conspicuous cracks in ground. In alluviated areas sand and mud ejected, earthquake fountains, sand craters.
- X:** Most masonry and frame structures destroyed with their foundations. Some well-built wooden structures and bridges destroyed. Serious damage to dams, dikes, embankments. Large landslides. Water thrown on banks of canals, rivers, lakes, etc. Sand and mud shifted horizontally on beaches and flat land. Rails bent slightly.
- XI:** Rails bent greatly. Underground pipelines completely out of service.
- XII:** Damage nearly total. Large rock masses displaced. Lines of sight and level distorted. Objects thrown into the air.

#### *2.2.4. The Medvedev–Sponheuer-Karnik scale (1964)*

The Medvedev-Sponheuer-Karnik scale, also known as the MSK or MSK-64, was first proposed by Sergei Medvedev (USSR), Wilhelm Sponheuer (East Germany), and Vít Kárník (Czechoslovakia) in 1964. It was based on the experiences being available in the early 1960s from the application of the Modified Mercalli scale and the 1953 version of the Medvedev scale, known also as the GEOFIAN scale. With minor modifications in the mid-1970s and early 1980s, the MSK scale became widely used in Europe and the USSR. MSK-64 is still being used in India, Israel, and countries which were parts of the former USSR. The MSK scale is somewhat similar to the MM scale used in the United States. The MSK scale has 12 intensity degrees expressed in Arabic numerals.

- 1: Not perceptible.** Not felt, registered only by seismographs. No effect on objects. No damage to buildings.
- 2: Hardly perceptible.** Felt only by individuals at rest. No effect on objects. No damage to buildings.
- 3: Weak.** Felt indoors by a few. Hanging objects swing slightly. No damage to buildings.
- 4: Largely observed.** Felt indoors by many and felt outdoors only by very few. A few people are awakened. Moderate vibration. Observers feel a slight trembling or swaying of the building, room, bed, chair etc. China, glasses, windows and doors rattle. Hanging objects swing. Light furniture shakes visibly in a few cases. No damage to buildings.
- 5: Fairly strong.** Felt indoors by most, outdoors by few. A few people are frightened and run outdoors. Many sleeping people awake. Observers feel a strong shaking or rocking of the whole building, room or furniture. Hanging objects swing considerably. China and glasses clatter together. Doors and windows swing open or shut. In a few cases window panes break. Liquids oscillate and may spill from fully filled containers. Animals indoors may become uneasy. Slight damage to a few poorly constructed buildings.
- 6: Strong.** Felt by most indoors and by many outdoors. A few persons lose their balance. Many people are frightened and run outdoors. Small objects may fall and furniture may be shifted. Dishes and glassware may break. Farm animals may be frightened. Visible damage to masonry structures, cracks in plaster. Isolated cracks on the ground.



- 7: Very strong.** Most people are frightened and try to run outdoors. Furniture is shifted and may be overturned. Objects fall from shelves. Water splashes from containers. Serious damage to older buildings, masonry chimneys collapse. Small landslides.
- 8: Damaging.** Many people find it difficult to stand, even outdoors. Furniture may be overturned. Waves may be seen on very soft ground. Older structures partially collapse or sustain considerable damage. Large cracks and fissures opening up, rockfalls.
- 9: Destructive.** General panic. People may be forcibly thrown to the ground. Waves are seen on soft ground. Substandard structures collapse. Substantial damage to well-constructed structures. Underground pipelines ruptured. Ground fracturing, widespread landslides.
- 10: Devastating.** Masonry buildings destroyed, infrastructure crippled. Massive landslides. Water bodies may be overtopped, causing flooding of the surrounding areas and formation of new water bodies.
- 11: Catastrophic.** Most buildings and structures collapse. Widespread ground disturbances, tsunamis.
- 12: Very catastrophic.** All surface and underground structures completely destroyed. Landscape generally changed, rivers change paths, tsunamis.

### *2.2.5. The European Macroseismic Scale*

In 1988 the European Seismological Commission (ESC) agreed to initiate a radical revision of the MSK Scale. A Working Group "Macroseismic Scales" was established under the chairmanship of G. Grünthal. At the first meeting in 1990 in Zürich, the framework of the new scale was agreed. The bulk of the text was composed at the second meeting at Munich in 1991. The third meeting, at Walferdange (Luxembourg) in 1992 dealt with the accompanying material (guide to the use, annexes, illustrations, etc.). It was decided at Walferdange to drop the name MSK in favour of "European Macroseismic Scale" (EMS). The material was finalised at a meeting of key members of the Working Group in Potsdam later in 1992. The scale was published in draft form by the Council of Europe in the spring of 1993, and was ratified at the ESC meeting in Reykjavik in September 1996, following a three-year testing period. In fact, this new scale was recommended by the 23<sup>rd</sup> General Assembly of the ESC in 1992 to be used in parallel with existing scales for a time period of three years, in order to gather experience under realistic conditions, especially on the more experimental parts of the scale: on the vulnerability classes and engineered constructions. This testing was not restricted to Europe. As a result of experiences gained during testing, further modifications were made, experimental parts were confirmed, and the presentation of the scale was improved. The final version was published in 1998. Since its 1993 publication the new scale has been widely adopted outside Europe as well. The EMS is the first intensity scale that actually comes with instructions for use. Previous scales assumed that the reader would always correctly understand the author's intentions (Musson, 2006). It is also the first scale with graphic illustrations, i.e., pictures demonstrating what is meant by the different grades of damage to buildings.

The basis for establishing the EMS was the MSK scale, which itself is an update relying on the experiences being available in the early 1960s from the application of the MCS, the MM scale and the Medvedev scale from 1953. Although slight, barely noticeably changes to the MSK-64 were proposed by Medvedev in 1976 and 1978, it became evident to many users that the scale needed several improvements, more clarity, and adjustment to incorporate newly introduced construction techniques.

One of the main intentions for the creation of the new scale was not to change the internal consistency of the scale. This would result in intensity evaluations which would be different from earlier applications of the widely used twelve degree scales and which would require a reclassification of all earlier intensity assessments. This should be avoided at all costs. It would result in a complete confusion in all studies on seismicity and seismic hazard which depend heavily on macroseismic data.

Other general aspects considered to be fundamental to the updating were as follows:

- the robustness of the scale, i.e., minor differences in diagnostics should not make large differences in the assessed intensity; further to this, the scale should be understood and used as a compromise solution, since no intensity scale can hope to encompass all the possible disagreements between diagnostics that may occur in practice;

- such disagreements may also reflect differences in cultural conditions in the regions where the scale is used;
- the simplicity of the use of the scale;
- the rejection of any intensity corrections for soil conditions or geomorphological effects, because detailed macroseismic observations should just be a tool for finding and elaborating such amplification effects;
- the understanding of intensity values as being representative for any village, small town or part of a larger town instead of being assigned to a point (for one house, etc.).

The specific problems to be solved by the WG on Macroseismic Scales, on the basis of the above mentioned aspects, were:

- the need to include new types of buildings, especially those including earthquake-resistant design features, which were not covered by existing versions of the scale;
- the need to address a perceived problem of non-linearity in the scale arrangement at the junction of the degrees VI and VII (which, after thorough discussion for preparing the EMS-92, as well as for the EMS-98, proved to be illusory);
- the need to generally improve the clarity of the wording in the scale;
- the need to decide what allowance should be made for including high-rise buildings for intensity evaluations;
- whether guidelines for equating intensities to physical parameters of strong ground motions, including their spectral representations, should be included;
- to design a scale that not only meets the needs of seismologists alone, but which also meets the needs of civil engineers and other possible users;
- to design a scale which should be suitable also for the evaluation of historical earthquakes;
- the need for a critical revision of the usage of macroseismic effects visible in the ground (rock falls, fissures etc.) and the exposure of underground structures to shakings.

The term "macroseismic intensity" is used in the EMS-98 entirely in the meaning of a classification of the severity of ground shaking on the basis of observed effects in a limited area.

The twelve-degree macroseismic scales are in fact ten-degree scales; i.e., intensity I means nothing was observable and intensities XI and XII are, apart from their very limited practical importance, difficult to distinguish. If one takes into account the rare practical use of the intensities II and XI as well as the fact that intensity XII defines maximum effects, which are not to be expected to occur in reality, the result is even an eight-degree scale. But, as mentioned above, to avoid any confusion, the classical numbering is kept.

Serious problems arose with the treatment of engineered or antiseismic constructions for intensity evaluation. Reasons for these were:

- the limited knowledge and experience up to now on the systematics of earthquake damage patterns for this category of buildings;
- the great variety of systems for classifying engineered constructions in seismic codes;
- disagreements between engineers and seismologists in the use of intensity and related research topics (e.g., a tendency among engineers to overestimate the importance of instrumental data in connection with intensities and therefore the danger to overcharge the concept of intensity);
- the often imprecise seismological approach to intensity assignment with regard to building types previously used in the MSK-64 or in the MM-56 scales; i.e., the general neglect of the quality of workmanship, the structural regularity, the strength of materials, the state of repair, and so on, as well as the need to consider such features as scaling conditions.

It was accepted already for the EMS-92 that engineered buildings can be used for intensity assignment only on the basis of earthquake-resistant design principles. An essential step for overcoming these problems was the introduction of the vulnerability table which provides the possibility to deal in one scheme with different kinds of buildings and the variety of their actual ranges of vulnerability (Fig. 2.4). In former scale versions building types were defined in a rather strict way, by construction type alone. This vulnerability table, as an essential part of the EMS, incorporates engineered and non-engineered buildings into a single frame. It was clear from the beginning that the

EMS-92 version with its adopted compromises had to be understood as an experimental or tentative solution, connected with the commitment to gather more information and experience on this subject, in order to become able to introduce necessary improvements.

At the final stage of the anticipated three-year testing period of the EMS-92 and after applications throughout the world it became clear that the personal judgement used in assigning intensity can be decreased with the new scale. This does not mean that assessing intensity with the new scale is easier in every case, but users become aware of problematic cases in a more direct way. The introduction of the vulnerability table was highly acknowledged, as well as the introduction of the new definitions of damage grades (Figs. 2.5 and 2.6) and especially the Guide to the Use of the Intensity Scale and the different Annexes. New building types or those which are not covered by the present vulnerability table can be added in an appropriate way. Generally, the engineering aspects incorporated into the new scale were appreciated by the engineers. The new elements of the EMS in the form of the vulnerability table and the damage grades have facilitated the use of the scale by insurers, planners, and decision makers to derive damage or risk scenarios for given intensities. Criticism has been expressed mainly on the downplaying of the role of effects in natural surroundings in the intensity assignment. The applications of the EMS-92 made clear that only its tentative parts, i.e., the use of engineered buildings, needed significant modification.

Type of Structure	Vulnerability Class					
	A	B	C	D	E	F
MASONRY	○					
	○—					
	—○					
	—○—					
	—○—					
	—○—					
	—○—					
REINFORCED CONCRETE (RC)	—○—					
	—○—					
	—○—					
	—○—					
	—○—					
	—○—					
STEEL						
WOOD						

○ most likely vulnerability class; — probable range;  
 ..... range of less probable, exceptional cases

Fig. 2.4 – Definition of structural vulnerability classes in EMS (from Grünthal, 1998).

The 25th General Assembly of the ESC in Reykjavik, 1996, passed a resolution recommending the adoption of the new macroseismic scale within the member countries of the ESC, considering that additional effort had to be invested to overcome several inconsistencies in the use of engineered structures.

While studies of the structural pattern of several earthquakes, e.g., Northridge (U.S.A.) 1994, Kobe (Japan) 1995, Aegion (Greece) 1995, were going on, several other damaging events, like Dinar

(Turkey) 1996, Cariaco (Venezuela) 1997 and central Italy 1997/98, provided further information and experience. They led finally, though with no complete agreement, to modifications of the vulnerability table with respect to reinforced concrete (RC) structures, their level of earthquake resistant design and their differentiation into RC wall and RC frame structures, as well as to the introduction of steel structures. The wording of the classifications of damage grades was in parts newly structured. Damage to buildings as part of the definitions of intensity degrees have been more clearly arranged.

The whole process of establishing first the EMS-92 and finally the EMS-98 went on for almost ten years. Further macroseismic practice may enable a deeper insight into the complex matters of assigning intensity. Future applications or future needs might be the basis for further improvements of this new tool in the seismological and engineering practice for classifying the effects of earthquakes on humans, on objects in the human's environment, or on buildings as an essential element of the human society.

The short form of the European Macroseismic Scale, abstracted from the Core Part, is intended to give a very simplified and generalized view of the EMS. It can be used for educational purposes, e.g., at schools or by the mass media, or otherwise to give a brief explanation of the significance of the numbers of the scale to an audience unable to digest the full version. This short form is not suitable for intensity assignments.

**I: Not felt.**

**II: Scarcely felt.** Felt only by very few individual people at rest in houses.

**III: Weak.** Felt indoors by a few people. People at rest feel a swaying or light trembling.

**IV: Largely observed.** Felt indoors by many people, outdoors by very few. A few people are awakened. Windows, doors and dishes rattle.

**V: Strong.** Felt indoors by most, outdoors by few. Many sleeping people awake. A few are frightened. Buildings tremble throughout. Hanging objects swing considerably. Small objects are shifted. Doors and windows swing open or shut.

**VI: Slightly damaging.** Many people are frightened and run outdoors. Some objects fall. Many houses suffer slight non-structural damage like hair-line cracks and fall of small pieces of plaster.

**VII: Damaging.** Most people are frightened and run outdoors. Furniture is shifted and objects fall from shelves in large numbers. Many well built ordinary buildings suffer moderate damage: small cracks in walls, fall of plaster, parts of chimneys fall down; older buildings may show large cracks in walls and failure of fill-in walls.

**VIII: Heavily damaging.** Many people find it difficult to stand. Many houses have large cracks in walls. A few well built ordinary buildings show serious failure of walls, while weak older structures may collapse.

**IX: Destructive.** General panic. Many weak constructions collapse. Even well built ordinary buildings show very heavy damage: serious failure of walls and partial structural failure.

**X: Very destructive.** Many ordinary well built buildings collapse.

**XI: Devastating.** Most ordinary well built buildings collapse, even some with good earthquake resistant design are destroyed.

**XII: Completely devastating.** Almost all buildings are destroyed.

### 2.3. Isoseismals

The isoseismals are the curves that join the points of the Earth where the earthquake was felt with the same intensity (Fig. 2.7). Theoretically the isoseismals should be circumferences having their centre in the epicentre. On the contrary one obtains in practice very strange curves depending principally on the nature of the ground at the observation points.



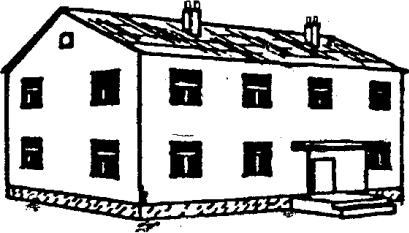
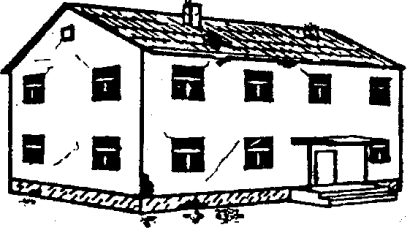
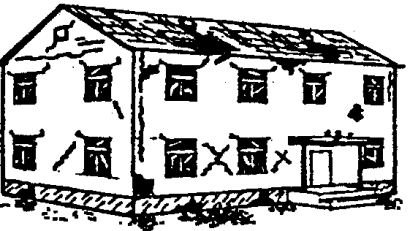

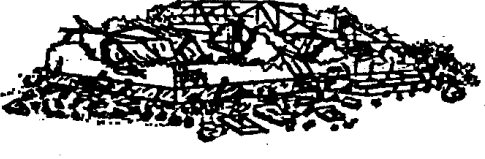
	<p><b>Grade 1: Negligible to slight damage</b> (no structural damage, slight non-structural damage) Hair-line cracks in very few walls. Fall of small pieces of plaster only. Fall of loose stones from upper parts of buildings in very few cases.</p>
	<p><b>Grade 2: Moderate damage</b> (slight structural damage, moderate non-structural damage) Cracks in many walls. Fall of fairly large pieces of plaster. Partial collapse of chimneys.</p>
	<p><b>Grade 3: Substantial to heavy damage</b> (moderate structural damage, heavy non-structural damage) Large and extensive cracks in most walls. Roof tiles detach. Chimneys fracture at the roof line; failure of individual non-structural elements (partitions, gable walls).</p>
	<p><b>Grade 4: Very heavy damage</b> (heavy structural damage, very heavy non-structural damage) Serious failure of walls; partial structural failure of roofs and floors.</p>
	<p><b>Grade 5: Destruction</b> (very heavy structural damage) Total or near total collapse.</p>

Fig. - 2.5 - Classification of damage to masonry buildings in EMS (from Grünthal, 1998).

The best method of obtaining field intensities is to examine effects as soon as possible after the earthquake; for the lower intensities, to interview several persons in each locality, being careful not to put questions so as to suggest particular answers. Newspaper reports are useful, if one becomes accustomed to journalistic phrases. Pieces of information from carefully designed questionnaires are reputed the most reliable source of data. The distribution of the isoseismals, and in particular the distance between them, reflect primarily the magnitude and the focal depth of the earthquake; the isoseismals of shallow earthquakes tend to be more closely spaced, whereas deeper earthquakes, in subduction zones, will generally produce lower values of intensity but with isoseismals enclosing much larger areas (Fig. 2.8).

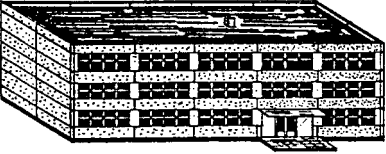
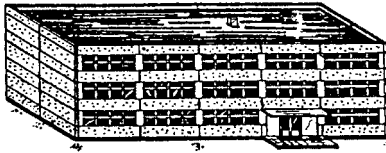

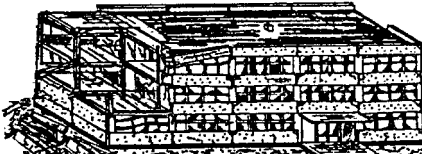

	<p><b>Grade 1: Negligible to slight damage</b> (no structural damage, slight non-structural damage)</p> <p>Fine cracks in plaster over frame members or in walls at the base.</p> <p>Fine cracks in partitions and infills.</p>
	<p><b>Grade 2: Moderate damage</b> (slight structural damage, moderate non-structural damage)</p> <p>Cracks in columns and beams of frames and in structural walls.</p> <p>Cracks in partition and infill walls; fall of brittle cladding and plaster. Falling mortar from the joints of wall panels.</p>
	<p><b>Grade 3: Substantial to heavy damage</b> (moderate structural damage, heavy non-structural damage)</p> <p>Cracks in columns and beam column joints of frames at the base and at joints of coupled walls. Spalling of concrete cover, buckling of reinforced rods.</p> <p>Large cracks in partition and infill walls, failure of individual infill panels.</p>
	<p><b>Grade 4: Very heavy damage</b> (heavy structural damage, very heavy non-structural damage)</p> <p>Large cracks in structural elements with compression failure of concrete and fracture of rebars; bond failure of beam reinforced bars; tilting of columns.</p> <p>Collapse of a few columns or of a single upper floor.</p>
	<p><b>Grade 5: Destruction</b> (very heavy structural damage)</p> <p>Collapse of ground floor or parts (e. g. wings) of buildings.</p>

Fig. - 2.6 - Classification of damage to RC buildings in EMS (from Grünthal, 1998).

Fig. 2.7b plots the MM intensity ratings of localities near the October 17, 1989 Loma Prieta earthquake. Intensities typically increase close to an earthquake's epicentre, allowing seismologists to interpret maps such as this for the general location of historical earthquakes. Note the locations of unusually high intensities (up to IX) far north of the earthquake's epicentre, near San Francisco Bay. During this earthquake, soft and water-saturated soils near the bay amplified the effects of the shaking. The amplified shaking, together with soil liquefaction effects, caused some well-built structures to collapse and yielded the intensity IX rating at those locations.

It is also possible to estimate the magnitude of an earthquake from the area of the map enclosed by isoseismal contours of certain intensities. Such estimates are, however, a subject of research and require verification.

A rough comparison between macroseismic and instrumental data can be done considering intensity and peak ground acceleration (PGA) although it must be pointed out that they represent two

different quantities: damage (intensity) and ground shaking (PGA), which are related through the building vulnerability (Fig. 2.9).

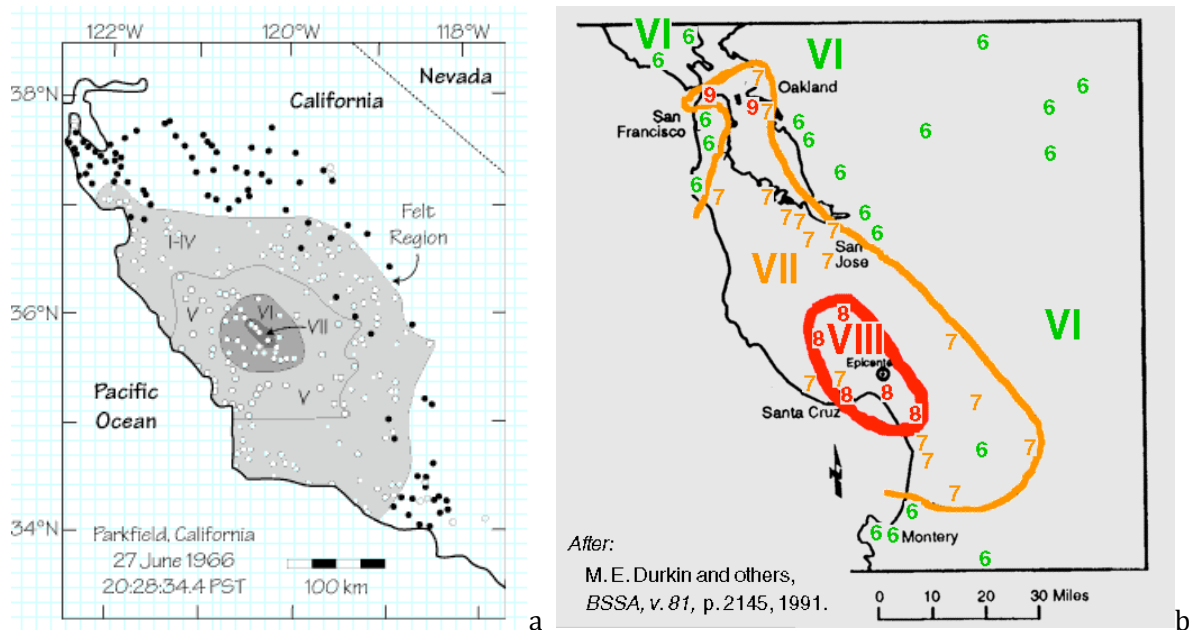


Fig. 2.7 – Isoseismal maps: a) 1966 Parkfield earthquake; b) 1989 Loma Prieta earthquake.

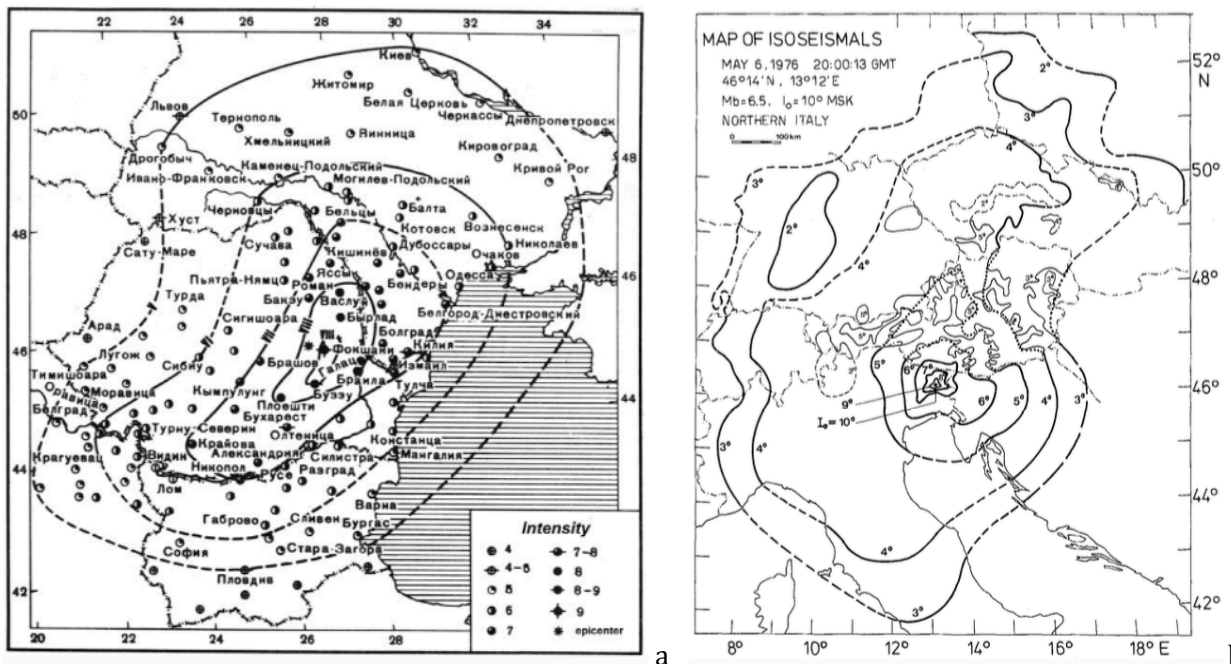


Fig. 2.8 – Comparison between the isoseismals of the 133 km deep M 7.7 Vrancea earthquake (a) of November 10, 1940 (from Bune et al., 1986) and those of the superficial (7 km deep) M 6.4 Friuli earthquake (b) of May 6, 1976 (from Karnik et al., 1978). It can be seen the much larger isoseismal areas of the deep event in comparison of the surficial one.

### 2.4. Macroseismic parameters

Although the macroseismic data are qualitative and not quantitative, interesting information can be derived from them about the source parameters of the earthquakes. Source parameters are the hypocentral coordinates (latitude, longitude, depth) and magnitude.

There are two basic approaches to deriving most earthquake parameters from macroseismic data. The first is to draw isoseismals and use the enclosed areas, or the average radii. The second is to

base the calculations on the intensity data points themselves, without drawing isoseismals. The advantage of the second approach is that any subjectivity in the isoseismal drawing is entirely circumvented. The disadvantage is that the results may be biased by heterogeneity in the distribution of intensity points as a result of variations in population distribution.

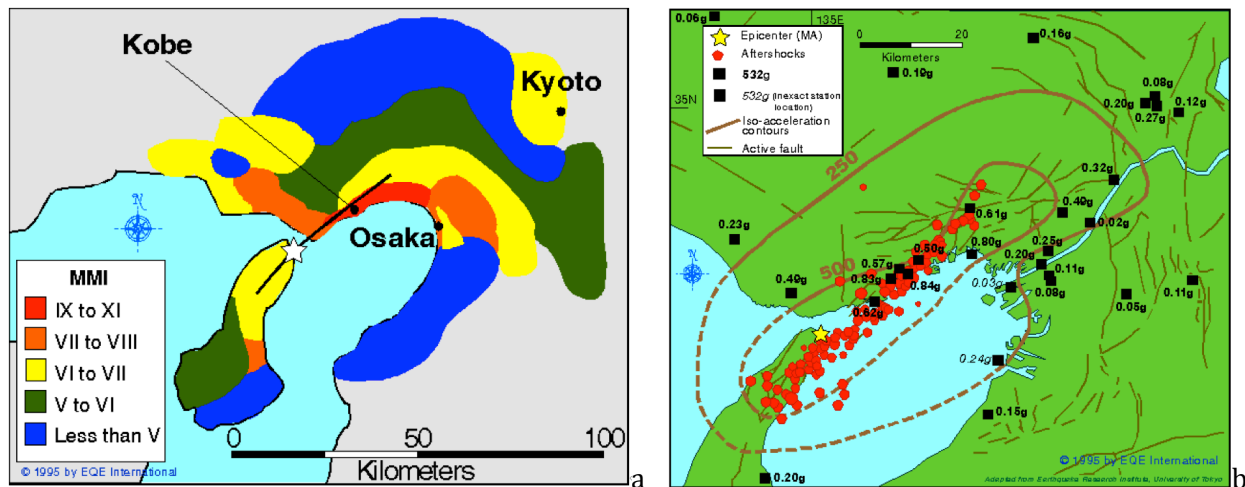


Fig. 2.9 – Comparison between macroseismic and instrumental data for the Kobe earthquake: a) MM macroseismic intensity contour; b) strong motion data and iso-acceleration contour.

A standard procedure for deriving the epicentral coordinates does not exist and in the past the common practise was to draw the isoseismals and to fix the epicentre as the gravity centre of the highest isoseismal. Considering that several times the highest isoseismal is biased by local effects, this procedure can drive to wrong estimates. Alternative more recent approaches are based on the intensity data points, without considering, then, the isoseismals. Among them, it is worth mentioning the “Boxer” algorithm (Gasperini et al., 1999) which is codified and suitable for automatic elaborations.

Procedures for estimating the focal depth were developed many years ago as the attenuation relations for macroseismic intensity take into account that parameter. Consequently, the Blake (1941) relation as well as that by Kovesligethy (Sponheuer, 1960) give an estimate of depth and were largely used in the past.

The estimation of focal depth from macroseismic data was first developed by Rado Kovesligethy. His first paper on the subject presented the formula

$$I - I_0 = 3 \log \sin e - 3\alpha \left( \frac{r}{R} \right) (1 - \sin e) \quad (2-1)$$

where  $e$  is the angle of emergence given by  $\sin e = h/r$  and  $R$  is the radius of the Earth (Kovesligethy, 1906). Eq. (2-1) was subsequently rewritten and modified slightly by Janosi (1907), to reach the better-known formula

$$I_0 - I_i = 3 \log \left( \frac{r}{R} \right) + 3\alpha(r - h) \quad (2-2)$$

where  $r$  is the radius of the isoseismal of intensity  $I_i$ ,  $h$  is depth, and  $\alpha$  is a constant representing anelastic attenuation. In this form the equation has been much used. The constant value of 3 represents an equivalence value between the degrees of the intensity scale and ground motion amplitudes. Some workers accept it, others prefer to find their own values by fitting to data. The attenuation parameter  $\alpha$  should usually be determined regionally by group optimisation on an appropriate data set rather than for individual earthquakes, since one assumes that this value, a property of the crust, does not alter from earthquake to earthquake.



This technique is also associated with the name of Blake (1941), whose contribution was essentially a reduction and simplification of Eq. (2-2); Blake's version is still used by some workers today, but Kovesligethy's original equation (in Janosi's version) is more commonly encountered. Kovesligethy's equation became more widely known, in the form of Eq. (2-2), through a paper by Sponheuer (1960).  $I_0$  is properly the barycentral intensity, which has to be solved for in addition to solving for  $h$ . This is usually done graphically; one can fit the isoseismal data to all possible values of  $h$  and  $I_0$  and find a minimum error value consistent with the observed maximum intensity.

More problematic is the estimation of the macroseismic magnitude: generally it was obtained from regressions between epicentral intensity and magnitude of recent events with relation of the type:

$$M = aI_0 + b \quad (2-3)$$

where  $a$  and  $b$  are constants calculated from regression analysis.

More articulated relations, which take into account the whole or part of the intensity data points, were developed as well and seem more robust. The total felt area ( $A$ ) of an earthquake, or the area enclosed by one of the outer isoseismals (usually degree III or IV), is, in fact, a much better indicator of magnitude, being not much affected by depth except in the case of truly deep earthquakes. For earthquakes below a threshold magnitude (about 5.5  $M_w$ ), magnitude and  $\log A$  scale more or less linearly, and so equations of the form

$$M = a \log A + b \quad (2-4)$$

can be established regionally by examination of data for earthquakes for which macroseismic data and instrumental magnitude are both available. For larger earthquakes, differences in spectral content may affect the way in which earthquake vibration is perceived, and a different scaling appears to apply.

Other forms that have been proposed include

$$M = aI_0 + b \ln r + c \quad (2-5)$$

where  $r$  is the radius, rather than the area, of the total macroseismic field, and

$$M = aI_0 + \sum b_i \ln r_i + c \quad (2-6)$$

in which all isoseismals (values for each  $i$ ) are used as well as the epicentral intensity.

The method of Bakun and Wentworth (1997) is of particular interest in making a joint determination of epicentre and magnitude by drawing contours of goodness-of-fit to the intensity data set of possible epicentres and magnitudes. This method is especially suited in cases where the intensity data set is sparse.

In the above equations,  $M$  has been used for generic magnitude; for any particular magnitude equation it is important to specify what magnitude type the derived values are compatible with ( $M_S$ ,  $M_L$ ,  $M_w$ , etc.). It is also useful to determine the standard error, which will give a measure of the uncertainty attached to estimated magnitude values.

## 2.5. Historical seismology

Historical seismicity is the historical records of earthquakes preserved in different form such as written history, chronicles, inscription etc., which plays an important role in the seismic hazard assessment because instrumentally recorded earthquakes are lacking before the 20<sup>th</sup> century. Historical events must be available for a long period of human civilization which should throw light on the extent of damage besides the date and place of occurrence. For older paleo-earthquakes, geological methods such as trenching surveys on active faults, identifications of liquefaction features at

archaeological sites or tsunami deposits in coastal environments, have been carried out in some countries.

A very good description of what the Historical Seismology is and what are its characteristics is reported in the introduction of the volume "Investigating the records of past earthquakes" by Albin et al. (2004), from which the following pages are taken.

The idea of making a compilation of past earthquakes, what we could call now an earthquake catalogue, is something that developed slowly. Early European examples can be found in the 16<sup>th</sup> and even the 15<sup>th</sup> centuries, but the purpose of these was hardly something that we would recognise today as scientific. In the Middle Ages and still in the Renaissance, earthquakes were generally regarded as signs and wonders, not as natural phenomena. In fact, to hold that an earthquake might be natural and not something sent by God was considered to be a heresy. Therefore, the motives for compiling a list of earthquakes would be most likely as a matter of antiquarian interest, or even have a religious purpose in order to record the number of times that God had revealed his anger. The concept of what we think of as seismicity was alien to these times, although writers were already noticing that some countries were more subject to earthquakes than others.

Approaches to the recording of earthquake data were also conditioned by thoughts about what sort of phenomena earthquakes were. Today we know that every earthquake has an epicentre from which the seismic energy radiates outwards; thus the idea of making a list of earthquakes according to place, or a map in which every event is indicated by a point symbol, is natural. At a period where it was often imagined that earthquakes travelled rather slowly round the world visiting one country at a time, in the manner of a thunderstorm, this false concept would be likely to influence how one thought about, and hence write about, earthquakes that had occurred.

By the second half of the 17<sup>th</sup> century, however, earthquakes were clearly becoming a subject for what we can recognise today as scientific studies; studies that required data, and thus antiquarian texts had to be raided for information about how earthquake phenomena had manifested themselves in the past.

This was even more pronounced in the 18<sup>th</sup> century, when a number of key earthquakes in Europe, of which the devastating 1755 Lisbon earthquake was the most important, triggered widespread public reaction, and gave a huge stimulus to earthquake studies, both scientific and those intended chiefly for a popular audience. Lacking the apparatus for collecting data on earthquakes that had just occurred (with some notable exceptions), many of these studies relied on historical accounts of previous events to supply the data for their speculations on the nature of earthquakes.

The 19<sup>th</sup> century saw this taken to new heights of elaboration with the compilation of great earthquake catalogues, which far exceeded in volume the works of previous centuries. Here one must mention the familiar names of von Hoff, Mallet and Perrey, culminating in the largest catalogue of all, the unpublished world earthquake catalogue of Montessus de Ballore, a manuscript famously occupying 30 m of shelf space, some of it written on scrap paper culled from the orders of the day of an artillery regiment. These global catalogues were supplemented by a variety of national catalogues of differing quality. Even at this period, although the intentions of the compilers were scientific, work consisted largely of collecting and ordering material from written sources (often secondary in nature) and arranging the result either by region or chronologically.

Parameterisation of earthquake data had to wait until the 20<sup>th</sup> century. The concept of magnitude was not invented until the 1930s and even intensity, which can be traced back in its modern sense to the 1820s, was not widely used in earthquake catalogues until the early 20<sup>th</sup> century. The production of parametric earthquake catalogues, where events are represented by date, time, epicentral coordinates, magnitude and perhaps depth, was stimulated by the work of Gutenberg and Richter for 20<sup>th</sup> century earthquakes. It was apparent soon in the second half of the 20<sup>th</sup> century that such catalogues were valuable for the study of plate tectonics and seismic hazard, and needed extension back in time using pre-instrumental, historical data. What was once a matter of antiquarian interest became a matter of primary scientific and also engineering importance.

This produced two significant problems, only one of which was immediately obvious.

The obvious problem was how to derive numerical parameters from textual data. Obviously, intensity was the key tool here. From an isoseismal map one could derive at least an estimate of epicentral coordinates (this was a procedure that by now was of long standing); the estimation of

depth from macroseismic data had been proposed by Kovesligethy as far back as 1906; and it remained to estimate the magnitude from maximum intensity or felt area.

The less-obvious problem was not less important. From the earliest antiquarian compilations, a simple procedure had been used, more or less, in most studies. If a historical document, of any character, attributed to a certain place and time the occurrence of an earthquake, then that was to be taken at face value, and an entry in the earthquake catalogue constructed corresponding to the data found. The amount of source criticism undertaken was extremely limited, and frequently non-existent entirely. No distinction was made between primary and secondary sources as these terms are understood by the historian, and the idea that a source might be seriously in error through tortured transmission seems not to have occurred. As a result, catalogues were filled with mistakes. These often arose from errors of dating. If chronicle A described an earthquake on 12 March 1247, and chronicle B copied from chronicle A and carelessly wrote the date as 12 March 1249, then one could be sure that the early catalogues of earthquakes would probably have two earthquakes in place of one, with both dates being respected. Problems due to the use of different dating systems are very common, and many are the errors committed through mistranslation of regnal years, or confusion between Julian and Gregorian calendars, or dates expressed as Anno Hejira treated as if they were Anno Domini.

These errors resulted in a large part from a simple failure to understand that the study of historical earthquakes is a multi-disciplinary study. Someone with no seismological training who attempts to interpret a seismogram using a basic textbook as a guide is liable to make errors that a trained seismologist would avoid. Likewise, someone without the insight of a professional historian is liable to fall into a variety of traps when dealing with historical documents that cannot necessarily be taken at face value, and usually need to be interpreted in the light of their historical and social context.

It is not just a matter of dealing with the issues revolving around the documents themselves; many contextual matters have to be resolved. The distribution of reports of an earthquake will be influenced by the distribution of population, and that will not be the same some hundreds of years ago as it is today. Social and linguistic divides can also affect the distribution of reports, and these have to be known about in order to appreciate properly how much of the final intensity map is due to seismological matters and how much due to social matters. The interpretation of historical damage reports is another minefield into which the seismologist must step warily. What sort of vulnerability was characteristic of the housing of the region and period under study? How can one find this out? Sometimes damage was reported to special structures indigenous to a particular place and time, and such damage can only be interpreted with great care. Forcing such data into rigid categories of an intensity scale written only with modern buildings in mind will lead to misjudgements.

It was really only in the last thirty years that these problems were properly faced, and the study of historical earthquakes started over again, sometimes almost from scratch, working with primary source data interpreted according to sound historical principles, and with seismologists and historians working in partnership. This partnership itself has been a rather fascinating one, and extended also to include archaeologists to take the record further back than purely written material can go. To the unenlightened layman, it might seem that historians and archaeologists belong to professions about as far removed from any practical importance or social relevance as one could possibly get. Despite this, now in many countries, historians and archaeologists are contributing findings of great significance to scientific studies that have as their extremely practical aim the elucidation of seismic hazard and the reduction of social losses from natural disasters.

Nevertheless, invariably, the situation is different in different parts of the world. Evidently, the length of literary history in a country is a restriction. In many parts of the world, earthquake information, other than that based on palaeoseismology, begins when settlers or colonists arrive in an area previously inhabited only by pre-literate people. Thus on the eastern seaboard of North America the potential length of the historical earthquake record is about 400 years; on the western seaboard, half that.

But other factors also affect the opportunities for historical earthquake research. The study of historical earthquakes in a region where settlements regularly suffer from destruction and heavy damage, is of a different character to studies in areas of lesser seismic activity where earthquakes usually cause surprise and alarm rather than physical damage. In the first case documents relating to bills for repair and requests for remission of taxes are significant sources; in the second case the

relative rarity of earthquakes occurring at all makes even quite low intensities a notable event, to be preserved for posterity.

Political experience and the passage of war impinge on the way that records are made and transmitted. Here one can point to the differences between the type and quantity of historical earthquake data in Italy and Greece in the Renaissance and Early Modern periods. Both countries have active seismicity and a literary tradition dated back to antiquity, but the experience of Greece under Ottoman occupation had a strong effect on how earthquakes were reported. Also, one has to consider not just how earthquakes were reported at the time, but also how those reports are transmitted to the present day. Archives are fragile things, and modern wars also impact on the material available for earthquake studies, as witness the destruction of irreplaceable archives in Sarajevo and Baghdad.

The situation facing those who would reconstruct the earthquake record of past centuries varies from country to country, not only as regards the material available for study, but also reflecting the differing traditions and opportunities relating to earthquake studies in the past: in some countries the modern earthquake historian has a pre-existing fabric of catalogues on which to build; in others it is necessary to start almost from scratch (which is not always a disadvantage).

But equally, many of the problems are the same: the problems of how to interpret different types of source, the discrimination of fake earthquakes, and the critical issues of deriving reliable parameters from documentary material. Additionally, material relating to historical earthquakes is often to be found distributed around the world in places far from where the earthquakes in question occurred. Key materials for the seismic history of the Caribbean are to be found in the maritime archives of New England ports; the archives of the major colonial powers contain material with a wide geographical scope; and so on.

Therefore, there is much advantage to be gained from earthquake historians in different countries and different parts of the world coming together, comparing experiences and exchanging ideas. In Europe, such exchanges had already started to take place, especially in the framework of different international projects sponsored by the European Community. In South America also, for some years there has been a well-established tradition of international cooperation between different countries in the frame of the Centro Regional de Sismología para América del Sur (CERESIS). However, the next stage, the formulation of contact between such specialists throughout the whole world, was something new.

### *2.5.1. Value of historical seismicity*

The purpose of an interesting note by Ambraseys (2002), and reported in the following, was to describe how historical evidence can be used to address some fundamental questions: when and where have earthquakes happened in the past? How can accounts of ancient events contribute to our scientific understanding of earthquake activity?

As we cannot know what will happen in the future, to estimate likely earthquake hazards we have to find out what happened in the past and extrapolate from there. Previous research has uncovered evidence of destructive earthquakes in areas where only small events have been experienced recently. This is not surprising: the timescale of geology is vastly different from that of human history, so some areas will suffer a short period of violent earthquakes only once in a few hundred years. It follows that if we took account only of information about the last century, in which earthquakes have been recorded by instruments (and even then not uniformly throughout the globe), we would have no way of knowing whether an apparently "quiet" area is in fact at risk from a damaging earthquake. The use of the historical record is invaluable, not only in the study of earthquakes but also of the climate and weather, and can guide the engineer to design structures to resist the forces of nature without being taken by surprise by unanticipated events.

The reappraisal of the seismicity of the eastern Mediterranean and the Middle East, east of the Adriatic and the Ionian seas all the way to India, shows that although the historical record is incomplete, careful reading of the available data can provide valuable insights into the long-term seismicity of the region. The pattern of seismic activity of many areas is seen to have changed little over the past 2,500 years, while other areas which are at present quiescent can be shown to be capable of generating earthquakes of significant size.



Some of the lessons we believe we have learned from these studies are noted here.

- Archaeological evidence for an earthquake is not always unambiguous and can seldom be used to provide a precise date for the damage caused. Nevertheless, archaeological evidence can provide confirmation of long-term seismicity in a given region and with greater collaboration between disciplines it is likely that many refinements of the existing database will be possible.
- For the Earth scientist and earthquake engineer the main objectives of historical research into primary sources are to refine and extend the information contained in secondary studies and catalogues, and to provide an objective measure of the reliability and completeness of the data retrieved.
- It is important to establish unambiguously the simultaneity of damage to different localities in an historical earthquake. Often one finds cases in which two separate events have been transformed into a large earthquake. This is understandable in view of the tendency of both contemporary and later writers to amalgamate seismic events, whether for lack of sufficiently precise information, from ignorance of the true nature of earthquakes, or from simple convenience. Such an amalgamation of effects will over-estimate the size of the damage area, and hence of the size of the event.
- While some of the problems of dating can be resolved, it is often more difficult to determine a sufficiently accurate location for historical earthquakes. The epicentral area of an historical event is not always certain and judgement has to be exercised to ascertain its location. The primary aim should be to avoid both the amalgamation and duplication of events.
- The size of an historical earthquake can be assessed in terms of its magnitude: such an assessment for historical events can be made only approximately and depends on the reliability of information regarding their effects at large epicentral distances or from the dimensions of their epicentral area. For events in which this information could be estimated, the magnitude of the event should be estimated using a calibration formula derived from 20th-century earthquakes for the region.
- In estimating intensities we find that at large distances an earthquake may cause the collapse of a few important but vulnerable constructions, for which there may be archaeological or historical evidence. This information alone should not always be taken to mean that all the other man-made structures at these sites have been destroyed. The observed effects can be the result of the high vulnerability of long-period structures to sustained ground motions, rather than of the severity of the shock.
- For many historical events, the data are wholly insufficient to permit assessment of intensity in terms of any of the scales currently in use, let alone to reckon the magnitude of an event, except in very general terms. We find that precise local or epicentral intensities assigned by modern cataloguers to many historical events, particularly in Greece and the Holy Land, are hypothetical and often grossly inflated.
- Earthquake catalogues are often used by Earth scientists and engineers to assess earthquake hazard. A more critical attitude is needed to rely only on those that combine the interpretation of primary sources with estimates of the reliability and completeness of the data provided.
- The location and size of historical earthquakes should not be used for scientific purposes without proper scrutiny of the associated historical material.
- The historical record confirms that some regions that are active today (e.g., the North Anatolian Fault zone) were also active 2,500 years ago, demonstrating the long-term nature of their seismicity. It also shows that some regions that are at present quiescent (such as the Jordan Rift Valley) are capable of generating relatively large earthquakes. For some of these events this is consistent with their known active tectonic environment.
- Too many modern catalogues of historical seismicity are not sufficiently rigorous to be treated with confidence. This has often been due to the inter-disciplinary nature of this field of study, which requires scientists to examine literary texts and historians to glean scientific information from their sources. The result has been the production of a large number of false earthquakes, or of seismic events of a size beyond the limits of the possible, often with a sensationalist tinge. This is of no technical consequence, provided the Earth scientist and engineer is aware of it.

2.5.2. The family tree of the historical earthquakes

A new approach to the study of the historical earthquakes was proposed by Stucchi in the 1980's. His approach is based on two main guidelines: 1) the collection of all (possible) documents about the studied event which were already cited by previous investigators, and 2) the systematic search in the archives and depository where it is likely that information about the studied event was stored.

Taking a catalogue as reference catalogue, all earthquakes with epicentral intensity greater than a selected level are considered. All sources cited in the reference catalogue are collected together with the sources they cite, as far as the documents coeval to the event (Fig. 2.10). A kind of family tree for the sources of the earthquake can be constructed in such a way and the transmission of the information from one source to another becomes clear (Fig. 2.11). When possible, only the sources coeval to the event are used to assess the macroseismic intensity and construct the intensity map of the earthquake.

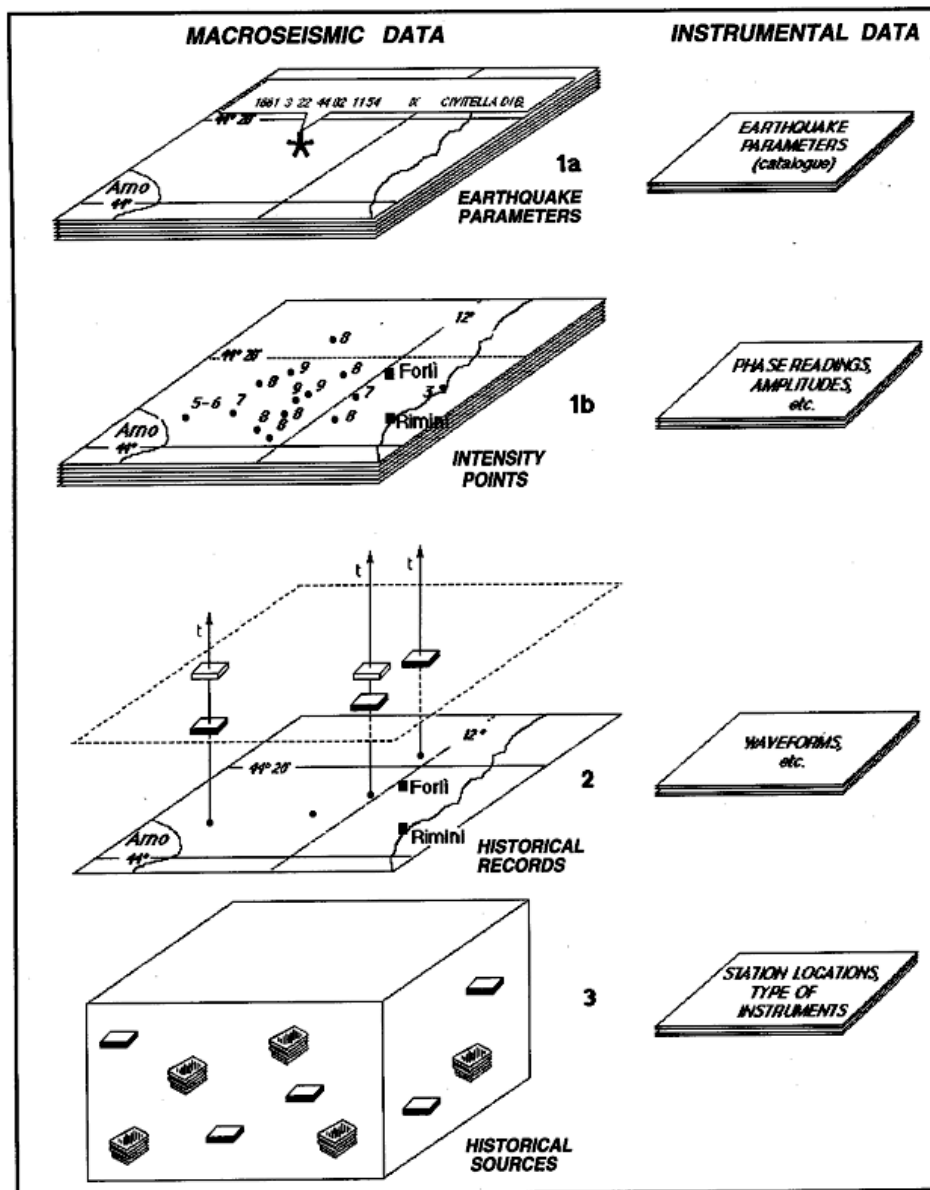


Fig. 2.10 – Scheme of macroseismic data processing compared to instrumental (from Stucchi, 1994).

On these bases the most recent Italian earthquake catalogues were compiled and also European quakes were studied in the framework of the EC project "Review of Historical Seismicity in Europe" which was developed in the years 1989 to 1993. In order to accomplish the goals of the European

project, the main attention was concentrated on transfrontier earthquakes in selected sub-areas and time-windows. The project developed according to the following basic ideas:

- a) each sub-area and time-window to be investigated included at least one destructive earthquake. Partners from both sides of the frontiers were asked to review the existing knowledge: catalogues, isoseismal maps, studies of single earthquakes, in order to evidence the quality of the available data. The main scope was to make clear upon which set of historical sources the present data relied. After this step, specific historical investigation was to be performed;
- b) other investigators were charged to explore the potential of some depositories of European interest, in order to extract historical records useful to all partners and to evaluate the opportunity of further, intensive investigation.

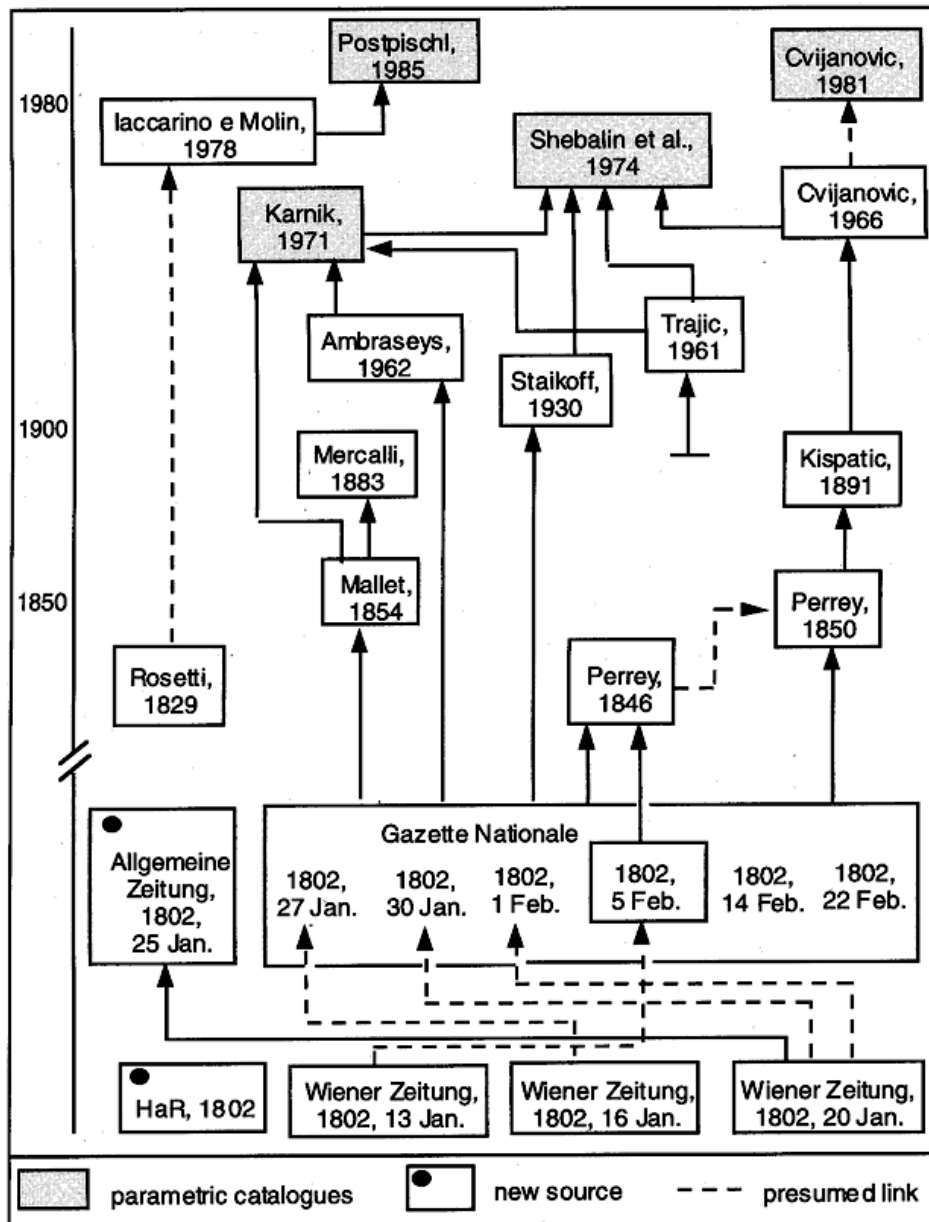


Fig. 2.11 - Simplified family-tree of the records of the 1564 Maritime Alps earthquake (from Moroni and Stucchi, 1993).

## 2.6. Palaeoseismology

In low seismicity areas large earthquakes are rare, but not necessarily absent. Consequently, the historical catalogue is generally limited in time and moreover the magnitude of most events is poorly

known. Fortunately there are methods to extend the observation period. Looking at an even longer timescale, palaeoseismology, the study of mainly prehistoric earthquakes, may add additional information. Looking in detail at the near surface geology of large faults, a search is made for traces of movements at the surface (surface rupture) that may be interpreted as being caused by large earthquakes.

Palaeoseismology can be defined as the identification and study of prehistoric earthquakes. Pre-instrumental seismicity can only be inferred by geological, archaeological, and historical investigation (Fig. 2.12). Geologists can read signs of past tremors imbedded in sedimentary sections (faults and fractures in the bedrock structures) and sometimes present as geomorphic features (marine landslides, etc.).

The concept of paleoseismicity was born in the 1970s with the precept that the geological record of large earthquakes could be used to extend the record beyond the historical and instrumental periods. Paleoseismology involves a multidisciplinary approach spanning geology, geomorphology, geochronology, and deformation modelling. Thus, paleoseismology has the potential to improve our knowledge of the seismic history of a region through several seismic cycles and to contribute some basic inputs for the assessment of seismic hazard. At the beginning of the 1990s, paleoseismology was still in its infancy and was applied mainly in the western United States, Japan and New Zealand with very few attempts in other regions.



Fig. 2.12 - Trace of a fault in the Gulf of Corinth that was activated during several ancient earthquakes and also during the 1981 seismic sequence.

### 2.6.1. Archaeoseismology

Many of the earthquakes that occurred in the last few thousand years have left their traces not only on the physical environment but in the archaeological record as well. The study of remains of ancient constructions to identify reliable indicators of ancient earthquakes and their parameters has led to the advent of a branch of Palaeoseismology, called Archaeoseismology.

Archaeological evidence is based on the effects of strong earthquakes on buildings and soil.



Generally, historical seismicity is based on descriptions of destructive earthquakes and can stretch back to 2000 years or more. When a written record is available, archaeological seismicity, which supplements the historical data, paints a very time and location specific picture, quite unlike the geological record.

Archaeological evidence in palaeoseismology is a relatively new source of investigation. It was put into a more scientific framework only in 1928 by Sir Arthur Evans. Based on evidence of a destruction layer, he established the tradition of regarding earthquake horizons as benchmarks in archaeological stratigraphy and chronology. Some archaeologists have gone as far as blaming major earthquakes for the destruction of several major constructions, even putting the blame for the collapse and disappearance of ancient civilisations.

The main contribution that seismic archaeology can offer to active tectonics is the localisation, dating and evaluation of seismic events (Fig. 2.13). The relationship between qualitative data (the description of effects) and quantitative data (magnitude, depth) is still approximate. Archaeologists need to interpret and place material and written clues into a wider temporal context in the appropriate socio-economic framework of the sampled region. In other words, to establish the extent and magnitude of a certain destructive episode, i.e., working within a rigorous scientific outline, the archaeological study has to look beyond the often scant written record of the event. Local patterns of destruction and damage, filtered through historical parameters, can point to a more precise description of an ancient earthquake.



Fig. 2.13 - Ruins of a tomb in Hierapolis, an ancient city in Turkey founded around 200 B.C. and abandoned after an earthquake in 1534. Many offsets can be observed between the different blocks: although gravity may be a primary driver of this tomb deformation, perhaps occasional seismic shakings contributed (taken from Callan Bentley in AGU Blogosphere).

First, we have to ask if an earthquake is at all possible within the present geophysical knowledge of a certain area.

- Could potential seismic evidence be confused with past landslides and falling rocks, avalanches, rushing water, mud flows, floods, tsunamis, storms, hurricanes, whirlwinds or gales?
- Would it be possible after millennia for slow-acting natural destructive forces such as deterioration, erosion, fissures and other surface effects, landslides, subsidence, produce the same effects as those generated by an earthquake?
- What about deformation resulting from gravitational forces, contraction or expansion of the ground,

leaching and even slow tectonic movements?

It is also crucial that a good stratigraphical check is carried out so that the observed deformations are not the result of later earthquakes.

Second, we need to establish that human factors are not at the origin of these seismic signs. Wars, fires, building over older structures, partial or complete demolition, restructuring, reconstruction and repair can all be confused with tectonic dynamics.

Finally we need to correlate the potential seismic event with the known historical setting of the site. We also have to establish the locality of the event, i.e., if neighbouring areas were also affected.

The following pieces of evidence are suggested as criteria for the identification of earthquakes from archaeological data (see also Fig. 2.14).

- Ancient constructions offset by seismic surface faults. A good example can be seen on the Great Wall of China, offset by the 1739 earthquake by about 3 m in the vertical and horizontal directions. On a lesser scale Greek and Roman mosaics in houses and temples in the Mediterranean show evidence of strike/slip movements. In these cases the amount and pattern of dislodgement can help estimating the magnitude and direction of the tremor.
- Skeletons of people killed and buried under the debris of fallen buildings. Deaths caused by earthquakes were so common in the ancient Greece that they had a name for describing these victims: *seismatias*. Unfortunately only earthquakes of great magnitude and destructiveness justified the abandonment of whole cities and stopped people resuming and giving a proper burial to the deceased. As a consequence the identification of skeletons of earthquake victims is a rare occurrence and often left out of archaeological reports.
- Certain abrupt geo-morphological changes, occasionally associated with destruction and/or abandonment of buildings and sites. Earthquakes may produce secondary, but locally very destructive effects such as landslides, liquefaction of unconsolidated sediments, tsunami, etc. Very often these secondary seismic products cause more damage on constructions than that resulting from ground shaking.
- Characteristic structural damage and failure of constructions as described in the following:
  - displacement drums of dry masonry columns. Seismic oscillation of a free-standing monolithic column produce strong extensional stresses at the base of the columns. At this point columns can fracture;
  - seismic oscillations of a multi-block column causes translation of the single drums if not reinforced by metal or wood. Toppled columns display a characteristic domino-style arrangement of its drums;
  - opened vertical joints and horizontally slided parts of walls in dry masonry walls;
  - diagonal cracks in rigid walls. Horizontal seismic acceleration can deform a rectangle to parallelograms. Fissures are often near openings and in corners and again they tend to arrange themselves into diagonal fractures in brick-and-mortar fillings;
  - triangular missing parts in corners of masonry buildings;
  - cracks at the base or top of masonry columns and piers. Because of the geometry and distribution of stress fields in vertical and solid constructions, cracks appear on the most rigid part of the building (the base) and the most oscillating part (the top);
  - inclined or sub-vertical cracks in the upper parts of rigid arches, vaults and domes, or their partial collapse along these cracks. An arch (vault or dome) under the influence of a seismic force is stretched and as a result, joints open in a dry and rigid masonry structure. As a consequence a total or partial collapse occurs;
  - down-slided keystones in dry masonry arches and vaults. Keystone (or even the uppermost voussoirs) may slide down and the entire structure collapse;
  - several parallel fallen columns. This exclude the natural and gradual fall of individual columns through the ages;
  - constructions deformed as by horizontal forces (rectangular transformed to parallelograms). Stress and strain applied by a ground motion of oscillatory nature can stretch and deform manmade objects such as pave-stones.
- Destruction and quick reconstruction of sites, with the introduction of what can be regarded as 'anti-seismic' building construction techniques, but with no change in their overall cultural character. This aspect is an obvious candidate to assert the past seismic tendency of certain areas. Because

humanity has always been struggling with limited resources, over-engineering in building practices are only applied when the danger of damage or collapse of constructions are potential and probable. Some peculiar reinforcement of certain structures such as temple columns in the Mediterranean can only be justified by an attempt to counteract oscillatory stresses due to ground movements.

<b>EARTHQUAKE ARCHAEOLOGICAL EFFECTS (EAE)</b>	<b>COSEISMIC PRIMARY EFFECTS (DIRECT EFFECTS)</b>	<b>GEOLOGICAL EFFECTS</b>	<i>Primary geological effects</i> - Fault scarps - Seismic Uplift / subsidence	
		<i>Secondary geological effects</i> - Liquefactions and dike injections - Landslides - Rock fall - Tsunamis/Seiches - Collapses in caves		
	<b>EFFECTS INTO THE BUILDING FABRIC</b>	<i>Strain structures generated by ground deformation</i> - Folded mortar pavements - Fractures, folds & pop-ups on regular pavements - Fractures, folds & pop-ups on irregular pavements - shock breakouts in flagstones - Rotated and displaced buttress walls - Tilted walls - Displaced walls - Folded walls		
<b>POSTSEISMIC 2<sup>nd</sup> EFFECTS (INDIRECT EFFECTS)</b>		<i>Strain structures generated in the building fabric</i> - Penetrative fractures in masonry blocks - Conjugated fractures in walls made of either stucco or bricks - Fallen and oriented columns - Rotated and displaced masonry blocks in walls and drums in columns - Displaced masonry blocks - Dropped key stones in arches or lintels in windows and doors - Folded steps and kerbs - Collapsed walls (including human remains and items of value under the rubble) - Collapsed vaults - Impact block marks - Broken pottery found in fallen position - Dipping broken corners		
		- Fires - Repaired buildings - Recycling anomalous elements - Settlement abruptly abandoned - Stratigraphic gap in the archaeological record - Flash floods generated by collapses of natural and human dams - Anti-seismic buildings		

Fig. 2.14 - A comprehensive classification of Earthquake Archaeological Effects (EAE), based on primary and secondary geological effects of earthquakes. Red arrows indicate the possible seismic wave orientation (from Giner-Robles et al., 2009).

### *2.6.2. Destruction of buildings correlating with historical earthquakes*

The partial collapse of the retaining wall of Acropolis in late 17th and 18th century is well documented. Historical evidence suggests that this destruction is associated with an earthquake dated 1705.

Along the river Jordan near Jericho there are written records of about 30 earthquakes which have occurred in the last 2000 years.

Ben Shean was destroyed by an earthquake under Roman occupation in A.D. 363. The damage extended 300 km from Petra in the south to Pnias in the north suggesting an unusually large magnitude, estimated at around 7. This event also destroyed dozens of synagogues in Galilee. From the direction in which these columns fell it is possible to infer the ground motion during this earthquake. In most of the investigated sites which are west of the Dead Sea Fault, columns fell north-westerly, whereas in sites east of the fault, columns fell south-westerly. Assuming that these more or less free-standing columns fell in the direction opposite to the initial horizontal strong ground motion, the directions may indicate the future direction of the fault dynamic.

Even the Bible can be a source for palaeoseismology; Zechariah's prophecy describes a large earthquake which occurred during the reign of king Uzziah around 760 B.C. The earthquake happened somewhere east of Jerusalem, most likely along the Jericho Fault. Apparently, the offset of the rocks across it was great enough to reveal the northward slip of the eastern side relative to the southward slip of the western side. This motion is remarkably similar to the motion observed in the 1927 Jericho earthquake, and is consistent with the N-S movement of the plates in this area. Many more examples includes new evidence of earthquake destruction in late Minoan Crete, in the south-western Peloponnese, the disappearance of Dioscura and Sebastopolis.

Other likely candidates are the Temple of Zeus Olympus in Sicily, the 6th city of Troy, and the destruction of the Rodi colossus in 224 B.C.

Palaeoseismology is not based only on destructive episodes. There is evidence that the uplifting of the ancient harbour of Aigeira in the Corinthian Gulf was also due to a well know seismic event. Carbon dating applied on a sample of fossil *Dendropoma* resulted in an estimated uplift centred around A.D. 1000-1200.

### **2.7. "ShakeMap": a new technology to aid emergency response**

ShakeMap is a product of the USGS Earthquake Hazards Program in conjunction with regional seismic network operators. ShakeMap sites provide near-real-time maps of ground motion and shaking intensity following significant earthquakes (Fig. 2.15). These maps are used by federal, state, and local organizations, both public and private, for post-earthquake response and recovery, public and scientific information, as well as for preparedness exercises and disaster planning.

The capability to automatically generate computer maps of the intensity of ground shaking and to provide them to the public on the Internet within minutes of a quake was developed after the 1994 Northridge, California, earthquake. ShakeMaps help greatly in the quick assessment of the scope of an earthquake emergency and in guiding emergency response. ShakeMap requires data from modern seismic networks with digital strong-motion recording capabilities and real-time telecommunication feeds.

A ShakeMap is constructed considering the hypocentral location provided by the data of the regional seismic network and applying an attenuation model of peak ground acceleration suitable for the investigated region. Data collected by the regional accelerometric network (if available) are, then, used to correct the acceleration estimates empirically calculated.



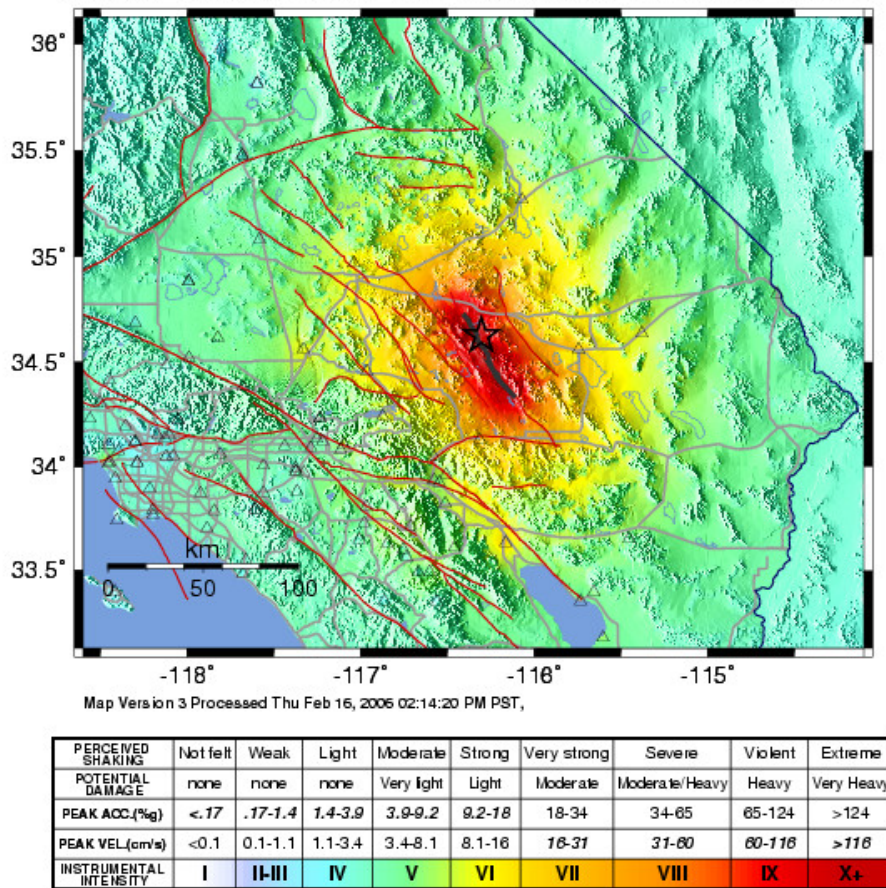


Fig. 2.15 – USGS ShakeMap of the M 7.1 Hector Mine earthquake of October 16, 1999.

## 2.8. The Community Internet Intensity Map

The Community Internet Intensity Map (CIIM) summarizes the questionnaire responses provided by Internet users in the U.S.A. An intensity value is assigned to each community from which a filled-out CIIM questionnaire is received; each intensity value reflects the effects of earthquake shaking on the people and structures in the community. For convenience, "communities" were defined to be ZIP code regions. All the filled-out questionnaires from a given ZIP code are considered and a single intensity to the ZIP code is assigned. The form of the questionnaire and the method for assignment of intensities are based on a published algorithm for determining a "Community Decimal Intensity". The decimal intensity values computed by the algorithm are rounded off to integers for the CIIM and represented by Roman numerals.

A CIIM is made and updated every five minutes following a significant earthquake and then less frequently as additional data are received (Fig. 2.16). ZIP code areas for which data are received are colour-coded according to the intensity scale below the map. At first only a few ZIP codes have intensities assigned, but over time others will be assigned as data come in. Individual ZIP code zones may change colour as a new consensus is reached (that is, data from more respondents may change the average intensity value for a ZIP code).

Since earthquake effects may vary significantly over small distances, the average intensity shown for an entire ZIP code may differ from the intensity that would be suggested by effects at a single location within the ZIP code. Further, the input data is raw and unchecked, and may contain errors.

The CIIM is made to be compatible with ShakeMap rapid instrumental intensity maps (compare Figs. 2.15 and 2.16). Like the ShakeMap, the CIIM's are centred on the epicentre (star) of the earthquake and have similar overall dimensions as the ShakeMaps. However, ShakeMap is based on point location measurements of the ground motion as recorded by seismometers, and the shaking intensity is inferred by empirically relating the recorded ground motions to intensities and then

interpolating the ground motions between the recording sites. ShakeMap does not represent any averaging over ZIP code regions.

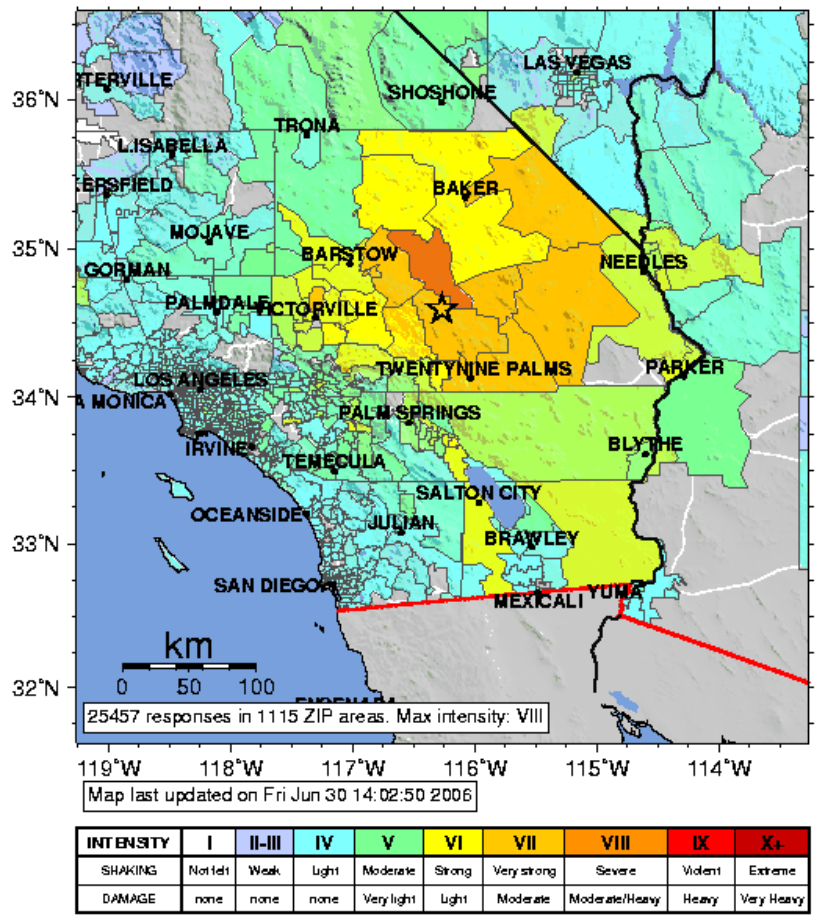


Fig. 2.16 – CIIM of the 7.1 Hector Mine earthquake of October 16, 1999.

### 3. INSTRUMENTAL SEISMOLOGY

The fundamental observations used in seismology (the study of earthquakes) are seismograms which are a record of the ground motion at a specific location. Seismograms come in many forms, on "smoked" paper, photographic paper, common ink recordings on standard paper, and in digital format (on computers, tapes, CD ROMs). Careful observation of ground vibrations during the last 80 years or so have led to our understanding these vibrations, which are caused by seismic waves.

A wave is a disturbance that transfers energy through a medium.

Waves are very common in nature: light is a wave, sound is a wave, ocean surf is generated by waves, and even matter has wave-like properties. The "disturbance" can be an alternating electromagnetic field strength (light), a variation in water height (ocean waves), a variation in material density (sound waves), or a distortion of the shape of the ground (seismic waves).

If you have felt Earth shake during an earthquake or explosion then you have felt seismic waves. These vibrations travel outwards in all directions from their source. Waves generated by large earthquakes can be detected throughout the world and are routinely recorded and analyzed by seismologists.

Seismic waves are generated by many different processes:

- . earthquakes,
- . volcanoes,
- . explosions (especially nuclear bombs),
- . wind,
- . planes (supersonic),
- . people,
- . vehicles.

#### 3.1. Elementary seismic waves

There are four elementary types of seismic waves which transmit the energy of an earthquake. Two wave types, the compressional and the transverse, are also called body waves because they penetrate the Earth's interior. Compressional waves are propagated through either solids, liquids or gases. Transverse waves, requiring rigidity, are transmitted only through solids. Love and Rayleigh waves are two types restricted of surface waves and both require rigidity in the transmitting media. They are also called long waves because of their long periods and wave lengths as compared with those of the compressional and transverse waves. With regard to the seismograph recordings, we may assume that the period of a wave as measured on a seismogram is also the actual period of the ground wave, because the seismograph pendulum, adequately damped, will be forced to oscillate in unison with any sustained ground vibration regardless of the seismograph pendulum period. There is, on the contrary, a great difference between the recorded amplitude of a wave and that of the ground motion: this fact is due to the dynamic magnification.

The compressional wave is analogous to a sound wave and it is sometimes called a longitudinal wave. When the compressional phase of such a wave passes a seismological station, the ground in its immediate surroundings is compressed and the seismograph frame moves slightly in the direction in which the wave is travelling, or away from the epicentre. On the contrary, when the rarefactional part of such a wave passes a station, the ground is dilated and the frame moves towards the epicentre. These directions are recorded on seismograms (see Fig. 3.1). The compressional wave is the faster ( $v_p \approx 6$  km/s) of the two body wave types and it is therefore called the first arrival: P-wave (from the Latin *unda prima*). The velocity of seismic waves increases regularly with depth. P-waves have periods of about 1 second either in the epicentral region or at very great distances and they are superposed on longer period waves of about 5 seconds. The short period part of P waves is of very small displacement and it is recorded by short period pendulums with high magnification, the long period part is of larger displacement and it is recorded by medium or long period instruments.

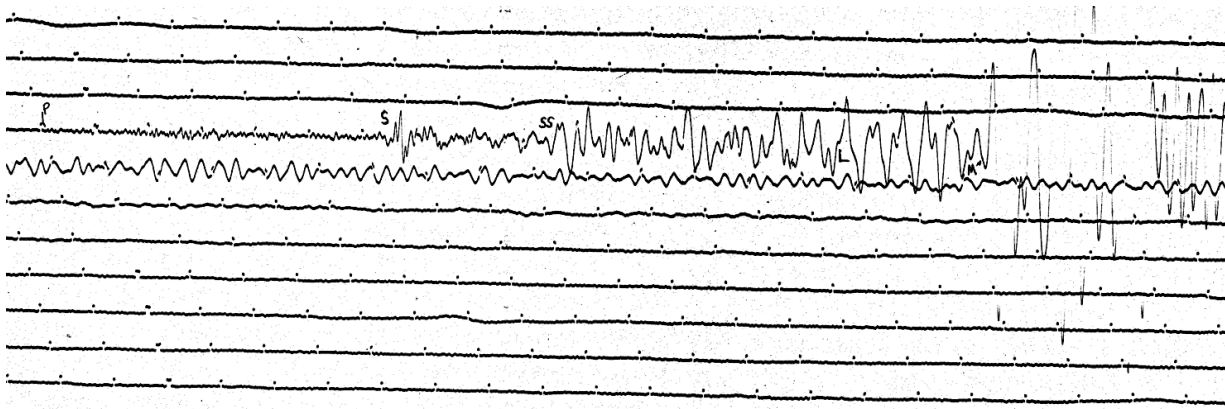


Fig. 3.1 -  $M_S$  5.6 Sinkiang earthquake of May 11, 1967 recorded by the N-S Ewing-Press seismometer of the WWSSN Trieste station (distance 4750 km).

The transverse or shear wave is analogous to a light wave or the transverse vibration of a string. The Earth particle is always displaced in a direction normal to the direction in which the wave is travelling. Shear waves travel at about 0.6 the speed of P waves and they appear as the second most conspicuous wave group on a record of a long period horizontal seismograph. They are also called the second arrival: S-wave (from the Latin *unda secunda*). Observations seem to imply that they do not penetrate the core of the Earth. We may assume that the periods of the S waves about double those of the long period part of P waves and, also the amplitude is roughly double (see Fig. 3.1). Only in near earthquakes the shear waves are recorded by short period seismographs.

If we now look at the theoretical expressions for the velocities of elastic waves:

$$v_P = \sqrt{(\lambda + 2\mu)/\rho} \quad (3-1)$$

for longitudinal waves and

$$v_S = \sqrt{\mu/\rho} \quad (3-2)$$

for transverse waves, where  $\lambda$  and  $\mu$  are the Lamé constants ( $\lambda$  = bulk modulus,  $\mu$  = shear modulus) and  $\rho$  is the mass density. It is clear that the increase in velocity with depth is not due to the increase in density since that alone would have the opposite effect. Therefore, we conclude that elasticity increases faster than density as we go deeper into the Earth.

The surface waves represent the greatest amount of wave energy recorded in shallow earthquakes and they are seen very well on records of long period seismographs. In deep earthquakes so little energy gets into the crustal layers that they may be missing from the record. There are two types of surface waves; the faster is a shear wave called Love wave and it is denoted as  $L_q$ , after Love, or  $G$ , after Gutenberg. Its wave length at long epicentral distances is a function of the thickness of the layered structure traversed and it has been used by investigators to determine crustal and mantle thickness. It has no vertical component and it appears on records of long period instruments as an emergence of a low amplitude wave of about 30 seconds period or more with successive waves of the group decreasing in period and increasing in amplitude. The speed of the  $L_q$  wave, 4.5 km/s, is similar to that of the S waves, when it is propagated over short epicentral distances. There is an appreciable variation in the velocity of the surface shear wave with path traversed.

The Rayleigh wave,  $L_r$ , arrives a short time after the  $L_q$  wave since its speed is about 0.92 that of the shear wave. In a Rayleigh wave the Earth particle follows a retrograde elliptical orbit in a vertical plane through the direction of the propagation. There is no motion transverse to the direction of propagation. Generally the  $L_r$  waves correspond to the group of waves of maximum amplitude, but sometimes the maximum is associated to the  $L_q$  waves. At short epicentral distances it is very difficult to identify true  $L_q$  and  $L_r$  surface waves because they are obscured by some waves of great trace amplitude associated principally with the S wave group. In the epicentral region, the entire ground motion, including surface wave activity, may be recorded for only a few minutes but a great distances



the surface waves may be recorded even for 24 hours. This duration is further emphasized by the fact that the surface waves travel over the major arc between station and epicentre as well as over the minor arc. In some great quakes the surface waves make several complete circuits of the globe plus the arc between station and earthquake.

### 3.2. Dependent seismic waves

The P- and the S-waves generate other types of waves obtained by reflection and refraction at the passage in a different medium. During this fact, part of the energy of a P-wave may be transformed into an S-wave and viceversa. When a wave strikes an interface at a certain critical angle it may be propagated horizontally in the lower medium and it may be continuously diffracted to the surface of the Earth where it will be recorded by seismographs.

For near shocks we must pay attention only to the discontinuities of Conrad and of Mohorovicic according to Jeffreys and so we obtain three types of waves (see Fig. 3.2).

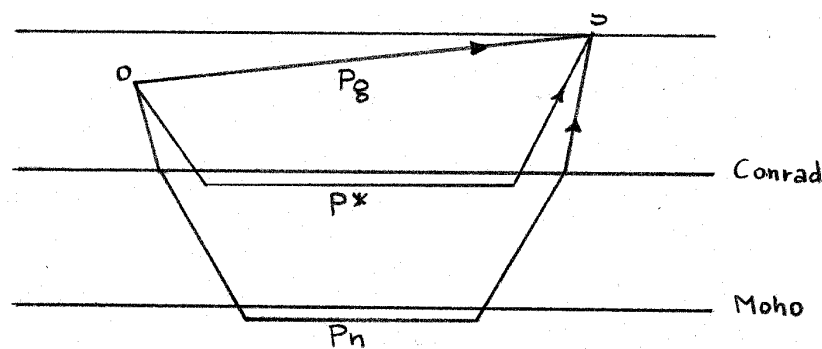


Fig. 3.2 - Paths of principal local shock waves in crustal layers according to Jeffreys.

- 1) The direct wave from the hypocentre O to the station S called  $P_g$  according to Jeffreys or P according to Mohorovicic. The velocity of this wave changes very much in different parts of the world and it is a good thing to find out the right travel-time with a special regional study.
- 2) Other P-wave rays dip downwards penetrating the Conrad discontinuity. Some of the energy is transmitted along the high velocity side of this interface and generates a diffracted wave. It is called  $P^*$  and it is not very easy to identify it in the group of the P waves (see Fig. 3.3).
- 3) Other P-wave rays penetrate the Moho and travel along the high velocity side of this interface and generate a diffracted wave having the surface speed of about 8.2 km/s: this wave is called  $P_n$ .

So, for shocks far no more than 100 km, the first arrival is the direct wave with a velocity of about 6.0 km/s. Beyond that, up to approximately 1500 km the first arrival, with a velocity of about 8.2 km/s, there is a combination of the  $P_n$ -wave and the normal P, travelling through the upper portion of the rock mantle.

S-waves generally duplicate the P-wave phenomena except for the slower speed, the velocity of the S-wave being roughly 0.6 times that of P-wave.

For far quakes we have to consider all possible reflections and refractions. Let us begin with the reflection on the Earth surface. This fact generates the waves called PP, PPP, SS, SSS. The travel-times of these waves will be twice or three times that of the unreflected wave. But the reflection generates also waves of opposite type so we will have PS and SP. All these kinds of waves are recorded very well on seismograms of long period instruments. P- and S-waves are also reflected from the core of the Earth,  $P_cP$ ,  $S_cS$  and  $P_cS$  and  $S_cP$  (see Fig. 3.4); also  $P'P'$ , transmitted through the core and reflected from the Earth's surface through the core a second time.  $P'P'$  is well recorded only on short period, high magnification seismographs.

In the core only a compressional wave is possible which is called K. It is generated either by a P or by a S wave and it generates both of these types, so we will have PKP, SKS, PKS, SKP and also many reflections from the interior interface of the core: PKKKKP and so on.

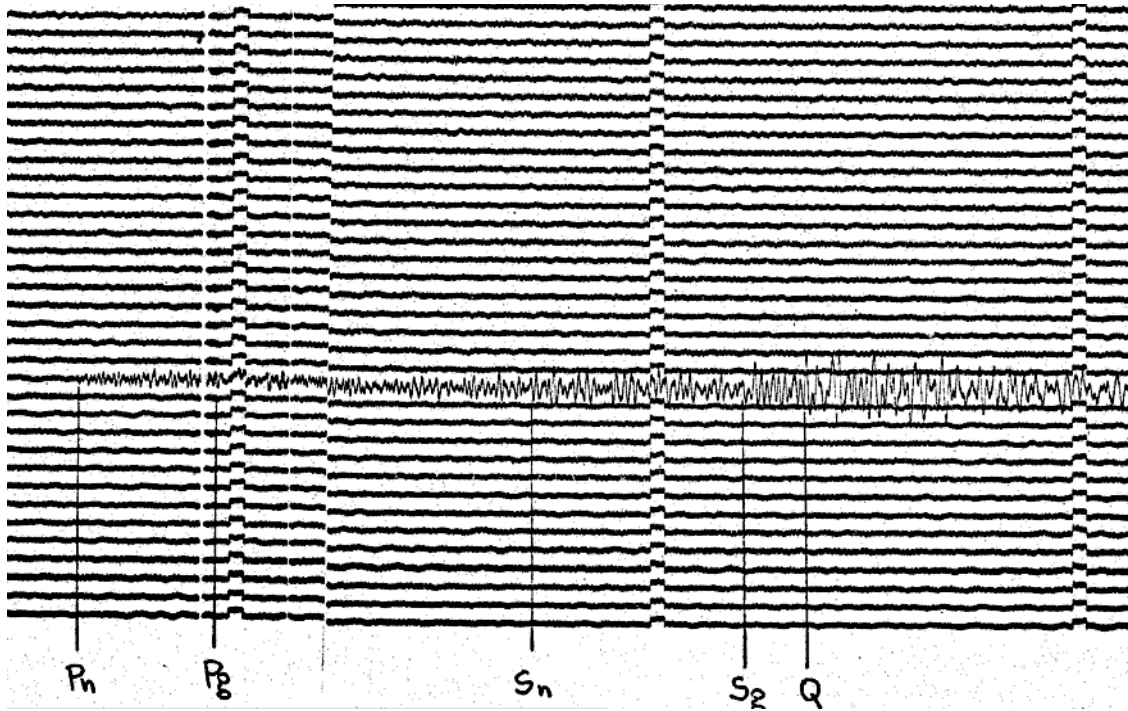


Fig. 3.3 - Albania earthquake of March 8, 1977 recorded by the N-S Benioff seismometer of the WWSSN Trieste station.

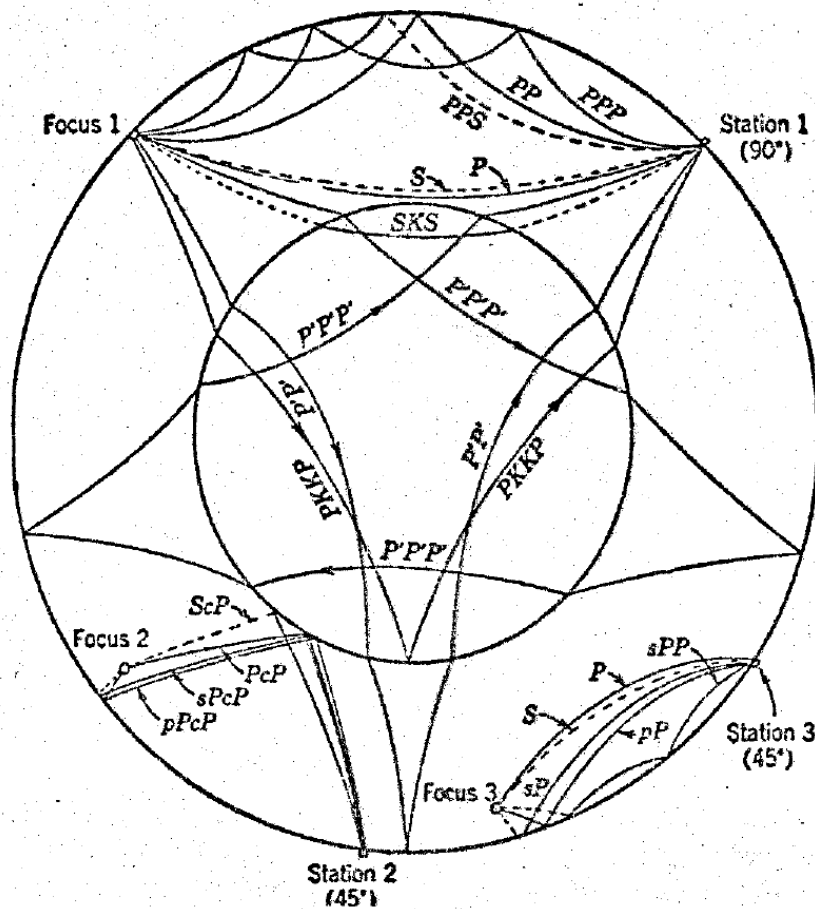


Fig. 3.4 - Paths of some of the more important waves for shallow and deep focus earthquakes.

Earthquakes with a deep focus have a P wave reflected, with angle of reflection equal to angle of incidence, at a point near the epicentre. The short leg of the ray from focus to reflecting point is designed p; the long leg from reflecting point to station P. The combination, pP, represents perhaps the

most important phase that is indicative of the deep focus character of an earthquake. The phenomenon is repeated in the case of the elementary S wave.

### 3.3. Travel-time tables

Travel-time tables show the times required for the various types of seismic waves to travel from an earthquake focus to any point of the Earth's surface (see Fig. 3.5). They are used principally to determine distance between epicentre and station after certain time intervals, usually S-P, have been measured on a seismogram.

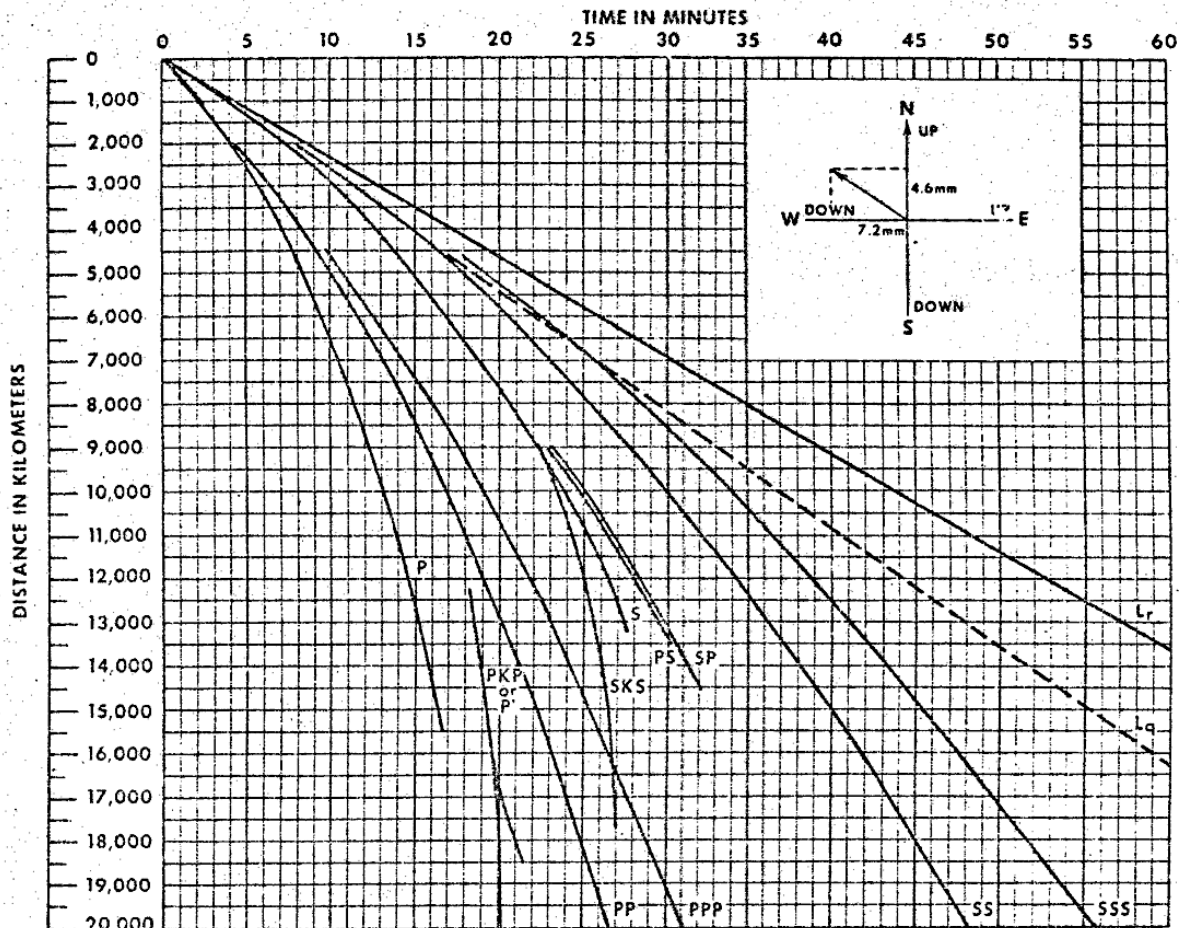


Fig. 3.5 - A simplified form of travel-time chart showing approximate travel times of principal phases for shallow-focus earthquakes. Insert illustrates method of computing direction of ground motion from impulsive P phase.

These intervals increase with epicentral distance and therefore become measures of the epicentral distances. The origin time,  $H$ , that is the true time when the earthquake happened, is also ascertained from travel-time tables. The travel time for waves from a surface source in a medium in which their velocity is constant is a straight line and its slope is equal to the reciprocal of the velocity of the waves. The travel-time tables are needed because the velocity of the waves is not a constant being the seismic rays bent towards the centre of the Earth because of increase of velocity with depth. Travel-time tables are based entirely on observational data; they are obtained by plotting the epicentral distances versus the arrival times in different places of the Earth. The most famous travel-time tables used are the following:

- 1) the Gutenberg-Richter table, that assumes for long distances an average focal depth of 25 km in a crustal structure similar to that of southern California;
- 2) the Macelwane table, that assumes a 12 km depth in continental structure;

3) the Jeffreys and Bullen table, that assumes a focus 33 km deep at the bottom of a typical continental structure.

For distances under 1000 km it is necessary to develop a local travel-time table because of the great difference in velocity values due to the local geology. In this case it is possible to consider velocities as straight lines, and we will have:

$$D = v_P (P-H) = v_S (S-H) \quad (3-3)$$

$$S-P = (S-H) - (P-H) = D/v_S - D/v_P \quad (3-4)$$

We will obtain the Omori's formula:

$$D = K (S-P) \quad (3-5)$$

that permit to calculate directly the distance knowing the two velocities.

In the formula  $S$  and  $P$  are the S- and P-arrival times and  $K$  is equal to  $v_P v_S / (v_P - v_S)$  and it is called the velocity of the fictitious wave.

Let us consider now a local shock and let us try to obtain the travel-time curves.

In Fig. 3.6 the x-axis represents the surface of the ground, below it rays indicating wave paths in the Earth are drawn. Above, the arrival times, corresponding to the various paths at the different distances, are plotted.

1) The direct wave is represented by the branch ABCD but the point A or neighbouring points are rarely observed because of the difficulty to have a station very near the hypocentre, also for very shallow shocks. The travel time is given by:

$$t_1 = \frac{\sqrt{x^2 + h^2}}{v_1} \quad (3-6)$$

where  $h$  is the depth of the focus. The function is a straight line.

2) The travel time of the reflected wave is given by the branch EFG and, if  $h$  is very small in comparison with  $h_1$  the function

$$t_2 = \frac{2}{v_1} \sqrt{\left(\frac{x}{2}\right)^2 + h_1^2} = \frac{1}{v_1} \sqrt{x^2 + 4h_1^2} \quad (3-7)$$

is the equation of an equilateral hyperbole, tangent to the direct wave at infinity and with the origin ordinate equal to  $2h_1/v_1$ .

3) The first refracted wave, represented by the branch FCH, incides to the discontinuity surface with the limit angle  $i_{12}$ , it propagates in the second medium parallelly to the discontinuity and therefore it emerges at the surface after the time:

$$t_3 = \frac{(h_1 - h) \sec i_{12}}{v_1} + \frac{x - (h_1 - h) \operatorname{tg} i_{12} - h_1 \operatorname{tg} i_{12}}{v_2} + \frac{h_1 \sec i_{12}}{v_1} \quad (3-8)$$

and if  $h$  is negligible and  $\sin i_{12} = \frac{v_1}{v_2}$  we obtain:



$$t_3 = \frac{x}{v_2} + 2h_1 \sqrt{\frac{1}{v_1^2} - \frac{1}{v_2^2}} \tag{3-9}$$

that is the equation of a straight line of slope  $1/v_2$  and origin ordinate equal to  $2h_1 \sqrt{\frac{1}{v_1^2} - \frac{1}{v_2^2}}$ .

The angular point C is the point in which the direct wave and the first refracted wave arrive at the same time  $t_1=t_3$ , so knowing the epicentral distance, the velocities  $v_1$  and  $v_2$ , and setting  $h=0$  we have

$$h_1 = \frac{x}{2} \sqrt{\frac{v_2 - v_1}{v_2 + v_1}} \tag{3-10}$$

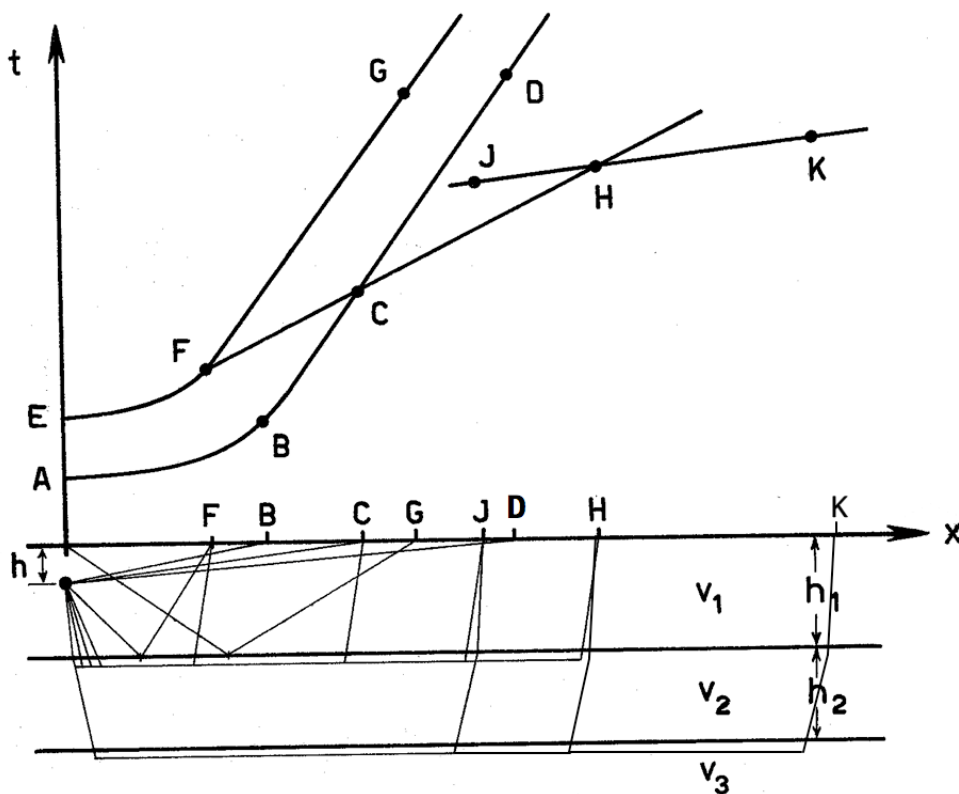


Fig. 3.6 - Wave paths and travel-time curves for local quakes.

4) The second refracted wave penetrates a lower medium of speed  $v_3$  it is represented by the branch JHK and its travel-time is:

$$t_4 = \frac{x}{v_3} + 2(h_1 - h) \frac{\cos i_{13}}{v_1} + 2h_2 \frac{\cos i_{13}}{v_2} \tag{3-11}$$

$$t_4 = \frac{(h_1 - h) \sec i_{12}}{v_1} + 2 \frac{h_2 \sec i_{13}}{v_2} + \frac{x - [(h_1 - h) \operatorname{tg} i_{12} + 2h_2 \operatorname{tg} i_{23} + h_1 \operatorname{tg} i_{12}]}{v_3} + \frac{h_1 \sec i_{12}}{v_1}$$

with  $\sin i_{13} = \frac{v_1}{v_3}$  and  $\sin i_{23} = \frac{v_2}{v_3}$  within our limits of accuracy of observation Eq. (3-11) is a straight line.

### 3.4. Seismic instruments

The motion of the ground under the effects of an earthquake can be measured using different detectors:

- 1) seismometers: if the recorded amplitude is proportional to the amplitude of the ground motion;
- 2) velocity meters: if the recorded amplitude is proportional to the amplitude of the ground velocity;
- 3) accelerometers: if the recorded amplitude is proportional to the amplitude of the ground acceleration.

Since the three measured quantities are vectors we will use three instruments to obtain the value of the vector: one vertical and two horizontal ones placed in directions perpendicular to each other, generally one in the N-S direction and one in the E-W direction.

A seismograph is a device for measuring the movement of the Earth, and it consists of a ground motion detection sensor, called a seismometer, coupled with a recording system (Fig. 3.7). A simple seismometer that is sensitive to up-down motions of the Earth can be understood by visualizing a weight hanging on a spring. The spring and weight are suspended from a frame that moves along with the Earth's surface. As the Earth moves, the relative motion between the weight and the Earth provides a measure of the vertical ground motion. If a recording system is installed, such as a rotating drum attached to the frame, and a pen attached to the mass, this relative motion between the weight and Earth can be recorded to produce a history of ground motion, called a seismogram. Seismographs operate on the principle of inertia (stationary objects, such as the weight in the above picture, remain stationary unless a force is applied to them). The weight thus tends to remain stationary while the frame and drum are moving. Seismometers used in earthquake studies are designed to be highly sensitive to ground movements, so that movements as small as 1/10,000,000 centimetres can be detected at very quiet sites. Modern research seismometers are electronic, and instead of using a pen and drum, the relative motion between the weight and the frame generates an electrical voltage that is recorded by a computer. By modifying the arrangement of the spring, weight and frame, seismometers can record motions in all directions.

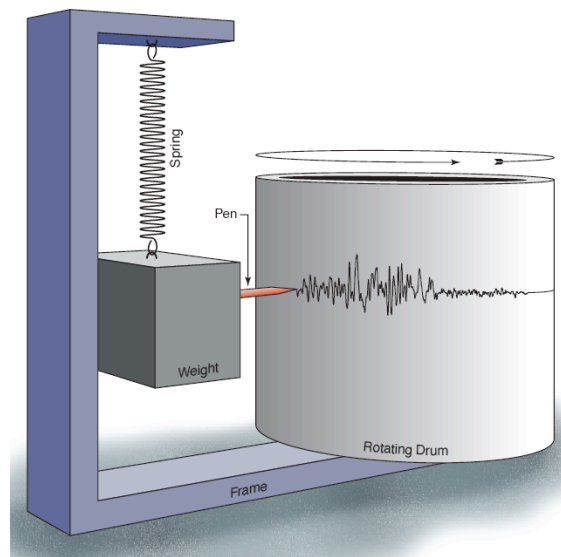


Fig. 3.7 – Scheme of a seismograph.

Seismograms can be used to determine many characteristics of the earthquake source.

The first seismographs were developed by a group led by John Milne working in Japan at the end of the 19<sup>th</sup> century. Instruments were installed in several locations around the world (Fig. 3.8) and the seismic waves of many large earthquakes were recorded, enabling the location and size of earthquakes to be calculated. The period of instrumental seismology is generally considered to have begun in 1898 although at that time the number of instruments in operation around the world was

very small, their distribution uneven and their accuracy limited. During the first half of the 20<sup>th</sup> century seismograph networks were expanded and instrumentation was improved (Fig. 3.9). A very notable contribution to the expansion of instrumental seismology was made by the Jesuits who established seismic observatories in many of their astronomical observatories around the world taking advantage of the accurate chronometry. After the Second World War many seismograph stations were established by government agencies such as geological surveys although the Jesuits, in common with many universities, continue to operate many of their observatories (Fig. 3.10).

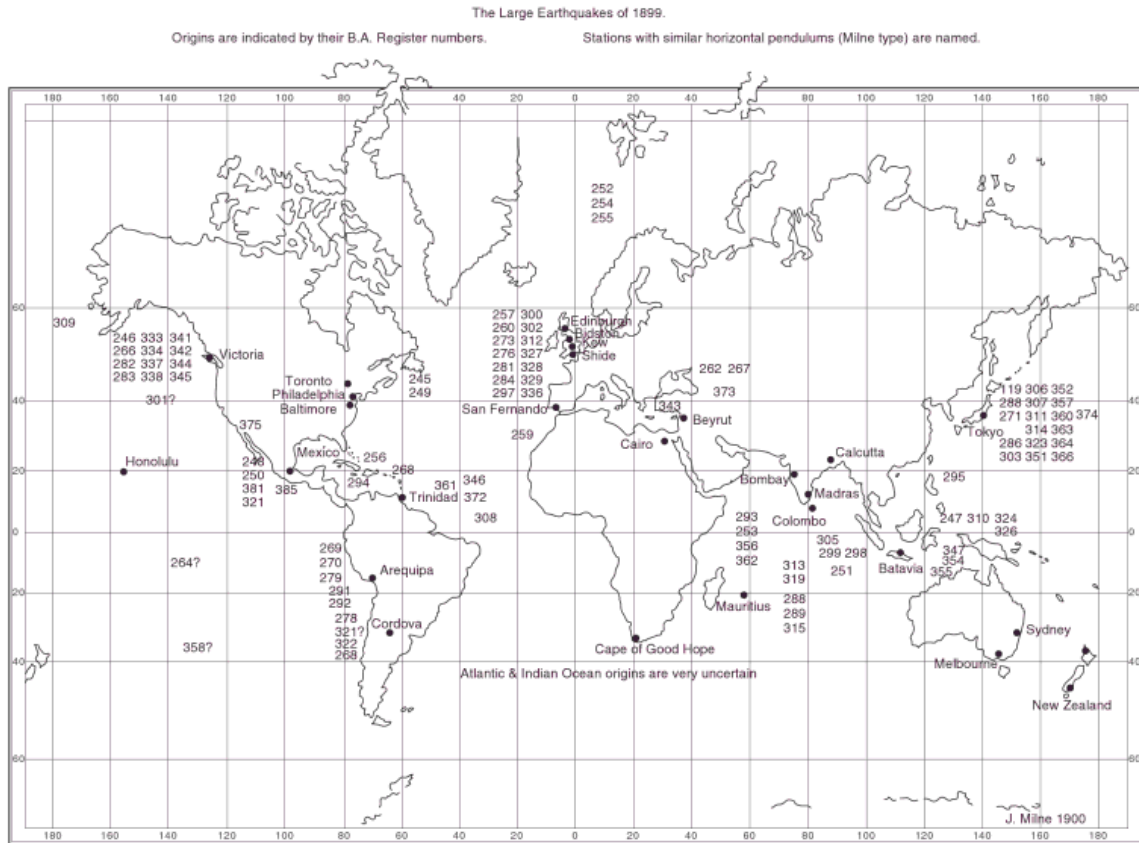


Fig. 3.8 – Global earthquakes and seismographic stations in 1899 (after Milne, 1900). Number refer to earthquakes listed in the Milne’s catalogue, and show approximate positions.

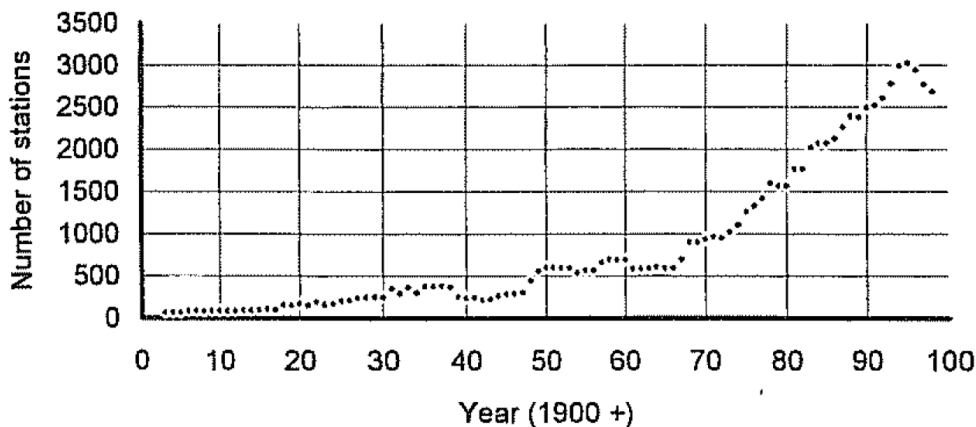


Fig. 3.9 – Distribution of the number of seismographic stations reporting data to international agencies plotted by year after 1902 (from Ambraseys, 2003).

Analogue seismographs record on paper on revolving drums, with time marks generated usually every minute and the absolute time noted on each change of paper on the drum. A very important feature of seismographs is that the recording is always made against absolute UTC (GMT) time so that

there is a common reference for stations throughout the world. The main task of observatory seismologists is to identify the arrivals of different waves and phases on the seismograms and note the exact time of their arrivals.

There are many different types of seismograph networks. Local networks are operated by government agencies in most countries and also by the operators of utilities for which seismic monitoring is important, particularly dams and reservoirs. On the seismograms obtained from local networks, it is generally crustal phases that can be identified.

During the 1960s instrumental seismicity was boosted by the establishment of the World-Wide Standardized Seismograph Network (WWSSN) that consisted of 120 stations in 60 countries (Fig. 3.10), each equipped with accurate chronometry, a triaxial Benioff short-period seismograph and a triaxial Ewin-Press long-period seismograph (Figs. 3.11 and 3.12). The establishment of the WWSSN had as much to do with monitoring atomic test ban treaties as with the study of earthquakes but the benefits for seismology were enormous. It could be considered that a second era of instrumental seismology began in 1964 with establishment of the WWSSN and the International Seismological Centre, an agency placed in England where data from all contributing stations are collected and elaborated for earthquake location (Bommer, 2004).



Fig. 3.10 – World-wide standardized seismograph network (WWSSN) established in the early 1960s. It used analogue short-period (1 s) and long-period (15 or 30 s) 3-component standardized seismographs and crystal clock. More recently (1980-1990s), the WWSSN has been gradually replaced by global initiatives that have utilized broad-band digital instruments.

The most modern seismographs record digitally and have a flat response over wide ranges of period (broad-band seismometers), enabling complete information to be obtained on the nature of the ground motion.

World-wide, national, and regional seismometric networks allow a rapid collection and elaboration of the seismic data and are particularly useful for surveillance. After an earthquake we often descend on the epicentral region with portable seismic instruments to carefully and closely monitor aftershock sequences that follow most large earthquakes. Portable seismic recording systems have been designed for this purpose and they are similar to the permanent stations but often run on





relatively large. Five sample instrument response curves are shown in Fig. 3.13. The frequency is shown along the horizontal axis, the equivalent period (period = 1/frequency) is shown along the top horizontal axis. The vertical axis shows the ground-motion amplification factor.

The broad-band instrument senses most frequencies equally well; the long-period and short-period instruments are called "narrow" band, because they preferentially sense frequencies near 1/(15 s) and 1 Hz respectively.

The left panel of Fig. 3.13 is a comparison of a modern broad-band seismometer response and the classic World-Wide Standard Seismic Network (WWSSN) long- and short-period instruments. The same broad-band response is shown in the right panel, to compare the response with a special short-period instrument, the Wood-Anderson, and an accelerometer. The Wood-Anderson short-period instrument (Fig. 3.14) was the one that Charles Richter used to develop his magnitude scale for southern California. The accelerometer is an instrument designed to record large amplitude and high-frequency shaking near large earthquakes. Those are the vibrations that are important in building, highway, etc. design.

Fig. 3.15 shows the results of different recording instruments on the measurements of ground motion (displacement) near Tucson, Arizona for an earthquake that occurred in Texas, in 1995. The observations were recorded on a broad-band instrument and the signals that would have been recorded on the WWSSN instrument types were simulated using a little mathematics since all the vibrations that would be detected by the long- and short-period seismometers are also recorded by the broad-band seismometer.

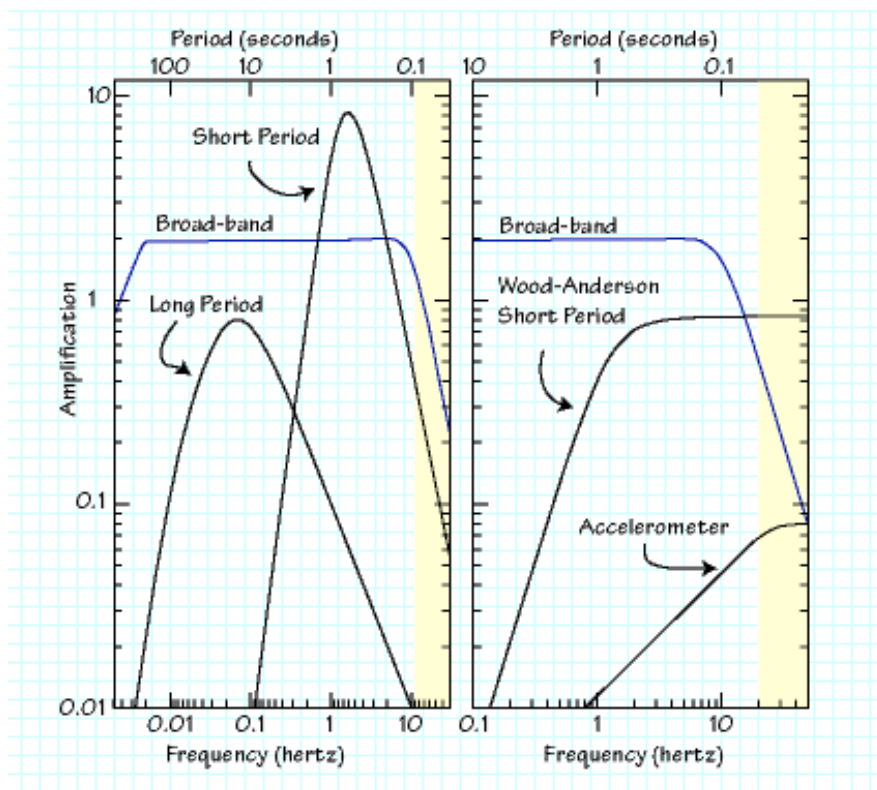


Fig. 3.13 – Amplification curves for different kinds of sensors.

The top panel of Fig. 3.15 shows the vibrations measured using a broad-band seismometer, the middle panel shows the vibrations as they would be detected by the long-period sensor, and the bottom panel the vibrations that would be sensed by a short-period sensor (scaled by a factor of 10 so we can see them better). The displacements are shown in microns, which are  $1 \times 10^{-6}$  metres.

In the force-balance instruments (Fig. 3.16) the displacement of a mass object by an unknown force is sensed using a very high-resolution displacement sensor. The position of the object is then stabilized by applying an equal and opposite force to it. The magnitude of the stabilizing force is easily measured, and is assumed to be equivalent to the unknown force. These systems are critically dependent on the displacement sensor.



Fig. 3.14 - The short-period Wood-Anderson torsion seismometer, showing cover and sensitivity mirror in place (left) and the same without cover, showing damping magnet, lens etc. (right).

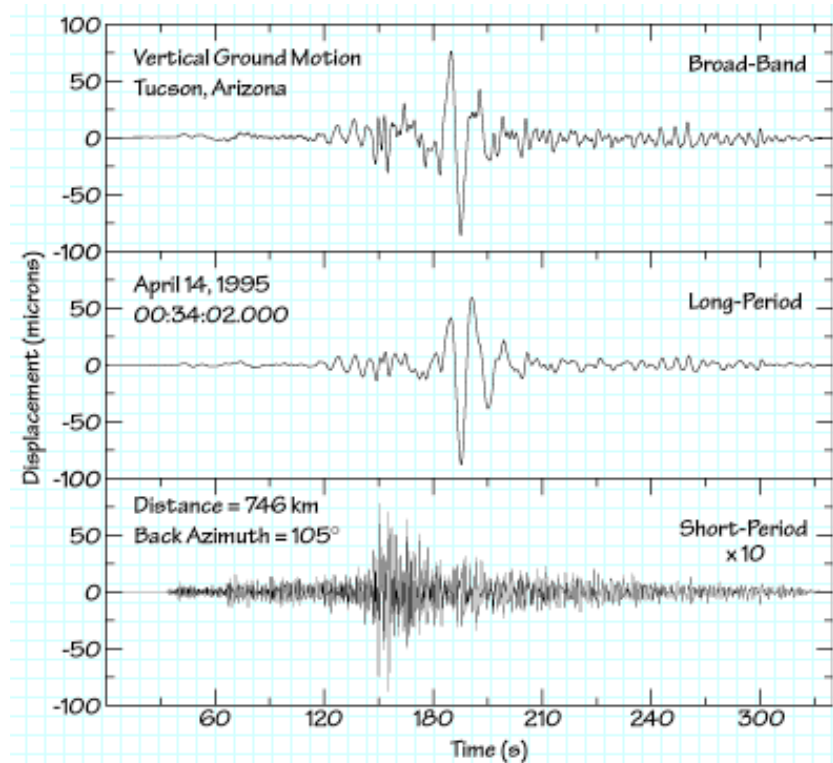


Fig. 3.15 – Recordings of the same event obtained by different seismometers.

Another important class of seismometers was developed for recording large amplitude vibrations that are common within a few tens of kilometres of large earthquakes: these are called strong-motion seismometers. Strong-motion instruments were designed to record the high accelerations that are particularly important for designing buildings and other structures. An example set of accelerations from a large earthquake that occurred near the coast of Mexico in September of 1985 is shown in Fig. 3.17.

The diagram in Fig. 3.17 shows the ground displacement recorded at a strong-motion seismometer that was located directly above the part of a fault that ruptured during the 1985  $M_w$  8.1, Michoacan, Mexico earthquake. The left panel is a plot of the three components of acceleration (one

vertical and two horizontal). From the curve we can see that strong, high-frequency shaking lasted almost a minute in the region. The peak acceleration was about 150 cm/s<sup>2</sup>, or about 0.15 g.

The middle panel shows the velocity of ground movement, which we can calculate using calculus (the velocity is the integral of the acceleration). The peak velocity for this site during that earthquake was about 20-25 cm/s. And if we integrate the velocity, we can compute the displacement, which is shown in the right-most panel. From the displacement plot, we can see that the permanent offsets near the seismometer were up, west, and south, for a total distance of about 125 cm.

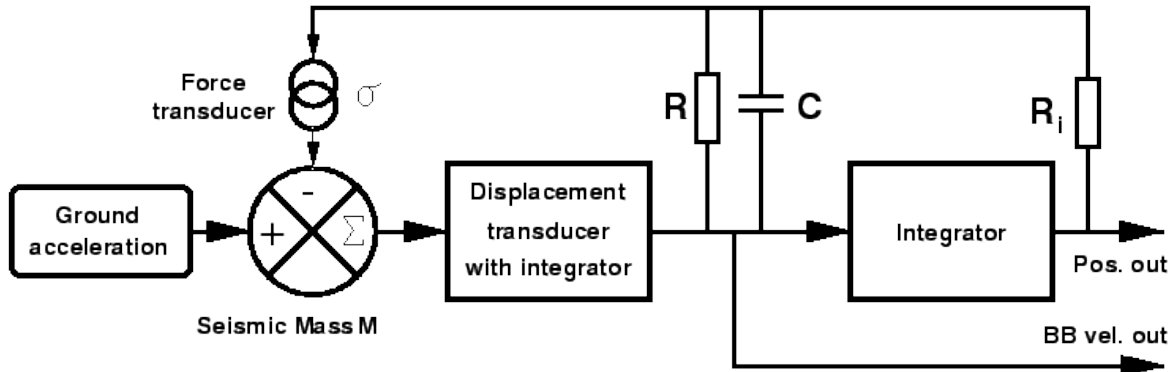


Fig. 3.16 – Scheme of a force-balance instrument.

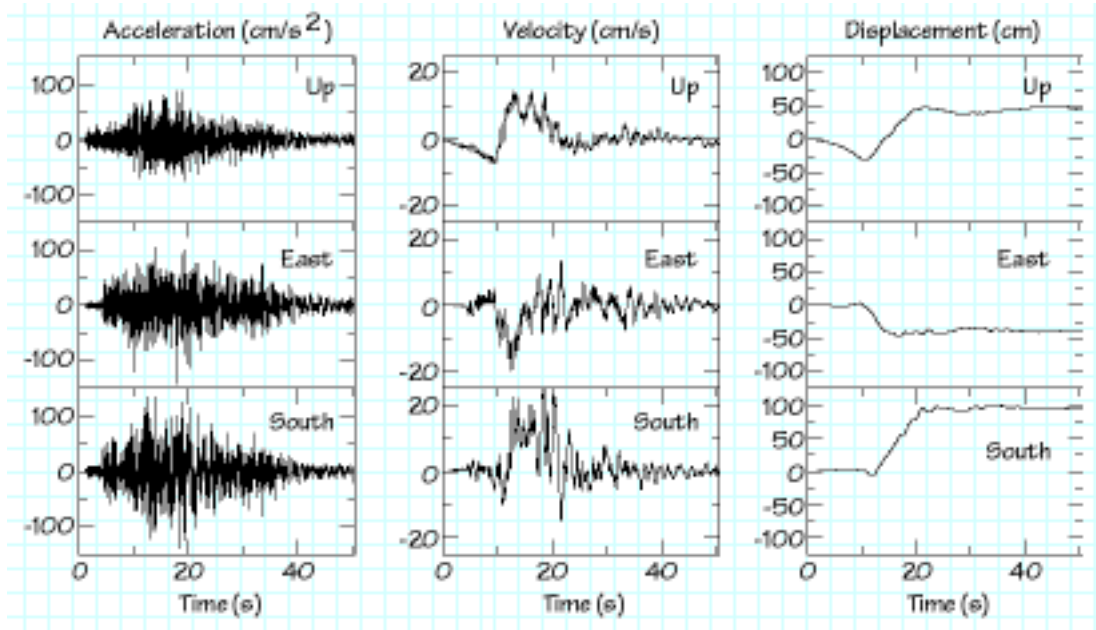


Fig. 3.17 – Integration and double integration of an accelerometer recording.

3.4.1. Theory of the seismograph

The physics behind the sensor is Newton's Law of Inertia: "a body in motion tends to stay in motion unless acted upon by a force, and a body at rest tends to remain at rest unless acted upon by another force."

A seismograph is a pendulum formed by two parts, one, the frame, which moves as the ground motion does, and one, the mass, that remains fixed for the inertia reaction and then it oscillates in a manner different from that of the ground that supports the pendulum. To obtain the ground motion it is necessary to record the relative motion of the mass with respect to the frame.

Let us consider a pendulum (see Fig. 3.18) with one degree of freedom and let us indicate:  $x$  = position of the centre of gravity of the pendulum, referred to a fixed point of origin,



$y$  = position of a specified point of the frame, referred to the same fixed point of origin, so that  $x=y$  in the position of equilibrium,

$K$  = a spring constant, so that the restoring force on the pendulum is:  $-K(x-y)$ ,

$m$  = mass of the pendulum,

$u = x-y$  is the displacement of the pendulum relative to the frame; the deflection on the seismogram will be a measure of  $u$ .

The equation of motion is:

$$m\ddot{x} = -K(x - y). \quad (3-12)$$

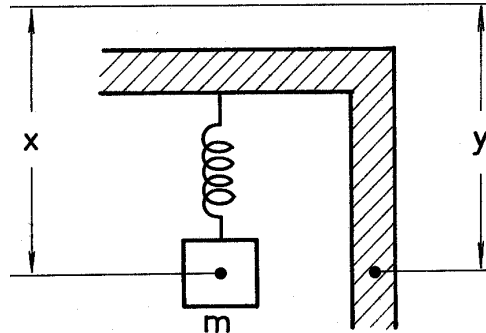


Fig. 3.18 - Scheme of a seismograph.

Introducing  $u$  and setting  $w_1^2 = K/m$ , where  $w_1$  is the pulsation of the pendulum  $w_1 = 2\pi/T_1$  we obtain:

$$\ddot{u} + \omega_1^2 u = -\ddot{y}. \quad (3-13)$$

This relates the seismogram deflection, represented by  $u$ , to the actual ground displacement  $y$ . If the ground is at rest,  $y=0$  and Eq. (3-13) represents a simple harmonic motion; that is:

$$u = B \sin(\omega_1 t + b) \quad (3-14)$$

here  $B$  and  $b$  are constants specifying amplitude and phase.

Now suppose that the ground is in motion, and begin by assuming that this motion is simple harmonic, with its own period  $T_2$ . Put  $w_2 = 2\pi/T_2$  and write:

$$y = A \sin \omega_2 t. \quad (3-15)$$

It is possible, but not necessary, for the pendulum to respond with forced oscillations of period  $T_2$ , in phase or out of phase. To show this, let us substitute the expression for  $y$  from Eq. (3-15) into Eq. (3-13) and the following expression for  $u$ :

$$u = B \sin \omega_2 t. \quad (3-16)$$

Carrying out the differentiations and dividing out common terms, the following condition is found:

$$\frac{B}{A} = \frac{\omega_2^2}{\omega_2^2 - \omega_1^2} \quad (3-17)$$

that is necessary condition to obtain the following general solution:

$$u = B \sin \omega_2 t + C \sin(\omega_1 t + c). \quad (3-18)$$

Eq. (3-16) is a particular case of Eq. (3-18) with  $C=0$ .

$B$  is given by Eq. (3-17) and  $C$  and  $c$  are arbitrary constants specifying the amplitude and phase of a free oscillation called transient superposed on the forced oscillation. A second undesirable feature of the instrumental performance represented by Eq. (3-18) is the fact that  $B$  becomes theoretically infinite when  $\omega_2 = \omega_1$ . This fact is called resonance. The quantity  $B/A$  obtained by Eq. (3-17) can be given also by:

$$\frac{B}{A} = \frac{T_1^2}{T_1^2 - T_2^2} \quad (3-19)$$

and it is called the dynamic magnification.

If  $T_2$  is much smaller than  $T_1$ :  $B/A \approx 1$ , that is, if the pendulum period is much greater than that of the ground oscillation, the instrument becomes a displacement meter. If  $T_2$  is much larger than  $T_1$ :  $B/A \approx -(T_1^2/T_2^2)$  but, since the acceleration is  $4\pi^2(A/T_2^2)$ ,  $B$  is proportional to the acceleration and the instrument becomes an accelerometer. To make satisfactory use of either of these properties it is necessary to diminish the effects of resonance and of the transient free oscillation. This is done by introducing damping, that is a force that opposes the pendulum motion and increases with its velocity.

Fig. 3.19 shows how the harmonic magnification factor becomes indeterminable for undamped pendulums when recording earthquake waves having periods near the pendulum period. The magnitude of a damping force may be measured in terms of a damping ratio or in terms of a fractional part of the critical damping:  $h$ . If the mass is moved 10 mm from the zero position and, on returning, it overswings the zero position by 1 mm, the damping ratio is 10:1. Damping is critical when it is just sufficient to prevent the pendulum from overswinging the zero position: under this condition  $h=1$ . When  $h$  is greater than this a pendulum is overdamped; underdamping is preferable as it increases rather than decreases the mass motion.

So introducing damping into Eq. (3-12) we obtain:

$$m\ddot{x} = -K(x - y) - Q(\dot{x} - \dot{y}). \quad (3-20)$$

Setting:  $u=x-y$ ,  $\omega_1^2=K/m$ , and  $Q=2hm\omega_1$ , where  $h$  is a new instrumental constant, we obtain:

$$\ddot{u} + 2h\omega_1\dot{u} + \omega_1^2 u = -\ddot{y} \quad (3-21)$$

The free motion of the pendulum ( $\ddot{y}=0$ ) is no longer a simple harmonic motion and a complete solution is:

$$u = Be^{-h\omega_1 t} \sin(j\omega_1 t + b) \quad (3-22)$$

in which  $j$  is defined so that:

$$h^2 + j^2 = 1. \quad (3-23)$$

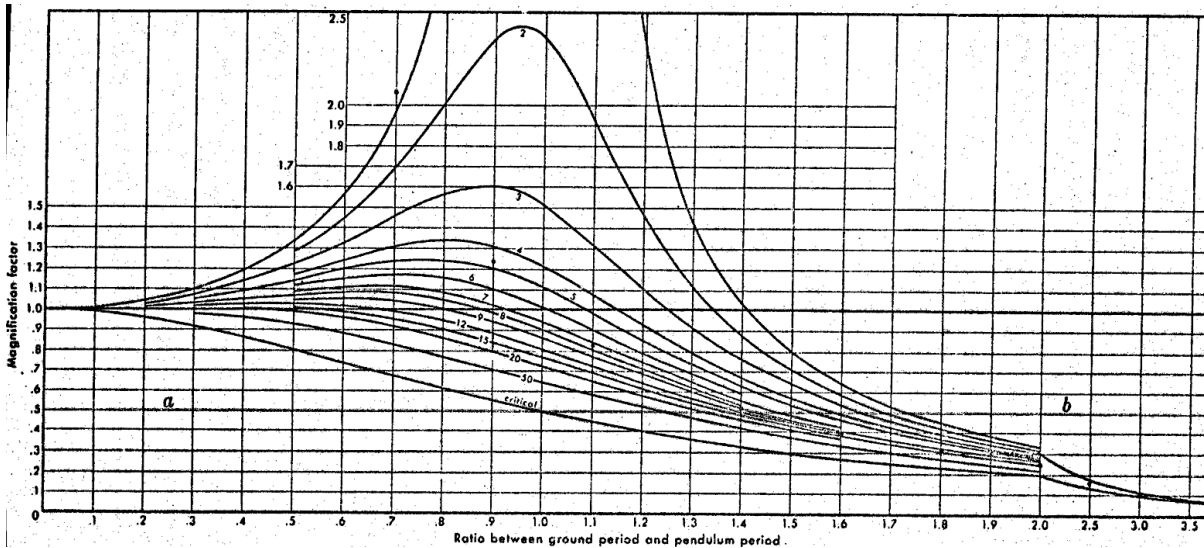


Fig. 3.19 - Magnification curves for direct-recording pendulums with varying damping ratios.

If  $h < 1$ , Eq. (3-22) represents a damped harmonic oscillation, if  $h > 1$  the pendulum is overdamped and there is no oscillation, if  $h = 1$  the damping is critical.

Now suppose that the ground is in motion ( $y = A \sin \omega_2 t$ ). It is not possible to obtain a solution  $u = B \sin \omega_2 t$  as we have obtained for  $h = 0$ . We have to include a phase difference between the ground and the pendulum, so that:

$$u = B \sin(\omega_2 t + b) = B(\sin \omega_2 t \cos b + \cos \omega_2 t \sin b). \tag{3-24}$$

If we substitute Eq. (3-24) into Eq. (3-21), put  $y = A \sin \omega_2 t$  and carry out the differentiations we obtain the two conditions:

$$\left(\frac{A}{B}\right)^2 = \left(1 - \frac{\omega_1^2}{\omega_2^2}\right)^2 + \frac{4h^2 \omega_1^2}{\omega_2^2} \tag{3-25}$$

$$\tan b = \frac{2h\omega_1\omega_2}{\omega_2^2 - \omega_1^2}. \tag{3-26}$$

The complete solution of Eq. (3-21) for  $y = A \sin \omega_2 t$  is:

$$u = B \sin(\omega_2 t + b) + Ce^{-h\omega_1 t} \sin(j\omega_1 t + c) \tag{3-27}$$

where  $B$  and  $b$  are calculated from Eqs. (3-25) and (3-26),  $C$  and  $c$  are arbitrary constants and  $j$  is given by Eq. (3-23). The unwanted oscillation with coefficient  $C$  falls off exponentially and the resonance also disappears; if in Eq. (3-25) we put  $T_1 = T_2$  we find  $B/A = 1/(2h)$  which is not seriously exaggerated.

### 3.4.2. Characteristics of the seismographs

The pendulum that operates as a seismometer must have its own period rather long. This can be obtained in different ways. A solution is to make the pendulum support nearly, but not quite, vertical, so that the pendulum lies nearly horizontal but can swing slowly like a farmyard gate about the position of equilibrium. If in the undisturbed position the pendulum rod points to the north, it will be twisted about the support by a displacement of the ground to the east or west. This principle is the basis of the Milne-Shaw, Mainka, and Galitzin seismographs. Another solution is obtained using a

small cylinder, with its axis vertical, attached along a generator to a fine vertical wire; it will have a natural position of equilibrium maintained by the torsional rigidity of the wire. Conversely, a motion of the wire, if sufficiently sudden, gives a twist. The wire is mounted in a frame attached to the ground. This principle is used in the Wood-Anderson and Nikiforov instruments and, in a different form, in that of Benioff. In the Wiechert instrument a heavy mass is supported on a stiff spring, clamped at its lower end, and it is kept stable by springs on four sides (Fig. 3.20). In this case a single instrument is sensitive to displacements in both horizontal components.

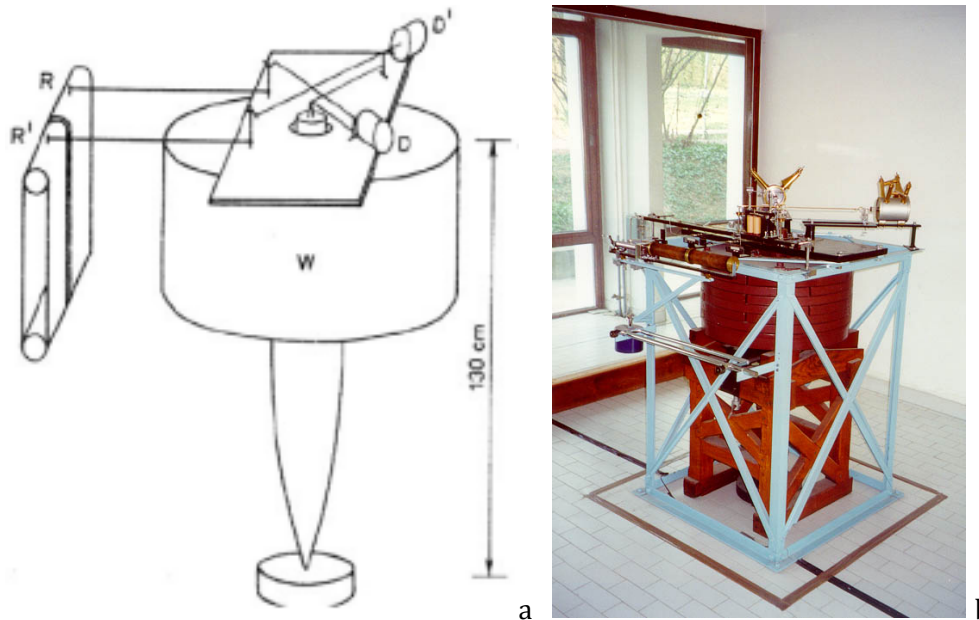


Fig. 3.20 - The Wiechert seismograph: a) the mass horizontal motion is captured by two arms that, by using a system of levers, can amplify the motion and record it on two rotating drums (R), the seismograph can record horizontal motions in E-W and N-S directions at the same time; b) the Wiechert seismograph of Zagreb.

Seismographs are divided into two main classes as follows.

- 1) Direct recorders record the motion of the pendulum directly on the recording paper through a simple mechanical or optical lever system. The mechanical system can be a pen scratching smoked paper, a pen writing with ink on paper or a thermic pen writing on special paper. An optical lever is obtained by the reflection of a light ray on a mirror turning according to the movement of the pendulum. In fact the relative movement between the mass and the frame determines a movement of a magnet; inside the poles of the magnet a piece of iron, connected to a mirror, moves following the variations of the magnetic field. This type of seismograph is called Alfani.
- 2) Electrical recorders measure the motion indirectly by generating an electrical current into a coil of wire fixed to the mass that moves between the poles of a strong permanent magnet (see Fig. 3.21). The current thus generated is proportional to the velocity of the relative motion between pendulum and ground, because if we have a relative movement between the coil and the magnet we obtain an induced electromotive force according to the Faraday's law:

$$E = - \frac{d(N\Phi)}{dt} \quad (3-28)$$

where  $N$  is the number of turns and  $F$  is the magnetic flux across the coil. Setting  $F=Blx$  where  $B$  is the magnetic field and  $lx$  is the area of the coil we obtain:

$$E = - \frac{d(NBlx)}{dt} = -NBl \frac{dx}{dt} = -NBlv \quad (3-29)$$



where  $v$  is the velocity of the relative movement.

The current induced in the circuit is:

$$i = \frac{NBlv}{R} \quad (3-30)$$

where  $R$  is the resistance of the circuit.

The current can move a pen and so it is possible to record on paper or the signal can be sent to a magnetic tape recorder, to a computer, or the intensity of the current can be detected by a mirror galvanometer reflecting a light ray that is recorded on photographic paper. The galvanometer has oscillatory characteristics of its own that can control the entire character of the seismographic record. The recording can be continuous during the time or it can start when the seismic signal exceeds a fixed value. In this case a codified timing is needed. The recording on magnetic tapes may be analogic or digital also compatible for automatic processing. An analogic recording is called seismogram.

On the recordings it is very important to have a great accuracy in timing which is generally obtained from a quartz clock with an average error of some milliseconds per day. The error is daily corrected comparing the clock with a radio signal on a stroboscope. Modern stations record and transmit the timing received by GPS signal.

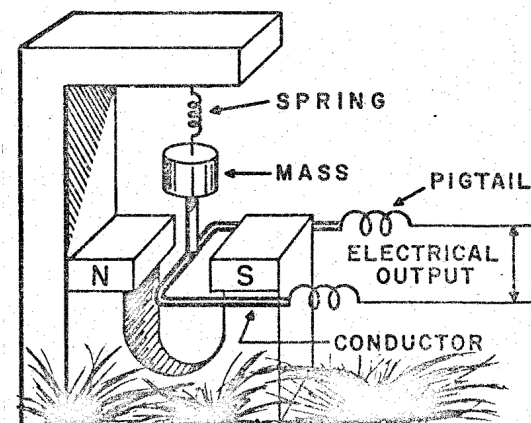


Fig. 3.21 - Scheme of an electrical seismometer.

The range of the seismograph pendulum periods goes from 0.1 s to 20 s, according to the different types of waves that one wants to detect. The stations belonging to the WWSSN, installed by the USGS in the early 1960s for monitoring both earthquakes and nuclear testing, have in operation short-period pendulums of 1 s and long-period pendulums of 15 s. The magnification depends upon the stability of the sites and it is variable from about 10,000 to 400,000 for short period seismographs and from about 500 to 6,000 for long period instruments.

### 3.5. Interpretation of seismograms

We have seen that the seismographs record the earthquakes, but if their magnification is very high they record also a lot a disturbances caused by different sources (see Table 3.1).

The most usual are the microseisms, that are not small earthquakes but continuous disturbances in the ground. Most of them appear to be connected with weather, and the smaller amplitudes are generally associated with periods of approximately 0.1 second and over (see Fig. 3.22a), largely local in character, the largest ones are associated with microseisms of 4-7 seconds period which may travel thousands of kilometres from their sources over either continental or oceanic paths (see Fig. 3.22b).

These disturbances make sometimes hard the seismogram interpretation, which consists in the reading of arrival times of some phases and in their identification to obtain the epicentral distance, the direction and the origin time of the earthquake. The beginning time of an activity may be measured to the nearest second or tenth of a second, or even more, depending upon the sharpness of the onset and the type of recording. In regional investigations with seismographs employing 60 mm/min paper speeds, important impulsive phases were read to the nearest 0.1 second; if the measured times of the first impulse on two components differ by 1 or 2 seconds the earliest arrival time was used. The onsets of surface waves were often so questionable that it may be sufficient to record them to the nearest minute. The arrivals of compressional waves are well recorded by the vertical component of the seismographs, the arrivals of transverse waves by the horizontal component perpendicular to the epicentral direction. In some seismological bulletins Lq and Lr waves are not reported but the group of surface waves is divided into L and M waves, where L are generally long period waves and M is the group of waves with maximum amplitude.

Table 3.1 - Earth disturbances recorded by seismographs.

<b>A. Continuous disturbances</b>
<b>1. Artificial</b>
Traffic
Machinery
<b>2. Natural (microseisms)</b>
Meteorological: storms, wind, frost
Water in motion: surf, streams, waterfalls
Volcanic tremor
<b>B. Single disturbances</b>
<b>1. Artificial (chiefly explosions)</b>
Blasting: quarry or road work, geophysical exploration
Explosives tests
Demolitions
Bombing and bomb tests
Gunfire
Accidental large detonations
<b>2. Natural (including earthquakes)</b>
<b>I. Minor causes</b>
Collapse of caves
Large slides and slumps
Rockbursts in mines
Meteorites
<b>II. Volcanic shocks</b>
Superficial, explosive
Magmatic or eruptive
<b>III. Tectonic shocks</b>
Shallow or normal (depths not over 60 kilometers)
Intermediate (depths 70 to 300 kilometers)
Deep (depths 300 to 720 kilometers)

Sometimes the analysis is rather hard because of poor signals on the seismograms or because of an overload recording. In this case the seismologist may be helped by information received from press agencies or, if the earthquake is local, directly from people who felt the shock. Modern technologies

facilitate notably the seismogram readings and following processing because the seismic traces are plotted on the computer screen, signal zooming is possible, and the phase picking is both automatic and manual.

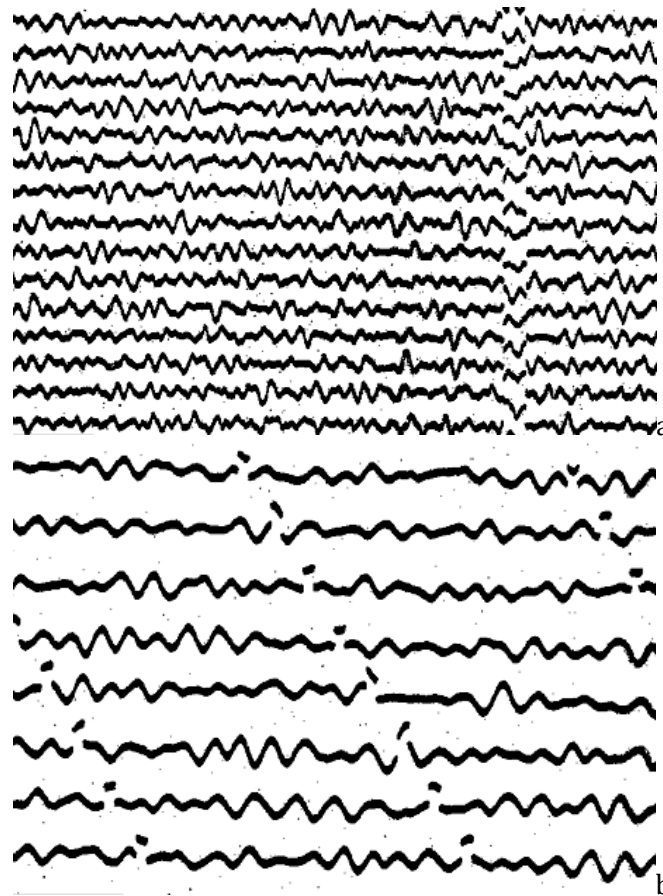


Fig. 3.22 - Microseisms recorded in Trieste: a) on a vertical Benioff seismometer; b) on a N-S Ewing-Press seismometer.

The seismologist may control his interpretations using the determination of the hypocentres made by organisations that collect the data from all the stations in the world. The most famous organisations are; the USGS (<http://quake.usgs.gov>), the Centre Seismologique Europeo-Mediterraneen (<http://www.emsc-csem.org>), and the International Seismological Centre (<http://www.isc.ac.uk/>).

### 3.5.1. Locating earthquakes

There are two main procedures for locating earthquakes: the first is the graphical one and was used when computers and seismometric networks did not exist, the second is based on the use of a computer software.

Both procedures, of course, are based on the readings of the P- and S-waves arrival times obtained from the seismograms of one or more stations

#### 3.5.1.1. The graphical procedure

This procedure can be used having available the data of one single station or several ones. To obtain the epicentral distance it is sufficient to read accurately the arrival times of P and S waves and report them on a travel-time table. But it is not always so easy to identify the S-wave on a seismogram so a good advise is to read all the sharp impulses recorded and also the arrival times of the surface

waves. Reporting all these phases on a travel-time table, it will not be very hard to obtain a solution, also if it is clear that many of the phases read will be neither principal nor dependent phases and some will have a delay according to the theoretical curves. The origin time is also obtained directly from the travel-time table. If the arrival times read on the seismograms are reported on a strip of paper, moving it horizontally on the travel-time table, we obtain the position that fits best the velocities curves: on the y-axis we may read the epicentral distance and on the strip for travel-time equal to zero we have the origin time.

The direction of ground motion of the arrival of the first impulsive longitudinal wave will be away from the hypocentre if it is compressional and towards the hypocentre if it is rarefactional. By measuring the amplitudes of the first N-S and E-W impulses (exactly at the arrival time of the first motion on the vertical component) and knowing the directional constants of the pendulums, the direction of the resultant motion can be determined by a simple vector analysis: if we have, for example, on the seismograms, a direction NE with a dilatation on the vertical component, we know that the movement of the ground is directed SW with a compressional phase of the first longitudinal arrival; this is the ray away from the hypocentre, that will be to NE. So, if on the seismogram of the vertical component we have a dilatation of the first impulse, the vector obtained is towards the focus, if we have a compression the vector is away from the focus.

With distance and azimuth, it is possible to identify on a map the epicentre of the quake. The weakest point of this procedure is the determination of the azimuth because little uncertainties in measures of the first motion amplitudes can lead to large differences on the map. If the quake is not very strong it is possible to determinate only the distance and so it is necessary to have data from three stations at least to obtain the epicentre by drawing circles with the corresponding stations at the centre. Naturally before making this it is necessary to control all the interpretations using the origin time determined best.

### 3.5.1.2. The automatic procedure

We want to find the location, depth and origin time of an earthquake whose waves arrive at the times measured on each seismograms. We want a straightforward and general procedure that we can also program in a computer. The procedure is simple to state: guess a location, depth and origin time; compare the predicted arrival times of the wave from your guessed location with the observed times at each station; then move the location a little in the direction that reduces the difference between the observed and calculated times. Then repeat this procedure, each time getting closer to the actual earthquake location and fitting the observed times a little better. Quit when your adjustments have become small enough and when the fit to the observed wave arrival times is close enough. You can try to fit an earthquake location on the map just to see how the procedure goes. Note that the earthquake arrives first on station C, thus C is a good first guess for the location. If the majority of quakes in the study region are crustal, the trial hypocentral depth can be set as the half of the crust thickness in the region. The origin time should be a few seconds before the time of the wave at the first station. Let us guess an origin time of 10 seconds, measured on the same clock that made the time scale at the bottom of the figure and timed the seismograms.

Mathematically, the problem is solved by setting up a system of linear equations, one for each station. The equations express the difference between the observed arrival times and those calculated from the previous (or initial) hypocentre, in terms of small steps in the 3 hypocentral coordinates and the origin time. We must also have a mathematical model of the crustal velocities (in km/s) under the seismic network to calculate the travel times of waves from an earthquake at a given depth to a station at a given distance. The system of linear equations is solved by the method of least squares which minimizes the sum of the squares of the differences between the observed and calculated arrival times. The process begins with an initial guessed hypocentre, performs several hypocentral adjustments each found by a least squares solution to the equations, and iterates to a hypocentre that best fits the observed set of wave arrival times at the stations of the seismic network.



### 3.5.1.3. Software for earthquake location

A long series of computer codes were developed during the years at U.S.G.S. since 1969, when Eaton (1969) wrote and disseminated HYPOLAR, the first public domain software for earthquake location. Some years after HYPOLAR, Lee and Lahr (1972) presented HYPO71, whose revised version (Lee and Lahr, 1975) is still in use for the management of seismic networks. HYPOINVERSE by Klein (1978, 2002) and HYPOELLIPSE by Lahr (1979, 1999) followed with interesting improvements with respect to HYPO71. The original version of those programs were written to run on powerful (for that time) mainframes, later most of them were modified for PCs.

HYPO71 (Lee and Lahr, 1972, 1975; Lee and Valdes, 1985) is a computer program for determining hypocentre, magnitude, and first motion pattern of local earthquakes. It is perhaps the first earthquake location program that achieved worldwide usage, as evidenced by the fact that about 1,000 copies of the HYPO71 manual were requested and distributed. Although Geiger (1912) introduced an earthquake location procedure based on the least squares in 1910, it was not a practical procedure until digital computers become common in the 1960s when Eaton (1969) wrote HYPOLAR.

HYPOINVERSE (Klein, 1978, 2002) is a computer program that processes files of seismic station data for an earthquake (like P wave arrival times and seismogram amplitudes and durations) into earthquake locations and magnitudes. It locates any number of events in an input file, which can be in one of several different formats. Any or all of printout, summary or archive output may be produced. HYPOINVERSE is driven by user commands, that define input and output files, set adjustable parameters, and solve for locations of a file of earthquake data using the parameters and files currently set. It is both interactive and "batch" in that commands may be executed either from the keyboard or from a file.

HYPOELLIPSE (Lahr, 1979, 1999) is a computer program for determining the hypocenters of local or near regional earthquakes and for each event the ellipsoid that encloses the 68% confidence volume. Travel times are determined from a horizontally-layered velocity-structure, from a linear increase of velocity with depth, from a linear increase of velocity over a halfspace, or from a previously generated travel-time table. With the travel-time-table option, gradients are allowed in all layers, but there can be no velocity discontinuities.

## 3.6. Magnitude

The idea of an earthquake magnitude scale based purely on instrumental records arose out of the great discrepancy that sometimes exists between the amount of popular excitement caused by an earthquake and its actual character as indicated by seismograms.

The magnitude is a number characteristic of the earthquake depending on the release of energy at the focus and independent of the location of the recording station. This concept was introduced for the first time by Richter in 1935. The term magnitude was selected by analogy with the corresponding usage in astronomy: earthquake magnitude corresponds logically to absolute stellar magnitude, apparent star magnitude corresponds to earthquake-intensity.

The concept of magnitude was introduced by Richter (1935), who recognized that the seismic waves radiated by all earthquakes can provide good estimates of their magnitudes. He collected the recordings of seismic waves from a large number of earthquakes, and developed a calibrated system of measuring them for magnitude. Richter showed that, the larger the intrinsic energy of the earthquake, the larger the amplitude of ground motion at a given distance. He calibrated his scale of magnitudes using measured maximum amplitudes of shear waves on seismometers particularly sensitive to shear waves with periods of about one second. More precisely, the records had to be obtained from a specific kind of instrument, called Wood-Anderson seismograph ( $T_0=0.8$  s, dynamic magnification = 2800,  $h = 0.8$ ). Although his work was originally calibrated only for these specific seismometers, and only for earthquakes in southern California, seismologists have developed scale factors to extend Richter's magnitude scale to many other types of measurements on all types of seismometers, all over the world. In fact, magnitude estimates have been made for thousands of Moon-quakes and for two quakes on Mars.

The diagram in Fig. 3.23 demonstrates how to use Richter's original method to measure a seismogram for a magnitude estimate in southern California: the scales in the diagram form a nomogram that allows us to do the mathematical computation quickly by eye.

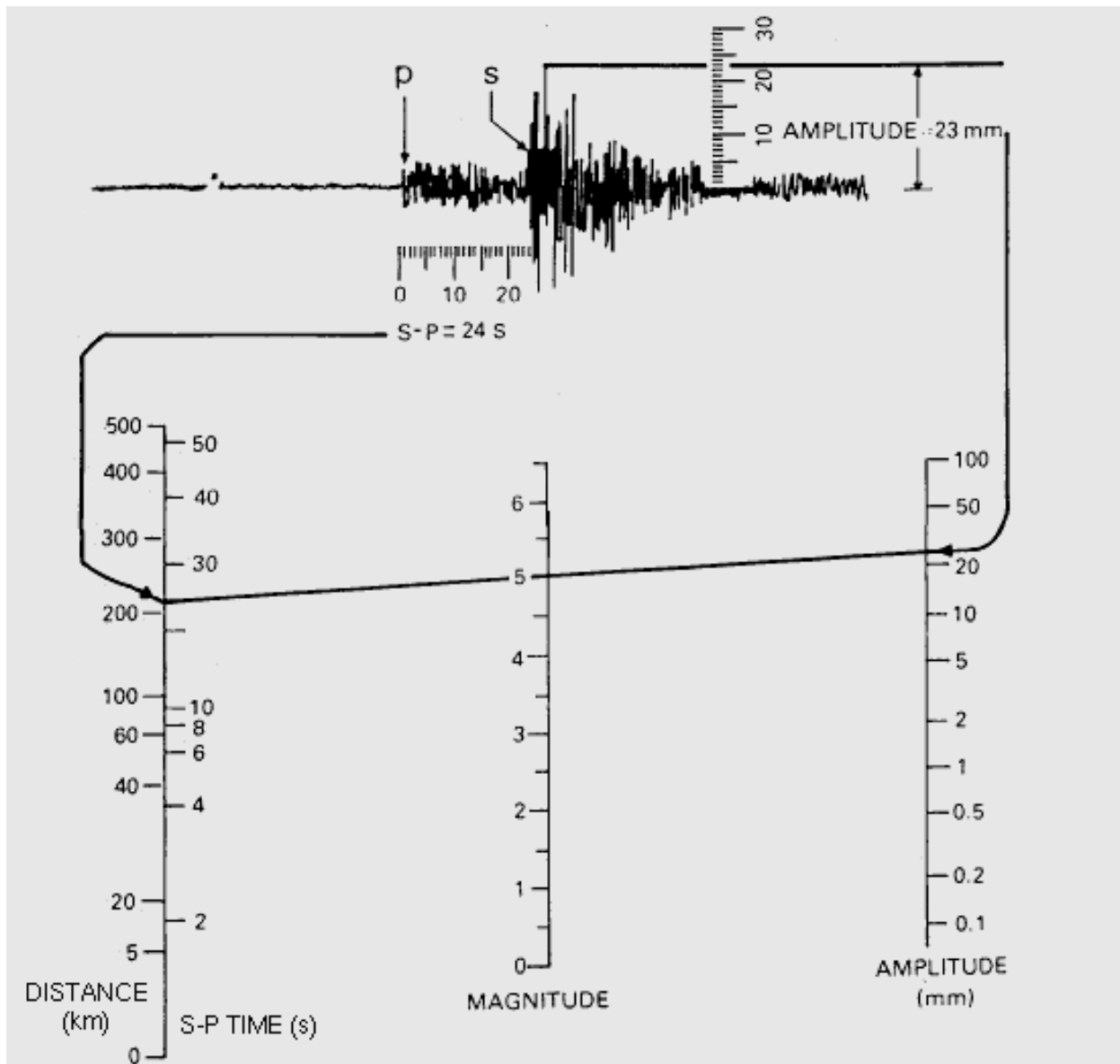


Fig. 3.23 - Nomogram for the graphical determination of the earthquake local magnitude.

The formulation of the local magnitude is the following: the magnitude of any shock is taken as the logarithm of the maximum trace amplitude with which the standard torsion seismometer would register that shock at an epicentral distance of 100 km:

$$M_L = \log A - \log A_0 \quad (3-32)$$

where  $A$  is the maximum trace amplitude in millimetres measured directly from the photographic paper record of the Wood-Anderson seismometer, and  $A_0$  is the amplitude in millimetres with which the standard seismograph should register an earthquake of magnitude zero.

$A_0$  is less than 1 and its logarithm is negative, their values were tabulated versus distance (shorter than 600 km) for shallow earthquakes by Richter (1935) for California and by Finetti and Morelli (1972) for the Trieste station (see Table 3.2).

Table 3.2 - Logarithms of the amplitudes  $A_0$  (in mm) with which a standard torsion seismometer should record an earthquake of magnitude zero (Finetti and Morelli, 1972).

$\Delta$ km	$-\log A_0$	$\Delta$ km	$-\log A_0$	$\Delta$ km	$-\log A_0$
0	1.4	160	3.3	410	4.5
5	1.4	170	3.4	420	4.5
10	1.5	180	3.4	430	4.6
15	1.6	190	3.5	440	4.6
20	1.7	200	3.5	450	4.6
25	1.9	210	3.6	460	4.6
30	2.1	220	3.65	470	4.7
35	2.3	230	3.7	480	4.7
40	2.4	240	3.7	490	4.7
45	2.5	250	3.8	500	4.7
50	2.6	260	3.8	510	4.8
55	2.7	270	3.9	520	4.8
60	2.8	280	3.9	530	4.8
65	2.8	290	4.0	540	4.8
70	2.8	300	4.0	550	4.8
80	2.9	310	4.1	560	4.9
85	2.9	320	4.1	570	4.9
90	3.0	330	4.2	580	4.9
95	3.0	340	4.2	590	4.9
100	3.0	350	4.3	600	4.9
110	3.1	360	4.3	700	5.1
120	3.1	370	4.3	800	5.3
130	3.2	380	4.4	900	5.5
140	3.2	390	4.4	1000	5.7
150	3.3	400	4.5		

This method can be used only for earthquakes distant not more than 600 km (Richter, 1935) or 1000 km (Finetti and Morelli, 1972) from the recording station. For applying the formula it is necessary to know the epicentral distance, but small errors in distance effect only slightly the magnitude determination. It is very important to control the magnitude determinations using data from other stations to see if it is necessary to introduce into Eq. (3.29) a station correction.

Seismologists will try to get a separate magnitude estimate from every seismograph station that records the earthquake, and then average them. This accounts for the usual spread of around 0.2 magnitude units that you see reported from different seismological laboratories right after an earthquake. Each laboratory is averaging in different stations that they have access to. It may be several days before different organizations will come to a consensus on what was the best magnitude estimate.

With the availability of broad-band instruments, the photographic Wood-Anderson recordings were dismissed and the computation of the local magnitude is performed simulating the Wood-Anderson recordings by filtering properly the broad-band records.

There are many different ways to calculate the magnitude of a quake according to which type of wave and which kind of seismometer is used. The most utilized magnitudes in the 20<sup>th</sup> century were the following:

- 1) original magnitude for local shocks obtained using the standard Wood-Anderson torsion seismometer indicated as  $M_L$ , or  $MAW$  according to the Karnik nomenclature (circular of 1976);
- 2) magnitude from body waves obtained using short or long period instruments, for epicentral distance greater than 1800 km, called  $m_B$  if it is derived from the long period recording and  $m_b$  if derived from the short period one, respectively  $MPV$  and  $M$  according to the Karnik nomenclature (circular of 1976);
- 3) magnitude from surface waves recorded by long period seismometers, for epicentral distance greater than 2200 km, indicated as  $M_S$ , or  $MLH$  according to the Karnik nomenclature (circular of 1976).

There is also a magnitude calculated from the duration of the recording of a local shock: the equation has to be derived empirically by comparison with actual  $M_L$  estimates. Duration magnitude is indicated with  $M_D$  and the general relation has the form:

$$M_D = a + b \log \tau + c \Delta \quad (3-31)$$

where  $\tau$  is the duration of the signal, computed from the P-wave arrival to the moment when the earthquake wave amplitude has the same amplitude as the background noise,  $\Delta$  is the epicentral distance and  $a$ ,  $b$ , and  $c$  are parameters calculated by regression analysis. In practice,  $c$  is very small indicating a slight dependence of  $M_D$  on distance.

To determinate the magnitude from body waves (Fig. 3.24) it is possible to use P, PP or S waves recorded by vertical or horizontal, short or long period seismographs. The most common determination is obtained from P waves recorded by vertical short or long period instrument. The general formula recommended from the IASPEI's Committee of Zurich 1967 is the following, given by Gutenberg (1945):

$$m = \log \left( \frac{A}{T} \right)_{\max} + Q + \varepsilon \quad (3-32)$$

where  $A$  is the maximum true amplitude and  $T$  the period of the used wave,  $Q$  is the Gutenberg-Richter's correction value for hypocentral depth and distance (see Table 3.3) and  $\varepsilon$  is the station correction obtained by statistical analysis of the resulting systematic divergences. The station correction is not a constant but it is variable with the wave used and the focal depth.

For magnitudes lesser than about 4.8 in the case of earthquakes with long epicentral distances, it is often hard to read with reliable accuracy the body waves trace amplitude. In this case it is better to determine the magnitude from surface waves.

The magnitude from surface waves (Fig. 3.24) can also be computed using different waves and vertical or horizontal components. The most common is the one computed with the waves of maximum amplitude having period from 10 to 30 seconds. The magnitude expression, given by Karnik et al. (1962) is:

$$M = \log \left( \frac{A}{T} \right)_{\max} + 1.66 \log d + 3.3 \quad (3-33)$$

where  $A$  is the maximum true amplitude of the wave used, computed as the square root of the sum of the squares of the two horizontal components,  $T$  is the period and  $d$  is the epicentral distance in degrees. Magnitude determination curves can be plotted on bilogarithmic paper, so it is possible to get immediately the magnitude knowing the true ground motion, the period and the epicentral distance (see Fig. 3.25).

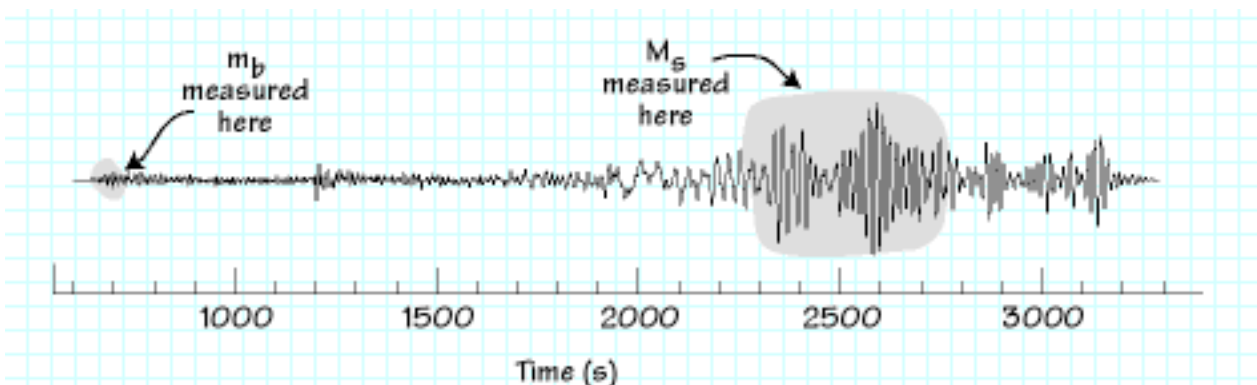


Fig. 3.24 – Scheme of the waves used for magnitude computation.

Table 3.3 - Values of 10 Q for shallow shocks (Gutenberg and Richter, 1956).

Δ	PZ	PH	PPZ	PPH	SH	Δ	PZ	PH	PPZ	PPH	SH	Δ	PZ	PH	PPZ	PPH	SH
16	59	60			72	56	68	71	69	70	66	96	73	76	72	74	71
17	59	60			68	57	68	71	69	70	66	97	74	78	72	74	72
18	59	60			62	58	68	71	70	71	66	98	75	78	72	74	73
19	60	61			58	59	68	71	70	72	66	99	75	78	72	74	73
20	60	61			58	60	68	71	71	73	66	100	74	77	72	74	74
21	61	62			60	61	69	72	72	74	67	101	73	76	72	74	74
22	62	63			62	62	70	73	73	74	67	102	74	77	72	74	74
23	63	64			62	63	69	73	73	74	67	103	75	79	72	74	73
24	63	65			62	64	70	73	73	75	68	104	76	79	73	75	73
25	65	66			62	65	70	74	73	75	69	105	77	81	73	75	72
26	64	66			62	66	70	74	73	74	69	106	78	82	74	76	72
27	65	67			63	67	70	74	72	74	69	107	79	83	74	76	72
28	66	67			63	68	70	74	71	73	69	108	79	83	74	76	72
29	66	67			63	69	70	74	70	72	69	109	80	84	74	76	72
30	66	68	67	68	63	70	69	73	70	72	69	110	81	85	74	76	72
31	67	69	67	68	63	71	69	73	71	73	70	112	82	86	74	76	
32	67	69	68	69	64	72	69	73	71	73	70	114	86	90	75	77	
33	67	69	68	69	64	73	69	72	71	73	69	116	88		75	77	
34	67	69	68	69	65	74	68	71	70	72	68	118	90		75	77	
35	67	69	68	69	66	75	68	71	69	71	68	120			75	77	
36	66	68	67	68	66	76	69	72	69	71	68	122			74	76	
37	65	67	67	68	66	77	69	72	69	71	68	124			73	75	
38	65	67	67	68	66	78	69	73	69	71	69	126			72	74	
39	64	66	66	67	67	79	68	72	69	71	68	128			71	74	
40	64	66	66	67	67	80	67	71	69	71	67	130			70	73	
41	65	67	65	66	66	81	68	72	70	72	68	132			70	73	
42	65	67	65	66	65	82	69	72	71	73	69	134			69	72	
43	65	67	66	67	65	83	70	74	72	74	69	136			69	72	
44	65	67	67	68	65	84	70	74	73	75	69	138			70	73	
45	67	69	67	68	65	85	70	74	73	75	68	140			71	74	
46	68	71	67	68	66	86	69	73	73	75	67	142			71	74	
47	69	72	67	68	66	87	70	73	72	74	68	144			70	73	
48	69	72	67	68	67	88	71	75	72	74	68	146			69	72	
49	68	71	67	68	67	89	70	74	72	74	68	148			69	72	
50	67	70	67	68	66	90	70	73	72	74	68	150			69	72	
51	67	70	67	68	65	91	71	75	72	74	69	152			69	72	
52	67	70	67	68	65	92	71	74	72	74	69	154			69	72	
53	67	70	67	68	66	93	72	75	72	74	69	156			69	72	
54	68	71	68	69	66	94	71	74	72	74	70	158			69	72	
55	68	71	69	70	66	95	72	76	72	74	70	160			69	72	
												170			69	72	

For earthquakes with a deep focus the determination of magnitude from body waves is preferred, but it is possible to calculate the magnitude also from surface waves introducing a statistical correction.

There is a relationship between  $m_b$  and  $M_s$  for shallow earthquakes and the conversion formula recommended by IASPEI's Committee is the following:

$$m_b = 0.56M_s + 2.90. \tag{3-34}$$

The two values agree at  $m = M = 6.6$ ; above this  $M > m$ , below it  $M < m$ .



Kanamori (1977) developed a standard magnitude scale that is completely independent of the type of instrument. It is called the moment magnitude, indicated with  $M$  or  $M_w$ , and it comes from the seismic moment  $M_0$  (see chapter 3.7).

There is a standard way to convert a seismic moment to a magnitude (Hanks and Kanamori, 1979). The equation is:

$$M_w = \frac{\log M_0}{1.5} - 10.7 \tag{3-35}$$

with  $M_0$  in dyne-cm. This  $M_w$  is uniformly valid with respect to  $3 \leq M_L \leq 7$ , and  $5 \leq M_S \leq 7.5$ .

Fig. 3.26 shows a relative comparison of moment magnitude with some other magnitude scales. It is important to note how the different magnitude scales saturate, or stop increasing with increasing earthquake size or moment. This occurs because each magnitude scale, aside from moment magnitude, is determined using a seismic wave of a particular period and wavelength. Seismic waves, whose wavelengths are much smaller than the earthquake source, do not increase in amplitude as the earthquake source size, moment, and energy release increase. Thus  $m_b$ , which uses P waves of about one second period and less than 10 km wavelength cannot really reflect the energy release or deformation from faults whose rupture dimension is tens of kilometres or greater.  $m_b$  saturates at about magnitude 6.5. Similarly  $M_S$ , which uses surface waves of about 20 seconds period and 80 km wavelength, cannot really reflect the energy release or deformation from faults whose rupture dimension is many hundreds of km long.  $M_S$  saturates at about magnitude 8.5. Except for  $M_S$  less than about magnitude 5.5, all the magnitude scales approach, and become approximately equal to, moment magnitude below their respective saturation points. Saturation explains the observation that earthquakes of obviously different sizes and energy releases often have the same magnitude. The 1906 San Francisco earthquake and the 1960 Chile earthquake both have estimated surface wave magnitudes of about 8.3. Yet, while the 1906 earthquake rupture was confined to a long, narrow fault segment believed to be about 5800 km<sup>2</sup> in area, the 1960 earthquake, the largest in the 20<sup>th</sup> century, was associated with a fault rupture some 35 times greater in area, equivalent in size to about one half of the whole state of California. When the moment magnitude is computed, it turns out that the 1906 earthquake is "only" about magnitude 8 while the 1960 earthquake has a moment magnitude of 9.5.

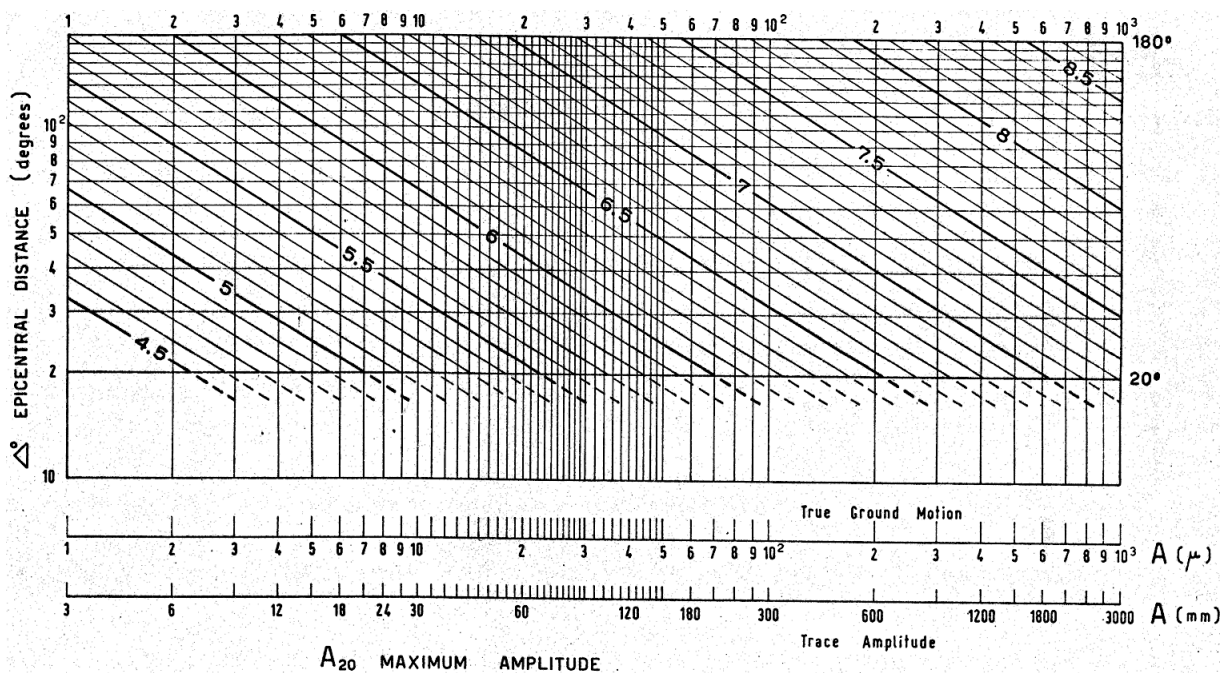


Fig. 3.25 - Curves for the determination of surface wave magnitude.

### 3.7. Seismic moment

The orientation of the fault, direction of fault movement, and size of an earthquake can be described by the fault geometry and seismic moment. These parameters are determined from waveform analysis of the seismograms produced by an earthquake. The differing shapes and directions of motion of the waveforms recorded at different distances and azimuths from the earthquake are used to determine the fault geometry, and the wave amplitudes are used to compute moment.

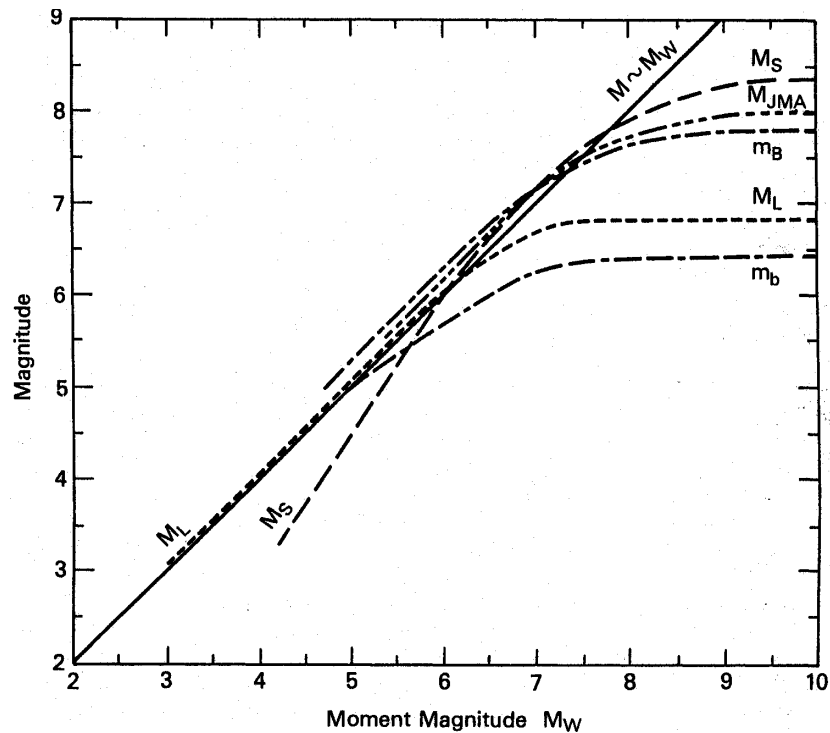


Fig. 3.26 - Saturation of various magnitude scales (after Reiter, 1990):  $M$  (moment magnitude),  $M_L$  (Richter local magnitude),  $M_S$  (surface wave magnitude),  $m_b$  (short-period body wave magnitude),  $m_B$  (long-period body wave magnitude), and  $M_{JMA}$  (Japanese Meteorological Agency magnitude;  $M_{JMA} = \log(A_N^2 + A_E^2)^{1/2} + 1.73 \log d - 0.83$ , where  $d$  is the epicentral distance in degrees).

To get an idea of the seismic moment, we refer to the elementary physics concept of torque. A torque is a force that changes the angular momentum of a system. It is defined as the force times the distance from the centre of rotation. Earthquakes are caused by internal torques, from the interactions of different blocks of the Earth on opposite sides of faults. After some rather complicated mathematics, it can be shown that the moment  $M_0$  of an earthquake is simply expressed by:

$$M_0 = \mu A d \quad (3-36)$$

where  $\mu$  is the shear strength (rigidity modulus) of the faulted rock (about  $3.3 \cdot 10^{10}$  N/m<sup>2</sup>),  $A$  is the area of the fault (i.e.: the product of its length and width), and  $d$  is the average displacement on the fault (i.e.: the slip which is the length of the slip vector of the rupture measured in the plane of the fault). Because fault geometry and observer azimuth are a part of the computation, moment is a more consistent measure of earthquake size than is magnitude, and more importantly, moment does not have an intrinsic upper bound.

Eq. (3-36), for the moment of an earthquake, is fundamental to seismologists' understanding of how dangerous faults of a certain size can be.

Now, let us imagine a chunk of rock on a laboratory bench, the rigidity, or resistance to shearing, of the rock is a pressure in the neighbourhood of a few hundred billion dyne/cm<sup>2</sup>. The pressure acts over an area to produce a force. Now if we guess that the distance the two parts grind together before they fly apart is about a centimetre, then we can calculate the moment, and we obtain  $M_0 = 3 \times 10^{13}$  dyne·cm (1 N·m =  $10^7$  dyne·cm).

Now let us consider a second case, the September 12, 1994 Double Spring Flat earthquake, which occurred about 25 km SE of Gardnerville. Considering a fault which is 15 km long and 10 km deep, we obtain that this earthquake, the largest in Nevada in 28 years, had  $2 \cdot 10^{12}$ , or 2 trillion, times as much moment as breaking the rock on the laboratory table  $M_0 = 1.4 \times 10^{25}$  dyne-cm.

Now let us use Eq. (3-35) (meant for energies expressed in dyne-cm units) to estimate the magnitude of the tiny earthquake we can make on a laboratory table:  $M_w \cong -1.7$ .

Negative magnitudes are allowed on Richter's scale, although such earthquakes are certainly very small.

Next let us take the energy we found for the Double Spring Flat earthquake and estimate its magnitude: 6.1. The value we get is about equal to the magnitude reported by the UNR Seismological Laboratory, and by other observers.

Most seismologists prefer to use the seismic moment to estimate earthquake magnitudes. Finding an earthquake fault's length, depth, and its slip can take several days, weeks, or even months after a big earthquake. Geologists' mapping of the earthquake's fault breaks, or seismologists' plotting of the spatial distribution of aftershocks, can give these parameters after a substantial effort. But some large earthquakes, and most small earthquakes, show neither surface fault breaks nor enough aftershocks to estimate magnitudes the way we have above. However, seismologists have developed ways to estimate the seismic moment directly from seismograms using computer processing methods. The Centroid Moment Tensor Project at Harvard University has been routinely estimating moments of large earthquakes around the world by seismogram inversion since 1982.

The two largest reported moments are  $2.5 \cdot 10^{30}$  dyne-cm for the 1960 Chile earthquake ( $M_S$  8.5;  $M_W$  9.6) and  $7.5 \cdot 10^{29}$  dyne-cm for the 1964 Alaska earthquake ( $M_S$  8.3;  $M_W$  9.2).  $M_S$  approaches its maximum value at a moment between  $10^{28}$  and  $10^{29}$  dyne-cm.

### 3.8. Energy

As we have seen before the magnitude of an earthquake is related to the energy which is radiated in the form of elastic waves. Part of the original potential energy of strain stored in the rock must go into mechanical work, as in raising crustal blocks against gravity, or incrusting material in the fault zone; part must be dissipated as heat.

The energy in an elastic wave of a given period is proportional to the square of the amplitude. If seismograms of different earthquakes at a fixed distance actually differ only in amplitude, the periods would be unchanged, and we should have a relationship of the form:

$$\log E + c + 2M \tag{3-37}$$

where  $c$  is a constant and  $M$  is the magnitude.

Both the magnitude and the seismic moment are related to the amount of energy that is radiated by an earthquake. Gutenberg and Richter (1956) developed a relationship between magnitude and energy. Their relationship is:

$$\log E = 11.8 + 1.5M \tag{3-38}$$

giving the energy  $E$  in erg from the magnitude  $M$ . Note that  $E$  is not the total "intrinsic" energy of the earthquake, transferred from sources such as gravitational energy or to sinks such as heat energy. It is only the amount radiated from the earthquake as seismic waves, which ought to be a small fraction of the total energy transferred during the earthquake process.

The drawback of this method is that  $M_S$  is computed from a bandwidth between approximately 18 to 22 s. It is now known that the energy radiated by an earthquake is concentrated over a different bandwidth and at higher frequencies. With the worldwide deployment of modern digitally recording seismograph with broad bandwidth response, computerized methods are now able to make accurate and explicit estimates of energy on a routine basis for all major earthquakes. A magnitude based on energy radiated by an earthquake,  $M_E$ , can now be defined,

$$M_E = 2/3 \log E - 2.9. \quad (3-39)$$

For every increase in magnitude by 1 unit, the associated seismic energy increases by about 32 times.

Although  $M_W$  and  $M_E$  are both magnitudes, they describe different physical properties of the earthquake.  $M_W$ , computed from low-frequency seismic data, is a measure of the area ruptured by an earthquake.  $M_E$ , computed from high frequency seismic data, is a measure of seismic potential for damage. Consequently,  $M_W$  and  $M_E$  often do not have the same numerical value.

The annual total energy of seismic activity gives a figure near  $9 \cdot 10^{24}$  erg, which is hardly more than a thousandth of the annual flow of the heat from the interior through the surface of the Earth. We may also do a comparison between large earthquakes and atomic bombs. The official figure for the energy released by a "nominal" atomic bomb of the Hiroshima type is about  $8 \cdot 10^{20}$  erg; the largest earthquakes are found to have an energy not much over  $10^{25}$  erg, roughly equivalent to 12,000 of the nominal bombs.

Although the frequency of earthquakes increases rapidly with decreasing magnitude, the energy released in the individual shocks decreases yet more rapidly: so the release of energy takes place principally in the relatively few shocks of largest magnitude and the minor earthquakes are rather incidental indication of the accumulation of regional strain. This agrees with the geographic evidence that the great earthquakes occur in association with the principal faults and active structures, while earthquakes of low magnitude are generally associated with minor tectonic features. Benioff took the strains as proportional to the square roots of the energies; if these quantities are then combined linearly, the total contribution from small quakes is often of the same order as that of the few large shocks. Following Richter, we may conclude that small shocks may release strain sufficiently to delay a major event, nevertheless once a major strain has accumulated it can only be relieved by a great earthquake or by a highly abnormal number of small shocks.

Hiroo Kanamori (1977) came up with a relationship between seismic moment and seismic wave energy. It gives:

$$E = M_0/20,000 \quad (3-40)$$

where  $M_0$  is in dyne-cm, and  $E$  is in erg. It comes that dyne-cm and erg are unit equivalents, but have different physical meaning.

In Table 3.4, the seismic wave energy yielded by the two examples of chapter 3.7 is compared to that of a number of earthquakes and other phenomena (see Fig. 3.27). For this a larger unit of energy, the seismic energy yield of quantities of the explosive TNT (we assume one ounce of TNT exploded below ground yields 640 million erg of seismic wave energy) is used.

### 3.9. Focal mechanisms

Seismic energy radiating from an earthquake can be used to infer the orientation of the fault on which the earthquake occurred and the direction of slip on that fault. But unless measurements are made very close to the earthquake, there will not be enough information to decide between two fault orientations.

The two planes on which the fault might have taken place will be perpendicular to each other. In fact, each plane will be perpendicular to the direction in which slip might have occurred in the other plane. Suppose, for example, the left-lateral slip on a vertical, N-S fault results in an earthquake. Measurements made far from the earthquake would be consistent both with the true orientation of fault slip and with right-lateral slip on a vertical, E-W fault (Fig. 3.28).

In most parts of the world there are not nearly enough seismic stations to find one close to every possible earthquake location. Thus, for many earthquakes, the best estimate of the fault orientation and slip is the focal mechanism, that is, a pair of perpendicular planes and a vector in each plane. The earthquake might have resulted from slip in the direction of either of the vectors, on a fault parallel to the plane of that vector (Fig. 3.29).

Although 160 trillion tons of dynamite is a frightening yield of energy, the Earth receives that amount in sunlight every day.

Table 3.4 – Energy released in some physical phenomena.

Richter Magnitude	TNT for Seismic Energy Yield	Example (approximate)
1.5	6 ounces	Breaking a rock on a laboratory table
1.0	30 pounds	Large Blast at a Construction Site
1.5	320 pounds	
2.0	1 ton	Large Quarry or Mine Blast
2.5	4.6 tons	
3.0	29 tons	
3.5	73 tons	
4.0	1,000 tons	Small Nuclear Weapon
4.5	5,100 tons	Average Tornado (total energy)
5.0	32,000 tons	
5.5	80,000 tons	Little Skull Mtn., NV Quake, 1992
6.0	1 million tons	Double Spring Flat, NV Quake, 1994
6.5	5 million tons	Northridge, CA Quake, 1994
7.0	32 million tons	Hyogo-Ken Nanbu, Japan Quake, 1995; Largest Thermonuclear Weapon
7.5	160 million tons	Landers, CA Quake, 1992
8.0	1 billion tons	San Francisco, CA Quake, 1906
8.5	5 billion tons	Anchorage, AK Quake, 1964
9.0	32 billion tons	Chilean Quake, 1960
10.0	1 trillion tons	(San-Andreas type fault circling Earth)
12.0	160 trillion tons	(Fault Earth in half through centre, OR Earth's daily receipt of solar energy)

One reason why the focal mechanism is valuable to geophysicists is that it provided unambiguous information about the change of stress within the Earth that was caused by the earthquake. That is, the two possible orientations of fault and slip are both compatible with the same orientation of pressure (P), tension (T), and neutral (B) axes. The P and T axes are both 45° from both planes, while the B axis is along the intersection of the two planes.

The focal mechanism can be expressed numerically in several different ways.

- a) **Fault plane solution.** The orientation of a plane can be represented by two angles, the strike and dip. The orientation of a vector in that plane can then be specified with just one more angle, the rake. The orientation of the other plane is known from this information, since it is perpendicular to the slip vector in the first plane. The orientation of the slip vector in the other plane is known since it must be perpendicular to the plane given. Giving the strike and dip of both planes requires four numbers and provides slightly less information, since it fails to tell of which of the planes the slip must have been leftwards, if that was the fault, and on which it must have been rightwards).
- b) **Principal axes and values.** Each of the P, T and B axes is perpendicular to both of the other axes. If the azimuth and plunge of any two axes are given, then the orientation of the third axis, the two planes, and the slip vectors can all be computed (if the orientation of only two axes is given, they are almost always the P and T axes). Sometimes, in addition, the value of stress change on each axis is given. Unless the earthquake involved an explosion or implosion (in addition to slip on a fault) the sum of the three stress changes is 0. That is, if the stress change on the P axis is not exactly negative to the change on the T axis, then the stress change on the "neutral" B axis will not be exactly 0. This allowance for a non-zero stress change in the B direction makes this way of expressing the focal mechanism more general than the fault plane solution. For example, slip on complexly curved faults can result in stress changes that are only imperfectly expressed by a fault plane solution. Also, the average of the absolute values of the principal values is one way measure of the size of an earthquake.



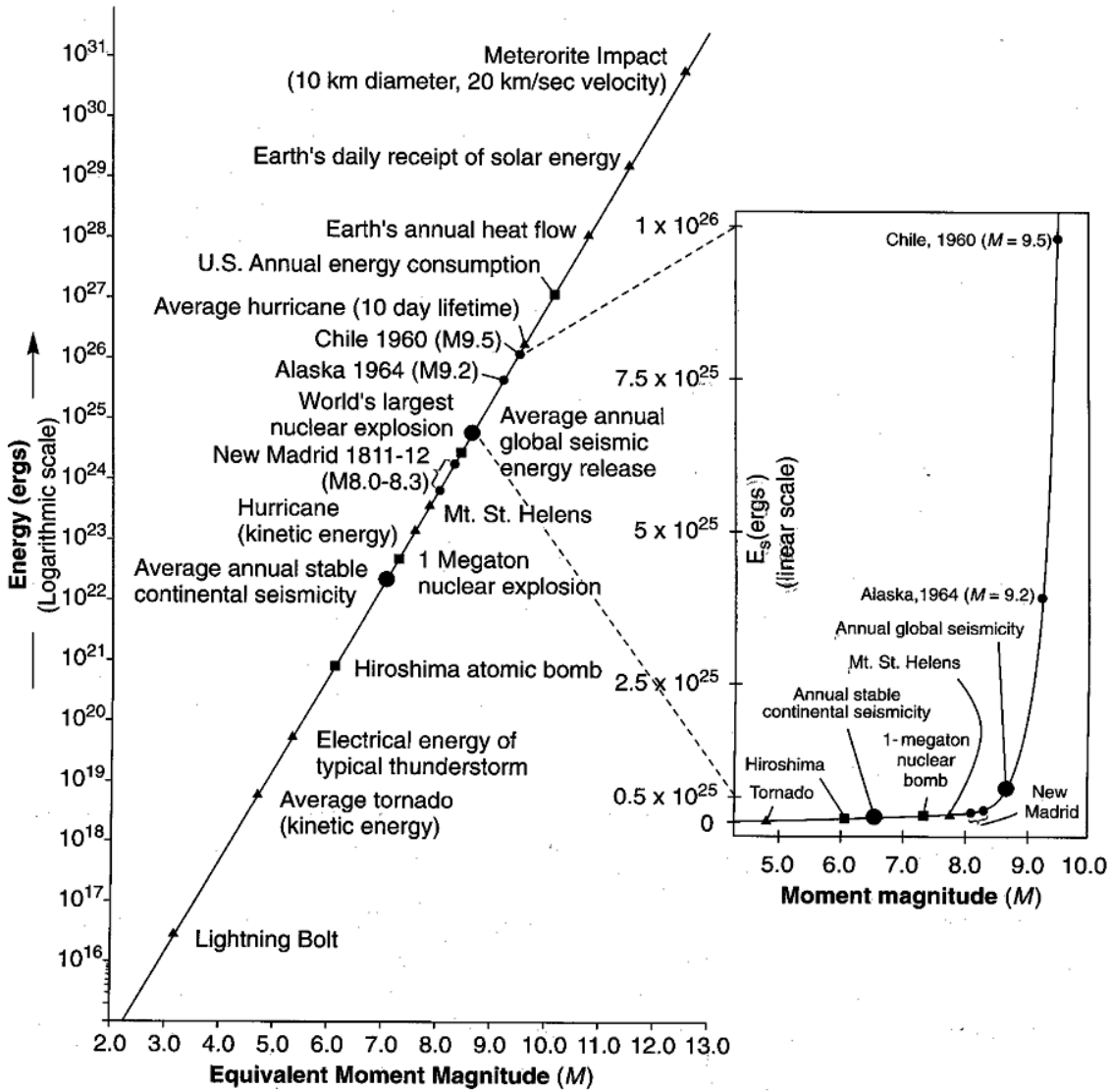


Fig. 3.27 - Relative energy of various natural and human-made phenomena (from Kramer, 1996).

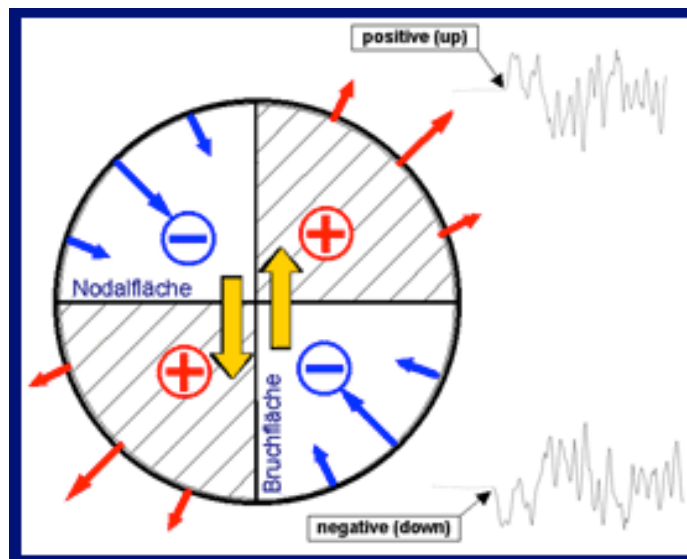


Fig. 3.28 - Example of a fault plane solution based on first motion observations. For a double-couple source mechanism (or only shear motion on the fault plane), the compression first-motions should lie only in the quadrant containing the tension axis, and the dilatation first-motions should lie only in the quadrant containing the pressure axis.

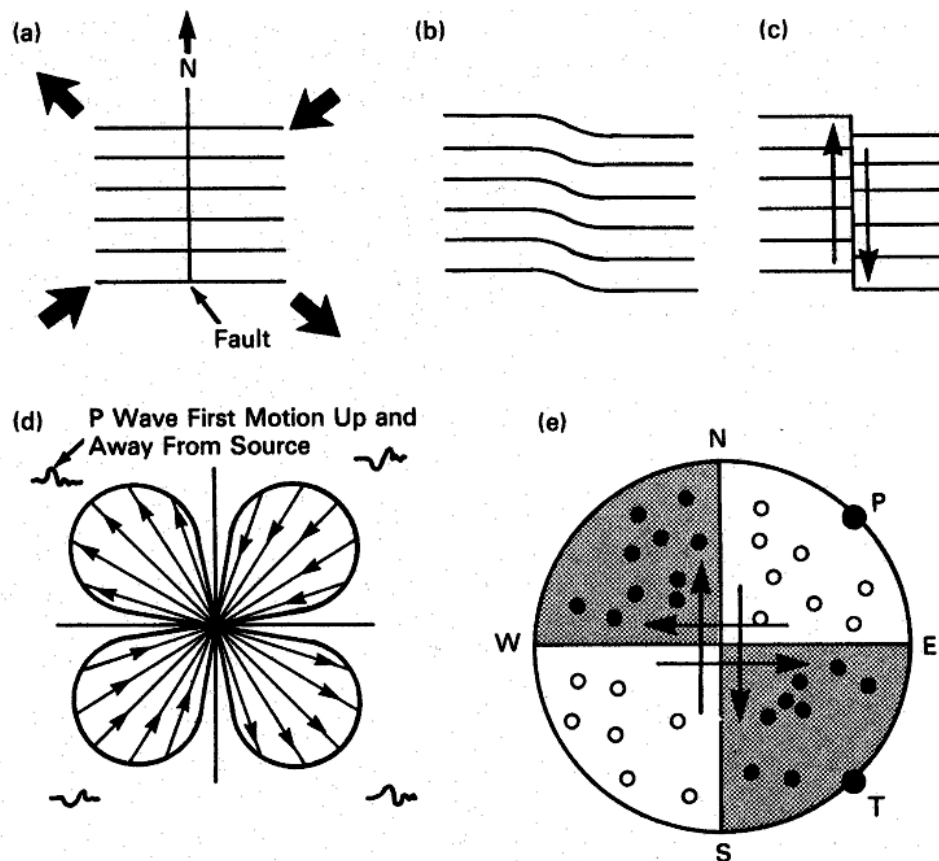


Fig. 3.29 - Elastic rebound, radiation pattern and focal-mechanism solution (from Reiter, 1990); a) after an earthquake a N-S vertical fault is subject to tectonic stresses shown by the large arrows; b) under stress, the region is deformed (strained) as shown by lines that were originally perpendicular to fault immediately after the earthquake. While the eastern and western sides of the fault have moved in the directions shown by the arrows, the fault itself has not yet ruptured; c) rupture occurs allowing built up strain energy to be released in the form of an earthquake; d) radiation pattern of P waves from rupture (earthquake) shown in (c). Length and direction of arrow indicate strength and direction of P wave first motion at that azimuth. Idealized seismograms of P waves are shown for each quadrant; e) focal mechanism solution. P and T are pressure and tension axes.

c) **Moment tensor.** The six independent elements of a  $3 \times 3$  symmetrical matrix represent the sudden change in three normal stresses (pressure and tension in three directions) and three shear stresses (on the face of each side of a cube) that all together would account for the seismic energy that radiated from the earthquake. The moment tensor is actually identical to the principal axes and values, but moment tensor values relate to some convenient coordinate system (such as up, north, east) rather than values on axes oriented with respect to the earthquake. In a coordinate system oriented along the principal axes the "off-diagonal" terms are always zero, so they simply were not stated among the principal values. There are rules for computing the values of a matrix to represent the same tensor in any other coordinate system. If you start with a moment tensor and use the rules to rotate to a coordinate system that matches the P, T and B axes, then all of the off-diagonal values will be zero and the values on the diagonal of the matrix will be the principal values.

To represent focal mechanisms graphically, seismologists use techniques that were originally developed by structural geologists to represent the orientation of rock surfaces and lineations that they measured in the field. The starting point is to imagine a small sphere around the place where the earthquake occurred. Each plane through the centre intersects the sphere along a great circle, and two perpendicular planes divide the sphere into four quadrants (Fig. 3.30).

Each axis through the centre intersects the sphere at two points, on opposite sides. The P axis, which is  $45^\circ$  from each plane, will intersect the sphere in the middle of two of the quadrants, while the T axis will intersect the middle of the other two quadrants. Suppose that we paint the two quadrants intersected by either end of the P axis red.

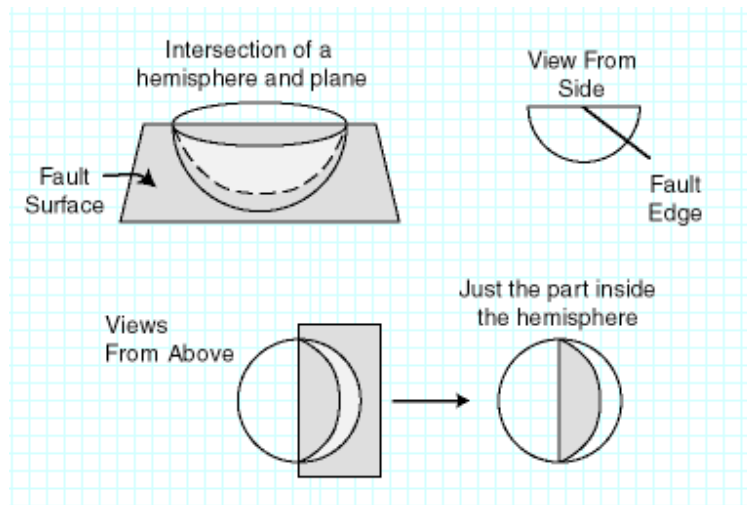


Fig. 3.30 – Meaning of a fault plane solution.

We have created a red and white "beach ball" that represents the focal mechanism. The two planes that separate the red and white quadrants are the two planes that might be a fault that slipped to cause the earthquake. The red and white quadrants always have the same shape, but the beach ball can be rotated to represent the orientation of the focal mechanism.

Waves radiated from the earthquake in directions of the quadrants painted white will initially compress the rocks through which they travel. Waves radiated in directions of the quadrants painted red will initially dilate the rocks through which they travel.

The standard way of creating a two-dimensional figure from the three-dimensional visualisation harkens back to the structural geologists, who originally developed all of this. The geologist would have been standing in the field, looking down at the planes and lineations that extend downwards into the Earth. So after orienting the beach ball, imagine cutting away the top half of the beach ball and just keeping the lower hemisphere inside the Earth where the planes and lineations exist. Now each plane intersects the lower hemisphere along a semicircle and each axis intersects the lower hemisphere at one point.

To create a two-dimensional figure, the intersection points and circles must be projected up to the horizontal plane at the top of the hemisphere. This is analogous to making a two-dimensional map of half of the Earth, and any projection will distort things in some way. Most seismologists use an "equal area" projection, which distorts angles between curves but avoids bunching together or spreading apart points that are equally spaced on the hemisphere.

If the fault on which the earthquake occurred is complexly curved then the boundaries between the initially compressive and initially dilatational waves will not be planes. Instead these boundaries will be gently curving surfaces, tending towards a pair of cones centred on either the P or T axis in the most extreme cases.

A beach ball can represent an earthquake on a complexly curved fault if the quadrants are distorted to representing directions of initially compressive and dilatational waves. Among the numerical representations of the focal mechanism, that with the principal axes and values shows the effect of complex curvature most readily, since the intermediate principal value that is not 0, even though the three principal values still sum to 0.

The representation of a focal mechanism as a fault plane solution cannot perfectly match radiation from certain types of rupture on complexly curved faults. In these cases, the fault plane solution is only an approximation of the complete focal mechanism (Fig. 3.31).

There are a few programs available on the Internet that are useful for determining or displaying focal mechanisms, including "Cliffs Nodes" by Cliff Frohlich and "FOCMEC" by Arthur Snoke, which are both available from <ftp://ftp.iris.washington.edu/pub/programs/sel/sun/>.

Sometimes a series of earthquakes, such as microearthquakes, for which separate focal mechanisms cannot be computed, can be treated as a single earthquake, and the pooled data can be used to compute a composite focal mechanism solution. These earthquakes should be near each other and result from the same causative mechanism.

Focal mechanisms are useful to study the evolution of a seismic sequence (Fig. 3.32) or the general characteristics of the stress pattern in a region (Fig. 3.33).

### 3.9.1. Stress tensor inversion

Fault plane solutions can be used for determining the stress regime of a region: this is done by a process of inversion of a large number of focal mechanism aiming at identifying the tensors suitable to produce the studied mechanisms.

The inversion algorithms of Gephart and Forsyth (1984) is based on the assumption that, if various orientations of focal mechanisms exist within a region of uniform stress, one may determine the directions of the principal stresses ( $\sigma_1$  and  $\sigma_3$ ) and a relative stress magnitude ( $R$ ) from the condition that slip occurs in the direction of the maximum shear stress. The conditions are, then: 1) stress is uniform in the rock volume under investigation; 2) earthquakes are shear dislocation episodes on pre-existing faults; 3) slip occurs in the direction of the resolved shear stress on the fault plane. The algorithm searches for the stress tensor showing the best agreement with the available focal mechanisms by minimizing the sum of the misfits. For a given stress model, the misfit of a single focal mechanism is defined as the smallest rotation about any arbitrary axis that brings the slip direction and sense of slip of either of the two nodal planes into an orientation that is consistent with the stress model. The average of the focal mechanism misfits to the best stress model provides a guide to how well the assumption of stress homogeneity is fulfilled in relation to the seismic data used in the inversion.

## 3.10. Foreshocks and aftershocks

A foreshock is a smaller earthquake preceding a much larger earthquake. Many scientists hope to use foreshocks to predict upcoming earthquakes.

In particular, the East Pacific Rise transform faults show foreshock activity before the main seismic event. Reviews of data of past events and their foreshocks showed that they have a low number of aftershocks and high foreshock rates compared to continental strike-slip faults. The 9.5-magnitude great Chilean earthquake had a 7.9-magnitude foreshock.

Aftershocks are earthquakes in the same region of the mainshock (generally within a few rupture length) but of smaller magnitude and which occur with a pattern that follows Omori's law (Omori, 1894). Omori's law, or more correctly the modified Omori's law, is an empirical relation for the temporal decay of aftershock rates. Omori published his work on the aftershocks of earthquakes, in which he stated that aftershock frequency decreases by roughly the reciprocal of time after the main shock:

$$n(t) = \frac{K}{c + t} \quad (3-41)$$

where  $n(t)$  is the number of earthquakes  $n$  measured in a certain time  $t$ ,  $K$  is the decay rate; and  $c$  is the "time offset" parameter.

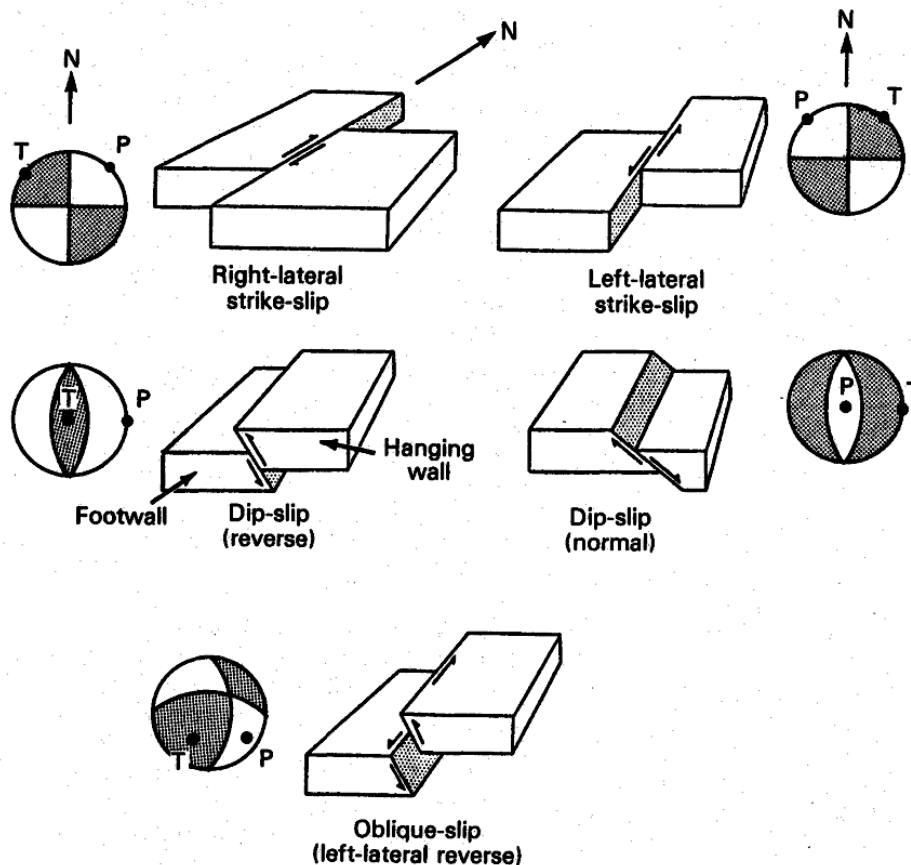


Fig. 3.31 - Different types of faults classified by the orientation of relative movement along the fault plane during an earthquake (from Reiter, 1990). Also shown are the corresponding focal mechanism solutions with pressure (P) and tension (T) axes.

The modified version of the law, now commonly used, was proposed by Utsu (1961):

$$n(t) = \frac{K}{(c+t)^p} \quad (3-42)$$

where  $p$  typically falls in the range 0.7-1.5.

What these equations describe is that the rate of aftershocks dies off quickly with time. The rate of aftershocks is proportional to the inverse of time since the mainshock. Thus whatever the odds of an aftershock are on the first day, the second day will have 1/2 the odds of the first day and the tenth day will have approximately 1/10 the odds of the first day (when  $p$  is equal to 1). These patterns describe only the mass behaviour of aftershocks; the actual times, numbers and locations of the aftershocks are 'random', while tending to follow these patterns. As this is an empirical law, values of the parameters are obtained by fitting to data after the mainshock occurred and they have no physical basis/meaning.

The other main law describing aftershocks is known as Bath's Law (Richter, 1958; Bath, 1965) and it says that any mainshock typical has an aftershock approximately 1 magnitude (on average 1.2) less than its mainshock. Aftershock sequences also typical follow the Gutenberg-Richter scaling (see chapter 3.11.1).

Aftershocks are dangerous because they are usually unpredictable, they can be of a large magnitude, and they can collapse buildings that are damaged from the mainshock. Bigger earthquakes have more and larger aftershocks and the sequences can last for years or even longer especially when a large event occurs in a seismically quiet area, see New Madrid Seismic Zone where events still follow Omori's law from the mainshocks in 1811/1812. An aftershock sequence is deemed to be over when the rate of seismicity drops back to a background level i.e., no further decay in the number of events with time can be detected.



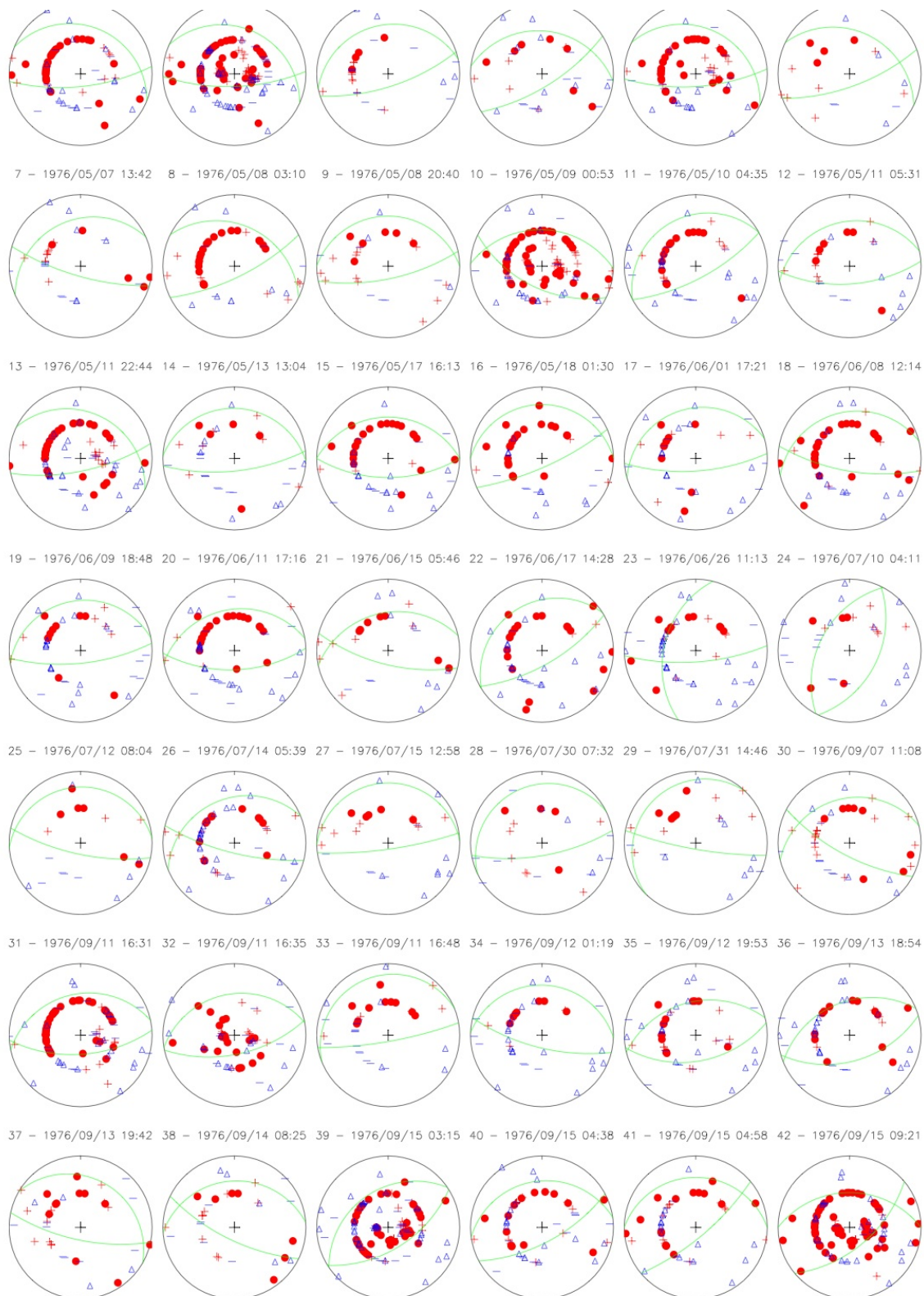


Fig. 3.32 – Fault plane solutions for the main events of the 1976 Friuli seismic sequence.

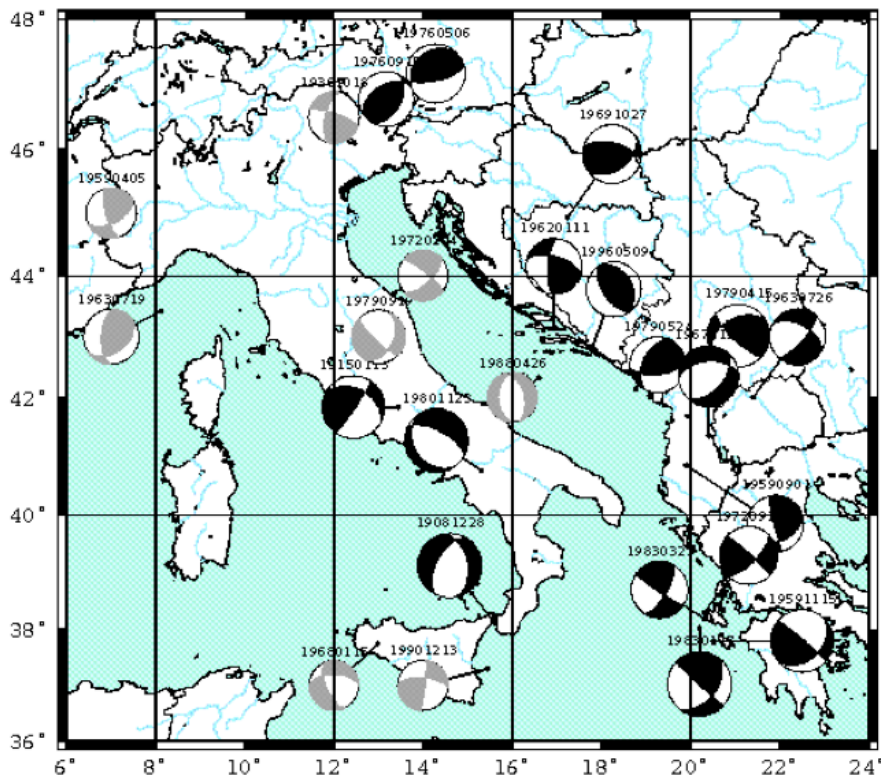


Fig. 3.33 – Fault plane solutions for the Adriatic region. They identify the stress pattern (compressional, extensional, transcurrent) characteristic of the different sectors of the region.

### 3.11. Earthquake statistics

As the earthquake spatial distribution is not random but it follows specific geodynamic features, also their size distribution is not random but it follows a specific relation that states that the number of small events is much larger than that of the strong ones.

Table 3.5 gives a general idea about the number of earthquakes that occur annually according to their magnitude. It derives that the number of the potentially damaging events (e.g.: magnitude larger than 5) is about 1000.

Table 3.5 - Frequency of occurrence of earthquakes based on observations since 1900.

Descriptor	Magnitude	Average Annually
Great	8 and higher	1
Major	7 - 7.9	18
Strong	6 - 6.9	120
Moderate	5 - 5.9	800
Light	4 - 4.9	6,200 (estimated)
Minor	3 - 3.9	49,000 (estimated)
Very Minor	< 3.0	Magnitude 2 - 3: about 1,000 per day Magnitude 1 - 2: about 8,000 per day

Considering the strongest events (Table 3.6), it can be seen that there are a very few that exceeded magnitude 9 and those that hit Chile is remarkably high.

Effects of earthquakes are recorded by seismometers and accelerometers. Although the number of stations has increased greatly in the last decades, it is not easy to find a record referred to a station located in the near field. Table 3.7 shows the largest PGAs recorded: it is interesting to compare the

data in Table 3.7 with those in Table 3.6, and it comes that there is no correspondence between the two lists. It depends on two reasons: the lack of a recording in the near field and the local effects that can amplify notably the ground motion.

Table 3.6 – Largest earthquakes according to magnitude.

N.	Date	Location	Magnitude
1	May 22, 1960	Valdivia, Chile	9.5
2	March 27, 1964	Prince William Sound, Alaska, USA	9.2
3	December 26, 2004	Indian Ocean, Sumatra, Indonesia	9.1-9.3
4	November 4, 1952	Kamchatka, Russia (then USSR)	9.0
5	March 11, 2011	Pacific Ocean, Tohoku region, Japan	9.0
6	November 25, 1833	Sumatra, Indonesia	8.8-9.2 (est.)
7	January 31, 1906	Ecuador - Colombia	8.8
8	February 27, 2010	Maule, Chile	8.8
9	January 26, 1700	Pacific Ocean, USA and Canada	8.7-9.2 (est.)
10	July 8, 1730	Valparaiso, Chile	8.7-9.0 (est.)
11	November 1, 1755	Atlantic Ocean, Lisbon, Portugal	8.7 (est.)
12	February 4, 1965	Rat Islands, Alaska, USA	8.7
13	July 9, 869	Pacific Ocean, Tohoku region, Japan	8.6 (est.)
14	October 28, 1707	Pacific Ocean, Shikoku region, Japan	8.6 (est.)
15	August 15, 1950	Assam, India - Tibet, China	8.6
16	March 9, 1957	Andreanof Islands, Alaska, USA	8.6
17	March 28, 2005	Sumatra, Indonesia	8.6
18	April 11, 2012	Off the West Coast of Northern Sumatra	8.6
19	August 13, 1868	Arica, Chile (then Peru)	8.5-9.0 (est.)
20	December 16, 1575	Valdivia, Chile (Kingdom of Chile)	8.5 (est.)
21	October 20, 1687	Lima, Peru (Viceroyalty of Peru)	8.5 (est.)
22	May 24, 1751	Concepción, Chile (Kingdom of Chile)	8.5 (est.)
23	November 11, 1922	Atacama Region, Chile	8.5
24	February 3, 1923	Kamchatka, Russia (USSR)	8.5
25	February 1, 1938	Banda Sea, Indonesia	8.5
26	October 13, 1963	Kuril Islands, Russia (USSR)	8.5
27	November 1, 1755	Lisbon, Portugal	8.5-9.0 (est.)
28	September 12, 2007	Sumatra, Indonesia	8.5

### 3.11.1. The Gutenberg – Richter law

The frequency-magnitude law of Gutenberg and Richter (G-R) is one of the three relations for earthquakes presumed to be globally valid (Knopoff, 2000). The other two are the Omori (1894) decay rate law for the aftershocks of great earthquakes and the G-R law for aftershocks.

Although a power-law distribution for earthquake energies was already suggested by Wadati (1932), the exponential distribution for earthquake magnitudes was proposed by Gutenberg and Richter (1944) with the relation:

$$\log N = a + b (8 - M_L) \quad (3-43)$$

where  $N$  is the number of earthquakes in each magnitude class and  $M_L$  is the local magnitude. The authors considered Eq. (3-43) valid in the magnitude range 3.0 to 8.5. Formulae for  $M_S$  were developed by Gutenberg (1945) by equalizing  $M_S$  to  $M_L$ . The method of the least squares was applied by Gutenberg and Richter (1949) to fit by Eq. (3-43), equalizing  $M_L$  and  $M_S$ , the data of southern California and New Zealand separately in the magnitude range 6.0 to 8.6 and found a  $b$ -value of 0.88 and 0.87, respectively. Richter (1958) modified slightly Eq. (3-43) in:

$$\log N = a - b M \quad (3-44)$$

where  $N$  is the number of earthquakes of magnitude  $M$  or greater. Eq. (3-44) is now known as G-R law and is considered valid for  $M_L$  as well as for  $M_S$ .

The spatial or temporal variation of the  $b$ -value has been one of the frequently discussed topics in seismology. Some authors are of the opinion that the  $b$ -value for tectonic earthquakes in general does not differ significantly from a universal value (e.g.: Isacks and Oliver, 1964). Some tried to relate the spatial variations of the  $b$ -value to tectonics, degree of fracturing, material properties, degree of stress concentration, etc. (e.g.: Karnik and Klima, 1993). Some tries to relate the temporal variations to changes in stress level, pore-fluid pressure, fracture growth conditions, etc. (e.g., Imoto, 1991). According to Isacks and Oliver (1964), a large part of the variation of the  $b$ -value from region to region can be attributed to statistical fluctuation of observational uncertainties.

Table 3.7 – Maximum PGA (in g) recorded in the last 50 years: PGA sd = PGA recorded along a single direction (E-W, N-S or vertical); PGA sv = vectorial sum of the 3 components; M = earthquake magnitude; h = earthquake depth. The highest PGAs were recorded in the last 15 years, when the number of strong-motion recording stations has increased notably, consequently also in the near field.

PGA sd	PGA vs	M	h (km)	Fatalities	Earthquake
2.7	2.99	9.0	32	>10.035	2011 Tohoku
2.2		6.3	5	182	2011 Christchurch
	4.36	6.9/7.2	8	12	2008 Iwate-Miyagi Nairiku
1.7		6.7	19	57	1994 California
	1.47	7.1	42	4	April 2011 Miyagi
1.26		7.1	10	0	2010 Canterbury
1.01		6.6	10	11	2007 Chuetsu
1.01		7.3	8	2.415	1999 Jiji
1.0		6.0	8	0	December 2011 Christchurch
0.8		6.8	16	6.434	1995 Kobe
0.78		8.8	35	521	2010 Chile
0.6		6.0	10	143	1999 Athens
0.51		6.4		612	2005 Zarand
0.5		7.0	13	92,000-316,000	2010 Haiti
0.438		7.7	44	27	1978 Miyagi (Sendai)
0.4		5.7	8	0	2016 Christchurch
0.367		5.2	1	9	2011 Lorca
0.25-0.3		9.5	33	1.655	1960 Valdivia
0.24		6.4		628	2004 Morocco
0.18		9.2	23	143	1964 Alaska
0.125		7.7	44	27	1978 Miyagi (Sendai)

The frequency vs. magnitude plots for some data sets exhibit considerable deviation from a straight line and, consequently, modifications of the G-R relation have been proposed to represent such character, such as the truncated G-R equation, two-range G-R equation, and equations with various additional terms to the original G-R equation.

It is well known that most widely used earthquake magnitude scales,  $M_L$ ,  $M_S$ , and  $m_b$  saturate at large magnitude:  $m_b$  and  $M_L$  at around 7,  $M_S$  at around 8.3. It is possible to explain the saturation effect in terms of the source dimensions and mechanism. Hanks and Thatcher (1972) pointed out that a magnitude scale based directly on an estimate of the radiated energy would circumvent this drawback.

Different methodologies for assessing the  $b$ -value of the G-R relation are available in literature. The least-squares method (LSM) is often used, although not formally suitable since magnitude is not error free, cumulative event counts are not independent, and the error distribution of the number of earthquake occurrences does not follow a Gaussian distribution. The maximum likelihood method (MLM) has been widely applied (Aki, 1965; Utsu, 1965, 1966): Weichert (1980) proposed a general routine suitable also for different completeness periods of the earthquake catalogue. This aspect is particularly important for the correct estimation of the standard error associated with the  $b$ -value ( $\sigma_b$ ). In fact,  $\sigma_b$  depends strongly on the number of samples constituting each magnitude class. It derives that longer the completeness period and larger the sample number. An example is given in Table 3.8, where the activity rate computed in a suitable way (it does not matter what this way is in

the present example) is referred either to 1 year or to 1000 years. This implies that in the first case you consider the completeness period of your catalogue very short (1 year), while in the second case you consider it very long (1000 years). The results obtained with the Weichert (1980) code is  $a = 9.54$  and  $b = 1.61$  in both cases, but  $\sigma_b$  is 3.60 when considering annual rates and 0.11 when considering 1000-year rates.

Table 3.8 – Activity rates used for computing the parameters of the G-R law by the MLM of Weichert (1980). As  $I_1$  is the annual activity rate and  $I_{1000}$  refers to 1000 years, they represent the same G-R relation ( $\log N = 9.54 - 1.61M$ ) but the value of  $s_b$  is remarkably different: 3.60 using  $I_1$  and 0.11 with  $I_{1000}$ .

$M$	$I_1$	$I_{1000}$
6.4	0.100	100.0
6.7	0.050	50.0
7.0	0.010	10.0
7.3	0.005	5.0
7.6	0.001	1.0

We can consider three theoretical cases, where we have a G-R relation referred to a completeness period of 100 years for all magnitude classes, described by the equation:

$$\log N = 5 - b M_S \quad (3-45)$$

with  $b$  equal to 0.7, 1.0, and 1.3, respectively. We define this relation in the range 4.5 to 7.5, range of applicability of the  $M_S$  to  $M_W$  scaling law (Ekstrom and Dziewonski, 1988). From it, the non-cumulative number of earthquakes for each  $M_S$  class, considering a magnitude step of 0.1, has been calculated. The  $M_S$  values were transformed into  $M_W$  values by the Ekstrom and Dziewonski (1988) relations:

$$\begin{aligned} M_W &= 2/3 M_S + 2.13 && (M_S < 5.3) \\ M_W &= 9.40 - \sqrt{41.09 - 5.07 M_S} && (5.3 \leq M_S \leq 6.8) \\ M_W &= M_S + 0.03 && (M_S > 6.8). \end{aligned} \quad (3-46)$$

obtaining the values reported in Table 3.9.

By analyzing Table 3.9 and considering only one decimal figure, it derives that a few contiguous  $M_S$  classes are merged together in the same  $M_W$  class and, in general, that the  $M_S$  range 4.5-6.8 is compressed into the  $M_W$  range 5.1-6.8.

Table 3.9 –  $M_W$  values obtained by applying the Ekstrom and Dziewonski (1988) relation.

$M_S$	$M_W$	$M_S$	$M_W$	$M_S$	$M_W$
4.5	5.13	5.6	5.84	6.6	6.64
4.6	5.20	5.7	5.91	6.7	6.73
4.7	5.26	5.8	5.98	6.8	6.83
4.8	5.33	5.9	6.06	6.9	6.93
4.9	5.40	6.0	6.13	7.0	7.03
5.0	5.46	6.1	6.21	7.1	7.13
5.1	5.53	6.2	6.29	7.2	7.23
5.2	5.60	6.3	6.38	7.3	7.33
5.3	5.63	6.4	6.46	7.4	7.43
5.4	5.70	6.5	6.55	7.5	7.53
5.5	5.77				

Passing to the cumulative number of events and computing the  $b$ -value by both the LSM, which better fits the high-magnitude data because all data points are weighted equally, and MLM [according to Weichert (1980)], the results reported in Fig. 3.34 have been obtained. It can be seen that the  $b$ -value calculated by considering the  $M_W$  scale is remarkably larger than the one fixed a priori for  $M_S$ .



The difference in the  $b$ -value estimates in terms of  $M_S$  and  $M_W$  remains within 0.3 when using the LSM, while it is larger and variable according to the  $b$ -value itself when using the MLM.

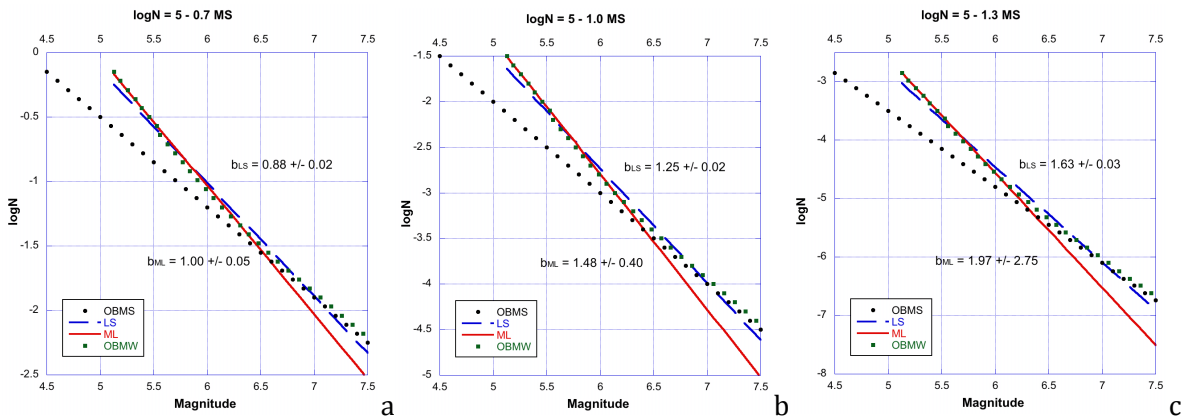


Fig. 3.34 -  $b$ -value computation according to 3 theoretical cases: a)  $b=0.7$ ; b)  $b=1.0$ ; c)  $b=1.3$ . OBMS indicates the rates expressed in  $M_S$  while OBMW the same rates but transformed into  $M_W$ . LS is the least squares fit and ML is the maximum likelihood one.



## 4. STRONG GROUND MOTION

Instrumental recordings of the strong, and potentially destructive, ground movements during earthquakes provide the foundation stone for earthquake engineering since they are the clearest and most comprehensive definition of the actions against which structures and lifelines must be designed.

The instruments that record strong ground motion are called accelerographs because they record the acceleration of the ground as a function of time, unlike seismographs which record the displacement or velocity of the ground. The first accelerographs were developed and installed in California in 1932, more than three decades after the first seismographs came into operation. The reason that it took much longer to develop accelerographs is that they are required to be sufficiently sensitive to produce detailed records of the ground motion and at the same time robust enough to operate while being subjected to very strong vibrations.

Accelerograms, the records obtained from accelerographs, contain a wealth of information about the nature of the ground shaking in strong earthquakes and also about the highly varied characteristics that different earthquakes can produce at different locations (Fig. 4.1).

In addition to the information about the variation of acceleration with time during the earthquake, double integration of the accelerogram provides the velocity and displacement time-histories to be recovered as well (Fig. 4.1). However, the nature of the integrated motions, especially the displacements, are highly sensitive to the processing applied to remove the digitisation noise from the record and the reported values of velocity and displacement must always be interpreted with some caution.

### 4.1. Ground motion parameters

Ground motion parameters are essential for describing the important characteristics of strong ground motion in compact, quantitative form. Many parameters have been proposed to characterize the amplitude, frequency content, and duration of strong ground motions; some describe only one of these characteristics, while others may reflect two or three. Because of the complexity of earthquake ground motions, identification of a single parameter that accurately describes all important ground motion characteristics is regarded as impossible.

#### 4.1.1. Amplitude parameters

The most common way of describing a ground motion is with a time history. The motion parameter may be acceleration, velocity, or displacement, or all three may be displayed as shown in Fig. 4.1. Typically, only one of these quantities is measured directly with the others computed from it by integration and/of differentiation. Note the different predominant frequencies in the acceleration, velocity, and displacement time histories. The acceleration time history shows a significant proportion of relatively high frequencies. Integration produces a smoothing or filtering effect [in the frequency domain,  $v(\omega) = a(\omega)/\omega$  and  $u(\omega) = v(\omega)/\omega$ , where  $u$ ,  $v$ , and  $a$  are the transformed displacement, velocity, and acceleration, respectively, and  $\omega=2\pi f$ ]. Therefore, the velocity time history shows substantially less high-frequency motion than the acceleration time history. The displacement time history, obtained by another round of integration, is dominated by relatively low frequency motion.

The most commonly used measure of the amplitude of a particular ground motion is the horizontal peak ground acceleration (PGA). The PGA for a given component of motion is simply the largest (absolute) value of horizontal acceleration obtained from the accelerogram of that component. By taking the vector sum of two orthogonal components, the maximum resultant PGA (the direction of which will usually not coincide with either of the measured components) can be obtained.

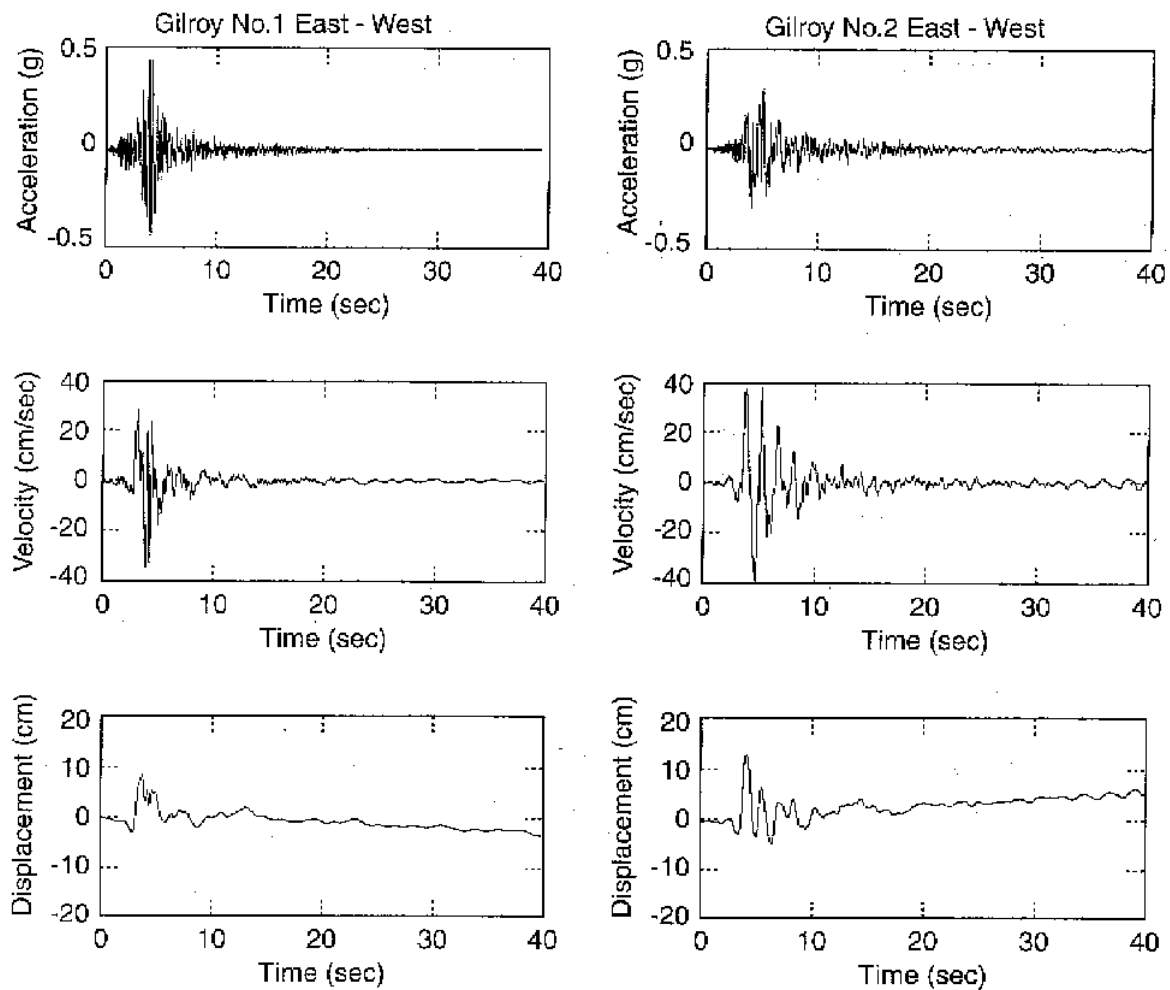


Fig. 4.1 – Acceleration, velocity, and displacement time histories for the E-W components of the Gilroy No 1 (rock) and Gilroy No. 2 (soil) strong motion records. The velocities and displacements were obtained by integrating the acceleration records using the trapezoidal rule. Note that the Gilroy No. 1 (rock) site experienced higher accelerations, but the Gilroy No. 2 (soil) site experienced higher velocities and displacements.

Horizontal PGAs have commonly been used to describe ground motions because of their natural relationship to inertial forces; indeed, the largest dynamic forces induced in certain types of structures (i.e., very stiff structures) are closely related to the PGA. The PGA can also be correlated to earthquake intensity (Table 4.1). Although this correlation is far from precise, it can be very useful for estimation of PGA when only intensity information is available, as in the cases of earthquakes that occurred before strong motion instruments were available (pre-instrumental earthquakes). A number of intensity-acceleration relationships have been proposed, several of which are shown in Fig. 4.2. The use of intensity-attenuation relationships also allows estimation of the spatial variability of peak acceleration from the isoseismal maps of historical earthquakes.

Vertical PGAs have received less attention in earthquake engineering than horizontal accelerations, primarily because the margins of safety against gravity-induced static vertical forces in constructed works usually provide adequate resistance to dynamic forces induced by vertical accelerations during earthquakes. For engineering purposes, the vertical PGA is often assumed to be two-thirds of the horizontal PGA. The ratio of vertical to horizontal PGA, however, has more recently been observed to be quite variable but generally to be greater than two-thirds near the source of moderate to large earthquakes and less than two-thirds at large distances. Vertical PGAs can be quite large; a vertical PGA of 1.74 g was measured between the Imperial and Brawley faults in the 1979 Imperial Valley earthquake (Table 4.2).

Tab. 4.1 – Correlations between PGA (in cm/s<sup>2</sup>) and MM intensity (from Linkimer, 2008).

Reference	Correlation	Region	Range
Gutenberg & Richter (1942, 1956); Richter (1958)	$MMI=3.00 \cdot \log PGA_{ave} + 1.50$	West USA	
Hershberger (1956)	$MMI=2.33 \cdot \log PGA_{ave} + 2.1$	West USA	
Trifunac & Brady (1975)	$MMI=3.33 \cdot \log PGA_{ave} - 0.47$	West USA	IV < MMI < X
Murphy & O'Brien (1977)	$MMI=2.86 \cdot \log PGA_{ave} + 1.24$	West USA, Japan & southern Europe	IV < MMI < X
Murphy & O'Brien (1977)	$MMI=4.00 \cdot \log PGA_{max} - 1.00$	West USA, Japan & southern Europe	IV < MMI < VIII
Sauter & Shah (1978)	$MMI=3.62 \cdot \log PGA_{ave} - 0.90$	Unspecified	
Wald et al. (1999)	$MMI=2.20 \cdot \log PGA_{max} + 1.00$	California	MMI < V
Wald et al. (1999)	$MMI=3.66 \cdot \log PGA_{max} - 1.66$	California	V < MMI < VIII

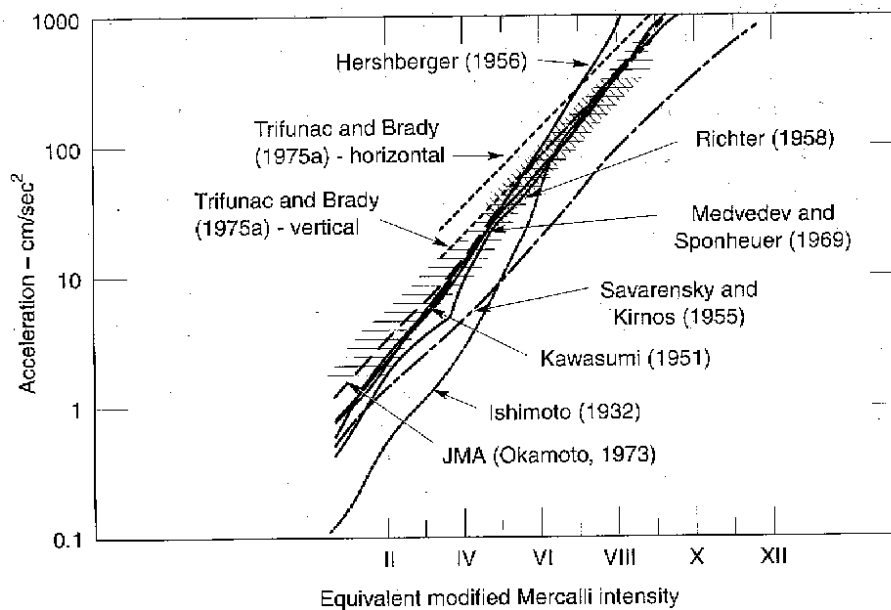


Fig. 4.2 - Proposed relationships between PGA and MM intensity (from Kramer, 1996).

Table 4.2 - Earthquakes with a vertical acceleration (recorded or estimated from field evidence) larger than 1 g in the near field.

Year	Earthquake	Magnitude	Dist	H-PGA (g)	V-PGA (g)
1897	Assam	8.1			>1.0
1976	Gazli, U.S.S.R.	6.9	?	0.72	1.36
1979	Imperial Valley, U.S.A.	6.6	4	0.44	1.64
1984	West Hagano, Japan	6.9			>1.0
1985	Nahanni, Canada	6.9	?	1.34	2.37
1990	Philippine	7.8			>1.0
1994	Norridge, U.S.A.	6.7	29	0.94	1.56
1997	Umbria-Marche, Italy	6.0			>1.0
2003	Miyagi-Oki	7.0	81	0.74	1.30
2008	East Honshu, Japan	6.9	8	1.46	3.94
2011	Tohoku, Japan	9.0	131	2.75	1.92

Ground motions with high PGAs are usually, but not always, more destructive than motions with lower peak accelerations. Very high peak accelerations that last for only a very short period of time may cause little damage to many types of structures. A number of earthquakes have produced peak accelerations in excess of 0.5 g but caused no significant damage to structures because the peak accelerations occurred at very high frequencies and the duration of the earthquake was not long. Although peak acceleration is a very useful parameter, it provides no information on the frequency



content or duration of the motion; consequently, it must be supplemented by additional information to characterize a ground motion accurately.

The horizontal peak ground velocity (PGV) is another useful parameter for characterization of ground motion amplitude. Since the velocity is less sensitive to the higher-frequency components of the ground motion, as illustrated in Fig. 4.1, the PHV is more likely than the PGA to characterize ground motion amplitude accurately at intermediate frequencies. For structures or facilities that are sensitive to loading in this intermediate-frequency range (e.g., tall or flexible buildings, bridges, etc.), the PHV may provide a much more accurate indication of the potential for damage than the PGA. PGV has also been correlated to earthquake intensity.

Recent developments have highlighted the importance of displacement in capacity designing and the earthquake resistant design of structures has become performance-based. For this reason, the basic descriptor of the seismic demand is the structure displacement caused by the ground shaking, that can be represented by the displacement response spectrum (Cauzzi and Faccioli, 2008). Peak ground displacements (PGDs) are generally associated with the lower-frequency components of an earthquake motion. They are, however, often difficult to determine accurately, due to signal processing errors in the filtering and integration of accelerograms and due to long-period noise. As a result, peak displacement is less commonly used as a measure of ground motion than is peak acceleration or peak velocity.

Although the parameters discussed previously are easily determined, they describe only the peak amplitudes, of single cycles within the ground motion time history. In some cases, damage may be closely related to the peak amplitude, but in others it may require several repeated cycles of high amplitude to develop. Newmark and Hall (1982) described the concept of an effective acceleration as "that acceleration which is most closely related to structural response and to damage potential of an earthquake. It differs from, and is less than, the PGA. It is a function of the size of the loaded area, the frequency content of the excitation, which in turn depends on the closeness to the source of the earthquake, and to the weight, embedment, damping characteristic, and stiffness of the structure and its foundation".

Some time histories are characterized by single-cycle peak amplitudes that are much greater than the amplitudes of other cycles. An example of such a case is the Stone Canyon record shown in Fig. 4.3a. These single cycles often occur at high frequencies and consequently have little effect on structures with lower natural frequencies. In other time histories, such as the Koyna record of Fig. 4.3b, a number of peaks of similar amplitude are observed.

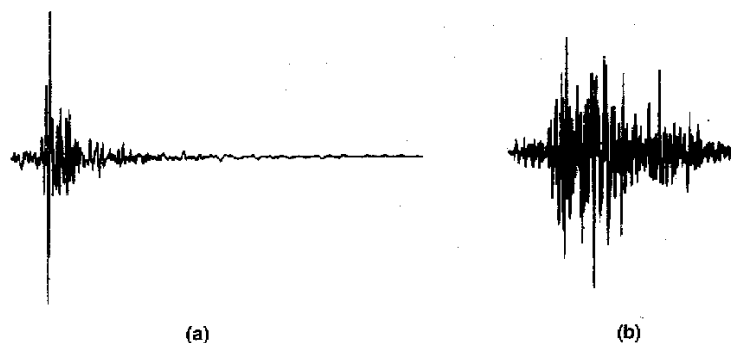


Fig. 4.3 - Accelerograms of: a) the 1972 Stone Canyon ( $M=4.6$ ) earthquake and b) the 1967 Koyna ( $M=6.5$ ) earthquake. The time and acceleration scales are identical for both records. Peak accelerations are very close, illustrating the limitations of using peak amplitude as a sole measure of strong ground motion (from Kramer, 1996).

Nuttl (1979) used lower peaks of the accelerogram to characterize strong motion by defining the sustained maximum acceleration for three (or five) cycles as the third (or fifth) highest (absolute) value of acceleration in the time history. The sustained maximum velocity was defined similarly. Although the PGA values for the 1972 Stone Canyon earthquake and 1967 Koyna earthquake records (Fig. 4.3) were nearly the same, a quick visual inspection indicates that their sustained maximum accelerations (three- or five-cycle) were very different. For a structure that required several repeated cycles of strong motion to develop damage, the Koyna motion would be much more damaging than the

Stone Canyon motion, even though they had nearly the same PGA. For these motions, the sustained maximum acceleration would be a better indicator of damage potential than the PGA.

The notion of an effective design acceleration, with different definitions, has been proposed. Since pulses of high acceleration at high frequencies induce little response in most structures. It was proposed that an effective design acceleration be taken as the peak acceleration that remains after filtering out accelerations above 8 to 9 Hz. It was also proposed that the effective design acceleration be 25% greater than the third highest (absolute) peak acceleration obtained from a filtered time history.

#### 4.1.2. Frequency content parameters

Only the simplest of analyses are required to show that the dynamic response of compliant objects, be they buildings, bridges, slopes, or soil deposits, is very sensitive to the frequency at which they are loaded. Earthquakes produce complicated loading with components of motion that span a broad range of frequencies. The frequency content describes how the amplitude of a ground motion is distributed among different frequencies. Since the frequency content of an earthquake motion will strongly influence the effects of that motion, characterization of the motion cannot be complete without consideration of its frequency content.

##### 4.1.2.1. Ground motion spectra

Any periodic function (i.e., any function that repeats itself exactly at a constant interval) can be expressed using Fourier analysis as the sum of a series of simple harmonic terms of different frequency, amplitude, and phase. Using the Fourier series, a periodic function,  $x(t)$ , can be written as

$$x(t) = c_0 + \sum_{n=1}^{\infty} c_n \sin(\omega_n t + \Phi_n) \quad (4-1)$$

In this form,  $c_n$  and  $\Phi_n$  are the amplitude and phase angle, respectively, of the  $n$ th harmonic of the Fourier series. The Fourier series provides a complete description of the ground motion since the motion can be completely recovered by the inverse Fourier transform.

A plot of Fourier amplitude versus frequency [ $c_n$  versus  $\omega_n$  from Eq. (4-1)] is known as a Fourier amplitude spectrum; a plot of Fourier phase angle ( $\Phi_n$  versus  $\omega_n$ ) gives the Fourier phase spectrum. The Fourier amplitude spectrum of a strong ground motion shows how the amplitude of the motion is distributed with respect to frequency (or period). It expresses the frequency content of a motion very clearly.

The Fourier amplitude spectrum may be narrow or broad. A narrow spectrum implies that the motion has a dominant frequency (or period), which can produce, a smooth, almost sinusoidal time history. A broad spectrum corresponds to a motion that contains a variety of frequencies that produce a more jagged, irregular time history. The Fourier amplitude spectra for the E-W components of the Gilroy No. 1 (rock) and Gilroy No. 2 (soil) motions (Fig. 4.1) are shown in Fig. 4.4. The jagged shapes of the spectra are typical of those observed for individual ground motions. The shapes of the spectra are quite different: the Gilroy No. 1 (rock) spectrum is strongest at low periods (or high frequencies) while the reverse is observed for the Gilroy No. 2 (soil) record. A difference in frequency content can be detected by closely examining the motions in the time domain, but the difference is explicitly illustrated by the Fourier amplitude spectra.

When the Fourier amplitude spectra of actual earthquake motions are smoothed and plotted on logarithmic scales, their characteristic shapes can be seen more easily. As illustrated in Fig. 4.5, Fourier acceleration amplitudes tend to be largest over an intermediate range of frequencies bounded by the corner frequency  $f_c$  on the low side and the cutoff frequency  $f_{max}$  on the high side. The corner frequency can be shown theoretically to be inversely proportional to the cube root of the seismic moment. This result indicates that large earthquakes produce greater low-frequency motions than do

smaller earthquakes. The cutoff frequency is not well understood; it has been characterized both as a near-site effect and as a source effect, and is usually assumed to be constant for a given geographic region.

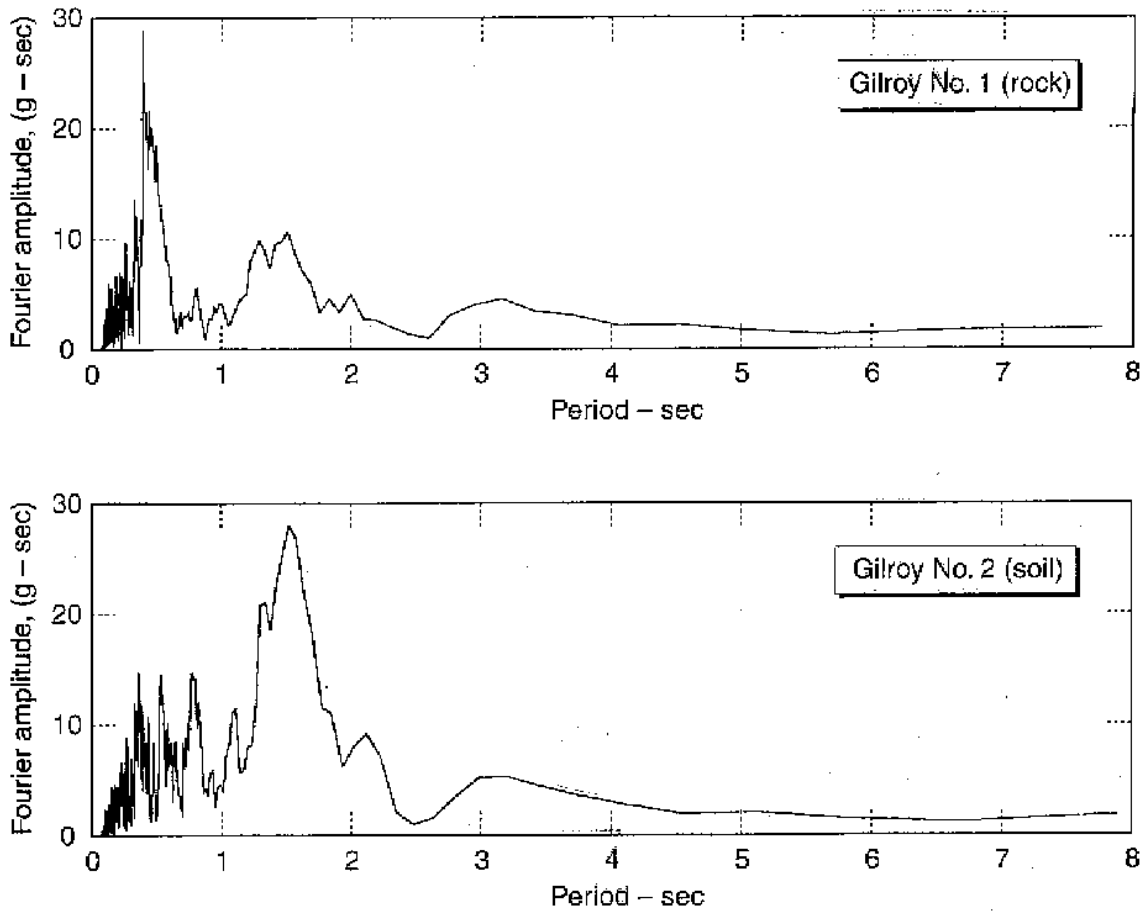


Fig. 4.4 - Fourier amplitude spectra for the E-W components of the Gilroy No. 1 (rock) and Gilroy No. 2 (soil) strong motion records (Fig. 4.1). Fourier spectra were obtained by discrete Fourier transform and consequently have units of velocity. Fourier amplitude spectra can also be plotted as functions of frequency.

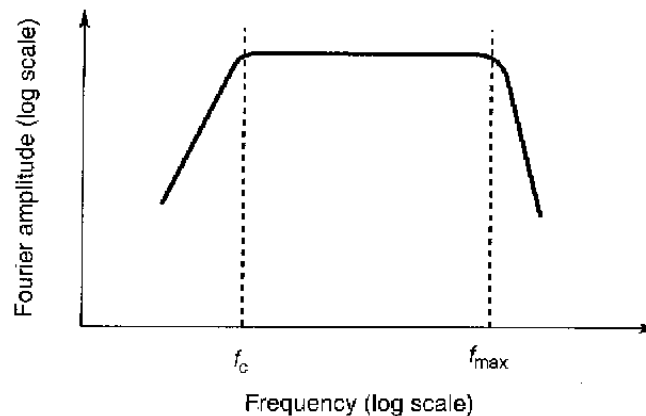


Fig. 4.5 - Idealized shape of smoothed Fourier amplitude spectrum illustrating the corner frequency  $f_c$  and cutoff frequency  $f_{max}$ .

The frequency content of a ground motion can also be described by a power spectrum or power spectral density function. The power spectral density function can also be used to estimate the statistical properties of a ground motion and to compute stochastic response using random vibration

techniques. The power spectral density function is useful in characterizing the earthquake as a random process. The power spectral density function by itself can describe a stationary random process (i.e., one whose statistical parameters do not vary with time). Actual strong motion accelerograms, however, frequently show that the intensity builds up to a maximum value in the early part of the motion, then remains approximately constant for a period of time, and finally decreases near the end of the motion. Such nonstationary random process behaviour is often modelled by multiplying a stationary time history by a deterministic intensity function.

A third type of spectrum is used extensively in earthquake engineering practice. The response spectrum describes the maximum response of a single-degree-of-freedom (SDOF) system to a particular input motion as a function of the natural frequency (or natural period) and damping ratio of the SDOF system. Computed response spectra for the Gilroy No. 1 (rock) and Gilroy No. 2 (soil) records (Fig. 4.1) are illustrated in Fig. 4.6.

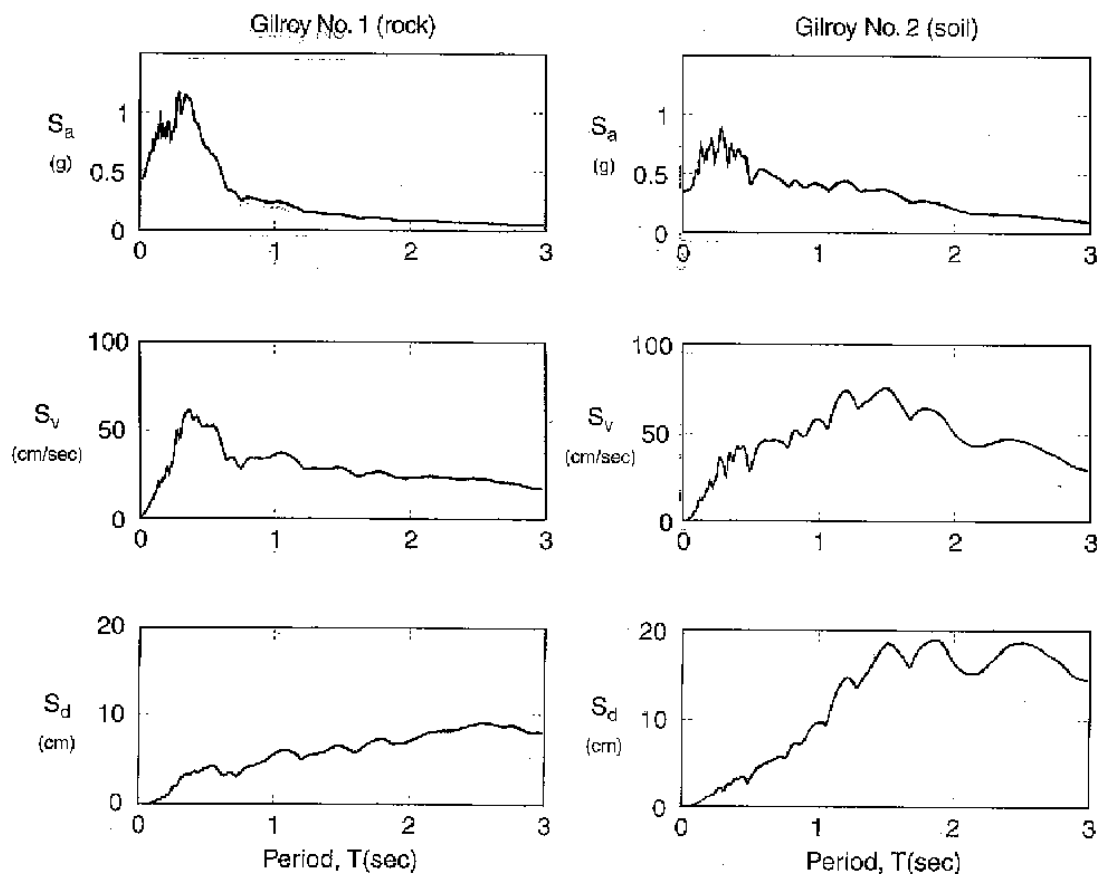


Fig. 4.6 - Response spectra (5% damping) for Gilroy No. 1 (rock) and Gilroy No. 2 (soil) strong motion records (Fig. 4.1). The frequency contents of the two motions are reflected in the response spectra. The Gilroy 1 (rock) motion, for example, produced higher spectral accelerations at low periods than did the Gilroy 2 (soil) motion, and lower spectral accelerations at higher periods. The higher long period content of the Gilroy 2 (soil) motion produced spectral velocities and displacements much higher than those of the Gilroy (rock) motion.

A response spectrum is simply a plot of the peak or steady-state response (displacement, velocity, or acceleration) of a series of oscillators of varying natural frequency, that are forced into motion by the same base vibration (Fig. 4.7a). The resulting plot can then be used to pick off the response of any linear system, given its natural frequency of oscillation (Fig. 4.7b). One such use is in assessing the peak response of buildings to earthquakes. The science of strong ground motion may use some values from the ground response spectrum (calculated from recordings of surface ground motion from seismographs) for correlation with seismic damage.

If the input used in calculating a response spectrum is steady-state periodic, then the steady-state result is recorded. Damping must be present, or else the response will be infinite. For transient input (such as seismic ground motion), the peak response is reported. Some level of damping is

generally assumed, but a value will be obtained even with no damping. The main limitation of response spectra is that they are only universally applicable for linear systems.

Response spectra are very useful tools for analyzing the performance of structures and equipment in earthquakes, since many behave principally as SDOFs. Thus, if you can find out the natural frequency of the structure, then the peak response of the building can be estimated by reading the value from the ground response spectrum for the appropriate frequency. In most building codes in seismic regions, this value forms the basis for calculating the forces that a structure must be designed to resist (seismic analysis).

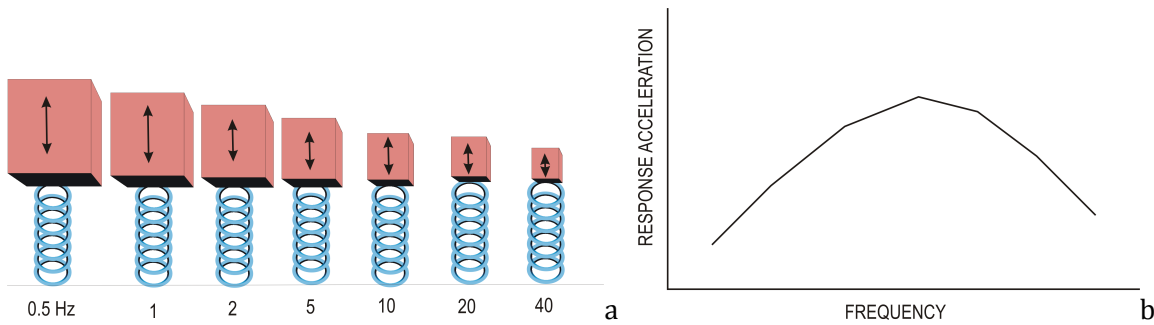


Fig. 4.7 – Basics of response spectrum: a) series of mixed vertical oscillators; b) a plot of the peak acceleration for the mixed vertical oscillators.

As mentioned earlier, the ground response spectrum is the response plot done at the free surface of the Earth. Significant seismic damage may occur if the building response is 'in tune' with components of the ground motion (resonance), which may be identified from the response spectrum. This was observed in the 1985 Mexico City earthquake where the oscillation of the deep-soil lakebed was similar to the natural frequency of mid-rise concrete buildings, causing significant damage. Shorter (stiffer) and taller (more flexible) buildings suffered less damage.

In 1941 at Caltech, George Housner began to publish calculations of response spectra from accelerographs (Housner, 1941). In the 1982 EERI Monograph on "Earthquake Design and Spectra", Newmark and Hall (1982) describe how they developed an "idealized" seismic response spectrum based on a range of response spectra generated for available earthquake records (Fig. 4.8). This was then further developed into a design response spectrum for use in structural design, and this basic form (with some modifications) is now the basis for structural design in seismic regions throughout the world (typically plotted against structural "period", the inverse of frequency). A nominal level of damping is assumed (5% of critical damping). The design response spectrum is, then, a simplified spectrum that simulates in a quasi conservative way all response spectra expected for the site. It is presently obtained from the values of PGA, spectral acceleration at 0.2 s (SA0.2), and spectral acceleration at 1.0 s (SA1.0) reported in the seismic hazard maps (Fig. 4.9).

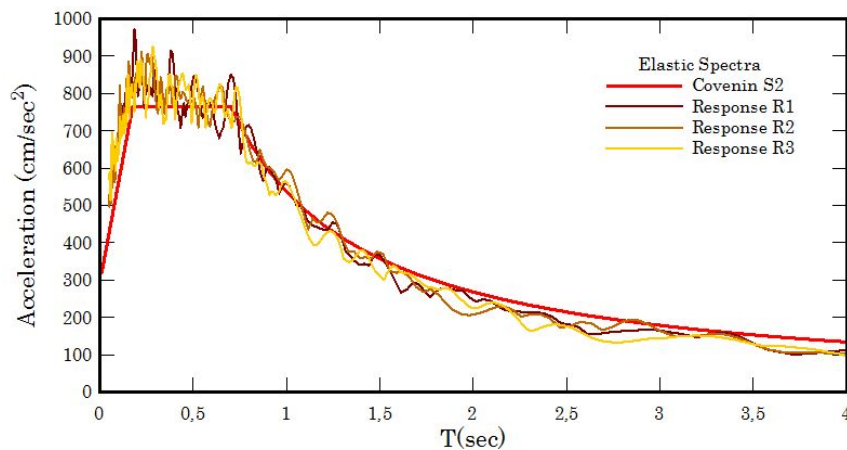


Fig. 4.8 – The design response spectrum.



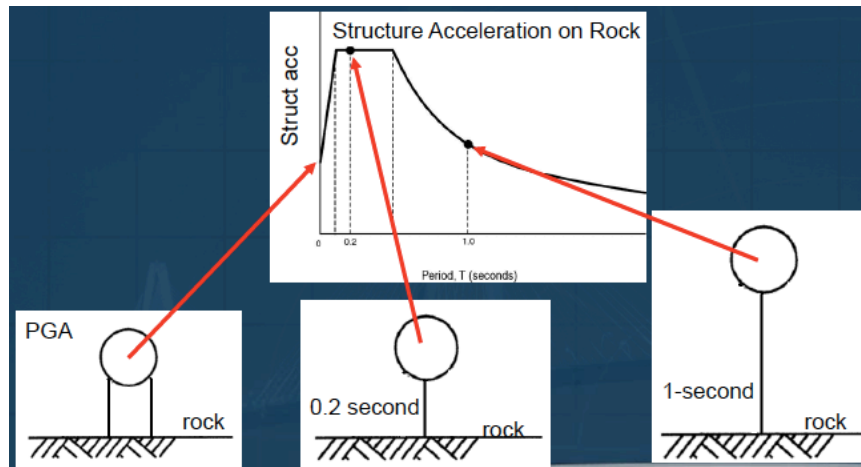


Fig. 4.9 – The construction of the design response spectrum.

For "regular" low-rise buildings, the structural response to earthquakes is characterized by the fundamental mode (a "waving" back-and-forth), and most building codes permit design forces to be calculated from the design spectrum on the basis of that frequency, but for more complex structures, combination of the results for many modes (calculated through modal analysis) is often required. In extreme cases, where structures are either too irregular, too tall or of significance to a community in disaster response, the response spectrum approach is no longer appropriate, and more complex analysis is required, such as non-linear static or dynamic analysis. The behaviour of a complex structure can be, then, modelled as a superposition of SDOFs. The elastic response spectrum presents the maximum response of a suite of damped SDOF oscillators to a given ground motion (Newmark and Hall, 1982).

Response spectra may be plotted individually to arithmetic scales, or may be combined in tripartite plots. The tripartite plot displays spectral velocity on the vertical axis, natural frequency (or period) on the horizontal axis, and acceleration and displacement on inclined axes. The acceleration and displacement axes are reversed when the spectral values are plotted against natural period rather than natural frequency. The shapes of typical response spectra indicate that peak spectral acceleration, velocity, and displacement values are associated with different frequencies (or periods). At low frequencies the average spectral displacement is nearly constant; at high frequencies the average spectral acceleration is fairly constant. In between lies a range of nearly constant spectral velocity. Because of this behaviour, response spectra are often divided into acceleration-controlled (high-frequency), velocity-controlled (intermediate-frequency), and displacement-controlled (low-frequency) portions.

Elastic response spectra assume linear structural force-displacement behaviour. For many real structures, however, inelastic behaviour may be induced by earthquake ground motions. Fig. 4.10 shows inelastic response spectra for acceleration and yield displacement for various values of the ductility factor  $\mu = u_{max} / u_y$ , where  $u_{max}$  is the maximum allowable displacement and  $u_y$  is the yield displacement. A separate inelastic spectrum must be plotted to show total (elastic plus plastic) displacement. Spectral accelerations decrease with increasing ductility, but total displacements increase.

Response spectra reflect strong ground motion characteristics indirectly, since they are "filtered" by the response of a SDOF structure. The amplitude, frequency content, and to a lesser extent, duration of the input motion all influence spectral values. The different frequency contents of the Gilroy No. 1 (rock) and Gilroy No. 2 (soil) ground motions are clearly illustrated by the different shapes of their respective response spectra (Fig. 4.6).

It is important to remember that response spectra represent only the maximum responses of a number of different structures. However, the response of structures is of great importance in earthquake engineering, and the response spectrum has proven to be an important and useful tool for characterization of strong ground motion.

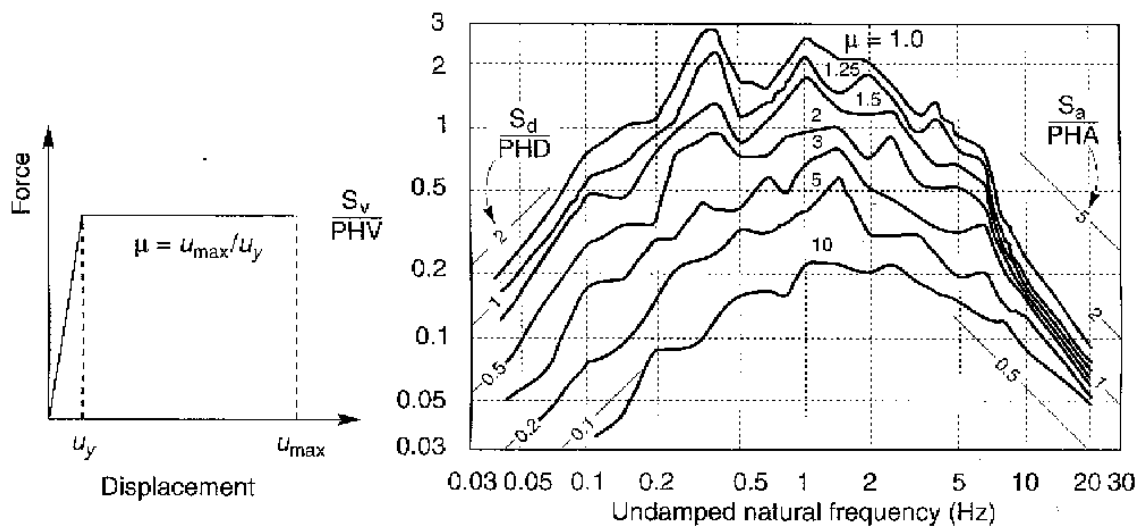


Fig. 4.10 – Inelastic response spectra for the El Centro N-S component of the 1940 Imperial Valley earthquake. Only the elastic component of the displacement is plotted. Spectral accelerations are correct, but spectral velocities are not (from Kramer, 1996).

The spectral displacement (SD) response spectrum can be expressed as:

$$SD(w,b) = \max a(t) * I(t | w, b) \quad (4-2)$$

where  $w$  and  $b$  are the natural frequency and damping coefficients of a SDOF oscillator,  $a(t)$  is the ground acceleration at time “ $t$ ”,  $I(t | w, b)$  is the relative displacement of the oscillator with respect to the ground in response to an acceleration impulse (a Dirac delta function). For a given time series and damping coefficient, a spectrum can be constructed by convolving the acceleration time series with the impulse response and determining the maximum response values for a suite of oscillator frequencies ( $w$ ). Such a spectrum constitutes the relative displacement response spectrum for a specific value of damping. Note that the spectrum is a function of the driving acceleration,  $a(t)$ . To the extent that a structure can be represented by a SDOF oscillator, the maximum deflection of the centre of mass can be determined directly from the SD spectrum. More complex structures can be analyzed using the principle of modal superposition (Newmark and Hall, 1982).

The pseudo-spectral velocity (PSV) spectrum is related to the relative displacement spectrum by:

$$PSV(w, b) = wSD(w, b) \quad (4-3)$$

The PSV spectrum closely approximates the maximum relative velocity of the oscillator at oscillator frequencies close to the dominant frequency of the ground acceleration. At very high and very low oscillator frequencies, the PSV spectrum approaches zero. The PSV spectrum closely follows the Fourier amplitude spectrum of the ground acceleration, for  $b=0$ . Usually, the PSV response spectrum is calculated for 5% critical damping ( $b=0.05$ ).

In the past, much engineering analysis was performed using “standard” response spectra scaled according to the PGA expected for a given hazard scenario at a particular site. With the availability of a huge variety of records in the strong motion data bank, it is now possible to choose a specific accelerometric time history for the study site according to the magnitude and distance of its scenario earthquake, and derive directly the response spectrum from the accelerometric time history. Recently, models have been developed that allow prediction of the spectrum over a range of oscillator frequencies for an earthquake of given magnitude at a given distance from a site. Uniform hazard response spectra, which have equal probability of exceedance at all oscillator frequencies, can be derived from probabilistic seismic hazard analysis, in which proper spectral attenuation relations are used.

#### 4.1.3. Duration

The duration of strong ground motion can have a strong influence on earthquake damage. Many physical processes, such as the degradation of stiffness and strength of certain types of structures and the buildup of porewater pressures in loose, saturated sands, are sensitive to the number of load or stress reversals that occur during an earthquake. A motion of short duration may not produce enough load reversals for damaging response to build up in a structure, even if the amplitude of the motion is high. On the other hand, a motion with moderate amplitude but long duration can produce enough load reversals to cause substantial damage.

The duration of a strong ground motion is related to the time required for release of accumulated strain energy by rupture along the fault. As the length, or area, of fault rupture increases, the time required for rupture increases. As a result, the duration of strong motion increases with increasing earthquake magnitude. While this relationship has been supported by empirical evidence for many years, advances in source mechanism modelling have provided theoretical support, indicating that the duration should be proportional to the cube root of the seismic moment. When bilateral rupture [i.e., rupture that propagates in opposite directions from the focus (as in the case of the 1989 Loma Prieta earthquake)] occurs, the strong motion duration may be considerably lower.

An earthquake accelerogram generally contains all accelerations from the time the earthquake begins until the time the motion has returned to the level of background noise. For engineering purposes, only the strong-motion portion of the accelerogram is of interest. Different approaches have been taken to the problem of evaluating the duration of strong motion in an accelerogram. The bracketed duration (Bolt, 1969) is defined as the time between the first and last exceedances of a threshold acceleration (usually 0.05 g). Another definition of duration (Trifunac and Brady, 1975) is based on the time interval between the points at which 5% and 95% of the total energy has been recorded. Boore (1983) has taken the duration to be equal to the corner period (i.e., the inverse of the corner frequency). Because it implicitly reflects the strength of shaking, the bracketed duration is most commonly used for earthquake engineering purposes.

The duration of strong motion has been investigated by interpretation of accelerograms from earthquakes of different magnitudes. Using a 0.05 g threshold acceleration, Chang and Krinitzky (1977) estimated the bracketed durations for soil and rock sites at short (less than 10 km) epicentral distances shown in Table 4.3.

Duration has also been expressed in terms of equivalent cycles of ground motion. One such approach was developed in conjunction with an early procedure for evaluation of liquefaction potential (Seed et al., 1975).

Table 4.3 - Typical earthquake durations at epicentral distances less than 10 km.

Magnitude	Duration	
	Rock sites	Soil sites
5.0	4	8
5.5	6	12
6.0	8	16
6.5	11	23
7.0	16	32
7.5	22	45
8.0	31	62
8.5	43	86

#### 4.1.4. Other ground motion parameters

The preceding parameters are related primarily to the amplitude, frequency content, or duration of a ground motion. Since all of these characteristics are important, ground motion parameters that reflect more than one are very useful. The following paragraphs present a number of parameters that reflect two or three important ground motion characteristics.

A single parameter that includes the effects of the amplitude and frequency content of a strong motion record is the rms acceleration, defined as

$$a_{rms} = \sqrt{\frac{1}{T_d} \int_0^{T_d} [a(t)]^2 dt} = \sqrt{\lambda_0} \quad (4-4)$$

where  $T_d$  is the duration of the strong motion and  $\lambda_0$  is the average intensity (or mean-squared acceleration). Because the integral in Eq. (4-4) is not strongly influenced by large, high-frequency accelerations (which occur only over a very short period of time) and because it is influenced by the duration of the motion, the rms acceleration can be very useful for engineering purposes. Its value, however, can be sensitive to the method used to define strong motion duration.

A parameter closely related to the rms acceleration is the Arias intensity, (Arias, 1970), defined as

$$I_a = \frac{\pi}{2g} \int_0^{\infty} [a(t)]^2 dt. \quad (4-5)$$

where  $t$  and  $a$  are the total duration and acceleration of the ground motion, respectively.

The Arias intensity has units of velocity and represents the sum of the total energies, per unit mass, stored, at the end of the earthquake ground motion, in a population of undamped linear oscillators. Since it is obtained by integration over the entire duration rather than over the duration of strong motion, its value is independent of the method used to define the duration of strong motion. Consequently, it could overestimate the intensity of an earthquake with long duration, high acceleration and broad band frequency content.

The characteristic intensity, defined as

$$I_c = a_{rms}^{1.5} T_d^{0.5} \quad (4-6)$$

is related linearly to an index of structural damage due to maximum deformations and absorbed hysteretic energy.

The cumulative absolute velocity (CAV) is simply the area under the absolute accelerogram:

$$CAV = \int_0^{T_d} |a(t)| dt. \quad (4-7)$$

The CAV has been found to correlate well with structural damage potential. For example, a CAV of 0.30 g-s (obtained after filtering out frequencies above 10 Hz) corresponds to the lower limit for VII MM intensity shaking (Benjamin and Associates, 1988).

Since many structures have fundamental periods between 0.1 and 2.5 s, the response spectrum ordinates in this period range should provide an indication of the potential response of these structures. The response spectrum intensity (Housner, 1959) was therefore defined as

$$SI(\xi) = \int_{0.1}^{2.5} PSV(\xi, T) dt \quad (4-8)$$

(i.e., the area under the pseudovelocity response spectrum between periods of 0.1 s and 2.5 s. The response spectrum intensity, as indicated in Eq. (4-8), can be computed for any structural damping ratio. It captures important aspects of the amplitude and frequency content (in the range of primary importance for structures) in a single parameter.

Von Thun et al. (1988) referred to the response spectrum intensity for 5% damping as the velocity spectrum intensity. The velocity spectrum intensity was suggested as being useful for evaluation of the response of Earth and rockfill dams, which typically have fundamental periods between 0.6 and 2.0 s. To characterize strong ground motion for analysis of concrete dams, which

generally have fundamental periods of less than 0.5 s, Von Thun et al. (1988) introduced the acceleration spectrum intensity, defined as

$$ASI = \int_{0.1}^{0.5} S_a(\xi = 0.05, T) dt \quad (4-9)$$

(i.e., the area under the acceleration response spectrum between periods of 0.1 and 0.5 s).

The Applied Technology Council (1978) defined two factors by which standard response spectra could be normalized. The effective peak acceleration (EPA) was defined as the average spectral acceleration over the period range 0.1 to 0.5 s divided by 2.5 (the standard amplification factor for a 5% damping spectrum). The effective peak velocity (EPV) was defined as the average spectral velocity at a period of 1 s divided by 2.5. Determination of EPA and EPV is shown schematically in Fig. 4.11. The process of averaging the spectral accelerations and velocities over a range of periods minimizes the influence of local spikes in the response spectrum on the EPA and EPV. The EPA and EPV have been used in the specification of smoothed design response spectra in building codes.

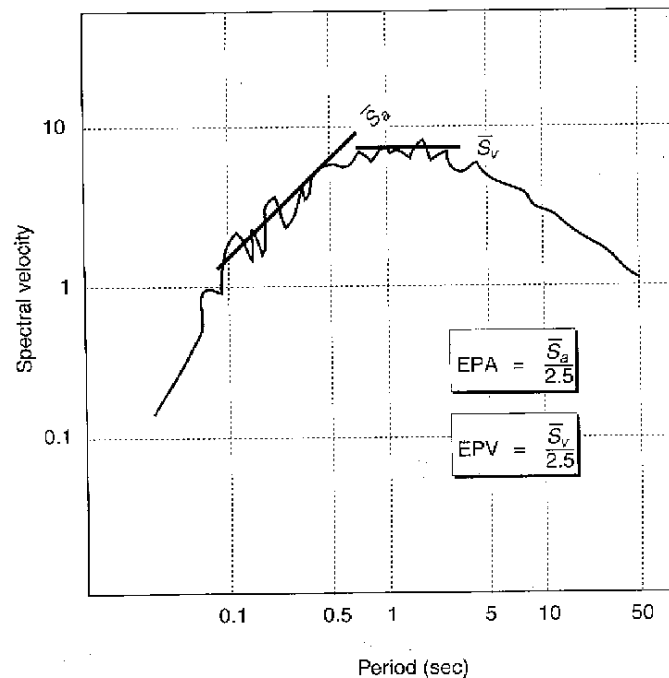


Fig. 4.11 - Determination of EPA and EPV from response spectra (from Kramer, 1996).

## 4.2. Development of predictive relationships

Earthquake ground motions have been recorded by seismographs since the early 20th century. Major initiatives to instrument seismically active regions around the world were then undertaken, and these instruments have provided a large inventory of recordings. Data from this inventory are used to develop attenuation relationships (ground motion prediction equations: GMPEs), which are either fully empirical, or rely on empirical data to calibrate theoretical stochastic models.

Two types of attenuation relations [presently, the term ground motion prediction equations (GMPEs) is widely used] can be computed:

- **empirical:** based on recorded data
- **stochastic:** computed according to a model.

If there is insufficient amount of ground motion recordings to develop empirically-based equations it is possible to generate ground motions using stochastic methods to supplement existing recordings. These methods are commonly used for ground motion estimation in stable tectonic



regions and for high frequency motions characterized by a large magnitude and short source-to-site distance.

The standard stochastic method is based on the assumption that the far-field shear wave energy generated by an earthquake source can be represented as a band-limited random process. Under this assumption ground motions can be represented as a band-limited, finite duration, white Gaussian noise.

A general form of the ground motion amplitude spectrum can be expressed as:

$$Y(M_0, R, f) = E(M_0, f) \times P(R, f) \times G(f) \times I(f) \quad (4-10)$$

where  $E$  is the source contribution [e.g.,  $\omega^2$  model by Aki (1967)],  $P$  is the path contribution (geometric spreading and anelastic attenuation),  $G$  is the site contribution,  $I$  is the type of motion contribution (displacement, velocity, acceleration or the response of oscillator (from which response spectra can be derived).

Predictive relationships of the expected ground motion (in the past mainly PGA) are nearly always obtained empirically by least squares regression on a particular set of strong motion data. Despite attempts to remove questionable data and the use of quality-based weighting schemes, some amount of scatter in the data is inevitable. The scatter results from randomness in the mechanics of rupture and from variability and heterogeneity of the source, travel path, and site conditions. Scatter in the data can be quantified by confidence limits or by the standard deviation of the predicted parameter. Reflecting the form of most predictive relationships, the standard deviation of the logarithm of the predicted parameter is usually computed. This considerable (aleatory) uncertainty must be accounted for in computation of seismic hazard.

Moreover, despite the large ground motion inventory, the strong motion data set remains poorly sampled for the development of attenuation relations. To illustrate this point, Fig. 4.12 shows the magnitudes and distances that are sampled in the worldwide ground motion inventory of recordings from shallow crustal earthquakes in active tectonic regions. The horizontal lines of dots are in most cases single events that were well recorded. The sampling problems with the inventory are twofold. First, there are only 82 recordings of large magnitude earthquakes ( $m > 7$ ) at close distance ( $r < 20$  km), and 59 of these are from a single event ( $m 7.6$  1999 Chi Chi, Taiwan). This range of  $m$  and  $r$  is critical for seismic design practice in active tectonic regions, and the lack of data leads to significant epistemic uncertainty (i.e., uncertainty about the proper form of attenuation functions).

The second sampling problem is associated with the fact that the data set is dominated by a few well-recorded events. For example, the data set in Fig. 4.12 contains approximately 1800 recordings, but 1055 of these are from only 8 earthquakes ( $m 6.6$  1971 San Fernando, California;  $m 6.5$  1979 Imperial Valley, California;  $m 6.4$  1983 Coalinga, California;  $m 6.0$  1987 Whittier, California;  $m 6.9$  1989 Loma Prieta, California;  $m 7.3$  1992 Landers, California;  $m 6.7$  1994 Northridge, California;  $m 7.6$  1999 Chi Chi, Taiwan). While these well-recorded events allow for robust quantification of intra-event aleatory variability of ground motion (random variability within an event), this clustering of data in a few events is not sufficient to unambiguously evaluate inter-event aleatory variability (random variability across events). Stated another way, if inter-event variability were negligible, attenuation relations could be developed by weighting each data point equally, whereas if intra-event variability were negligible, the collective data from each event would be weighted equally. As neither source of variability is small, an important question is how data from sparsely and well-recorded events should be weighted relative to each other in the regression analysis.

A wide range of procedures for data analysis of GMPEs have been developed, each attempting to properly quantify the overall aleatory variability (i.e., sum of inter- and intra-event variability). Among the many, two procedures are the simplest and most popular. A two-step regression procedure was proposed by Joyner and Boore (1981) in which: 1) all data points are weighted equally to derive the shape of the function describing the variation of ground motion with distance (i.e., the change of PGA with changes in  $r$ ), and 2) all events are weighted equally to derive the magnitude dependence of ground motion (i.e., the change of PGA with changes in  $m$ ). Campbell (1981) suggested a weighted least squares regression in which: 1) the ground motion inventory (e.g., Fig. 4.12) is first binned according to  $m$  and  $r$  (i.e., all data within a limited range of  $m$  and  $r$  is placed into a bin), 2) each bin of data is given equal weight in the regression, and 3) within a bin, the collective data from each event

are weighted equally.

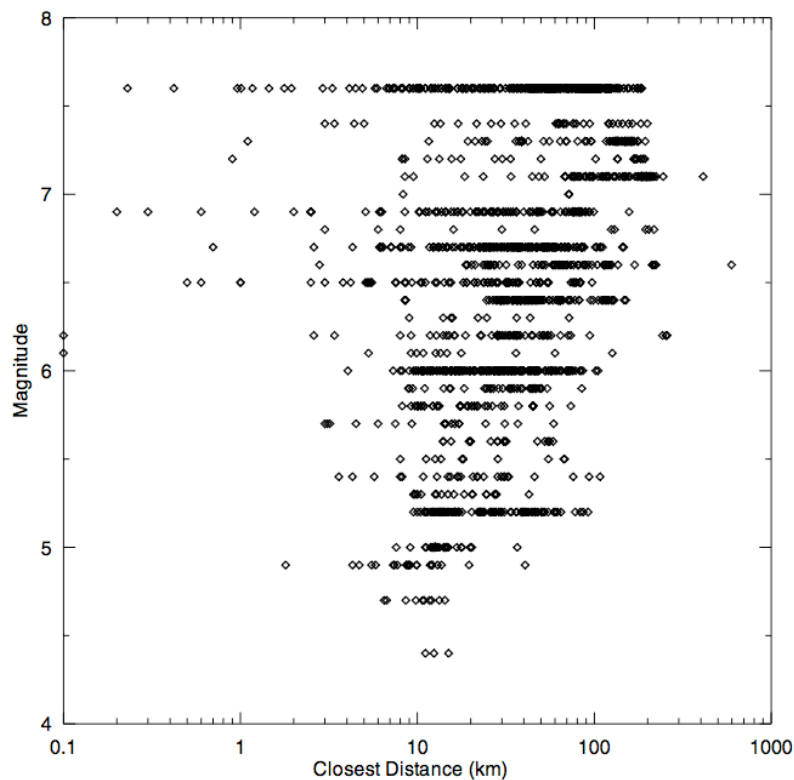


Fig. 4.12 - Inventory of strong motion recordings (1933 to 1999) from shallow crustal earthquakes in active tectonic regions (from Stewart et al., 2001).

Predictive relationships usually express ground motion parameters as function of magnitude, distance, and in some cases, other variables, for example

$$Y = f(M, R, P_i) \quad (4-11)$$

where  $Y$  is the ground motion parameter of interest,  $M$  the magnitude of the earthquake,  $R$  a measure of the distance from the source to the site being considered, and the  $P_i$  are other parameters (which may be used to characterize the earthquake source, wave propagation path, and/of local site conditions). Predictive relationships are developed by regression analyses of recorded strong motion databases. As such, they change with time as additional strong motion data become available. Most predictive relationships are updated in the literature every 3 to 5 years or shortly after the occurrence of large earthquakes in well-instrumented regions.

The functional form of the predictive relationship is usually selected to reflect the mechanics of the ground motion process as closely as possible. This minimizes the number of empirical coefficients and allows greater confidence in application of the predictive relationship to conditions (magnitudes and distances) that are poorly represented in the database. Common forms for predictive relationships are based on the following observations.

1. Peak values of strong motion parameters are approximately lognormally distributed (i.e., the logarithms of the parameters are approximately normally distributed). As a result, the regression is usually performed on the logarithm of  $Y$  rather than on  $Y$  itself.
2. Earthquake magnitude is typically defined as the logarithm of recorded peak amplitude. Consequently, the logarithm of  $Y$  should be approximately proportional to  $M$ .
3. The spreading of stress waves as they travel away from the source of an earthquake causes body wave (P- and S-wave) amplitudes to decrease according to  $1/R$  and surface wave (primarily Rayleigh wave) amplitudes to decrease according to  $1/R^{1/2}$ .
4. The area over which fault rupture occurs increases with increasing earthquake magnitude. As a result, some of the waves that produce strong motion at a site arrive from a distance,  $R$ , and some

arrive from greater distances. The effective distance, therefore, is greater than  $R$  by an amount that increases with increasing magnitude.

5. Some of the energy carried by stress waves is absorbed by the materials they travel through (material damping). This material damping causes ground friction amplitudes to decrease exponentially with  $R$ .
6. Ground motion parameters may be influenced by source characteristics (e.g., strike-slip, normal or reverse faulting) or site characteristics (e.g., hard rock, soft rock, alluvium, etc.).

The general form of the GMPEs is the following:

$$\ln y = \underbrace{c_1}_{(1)} + \underbrace{c_2 m + c_3 m^{c_4}}_{(2)} + \underbrace{c_5 \ln r}_{(3)} + \underbrace{f(F) + f(HW) + f(S)}_{(4)} \quad (4-12)$$

where  $c_1$  to  $c_5$  are constants computed by the regression,  $F$  is a factor related to the source rupture mechanism,  $HW$  is a hanging wall factor for dip-slip faults, and  $S$  is a site factor. Term  $m$  represents magnitude. Term  $r$  represents site-source distance, and is measured differently by different investigators (Fig. 4.13). Explanations for the numbered terms in Eq. (4-12) are as follows:

1. as noted previously,  $y$  is generally log-normally distributed, hence regressions are performed on the natural or decimal logarithm of the data, which is normally distributed;
2. source: several magnitude scales are derived from the logarithm of various peak ground motion parameters. Consequently,  $\ln y$  is approximately proportional to  $m$ . However, data from recent earthquakes suggest that this proportionality may break down for high-frequency ground motion parameters (e.g., PGA) at large magnitudes;
3. path: as body waves travel away from a seismic source, geometric spreading reduces their amplitude by  $1/r$  (term  $c_5$  is usually close to  $-1.0$ );
4. site: fault rupture mechanism ( $F$ ), the location of a site on or off the hanging wall of dip-slip faults ( $HW$ ), and local site conditions ( $S$ ) are observed to affect ground motion.

The geometrical spreading is caused by the fact that, as the seismic wave moves away from the source, the area that the energy covers becomes larger and thus intensity decreases. The anelastic attenuation factor, often expressed as seismic quality factor or  $Q$  (which is inversely proportional to attenuation factor), quantifies the effects of anelastic attenuation on the seismic wavelet caused by fluid movement and grain boundary friction. As a seismic wave propagates through a medium, the elastic energy associated with the wave is gradually absorbed by the medium, eventually ending up as heat energy. This is known as absorption (or anelastic attenuation) and will eventually cause the total disappearance of the seismic wave.

Worldwide earthquakes occur in one of three tectonic regimes: active tectonic regions, subduction zones, and stable continental regions. Very little strong motion data are available for stable continental regions, and as a result, attenuation relationships are generally based on simulated ground motions instead of recordings (stochastic models).

The strike-slip mechanism is generally taken as a "reference" mechanism, and no correction is necessary [i.e.,  $f(F) = 0$  in Eq. (4-12)]. Significant differences are observed between reverse earthquake motions and strike-slip. No corrections are generally made for normal-slip earthquakes, although a separate set of attenuation relations is necessary for extensional tectonic regimes. Relatively little data are available for oblique-slip earthquakes, and the  $f(F)$  correction for oblique-slip is often taken as half of  $f(F)$  for reverse earthquakes. Studies have shown that there is a significant increase in ground motions for sites located over the hanging wall of dipping faults. In the case of the 1994 Northridge earthquake, analyses have shown that this increase can be by as much as 50%. This effect is primarily a geometric effect since sites located on the hanging wall are closer to a larger area of the source than the footwall sites.

Some attenuation models use a simple rock/soil classification of ground conditions, setting  $S=1$  for soil and  $S=0$  for rock. Alternatively, a site classification in rock, stiff soil, soft soil, and very soft soil has been proposed and the related parameters have been computed (e.g., Ambraseys et al., 1996). The

limited number of strong motion recordings for the different terrains and the uncertain site classification have weakened the results of the analyses performed.

Some simulation studies using finite faults have shown the need to consider a magnitude-dependent form in the general attenuation relation:

$$\log Y = c_1 + c_2 M + c_3 r + c_4 \log r \quad (4-13)$$

In such models  $dY/dM$  increases with increasing distance at the same time that it decreases with increasing magnitude. Distance attenuation curves become closer as magnitude increases, while their slope tends to diminish. It was often demonstrated as well that the term for anelastic attenuation does not contribute significantly to a better description of the data. Then, the following functional form is adopted:

$$\log Y = a + (b + cM)M + (d + eM^3) \log r \quad (4-14)$$

In the equation the term for anelastic attenuation is dropped, while magnitude scaling ( $c_2$ ) decreases linearly with  $M$  through parameters  $b$  and  $c$ , where  $c$  is expected to be negative. The slope in the far field ( $c_4$ ) depends on the cube of  $M$  through parameters  $d$  and  $e$ . Such parameters should be negative and positive respectively.

The error term ( $\sigma_{mY}$ ) in attenuation relations are generally either constant or functions of magnitude: available data generally indicate a decrease of standard error with increasing magnitude.

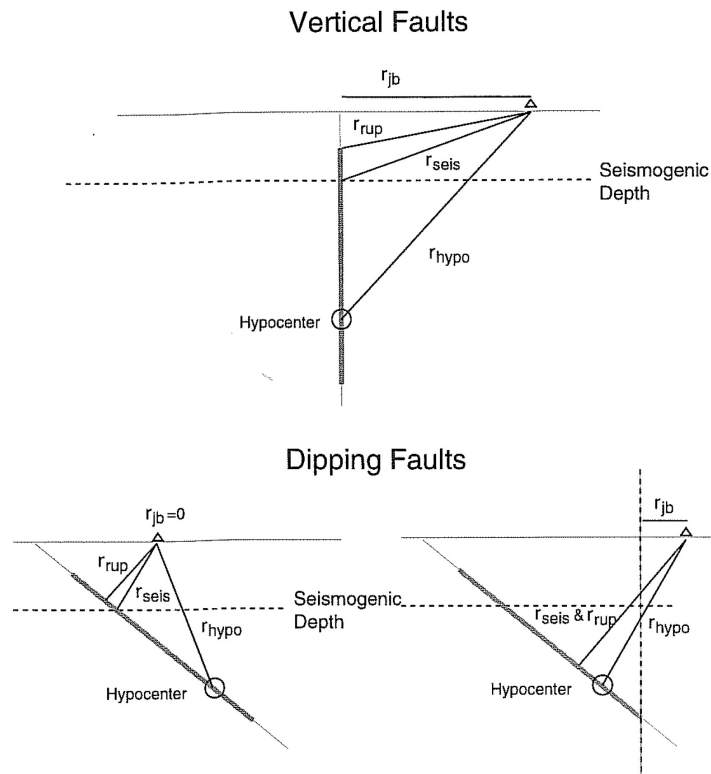


Fig. 4.13 - Site-to-source distance measures for ground motion attenuation models (from Abrahamson and Shedlock, 1997).

The  $\sigma_{mY}$  term describes uncertainty in the value of the ground motion parameter given by the predictive relationship. Statistically, it represents an estimate of the standard deviation of  $\ln Y$  at the magnitude and distance of interest. At a given magnitude, therefore, the probability that the ground motion parameter will exceed a value  $Y^*$  would be  $1 - F_Z(z^*)$  where  $F_Z(z^*)$  is the value of the standard CDF at  $z^* = (\ln Y^* - \overline{\ln Y}) / \sigma_{\ln Y}$  (introducing the standard normal variable of the Gaussian distribution).

When using any predictive relationship, it is very important to know how parameters such as  $M$  and  $R$  are defined and to use them in a consistent manner. It is also important to recognize that different predictive relationships are usually obtained from different data sets. To make reasonable predictions of ground motion parameters, a predictive relationship based on data that are consistent with the conditions relevant to the prediction is required.

Concerning the distance, it is important to point out the different metrics used in the attenuation models (Fig. 4.14):

1.  $r_{jb}$ , the closest horizontal distance to the vertical projection of the rupture (Joyner-Boore distance);
2.  $r_{rup}$ , the closest distance to the rupture surface;
3.  $r_{seis}$ , the closest distance to the seismogenic rupture surface (assumes that near-surface rupture in the sediments is not seismogenic);
4.  $r_{hyp}$ , the hypocentral distance.

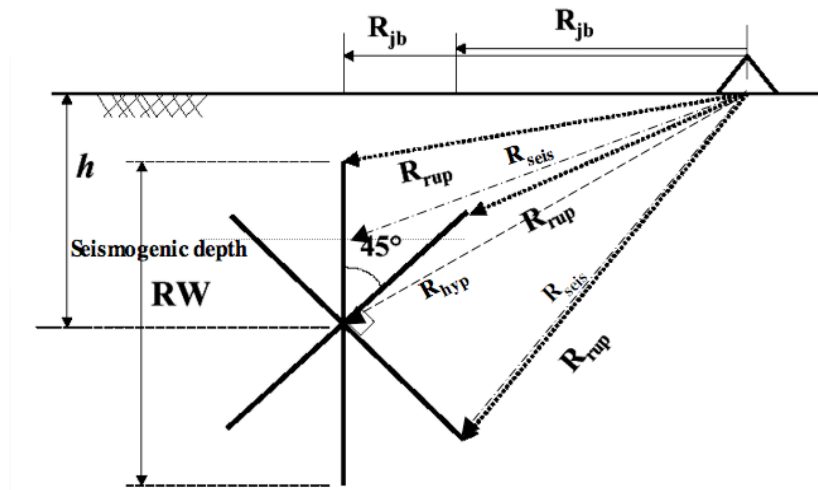


Fig. 4.14 – Definition of distance used in attenuation models.

#### 4.2.1. Peak acceleration

Predictive relationships for parameters that decrease with increasing distance (such as peak acceleration and peak velocity) are often referred to as attenuation relationships and, recently, as ground motion prediction equations (GMPEs). A few of a large number of useful attenuation relationships for different geographic and tectonic environments are described in the following sections. A complete summary of the PGA attenuation relations available in the literature can be found in Douglas (2003, 2011).

Since peak acceleration is the most commonly used ground motion parameter, many peak acceleration attenuation relationships have been developed. The most popular attenuation model is represented by the following parametric relation:

$$\log_{10}(Y) = c_1 + c_2 M + c_3 r + c_4 \log_{10}(r) \quad (4-15)$$

where  $Y$  is the ground motion quantity under study,  $M$  is the earthquake magnitude, and  $r$  is a quantity related to the source-to-station distance. The two terms that include  $r$  model the anelastic attenuation and the geometrical spreading respectively. The quantity  $r$  is generally expressed as:

$$r = \sqrt{d^2 + h^2} \quad (4-16)$$

where  $d$  represents the distance on the surface between the source (or rupture) and the recording station, and  $h$  a further parameter to estimate through regression, which is roughly related to the source (or rupture) depth. More precisely,  $h$  includes all the factors limiting the ground shaking close



to the source. From the mathematical point of view,  $h$  decreases the curve's slope at small distances. It makes Eq. (4-15) non linear with respect to the parameters.

Eq. (4-15) is characterized by a constant magnitude scaling, with  $dY/dM$  equal to  $c_2$ : distance attenuation curves obtained for different values of magnitude have the same shape and are simply scaled by the quantity  $c_2M$ . Some simulation studies using finite faults have shown the need to consider a magnitude-dependent form for attenuation. In such models  $dY/dM$  increases with increasing distance at the same time that it decreases with increasing magnitude. Distance attenuation curves become closer as magnitude increases, while their slope tends to diminish. It was often demonstrated as well that the term for anelastic attenuation [ $c_3$  in Eq. (4-15)] does not contribute significantly to a better description of the data. Then, the following functional form is adopted

$$\log_{10}(Y) = a + (b + cM)M + (d + eM^3) \log_{10}(r) \quad (4-17)$$

In Eq. (4-17), the term for anelastic attenuation is dropped, while magnitude scaling [ $c_2$  in Eq. (4-15)] decreases linearly with  $M$  through parameters  $b$  and  $c$ , where  $c$  is expected to be negative. The slope in the far field [ $c_4$  in Eq. 4-15)] depends on the cube of  $M$  through parameters  $d$  and  $e$ . Such parameters should be negative and positive respectively.

PGA attenuation relations are best suited to conditions similar to those in the databases from which they were developed. As additional strong motion data have become available, attenuation relationships have become more refined. Consider, for example, two attenuation relationships developed some 13 years apart. In 1981, Campbell (1981) used worldwide data to develop an attenuation relationship for the mean horizontal PGA (expressed in g) for sites within 50 km of the fault rupture and earthquakes in the magnitude range 5.0 to 7.7:

$$\ln PGA = -4.141 + 0.868M - 1.09 \ln(R + 0.0606e^{0.7M}) \quad (4-18)$$

$$\sigma_{\ln PGA} = 0.37$$

where  $M$  is the local magnitude or surface wave magnitude for magnitudes less than or greater than 6, respectively, and  $R$  is the closest distance to the fault rupture in kilometers. In this relatively simple attenuation relationship, which represented the state of the art in 1981, the peak acceleration was taken as a function of  $M$  and  $R$  only and  $\sigma_{\ln PGA}$  was constant. In 1994, Campbell and Bozoinia (1994) used worldwide accelerograms from earthquakes of moment magnitude ranging from 4.7 to 8.1 to develop the attenuation relationship for horizontal PGA (in Gal, i.e., cm/s<sup>2</sup>)

$$\begin{aligned} \ln PGA = & -3.512 + 0.904M_w - 1.328 \ln \sqrt{R^2 + [0.149 \exp(0.647M_w)]^2} + \\ & + (1.125 - 0.112 \ln R - 0.0957M_w)F + (0.440 - 0.171 \ln R)S_{SR} + (0.405 - 0.222 \ln R)S_{HR} \end{aligned} \quad (4-19)$$

$$\sigma_{\ln PGA} = 0.889 - 0.0691M \quad \text{for } M \leq 7.4$$

$$\sigma_{\ln PGA} = 0.38 \quad \text{for } M > 7.4$$

where  $R$  is the closest distance ( $\leq 60$  km) to seismic rupture in kilometers (with minimum values of 7.3, 5.8, 3.5, and 3.0 km for magnitudes of 5.0, 5.5, 6.0, and 6.5, respectively); the source term,  $F$ , takes values of 0 for strike-slip and normal faulting, and 1 for reverse, reverse-oblique, and thrust faulting;  $S_{SR}=1$  for soft-rock sites (sedimentary deposits of Tertiary age),  $S_{HR}=1$  for hard-rock sites (primarily older sedimentary deposits, metamorphic rock, and crystalline rock), and  $S_{SR}=S_{HR}=0$  for alluvium sites. The 1994 relationship, which is based on more data, is clearly more specific (and more complicated) than the 1981 relationship. The incorporation of additional terms reflecting source and site characteristics are typical of the refinement of GMPEs that has taken place in recent years.

Boore et al. (1993) used data from western North American earthquakes of magnitude 5.0 to 7.7 at distances within 100 km of the surface projection of the fault to develop the predictive relationship for horizontal PGA (in g)

$$\log PGA = b_1 + b_2(M_w - 6) + b_3(M_w - 6)^2 + b_4R + b_5 \log R + b_6G_B + b_7G_C \quad (4-20)$$

where  $R = \sqrt{d^2 + h^2}$ ,  $d$  is the closest distance to the surface projection of the fault in kilometers, and

$G_B = 0$  for site class A  
 $G_B = 1$  for site class B  
 $G_B = 0$  for site class C

$G_C = 0$  for site class A  
 $G_C = 0$  for site class B  
 $G_C = 1$  for site class C.

Note that the Boore et al. (1993) attenuation relationship is expressed in terms of the common (base 10) logarithm rather than the natural logarithm. The site classes are defined on the basis of the average shear wave velocity in the upper 30 m (Table 4.4). Coefficients for the Boore et al. (1993) GMPE were developed for two measures of peak acceleration: the randomly oriented component and the larger horizontal component (the former considers two orthogonal horizontal records at a particular site as separate events and the latter considers only the larger of the two). The coefficients are given in Table 4.5.

Table 4.4 - Definitions of site classes for Boore et al. (1993) attenuation relation.

Site Class	$v$ in upper 30 m
A	> 750 m/s
B	360-750 m/s
C	130-360 m/s

Table 4.5 - Coefficients for Boore et al. (1993) attenuation relation.

	$b_1$	$b_2$	$b_3$	$b_4$	$b_5$	$b_6$	$b_7$	$h$	$\sigma_{0gPGA}$
Random	-0.105	0.229	0.0	0.0	-0.778	0.162	0.251	5.57	0.230
Larger	-0.038	0.216	0.0	0.0	-0.777	0.158	0.254	5.48	0.205

Since the continental crust in eastern North America is stronger and more intact than the crust in western North America, peak accelerations tend to be higher. For the mid-continental portion of eastern North America, Toro et al. (1997) developed an attenuation relationship for horizontal PGA (in g) on rock sites:

$$\ln PGA = 2.20 + 0.81(M_w - 6) - 1.27 \ln R_m + 0.11 \max\left(\ln \frac{R_m}{100}, 0\right) - 0.0021R_m \quad (4-21)$$

$$\sigma_{\ln PGA} = \sqrt{\sigma_M^2 + \sigma_R^2}$$

where  $R_m = \sqrt{R^2 + 9.3^2}$ ,  $R$  is the closest horizontal distance to the earthquake rupture (in km),  $\sigma_m = 0.36 + 0.07(M_w - 6)$ , and

$$\sigma_R = 0.54 \quad \text{for } R < 5 \text{ km}$$

$$\sigma_R = 0.54 - 0.0227(R - 5) \quad \text{for } 5 \text{ km} \leq R \leq 20 \text{ km}$$

$$\sigma_R = 0.20 \quad \text{for } R > 20 \text{ km.}$$

Subduction zone earthquakes generally occur at greater hypocentral depths than earthquakes that occur on transform faults. Consequently, the seismic waves that emanate from subduction zone earthquakes follow different paths from those of transform faults. Youngs et al. (1988) used strong-motion measurements obtained on rock from 60 earthquakes and numerical simulations of  $M_w \geq 8$  earthquakes to develop a subduction zone GMPEs for horizontal PGA (in g):

$$\ln PGA = 19.16 + 1.045 M_W - 4.738 \ln [R + 205.5 \exp(0.0968 M_W)] + 0.54 Z_r \quad (4-22)$$

$$\sigma_{\ln PGA} = 1.55 - 0.125 M_W$$

where  $R$  is the closest distance to the zone of rupture in kilometers and  $Z_r$  is 0 for interface events and 1 for intraslab events.

The four preceding attenuation relationships are shown graphically for earthquake magnitudes 5.5, 6.5, and 7.5 in Fig. 4.15. The shapes of the attenuation relationships are similar, despite the fact that they represent different geographic regions and different source mechanisms and use different measures of distance.

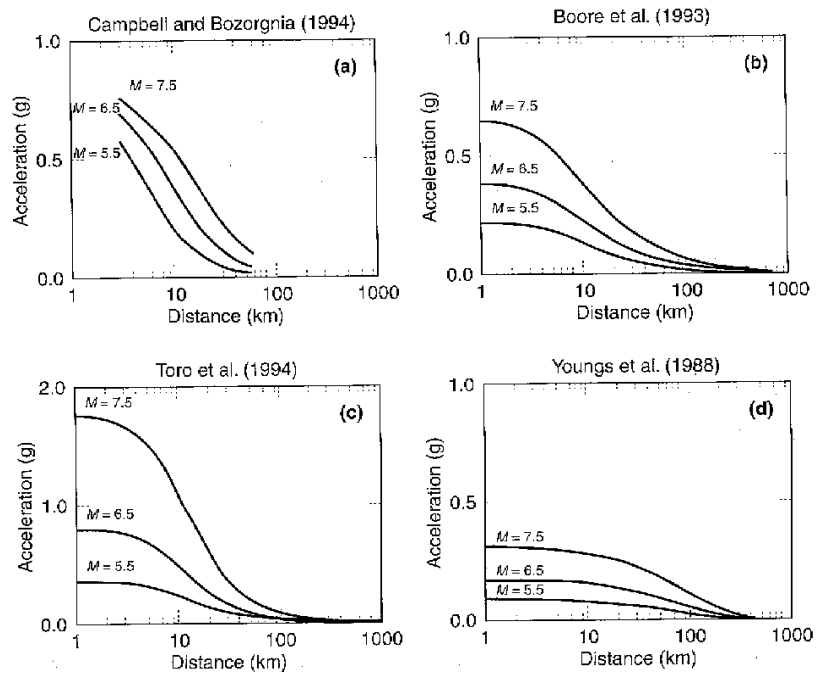


Fig. 4.15 - Variation of horizontal PGA with distance for  $M=5.5$ , 6.5, and 7.5 earthquakes according to various attenuation relationships: a) Campbell and Bozorgnia (1994), soft rock sites and strike-slip faulting; b) Boore et al. (1993), site class B; c) Toro et al. (1994); and d) Young et al. (1988), intraslab event (from Kramer, 1996).



## 5. SEISMIC HAZARD

The seismic hazard analysis provides an estimate of the expected ground motion at a site caused by the occurrence of earthquakes. The process of seismic hazard assessment can be summarized as follows: selection of the suitable approach for the seismic hazard analysis, characterization of the seismic sources, characterization of the ground motion attenuation, development of the seismic hazard analysis, computation of the seismic hazard curve for the studied site, computation of the response spectrum for the studied site, computation of ground motion time histories for the studied site.

Similarly to most of the subjects in physics, the approaches for seismic hazard assessment can be grouped into two broad categories: deterministic and probabilistic. Simply speaking, a deterministic approach is applicable when the physic process is known and, consequently, it is possible to write the equation describing the process (the model). Conversely, a probabilistic approach is applicable when the process is not known and it is possible to approximate the outcome by statistics applied to the observations.

According to McGuire (2001), both deterministic and probabilistic approaches for seismic hazard assessment have advantages and disadvantages that often make the use of one advantageous over the other (Table 5.1). Probabilistic methods can be considered as inclusive of all deterministic events with a finite probability of occurrence. In this context, the deterministic methods that focus on a single earthquake are based on the fact that that event is realistic, i.e., that it has a finite probability of occurrence. There is, then, a complementary nature of deterministic and probabilistic analyses: deterministic events can be checked with a probabilistic analysis to verify that the event is realistic (and reasonably probable), and probabilistic analyses can be checked with deterministic events to verify that the event has been properly modelled.

Determinism vs. probabilism should not be a bivariate choice but a continuum where both analyses are conducted, but more emphasis is given to one over the other (Fig. 5.1). Emphasis here means weight assigned to one method or the other in the decision-making process. The best result will be obtained if both deterministic and probabilistic analyses are conducted.

Table 5.1 – Examples of earthquake decisions (from McGuire, 2001).

Decision	Quantitative aspects	Predominat approach
Seismo design levels	Highly quantitative	Probabilistic
Retrofit design	Highly quantitative	Probabilistic
Insurance / reinsurance	Highly quantitative	Probabilistic
Design of redundant industrial systems	Quantitative or qualitative	Both
Training and plans for emergency response	Mostly qualitative	Deterministic
Plans for post-earthquake recovery	Mostly qualitative	Deterministic
Plans for long-term recovery, local	Mostly qualitative	Deterministic
Plans for long-term recovery, regional	Mostly quantitative	Probabilistic

Factors that influence the choice include: 1) the decision to be made (i.e., the purpose of the hazard study), 2) the seismic environment (whether the investigated site is located in a high, moderate, or low seismic region), and 3) the scope of the assessment (whether the study focuses on a site, several sites, or a region).

The advantage of the PSHA is that it models the fundamentally probabilistic nature of seismic hazard. Future earthquakes can occur at a variety of locations and over a range of magnitudes. Because many combinations of magnitude and distance could result in damage to a given structure, the probabilistic approach is the more suitable of the two for most cases. It derives that the probabilistic approach is preferable when the aim is a quantitative estimate of the expected hazard, conversely, the deterministic approach is used to construct a specific hazard scenario.



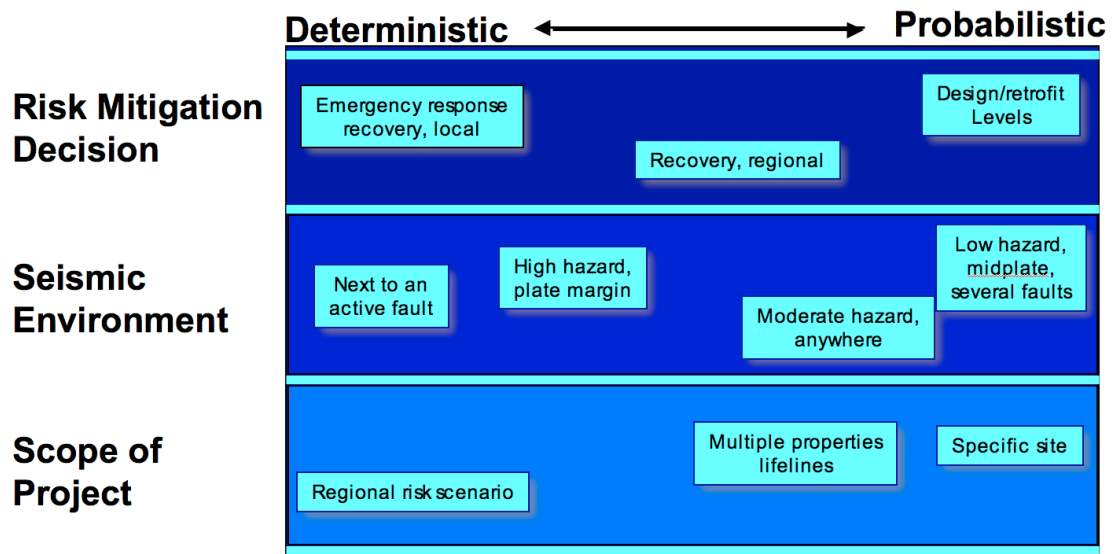


Fig. 5.1 – Seismic risk application in the deterministic-probabilistic spectrum (from McGuire, 2001).

### 5.1. Deterministic approach

In the early years of earthquake engineering, the use of deterministic seismic hazard assessment (DSHA) was prevalent. A DSHA involves the development of a particular seismic scenario upon which a ground motion evaluation is based. The scenario consists of the occurrence of an earthquake of a specified size at a specified location. A typical DSHA can be described as a four-step process (Reiter, 1990; Kramer, 1996) consisting of the steps described in the following.

1. Identification and characterization of all earthquake sources capable of producing significant ground motion at the site. Source characterization includes definition of each source's geometry (the source zone) and earthquake potential.
2. Selection of a source-to-site distance parameter for each source zone. In most DSHAs, the shortest distance between the source zone and the site of interest is selected. Several are the distance metrics (epicentral distance, hypocentral distance, fault distance, rupture distance, etc.) depending on the measure of distance of the predictive relationship(s) used in the following step.
3. Selection of the controlling earthquake (i.e., the earthquake that is expected to produce the strongest level of shaking), generally expressed in terms of some ground motion parameters, at the site. The selection is made by comparing the levels of shaking produced by earthquakes (identified in Step 1) assumed to occur at the distances identified in Step 2. The controlling earthquake is described in terms of its size (usually expressed as magnitude) and distance from the site.
4. The hazard at the site is formally defined, usually in terms of the ground motions produced at the site by the controlling earthquake. Its characteristics are usually described by one or more ground motion parameters obtained from predictive relationships. Peak acceleration, peak velocity, and response spectrum ordinates are commonly used to characterize the seismic hazard.

The DSHA procedure is shown schematically in Fig. 5.2. Expressed in these four compact steps, DSHA appears to be a very simple procedure, and in many respects it is.

When applied to structures for which failure could have catastrophic consequences, such as nuclear power plants and large dams, DSHA provides a straightforward framework for evaluation of worst-case ground motions. However, it provides no information on the likelihood of occurrence of the controlling earthquake, the likelihood of the selected hypocentre, the level of shaking that might be expected during a finite period of time (such as the useful lifetime of a particular structure or facility), or the effects of uncertainties in the various steps required to compute the resulting ground motion characteristics.

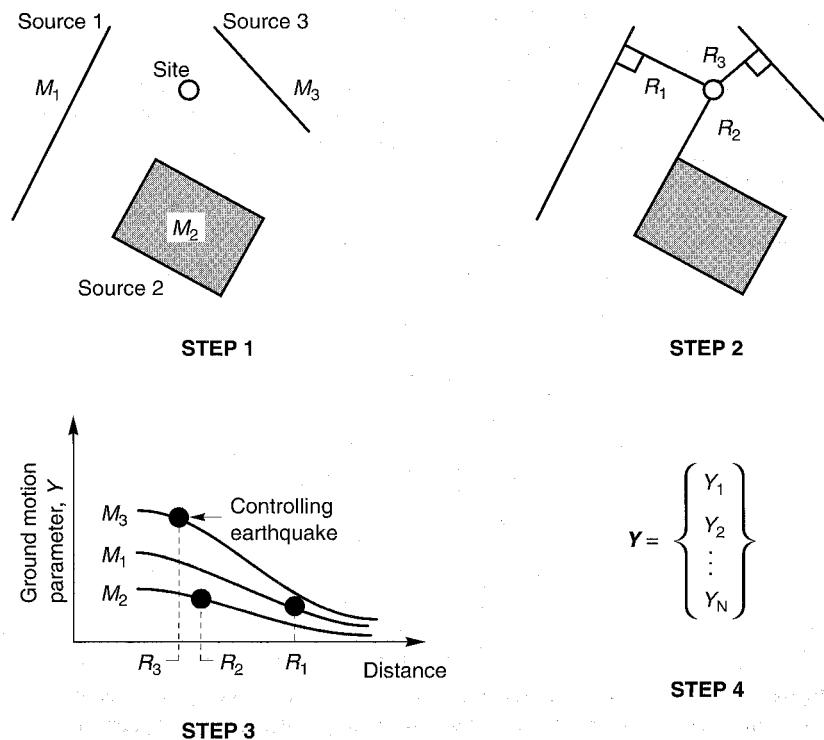


Fig. 5.2 - Four steps of a DSHA (from Kramer, 1996).

Perhaps most important, DSHA involves subjective decisions, particularly regarding earthquake potential (step 1), that can require the combined expertise and opinions of seismologists, seismic geologists, engineers, risk analysts, economists, social scientists, and government officials. The broad range of backgrounds and often divergent goals of such professionals can cause difficulty in reaching a consensus on earthquake potential. Likewise, the identification of the control earthquake, as provided in Step 3, may be complicated. This operation implies, among others, socio-economic considerations related to a purely qualitative selection of acceptable risk in terms of cost-benefit analysis, without any quantitative basis. Over the years there have been many terms used to describe earthquake potential; among them the maximum credible earthquake (MCE), design basis earthquake (DBE), safe shutdown earthquake (SSE), maximum probable earthquake (MPE), operating basis earthquake (OBE), and seismic safety evaluation earthquake. The MCE, for example, is usually defined as the maximum earthquake that appears capable of occurring under the known tectonic framework. The DBE and SSE are usually defined in essentially the same way. The MPE has been defined as the maximum historical earthquake and also as the maximum earthquake likely to occur in a 100-year interval. Many DSHAs have used the two-pronged approach of evaluating hazards for both the MCE and MPE (or SSE and OBE). Disagreements over the definition and use of these terms have forced the delay, and even cancellation, of a number of large construction projects. The Committee on Seismic Risk of the Earthquake Engineering Research Institute (EERI) has stated that terms such as MCE and MPE "are misleading ... and their use is discouraged" (EERI Committee on Seismic Risk, 1984).

In summary, in DSHA all distances from the studied site to the potential earthquake sources, as well as the magnitudes of the earthquakes within the potential sources, are fixed (Steps 1 and 2). The result is an estimate of the ground motion that the site would experience given the occurrence of an earthquake at some fixed distance and magnitude. DSHA defines, generally, the worst-case ground motion and is useful for site-specific studies, particularly those involving critical facilities in which the design criteria are based upon the occurrence of the largest possible seismic event (Reiter, 1990). The disadvantage of this type of analysis is that 1) the likelihood of occurrence of the events is not considered; 2) uncertainty in the hazard estimate cannot be analysed explicitly in a formal, quantitative manner; and 3) the procedure involves subjective decisions.

## 5.2. The probabilistic approach

A probabilistic seismic hazard analysis provides an estimate of the frequency of exceeding specified levels of ground motion at a site by integrating the contributions of earthquakes of all possible magnitudes and locations in a consistent manner. This method has many applications in the field of earthquake engineering, including the design or retrofitting of critical facilities (for example, nuclear reactors, bridges, dams, and hospitals) and the containment of hazardous waste. More recently, seismic hazard analyses have also been used for the determination of earthquake insurance coverage of private homes and businesses.

In the past 20 to 30 years the use of probabilistic concepts has allowed uncertainties in the size, location, and rate of recurrence of earthquakes and in the variation of ground motion characteristics with earthquake size and location to be explicitly considered in the evaluation of seismic hazards. Probabilistic seismic hazard analysis (PSHA) provides a framework in which these uncertainties can be identified, quantified, and combined in a rational manner to provide a more complete picture of the seismic hazard.

Understanding the concepts of PSHA requires familiarity with some of the terminology and basic concepts of probability theory. Such background information can be found in Appendix C.

According to Muir-Wood (1993), one can trace the evolution of seismic hazard in the form of a series of methodological generations, from simpler ones, where the results are nothing more than the future projection of past observations, to the most sophisticated ones of strong seismotectonic character, where it is requested information derived from the global geodynamic analysis, elements of regional geology, and knowledge about the past and present seismicity. The probabilistic seismic hazard analyses were, therefore, grouped into five different generations, in terms of increasing complexity: the historical determinism, the historical probabilism, the seismotectonic probabilism, the non-Poissonian probabilism, and the earthquake prediction. The last two generations are still mainly advanced research topics.

- a) **Historical determinism.** The first generation of seismic hazard involved mapping the maximum intensity of earthquake effects recorded in the known historical period (Fig. 5.3). These were assumed to represent the highest intensity to be expected in the future. The method was very simple, took no account of the duration or completeness of the historical record, and required no knowledge of earthquake causes. Modified first generation hazard, as employed for critical facilities, involved adding some ad hoc factor to the mapped intensity (typically one or two intensity grades) to obtain a more extreme hazard.
- b) **Historical probabilism.** The second generation of hazard took the historical record of seismicity and considered it in terms of its duration to achieve some kind of annual probability of the recurrence of earthquake effects. This could be the annual probability of exceeding an intensity, or some other ground motion parameter calibrated with intensity. The annual probability of more extreme effects is simply extrapolated. Modified second generation hazard employs some conversion to translate historical earthquakes into magnitudes and then, through the use of an attenuation relationship, computes the recurrence of some magnitude-distance related ground motion parameter at a site or within a region. No geological information is used in this approach. Many seismic hazard cultures remain at this stage.
- c) **Seismotectonic probabilism.** Third generation seismic hazard recognizes the danger of relying solely on the historical record of past earthquakes and incorporates geological evidence, including the prehistoric record of palaeoseismic ground motion and neotectonic surface faulting, as well as the scientific seismotectonic understanding of earthquake causes. These different data sources can only be combined through a seismic source model. In recognition of the uncertainty and judgement involved in determining the input parameters of such a model, all parameters are assigned in the form of a weighted range of values, through a logic tree. The most famous theoretical development of this approach is the one proposed by Cornell (1968). It is based on specific assumptions about space-time distribution of earthquakes: inside a seismic source, the seismicity is assumed to be homogeneous and stationary, i.e., each point can be the focus of an earthquake, and earthquakes occur randomly in time, governed only by a predetermined ratio between the number of large and small events. Empirical relationships simulate the radiation of the ground shaking around each source. The result of applying this

approach to a generic studied site is obtained by integrating statistically the contributions from all sources. For this reason the results are represented by maps of expected shaking in a fixed time interval at a certain level of probability of exceedance, or in terms of exceedance probability curves of the shaking parameter chosen. Although some assumptions may seem inadequate, or simplifications too reductive, the seismotectonic probabilism is based on reasonable and robust assumptions and it is certainly the more established and widely used internationally approach with regard to urban planning strategies.

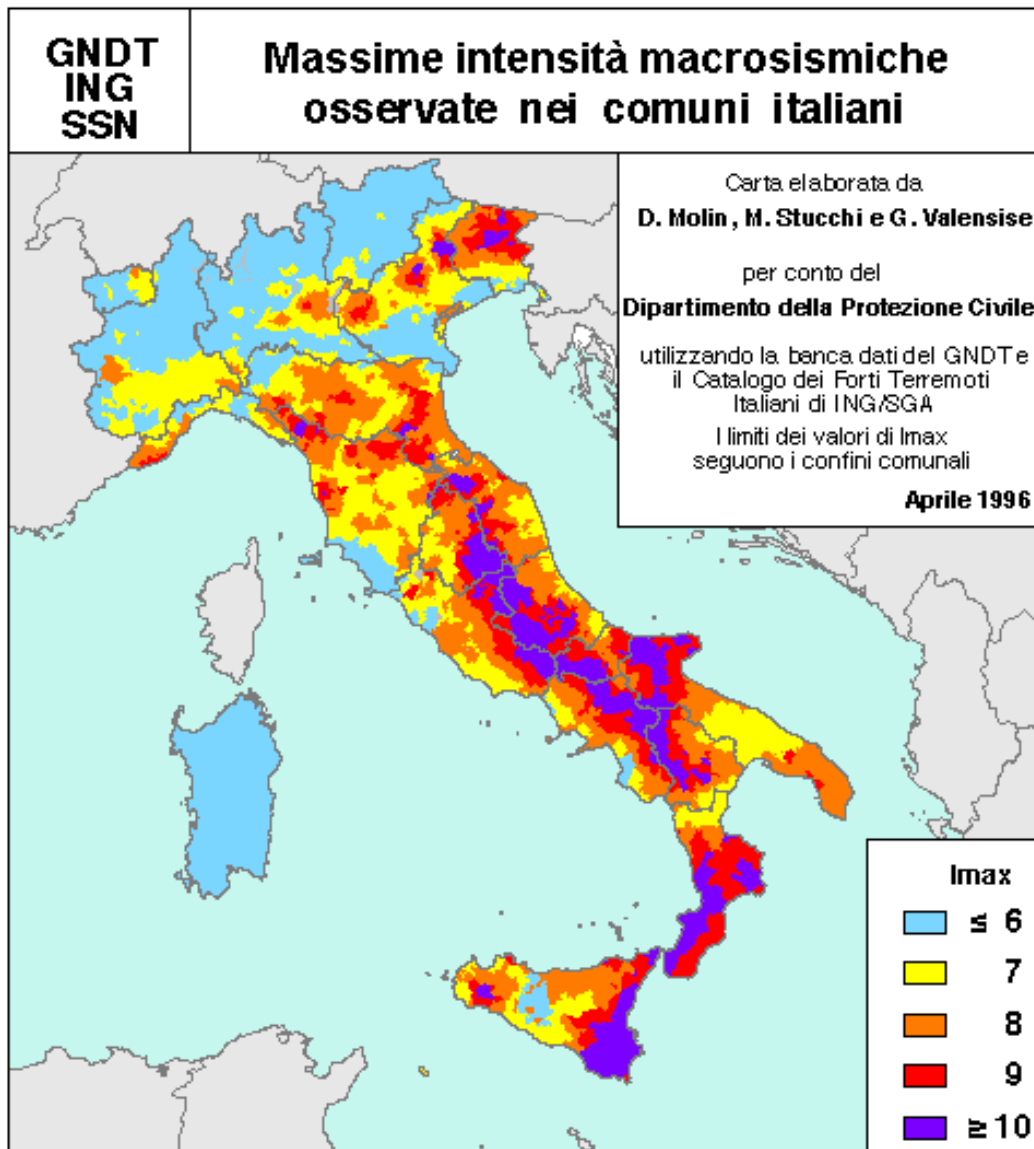


Fig. 5.3 – Maximum observed macroseismic intensities in Italy.

- d) **Non-Poissonian probabilism.** Fourth generation hazard is time-dependent. The more that is learnt about earthquake recurrence the more it becomes clear that major earthquakes do not occur randomly in time. The occurrence of any major earthquake will affect the likelihood of other events in its vicinity and in particular the repeat of the same event. Time-dependent hazard models have been explored in a number of the most seismically active regions. The hazard has to be computed through the use of fully probabilistic seismic source models employing non-Poissonian earthquake recurrence. As seismotectonic knowledge increases, non-Poissonian hazard models will become employed in medium and even low-seismicity areas. Initially concerned with time dependence, such models are now evolving towards the full spatio-temporal properties of earthquake activity. This is a reasonable and intuitive assumption, but it is very difficult to validate, for the complexity of seismic phenomenon and even more for the

limited observations available. It may, in fact, introduce large uncertainties, exceeding even the level of the forecast itself, thus making these estimates of the hazard without any practical utilities. Among these models, those “time-predictable” and “slip-predictable” (Shimazaki and Nakata, 1980) and the Brownian Passage Time Model (Kagan and Knopoff, 1987) are the most famous.

- e) **Earthquake prediction.** Fifth generation hazard is earthquake prediction. Where sufficient knowledge is accumulated to indicate that an earthquake is imminent, the concept of seismic hazard enters a new phase, concentrating on the probability of constraining the time of the earthquake, as well as its size and location and their associated uncertainties. Short, medium, and long term earthquake prediction can be considered the ultimate objective of seismic hazard. This would be a step of crucial importance for the subsequent simulation of earthquake effects on the environment and human settlements. Unfortunately, although there have been a few positive cases in the world of short-term forecast, by far the most important were, however, failures. In the literature, it is reported as successful predictions of earthquakes those of Blue Mountain Lake (U.S.A.) in 1973, Haicheng (China) in 1975, Oaxaca (Mexico) in 1978, and Izu (Japan) in 1978. The optimism generated by the positive prediction of the Haicheng earthquake was dampened by the unpredicted event in Tangshan (China) in 1976 which caused about 650,000 casualties. In the mid-1980s, the USGS, along with several universities, began a program of intensive monitoring of many geophysical parameters in the Parkfield area (California), where an earthquake of magnitude 6 around 1987 was expected. Only in 2004, without any obvious precursory phenomena, there was an earthquake of magnitude 6, while it was expected a lot stronger. The possibility that, in the future, earthquake prediction can play a useful role for civil protection remains, then, extremely controversial. Earthquake prediction is, therefore, at the present state of knowledge, a research topic that does not apply operationally to the seismic risk reduction.

These hazard generations blur into one another. Different regions of the world exist in different generations of hazard. Some countries have become stuck in first generation hazard for political reasons, others because there has never been the initiative or funding to attempt anything better. A number of researchers in plate boundary regions are strongly involved in developing and implementing fourth generation time-dependent hazard models (see for example Working Group on California Earthquake Probabilities, 1990).

These hazard generations can make profound differences to seismic hazard estimates (Muir-Wood, 1993). One can follow their implications for hazard by comparing two cities lying above subduction zones: Valdivia in southern Chile, and Portland, in Oregon U.S.A. The city of Valdivia has been destroyed four times (1575, 1737, 1837 and 1960) by major plate boundary earthquakes since it was founded by the Spanish in the mid 16th century. In contrast the city of Portland has suffered no serious earthquake damage since it was founded in the mid 19th century.

Second generation hazard assigns a very high hazard to Valdivia and a very low hazard to Portland (see Fig. 5.4). On reaching third generation hazard the subduction zone setting of Portland, and the evidence for major coseismic land-level changes and tsunami sand deposits along the neighbouring coast, indicate that the hazard is much higher than is suggested by historical seismicity alone. However this averaged hazard remains below that of Valdivia as the Cascadian convergence between the Juan da Fuca and North American plates is slower than that between the Nazca and South American plates, and the recurrence of major earthquakes appears to be 400-600 years in Cascadia, in contrast to 100-200 years in southern Chile. However on reaching fourth generation hazard, the position becomes reversed: the last major subduction zone earthquake in Valdivia was in 1960, while on the Washington State coast to the west of Portland it was around 1690. Hence the seismic cycle in the region of Portland is becoming mature; that close to Valdivia is very immature.

Any attempt to achieve a global seismic hazard program has to attempt to bring all regions up to a third generation hazard culture. However for some regions of the world it may prove impossible to move beyond second generation hazard while at a number of plate boundaries the hazard culture has already moved into the fourth generation, from which it cannot be returned. At present, global seismic hazard has inevitably to be a mixture of third and fourth generation philosophies. Hazard methodology is defined by the state of seismotectonic knowledge. Hence it is not possible to employ a



single uniform model of earthquake hazard globally. Fifth generation earthquake prediction hazard remains a much debated drawing-board research program that is taking a long time to fly.

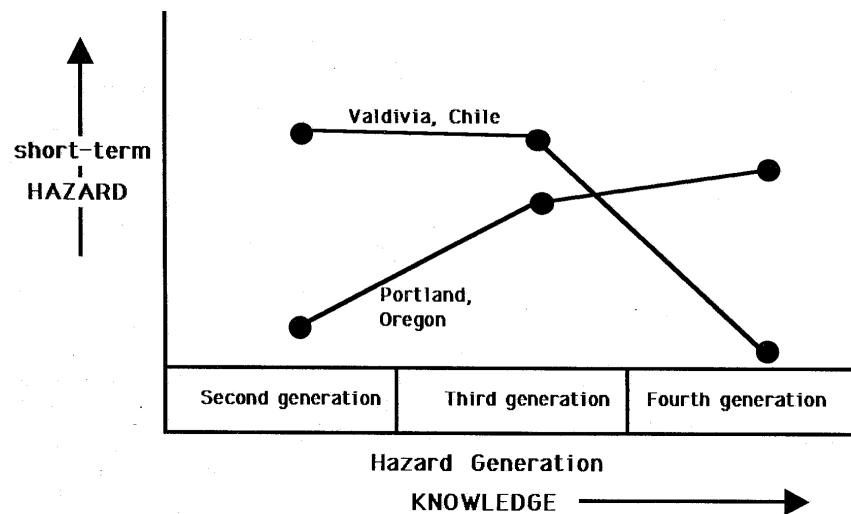


Fig. 5.4 – Hazard generations for Valdivia and Portland (from Muir-Wood, 1993).

In conclusion, it is not possible to suggest a single approach to be applied worldwide: the choice depends on the seismotectonic knowledge, that at present, allows to calculate seismic hazard of most of the countries according to the approach of the seismotectonic probabilism. There are special areas where it is not reasonable to use approaches better than that of the historical probabilism, while the method of non-Poissonian probabilism is applied in many regions located at plate margins. The fifth generation, namely that of earthquake prediction, remains an area of advanced research for which is not yet possible to estimate the timing of its translation into practical applicability, if ever it will be possible, and if the consequences of any erroneous forecasts may be considered acceptable in terms of cost-benefit analysis.

National seismic codes and zonation are based on seismic hazard estimates computed with the most suitable approach for the seismotectonic knowledge available (see McGuire, 1993). The first three of the above types of hazard maps are very popular, while non-Poissonian probabilism, and its hybrid variation (Wu et al., 1995), are still mainly research topics. UNDR's GSHAP project (Giardini and Basham, 1993) has proposed the Cornell (1968) approach as the reference method for all countries where seismotectonic knowledge supports this approach.

The theoretical basis of the calculation of seismic hazard were posed by some seminal papers published since the early 1960s by Rosenblueth (1964), Epstein and Lomnitz (1966), Esteva (1967, 1968, 1969, 1970), Cornell (1968, 1971), Merz and Cornell (1973) and Cornell and Merz (1975). Among these, those of Epstein and Lomnitz (1966) and Cornell (1968) still remain the most cited in the literature and used: they opened the way for two different but converging lines of calculation of seismic hazard. Epstein and Lomnitz (1966) applied the method of extreme values to the probabilistic estimate of the occurrence of strong earthquakes. Cornell (1968) developed analytically the seismic hazard assessment at a site under specific conditions about the geometry of the seismic source. In the second half of the 1970s with the spread of computers, the method of Cornell (1968) found its development in some numerical calculation programs, still in use today: RISK4a (Algermissen et al., 1976) and EqRisk (McGuire, 1976).

The first dissertation on PSHA can be considered the paper by Epstein and Lomnitz (1966) published in the scientific journal "Nature". Those authors presented some hazard estimates for California considering the Gumbel asymptotic distribution. A similar approach was applied frequently in the following years and it is possible to find some hazard studies based on the Epstein and Lomnitz (1966) approach even nowadays. Following to the Muir-Wood (1993) classification of hazard generations, this approach refers to the second hazard generation.

The methodological basis of the modern PSHA can be considered the paper by Cornell (1968) published in the Bulletin of the Seismological Society of America. In the Cornell approach, distances to potential seismic sources and the magnitudes of earthquakes generated by those sources are treated

as random variables. The result is a single hazard curve or set of hazard curves that represent the expected frequency of exceedance of a pre-specified value of motion at a given site. In the Cornell approach a great importance is given by the seismogenic sources, which can be designed as wide areas (seismogenic zones, SZs) or as lines (seismogenic faults, SFs). Consequently, the Cornell approach is the main example of a third generation hazard, according to the Muir-Wood (1993) classification.

In the following years some attempts were made to introduce a time-dependent model for the earthquake occurrence in the Cornell (1968) approach (Wu et al., 1995) and a method to smooth the seismicity was developed where the seismogenic sources are not well defined (Frankel, 1995).

### 5.2.1. The historical probabilism

The statistical analysis of seismic data in a specific area shows that the number of low magnitude earthquakes is much higher than those of high magnitude, and a relationship of the following type holds (Gutenberg and Richter, 1944):

$$\log n_m = a - bm \quad (5-1)$$

where  $n_m$  is the number of earthquakes with magnitude greater than, or equal to,  $m$ ,  $a$  is a parameter related to the total number of earthquakes in the region (number of earthquakes of magnitude greater than, or equal to, zero), and  $b$  is a variable that characterizes the relationship between the number of high and low magnitude events. It has been shown experimentally that the model of Gutenberg - Richter (G-R) is valid both on a global scale and for sources of limited size, and laboratory tests have verified its validity on rock samples. This has led some researchers to assert that the G-R model is an invariant law in seismology. Generally, the application of this relationship is strongly influenced by the lack of historical data, namely incompleteness of the catalogue for earthquakes of low magnitude.

A useful approach to overcome this problem is offered by the method of statistical analysis based on extreme values (Fisher and Tippett, 1928; Gumbel, 1945, 1958). This method was applied to seismicity (Epstein and Lomnitz, 1966; Lomnitz, 1966, 1974) after Nordquist (1945) showed that the strongest earthquakes occurred in California are in agreement with the theory of extreme values. The approach of extreme values has the disadvantage that it operates with a selection of data and not with all the available information. As it considers only the strongest earthquakes, it has the advantage to use the events that are better known.

The statistical bases of extreme values theory (Gumbel, 1958) can be summarized as follows. Let's consider many independent and identically distributed random variables  $X_i$ . Be the distribution of  $X_i$  unbounded from above and with an exponential decay, i.e., the cumulative distribution function (CDF) of all the  $X_i$ , at least in the tail, has the form:

$$F_X(x) = 1 - e^{-g(x)}. \quad (5-2)$$

The above conditions are not very restrictive because the normal, lognormal, exponential, and gamma distributions are of this type. It is shown that  $Y$ , the maximum value of  $X_i$ , has the following distributions:

$$\begin{aligned} F_Y(y) &= e^{-e^{-c(y-u)}} \\ f_Y(y) &= ce^{-c(y-u)}e^{-e^{-c(y-u)}} \end{aligned} \quad (5-3)$$

where  $-\infty \leq y \leq +\infty$  and  $c$  and  $u$  are parameters calculated from the data and where  $f_Y(y)$  and  $F_Y(y)$  are, respectively, the probability density function (PDF) and the CDF of  $Y$ . Eq. (5-3) is called Type 1 Gumbel asymptotic distribution.

Consequently, the mean value  $\mu$ , the variance  $\sigma^2$ , and the standard deviation  $\sigma$  are:

$$\begin{aligned}\mu &\approx u + \frac{0.577}{c} \\ \sigma^2 &\approx \frac{1.645}{c^2} \\ \sigma &\approx \frac{1.282}{c}.\end{aligned}\tag{5-4}$$

If we introduce the reduced variable  $z = \ln[-\ln F_Y(y)]$ , we obtain:

$$z = -c(y - u).\tag{5-5}$$

Eq. (5-5) is a linear equation and allows us to find an easy solution for the parameters  $c$  and  $u$  of the Type 1 Gumbel asymptotic distribution.

Conversely, if the  $X_i$  do not verify Eq. (5-2) but have a finite limit:

$$F_X(x) = 1 - e^{-(w-x)^k}\tag{5-6}$$

with  $x \leq w$  and  $k > 0$ , the extreme value distribution is:

$$\begin{aligned}F_Y(y) &= e^{-\left(\frac{w-y}{w-u}\right)^k} \\ f_Y(y) &= \frac{k}{w-u} \left(\frac{w-y}{w-u}\right)^{k-1} e^{-\left(\frac{w-y}{w-u}\right)^k}\end{aligned}\tag{5-7}$$

with  $y > w$ .

Eq. (5-7) is called Type 3 Gumbel asymptotic distribution (or Weibull distribution) and, introducing the reduced variable  $z$ , it becomes

$$z = c - k \cdot \ln(w-y),\tag{5-8}$$

with  $c$  a constant that can be obtained, together with  $k$  and  $w$ , by regression analysis.

Epstein and Lomnitz (1966) combined a distribution suitable to describe the number of earthquakes of a particular magnitude (G-R distribution) with their annual frequency of occurrence, expressed by the Poisson distribution. The model thus obtained proved to be equivalent to the Type 1 Gumbel distribution of extreme values. The main applications that followed, including seismic hazard assessment of central and eastern Mediterranean basin, can be found in Burton (1979).

In detail, the application of Epstein and Lomnitz (1966) requires the following two working hypotheses: a) the annual number of earthquakes  $N$  is a Poisson random variable with mean value  $\alpha$  (see below):

$$P[N = k] = \frac{\alpha^k e^{-\alpha}}{k!}\tag{5-9}$$

and b) the earthquake magnitude  $X$  is a random variable with a CDF of exponential type (G-R relation):

$$F_X(x) = P[X \leq x] = 1 - e^{-\beta x} \quad \text{with } x \geq 0\tag{5-10}$$

and it satisfies, then, the condition expressed by Eq. (5-2).

From these hypotheses, according to Eq. (5-3), it follows that (Epstein and Lomnitz, 1966)  $Y$ , the maximum annual magnitude has a CDF  $G_Y(y)$ :

$$G_Y(y) = P[Y \leq y] = \sum_{k=0}^{\infty} \frac{e^{-\alpha} \alpha^k}{k!} [F_Y(y)]^k = e^{-\alpha[1-F_Y(y)]} = e^{-\alpha e^{-\beta y}} \quad \text{with } y \geq 0 \quad (5-11)$$

where  $y$  is the magnitude of the strongest earthquake in the time interval of one year. The CDF (5-11) corresponds to the Type 1 Gumbel asymptotic distribution [see Eq. (5-5)].

To estimate the parameters  $\alpha$  and  $\beta$  in Eq. (5-11), the time span of the earthquake catalogue is subdivided into  $\Delta t$  wide intervals (one year each in our case, but time intervals of any length can be considered by referring all processing to the maximum magnitude in the chosen interval). Each interval is a random variable whose elements are the magnitudes. The extreme value  $y_i$ , i.e., the maximum magnitude that the variable  $x$  assumes in each  $t_i$  interval, is, then, considered and the set  $\{y_1, y_2, \dots, y_n\}$  of maximum magnitudes, covering the time span of the catalogue, is obtained. The so constructed random variable  $Y$  follows the asymptotic Gumbel distribution [Eq. (5-11)]. The  $n$   $y_i$  magnitudes are arranged in order of increasing magnitude, so that  $y'_1 \leq y'_2 \leq \dots \leq y'_n$ .

The values of  $G_Y(y')$ , i.e., the probability of not exceeding  $y$ , are estimated using the Plotting Rule proposed by Gumbel (1958):

$$G_Y(y'_j) = \frac{j}{n+1} \quad (5-12)$$

where  $j$  is 1, 2, 3, ...,  $n$  and  $n$  is the number of time intervals in which the catalogue has been divided.

Other different versions of the Plotting Rule  $G_Y(y')$  are available in the literature:

$$G_Y(y'_j) = \frac{j-0,5}{n} \quad (5-13)$$

proposed by Jenkinson (1955);

$$G_Y(y'_j) = \frac{j-0,44}{n+0,12} \quad (5-14)$$

proposed by Gringorten (1963).

Taking the natural logarithm of the first and second members of Eq. (5-11) and introducing the values of  $G_Y(y')$  obtained for each  $y'$  from the Plotting Rule, a system of  $n$  linear equations:

$$\ln[-\ln G_Y(y'_j)] = \ln \alpha - \beta y'. \quad (5-15)$$

The estimate of  $\alpha$  and  $\beta$  derives from the application of least squares method.

The slope of the straight line (Fig. 5.5) gives the value of  $\beta$ , while the intercept with the y-axis gives the value of  $\ln \alpha$ .

It is interesting to notice that  $n_y = \alpha e^{-\beta y}$  represents the expected number of earthquakes in a given year that have magnitudes above  $y$  (Epstein and Lomnitz, 1966). It follows that:

$$\ln n_y = \ln \alpha - \beta y \quad (5-16)$$

and this relation has the same shape as the famous G-R law  $\log n_m = a - bm$ .

As, from the previous relations it results that:

$$n_m = \frac{e^{\ln \alpha}}{e^{\beta m}} = \frac{10^a}{10^{bm}} \quad (5-17)$$

and, consequently,

$$e^{\ln \alpha} = 10^a \quad \text{and} \quad e^{\beta m} = 10^{bm}, \quad (5-18)$$

it follows that the parameters  $a$  and  $b$  are related to  $\alpha$  and  $\beta$  as follows:

$$a = \frac{\ln \alpha}{\ln 10} \quad \text{and} \quad b = \frac{\beta}{\ln 10}. \quad (5-19)$$

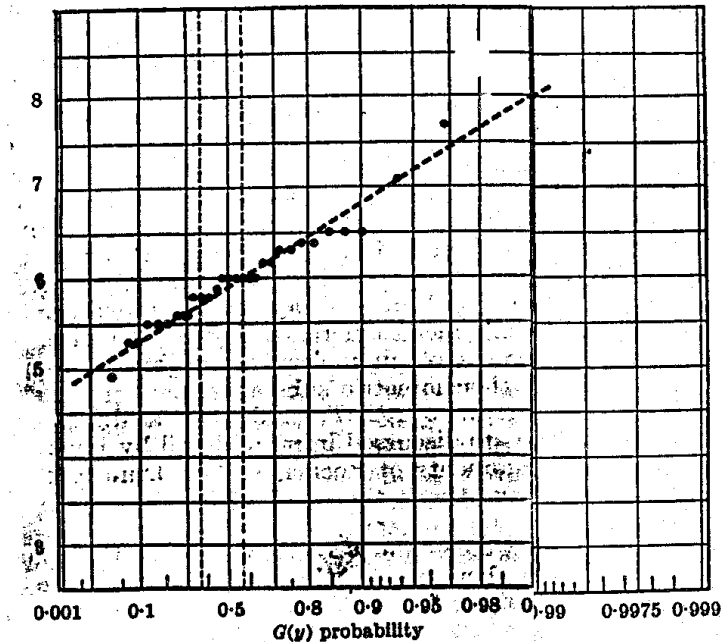


Fig. 5.5 – Gumbel interpolation of the earthquake annual maxima in California (from Epstein and Lomnitz, 1966).

The parameter  $\beta$  also has a physical meaning, since  $1/\beta$  is the mean magnitude of all earthquakes of magnitude  $x > 0$ . If  $x_0$  is the magnitude threshold of the observations then  $x_0 + 1/\beta$  is the mean magnitude over the data range used.

Given  $\alpha$  and  $\beta$ , it is, then, possible to compute all the parameters defining the seismic hazard of a studied area.

- a) The **mean recurrence interval**  $T_y$  in years between earthquakes having magnitude larger than  $y$  is obtained from Eq. (5-16) and it is:

$$T_y = \frac{1}{N_y} = \frac{e^{\beta y}}{\alpha}. \quad (5-20)$$

- b) The **modal annual maximum** (most probable or most frequently observed) magnitude  $\tilde{y}$ , is the value for which the first derivative of Eq. (5-11) becomes maximum [i.e.,  $g(y) = G'(y)$ ] and, then, the value for which the second derivative of Eq. (5-11) is equal to zero. It is given by:

$$\tilde{y} = \frac{\ln \alpha}{\beta}. \quad (5-21)$$

As  $n_y = \alpha e^{-\beta y}$  [Eq. (5-16)], it derives that  $n_{\tilde{y}} = 1$ , that is,  $\tilde{y}$  is the magnitude such that we can expect one earthquake having magnitude  $\tilde{y}$  or more in a given year (i.e.: the mean recurrence interval of  $\tilde{y}$  is  $T_{\tilde{y}} = 1$ ). Also,  $G_y(\tilde{y}) = e^{-1}$ , that is,  $\tilde{y}$  is that maximum annual magnitude which is exceeded in the long run 63% of the time.

The modal earthquake magnitude in a  $T$  year period is



$$\tilde{y}_T = \frac{\ln \alpha T}{\beta} = \tilde{y} + \frac{\ln T}{\beta}. \quad (5-22)$$

- c) The value  $y_p$  of the **maximum annual earthquake magnitude which is exceeded with probability  $p$**  derives directly from Eq. (5-11) and is found by solving the equation

$$\exp(-\alpha e^{-\beta y_p}) = 1 - p \quad (5-23)$$

which, together with Eq. (5-21) yields

$$y_p = \tilde{y} - \frac{\ln[-\ln(1-p)]}{\beta}, \quad y_p = \tilde{y} - \frac{\ln[-\ln(1-p)]}{\beta} = \frac{\ln \alpha}{\beta} - \frac{\ln[-\ln(1-p)]}{\beta}. \quad (5-24)$$

More generally,  $y_p(D)$ , the value of the **maximum earthquake magnitude which is exceeded with probability  $p$  in a  $D$  year period**, is given by combining Eqs. (5-21), (5-22), and (5-24):

$$y_p(D) = y_p + \frac{\ln D}{\beta} = \frac{\ln \alpha}{\beta} - \frac{\ln[-\ln(1-p)]}{\beta} + \frac{\ln D}{\beta}. \quad (5-25)$$

- d) Finally, the **occurrence probability of an earthquake of magnitude  $y$  or more in a  $D$  year period**  $R_D(y)$  derives from Eq. (5-11) and can be written as

$$R_D(y) = 1 - e^{-\alpha D e^{-\beta y}}. \quad (5-26)$$

The application of the theory of extreme values to seismic hazard has been criticized by Knopoff and Kagan (1977) on the basis that the application of methods that use the entire seismic process provides more accurate results. This deficiency does not belong to the Type 3 Gumbel distribution, which takes into account the physical reality represented by the asymptotic behaviour, in the upper tail, of the magnitude, evidence, however, not covered by the G-R law in its basic formulation (Burton et al., 1983).

### Numerical example

Calculations based on this model were carried out for earthquakes in California for the period 1932-62. Table 5.2 lists the magnitude maxima by increasing size.

The values given in Table 5.2, plotted on extreme probability paper, yield an acceptable straight line fit (Fig. 5.5). From this graph it is possible to determine approximate values for the parameters  $a$  and  $b$  of the distribution  $G(y)$  of annual extreme earthquakes in California. More accurately, the data given in Table 5.2 can be fitted to Eq. (5-15) by a least squares regression procedure. Application of this procedure to the data in Table 5.2 yields 11.43 and 2.00 as estimates, respectively, of  $\ln a$  and  $b$ . The standard deviation of  $b$  was estimated as 0.08 by the same program.

Gutenberg and Richter (1949) give  $0.88 \pm 0.03$  as an estimate of their parameter  $b$  for southern California, which yields [see Eq. (5-19)]

$$\beta = 2.03 \pm 0.07$$

which gives reasonable agreement with our estimate derived from only 31 annual maxima. Our predicted modal annual maximum [Eq. (5-21)] is:

$$\tilde{y} = 11.43/2.00 = 5.715$$

Table 5.2 - California yearly earthquake maxima (1932-62) by order of increasing size (from Epstein and Lomnitz, 1966).

j	y(j)	G[y(j)]
1	4.9	0.03125
2	5.3	0.06250
3	5.3	0.00375
4	5.5	0.12500
5	5.5	0.15625
6	5.5	0.18750
7	5.5	0.21875
8	5.6	0.25000
9	5.6	0.28125
10	5.8	0.81250
11	5.8	0.34375
12	5.8	0.37500
13	5.8	0.40625
14	5.0	0.43750
15	6.0	0.46875
16	6.0	0.50000
17	6.0	0.53125
18	6.0	0.56250
19	6.0	0.59375
20	6.0	0.62500
21	6.2	0.65625
22	6.2	0.68750
23	6.3	0.71875
24	6.3	0.75000
25	6.4	0.78125
26	6.4	0.81250
27	6.5	0.84375
28	6.5	0.87500
29	6.5	0.00625
30	7.1	0.93750
31	7.7	0.96875

In view of the fact that, according to the Poisson distribution, the modal value  $\tilde{y}$  is exceeded 63 per cent of all years we have  $G(\tilde{y}) = 0.37$ , which corresponds to a magnitude  $\tilde{y} = 5.8$  in Table 5.2. Again, the agreement is excellent.

Let us now compute  $N_y$ , the expected number of earthquakes per year, and  $T_y$ , the mean, return period, for shocks of magnitude greater than or equal to  $y$  in California. Using Eqs. (5-16) and (5-20) with the values of  $\alpha$  and  $\beta$  already obtained we find the estimates given in Table 5.3.

Table 5.3 - Predicted yearly number ( $N_y$ ) and return periods ( $T_y$ ) in each magnitude ( $M$ ) class for California earthquakes.

$M$	$N_y$	$T_y$
3	228	1.6 days
4	20.7	17.6 days
5	4.18	87.3 days
6	0.57	1.8 years
7	0.076	13.2 year
8	0.010	100 years
9	0.0014	720 years

The model presented in this note should be considered as a first approximation to the real situation. In an area as large and complex as California there is considerable geographical variation both as to frequency and magnitude of occurrence of earthquakes. A more refined model would be obtained by dividing the area into two or more regions and fitting the seismicity in each of these regions by the model. However, despite the known lack of homogeneity of earthquake occurrence in California the present simplified approach provides reasonable estimates for the occurrence of large earthquakes within the uncertainty due to the shortness of the available historical record. A similar application can be done considering a single site: in this case, local ground motion

parameters (e.g., intensity or peak ground acceleration) are considered. These parameters can have been locally recorded or computed from the hypocentral ones by proper attenuation models.

### 5.2.2. The seismotectonic probabilism

The method of the seismotectonic probabilism was originally proposed by Cornell (1968) and was later translated into computer programs by many researchers. Seismic hazard is computed analytically in the Cornell (1968) seminal paper and for this reason the method requires some working hypotheses that can be damped in the numerical solution. These working hypotheses are as follows:

- 1) the earthquake magnitude is exponentially distributed, i.e., the G-R law is valid;
- 2) seismicity is a Poisson process, i.e., time intervals between earthquakes are distributed exponentially;
- 3) the seismicity is uniformly distributed inside the seismic sources.

#### 5.2.2.1. The original Cornell (1968) approach for PSHA

In his original formulation, Cornell (1968) considered initially a very simple form of seismic source (line segment, corresponding in geology to the surface projection of a fault) in order to calculate analytically the CDF of the macroseismic intensity at the site,  $I$ , given the occurrence of an earthquake in the source. To do this, the conditional probability of exceeding a fixed level of intensity  $i$  at the site is calculated, given the occurrence of an earthquake at a distance  $r$  from the site itself. In order to consider all possible distances, the product of the conditional probability times the probability of the distance (PDF of  $R$ ) is integrated over the range of possible distances:

$$1 - F_I(i) = P[I \geq i] = \int P[I \geq i | R = r] f_R(r) dr \quad (5-27)$$

where  $F_I(i)$  is the CDF of  $I$  and  $f_R(r)$  is the PDF of  $R$ .

Cornell (1968), then, developed his original approach considering different geometries for the seismogenic sources.

##### 5.2.2.1.1. Line source

The first methodological application of PSHA refers to a line source and the distribution of the annual maximum intensity at a site due to potential earthquakes along a neighbouring fault is considered. As illustrated in Fig. 5.6a, the site is assumed to lie a perpendicular distance,  $\Delta$ , from a line on the surface vertically above the fault at the focal depth,  $h$ , along which future earthquake foci are expected to lie. The length of this fault is  $l$ , and the site is located symmetrically with respect to this length.

Concern with focal distances restricts attention to the ABD plane (Fig. 5.6b). The perpendicular slant distance to the source is  $d = \sqrt{h^2 + \Delta^2}$ .

The focal distance  $R$  to any future focus located a distance  $X$  from the point B is

$$R = \sqrt{d^2 + X^2} \quad (5-28)$$

Since  $-l/2 \leq X \leq l/2$ , the distance from the studied site to any earthquake focus is restricted to  $0 \leq R < r_0$  in which  $r_0 = \sqrt{d^2 + l^2/4}$ . In general the size and location of a future earthquake are uncertain. They shall be treated therefore as random variables (as usual random variables are denoted by capital letters).

It is first sought the conditional distribution of the intensity,  $I$ , at the site given that an earthquake occurs at a focal distance  $R=r$  from the site. For illustration it is used the common assumption that in the range of interest the intensity has the following dependence on magnitude,  $M$ , and focal distance,  $R$ :

$$I = c_1 + c_2 M + c_3 \ln R \tag{5-29}$$

in which  $\ln$  denotes natural logarithm and  $c_i$ ,  $i = 1, 2, 3$ , are semiempirical constants on the order of 8, 1.5, and -2.5, respectively for firm ground in southern California.

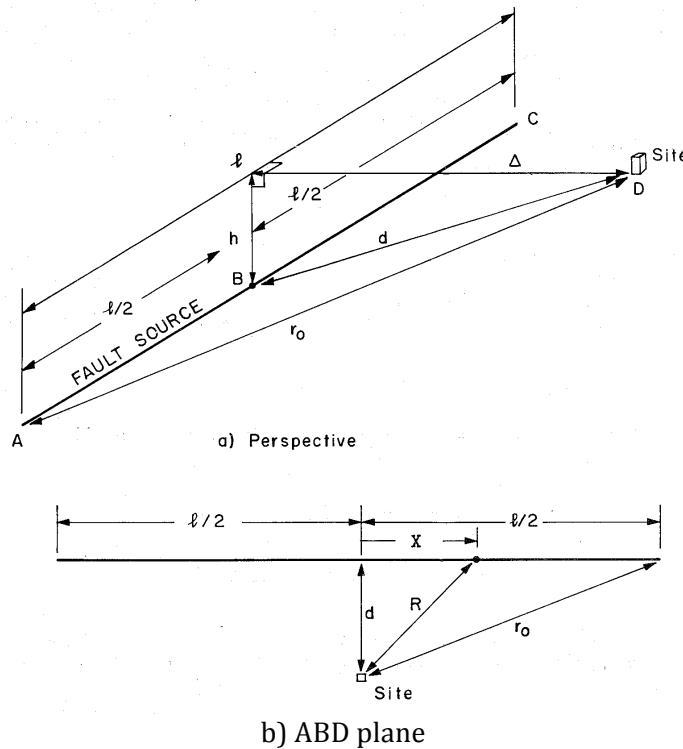


Fig. 5-6 - Line source (from Cornell, 1968).

Given that an earthquake occurs at focal distance  $R=r$ , the probability that  $I$ , the intensity at the site, is greater than any number  $i$  is, using Eq. (5-29),

$$P[I \geq i | R = r] = P[c_1 + c_2 M + c_3 \ln r \geq i | R = r], \tag{5-30}$$

in which  $P[I|R]$  is the conditional probability of  $I$  given  $R$ . Assuming probabilistic independence of  $M$  and  $R$ ,

$$P[I \geq i | R = r] = P[M \geq (i - c_3 \ln r - c_1)/c_2] = 1 - F_M[(i - c_3 \ln r - c_1)/c_2] \tag{5-31}$$

in which  $F_M(m)$  is the CDF of earthquake magnitudes. For example, Gutenberg and Richter (1944) proposed the relationship between number,  $n_m$ , and magnitude  $m$ ,  $\log n_m = a - bm$  corresponding to

$$n_m = 10^{a-bm} = e^{\alpha-\beta m} = v_0 e^{-\beta m} \tag{5-32}$$

where

$$\alpha = a \ln 10, \beta = b \ln 10, \text{ and } v_0 = 10^a = e^\alpha. \tag{5-33}$$

$\nu_0$  is, then, the average annual number of earthquakes greater than, or equal to, 0. Introducing a threshold magnitude  $m_0$ , that is some magnitude small enough, say 4, that events of lesser magnitude may be ignored by engineers because they should not produce damage, we obtain

$$\log n_m = a - bm_0 - b(m - m_0) \quad (5-34)$$

corresponding to

$$\ln n_m = \ln\left(e^{\alpha - \beta m_0} \cdot e^{-\beta(m - m_0)}\right) \quad (5-35)$$

that is

$$n_m = \nu e^{-\beta(m - m_0)} \quad (5-36)$$

in which

$$\nu = e^{\alpha - \beta m_0} \quad (5-37)$$

is the average annual number of earthquakes greater than, or equal to,  $m_0$ . This implies

$$1 - F_M(m) = P[M \geq m] = \frac{n_m}{n_{m_0}} = \frac{\nu e^{-\beta(m - m_0)}}{\nu} = e^{-\beta(m - m_0)} \quad (5-38)$$

This restriction to larger events (larger than  $m_0$ ) implies that the probabilities above are conditional on the occurrence of an event of interest, that is, one where  $M \geq m_0$ . The parameter  $b$  is typically such that  $\beta$  is about 1.5 to 2.3.

Combining Eqs. (5-31) and (5-38), the result is

$$P[I \geq i | R = r] = P[c_1 + c_2 M + c_3 \ln R \geq i | R = r] = P\left[M \geq \frac{i - c_1 - c_3 \ln r}{c_2}\right] = e^{-\beta\left(\frac{i - c_1 - c_3 \ln r}{c_2} - m_0\right)} \quad (5-39)$$

The limit on the definition of  $F_M(m)$ , namely  $m \geq m_0$ , implies that Eq. (5-39) holds for

$$(i - c_3 \ln r - c_1)/c_2 \geq m_0$$

or

$$i \geq c_2 m_0 + c_1 + c_3 \ln r. \quad (5-40)$$

At smaller values of the argument,  $i$ , the probability [Eq. (5-39)] is unity that  $I$  exceeds  $i$  (given the occurrence of an event of magnitude greater than  $m_0$  at distance  $r$ ).

In order to consider the influence of all possible values of the focal distance and their relative likelihoods, it is necessary to integrate. It is sought the CDF of  $I$ ,  $F_I(i)$ , given an occurrence of  $M \geq m_0$ ,

$$1 - F_I(i) = P[I \geq i] = \int P[I \geq i | R = r] f_R(r) dr \quad (5-41)$$

in which  $f_R(r)$  is the PDF of  $R$ , the uncertain focal distance. Considering Fig. 5.6, it is assumed that, given an occurrence of an event of interest along the fault, it is equally likely to occur anywhere along the fault. Formally, the location variable  $X$  is assumed to be uniformly distributed on the interval  $(-l/2,$

$+l/2$ ). Thus  $|X|$ , the absolute magnitude of  $X$ , is uniformly distributed on the interval  $(0, l/2)$ . The CDF  $F_R(r)$  of  $R$  follows immediately:

$$\begin{aligned} F_R(r) &= P[R \leq r] = P[R^2 \leq r^2] = P[X^2 + d^2 \leq r^2] \\ &= P[|X| \leq \sqrt{r^2 - d^2} = \sqrt{r^2 - d^2} / (l/2)] \end{aligned} \quad (5-42)$$

with  $d \leq r \leq r_0$

Therefore, the PDF of  $R$  is

$$f_R(r) = \frac{dF_R(r)}{dr} = \frac{d}{dr} \left( \frac{2\sqrt{r^2 - d^2}}{l} \right) = \frac{2r}{l\sqrt{r^2 - d^2}} \quad (5-43)$$

with  $d \leq r \leq r_0$ .

This PDF is plotted in Fig. 5.7.

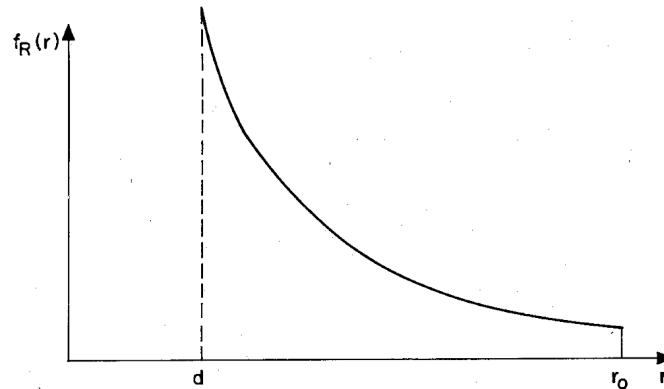


Fig. 5.7 - PDF of focal distance,  $R$  (from Cornell, 1968).

After the substitution of Eq. (5-43) into Eq. (5-41), the integration is complicated by the awkward limits of definition of the functions, but in the region of greatest interest, namely larger values of the intensity, the result is

$$1 - F_I(i) = P[I \geq i] = \frac{1}{l} CG \exp \left[ -\frac{\beta}{c_2} i \right] \quad (5-44)$$

with  $i \geq i'$

in which  $i'$  is the lower limit of validity for Eq. (5-44) and equals

$$i' = c_1 + c_2 m_0 - c_3 \ln d \quad (5-45)$$

and in which  $C$  and  $G$  are constants. The first constant is related to parameters in the various relationships used above:

$$C = \exp \left[ \beta \left( \frac{c_1}{c_2} + m_0 \right) \right] \quad (5-46)$$

The second constant is related to the geometry illustrated in Fig. 5.6:



$$G = 2 \int_d^{r_0} \frac{dr}{r^\gamma \sqrt{r^2 - d^2}} = \frac{2}{d^\gamma} \int_0^{\sec^{-1}(r_0/d)} (\cos u)^{\gamma-1} du \quad (5-47)$$

in which

$$\gamma = \beta \frac{c_3}{c_2} - 1 \quad (5-48)$$

The integral in Eq. (5-47) must be evaluated numerically. Results appear in Fig. 5.8. For typical parameter values and sufficiently long faults, it is conservative and reasonable to replace  $r_0$  by infinity. In this case  $G$  is given by

$$G = \frac{2\pi}{(2d)^\gamma} \frac{\Gamma(\gamma)}{\left[\Gamma\left(\frac{\gamma+1}{2}\right)\right]^2} \quad (5-49)$$

in which  $\Gamma(g)$  is the complete gamma function and  $g$  is restricted to positive values.

The results above yield the probability that the site intensity,  $I$ , will exceed a certain value,  $i$ , given that an event of interest ( $M \geq m_0$ ) occurs somewhere along the fault.

Next it must be considered the question of the random number of occurrences in any time period. For illustration, it is assumed that the occurrences of these major events follow a Poisson arrival process with average occurrence rate (along the entire fault) of  $\nu$  per year (annual number of events exceeding  $m_0$ ). Then,  $\tilde{N}$ , the number of events of interest along the fault in a time interval of length  $t$  years

$$\tilde{N} = \nu t \quad (5-50)$$

is known to be Poisson distributed with a PDF [see also Eq. (5-9), where  $\alpha$  corresponds to  $\nu$  and  $t=1$ ]

$$f_{\tilde{N}}(n) = P[\tilde{N} = n] = \frac{e^{-\nu t} (\nu t)^n}{n!} \quad n = 0, 1, 2, \dots \quad (5-51)$$

It is easily established that, if certain events are Poisson arrivals with average arrival rate  $\nu$  and if each of these events is independently, with probability  $p$ , a "special event," then these special events are Poisson arrivals with average rate  $p\nu$ . This is said to be a Poisson process with "random selection". In our case the special events are those which cause an intensity at the site in excess of some value  $i$ . The probability,  $p_i$ , that any event of interest ( $M \geq m_0$ ) will be a special event is given by Eq. (5-52), equivalent to Eq. (5-44).

$$p_i = P[I \geq i] = \frac{1}{l} CG \exp\left[-\frac{\beta}{c_2} i\right] \quad (5-52)$$

Thus the number of times  $N$  that the intensity at the site will exceed  $i$  in an interval of length  $t$  is

$$f_N(n) = P[N = n] = \frac{e^{-p_i \nu t} (p_i \nu t)^n}{n!} \quad n = 0, 1, 2, \dots \quad (5-53)$$

Such probabilities are useful in studying losses due to a succession of moderate intensities or cumulative damage due to two or more major ground motions.

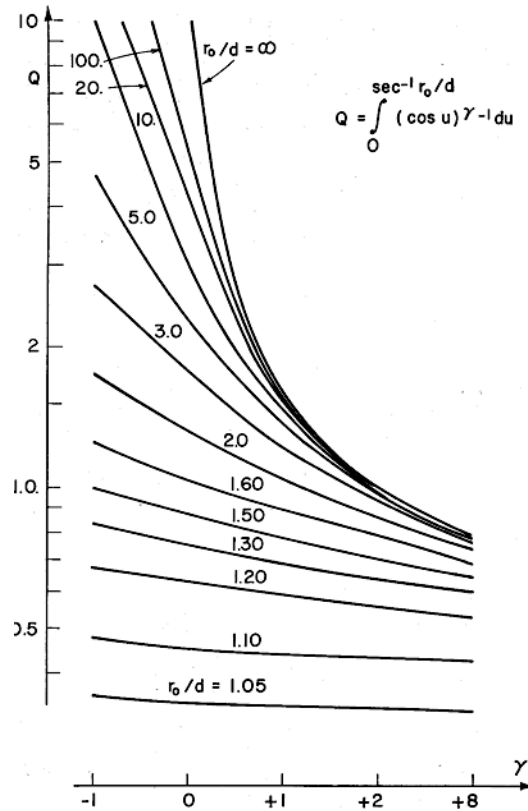


Fig. 5.8 - Numerical values of integral in Eq. (5-47) (from Cornell, 1968).

Of particular interest is the probability distribution of  $I_{max}^{(t)}$  the maximum intensity over an interval of time  $t$  (often one year). Observe that

$$F_{I_{max}^{(t)}}(i) = P[I_{max}^{(t)} \leq i] = P[\text{exactly zero special events in excess of } i \text{ occur in the time interval } 0 \text{ to } t] \tag{5-54}$$

which from Eq. (5-53) is

$$F_{I_{max}^{(t)}}(i) = P[I_{max}^{(t)} \leq i] = P[N = 0] = e^{-p_i t} \tag{5-55}$$

If we let  $I_{max}$  equal  $I_{max}^{(t)}$ , the annual maximum intensity,  $t = 1$ , and

$$F_{I_{max}}(i) = e^{-p_i} = \exp\left[-\tilde{\nu}CG \exp\left(-\frac{\beta}{c_2} i\right)\right] \quad i \geq i' \tag{5-56}$$

in which now the ratio  $\tilde{\nu} = \nu/l$  appears. This ratio is the average number of occurrences per unit length per year.

The conclusion is that for the larger intensities of engineering interest, the annual maximum intensity has a distribution of the double exponential or Gumbel type. This distribution is widely used in engineering studies of extreme events. It is important to realize that, here, this conclusion is *not* based on the intuitive appeal to the familiar asymptotic extreme value argument (Gumbel, 1958), which has caused other investigators to seek and find empirical verification of the distribution for maximum magnitudes or intensities in a given region. The form of the distribution is dependent on the functional form of the various relationships assumed above. Others, too, have found (Epstein and Lomnitz, 1966) that the combination of Poisson occurrences of events and exponentially distributed

sizes of events will invariably lead to the conclusion that the largest event has a Gumbel-like distribution (the true Gumbel distribution is non-zero for negative as well as positive values of the argument). Any combination of assumptions which leads to the exponential form of the distribution of  $I$  will, in combination with Poisson assumption of event occurrences, yield this Gumbel distribution. The exponential form of  $F_I(i)$  does not require the exponential form of  $F_M(m)$ . If the logarithmic dependence of  $I$  on  $R$  [Eq. (5-29)] is retained, for example, even polynomial distributions of magnitude will lead to the exponential distribution of  $I$ .

If the annual probabilities of exceedance are small enough (say  $\leq 0.05$ ), the distribution of  $I_{max}$  can be approximated by

$$1 - F_{I_{max}}(i) = 1 - e^{-p_i v} \cong 1 - (1 - p_i v) \cong p_i v \quad i \geq i' \quad (5-57)$$

and we obtain

$$1 - F_{I_{max}}(i) \cong \bar{v}CG \exp\left(-\frac{\beta}{c_2} i\right) \quad i \geq i'. \quad (5-58)$$

The average return period,  $T_i$ , of an intensity equal to or greater than  $i$  is defined as the reciprocal of  $1 - F_{I_{max}}(i)$  or

$$T_i \cong \frac{1}{\bar{v}CG} \exp\left(\frac{\beta}{c_2} i\right) \quad i \geq i' \quad (5-59)$$

or, the " $T$ -year" intensity is

$$i \cong \frac{c_2}{\beta} \ln(\bar{v}CGT_i) \quad i \geq i'. \quad (5-60)$$

### Numerical example

Consider the following typical numerical values of the parameters and site constants, applicable to a particular site in Turkey, where in one region in 1953 years it was found that

$$\log n_m = a - bm = 5.47 - 0.644 m$$

in which  $n_m$  is the number of earthquakes greater than  $m$  in magnitude. Assuming these earthquakes all occur along the 650 km of the major fault system in the region, the average number of earthquakes in excess of magnitude 5 (i.e.,  $m_0 = 5$ ) per year per unit length of fault is

$$\bar{v} = \frac{n_5}{(1953)(650)} = 1.5 \times 10^{-4} (\text{year})^{-1} (\text{kilometer})^{-1}$$

Also

$$\beta = b \ln 10 = 0.644(2.30) = 1.48.$$

Using attenuation constants found empirically for California

$$c_1 = 8.16; c_2 = 1.45; c_3 = 2.46$$

the following numerical results are obtained for a site located at a minimum surface distance,  $\Delta$ , of 40 km from a line source of earthquakes at depth  $h = 20$  km:

$$d = \sqrt{h^2 + \Delta^2} = 44.6 \text{ km}$$

$$v = \beta \frac{c_3}{c_2} - 1 = 1.52$$

$$C = \exp \left[ \beta \left( \frac{c_1}{c_2} + m_0 \right) \right] = 6.85 \times 10^6,$$

$$G = \frac{2\pi}{(2d)^\gamma} \frac{\Gamma(\gamma)}{\left[ \Gamma\left(\frac{\gamma+1}{2}\right) \right]^2} = 7.04 \times 10^{-3}.$$

Numerical integration gives  $G = 6.58 \times 10^{-3}$ . Thus, the intensity at this site with return period  $T_i$  is

$$i \cong \frac{c_2}{\beta} \ln(\bar{v}CGT_i) + 0.98 \ln(6.9T_i).$$

Note the logarithmic relationship between  $i$  and  $T_i$ . The risk that a design intensity will be exceeded can be halved ( $T$  doubled) by increasing the design intensity by about 0.7. This equation is plotted in Fig. 5.9 for the range of validity  $i \geq i'$  where  $i' = c_1 + c_2 m_0 - c_3 \ln d = 6.08$ .

If interest extends to smaller intensities, it necessitates more cumbersome integrations neither shown here nor in Cornell (1968).

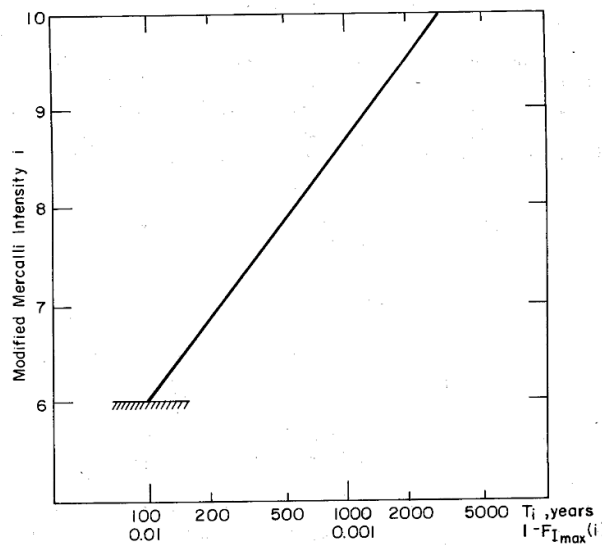


Fig. 5.9 - Numerical example: Intensity versus return period (from Cornell, 1968).

#### 5.2.2.1.2. Peak ground motion results

The previous section developed the desired distribution results for the intensity,  $I$ , and a uniform line source, with a particular set of assumptions on magnitude distribution and the intensity versus  $M$  and  $R$  relationship. Engineers are generally more directly concerned with such ground motion parameters as peak ground acceleration,  $A$ , peak ground velocity,  $V$ , or peak ground displacement,  $D$ , than with intensity itself.

An argument parallel to that in the preceding section can be carried out with any functional relationship between the site ground motion variable,  $Y$ , and  $M$  and  $R$ . For example, the particular form

$$Y = b_1 e^{b_2 m} R^{-b_3} \quad (5-61)$$

has been recommended for peak ground acceleration ( $Y=A$ ), peak ground velocity ( $Y=V$ ), and peak ground displacement ( $Y=D$ ). It was suggested that the constants  $[b_1, b_2, b_3]$  be  $[2000, 0.8, 2]$ ,  $[16, 1.0, 1.7]$ , and  $[7, 1.2, 1.6]$  for  $A$ ,  $V$ , and  $D$  respectively in southern California, with  $A$ ,  $V$ , and  $D$  in units of centimetres and seconds and  $R$  in kilometres.

For the general relationship in Eq. (5-61), an argument like that in the previous section yields for the annual maximum value of  $Y$  from a uniform line source

$$F_{Y_{\max}}(y) = \exp\left[-\tilde{\nu}CGy^{\frac{-\beta}{b_2}}\right] \quad y \geq y' \quad (5-62)$$

$$1 - F_{Y_{\max}}(y) \cong \tilde{\nu}CGy^{\frac{-\beta}{b_2}} \quad y \geq y' \quad (5-63)$$

$$T_y \cong \frac{1}{\tilde{\nu}CG} y^{\frac{-\beta}{b_2}} \quad (5-64)$$

in which

$$C = e^{\beta m_0} b_1^{b_2} \quad (5-65)$$

and  $G$  is as given in Eq. (5-47), or Eq. (5-49), with

$$\gamma = \beta \frac{b_3}{b_2} - 1. \quad (5-66)$$

The lower limit of the validity of these forms of  $F_{Y_{\max}}(y)$  is

$$y' = b_1 e^{b_2 m_0} d^{-b_3}. \quad (5-67)$$

For durations,  $t$ , other than one year,  $\tilde{\nu}$  should be replaced by  $\tilde{\nu}t$  in Eqs. (5-62) and (5-63). Notice that Eq. (5-62) is of the general form of the Type III asymptotic extreme value distribution of largest values (Gumbel, 1958). This distribution, too, is commonly used in the description of natural loadings on engineering structures, the most familiar being maximum annual wind velocities. The justification there is based on asymptotic (large  $N$ ) arguments while that here is not. The results here are a consequence of the forms of the relationships assumed.

Using results such as these, the designer can compute for his site the peak ground velocity,  $v$ , and peak ground acceleration,  $a$ , associated with the same, say the 200-year, return period. For the numerical example in the previous section and the values of the parameters referred to in this section, these values are approximately

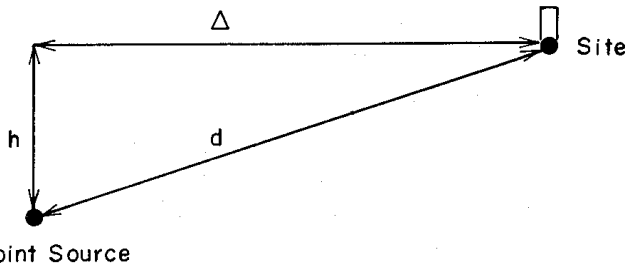
$$\begin{aligned} v &= 7.5 \text{ cm/s} \\ a &= 80 \text{ cm/s}^2 = 0.08 \text{ g.} \end{aligned}$$

### 5.2.2.1.3. General source results

In order to facilitate representing the geometry and potential source conditions at arbitrary sites, it is desirable to have additional results for point and area sources. It will be shown that these results can be used to represent quite general conditions.

If a potential source of earthquakes is closely concentrated in space relative to its distance,  $d$ , from the site, it satisfactorily may be assumed to be a point source (Fig. 5.10). In this case there is no uncertainty in the focal distance,  $d$ , and the previous results [e.g., Eqs. (5-56), (5-60), (5-62), (5-64)] hold with  $\tilde{\nu}$  equal to the average number of earthquakes of interest ( $M \geq m_0$ ) per year originating at this point and with a geometry term [in place of Eq. (5-47)] equal to

$$G = d^{-(\gamma+1)} \tag{5-68}$$



Point Source  
Fig. 5.10 - Point source, cross section (from Cornell, 1968).

For intensities,  $\gamma$  is given by Eq. (5-48) and for variables with relationships of the type shown in Eq. (5-61),  $\gamma$  is given by Eq. (5-66). For a point source, for values of the argument less than  $i'$  or  $y'$ , the CDF [Eq. (5-56) or (5-62)] is simply zero.

In some situations, owing to an apparent lack of correlation between geologic structure and seismic activity or owing to an inability to observe this structure due to deep overburdens, it may be necessary for engineering purposes to treat an area surrounding the site as if earthquakes were equally likely to occur anywhere over the area. It can be shown that for an annular areal source surrounding the site, as pictured in Fig. 5.11, the distributions above [Eqs. (5-56) and (5-62)] hold with a geometry term equal to

$$G = \frac{2\pi}{(\gamma-1)d^{\gamma-1}} \left[ 1 - \left( \frac{r_0}{d} \right)^{-(\gamma-1)} \right] \tag{5-69}$$

with  $\gamma$  given by Eq. (5-48) or (5-66). The value of  $\tilde{\nu}$  should now be the average number of earthquakes of interest ( $M \geq m_0$ ) per year per unit area. In terms of  $\nu$ , the average number per year over the entire annular region,  $\tilde{\nu}$  is

$$\tilde{\nu} = \frac{\nu}{\pi(l^2 - \Delta^2)} \tag{5-70}$$

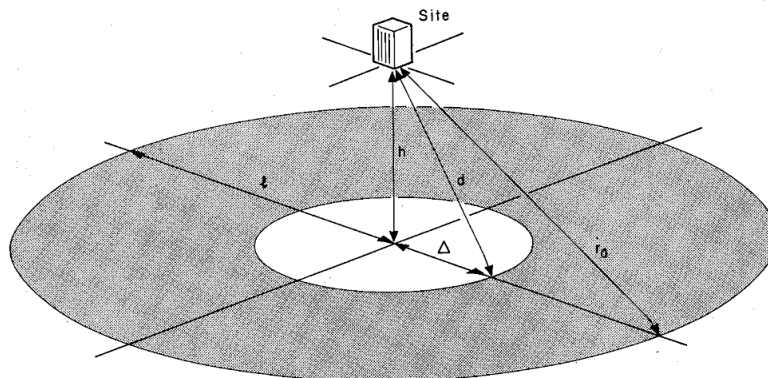


Fig. 5.11 - Annular sources, perspective (from Cornell, 1968).

For values of the argument less than  $i'$  or  $y'$ , the CDF [Eq. (5-56) or (5-62)] is zero. Note that  $d$  will never be less than  $h$ . Thus the geometry factor remains finite even when the site is "immersed" in



the areal source, i.e., when  $\Delta=0$ , and an earthquake directly below the site is an (improbable) possibility.

When more complex source configurations exist, the distribution function for the maximum value of some ground motion variable can be found by combining the results above. For example, if there exist independent sources (1, 2, ...,  $n$ ) of the various types discussed above, the probability that the maximum value of  $Y$ , the peak ground acceleration, for example, is less than  $y$  is the probability that the maximum values from sources 1 through  $n$  are all less than  $y$ , or

$$F_{Y_{\max}}(y) = F_{Y_{\max 1}}(y)F_{Y_{\max 2}}(y)\dots F_{Y_{\max n}}(y) = \prod_{j=1}^n F_{Y_{\max j}}(y) \quad (5-71)$$

in which  $F_{Y_{\max j}}(y)$  is the distribution of the maximum  $Y$  (say peak acceleration) from source  $j$ , as given by Eq. (5-62) with the appropriate values of the parameters  $\tilde{v}_j$ ,  $C_j$ ,  $G_j$ . Note that the different possible focal depths on the same fault can be accounted for in this manner.

For the exponential form of the  $F_{Y_i}(y)$  functions [Eq. (5-62)]

$$F_{Y_{\max}}(y) = \exp\left[-\sum_{j=1}^n \tilde{v}_j C_j G_j y^{\frac{-\beta_j}{b_{2j}}}\right] \quad y > y' \quad (5-72)$$

where  $y'$  is the largest of the  $y'_j$ . For  $y$  less than  $y'$ , the distribution can be found with ease (unless a line source is involved). If the constants  $b$ ,  $b_1$ ,  $b_2$ ,  $b_3$  are the same for all the sources in the region around the site, Eq. (5-72) becomes simply

$$F_{Y_{\max}}(y) = \exp\left[-\bar{v}CGy^{\frac{-\beta}{b_2}}\right] \quad y > y' \quad (5-73)$$

in which

$$\bar{v}G = \sum_{j=1}^n \tilde{v}_j G_j \quad (5-74)$$

A similar conclusion holds for intensities [Eq. (5-35)].

In short the distributions retain the same forms with the product,  $\tilde{v}G$ , equal to the sum of the corresponding products over the various sources. With respect to these products, then, linear superposition applies. This conclusion is a reflection of the fact that the sum of independent Poisson process is a Poisson process with an average arrival rate equal to the sum of individual rates.

This conclusion can be used to determine geometry factors for unsymmetrical source geometries. For example, for the condition in Fig. 5.12a, the geometry factor,  $G$ , must equal one half of that for the symmetrical situation. The geometry factor for the situation in Fig. 5.12b must equal one half of that for a symmetrical source length  $2b$  minus one half of that for a symmetrical source of length  $2a$ , or

$$G = \frac{1}{2}[G' - G''] \quad (5-75)$$

in which  $G'$  and  $G''$  are calculated from Eq. (5-47) with values  $r_o'$  and  $r_o''$  respectively. This result also permits an easy treatment of a fault with a (spatially) non-constant average occurrence rate, each different portion of the fault being treated independently.

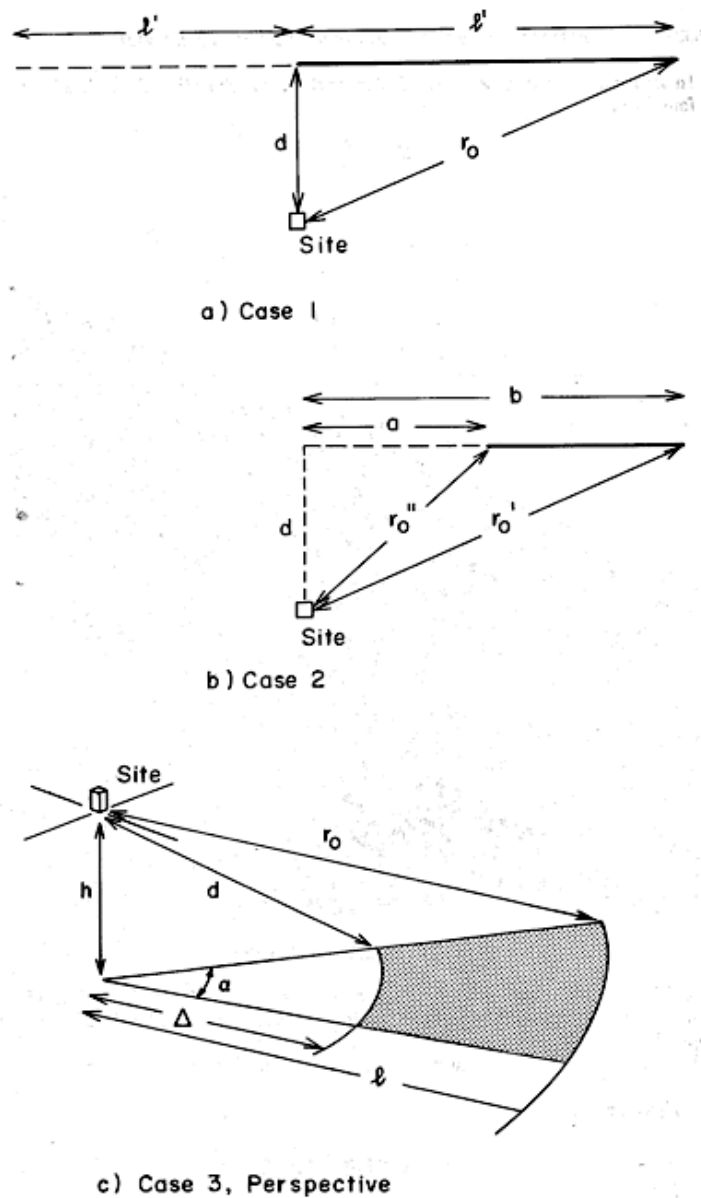


Fig. 5.12 - Unsymmetrical sources (from Cornell, 1968).

In the same manner the geometry factor for an area such as that shown in Fig. 5.12c is found to be

$$G_{\alpha} = \frac{\alpha}{2\pi} G_{2\pi} \tag{5-76}$$

in which  $G_{2\pi}$  is the result for the complete annulus [Eq. (5-69)]. An areal source of arbitrary shape can be modelled with ease by approximating it by a number of such shapes.

Note that the approximation to Eq. (5-73) for smaller values of the probability  $1 - F_{Y_{\max}}(y)$  becomes

$$1 - F_{Y_{\max}}(y) \cong Cy^{-\frac{\beta}{b_2}} \sum_{j=1}^n \tilde{v}_j G_j \tag{5-77}$$

suggesting that the (small) probability that the annual maximum,  $Y_{max}$ , exceeds  $y$  in any year is made up of the sum of the probabilities contributed by each of the sources. Also, for larger values the return period is approximately

$$T_y \cong \frac{1}{C \sum v_j G_j} y^{\frac{\beta}{b_2}}. \quad (5-78)$$

It is interesting to notice that all calculations refer to the occurrence of a single earthquake and Eq. (5-27) considers only the integration over distance, while the complete integration over distance and magnitude was presented by Whitman and Cornell (1976).

#### 5.2.2.2. The general probabilistic hazard model

The basic concept of probabilistic seismic hazard assessment is quite simple and consists 1) in calculating the probability for the shaking parameter  $Y$  to exceed at the study site a particular level,  $y$ , at the occurrence of an earthquake in one of the sources considered, and 2) in multiplying it by the probability that an earthquake of that particular magnitude occurs at that particular distance from the study site. The calculation is then repeated for all possible magnitudes and source to site distances, adding at the end all these probabilities.

In detail, the calculation of seismic hazard is based on the Total Probability Theorem:

$$P[E] = \int_S P[E|S] f_S(s) ds \quad (5-79)$$

where  $P[E]$  represents the probability that event  $E$  occurs,  $P[E|S]$  is the conditional probability of the event  $E$  given the occurrence of the event  $S$  and  $f_S(s)$  is the PDF of  $S$ , being  $S$  a continuous random variable.

If  $S$  is a discrete random variable taking the values  $S_1, S_2, \dots, S_n$ , the previous Eq. (5-79) takes the form:

$$P[E] = \sum_1^n P[E|S_i] P[S_i]. \quad (5-80)$$

With regard to the seismic hazard, the quantities that describe fully  $S$  are the magnitude  $M$  and the source to site distance  $R$ . Assuming that  $M$  and  $R$  are independent random variables, Eq. (5-50) becomes:

$$P[E] = \int_M \int_R P[E|M=m, R=r] f_M(m) f_R(r) dm dr \quad (5-81)$$

where  $P[E|M=m, R=r]$  is the conditional probability of  $E$  given the occurrence of an earthquake of magnitude  $m$  at distance  $r$  from the study site. The double integration takes into account all possible magnitudes of all possible distances.

If the event  $E$  consists in exceeding the shaking  $y$  at the site, and if  $N_S$  seismic sources concur to define the hazard of the site, Eq. (5-81) becomes:

$$P[Y > y] = \sum_1^{N_S} \int_M \int_R P[Y > y | M=m, R=r] f_M(m) f_R(r) dm dr. \quad (5-82)$$

Eq. (5-82) expresses the probability that a fixed value of ground motion  $y$  is exceeded the site, given the occurrence of an earthquake in each seismic source; it represents the core of the

probabilistic calculation of seismic hazard. The problem now is to solve the double integral by explicating the 3 probability functions  $P[Y>y|M=m, R=r]$ ,  $f_M(m)$  and  $f_R(r)$ .

The general procedure for calculating seismic hazard was originally proposed at U.S.G.S. both by Algermissen and Perkins (1976) and McGuire (1976) and then specified by Reiter (1990) and Kramer (1996). It basically refers to the original formulation proposed by Cornell (1968) and formalizes the procedure itself in 5 steps (Reiter, 1990) of which the first 3 are essentially very similar to those used in the DSHA. This procedure is based on the assumption that earthquakes form a stochastic, i.e., random, process. If the seismic events can be considered statistically independent, then the cumulative number of earthquakes of a certain magnitude class is a Poisson random variable and the distribution function of the elapsed times (inter event intervals) is exponential. An alternative model to the Poisson one is the “renewal” model, in which the occurrence probability of an event depends on the elapsed time since the previous one. Both the Poisson and renewal models will be considered in the following chapters.

The general procedure for a PSHA requires five steps (Fig. 5.13).

- Step 1.** The first step aims at making explicit  $f_R(r)$  and involves the identification and delineation of potential sources of seismicity that may affect the site or sites of interest. These sources of seismicity may be represented as area sources (SZs), fault sources (SFs), or, rarely, point sources, depending upon the geological nature of the sources and available data.
- Step 2.** In the second step  $f_M(m)$  is defined as the temporal behaviour of earthquakes is determined for each source by establishing a magnitude recurrence relationship over the range of magnitudes that are likely to be generated by each seismic source. Traditionally recurrence models have assumed a G-R relationship ( $\log N = a - bM$ ) where  $N$  is the number of earthquakes with magnitude greater than, or equal to,  $M$ . However, other recurrence models, such as the characteristic earthquake model, are certainly possible and can be applied, if appropriate. A description of the characteristic earthquake model is given in chapter 5.4.2.3.
- Step 3.** The third step makes explicit  $P[Y>y|M=m, R=r]$  and involves the use of a ground motion prediction model to establish the conditional probability of exceedance of a pre-specified ground motion value for each site given the occurrence of an earthquake at a particular magnitude and location. Ground motion prediction models are derived for several quantities describing the ground shaking [peak ground acceleration (PGA), peak ground velocity (PGV), peak ground displacement (PGD, spectral acceleration (SA), etc.] mainly from strong motion data; the resulting prediction equations usually consist of separate relations for elastic response spectral amplitudes for different soil types (hard rock, stiff soil, soft soil, etc.).
- Step 4.** The fourth step of the analysis consists in the integration of the first three steps over all possible magnitudes and earthquake locations to produce the ultimate result of a seismic hazard analysis: the seismic hazard curve, i.e., a function representing the annual probability (or the annual frequency) of exceeding various levels of ground shaking (in terms of PGA, PGV, PGD, SA, etc.) at a specific site. Response spectra are an advantage in areas of engineering concern because the response of a structurally complex building can be modelled as the superposition of a number of single degree-of-freedom oscillators (i.e., different values of SA). Therefore, hazard curves are calculated for a number of different single-degree-of-freedom oscillators which, in turn, can be used for the development of uniform hazard spectra. Uniform hazard response spectra are derived from hazard curves by selecting oscillator response values for a specific exceedance probability (frequency).
- Step 5.** The fifth step of the analysis consists in the introduction of the earthquake recurrence model (e.g., the Poisson model) for the computation of seismic hazard referred to different time periods.

In summary, the PSHA according to the seismotectonic probabilism (Fig. 5.13) requests the spatial identification of the earthquake sources and the distribution of earthquakes within each source (Step 1), requires the distribution of earthquake size for each source (Step 2), needs the definition of the attenuation model (Step 3), and, after having computed the annual seismic hazard (Step 4), requests the distribution of earthquakes with time (Step 5). Each of these characteristics involves some degree of uncertainty.

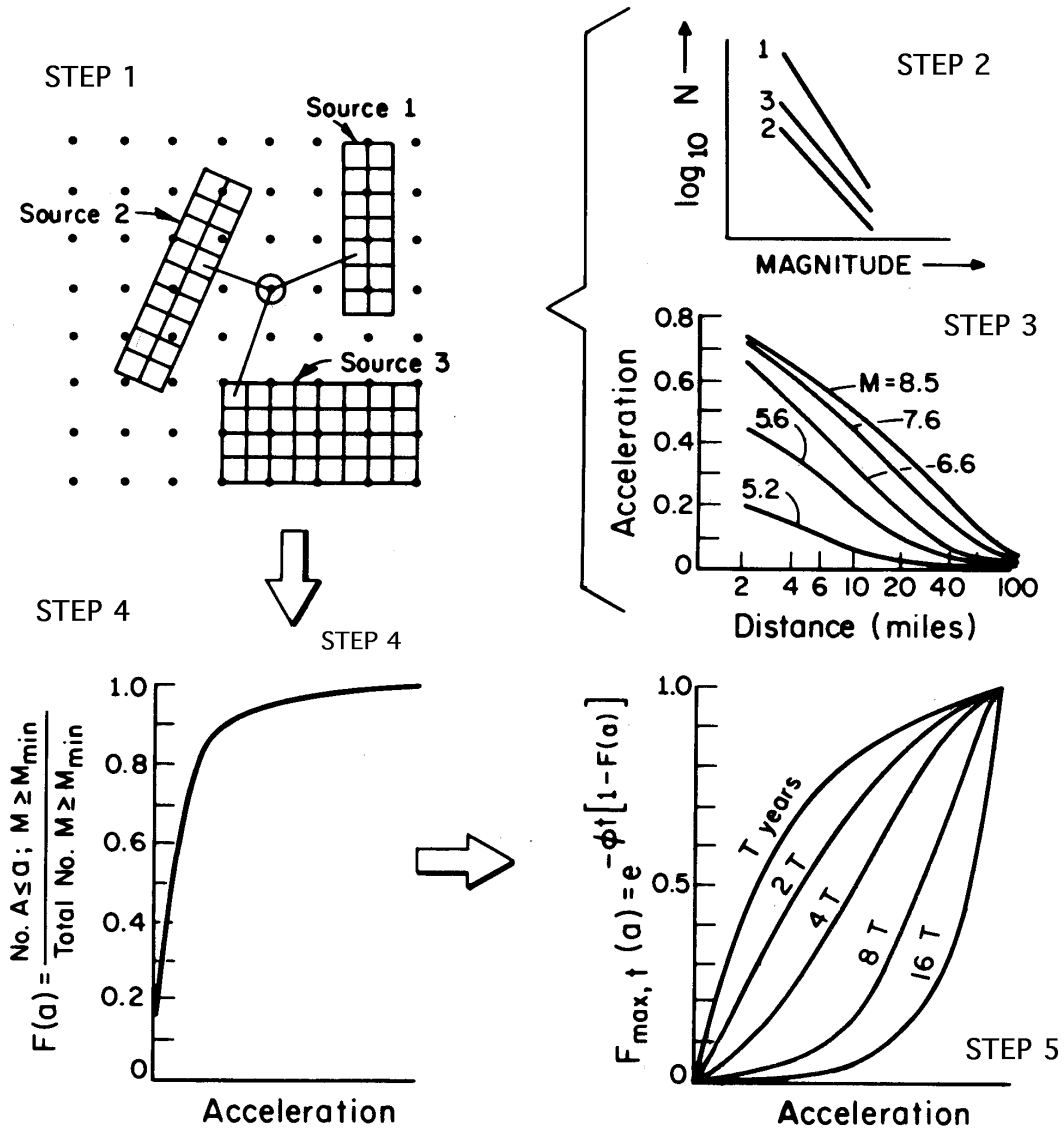


Fig. 5.13 – The five steps of a PSHA (from Algermissen and Perkins, 1976).

5.2.3.1. Step 1: spatial identification of the earthquake sources

The geometries of earthquake sources depend on the tectonic processes involved in their formulation. Earthquakes associated with volcanic activity, for example, generally originate in zones near the volcanoes that are small enough to allow them to be characterized as point sources. Well defined fault planes, on which earthquakes can occur at many different locations, can be considered as two-dimensional areal sources (SFs). Areas where earthquake mechanisms are poorly defined, or where faulting is so extensive as to preclude distinction between individual faults, can be treated as three-dimensional volumetric sources (SZs).

For the purposes of a PSHA, the earthquake source may be similar to, or somewhat different than, the actual source, depending on the relative geometry of the source and site of interest and on the quality of information about the sources. For example, the relatively short fault in Fig. 5.14a can be modelled as a point source since the distance between any point along its length and the site is nearly constant. Similarly, the depth of the vertical fault plane shown in Fig. 5.14b is sufficiently small that variations in hypocentral depth have little influence on hypocentral distance. In such a case the hazard analysis can be simplified with negligible loss of accuracy by approximating the planar source as a

linear source zone. In Fig. 5.14c, the available data are insufficient to determine accurately the actual geometry of the source, so it is represented as a volumetric source.

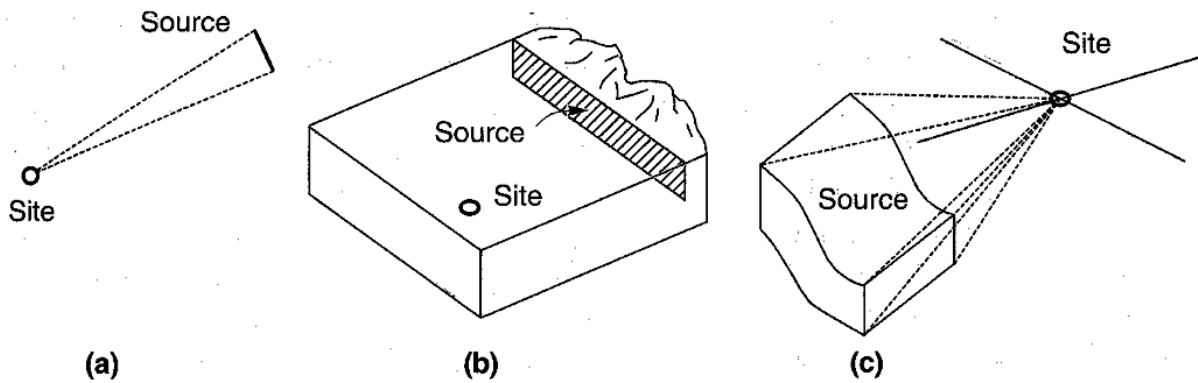


Fig. 5.14 – Examples of different earthquake source geometries: a) short fault that can be modelled as a point source; b) shallow fault that can be modelled as a linear source; c) 3D source zone modelled as an area source (from Kramer, 1996).

In the Cornell (1968) approach, earthquakes are usually assumed to be uniformly distributed within a particular source zone (i.e., earthquakes are considered equally likely to occur at any location). The assumption of uniformity is by no means required; non-uniform distributions may be used when sufficient information to justify them exists (or, more easily, the source can be subdivided in some uniform sub-sources). A uniform distribution within the source zone does not, however, often translate into a uniform distribution of source-to-site distance. Since predictive relationships express ground motion parameters in terms of some measure of source-to-site distance, the spatial uncertainty must be described with respect to the appropriate distance parameter. The uncertainty in source-to-site distance can be described by a PDF.

For the point source of Fig. 5.15a, the distance,  $R$ , is known to be  $r_s$ ; consequently, the probability that  $R=r_s$  is assumed to be 1, and the probability that  $R \neq r_s$  is zero.

Other cases are not so simple. For the linear source of Fig. 5.14b, as  $l^2 = r^2 - r_{\min}^2$  (see Fig. 5.15b), the CDF of  $R$  is:

$$F_R(r) = P[R \leq r] = P[R^2 \leq r^2] = P[L^2 + r_{\min}^2 \leq r^2] = P[|L| \leq \sqrt{r^2 - r_{\min}^2}] \quad (5-83)$$

and, considering the frequentistic approach (favourable cases over possible cases), we have:

$$F_R(r) = \frac{\sqrt{r^2 - r_{\min}^2}}{L_f} \quad (5-84)$$

It comes that:

$$f_R(r) = \frac{dF_R(r)}{dr} = \frac{d}{dr} \frac{\sqrt{r^2 - r_{\min}^2}}{L_f} = \frac{r}{L_f \sqrt{r^2 - r_{\min}^2}} \quad (5-85)$$

For source zones with more complex geometries, it is easier to evaluate  $f_R(r)$  by numerical rather than analytical methods. For example, dividing the irregular source zone of Fig. 5.15c into a large number of discrete elements of equal area, a histogram that approximates  $f_R(r)$  can be constructed by tabulating the values of  $R$  that correspond to the centre of each element.



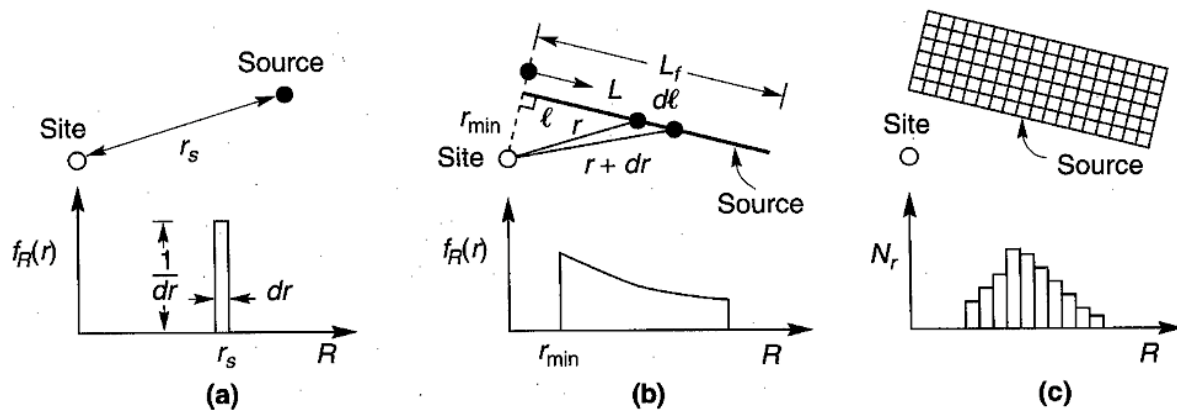


Fig. 5.15 - Examples of variations of source-to-site distance for different source zone geometries. The shape of the PDF can be visualized by considering the relative portions of the source zone that would fall between each of a series of circles (or spheres for 3D problems) with equal differences in radius (from Kramer, 1996).

Fig. 5-16 shows the SZs used in the construction of the most recent seismic hazard map of the Italian territory (Gruppo di Lavoro, 2004). Each source is associated with an average depth of earthquake foci and a typical mechanism of rupture (focal mechanism).

The preceding discussion assumes that all the energy is released at the hypocentre of the earthquake. However, energy is released over the entire fault rupture surface, parts of which may be much closer to the site than the hypocentre. Der Kiureghian and Ang (1977) noted that the rupture surface of a large earthquake with a distant hypocentre could release energy much closer to the site, and developed methods to account for rupture surface dimensions in PSHA.

### 5.2.3.2. Step 2: seismic characterization of the earthquake sources

Once an earthquake source is identified and its corresponding source zone characterized, the seismic hazard analyst's attention is turned toward the evaluation of the sizes of earthquakes that the source zone can be expected to produce. The strain energy may be released aseismically (and therefore not considered in PSHA), or in the form of earthquakes. The distribution of earthquake sizes in a given period of time is described by a recurrence law. A basic assumption of PSHA is that the recurrence law obtained from past seismicity is appropriate for the prediction of future seismicity: i.e., seismicity is assumed to be stationary in time. This assumption is clearly not realistic at a geological time scale, but it is for the time scale of our knowledge, according to contents of the earthquake catalogues (a few millennia at maximum). It is also not realistic during a seismic sequence, when the number of aftershocks decreases with time and, generally, the event magnitude is much smaller than that of the main event. Fluctuations during short time periods (years or decades) of the seismic activity are also possible in nature and this aspect must be considered in the estimation of the average seismicity of the seismic source.

The most popular models of seismicity are two: that of G-R that considers each source producing earthquakes of all magnitudes, from the smallest to a maximum value, variable from source to source, and that of the characteristic earthquake, which states that each source can produce only earthquakes with a magnitude of a certain value, different from source to source and dependent on the size of the source. The two models may coincide considering the characteristic earthquake model valid for individual faults and the G-R one for extended sources, which contain faults of different sizes.

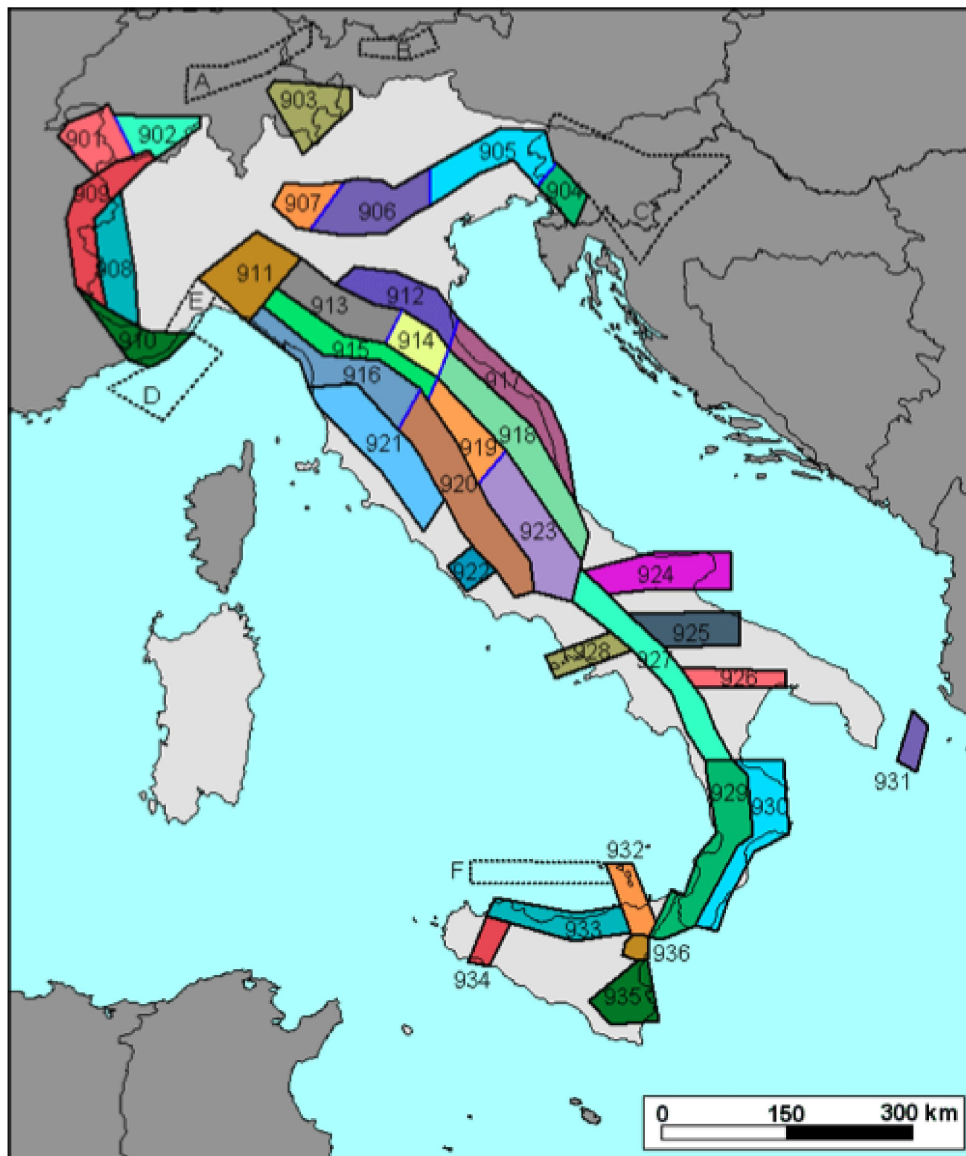


Fig. 5.16 – The SZs used in the most recent seismic hazard map of Italy (Meletti et al., 2008).

#### 5.2.2.2.1. Gutenberg-Richter recurrence law

Gutenberg and Richter (1944) gathered data for southern California earthquakes over a period of many years and organized the data according to the number of earthquakes that exceeded different magnitudes during that time period. They divided the number of exceedances of each magnitude by the length of the time period to define a mean annual rate of exceedance, of an earthquake of magnitude  $m$ . As would be expected, the mean annual rate of exceedance of small earthquakes is greater than that of large earthquakes. The reciprocal of the annual rate of exceedance for a particular magnitude is commonly referred to as the **recurrence interval** of earthquakes exceeding that magnitude. When the logarithm of the annual rate of exceedance of southern California earthquakes was plotted against earthquake magnitude, a linear relationship was observed. The resulting G-R law for earthquake recurrence was expressed as [see Eq. (5-1)]

$$\log n_m = a - bm \quad (5-1)$$

where  $n_m$  is the mean annual rate of exceedance of magnitude  $m$ , and  $b$  (the  $b$ -value) describes the relative likelihood of large and small earthquakes. For PSHA, Eq. (5-1) is usually expressed in the equivalent form:

$$n_m = 10^{a-bm} = e^{\alpha-\beta m} = v_0 e^{-\beta m} \tag{5-86}$$

where  $\alpha=2.303a$ ,  $\beta=2.303b$  [see Eq. (5-19)], and  $v_0=10^a$  is the mean yearly number of earthquakes of magnitude greater than, or equal to, zero. From this relation, it comes that the cumulative number of earthquakes of a certain magnitude is exponentially distributed or, more simply, that the magnitude has an exponential distribution.

The G-R relation in practice is valid in both cases: when considering the number of earthquakes with a magnitude of a specific class or when considering the cumulative number of events in the magnitude classes, i.e., the number of earthquakes of magnitude greater than, or equal to, the class value. As this is an experimental relationship, the small fluctuations that are obtained moving from the individual number of events to the cumulative one are largely in the scatter of data.

The G-R law is illustrated schematically in Fig. 5.17a. As the  $b$ -value increases, the number of larger magnitude earthquakes decreases compared to those of smaller magnitudes. The G-R law is not restricted to the use of magnitude as a descriptor of earthquake size; epicentral intensity has also been used: this is correct only if a linear scaling law between magnitude and macroseismic intensity is accepted. Worldwide recurrence data are shown in Fig. 5.17b.

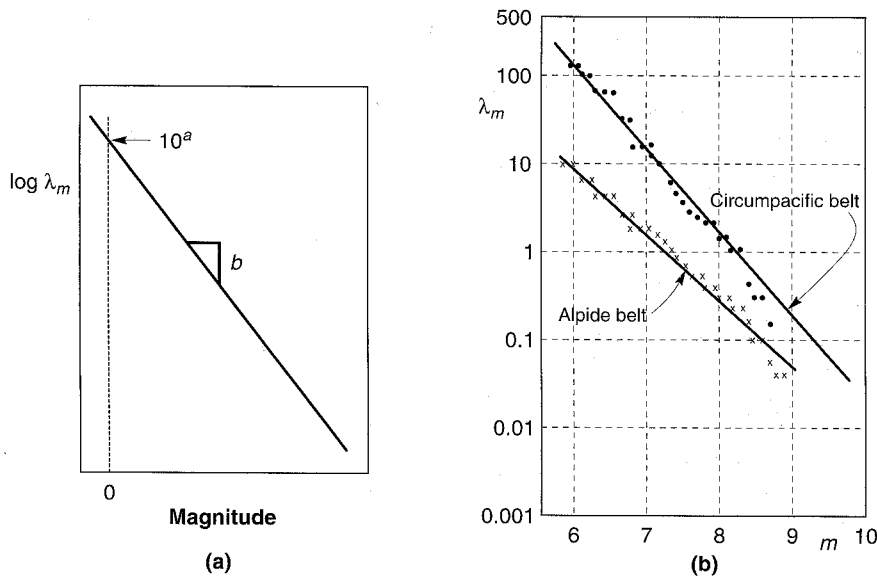


Fig. 5.17 - Gutenberg-Richter recurrence law: a) showing meaning of  $a$  and  $b$  parameters; b) application of G-R law to worldwide seismicity data (from Kramer, 1996).

The  $a$  and  $b$  parameters are generally obtained by regression on a database of seismicity from the source zone of interest. Unless the source zone is extremely active, the database is likely to be relatively sparse. Since the use of both instrumental and historical events is usually required, the database may contain both magnitude (possibly based on different scales) and intensity data, necessitating the conversion of one measure of size to the other. The instrumental data may require as well a conversion of magnitudes from one type to another. The utmost care must be taken in these conversion operations to avoid the introduction of a systematic error.

From Eq. (5-86), it derives that

$$F_M(m) = P[M < m] = \frac{n_0 - n_m}{n_0} = 1 - e^{-\beta m} \tag{5-87}$$

and the PDF:

$$f_M(m) = \frac{d}{dm} F_M(m) = \beta e^{-\beta m} \tag{5-88}$$

In some areas, the record of seismicity may be distorted by the presence of dependent events such as aftershocks and foreshocks (Merz and Cornell, 1973). Although such dependent events can cause significant damage, a PSHA, according to the Cornell (1968) approach, is intended to evaluate the hazard from discrete, independent releases of seismic energy. Therefore, dependent events must be removed from the seismicity database and their effects accounted for in separate analyses. It should be remembered that it is extremely difficult to identify objectively a dependent seismic event because it would need to know exactly the seismogenesis of each earthquake. The technique, called declustering, commonly used is based on defining a space-time window, depending on the magnitude of the main event, in which we assume that foreshocks and aftershocks can occur (Gardner and Knopoff, 1974).

Completeness of the database must also be considered. The historical record is usually more complete for large earthquakes than for small earthquakes; small earthquakes can go undetected for a variety of physical and demographic reasons. Fitting a straight line such as that implied by the G-R law through recurrence data in which the mean rate of exceedance of small earthquakes is underestimated will tend to flatten the line. As a result, the actual mean rate of small earthquakes will be underpredicted and the mean rate of large earthquakes will be overpredicted. The calculation of annual seismicity rates involves identifying the specific time periods for each magnitude class in which the catalogue is complete. Usually this analysis of completeness is done simply by checking the stability of the (annual or per decades) number of earthquakes (e.g., Nasir et al., 2013) by Stepp (1972) graphs. The Stepp (1972) test relies on the statistical property of the Poisson distribution highlighting time intervals during which the recorded earthquake recurrence rate is uniform. Supposing that earthquake recurrences follow a Poisson distribution, the Stepp test evaluates the stability of the mean rate of occurrences ( $\lambda$ ) of events which fall in a predefined intensity range in a series of time windows (T). If  $\lambda$  is constant, then the standard deviation ( $\sigma$ ) varies as  $1/\sqrt{T}$ . On the contrary, if  $\lambda$  is not stable,  $\sigma$  deviates from the straight line of the  $1/\sqrt{T}$  slope. The length of the time interval at which no deviation from that straight line occurs defines the completeness time interval for the given intensity range (Fig. 5.18). This interval is visually determined from the plots. This analysis does not verify the completeness of the catalogue but its stationarity. Since stationarity is also requested by the Cornell (1968) method, the operation is lawful even if a historical analysis based on the estimate of the changes in quality of the collection of seismic data during the time is suggested. The correct estimate of the annual rates is extremely important to avoid that the low magnitude classes, poorly documented in the past, result underestimated and, consequently, adversely affect the estimate of the  $b$ -value.

Several specific methods are available in the literature to compute the  $b$ -value. The least squares method, easy to apply, is not statistically correct for the seismicity rate computation since magnitude is not uncertainty free and the earthquake number does not follow the Gaussian distribution with uniform variance. If you consider the cumulative number of earthquakes, the least squares technique is even more inappropriate, because the values of the dependent variable are not independent of each other, as required by this method, since the number of earthquakes greater than 5 also includes that of events greater than 6, and so on. For seismological purposes, therefore, the maximum likelihood method, originally proposed by Aki (1965) and Utsu (1965), is applied. Weichert (1980) proposed a procedure of general applicability that also considers different completeness periods of the earthquake catalogue. We must, also, remember the characteristics of the various types of magnitude: only the moment magnitude ( $M_W$ ) is tied directly to a physical quantity (the seismic moment) and, therefore, its classes are evenly spaced. Given a scaling law between  $M_W$  and all other magnitude scales, one sees that even spacing is compromised with a resulting clustering of earthquakes in certain classes and rarefaction in others. The linearity of the G-R relationship is, in this way, compromised.

#### 5.2.2.2.2. Bounded Gutenberg-Richter recurrence law and maximum magnitude

The standard Gutenberg-Richter law covers an infinite range of magnitudes, from  $-\infty$  to  $+\infty$ . For engineering purposes, the effects of very small earthquakes are of little interest and it is common to disregard those that are not capable of causing significant damage [but they contribute to the seismic hazard estimate because, although they have a very low probability to produce strong ground

motions, they have a very high occurrence probability [Reiter, 1990]]. If earthquakes smaller than a lower threshold magnitude  $m_0$  are eliminated, the mean annual rate of exceedance can be written (McGuire and Arabasz, 1990) as

$$n_m = \nu e^{-\beta(m-m_0)} \quad m > m_0 \tag{5-89}$$

where

$$\nu = e^{\alpha - \beta m_0} \tag{5-90}$$

is the rate of occurrence of earthquakes exceeding  $m_0$ . In most PSHAs, the lower threshold magnitude is set at values from about 4.0 to 5.0 since magnitudes smaller than that seldom cause significant damage. The resulting probability distribution of magnitude for the G-R law with lower bound can be expressed in terms of the CDF:

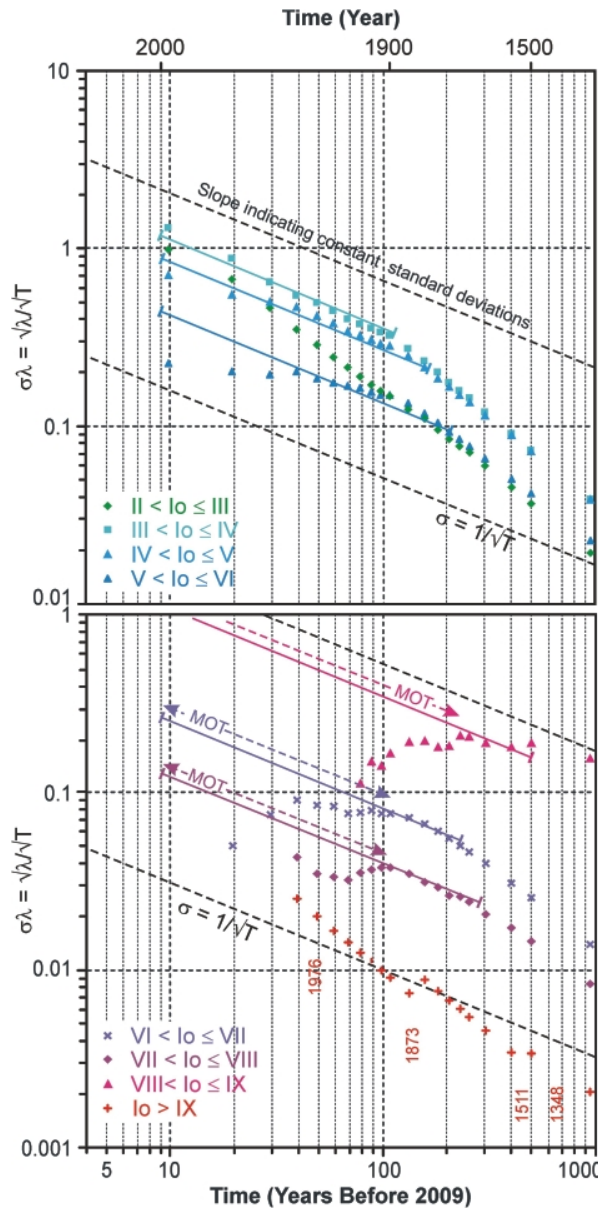


Fig. 5.18 – Stepp graphs for different intensity classes (from Nasir et al., 2013). Dashed arrows in the lower diagram indicate the minimum observation time (MOT) required for deriving reliable average recurrence intervals for the intensity class indicating that ~100 years observation are required for VI <  $I_0$  ≤ VIII and ~250 years for VIII <  $I_0$  ≤ IX. For the intensity class  $I_0$  > IX only four events are reported. A completeness time period with stable  $\sigma$  cannot be determined for the intensity class  $I_0 = X$ .

$$F_M(m) = P[M < m \mid M > m_0] = \frac{n_{m_0} - n_m}{n_{m_0}} = 1 - e^{-\beta(m-m_0)} \quad (5-91)$$

or the PDF:

$$f_M(m) = \frac{d}{dm} F_M(m) = \beta e^{-\beta(m-m_0)} \quad (5-92)$$

At the other end of the magnitude scale, the standard G-R law predicts nonzero mean rates of exceedance for magnitudes up to infinity. This implies, for example, that the Circumpacific belt (Fig. 5.17b) would produce a magnitude 10 earthquake at a mean annual exceedance rate of about 0.02 per year (a return period of only 50 years), even though earthquakes of that size have never been observed. Some maximum magnitude,  $m_{max}$ , is associated with all source zones. If it is known or can be estimated, the mean annual rate of exceedance can be expressed (McGuire and Arabasz, 1990) as

$$n_m = \nu \frac{e^{-\beta(m-m_0)} - e^{-\beta(m_{max}-m_0)}}{1 - e^{-\beta(m_{max}-m_0)}}. \quad (5-93)$$

This form was first proposed by Cornell and Van Marke (1969) motivated by the existence of an upper limit to the size of earthquakes that can be generated by an individual fault, or that can occur in a finite volume of crust encompassing a set of faults.

The bounded recurrence law of Eq. (5-93) is shown in Fig. 5.19a for conditions of constant rate of seismicity (i.e., constant mean annual rate of exceedance of  $m_0$ ). An alternative interpretation, based on a constant rate of seismic moment (hence energy) release, produces the recurrence curves of Fig. 5.19b. In the constant moment rate model, increasing the maximum magnitude requires a substantial decrease in the mean annual rate of exceedance of lower magnitude events to account for the extra energy released in large earthquakes. Since the seismic moment is proportional to the amount of slip (displacement) that occurs in an earthquake, the moment rate is proportional to the slip rate. Hence the constant-moment-rate model is equivalent to a constant-slip-rate model and can be used when the slip rate is known to be constant. The extent to which actual slip rates vary with time, however, appears to be different for different faults and can even fluctuate with time along the same fault.

The CDF and PDF for the G-R law with upper and lower bounds can be expressed as

$$F_M(m) = P[M < m \mid m_0 \leq M \leq m_{max}] = \frac{1 - e^{-\beta(m-m_0)}}{1 - e^{-\beta(m_{max}-m_0)}} \quad (5-94)$$

$$f_M(m) = \frac{\beta e^{-\beta(m-m_0)}}{1 - e^{-\beta(m_{max}-m_0)}}.$$

The maximum magnitude can be estimated in several ways, the simplest is to take for  $m_{max}$  the maximum value historically observed. Conservatively, sometimes, this value is slightly increased, for example by 0.2 magnitude units. More sophisticated methods consist in calculating statistically  $m_{max}$  from the earthquake catalogue of the source considered (e.g., Kijko and Graham, 1998) or from the geometry of the source (e.g., Wells and Coppersmith, 1994).

The Kijko and Graham (1998) approach requests the values of the maximum observed magnitude, the seismicity parameters, and the completeness interval of the catalogue used for the assessment of the parameters; then it computes  $m_{max}$  on a statistical base. The EPRI approach (Johnston et al., 1994) corrects a prior distribution of  $m_{max}$ , calculated for seismic sources in stable continental regions, according to the seismicity parameters of the studied source.

The geological approach for the determination of  $m_{max}$  for a seismogenic source is based on the scaling law between fault features (surface rupture length, rupture area, etc.; see, e.g., Fig. 5.20) and



maximum (or characteristic) magnitude and was established, among others, by Bonilla et al. (1984), for global faults, and Wells and Coppersmith (1994), for earthquakes in California, etc. (see Table 5.4).

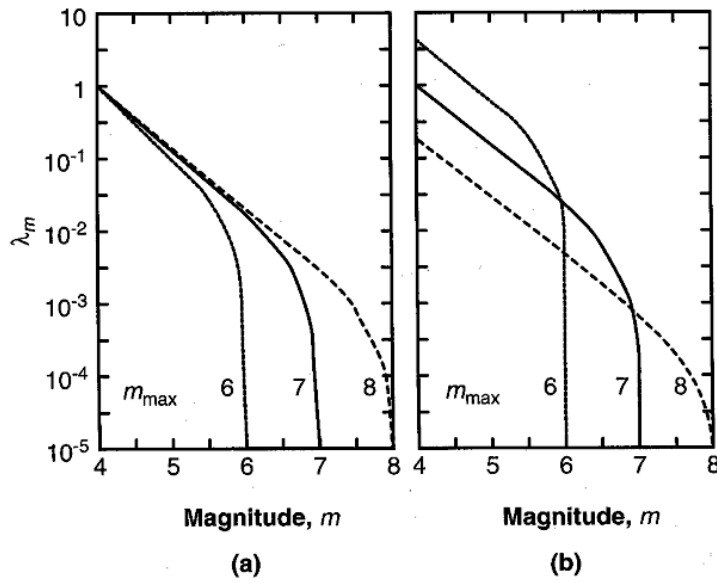


Fig. 5.19 - Bounded G-R recurrence laws for  $m_0=4$  and  $m_{max}=6, 7,$  and  $8$  constrained by: a) constant seismicity rate; b) constant moment rate (from Youngs and Coppersmith, 1985).

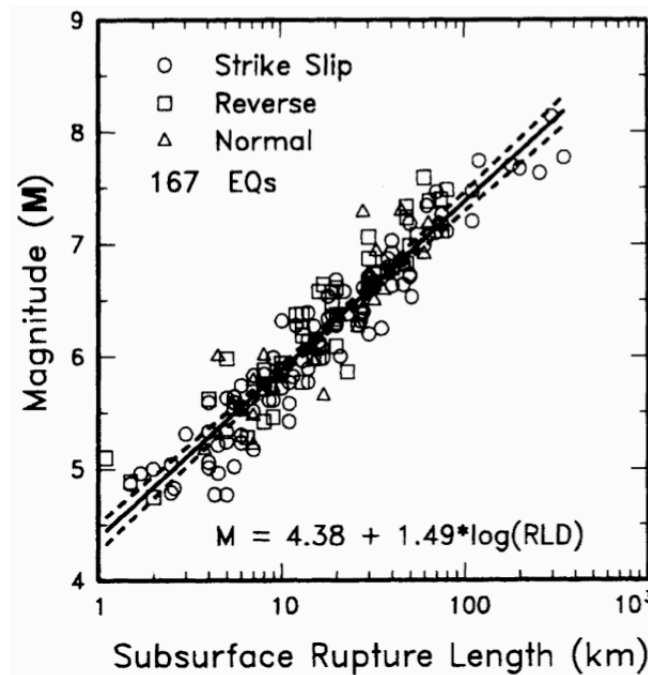


Fig. 5.20 - Regression of rupture length on magnitude by Wells and Coppersmith (1994). The dashed line shows 95% confidence intervals.

Table 5.4 – Scaling laws between fault dimensions and magnitude.

Wells & Coppersmith (1994) all fault types	$M=0.98 \cdot \log A+4.07$
Wells & Coppersmith (1994) Strike slip	$M=1.02 \cdot \log A+3.98$
Wells & Coppersmith (1994) reverse	$M=0.90 \cdot \log A+4.33$
Ellsworth (2001) Strike slip for $A>500 \text{ km}^2$	$M=\log A+4.2$
Sommerville et al. (1999) All fault types	$M=\log A+3.95$

## 5.2.2.2.3. Characteristic earthquake recurrence laws

The G-R law was developed from a set of regional data that included many different seismic sources. Since PSHAs are usually conducted for specific sites rather than large regions, the earthquake-generating characteristics of individual faults are important. The ability of the G-R law to represent the behaviour of a single source has been called into question (Schwartz and Coppersmith, 1984) because some regions repeatedly experience earthquakes and this suggests that perhaps earthquakes are part of a cycle of build in and release of deformation.

Paleoseismic studies indicate that individual points on faults and fault segments tend to move by approximately the same distance in each earthquake. This has suggested that individual faults repeatedly generated earthquakes of similar (within about one-half magnitude unit) size, known as characteristic earthquakes, at or near their maximum magnitude [this model is called “maximum magnitude model” by Wesnousky et al. (1984), see Fig. 5.21]. Characteristic earthquakes occur on a fault not at the exclusion of all other magnitudes (foreshocks, aftershocks, and generally low-level background activity), but with a frequency distribution that differs from an exponential magnitude distribution model. Alternatively, the apparently repetitive nature of fault movement at individual points may be controlled by localized geologic constraints and, consequently, not reflect earthquake magnitude very accurately. Resolution of these alternative interpretations awaits further paleoseismic research.

By dating these characteristic earthquakes, their historical rate of recurrence can be estimated. Geologic evidence indicates the characteristic earthquakes occur more frequently than would be implied by extrapolation of the G-R law from high exceedance rates (low magnitude) to low exceedance rates (high magnitude). The result is a more complex recurrence law that is governed by seismicity data at low magnitudes and geologic data at high magnitudes, as shown in Fig. 5.22.

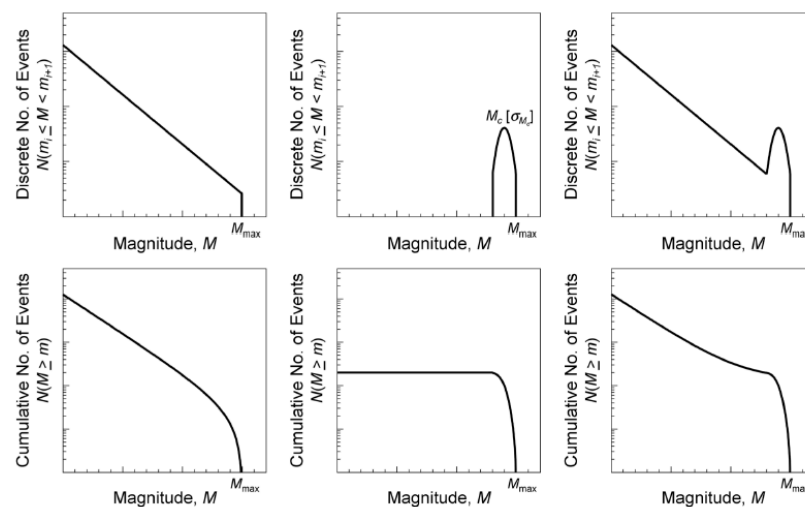


Fig. 5.21 – Number of earthquakes vs. magnitude according to the G-R model (left column), the characteristic earthquake model (central column), and G-R model for low to medium events and characteristic earthquake model for large events (right column).

Youngs and Coppersmith (1985) developed a generalized magnitude-frequency PDF that combined an exponential magnitude distribution at lower magnitudes with a uniform distribution in the vicinity of the characteristic earthquake. Recurrence relationships derived from the Youngs and Coppersmith (1985) model and the bounded G-R model, assuming the same  $m_{max}$ ,  $b$ -value, and slip rate, are shown in Fig. 5.23. The characteristic earthquake model predicts higher rates of exceedance at magnitudes near the characteristic earthquake magnitude and lower rates at lower magnitudes. Other models that account for characteristic earthquakes have been developed by Wesnousky et al. (1984) and Wu et al. (1995).

Wesnousky (1994) found that fault zones with highly irregular geometry, such as the San Jacinto fault in California, which has many offsets and branches, display universal G-R type power law

statistics over the entire range of observed magnitudes but if attention is limited to segments of the San Jacinto that are marked by the rupture zones of large historical earthquakes or distinct steps in fault trace, the observed distribution along each segment is consistent with the characteristic earthquake model. The G-R distribution observed for the entirety of the San Jacinto may reflect the sum of seismicity along a number of distinct fault segments, each of which displays a characteristic earthquake distribution. On the other hand, the available data show that faults with more regular geometry (presumably generated progressively with increasing cumulative slip), such as the San Andreas fault in California, display power law distributions only for small events, which occur between approximately periodically recurring events of a much larger characteristic size, which rupture the entire fault. There are practically no earthquakes of intermediate magnitudes observed in these faults.

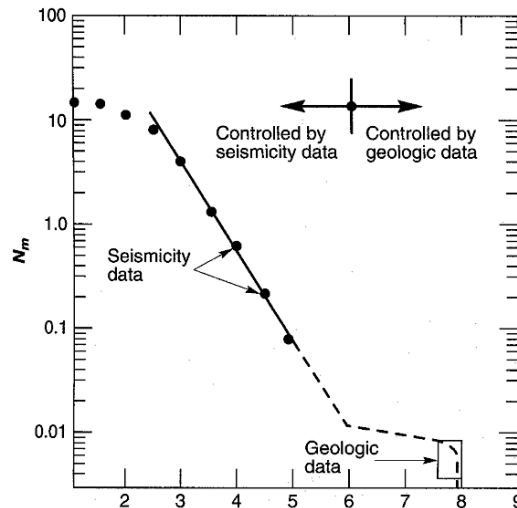


Fig. 5.22 - Inconsistency of mean annual rate of exceedance as determined from seismicity data and geologic data (from Schwartz and Coppersmith, 1984).

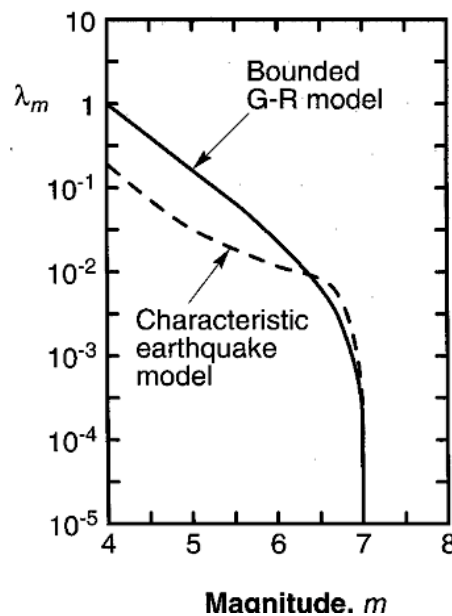


Fig. 5.23 - Comparison of recurrence laws from bounded G-R and characteristic earthquake models (modified from Youngs and Coppersmith, 1985).

Available evidence is insufficient to determine whether the G-R, characteristic earthquake, or some other recurrence law is correct. Evaluation of which model is most appropriate for a given source is hampered by the brevity of historical and/or instrumental records. The seismicity records of the last 5 decades for the major seismic sources of southern California suggest that, while the available data were not sufficient to disprove the G-R recurrence law, the characteristic earthquake model

better represented the observed distribution of earthquake magnitudes. Very seismic regions, such as California, have, in fact, only a short period of seismological observations (about two centuries), while well documented ones, such as Italy, where the earthquake catalogue covers nearly two millennia, are characterized by rare strong earthquakes. Additional research in this area is in progress and will undoubtedly be an active topic of discussion in the forthcoming seismology literature.

### 5.2.2.2.3. Step 3: attenuation relationships

The probability that a particular ground motion parameter  $Y$  exceeds a certain value,  $y$ , for an earthquake of a given magnitude,  $m$ , occurring at a given distance,  $r$ , is illustrated graphically in Fig. 5.24. In probabilistic terms, it is given by

$$P[Y > y | m, r] = 1 - F_Y(y) \quad (5-95)$$

where  $F_Y(y)$  is the value of the CDF of  $Y$  at  $m$  and  $r$ . The value of  $F_Y(y)$  depends on the probability distribution used to represent  $Y$ . In general, ground motion parameters are assumed to be lognormally distributed (the logarithm of the parameter is normally distributed). We, then, obtain:

$$P[\ln Y > y | m, r] = 1 - F_{\ln Y}(y) = \frac{1}{\sigma\sqrt{2\pi}} \int_y^{\infty} e^{-\frac{(v-\mu)^2}{2\sigma^2}} dv \quad (5-96)$$

where  $\mu$  and  $\sigma$  are respectively the mean value and the standard deviation of  $\ln y$  obtained from

$$\ln y = a - bm + c \ln r \quad (5-97)$$

and  $m$  and  $r$  are fixed [see also Eq. (5-29), where macroseismic intensity is considered although it is not a strictly physical quantity]. The right term is the complementary term of the CDF of the normal distribution. However, the unbounded characteristics of that distribution can attribute a nonzero probability to unrealistic values of the ground motion parameter. For example, a hypothetical GMPE for PGA that predicts a mean PGA of 0.5 g with  $\sigma_{\ln y} = 0.5$  would imply a 0.06% probability that the PGA would exceed 2.5 g. A problem that arises in the solution of Eq. (5-96) is the upper limit of integration, which is equal to infinity (see Fig 5.24). In practice, the integration is truncated to a value of  $\mu + n\sigma$ , where  $n$  is usually 2 or 3. The use of distributions that impose an upper limit on  $Y$  have been studied by several authors.

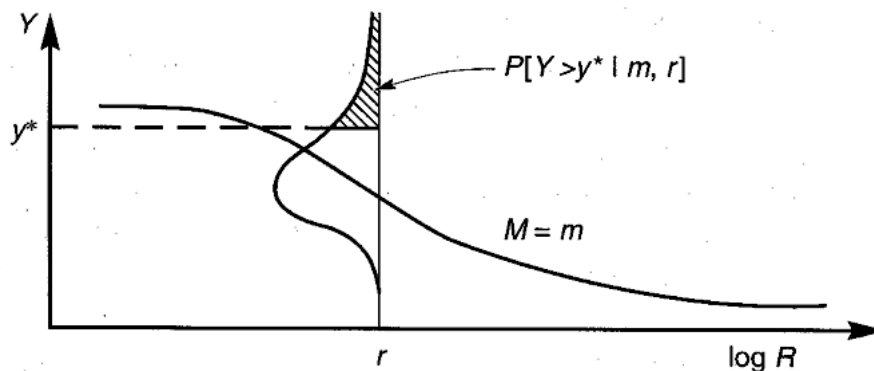


Fig. 5.24 - Schematic illustration of conditional probability of exceeding a particular value of a ground motion parameter for a given magnitude and distance (from Kramer, 1996).

It is interesting to note that Cornell (1968) in the original formulation of his method considered only the average value of  $I$  obtained from the attenuation relationship  $I=f(M, R)$  without taking into account the random variability ( $\sigma$ ) of attenuation [see Eqs. (5-29) and (5-39)].

## 5.2.2.2.4. Step 4: the hazard curve

The model in PSHA (McGuire, 2004) assumes that the magnitudes, distances, and resulting ground motions of earthquakes potentially affecting the site in question are random variables. This model reflects the fact that the exact size, location and time of occurrence of future earthquakes cannot be predicted deterministically.

The results of a PSHA can be expressed in many different ways. All involve some level of probabilistic computations to combine the uncertainties in earthquake size, location, frequency, and effects to estimate seismic hazards. The most common result of a hazard analysis is given by the hazard curve (Fig. 5.25), which represents the annual probability of exceeding certain levels of ground motion (Kramer, 1996). A slightly different definition for the hazard curve can be found in the literature as well, namely that it represents the annual frequency of exceeding certain levels of ground motion [see advantages of this definition in McGuire (2004)]. In practice the two definitions coincide (Cornell and Merz, 1975) because, given the small values considered, the frequencies can be regarded as probabilities [see Eq. (5-58)], the condition that the seismicity is a Poisson process is not, in practice, required to calculate the annual exceedance probability, and consequently for the hazard curve expressed in terms of annual frequency. From the hazard curve in terms of probabilities (not frequency, as an earthquake recurrence model is needed), it is possible to derive various hazard indicators as the probability of exceeding a certain level of shaking in a fixed period of time, or the shaking that has a certain probability not to be exceeded in a fixed time period. This last quantity is generally represented in the seismic hazard maps.

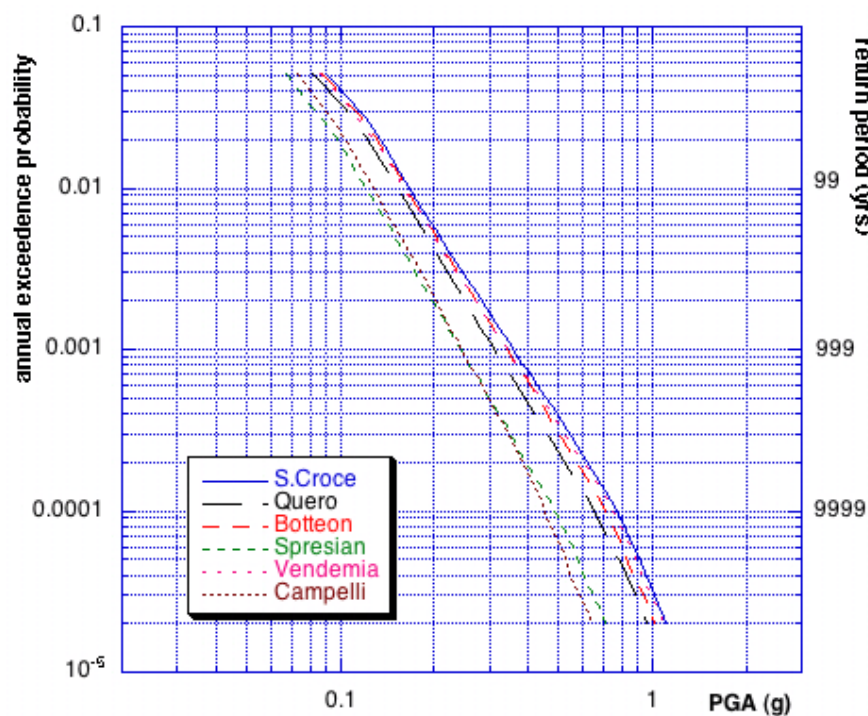


Fig. 5.25 – Hazard curve for six bridges in N.E. Italy.

Seismic hazard curves can be obtained for individual source zones and combined to express the aggregate hazard at a particular site. The basic concept of the computations required for development of seismic hazard curves is fairly simple. Compared to Eq. (5-81), which calculates the exceedance probability for a threshold level of shaking at the site when an earthquake occurs in each seismic source, we must now add the annual frequency of occurrence of earthquakes in the seismic sources. If each  $i$ -th source has an average annual number of earthquake occurrences (**mean annual rate of occurrence**) between minimum magnitude  $m_0$  and maximum magnitude  $m_{max}$  equal to  $\nu_i = e^{\alpha_i - \beta_i m_0}$  (this can be seen as the frequency/probability of earthquake occurrence in the source  $i$ ), and if the

source to site distance is between  $r_{min}$  and  $r_{max}$ , the expected annual number of exceedances  $\lambda_y$  (**mean annual rate of exceedance**) of the ground motion  $y$  to site will be given by:

$$\lambda_y = \sum_1^{N_S} v_i \int_{m_0}^{m_{max}} \int_{r_{min}}^{r_{max}} P[Y > y | M = m, R = r] f_M(m) f_R(r) dm dr \tag{5-98}$$

To explicitly take into account the attenuation of the dispersion relations see Fig. 5.24), Eq. (5-98) can be written in the form (McGuire, 1995):

$$\lambda_y = \sum_1^{N_S} v_i \int_{m_0}^{m_{max}} \int_{r_{min}}^{r_{max}} \int_{\epsilon} P[Y > y | M = m, R = r, E = \epsilon] f_M f_R(r) f_E(\epsilon) dm dr d\epsilon \tag{5-99}$$

where  $\epsilon$  expresses the offset (in terms of number of logarithmic standard deviations) of the logarithm of the shaking from its median value.

Eq. (5-98) represents the **seismic hazard curve, in terms of annual frequency of exceeding a threshold shaking** (McGuire, 1995, 2004). A summary of the hazard curve calculation is given by Fig. 5.26, where all terms of the equation are documented with their seismological meaning.

As the individual components of Eq. (5-98) are sufficiently complicated that the integrals cannot be evaluated analytically [only some simple situations (source with a regular shape) were investigated by Cornell (1968), who posed the basis for PSHA (see chapter 5.2.2.1.) and his approach, named from him, is still used worldwide], numerical integration, which can be performed by a variety of different techniques, is therefore required. The most used approach, used for simplicity rather than efficiency, is to divide the possible ranges of magnitude and distance into  $N_M$  and  $N_R$  segments, respectively. The average exceedance rate (expected number of exceedances of ground motion level  $y$ ) can then be estimated by:

$$\lambda_y = \sum_{i=1}^{N_S} \sum_{j=1}^{N_M} \sum_{k=1}^{N_R} v_i P[Y > y | M = m_j, R = r_k] f_{M_i}(m_j) f_{R_i}(r_k) \Delta m \Delta r \tag{5-100}$$

where  $m_j = m_0 + (j - 0.5)(m_{max} - m_0)/N_M$ ,  $r_k = r_{min} + (k - 0.5)(r_{max} - r_{min})/N_R$ ,  $\Delta m = (m_{max} - m_0)/N_M$  and  $\Delta r = (r_{max} - r_{min})/N_R$ . This is equivalent to assuming that each source is capable of generating only  $N_M$  different earthquakes of magnitude,  $m_j$ , at only  $N_R$  different source-to-site distances,  $r_k$ . Eq. (5-98) is then equivalent to

$$\lambda_y = \sum_{i=1}^{N_S} \sum_{j=1}^{N_M} \sum_{k=1}^{N_R} v_i P[Y > y | M = m_j, R = r_k] P[M = m_j] P[R = r_k] \tag{5-101}$$

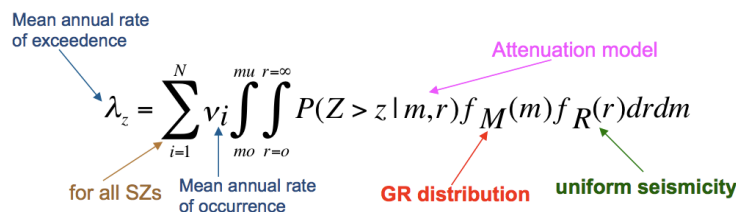


Fig. 5.26 – Seismological components of the seismic hazard curve.

The accuracy of the crude numerical integration procedure described above increases with increasing  $N_M$  and  $N_R$ . More refined methods of numerical integration will provide greater accuracy at the same values of  $N_M$  and  $N_R$ .



### 5.2.2.2.5. Step 5: time occurrence models

All what we have seen in the previous chapters refers to a specific time period (usually one year) and the hazard curve represents the related (annual) exceedance probability, or frequency (Fig. 5.26). To calculate the probabilities of various hazards occurring in a given time period, the distribution of earthquake occurrence with respect to time must be considered. Earthquakes have long been assumed to occur randomly with time, and in fact, examination of available seismicity records has revealed little evidence (when aftershocks are removed) of temporal patterns in earthquake recurrence. The assumption of random occurrence allows the use of simple probability models, but is inconsistent with the implications of elastic rebound theory. Nevertheless, the Poisson model remains the most used model in PSHA.

#### 5.2.2.2.5.1. Poisson model

The temporal occurrence of earthquakes is most commonly described by a Poisson model. The Poisson model provides a simple framework for evaluating probabilities of events that follow a Poisson process, one that yields values of a random variable describing the number of occurrences of a particular event during a given time interval. Poisson processes possess the following properties:

1. the number of occurrences in one time interval are independent of the number that occur in any other time interval;
2. the probability of occurrence during a very short time interval is proportional to the length of the time interval;
3. the probability of more than one occurrence during a very short time interval is negligible.

These properties indicate that the events of a Poisson process occur randomly, with no "memory" of the time, size, or location of any preceding event.

For a Poisson process, the probability of a random variable  $N$ , representing the number of occurrences of a particular event during a given time interval is given by

$$P[N = n] = \frac{\mu^n e^{-\mu}}{n!} \quad (5-102)$$

where  $\mu$  is the average number of occurrences of the event in that time interval.

The time between events in a Poisson process can be shown to be exponentially distributed. To characterize the temporal distribution of earthquake recurrence for PSHA purposes, the Poisson probability is usually expressed setting  $\mu=vt$ :

$$P[N = n] = \frac{(vt)^n e^{-vt}}{n!} \quad (5-103)$$

where  $v$  is the mean annual rate of occurrence of the event and  $t$  is the time period of interest. It derives that the probability of occurrence of at least one event in a period of time  $t$  is given by

$$P[N \geq 1] = P[N = 1] + P[N = 2] + \dots + P[N = \infty] = 1 - P[N = 0] = 1 - e^{-vt}. \quad (5-104)$$

Referring to a single seismic source, in Eq. (5-104)  $v$  can be obtained by a suitable recurrence law (e.g., the G-R law) to predict the probability of a particular earthquake magnitude. Similarly, Eq. (5-104) can be combined with the seismic hazard curve and we can predict the probability of at least one exceedance of  $y$  in a period of  $t$  years (the mean exceedance rate substitutes the mean occurrence rate):

$$F_{Y_t}(y) = P[Y_t > y | M = m, R = r] = 1 - e^{-\lambda_y t} \quad (5-105)$$

Eq. (5-105) represents the **hazard curve in terms of annual (putting  $t=1$ ) exceedance probability** of a fixed ground motion  $y$  at the site. There is a practical correspondence between the hazard curve expressed by Eq. (5-98) and that defined by Eq. (5-105) because for small values of  $\lambda_y$  (lower than 0.05),  $\lambda_y$  and  $1 - e^{-\lambda_y}$  can be regarded as similar [see Eq. (5-58)].

These types of analyses have been performed for a variety of seismically active areas all around the world. As the exposure time,  $t$ , increases, the probability of exceeding a particular ground motion parameter value also increases. Similarly, the value of a ground motion parameter with a particular probability of exceedance increases with increasing exposure time.

Introducing the return period  $T=1/\nu$  we obtain:

$$F_{Y_t}(y) = 1 - e^{-\frac{t}{T}} \quad (5-106)$$

and consequently

$$T = \frac{-t}{\ln[1 - F_{Y_t}(y)]}. \quad (5-107)$$

The annual non-exceedance probability of  $y$  is then:

$$1 - F_{Y_t}(y) = e^{-\frac{1}{T}}. \quad (5-108)$$

Fig. 5.27 illustrates the PGA with a 10% probability of exceedance for a number of metropolitan areas within the United States.

#### 5.2.2.2.5.2. Other time occurrence models

The elastic rebound theory suggests that the occurrence of earthquakes on a particular fault or fault segment should not be independent of past seismicity. If earthquakes occur to release strain energy that builds up over extended periods of time, the occurrence of a large earthquake should substantially reduce the chances of another independent, large earthquake (from the same source) occurring shortly thereafter. If earthquakes are triggered when the stress on a fault reaches some limiting value, the chances of occurrence should depend on the times, sizes, and locations of preceding events.

In the original version of the characteristic earthquake model (Fig. 5-21), only magnitude is defined within a limited range, and no assumptions are made about inter-event intervals (Schwartz and Coppersmith, 1984). Later, Bakun and Lindh (1985) calculated that in the area of Parkfield, in California, earthquakes showed a similarity not only in magnitude (around 6) but also in the recurrence period (about 22 years). This, on one hand, led to the creation of the Parkfield seismic prediction experiment, unfortunately without any good results, and, on the other hand, led to propose an earthquake model which is characteristic in the earthquake magnitude and in the recurrence intervals as well (Wu et al., 1995).

A number of models that account for prior seismicity have been proposed. Non-homogeneous Poisson models allow the annual rate of exceedance to vary with time. Renewal models use arrival-time distributions other than exponential (implied by the homogeneous Poisson model) to allow the hazard rate, which describes the instantaneous "failure rate" at any time,

$$h_T(t) = \frac{f_T(t)}{1 - F_T(t)} \quad (5-109)$$

to increase with time since the last event: gamma and Weibull distributions are most common. Time-predictable models specify a distribution of the time to the next earthquake that depends on the magnitude of the most recent earthquake; slip-predictable models consider the distribution of earthquake magnitude to depend on the time since the most recent earthquake (Fig. 1.62). More precisely, two stress values (the pre-seismic one  $\tau_1$  and the post-seismic one  $\tau_2$ , in Fig. 5.28) control the behaviour of the fault. If  $\tau_1$  is constant, the behaviour of the earthquake is called of "time predictable" type and stress release (i.e., the earthquake magnitude) is different from event to event and, consequently, the inter-event interval is different but it can be forecasted as it corresponds to the attainment of the stress state  $\tau_1$  (top panel in Fig 1.62b). If, instead, the fault accumulates a variable amount of stress but the stress release during the earthquake leads to a constant stress state  $\tau_2$ , the behaviour of the earthquake is called of "slip predictable" type and amount of stress released (i.e., the earthquake magnitude) can be deduced from the time elapsed since the last event (bottom panel in Fig. 1.62c).

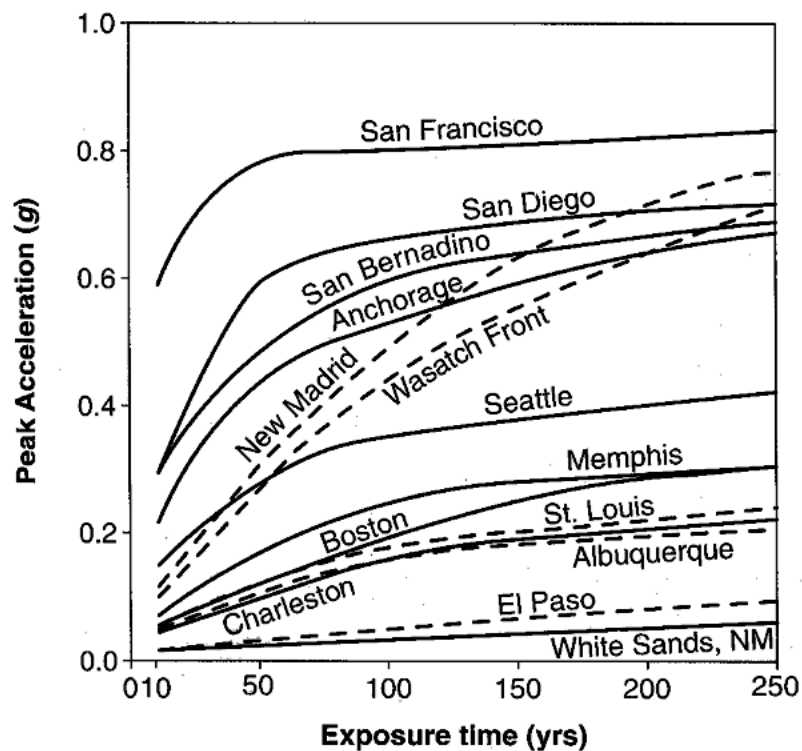


Fig. 5.27 - PGA with 10% exceedance probability over various exposure times for 14 areas in North America (from Kramer, 1996).

Markov models incorporate a type of memory that describes the chances that a process moves from some past "state" to a particular future state. The time for which the process stays in a particular state before moving to another state is exponentially distributed; semi-Markov models are not restricted to the exponential distribution. Both Markov models and semi-Markov models have been used in seismic hazard analysis. The semi-Markov models, for example, can relate the probability of future earthquakes of various sizes to the size of the most recent event and the elapsed time since its occurrence. Trigger models can account for clusters of events (aftershocks) that occur after triggering events.

The hybrid renewal model of Wu et al. (1995) can be used to calculate seismic hazard due to a potential characteristic earthquake source. The model represents a modification of the Poisson process to account for time-dependence of the rate of large magnitude earthquakes. Basically, the characteristic earthquake model assumes that the probability of a large characteristic earthquake is dependent upon the time since the occurrence of the previous characteristic earthquake. Thus, the model has memory and, unlike the Poisson model, hazard estimates are dependent upon the waiting time since the last large earthquake. Another element of the characteristic model is that the magnitude

distribution of large earthquakes is non-exponential but it is peaked (see Fig. 5.21) at the characteristic magnitude value (Schwartz and Coppersmith, 1984; Wu et al., 1995).

In the hybrid renewal model, the probability of motion exceeding some specified value,  $g$ , during a time period,  $w$ , given the time since the occurrence of the last characteristic event,  $t$ , is given by:

$$P[G > g | t] = 1 - e^{-w(\nu_p + \nu_r)} \quad (5-110)$$

where  $\nu_p$  is the rate of exceedance of  $g$  from earthquakes which follow a Poisson process and  $\nu_r$  is the rate of exceedance of  $g$  from earthquakes which follow a renewal process. The expression for  $\nu_p$  is:

$$\nu_p = \alpha_p \int_{m_p^-}^{m_p^+} \int_{r^-}^{r^+} f_R(r) f_M(m) P[G > g | m, r] dm dr \quad (5-111)$$

In the above equation the limits of magnitude integration represent the range over which the Poisson model is applicable. The rate of earthquakes assumed to follow a Poisson process is represented by  $\alpha_p$ . The expression for the mean rate of exceeding ground motion  $g$  due to large magnitude, characteristic earthquakes,  $\nu_r$ , is given by:

$$\nu_r = \frac{1}{w} \int_t^{t+w} h(\tau) d\tau \int_{m_c^-}^{m_c^+} \int_{r^-}^{r^+} f_R(r) f_M(m) P[G > g | m, r] dm dr \quad (5-112)$$

Here, the limits of integration for magnitude represent the range over which the renewal model is applicable. This represents the characteristic earthquake contribution to hazard. Note that the rate of characteristic earthquakes is given by the average value of the hazard function,  $h(t)$ , evaluated from time  $t$  to time  $t+w$ . Here,  $t$  is time since the occurrence of the previous characteristic earthquake and  $w$  is a time interval representing the exposure period during which hazard estimates are desired. The hazard function,  $h(t)$ , of the characteristic earthquake renewal process, is expressed as:

$$h(t) = \frac{f_T(t)}{1 - F_T(t)} \quad (5-113)$$

In Eq. (5-113)  $F_T(t)$  and  $f_T(t)$  are the CDF and PDF, respectively, of the characteristic earthquake interoccurrence times. Following Wu et al. (1995), a Weibull model for  $F_T(t)$  and  $f_T(t)$  is assumed, leading to:

$$h(t) = \left[ \frac{\Gamma(COV)}{T} \right] \left[ \frac{\Gamma(COV + 1)}{T} \right]^{1-COV} \quad (5-114)$$

In the above Eq. (5-114),  $T$  is the mean interoccurrence time for the characteristic events,  $\Gamma$  is the gamma function, and COV is the coefficient of variation of the interoccurrence times where

$$COV = \frac{\sigma_T}{T} \quad (5-115)$$

In Eq. (5-115),  $\sigma_T$  is the standard deviation of the characteristic earthquake interoccurrence times. Because of the assumed form of  $f_T(t)$ ,  $h(t)$  is an increasing function of time  $t$  since the last characteristic earthquake. Therefore, the probability of another characteristic earthquake increases with time since the occurrence of the last characteristic earthquake for coefficients of variation less than one. For a coefficient of variation equal to 1,  $\sigma_T = T$ , which indicates that the underlying

distribution of interoccurrence times is exponential. Therefore, the renewal model reduces to the Poisson process when the coefficient of variation equals 1.

Another model has been proposed for time-dependent seismic hazard computation. It is the Brownian Passage Time (BPT) model (Kagan and Knopoff, 1987; Ellsworth et al., 1999; Matthews et al., 2002; Working Group on California Earthquake Probabilities, 2003) and represents the tectonic loading of a fault by a variable which evolves by superposition of an increasing linear trend and a Brownian noise term, and an earthquake occurs when this variable reaches a given threshold. All the earthquakes in that model are identical to each other.

The BPT process is illustrated in Fig. 5.28. The PDF of passage times across the failure threshold [ $f(t)$ ] is known as the BPT distribution, described by

$$f(t) = \sqrt{\frac{\mu_t}{2\pi\alpha_t^2 t^3}} \exp\left[-\frac{(t - \mu_t)^2}{2\alpha_t^2 \mu_t t}\right] \quad (5-116)$$

where  $t$  is the time to the next event, and is reset after an event occurs. Parameter  $\mu_t$  is the mean time between events ( $\mu_t = Y_f / \dot{M}_0$ ) and the  $\alpha_t$  coefficient of variation of time between events ( $\alpha_t = \delta / \sqrt{Y_f \dot{M}_0}$ ). The parameter  $\alpha_t$  can be interpreted as representing randomness associated with accumulating tectonic stress on a fault, spatial variations in the stress and strength of the fault, or perturbations to the stress state due to external causes such as nearby earthquakes (Ellsworth et al., 1999). This function gives a zero failure probability at  $t=0$  and finite failure probability as  $t \rightarrow \infty$ . The randomness of the time to failure increases with  $\alpha_t$  up to a limiting value of  $\alpha_t = 1/\sqrt{2}$ , at which point the model is equivalent to a Poisson process with failure rate  $\mu_t$ .

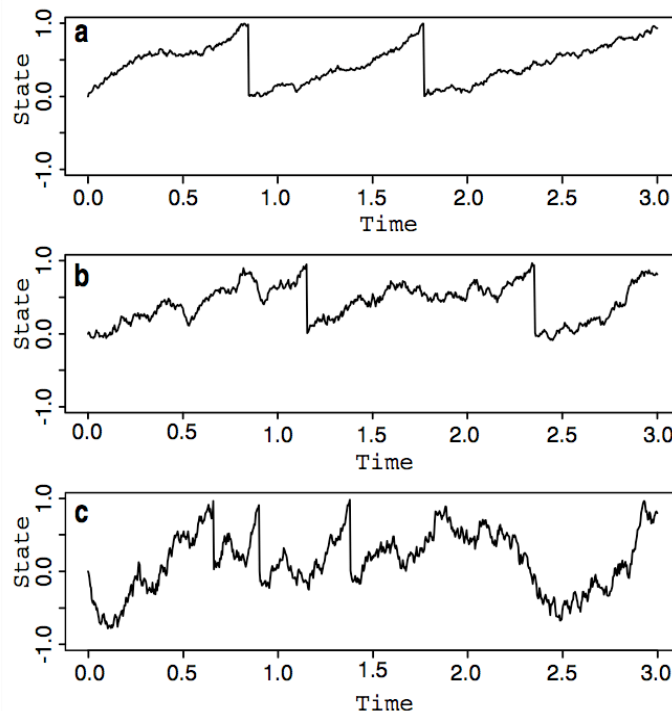


Fig. 5.28 - Load-state paths for a Brownian relaxation oscillator with  $\lambda=\delta=1$ : a)  $\sigma=1/4$ ; b)  $\sigma=1/2$ ; c),  $\sigma=1$  (from Matthews et al., 2002).

To apply the BPT model for time-predictable earthquake occurrence, the parameters  $\mu_t$  and  $\alpha_t$  are needed. The parameter  $\mu_t$  is generally derived from fault-specific studies of paleoseismic data. It should be noted that for faults modelled with a characteristic density function on magnitude,  $\mu_t$  can be approximated as  $1/v_c$ , the rate of the characteristic earthquake. The rate  $v_c$  has been tabulated by

Petersen et al. (1996) for major California faults. Parameter  $\alpha_t$  has been estimated by Ellsworth et al. (1999) from analysis of 37 recurrent earthquakes with  $m = -0.7$  to 9.2. It was found that  $\alpha_t = 0.5$  can serve as a working estimate for recurrent earthquake sequences of all sizes and in all tectonic environments. A BPT density function calculated for  $\alpha_t = 0.5$  and  $\mu_t = 300$  years is shown in Fig. 5.29.

Investigations of the applicability of Poisson and non-Poissonian models have shown that the Poisson model is useful for practical seismic risk analysis except when the seismic hazard is dominated by a single source for which the time interval since the previous significant event is greater than the average inter-event time and when the source displays strong "characteristic-time" behaviour. For this and other reasons related to simplicity, ease of use, and lack of sufficient data to support more sophisticated models, the Poisson model is the most widely used in contemporary PSHA.

Each of the more sophisticated models uses a pattern of earthquake occurrence to reconcile their computed probabilities with the mechanics of the elastic rebound process of earthquake generations. As a result, each requires additional parameters whose values must be evaluated from historical and instrumental seismicity records that are, in most cases, too sparse to permit accurate evaluation. As time passes and additional data becomes available, the use of these models will undoubtedly increase.

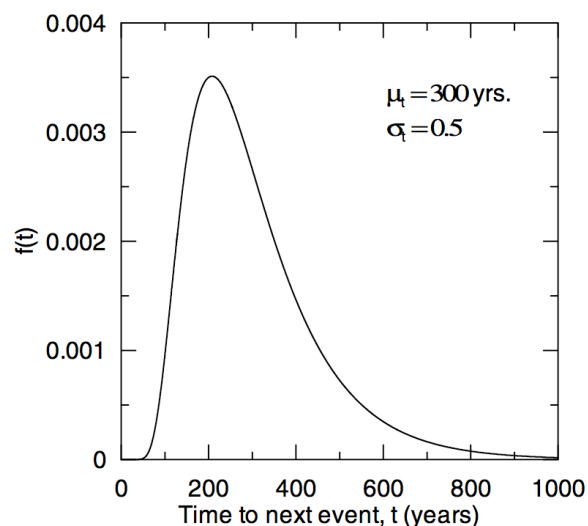


Fig. 5.29 - Probability density of the BPT distribution for mean period,  $\mu_t = 300$  years and coefficient of variation,  $\alpha_t = 0.5$  (from Stewart et al., 2001).

#### 5.2.3.6. Considerations on the hazard model parameters

From Eqs. (5-37) and (5-96) we observe that the seismic hazard is proportional to  $a$ . Other important parameters are the limits of integration and the functional forms of the probability functions in the integrand. Uncertainties on these parameters contribute to uncertainty in the results of the hazard analysis. The sources of uncertainty related to seismic hazard will be considered in a following chapter.

The estimation of  $a$  for each source involves an examination and assessment of the historical catalogue of seismicity. Because of the assumption of Poisson behaviour, foreshocks and aftershocks must be identified and removed from the catalogue before rates can be estimated. This is a somewhat subjective procedure because the analyst must assume a statistical model of foreshock and aftershock activity. For example, an often-used assumption is that the number of aftershocks decay exponentially with time. Therefore, a space-time window depending on the magnitude of the main shock was used to define the aftershocks (Gardner and Knopoff, 1974). The dimensions of the windows are based on an assessment of obvious aftershock sequences of the larger events in the catalogue. An additional source of uncertainty involves the assumption of stationarity. Due to variable population density and reporting, rates for earthquake activity apparently decrease with time. This is an artefact of catalogue



reporting (or completeness). Catalogues are considered complete for magnitudes less than 3 only during the past few decades when networks came into operation. These difficulties require that the catalogue be interpreted for completeness on a source-by-source basis prior to the estimation of a for each source.

The maximum earthquake,  $m_{max}$ , is an important parameter. Ideally, it would be estimated on the basis of a lengthy historical catalogue of earthquakes and geological evidence.

Another source of uncertainty is the ground motion prediction model. This is a general problem where the strong motion database is poor. However, important uncertainties in ground motion prediction remain with all databases, such as uncertainties due to the intrinsic variability of ground motion propagation. In the model, this variability is taken into account in the hazard computation by considering the standard deviation,  $\sigma$ , of the regression.

Another significant uncertainty is the delineation of seismic source zones. This uncertainty affects not only the functional form of  $f_R(r)$  but also estimates of  $a$  and  $f_M(m)$ . This is because the rates and magnitude distributions are estimated from the seismicity catalogue sorted according to geographic area. The use of an area source implies that the probability density of earthquake occurrence within the area is spatially uniform. This assumption cannot be tested for some areas due to limited catalogue length and completeness. The assignment of seismic source zones is generally determined by patterns of regional seismicity but may also be guided by geologic or geophysical information. A poor correlation between earthquake hypocentres and geologic structure compounded with a relatively poor earthquake catalogue, results in large uncertainties in the delineation of seismic source zones.

Finally, the assumption of the Poisson process is itself uncertain. This is particularly true for sites where the seismic hazard is dominated by one or a very few dominant faults. The G-R relationship combined with the assumption of Poisson behaviour has been found to represent adequately the seismicity behaviour of large regions. The explanation for this observation is that comparatively large areas include a large population of seismogenic faults having a very large range of potential rupture lengths. However, the seismicity observed on individual faults has been observed to deviate from the linear G-R relationship at the higher magnitudes. Also, geological investigations indicate that the inter-event times of pre-historic, large earthquakes cluster in a manner inconsistent with the exponential distribution function implied by the Poisson model. These observations form the basis for the characteristic earthquake model (Schwartz and Coppersmith, 1984; Youngs and Coppersmith, 1985).

#### 5.2.2.2.7. Deaggregation

The PSHA procedures described in the preceding sections allow computation of the mean annual rate of exceedance at a particular site based on the aggregate risk from potential earthquakes of many different magnitudes occurring at many different source-site distances. The rate of exceedance computed in a PSHA, therefore, is not associated with any particular earthquake magnitude or source-site distance.

In some cases, however, it may be useful to estimate the most likely earthquake magnitude and/or the most likely source-site distance. These quantities may be used, for example, to construct ground shaking and risk scenarios as well as to select existing ground motion records (recorded in earthquakes of similar magnitude at similar source-site distance) for response analyses. The methodology to identify the largest contributor, in the set of all earthquakes constructing the hazard at a site, is called deaggregation and was introduced by McGuire (1995). This process of deaggregation requires that the mean annual rate of exceedance be expressed as a function of magnitude and/or distance (Fig. 5.30).

Computationally, this simply involves the removal of terms from the summations of Eq. (5-101). For example, the mean annual rate of exceedance of  $y$  can be expressed as a function of magnitude by:

$$\lambda_y(m_j) \approx P[M = m_j] \sum_{i=1}^{N_S} \sum_{k=1}^{N_R} v_i P[Y > y | m_j, r_k] P[R = r_k] \quad (5-117)$$

Similarly, the mean annual rate of exceedance can be expressed as a function of source-site distance by:

$$\lambda_y(r_k) \approx P[R = r_k] \sum_{i=1}^{N_S} \sum_{j=1}^{N_M} v_i P[Y > y | m_j, r_k] P[M = m_j] \quad (5-118)$$

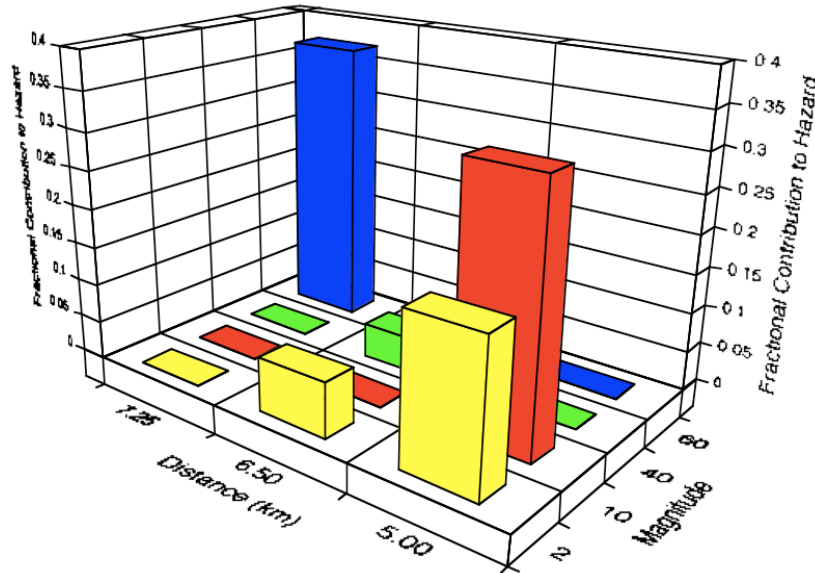


Fig. 5.30 – Deaggregation of hazard.

Finally, it is possible to compute the mean annual rate of exceedance as functions of both earthquake magnitude and source-site distance, i.e.

$$\lambda_y(m_j, r_k) \approx P[M = m_j] P[R = r_k] \sum_{i=1}^{N_S} v_i P[Y > y | M = m_j, R = r_k] \quad (5-119)$$

The full analysis can be conducted simply by appropriately discretizing the range of allowable magnitudes and distances (reference values can be  $Dm=0.1$  and  $Dr=5$  km). As the summation runs over all sources, in the case of many sources, placed at similar distances, it could be not trivial to identify the one hosting the dominant earthquake for the hazard at the site. The various sources must be, then, analyzed individually, eliminating the summation in Eq. (5-119).

#### 5.2.2.2.8. The treatment of uncertainties

The calculation of seismic hazard requires to hypothesize where earthquakes will occur and how strong they will be. This analysis calls into question many parameters and models that are not perfectly known and are, therefore, characterized by uncertainties due to lack of data or of knowledge regarding some aspects of the seismic phenomenon. The quantification of uncertainties was suggested by McGuire (1977) and formally introduced by McGuire and Shedlock (1981) and Toro et al. (1997). The Senior Seismic Hazard Analysis Committee (SSHAC, a group of U.S. experts with the task of verifying the results of two studies about the seismic hazard at a site of a nuclear power plant) has codified a methodology to be used in seismic hazard studies and a feature of this methodology consists in quantifying at the best the uncertainties inherent seismic hazard calculations.

Yet decisions on the siting and design of needed facilities must be made in the face of these uncertainties. No amount of statistical analysis, no matter how rigorously based and carefully done, can totally compensate for the incompleteness of available data and the defects of our evolving

scientific knowledge. A primary objective of the SSHAC methodology is to acknowledge and document uncertainties explicitly so that users of PSHA are able to make better-informed decisions.

The SSHAC methodology emphasizes the importance of how uncertainty is treated because the results of a PSHA can be influenced heavily by uncertainties in the data, the models, or both.

The two fundamental types of uncertainty are defined by SSHAC as:

- **aleatory**: the uncertainty due to variability inherent in a non-deterministic (stochastic, random) phenomenon;
- **epistemic**: the uncertainty attributable to incomplete knowledge about a phenomenon that affects our ability to model it.

Epistemic uncertainty may be reduced with time as more data are collected and more research is completed. Aleatory uncertainty, on the other hand, cannot be reduced by further study, as it expresses the inherent variability of a phenomenon.

After separation, these two components must be quantified for the model or parameter under consideration. Actually, making a rigorous separation between aleatory and epistemic uncertainty, as advocated by SSHAC, requires a great level of effort and expertise.

Recognition of the two kinds of uncertainty is useful initially when eliciting and combining expert inputs. Experts need to be aware of the sources of uncertainties (e.g., limitations of available data) so that they can make informed assessments of the validity of alternative hypotheses, the accuracy of alternative models, and the value of data and then transmit those uncertainties to the technical facilitator/integrator (TFI), who coordinates the project.

The classification of uncertainty as epistemic or aleatory depends on the model used to represent seismicity and ground motion. For example, epistemic uncertainty would be much greater if, in the assessment of seismic hazard at an eastern U.S. site, instead of representing random seismicity through homogeneous Poisson sources one used a model with an uncertain number of faults, each with an uncertain location, orientation, extent, state of stress, distribution of asperities, and so forth. As little is known about such faults, the total uncertainty about future seismicity and the calculated mean hazard curves would be about the same, irrespective of which model is used. However, the amount of epistemic uncertainty would be markedly different; it would be much greater for the more detailed, fault-based model. Consequently, the fractile hazard curves that represent epistemic uncertainty would also differ greatly.

It must be pointed out that the different terminology (aleatory versus epistemic) is not intended to imply that these uncertainties are of fundamentally different nature and the division between the two different types of uncertainty, epistemic and aleatory, is somewhat arbitrary. Consequently, the Panel on Seismic Hazard Evaluation (1997), who was charged to evaluate the SSHAC methodology, concluded that, unless one accepts that all uncertainty is fundamentally epistemic, the classification of PSHA uncertainty as aleatory or epistemic is ambiguous.

Furthermore, there is not a codified method which explicates how to separate the two uncertainties in practice.

It is established practice to take into account of the aleatory variability in seismic hazard calculations by introducing the standard deviation of the GMPE into the processing. Indeed, a hazard study which does not consider this uncertainty cannot be defined fully probabilistic (Bommer and Abrahamson, 2006). It is more difficult to consider other aleatory variabilities: the code SeisRisk III (Bender and Perkins, 1987), for example, allows us to take into account the uncertainty in defining the edges of the SZs by using a Gaussian distribution of the border position. This option, however, must be treated carefully, because it can lead to bizarre hazard estimates in the case of contiguous SZs.

#### 5.2.2.2.8.1. The logic tree method

The probability computations described previously allow systematic consideration of uncertainty in the values of the parameters of a particular seismic hazard model. In some cases, however, the best choices for elements of the seismic hazard model itself may not be clear. The use of logic trees (Kulkarni et al., 1984; Coppersmith and Youngs, 1986) provides a convenient framework for the explicit treatment of model (i.e., epistemic) uncertainty. The logic tree approach allows us to consider alternative models, to which a weight, representing the probability that that model is correct,

is assigned. The models considered in the logic tree must be exhaustive and mutually exclusive: this is not an easy request, especially for what concerns the exhaustiveness. Claiming that all the existing models were considered in a study is almost impossible, consequently, it is an accepted practice to consider those models that are most popular among the scientific community.

The logic tree approach allows the use of alternative models, each of which is assigned a weighting factor that is interpreted as the relative likelihood of that model being correct. It consists of a series of nodes, representing points at which models are specified and branches that represent the different models specified at each node. The sum of the probabilities of all branches connected to a given node must be 1. The relative likelihood of the combination of models and/or parameters implied by each terminal branch is given by the product of the relative likelihood of the terminal branch and all prior branches leading to it. The sum of the relative likelihoods of the terminal branches, or of those at any prior level, is equal to 1.

The simple logic tree shown in Fig. 5.31 allows uncertainty in selection of models for attenuation, magnitude distribution, and maximum magnitude to be considered. In this logic tree, attenuation according to the models of Campbell and Joyner-Boore are considered equally likely to be correct, hence each is assigned a relative likelihood of 0.5. Proceeding to the next level of nodes, the G-R magnitude distribution is considered to be 50% more likely to be correct than the characteristic earthquake distribution. At the final level of nodes, different relative likelihoods are assigned to the maximum magnitude. This logic tree terminates with a total of  $2 \times 2 \times 3 = 12$  (number of attenuation models  $\times$  number of magnitude distributions  $\times$  number of maximum magnitudes) branches. The relative likelihood of the combination of the Campbell attenuation model, G-R magnitude distribution, and maximum magnitude of 7.5 is  $0.5 \times 0.6 \times 0.3 = 0.09$ .

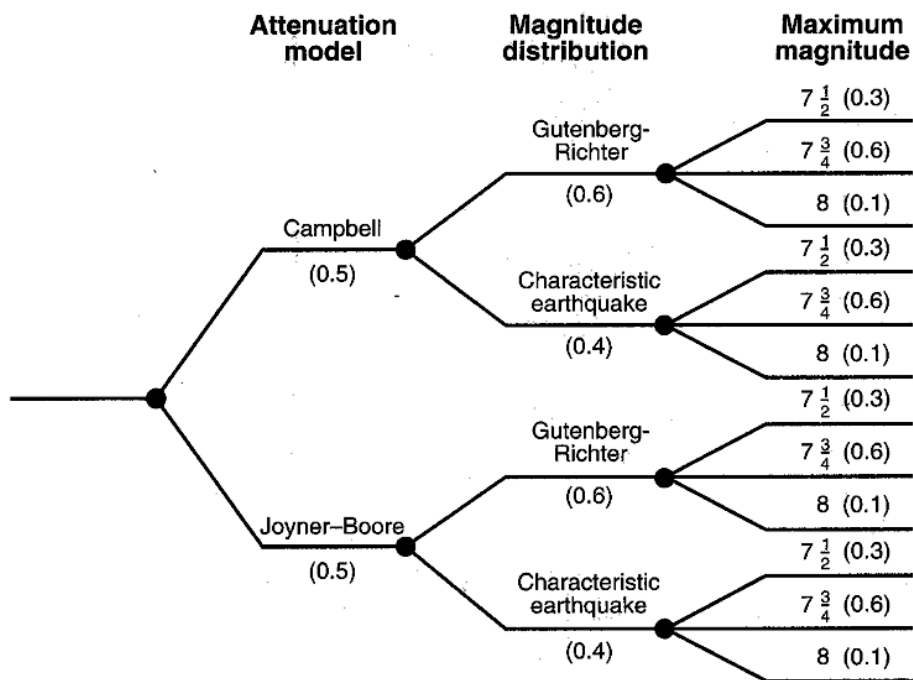


Fig. 5.31 - Simple logic tree for incorporation of model uncertainty (from Kramer, 1996).

The logic tree shown in Fig. 5.32 was used in the construction of the seismic hazard map of Italy (Gruppo di Lavoro, 2004), allows us to consider uncertainties related to the analysis about completeness of the earthquake catalogue, to the method for calculating seismicity rates, and to the attenuation model. All these alternative options lead to a logic tree with  $2 \times 2 \times 4 = 16$  branches.

The result at each terminal branch is weighted by the relative likelihood of its combination of branches, with the final result taken as the sum of the weighted individual results.

It is easy to see that the required computational effort increases quickly with increasing numbers of nodes and branches. Parameters best characterized by continuous distributions (e.g., the maximum magnitude in the example of Fig. 5.31) are difficult to treat in the logic tree without resorting to large numbers of branches. Nevertheless, the logic tree is a very useful tool for the analysis of seismic

hazards. When the number of branches is very large, the computation time may become too long and it is useful, then, to check if some branches have little contribution to the final estimate of the hazard or if different branches lead to the same result. As a result of this analysis we can identify a logic tree pruning (branch trimming) that can greatly reduce the computation time, without altering the final result (Barani et al., 2007).

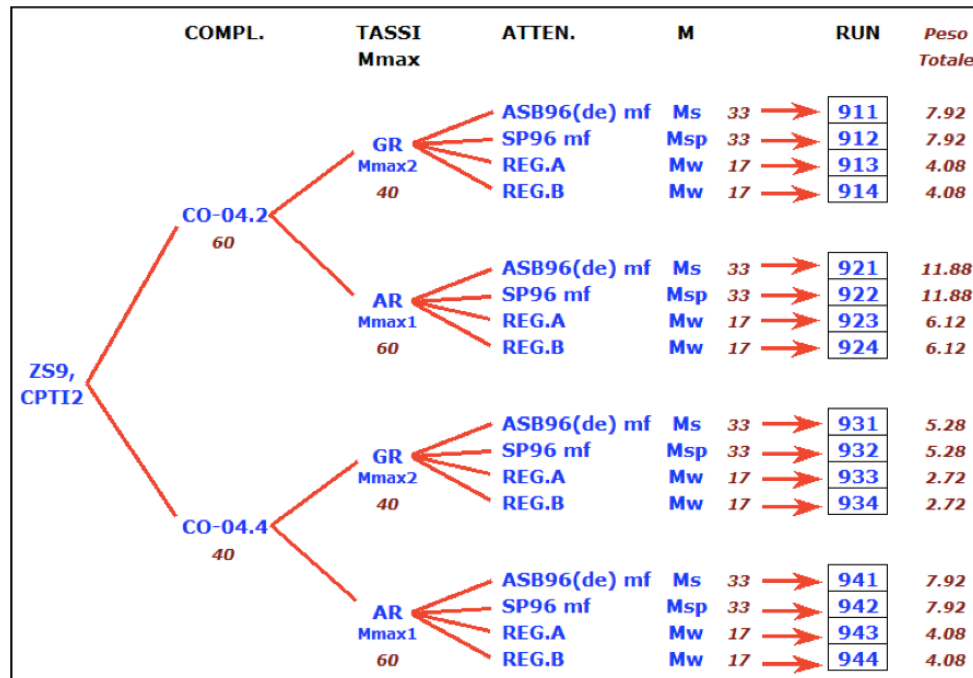


Fig. 5.32 – The logic tree used for the computation of the Italian seismic hazard map (Gruppo di Lavoro, 2004).

### 5.2.3. The smoothed seismicity approach

An alternative approach used in PSHA was proposed by Frankel (1995). In that approach, no delineation of seismic sources is needed, although SZs and SFs can be considered in the hazard computation. Seismic hazard is computed directly from seismicity spatially-smoothed in different ways. This approach, in its original form, can be considered referring to the Muir-Wood (1993) historical probabilism with aspects of seismotectonic probabilism in the case that SZs and/or SFs are applied.

The Frankel (1995) treatment of seismicity improves the concept of seismic activity already proposed by Riznichenko (1959) as the number of earthquakes in a given energy interval in a time and space unit: the seismic activity was used for the first quantitative estimations of seismic hazard, called seismic shakeability (Riznichenko et al., 1969). The main difference in the Frankel (1995) approach is in the use of a distribution function for seismicity, instead of its simple averaging. A similar approach, the “Historical Parametric Method” was proposed by Veneziano et al. (1984). Woo (1996) proposed also a methodology for seismic hazard assessment based statistically on kernel estimation of the activity rate density inferred from the regional earthquake catalogue. In his approach, the form of kernel is governed by the concepts of fractal geometry and self-organized criticality, with the bandwidth scaling according to magnitude.

Frankel (1995) retrieved the concept of seismic activity by computing seismic hazard directly through the  $a$ -values of the G-R distribution derived from different magnitude thresholds. With the addition of the hazard produced by the known seismogenic sources, the seismic hazard maps of the U.S.A. were computed (Frankel et al., 1996, 2002). This method, called the “Spatially-Smoothed Historical Seismicity” approach (Frankel, 1995), assumes that future large earthquakes will occur in areas that have experienced small-to-large earthquakes in the past. The main input data for the application of the Frankel (1995) approach are the earthquake catalogue, the completeness periods

for the different magnitude classes, the attenuation relations, and the correlation distance, used to smooth the seismicity. Furthermore, seismogenic sources, like SZs and SFs, can be introduced with their own seismicity too. The software for hazard computation is freely downloadable at <http://eqhazmaps.usgs.gov/html/hazsoft.html> in form of Fortran and C routines.

The hazard computation is based on the number  $n_i$  of earthquakes with magnitude greater than  $M_{ref}$  in each cell  $i$  of a grid: this count represents the maximum likelihood estimate of  $10^a$  for that cell.

The grid of  $n_i$  values is then smoothed spatially by multiplying by a Gaussian function with correlation distance  $c$ , obtaining  $\tilde{n}_i$ :

$$\tilde{n}_i(m_0) = \frac{\sum_j n_j(m_0) e^{-\Delta_{ij}^2/c^2}}{\sum_j e^{-\Delta_{ij}^2/c^2}} \quad (5-120)$$

where  $\tilde{n}_i$  is normalized to preserve the total  $\tilde{n}$  number of events and  $\Delta_{ij}$  is the distance between the  $i$ -th and  $j$ -th cells.

The annual probability of exceeding specific ground motions is calculated for a grid of sites using  $\tilde{n}_i$ . For each site, the values of  $\tilde{n}_i$  are binned by their distance from that site, so that  $N_k$  denotes the total of  $\tilde{n}_i$  values for cells within a certain distance increment of the site. The annual rate  $\lambda(u > u_0)$  of exceeding ground motion  $u_0$  at a specific site is determined from a sum over distance and magnitude

$$\lambda(u > u_0) = \sum_i \tilde{n}_i \int_{m_{\min}}^{m_u} P[u > u_0 | d_k, m_l] p_m(m) dm \quad (5-121)$$

where  $k$  is the index for the distance bin and  $l$  that for the magnitude bin, and  $T$  is the time in years of the earthquake catalogue used to determine  $N_k$ . The first factor in the summation is the annual rate of earthquakes in the distance bin  $k$  and magnitude bin  $l$ . The  $b$ -value is taken to be uniform throughout most of the area.  $P(u > u_0 | D_k, M_l)$  is the probability that  $u$  at the site will exceed  $u_0$ , for an earthquake at distance  $D_k$  with magnitude  $M_l$ , and it is dependent on the attenuation relation and its standard deviation.

#### 5.2.4. Earthquake prediction

Because earthquakes occur suddenly, often with devastating consequences, earthquake prediction is a matter of great interest among the public and emergency service officials and the prediction of individual earthquakes has proven to be one of the “holy grails” of geophysics (Main, 1996). Already at the beginning of the 20th century, Reid (1910) described the cyclic release of elastic energy build up over centuries in the Earth’s crust through large earthquakes, and he proposed that by understanding where in the cycle we are, upcoming earthquakes could be predicted. In the 1970’s many seismologists were optimistic that within a relatively short time reliable earthquake prediction could be achieved. The most famous successful earthquake prediction refers to the Haicheng (China) earthquake of 1975, when an evacuation warning was issued the day before an  $M$  7.3 earthquake. In the preceding months changes in land elevation and in ground water levels, along with widespread reports of peculiar animal behavior, and many foreshocks had led to a lower-level warning. An increase in foreshock activity triggered the evacuation warning. Unfortunately, most earthquakes do not have such obvious precursors. In spite of their success in 1975, there was no warning of the 1976 Tangshan earthquake, magnitude 7.6, which caused an estimated 250,000 fatalities.

The optimism turned into widespread pessimism in the 1990’s after numerous failures in predicting earthquakes.

Allen (1976) lists six attributes required for this type of prediction: 1) it must specify a time window; 2) it must specify a space window; 3) it must specify a magnitude window; 4) it must give some sort of indication of the author's confidence in the reliability of the prediction; 5) it must give some sort of indication of the chances of the earthquake occurring anyway, as a random event; 6) it



must be written and presented in some accessible form so that data on failures are as easily obtained as data on success.

Kanamori (2003) discusses some issues of long-term forecast and short-term prediction separately, because they have very different social implications. Sometimes forecasts on intermediate time scales are treated separately from long-term forecasts, but he treats them together as long-term forecasts. As there is no generally used definition of short-term, intermediate-term, and long-term predictions, that given by Sykes et al. (1999) can be considered a useful guideline: immediate alert (0 to 20 s), short-term prediction (hours to weeks), intermediate-term prediction (1 month to 10 years), long-term prediction (10 to 30 years), long-term potential (>30 years). The actual usage, however, may vary depending on the specific circumstances.

#### 5.2.4.1. Long-term forecast

The basis of long-term forecast is the elastic rebound theory (Reid, 1910). If the stress accumulates at a constant rate, and the strength of the crust is constant, one would expect a relatively regular recurrence of earthquakes on a given segment of fault. However, due to fault interactions, weakening of crust due to increase in pore pressures, or some non-linear processes, the actual occurrence can be more irregular than would be expected from the simple elastic rebound theory.

Even with this difficulty, long-term forecasts are useful because considerably large uncertainties can be tolerated for long-term applications. In general, such forecasts are easier for the places where stress accumulation rate is faster (e.g., plate boundaries with fast plate motion) than for the places with slower stress accumulation rates

##### 5.2.4.1.1. Seismic gap method

The basic premise is that large earthquakes occur more or less regularly in space and time as a result of gradual stress buildup and sudden stress release by failure. Consequently, a region that has historically experienced large earthquakes, but not recently is called a seismic gap and is more likely to produce a large earthquake in the next future than those regions that have recently experienced large events. Long-term forecasts made with the gap method are generally considered to have been successful for several large earthquakes (e.g., the 1978 Oaxaca, Mexico event) but the method is subject to all the uncertainties related to the elastic rebound theory, and it is not used for definitive forecasts.

##### 5.2.4.1.2. Stress transfer

In addition to secular loading by plate motion, the stress on a fault is affected by past earthquakes in adjacent areas. If the size and mechanism of earthquakes in the adjacent areas are known, it is possible to compute the stress changes on the fault on a time scale of a few decades. Coulomb Stress Transfer theory, which was first applied to earthquakes in the late 1980's (e.g., Roth, 1988; King et al., 1994), has been applied with increasing success to the understanding of earthquakes in recent years. The principle behind the application of stress transfer theory is an understanding of the stress regime within the rocks adjacent to a dynamic plate boundary, and the ability to create a mathematical model of how the stress changes when there is sudden movement (an earthquake) along some part of a fault at the boundary. While failure on one part of a fault plane will tend to reduce stress in the rocks surrounding the rupture zone, it is likely to increase the stress in some other part of the fault plane, or on other nearby fault planes. The immediate result of this stress transfer is the generation of aftershocks. Most of these occur within seconds of the original shock, but some are delayed for minutes, hours, days, months and even decades. In the case of the 1968 Borrego Mountain, California, earthquake, a significant aftershock cluster occurred in the area where shear stress was increased by the mainshock. This concept was more rigorously applied to several other earthquakes (e.g., 1992 Landers, 1994 Northridge, 1995 Kobe). In some cases [e.g., the 1992 Big Bear earthquake

( $M=6.4$ ) which occurred soon after the Landers earthquake; some aftershocks of the Landers, Northridge, and Kobe earthquakes], the hypothesis of triggering by stress transfer is well demonstrated. In other cases, the situation is not so obvious.

In general, if the geometry of the fault system, the loading mechanism, and the structure and properties of the crust are known in an area, it should be possible to compute the regional stress changes and infer the seismic behavior of the entire area. Stress transfer between different faults is an important mechanism controlling regional seismicity on decadal time scales, but the lack of detailed knowledge of the initial stress condition and the model parameters makes it difficult to make definitive forecasts of future seismicity.

#### 5.2.4.1.3. Seismicity patterns

The change in the stress or strength of the crust may manifest itself as spatial and temporal changes in seismicity patterns such as quiescence, increase, and doughnut patterns (Mogi, 1969). For some earthquakes, seismic quiescence had been identified before the occurrence (e.g., 1973 Nemuro-Oki, 1978 Oaxaca, Bear Valley, 1986 Andreanof Islands). In some retrospective studies, seismicity patterns were related to the occurrence of several large earthquakes (e.g., the 1868, 1906, and 1989 earthquakes in the San Francisco area), but the type of pattern may depend on the regional tectonic structure, fault geometries, and the loading system; it is unclear at present how to quantitatively relate seismicity patterns to an impending earthquake.

Another general approach along this line is a formal assessment of earthquake potential primarily using earthquake catalogues (e.g., Keilis-Borok et al., 1988). This approach is based on systematic examinations of earthquake catalogues to identify relations between some seismicity patterns (such as clustering, quiescence, and sudden increase in activity) and past large earthquakes, and using these relations to forecast future seismic activities on intermediate time scales. The method is being tested but its usefulness for practical purposes is still questionable.

#### 5.2.4.2. Short-term prediction

For the general understanding earthquake prediction means a short-term prediction of a specific earthquake on a relatively short time scale, e.g., a few weeks. Such prediction must specify the time, place, and magnitude of the earthquake in question with sufficiently high reliability and probability (Allen, 1976). However, any such short-term prediction, if made, is very uncertain.

Even uncertain predictions may be useful for those places where the social and economical environments are relatively simple and false alarms can be socially tolerated. However, in modern highly industrialized cities with complex lifelines, communication systems, and financial networks, such uncertain predictions could inadvertently damage local and global economies, so they are generally not useful unless the society involved is willing to accept the potential loss that could be inflicted by false alarms.

Despite this difficulty, many attempts to observe precursory phenomena for the purpose of short-term earthquake prediction have been made.

##### 5.2.4.2.1. Precursors and anomalous phenomena

The term "precursor" means two different things. In a restricted usage, "precursor" implies some anomalous phenomenon that always occurs before an earthquake in a consistent manner. This is the type of precursor one would wish to find for short-term earthquake prediction. As far as we know, universally accepted precursors that occur consistently before every major earthquake have not yet been found.

In contrast, "precursor" is often used in a second sense to mean some anomalous phenomena that may occur before large earthquakes. Because an earthquake may involve non-linear preparatory processes before failure, it is reasonable to expect a precursor of this type. However, it may not always

occur before every earthquake, or even if it occurs, it may not always be followed by a large earthquake. Thus, in this case, the precursor cannot be used for a definitive earthquake prediction. Nevertheless, it is an interesting physical phenomenon worthy of scientific study. Foreshocks are a good example of a precursor of this type. Some large earthquakes were preceded by distinct foreshock activity, but many earthquakes do not have foreshocks.

These precursors may be identified in retrospective studies, but it would be very difficult to identify some anomalous observations as a precursor of a large earthquake before its occurrence (Table 5.5). Even if an anomaly were detected, it would be difficult to use it for accurate predictions of the size and timing of the impending earthquake, considering the stochastic nature of earthquakes.

Table 5.5 – Earthquake precursors.

1	Increased emission of radon
2	Increased helium emission
3	Increased methane gas emission, with possible formation of colored methane clouds - Earthquake clouds
4	Increased activity of mud volcanoes
5	Occurrence of microseismicity
6	Changes in $v_p/v_s$
7	Changes in Gutenberg-Richter $b$ -value
8	Modification of ground electrical conductivity
9	Fluctuations in the Earth's magnetic field
10	Changes in the density of nearby rocks
11	Changes in well-water levels close to a fault
12	Light emissions
13	Magnetic anomalies
14	Anomalies in the behaviour of animals, such as mass migration of amphibians
15	Increased emission of carbon dioxide in volcanic areas; volcanic paroxysm
16	Occurrence of small sand volcanoes

Many anecdotal or qualitative reports on earthquake precursors can be found in the literature (Rikitake, 1986). Systematic efforts to detect precursors began in the 1960s. These efforts included measurements of seismicity, strain, seismic velocities, electric resistivity and potential, radio-frequency emission, ground water level, and ground water chemistry.

Encouraging reports of large (about 10%) precursory changes in the ratio  $v_p/v_s$  were made for several earthquakes especially in former Soviet Union and China.

These changes were interpreted as manifestations of rock-dilatancy and fluid diffusion in micro-cracks just before failure (Scholz et al., 1973). However, many precise measurements using not only earthquakes but also controlled sources, performed following the initial reports, failed to verify the large changes in the velocity reported by earlier studies. In most cases, the velocity changes, if detected at all, were less than 1% or below the experimental noise level.

Similarly, large changes in ground-water chemistry, especially the concentration of radon, were reported before several large earthquakes in the former Soviet Union and China. Some results in Japan, especially the change before the 1978 Izu-Oshima earthquake, are considered significant and intriguing changes in the chloride ion and radon concentrations in ground water were discovered before the 1995 Kobe (Japan) earthquake. However, the results in the United States were generally not encouraging, and most geochemical monitoring efforts have been discontinued. It is probably fair to say that the negative results from seismic velocity ratio and radon monitoring in the United States may not be entirely definitive because of the lack of instruments very close to the epicenters of large earthquakes, but most seismologists would agree that these precursors, if they exist, are not easily detectable.

Several intriguing hydrological precursors have been reported but more complete documentation of the data needs to be made before they can be used for a definitive interpretation of crustal processes leading to seismic failure.

An intriguing observation of very low-frequency (0.1 to 10 Hz) radio (RF) emission was reported for the 1989 Loma Prieta (California) earthquake. The level of RF emission detected by an

antenna located at about 7 km from the epicenter increased far above the background level about 3 hours before the earthquake. The emission also increased 12 days and 1 day before the earthquake. Although the exact cause of this emission is not established, this observation is probably one of the clearest anomalous signals detected before a large earthquake.

Efforts to detect slow strain precursors have been extensive in California, but no obvious strain precursors have been detected. It is important to note that a slow strain change was observed in 1993 near San Juan Bautista (California) but no large earthquake followed it. For some subduction-zone earthquakes (e.g., 1960 Chile, 1983 Akita-Oki, and 1944 Tonankai) slow deformations prior to the mainshock have been reported, but the instrumental data are not complete enough to make definitive cases.

A prediction method using changes in electric potential was extensively used for prediction of earthquakes in Greece since the 1980s [VAN method proposed by Varotsos and Alexopoulos (1984)], but its validity was vigorously debated.

Although many precursors have been reported, the study (Wyss, 1991) made by a committee under the International Association of Seismology and the Earth's Interior (IASPEI) concluded that only 3 out of 31 precursors subjected to review qualified as such. Although this type of evaluation depends on the criteria used, it is reasonable to say that reliable predictions using this type of precursor seem to be difficult at present.

Despite the limited value of precursors for short-term earthquake prediction, studies of such preparatory processes are important for a better understanding of the physics leading up to seismic failure in the Earth's crust, and careful, systematic, and quantitative investigations may be warranted.

#### 5.2.4.2.2. The 1975 Haicheng earthquake prediction

One intriguing example of a short-term prediction is that of the 1975 Haicheng, China, earthquake. A destructive earthquake ( $M=7.3$ ) occurred near Haicheng, China, on February 4, 1975. More than 1 million people lived near the epicentre. It has been widely reported that this earthquake was successfully predicted. Unfortunately, the Cultural Revolution was still taking place in 1975, and detailed information did not emerge in peer-reviewed scientific literature. Thus, it is not possible to assess this prediction with complete objectivity.

The sequence of precursor observations can be summarized as follows (Fig. 5.33). A seismicity migration towards the Heicheng area was observed since 1966. Seismicity around Heicheng increased from 1974 with several  $M5.0$  earthquakes and soil deformation was observed. Level variations in the wells and strange animal behaviour, radon emissions, magnetic anomalies were observed in January 1975 and the ground started to crack downtown Heicheng. A very vast area around Heicheng was alerted in January 1975. 500 earthquakes in the magnitude range 1 to 3.5 were recorded between February 1 and 4, 1975. Heicheng population was evacuated on February 1. Seismic activity stopped on February 4. An  $M7.2$  earthquake occurred during the night from February 4 to 5.

Judging from the various reports on the Haicheng earthquake, it appears that very extensive foreshock activity, including a few hundred instrumentally recorded events, played the most important role in motivating mass evacuation, which saved many thousands of lives. However, it is unclear: 1) how many false alarms had been issued before the final evacuation, 2) whether the evacuation was done under the direction of the local government or by more spontaneous decision by the local units or residents, and 3) what the total number of casualties was.

#### 5.2.4.2.3. The Parkfield experiment

The San Andreas fault passes through the small town of Parkfield, California, which is situated roughly halfway between Los Angeles and San Francisco (Fig. 5.34). Parkfield has experienced strong (at least magnitude 6) earthquakes six times between 1857 and 1966. These quakes, have an average repeat interval of 22 years (24, 20, 21, 12 and 32 years). Excluding the larger and more extensive 1857 earthquake, they have all occurred on almost exactly the same part of the fault. Furthermore, the 1934 and 1966 quakes have very similar-looking seismographs, and each was preceded by a magnitude 5

foreshock 17 minutes before the main shock. Another similar earthquake was expected to occur at Parkfield by around 1987: in 1985 USGS made a public forecast of 95% chance of an earthquake of magnitude 5.5 to 6.0 before 1993 but an earthquake of magnitude 6.0 occurred only in 2004 without any precursors (Fig. 5.35).

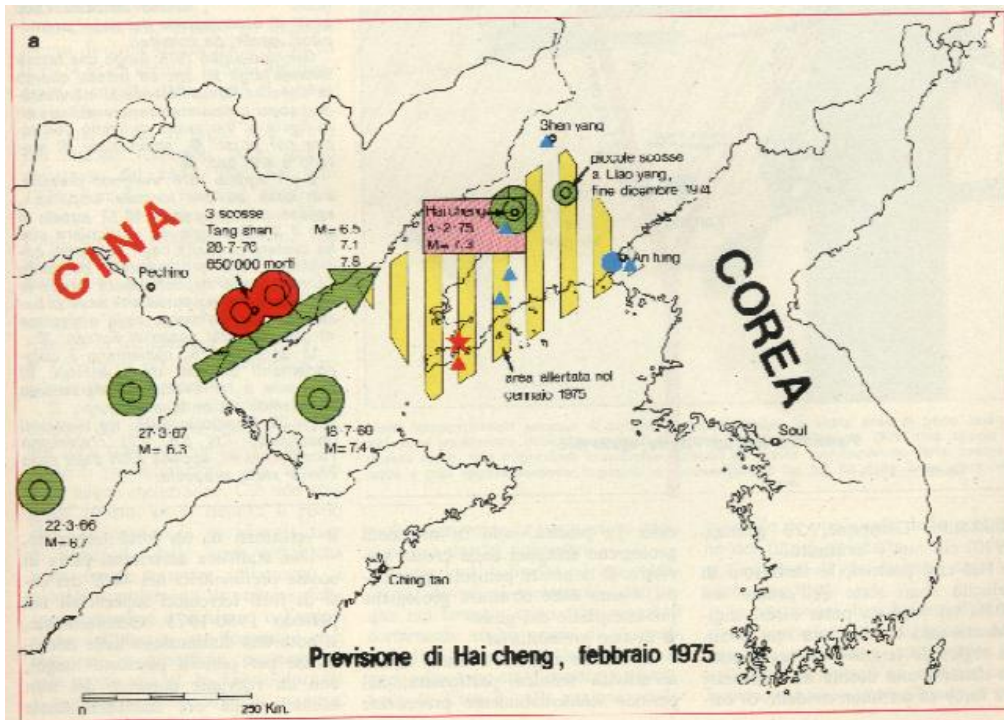


Fig. 5.33 – The Haicheng forecasts that motivated the successful alarm.



Fig. 5.34 – Location of Parkfield along the San Andreas fault.

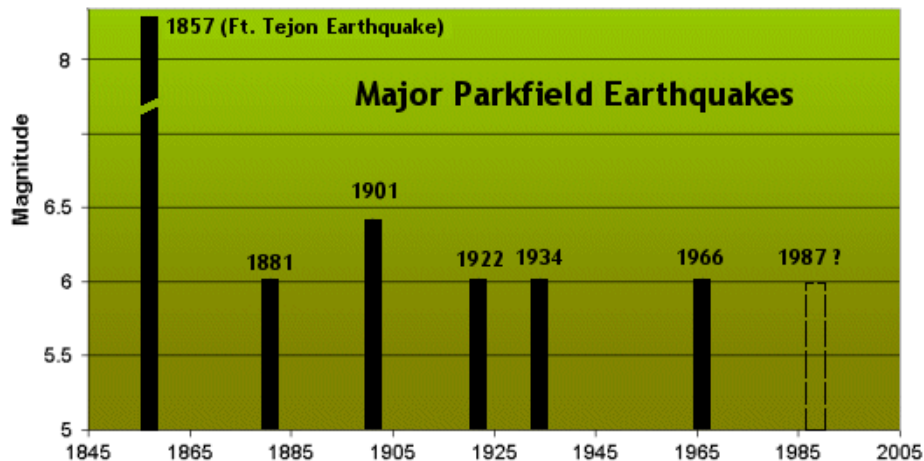


Fig. 5.35 - The sequence of the last earthquakes in the Parkfield area.

In the mid 1980s the USGS and several California universities initiated an intensive seismic monitoring program at Parkfield. The program includes the following instrumentation:

- 12 creep meters (to measure slow aseismic slip on the fault);
- 2 electronic distance measurement instruments (to monitor displacement);
- 12 GPS stations (to monitor displacement);
- 8 dilatational strain meters (to assess strain build-up in rocks);
- 3 tensor strain meters (to assess strain build-up in rocks);
- 12 short-period seismometers;
- 10 bore-hole seismometers;
- 30 strong motion sensors (to measure the ground motion associated with a large earthquake);
- a 2.2 km deep borehole with various instrumentation (SAFOD project started in 2004);
- a proposed 4 km deep borehole with various instrumentation.

Amongst numerous other studies, Earth scientists are monitoring water levels in wells and analysing data from satellites to assess ongoing ground displacement.

This unparalleled research effort was conducted for two main reasons. Firstly, the relatively simple geometry of the San Andreas Fault at Parkfield allows for a clear understanding of strain accumulation and release on the fault. Secondly, the apparent regularity of the historic earthquakes at Parkfield makes this an ideal site for testing the "time-predictable recurrence model" developed in the 1980s (Shimazaki and Nakata, 1980).

Some of the data gathered at Parkfield over the past few decades were analysed by geophysicists from Stanford University. Having estimated the rate of strain accumulation on the Parkfield segment of the San Andreas Fault, they concluded that the most of the strain released by the 1966 quake had re-accumulated by 1981, and that there was a 95% probability that another large quake should have occurred by 1987. In carrying out this analysis, the Stanford University geophysicists recognized that some of the strain at Parkfield could have been relieved by the nearby magnitude 6.5 Coalinga quake of 1983, and that this could have delayed Parkfield by about 2 years. On the other hand, they also calculated that two small earthquakes in the Parkfield area in 1992 and 1994 (around magnitude 4) actually increased strain on the Parkfield rupture zone, essentially countering the delaying effect of the Coalinga quake.

The only explanation offered was that local variations in pore-water pressure may have affected the tendency for failure on the Parkfield segment, although they had no means of measuring this parameter.

It was argued that the strain that accumulated at Parkfield was substantially more than that which had accumulated prior to the previous six large earthquakes, and therefore if the segment should have failed in 2002 or 2003 with a quake of magnitude between 6.6 and 6.9, which would have been significantly more damaging than any of the past Parkfield earthquakes. The only severe earthquake recorded since then was a  $M_w$  6.0 on September 28, 2004 and it ruptured roughly the same segment of the fault that broke in 1966.



### 5.3. Software for PSHA

Several computer codes for an automatic elaboration of hazard maps were prepared in the past: almost all of them refer to the historical probabilism or seismotectonic probabilism, according to Muir-Wood (1993).

Considering the second generation of hazard maps, it is worth mentioning the HAZAN code (Makropoulos and Burton, 1986): it considers both the first and third Gumbel distributions of extreme values and can handle several ground motion parameters (PGA, PGV, intensity, etc.). That software was used almost exclusively by the code's authors for PSHA of different regions (e.g., Greece), while similar home made software was used elsewhere.

The Cornell (1968) approach found translation into computer codes only some years after its publication. The USGS scientists developed two almost contemporary codes: RISK4a (Algermissen et al., 1976) and EqRisk (McGuire, 1976).

RISK4a (Algermissen et al., 1976) was used to create the 1976 seismic hazard maps of the U.S.A (Algermissen and Perkins, 1976) and of the Balkan region (Algermissen et al., 1976) and upgraded first as SeisRisk II (Bender and Perkins, 1982) and in its last version as SeisRisk III (Bender and Perkins, 1987), which is a free multiplatform code ([http://earthquake.usgs.gov/research/hazmaps/publications/Legacy\\_Code/index.php](http://earthquake.usgs.gov/research/hazmaps/publications/Legacy_Code/index.php)) applied all around the world till a few decades ago. SeisRisk III employs a model that allows earthquakes to occur as points within source zones and as finite-length ruptures along faults. SeisRisk III (Bender and Perkins, 1987) assumes the concept of seismic sources but allows earthquakes within a zone to be normally rather than uniformly distributed. This allows some of the earthquakes that would have occurred within the zone to occur outside the zone, permitting seismicity to vary smoothly across the boundaries of the zone. The result is that the calculated PGA varies smoothly at sites near the boundary. SeisRisk III does a partial magnitude smoothing that treats the closest distance ruptures as if they occurred over a range of magnitudes. Furthermore, the fault pattern may be quite complex within an active fault zone, and faults may be spread over a wide area. A peculiar aspect in SeisRisk III is represented by the individual seismicity rates used as input instead of the G-R parameters. This fact implies that there can be no proportionality among maps referring to different return periods.

Also EqRisk (McGuire, 1976) gave birth to a family of codes in which linear elements (faults) represent the seismogenic sources. The first version, Frisk (McGuire, 1978) is a USGS free code while the following versions [e.g., Frisk88™ (<http://www.riskeng.com/SoftwareHTML/software.html>)] are commercial products. Frisk88M™ is a sophisticated seismic hazard analysis tool: it allows you to look at multiple, weighted models of seismic sources, GMPEs, and correlation, and facilitates sensitivity studies on input parameters. It can be used on a site-specific basis or in a more efficient mode for seismic hazard mapping. It operates on multiple-weighted assumptions and accounts for both randomness and uncertainty.

In the 1970s also another code was prepared: its name is EqRisk (Anderson, 1978), hereafter referred as EqRisk-78 to differentiate it from the McGuire (1976) code. Also EqRisk-78 (Anderson, 1978) is based on the Cornell (1968) approach and its main difference with respect to the other cited codes is that it scales spectral amplitudes in several frequency bands.

STASHA (Guidi, 1979, Chiang et al., 1984) is a complete software for seismic hazard assessment developed at the Stanford University. The main difference with respect to the other codes is that two seismic hazard models are considered: the "classical" model, and the "probabilistic" model. Both models use a Poisson process for earthquake occurrence but in the "probabilistic" model it is also possible to treat earthquake occurrence and magnitude as a random variables of a Bayes model. Source geometry, tectonic model, and attenuation uncertainty are treated in different fashions according to the hazard model considered in the elaboration.

The most recent USGS maps for the U.S.A. were elaborated with a hazard package that mixes the Cornell (1968) approach with that of the smoothed seismicity (Frankel, 1995). It is a free software available at the USGS web page dedicated to current national seismic hazard maps (<http://earthquake.usgs.gov/research/hazmaps/publications/hazsoft.php>). The spatially-smoothed historic seismicity approach (Frankel, 1995) assumes that future damaging earthquakes will occur near areas which have had small ( $M > 3$  or  $M > 4$ ) or large earthquakes in the historic past.

Consequently,  $a$ -value grids are calculated using the maximum-likelihood formula. These  $a$ -value grids are smoothed with Gaussian smoothing functions and the hazard is calculated by summing the annual frequencies of exceedance for all of the grid cells. With this package, it is possible to use a combination of hazard curves calculated from gridded spatially-smoothed seismicity, large background zones, and specific fault sources.

Crisis99 (Ordaz et al., 1999), followed by various updated versions, is a computer program which computes seismic hazard in extended regions. It was developed at the Institute of Engineering, UNAM, Mexico, Crisis99 operates with completely arbitrary polygons for the definition of the source zones and dipping planes may also be defined. Seismicity of the sources can be modelled either as Poisson or characteristic earthquake process. In the first, magnitude frequency relations are smoothly truncated G-R curves, whereas for the second, the program assumes a Gaussian distribution of the magnitudes. Crisis99 allows different attenuation relations for different source zones, and hazard computations can be performed simultaneously for several ground motion measures. In the MS-Windows version, the source zones and the input parameters can be checked interactively through a user-friendly interface. In terms of the attenuation relations, Crisis99 allows different GMPEs for different source zones and takes into account the uncertainties through the standard deviations introduced on several input parameters. Crisis99 contains also a post-processing module that can be used to visualize the results, given in terms of maps of different parameters for arbitrary return periods or for exceedance rate curves for a selected site. Also, if several spectral ordinates are included in the computations as parameters, uniform-hazard response spectra can be produced. The updated version Crisis2003 considers different distances for the calculation of attenuation, and different values of the attenuation uncertainty as a function of magnitude. It has, also, a graphical interface, which displays all the data used and the geometry of seismic sources. The most important implementation, however, consists in the possibility of obtaining the deaggregation of the hazard results to identify the distance-magnitude pair that contributes most to the final result. Further updated releases of the code followed: Crisis2007, allows one to perform a chain of different elaborations in a single run; Crisis2015 (Aguilar-Meléndez et al., 2015) considers new options in area geometries, generalized Poissonian models, gridded seismicity, and site effects.

OpenSHA (Field et al., 2003) is an open-source, Java-based platform for conducting seismic hazard analysis. As an object-oriented framework, OpenSHA can accommodate arbitrarily complex (e.g., physics based) earthquake rupture forecasts, ground-motion models, and engineering-response models, which narrows the gap between cutting-edge geophysics and state-of-the-art hazard and risk evaluations.

OpenQuake ([www.globalquakemodel.org](http://www.globalquakemodel.org)) is a suite of open-source software that allows scientists to use data, best practice and applications collaboratively being developed. The suite comprises the Platform, the Engine, and a great variety of (desktop) Tools for modelling, and for accessing and exploring GEM products developed by the Global Earthquake Model (GEM), as well as uploading and sharing data and findings. The OpenQuake Engine is GEM's state-of-the-art software for seismic hazard and risk assessment at varying scales of resolution, from global to local. It can be used on a cluster, in the cloud or on a laptop. It is open-source, fully transparent and can be used with GEM or user-developed models to carry out scenario-based and probabilistic calculations and produce a great variety of outputs. The OpenQuake Engine combines hazard and risk calculations in a single software, but also supports hazard-only calculations and risk calculations with pre-computed hazard.

#### 5.4. Seismic hazard maps

In most of the countries in the world seismic hazard maps were prepared with different purposes: scientific studies or definition of national seismic codes. Those hazard maps were done according to the seismotectonic knowledge available: they can be roughly referred to the second (historical probabilism) and third (seismotectonic probabilism) hazard generation according to Muir-Wood (1993), with a few exceptions of maps referring to more advanced approaches. The use of non-Poissonian approaches, for example, may be useful as earthquake preparedness activity, but it is not suitable in the field of seismic zonation, because the zonation cannot be changed after the occurrence of every earthquake.

A comprehensive, although now dated, state-of-the-art of seismic hazard maps in the world can be found in McGuire (1993).

Without referring to the world map of earthquake occurrences, calculated in mid-19th century by Mallet and Mallet (1858), which is sometimes considered as the first seismic hazard map (Fig. 5.36), The first published seismic hazard map is very likely that of Canada (Milne and Davenport, 1969), in which the statistics of extreme values applied to seismicity (Epstein and Lomnitz, 1966) was considered. Some years later Algermissen and Perkins (1976) presented the seismic hazard map of the U.S.A. considering the Cornell (1968) approach and developing specific software (Algermissen et al., 1976): that is the first application of the seismotectonic probabilism at a national scale (prototype applications were done by the same authors only for individual states of the U.S.A.). Maps referred to the fourth hazard generation (non-Poissonian probabilism) were presented in recent years: generally the memory of the last event(s) is modelled only for some faults while the rest of the territory is treated with a Poisson approach (U.S.A. and Canada).

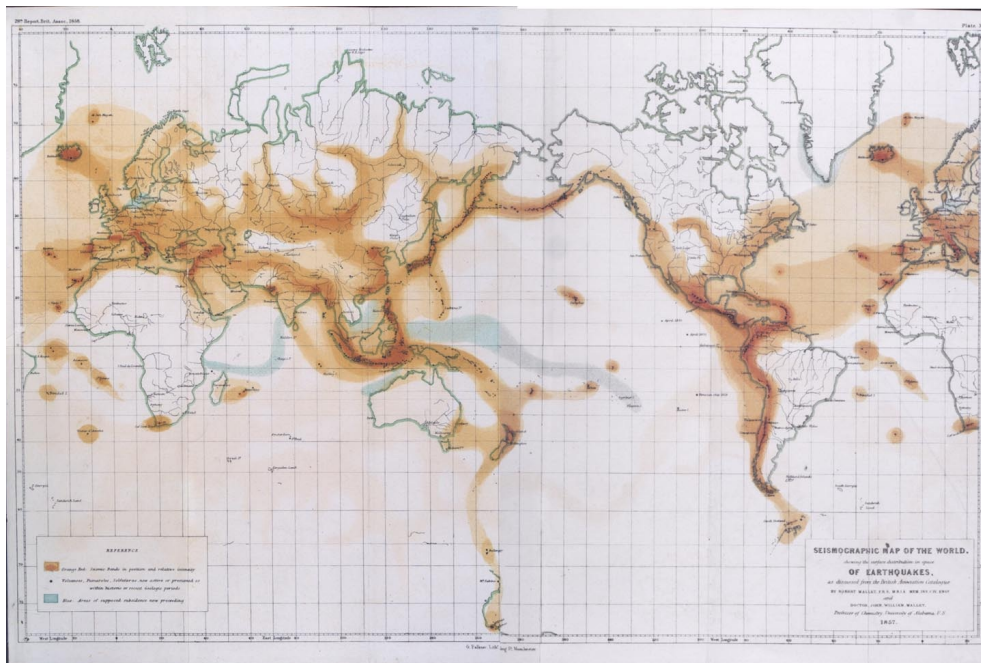


Fig. 5.36 - World map of earthquake occurrences calculated by Mallet e Mallet (1858).

It is interesting to describe briefly the evolution of the hazard maps in two emblematic situations: the U.S.A. and Italy.

The first national hazard map of the U.S.A. (Algermissen and Perkins, 1976) prepared by the USGS was revised some years later (Algermissen et al., 1982) by the same agency: in both maps the Cornell (1968) approach was used. More recently, the USGS scientists have developed a new methodology for PSHA, that merges the performances of the Cornell approach with those of the smoothed seismicity method. According this new methodology the national seismic hazard maps (Figs. 5.37 and 5.38) were prepared in 1996 (Frankel et al., 1996) and revised some years later (Frankel et al., 2002; Petersen et al., 2008, 2014).

The situation of Italy is different because in this case methodologies developed elsewhere were simply applied with a detailed analysis of the data used as input in the PSHA. The first national seismic hazard maps (Gruppo di Lavoro Scuoitibilità, 1979) were prepared in 1980 following the historical probabilism approach in the framework of a 3-year national project [called Progetto Finalizzato Geodinamica (PFG)] which involved a large number of Italian scientists. Macroseismic intensity was chosen as ground shaking parameter, because of the huge availability of macroseismic data, and the statistics of the extreme values was applied together with a national attenuation model (Fig. 5.39a). On the base of that map, it was set in the 1980s the first adjustment of the national seismic classification based on scientific criteria. New national maps (Slejko et al., 1998) were prepared in the 1990s in terms of both PGA and macroseismic intensity according to the Cornell (1968) approach. That study was developed the framework of a 6-year national project of the Gruppo Nazionale per la Difesa dai

Terremoti (GNDT) in which an earthquake catalogue (Camassi and Stucchi, 1997), a seismogenic zonation (Meletti et al., 2000), and both PGA and intensity national attenuation relations were applied (Slejko et al., 1998). Those maps were delivered in 1996 to the Italian Civil Protection Department and were revised together with the Servizio Sismico Nazionale (SSN) some years later (Albarelo et al., 2000) maintaining the same methodological approach (Figs. 5.39b and 5.39c). On the base of those maps and additional elaborations, a proposal of revision of the national seismic classification was presented in 1999 and applied in 2003. Recently, new national hazard maps (Gruppo di Lavoro, 2004) were prepared by the Istituto Nazionale di Geofisica e Vulcanologia, again following the Cornell (1968) approach but introducing a treatment of the uncertainties according to a logic tree approach (Fig. 5.39d). These maps are the base of the present national seismic zonation and building code.

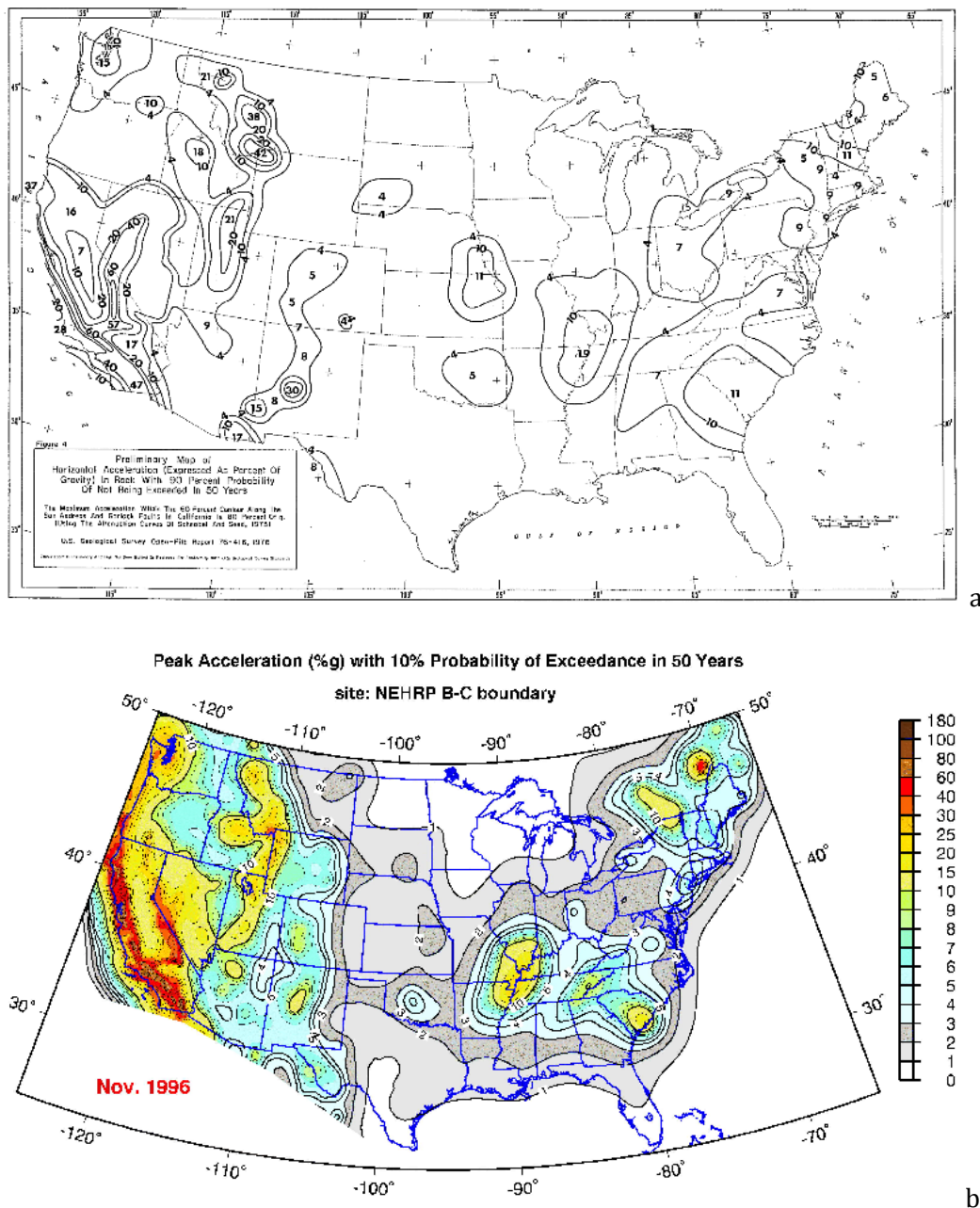


Fig. 5.37 – USGS seismic hazard maps of the U.S.A. of the 20th century, showing PGA with a 474-year return period for rock: a) 1976 release (from Algermissen et al., 1976); b) 1996 release (Frankel et al., 1996).



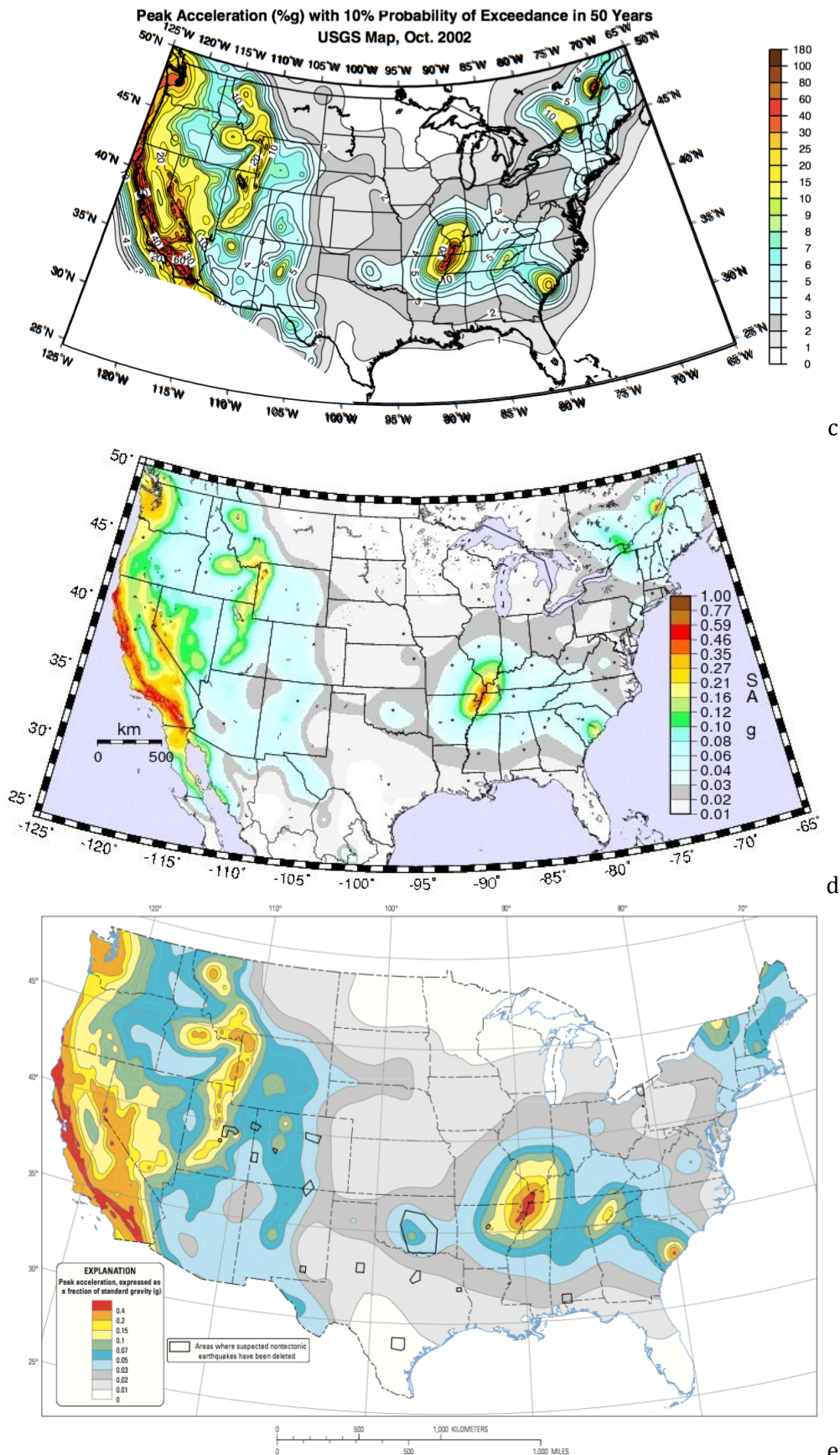


Fig. 5.38 – USGS seismic hazard maps of the U.S.A of the 21st century, showing PGA with a 474-year return period for rock: a) 2002 release (Frankel et al., 2002); b) 2008 release (Petersen et al., 2014); c) 2014 release (Petersen et al., 2014).

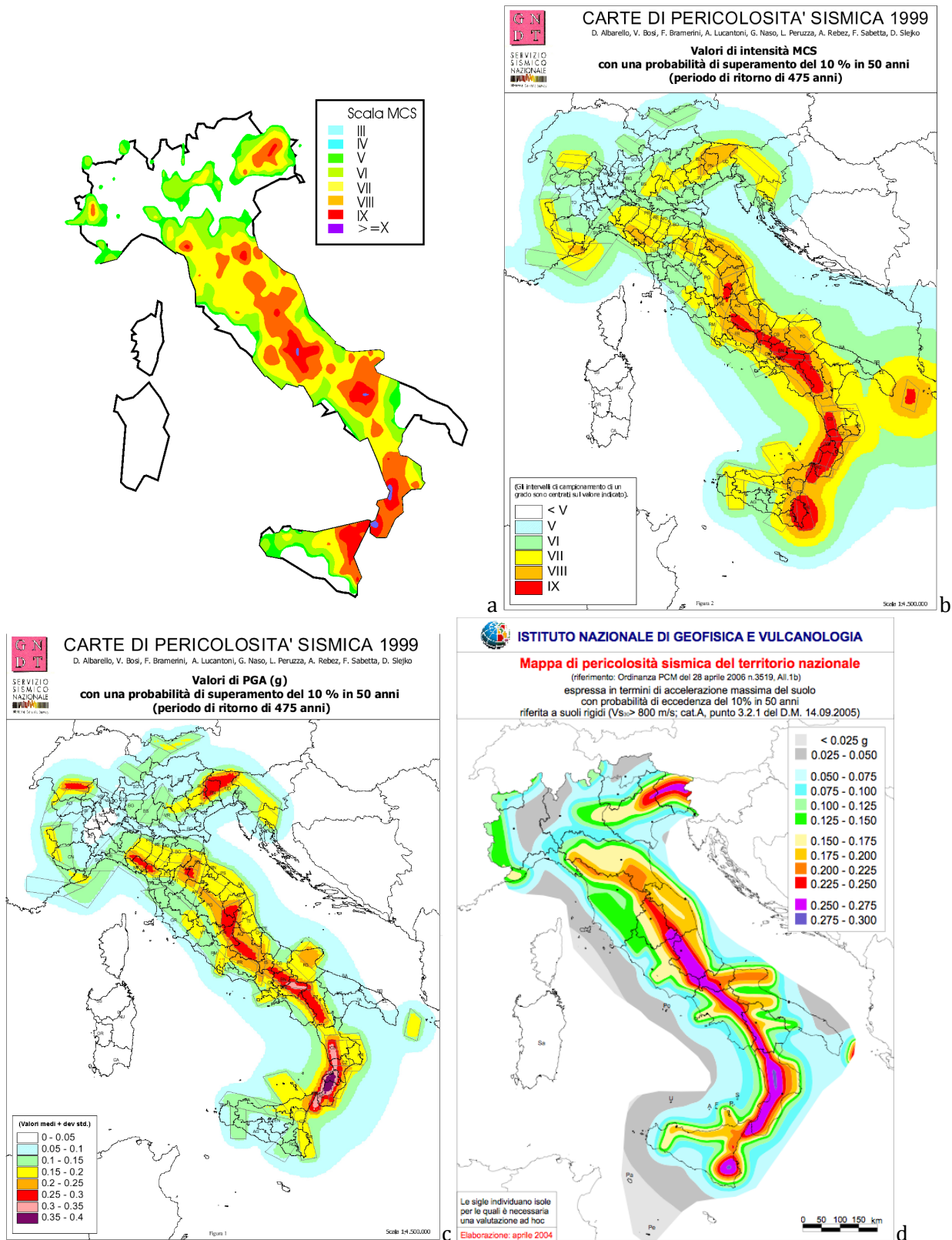


Fig. 5.39 – Seismic hazard maps of Italy: a) prepared in the frame of the PFG project and showing the expected macroseismic intensity with a 500-year return period (modified from Gruppo di Lavoro Scuotibilità, 1979); b) prepared by GNDT and SSN in 1999 and showing the expected macroseismic intensity with a 475-year return period (from Albarello et al., 2000); c) prepared by GNDT and SSN in 1999 and showing the expected PGA with a 475-year return period (from Albarello et al., 2000); d) prepared by INGV in 2004 and showing the expected PGA with a 475-year return period (from Gruppo di Lavoro, 2004).



Considering the whole planet, it must be mentioned the Global Seismic Hazard Assessment Project (GSHAP), in the framework of which a global map was prepared (Giardini et al., 1999). This map (Fig. 5.40) does not derive from a homogeneous elaboration of the global seismicity but it simply merge together national, or trans-national, maps obtained often with different approaches. This problem of heterogeneity of data treatment was overcome by the seismic hazard map of Europe and Mediterranean (Jimenez et al., 2003), elaborated in the framework of the European Seismological Commission. That map (Fig. 5.41) was an upgrade that of the Mediterranean region (Jimenez et al., 2001) and the elaboration, according to the Cornell (1968) approach, was based on a seismogenic zonation (geometry of the SZs and seismicity rates) valid for the whole studied region and derived from the GSHAP zonations.

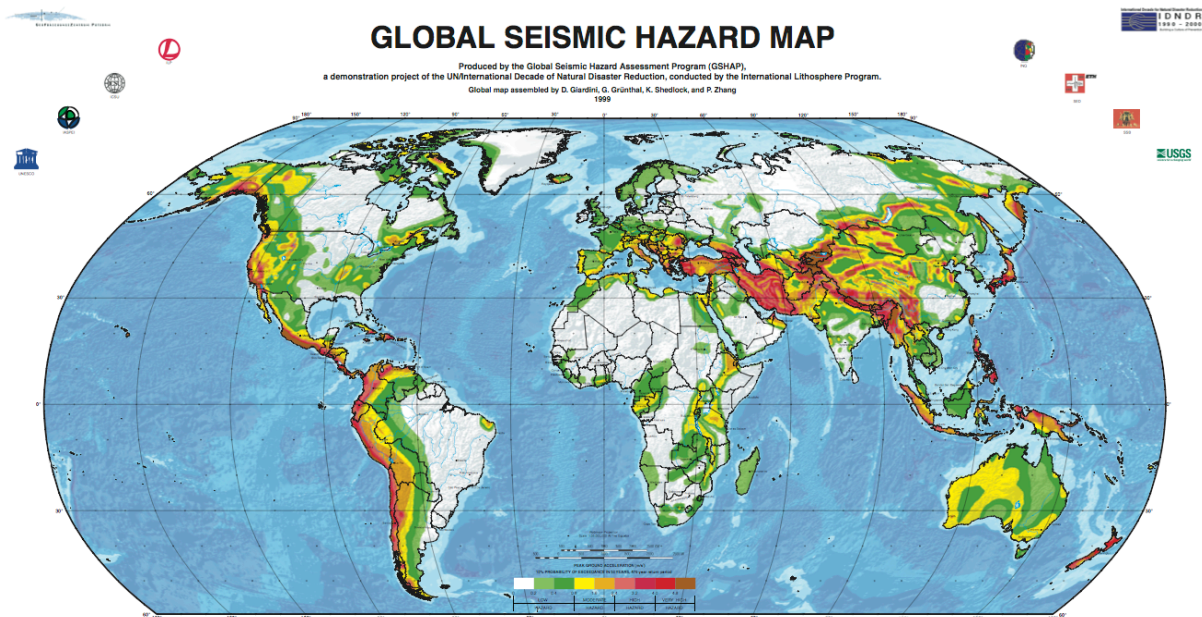


Fig. 5.40 – Seismic hazard map produced by GSHAP (Giardini et al., 1999).

Entering into details, it should be noted that both the Italian and European maps were computed using the computer code SeisRisk III (Bender and Perkins, 1987) while the GSHAP map is a collage of national maps obtained with different approaches. The seismic hazard maps generally refer to the return period of 475 years, corresponding to a 10% exceedance probability in 50 years [application of the relation (5-105)]. The genesis of this magic number is rather peculiar. In the 1960s and 1970s, seismic design in the U.S.A. referred to the recurrence interval of the design earthquake, i.e., 100 or 200 years. Algermissen and Perkins (1976) referred to the average life of ordinary buildings, i.e., 50 years, in their first hazard maps of the U.S.A., and chose the exceedance probability of 10%, among the many maps prepared. Therefore, the choice for the return period of 475 years was initially rather arbitrary, but it seemed justified on the basis of following considerations on the safety of buildings. Recently, seismic hazard maps of different countries (i.e., U.S.A. and Canada) refer to the return period of 2475 years (Frankel et al., 1996, 2000, 2002; Adams et al., 1999; Adams and Halchuk, 2003), corresponding to a 2% exceedance probability in 50 years.

### 5.5. Site effects in seismic hazard maps

The most intense shaking experienced during earthquakes generally occurs near the rupturing fault, and decreases with distance away from the fault. In a single earthquake, however, the shaking at one site can easily be 10 times stronger than at another site, even when their distance from the ruptured fault is the same. It is assumed that local geologic conditions are the cause of this difference in shaking intensity, but the particular conditions that are most responsible are still under debate, as well as the degree to which they affect earthquake shaking (Fig. 5.42). Combining this information

with estimates of where and how often earthquakes will occur would allow for better estimates of how intense shaking will be at the surface during future earthquakes.

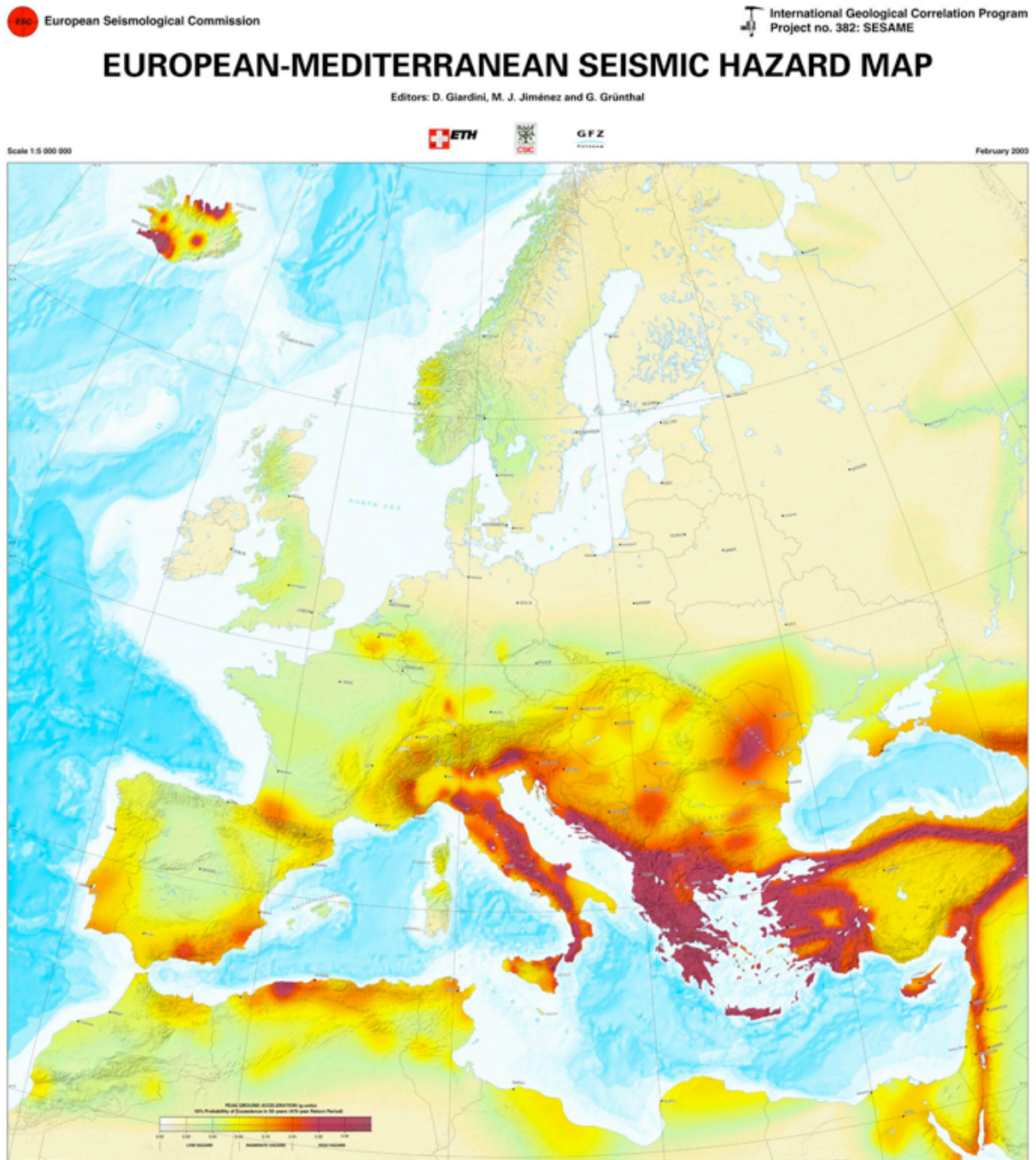


Fig. 5.41 – Seismic hazard map of the European – Mediterranean region (from Jimenez et al., 2003).

Ground motion attenuation relationships provide estimates of intensity measures that typically apply for broadly defined site conditions such as rock or soil.

The geologic factors that contribute most to the ground shaking at a site are: 1) the softness of the rock or soil near the surface (shaking is amplified in softer rock), 2) the thickness of the sediments above hard bedrock (shaking is amplified where sediments are thicker), and 3) the surface topography. Consequently, estimates from attenuation relationships necessarily represent averaged values across the range of possible site conditions. Analyses of site effects seek to improve the accuracy and reduce the dispersion of ground motion predictions using information about site conditions. The difficulty of quantifying the individual contribution of the site effects comes from observing that the observed ground shakings are generally different from those obtained theoretically

as they suffer at the same time the effects due to stratigraphy, buried morphology, topography, and directivity of the source mechanism.

It is possible to take into account these factors in different ways and a map showing where site effects will amplify the shaking can be produced. Nevertheless, even when these site effects are considered, each earthquake exhibits unique "hotspots" of anomalously strong shaking. Better predictions of strong ground shaking will therefore require additional geologic data and more comprehensive computer simulations of individual earthquakes.

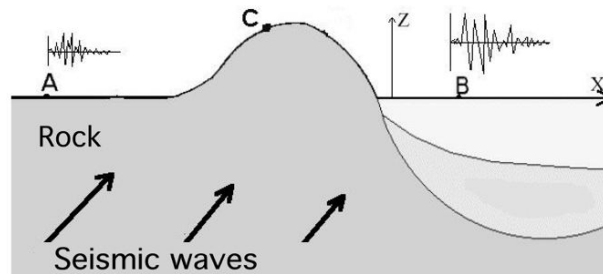


Fig. 5.42 – Scheme of the site effects.

### 5.5.1. The litho-stratigraphic site effects

The effect of the near-surface geology on the intensity of seismic shaking is difficult to quantify: we call this effect a site effect because it is local to each site. Several physical parameters can affect shaking intensity. The primary control of the site response is the rock or soil type, and a secondary control is the water content. The harder the rock the lower the level of shaking is a good rule of thumb. Igneous rocks such as granite are considered a hard rock, soft rocks are usually sedimentary rocks which include limestone, shale, and sandstone. Relative to a granitic site, a site underlain by sedimentary rocks could experience an increase of one-half to two intensity degrees at the same distance from the same earthquake. Sites underlain by young saturated soil or alluvium usually shake with the highest intensity: relative to granitic sites they may experience up to a three intensity degrees increase in shaking.

Local site conditions can profoundly influence all of the important characteristics (amplitude, frequency content, and duration) of strong ground motion. The extent of their influence depends on the geometry and material properties of the subsurface materials, on site topography, and on the characteristics of the input motion. The nature of local site effects can be illustrated in several ways: by simple, theoretical ground response analyses, by measurements of actual surface and subsurface motions at the same site, and by measurements of ground surface motions from sites with different subsurface conditions.

There are important theoretical reasons why ground surface motions should be influenced by local site conditions. At most sites the density  $\rho$  and S-wave velocity  $v_s$  of materials near the surface are smaller than at greater depths. If the effects of scattering and material damping are neglected, the conservation of elastic wave energy requires that the flow of energy (energy flux,  $\rho v_s \dot{u}^2$ ) from depth to the ground surface be constant. Therefore, since  $\rho$  and  $v_s$  decrease as waves approach the ground surface, the particle velocity,  $\dot{u}$ , must increase.

The characteristics of local soil deposits can also influence the extent to which ground motion amplification will occur when the specific impedance is constant. The basis for such amplification can be illustrated analytically using simple, theoretical ground response analyses. Consider, for example, the two soil deposits shown in Figs. 5.43a and 5.43b; their geometries are identical, but one is considerably stiffer than the other. If each soil is assumed to be linearly elastic and bedrock to be rigid, the amplification functions of each site are as illustrated in Fig. 5.43c. Clearly, the softer site (site A) will amplify low-frequency (long-period) bedrock motions more than the stiff site (site B); the reverse would be observed for high-frequency (short-period) motions. Since earthquakes produce bedrock motion over a range of frequencies, some components of an actual bedrock motion will be amplified more than others. For the more realistic condition of elastic bedrock, the nature of the local site

amplification will be influenced by the specific impedance of the bedrock. Consequently, any description of local site conditions should include the density and stiffness of the bedrock. For example, the harder crystalline bedrock found in much of the eastern U.S.A. would be expected to produce amplification factors about 50% higher than those associated with the softer rock conditions typically found in California for equivalent soil conditions.

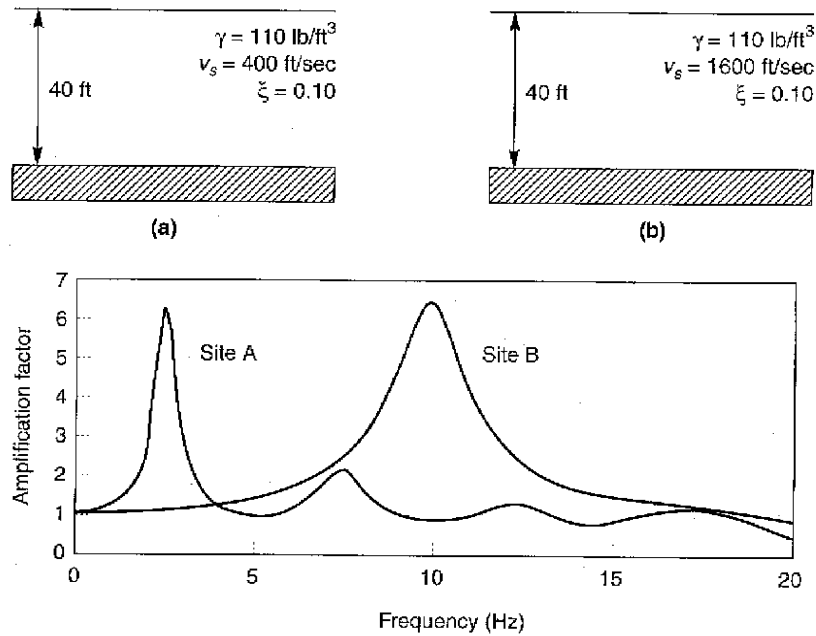


Fig. 5.43 – Site effects, soil deposits overlying rigid bedrock are identical, except the S-wave velocity of the soil at site B is four times greater than that at site A: a) site A; b) site B; c) amplification functions for sites A and B, note that the softer soil at site A will amplify low-frequency input motions much more strongly than will the stiffer soils of site B while at higher frequencies, the opposite behaviour would be expected (from <http://nptel.ac.in/courses>).

The common practice and the seismic building codes take into account the previous considerations defining different types of soils for which specific amplification factors (AFs) are applied. These amplification factors differ according to the entity of the ground motion. In fact, for strong ground motions a non-linear behaviour of the soil is expected and, consequently, the amplification is less than that in the case of a weak ground motion.

According to Vanini et al. (2017), the approaches to account for seismic site effects within a PSHA can be broadly classified as hybrid (deterministic and probabilistic) and fully probabilistic (Table 5.6). Hybrid approaches typically combine the results of a PSHA at a rock site with a suitable site-specific AF that multiplies the rock estimates. The AF may be derived either from a building code or by a site-specific 1D modelling based on ad hoc collected data. Bazzurro and Cornell (2004) noted that the hybrid approach, albeit easy to be applied, may produce exceedance rate estimates at the site not consistent with those on rock. The fully probabilistic approach implies either the application in the PSHA of GMPEs that take into account the soil characteristics or the convolution of the rock hazard curve with the curve representing the probabilistic AF derived by 1D modelling.

Table 5.6 – Approaches for site effect quantification in PSHA (modified from Vanini et al., 2017).

Hybrid		Fully probabilistic	
Generic site	Specific site	Generic site	Specific site
PSHA on rock + AF from building code	PSHA on rock + AF from 1D modelling	PSHA based on GMPE with site correction factor	PSHA on rock + convolution with AF curve from 1D modelling



The easiest way for introducing soil effects into PSHA considers soil AFs (e.g., those classified in a national building code) and increases the rock hazard map accordingly. Another way consists in the application of different GMPEs according to the specific soil types (Fig. 5.44). As the common GMPEs take into account five soil types as maximum (hard rock, soft rock, stiff soil, soft soil, and very soft soil) it is possible to construct different hazard maps for different soil types (Fig. 5.45). Combining together the five (or less according to the GMPE applied) hazard maps, according to the specific soil type, it is possible to obtain the soil hazard map, where the ground motion at the specific site is represented (Fig. 5.46). Figs. 5.44 to 5.46 show the main maps developed for the Friuli – Venezia Giulia region (NE Italy): the study region has been subdivided into three categories of soil types (rock, stiff soil, and soft soil) according to the guidelines of the European seismic code EC8 (CEN, 2002). Fig. 5.44 shows clearly the northern mountain sector (rock), cut by some valleys (stiff soil), and the southern Po Plain characterized by stiff and soft soils. The seismic hazard maps related to the three soil types are displayed in Fig. 5.45, where the expected ground motion amplification of the sedimentary deposits is evident. The final soil map (Fig. 5.46) was obtained by properly merging the previous maps by GIS technologies and points out many aspects of hazard which can be seen from the individual maps with some difficulties (areas with expected high amplification). The regular pattern of the usual hazard maps, in this case, is almost completely lost in favour of a representation related to the lithology of the studied region.

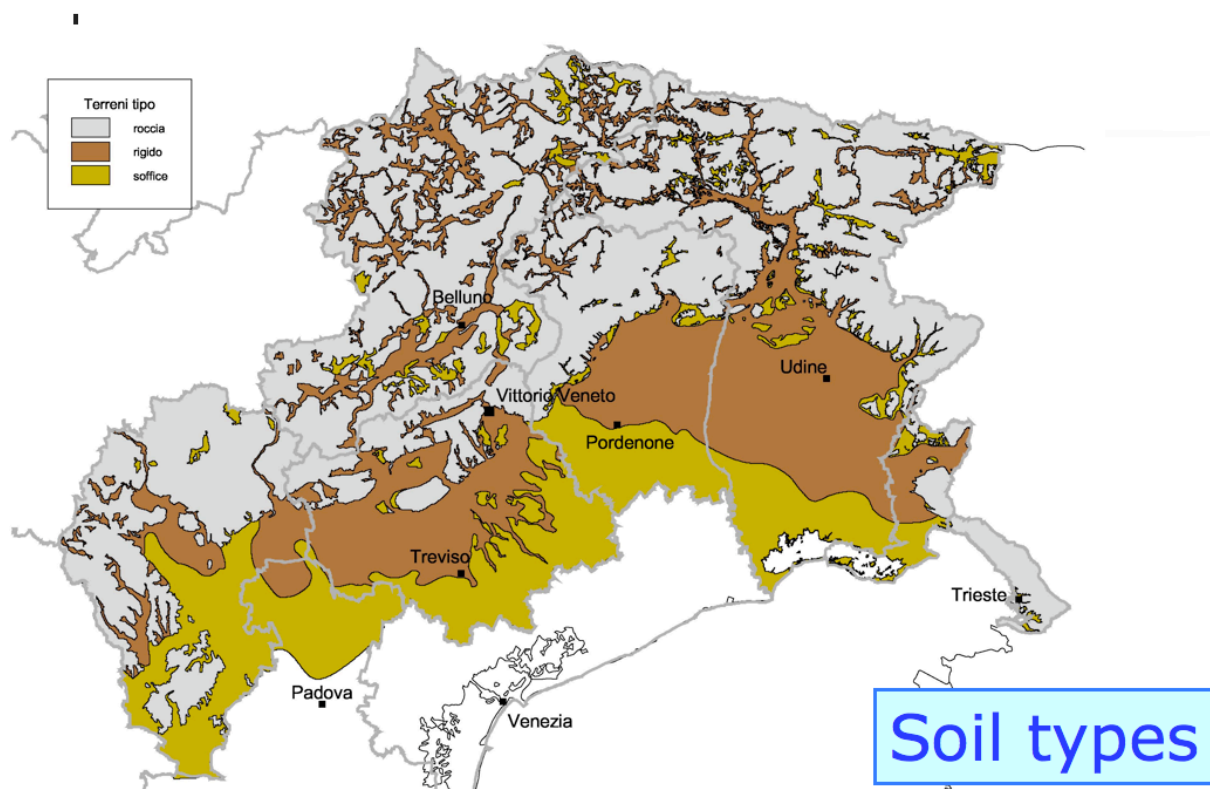


Fig. 5.44 – Soil types (rock, stiff soil, and soft soil) in NE Italy.

Another way to introduce simplified site effects in the seismic hazard maps is provided by the building codes and consists in modifying the rock estimates by proper AFs. Table 5.7 summarizes the AFs of the U.S. NEHRP (BSSC, 2004) provisions, European EC8 (CEN, 2002), and Italian (Ministro delle Infrastrutture; 2008) building codes. In addition to the application of different attenuation relations, also AFs from building codes were used for the soil seismic hazard assessment of the Friuli Venezia Giulia region, in NE Italy, and Fig. 5.47 shows the computed ground shaking. A comprehensive application of expeditious introduction of local effects is represented by the study of Rivera et al. (2004) for the province of Bayamo, in eastern Cuba. In addition to different attenuation relationships for the various soil types, the AFs of ground motion on soil with respect to that on rock were considered in agreement with the European and the U.S. seismic building codes (Fig. 5.48).

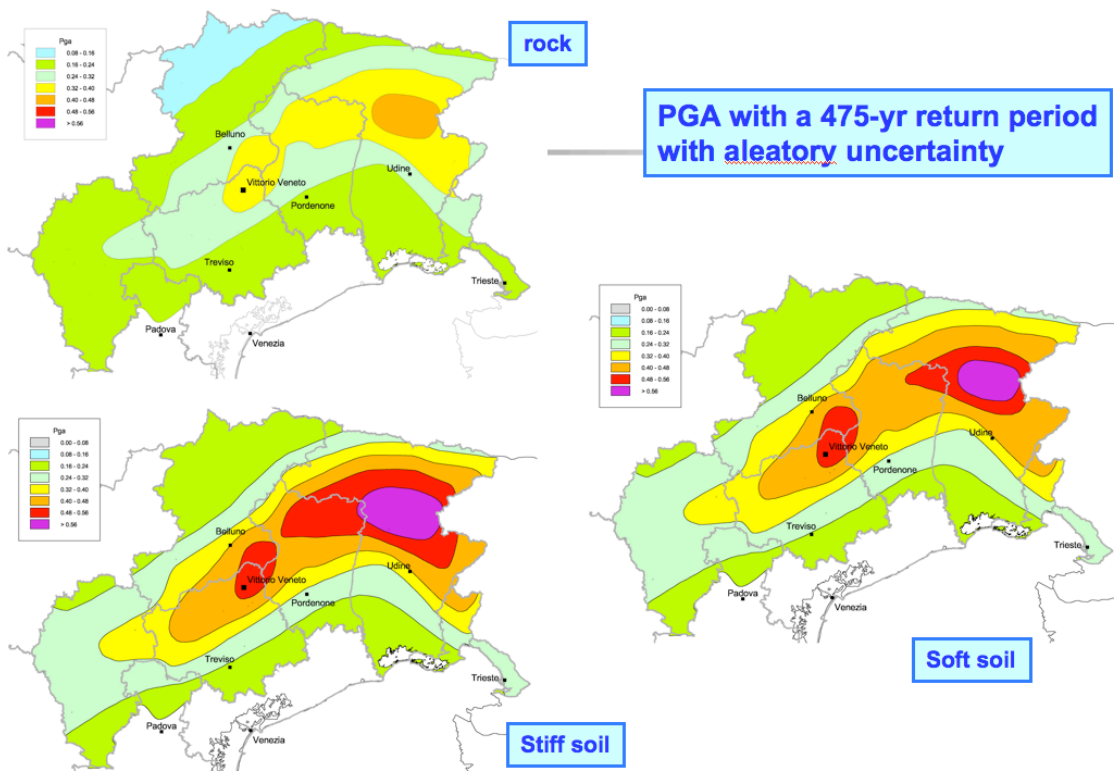


Fig. 5.45 – Seismic hazard maps of NE Italy for rock, stiff soil, and soft soil.

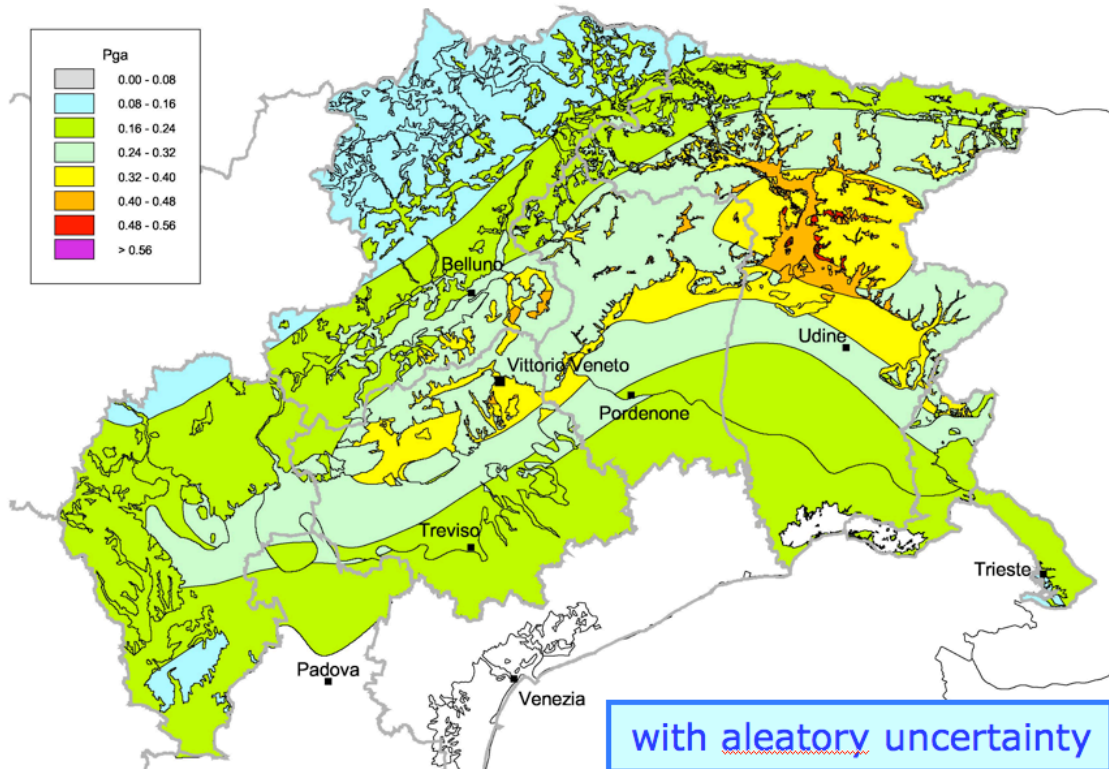


Fig. 5.46 – Seismic hazard map of NE Italy obtained applying different attenuation relations for different soil types.



Table 5.7 – Table of classification of soils a litho-stratigraphic Afs (from Slejko et al., 2011).

NEHRP Class	NEHRP V30 (m/s)	NEHRP AFs	Italian and EC8 Class	Italian and EC8 V30 (m/s)	EC8 AFs	Italian AFs	Local AFs
A - Hard rock	>1500	0.8					0.8
B - Rock	760-1500	1.0	Rock	>800	1	1	1
C - Very dense soil and soft rock	360-760	1.2	Stiff	800-360	1.2	1.25	1.2
D - Stiff soil	180-360	1.5	Soft	360-180	1.15	1.25	1.7
E - Soft soil	<180	2.1	Very soft	<180	1.35	1.35	1.9

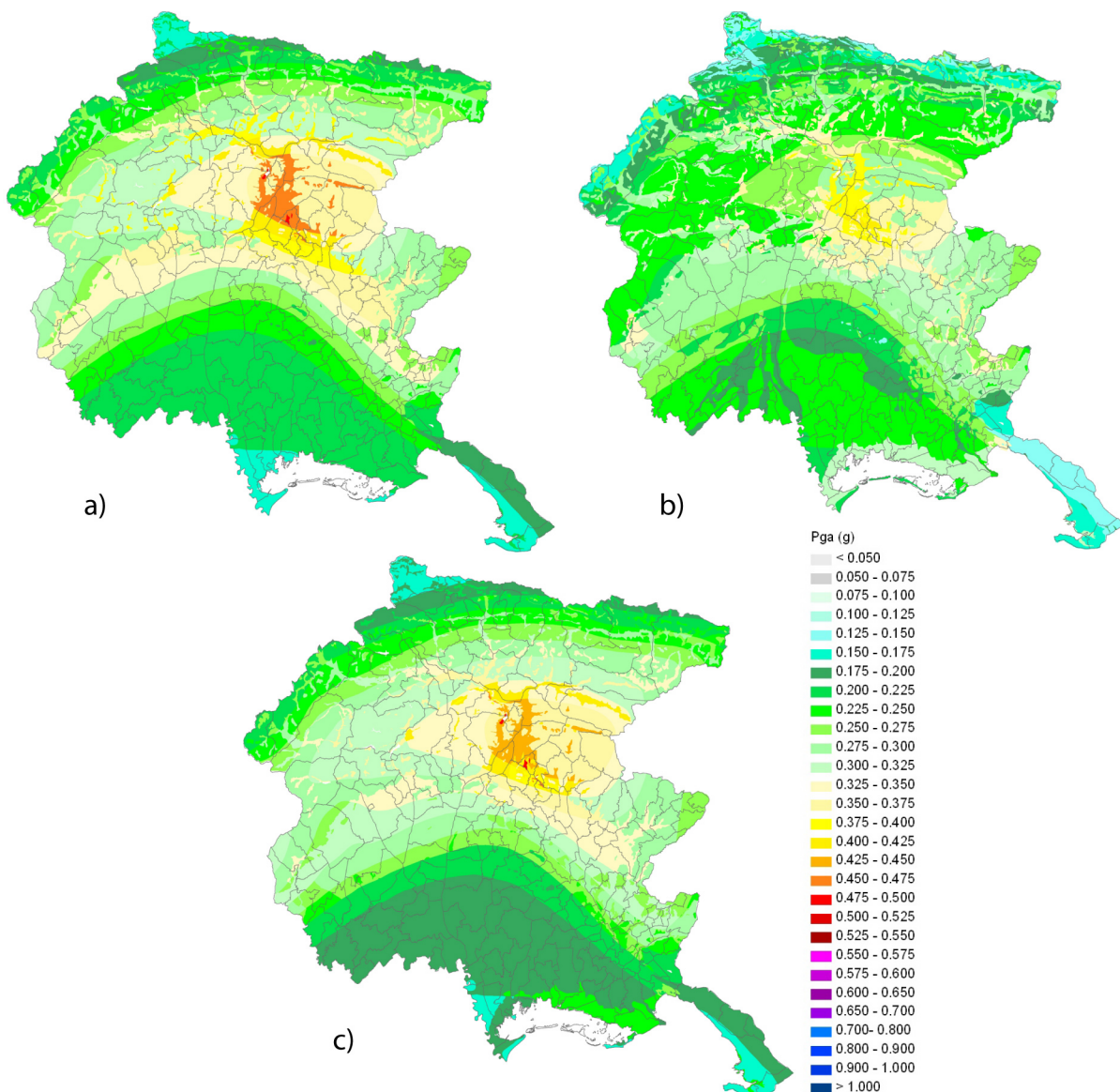


Fig. 5.47 – Soil seismic hazard map of the Friuli Venezia Giulia region (from Slejko et al., 2011) representing the PGA with a 475-year return period computed by considering building code lithological AFs (see Table 5.5): a) Italian (Ministro delle Infrastrutture, 2008); b) NEHRP (BSSC, 2004); c) EC8 (CEN, 2002).

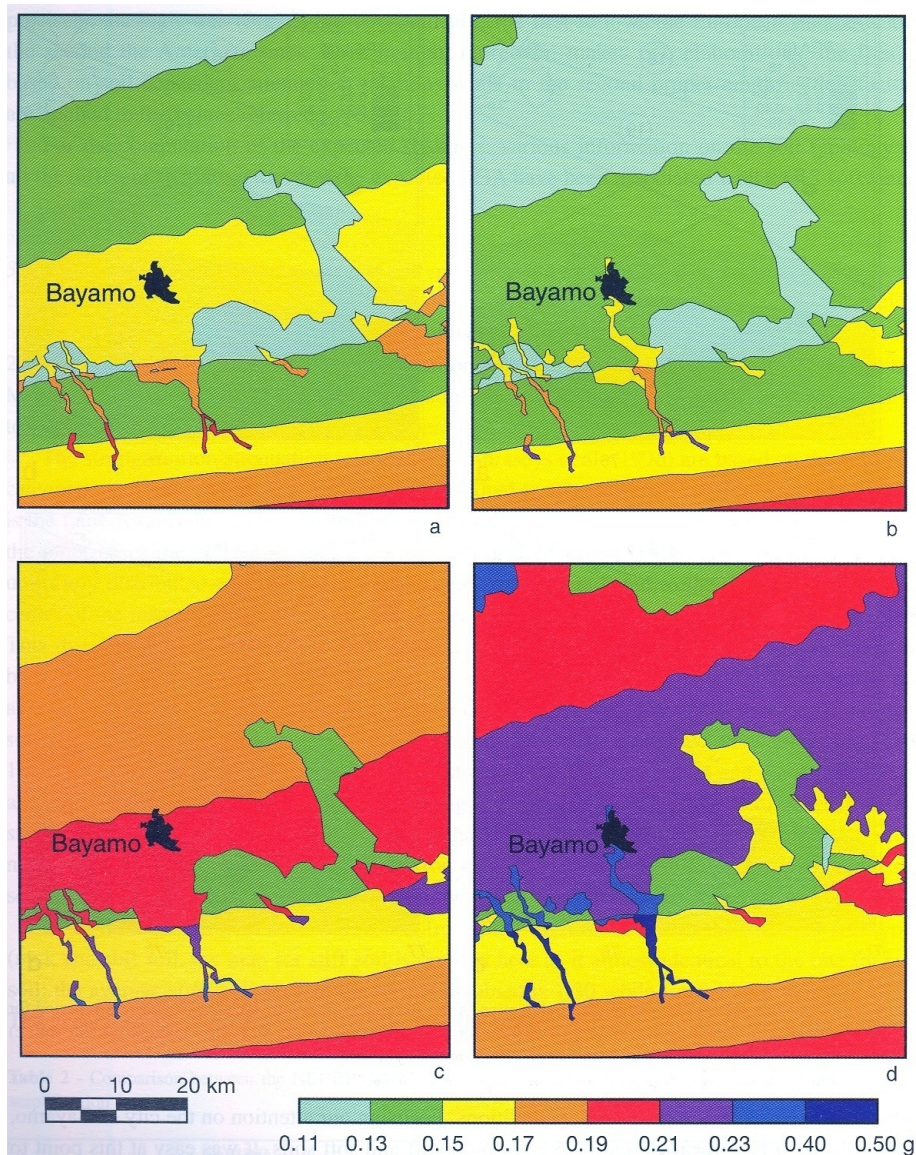


Fig. 5.48 – PGA with a 475-year return period for the Bayamo region (eastern Cuba) calculated according to the specific type of soil: a) using the European attenuation relationships; b) applying the European amplification factors; c) using American attenuation relationships; d) applying the U.S. amplification factors (from Rivera et al., 2004).

### 5.5.2. The morphological site effects

Amplification of ground motion may also be determined by the surface morphology. The relevance of these phenomena has been highlighted and documented during several earthquakes. In literature, topographic effects have been studied with reference to the following different morphological types (Stewart et al., 2001): 1) reliefs; 2) slopes; 3) canyons.

#### 5.5.2.1. Reliefs

Experimental observations and numerical simulations show that (Geli et al., 1988):

- at the top of a topographic relief the motion is amplified from the base;
- topographic amplification tends to grow with the relief steepness;
- topographic amplification is maximum in a frequency band corresponding to wavelengths

comparable to the width of the relief;

- if the incident wavelengths are less than the extension of the flanks of the hill, they can be affected by rapid alternations of amplification and attenuation phenomena, and consequently by important differential effects
- for non-vertical incidence waves, the zone of maximum amplification tends to move from the ridge to the side of the relief opposed to the direction of propagation;
- the adjacent topography, even if the relief is not homogeneous, leads to increase of amplification in the crest and deamplification at the foot.

#### 5.5.2.2. Slopes

Strong changes in ground motion have been observed in slope and step morphologies. In general it was observed that (Ashford et al., 1997):

- the ground motion is amplified close to the top of the slope and deamplified at the foot;
- a vertical motion is induced at the surface and the vertical accelerations can reach the same intensity as the horizontal ones;
- on the shelf behind the top of the slope, areas with amplification and with deamplification alternate, even within small distances;
- the change of the seismic motion extends from the edge up to about 2-8 times the height of the slope;
- the amplification increases with the steepness of the slope and is maximal in the presence of a vertical step.

#### 5.5.2.3. Canyons

In the case of canyons (as defined by Stewart et al. 2001) it was observed that (Sanchez-Sesma and Rosenblueth, 1979; Chuhan Zhang and Zhao Congbin, 1986):

- there is an amplification at the top of the canyon and a deamplification at the base;
- the amplification is very important for etched canyons ( $H/L > 2$ ; where  $2L$  and  $H$  are respectively the width and the depth of the canyon) and is negligible for shallow canyons ( $H/L < 0.05$ );
- if the stiffness of the upper layer is lower than that of the underlying bedrock, the amplification increases proportionally to the impedance contrast;
- the seismic response depends on the angle of incidence;
- the vertical component is more amplified as the angle of incidence approaches to vertical while the opposite occurs for the horizontal component.

#### 5.5.2.4. Quantification of the morphological site effects

2D and 3D numerical simulations show that, in the presence of strong morphological irregularities, the topographic factor alone can cause an amplification corresponding to more than one degree of macroseismic intensity (Paolucci, 2002).

It is interesting to note that with respect to topographic effects, the same Eurocode 8 (CEN, 2004), from a quantitative point of view, provides only minimum values (Table 5.8).

A very comprehensive study was done for the Friuli region in NE Italy and the following 9 morphotypes were identified (Fig. 5.49): plain, slope, wall, fluvial plain, alluvial fan, crest, terrace on slope, edge of scarp, and alluvial terrace. The related AFs were estimated on the basis of local geophysical surveys (Table 5.8) and compared with those coming from the building codes. Fig. 5.50 shows the influence of the morphological effects in the soil seismic hazard maps.



Table 5.8 - Morphological AFs calculated for Friuli compared with topographic AFs suggested by EC8 (from Slejko et al., 2011).

Morphotypes	$f_{MT}$	EC8
Plain	1.0	1.0
Slope	1.0	1.0
Alluvial fan	1.6	$\geq 1.2$
Fluvial plain (shallow)	1.8	$\geq 1.2$
Wall	3.5	$\geq 1.4$
Edge of scarp	3.5	$\geq 1.4$
Terrace on slope	3.5	$\geq 1.4$
Fluvial plain (deep)	3.9	$\geq 1.2$
Crest	4.0	$\geq 1.4$
Alluvial terrace	4.0	$\geq 1.4$

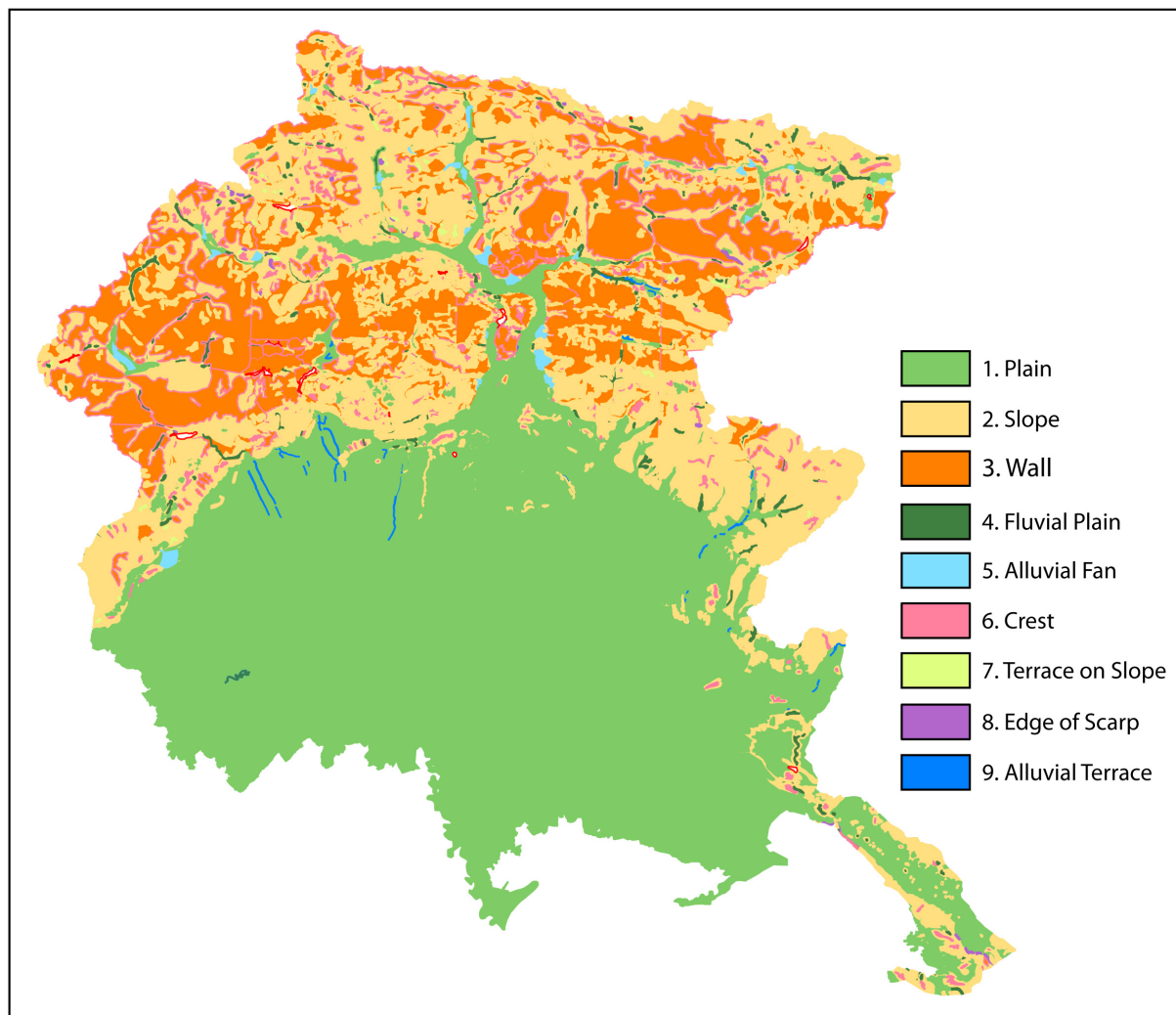


Fig. 5.49 – Morphotypes identified in the Friuli Venezia Giulia region in NE Italy (from Slejko et al., 2011)

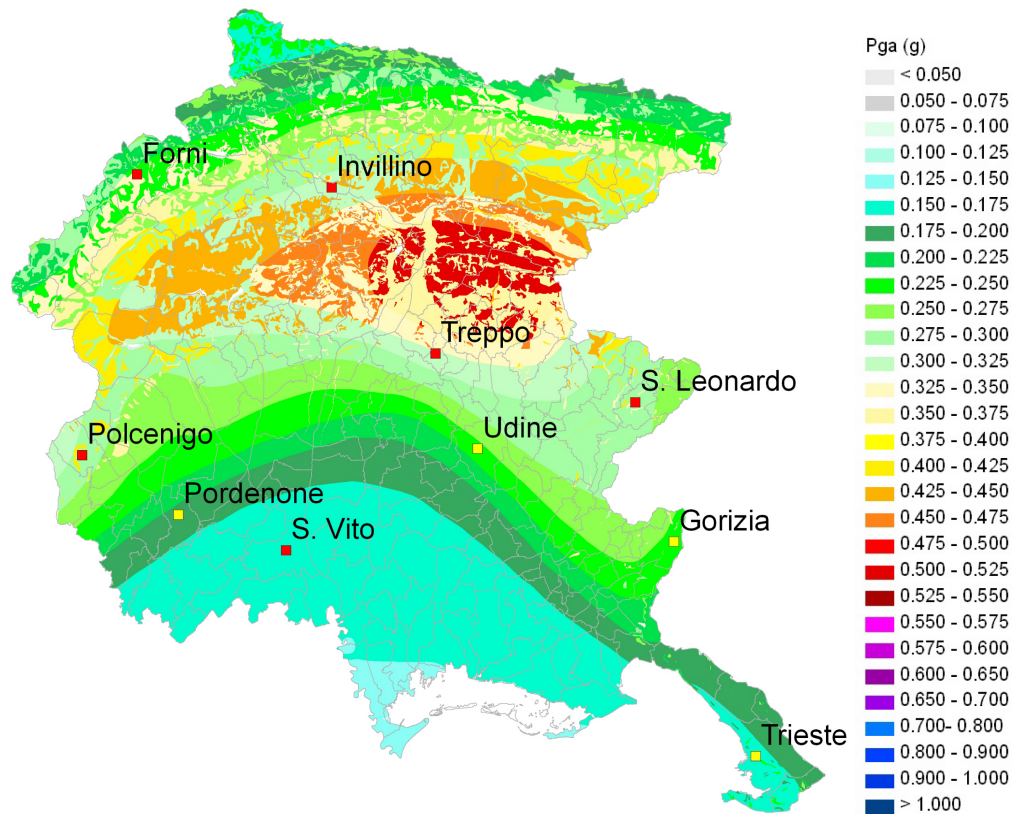


Fig. 5.50 - Soil seismic hazard map of the Friuli Venezia Giulia region (FROM slejko et al., 2011) representing the PGA with a 475-year return period computed by considering the EC8 (CEN, 2002) building code morphological AFs (see Table 5.7).

### 5.6. The SSHAC methodology in PSHA for strategic facilities

The methodology proposed by the Senior Seismic Hazard Analysis Committee (SSHAC) represents an up-to-date procedure for obtaining reproducible results from the application of PSHA principles established in past practice, not to advance the foundations of PSHA or develop a new methodology. This focus led to an emphasis on procedures for eliciting and aggregating data and models for performing a hazard analysis, rather than an examination of the Earth science foundations of PSHA. A second major theme in the SSHAC methodology is the treatment of uncertainties in data and models in arriving at stable estimates of seismic hazard at a selected site.

The SSHAC methodology for PSHA is an example of aggregating expert opinion on a scientific issue. In fact, due to large uncertainties in the geosciences data and in their modelling, multiple model interpretations are often possible, leading to disagreements among the experts. The objective of aggregation is to represent the scientific community's composite state of knowledge on a particular issue. The process should seek to capture the diversity of interpretations, as opposed to the judgment of any particular expert. What should be sought in a properly executed PSHA project are: a) a representation of the legitimate range of technically supportable interpretations among the entire informed technical community, and b) the relative importance or credibility (weight) that should be assigned to the various hypotheses across that range. The type of consensus being sought, therefore, is that all experts agree that a particular composite probability distribution represents, first, them as a panel, and secondly, perhaps modified, the informed community as a whole.

The SSHAC procedure at the highest level, recommended for nuclear power plants and other critical facilities, requests the presence of the TFI, who is essential to obtain a high degree of agreement among experts with many diverse viewpoints. The TFI approach is not recommended by SSHAC for every PSHA study.

In outlining its four levels of complexity, the SSHAC methodology visualizes three distinct roles that experts should play at various stages of the process. First, an expert may start out as the proponent of a particular position (data or model). Then, the expert is asked to become an objective evaluator of the positions of the other experts in the group. Finally, the expert becomes an integrator and aggregates all the positions to arrive at a putative position of the whole informed scientific community. This estimation of the position of the whole informed community by integration of the positions of a sample of well-qualified experts is the primary goal of the more complex SSHAC procedure.

It should be noted that the procedures recommended by SSHAC for the elicitation and aggregation of expert opinion as input to PSHA are equally applicable for compiling the input for DSHA.

The original task for which SSHAC was established consisted on the reconciliation of two studies done in the mid-1980s by the Lawrence Livermore National Laboratory (LLNL) and the Electric Power Research Institute (EPRI) of the earthquake hazard at nuclear power plant sites in the United States east of the Rocky Mountains. These studies were prompted by advice to the U.S. Nuclear Regulatory Commission (USNRC) from the USGS, based on its reconsideration of the likelihood that a major earthquake, such as the Charleston earthquake of 1886, could occur again in Charleston or elsewhere along the eastern seaboard. The possibility of such an earthquake could have implications for the safety of nuclear power plants in the eastern United States.

Although the two studies ranked the many sites approximately the same (from most hazardous to least hazardous in terms of the mean hazard estimates), the absolute hazard values for specific sites, in terms of the mean value of the annual probability of exceeding a specified level of ground motion, differed greatly, with the LLNL results consistently greater.

The problem is illustrated in Fig. 5.51, which displays the hazard at three widely separated sites as the annual frequency of occurrence of PGA. The median hazard curve from each study is shown, as well as the 85th and 15th percentile curves. Median rather than mean acceleration values are used in PSHA because log-acceleration is assumed to be normally distributed and, consequently, the median value of acceleration corresponds to the mean value of log-acceleration. In two of the three cases shown, the median hazard calculated by LLNL is well above that derived by EPRI, and the uncertainty, measured by the spread of the 15th and 85th percentile curves, is much greater for LLNL than EPRI. Also, the uncertainty is large, a factor of 5 or more at potentially damaging levels of ground motion (PGA greater than 200 cm/s<sup>2</sup>).

The mean hazard curves, not shown in the figure, differ by even greater factors in many cases. This is because the LLNL median and 85th percentile curves are above the EPRI results, and arithmetic averages spanning several orders of magnitude give greatest weight to the largest numbers. This explains the relatively high values of the mean hazard derived by LLNL but it does not get at the fundamental cause for the differences in the estimates.

The desirability of discovering the cause(s) of the discrepancies was obvious, not only for intellectual reasons (why did competent scientists working from the same or similar knowledge and data bases get vastly different answers?), but also for the practical reason that the quantitative estimate of seismic hazard is important in judging whether earthquakes represent a substantial threat, as well as the weight of earthquakes relative to other natural hazards in making design and retrofitting decisions. The U.S. National Research Council funded LLNL to investigate the problem. LLNL's study concluded that the factors involved in the discrepancy were: 1) different values were chosen for the lower-bound earthquake when the groups were integrated over seismicity to calculate the hazard, 2) different ground motion models were used, and 3) LLNL included a correction for local site effects and EPRI did not. This explained why the two studies obtained different answers but does not explain why competent analysts arrived at significantly different inputs to the hazard calculations.

As SSHAC was being assembled, the underlying cause of the discrepancies between the two studies was identified by further study at LLNL. Researchers there concluded that the differences were due to the ways in which the inputs provided by experts had been elicited. Once this was recognized and taken into account, the differences in the outputs (mean hazard curves) were reduced from orders of magnitude to small factors that represented satisfactory agreement, given the many uncertainties in every step of the analysis. SSHAC concluded its mandate presenting a recommended methodology and implementation guidelines, suitable for the performance of PSHA for seismic regulation of nuclear



power plants and other critical facilities.

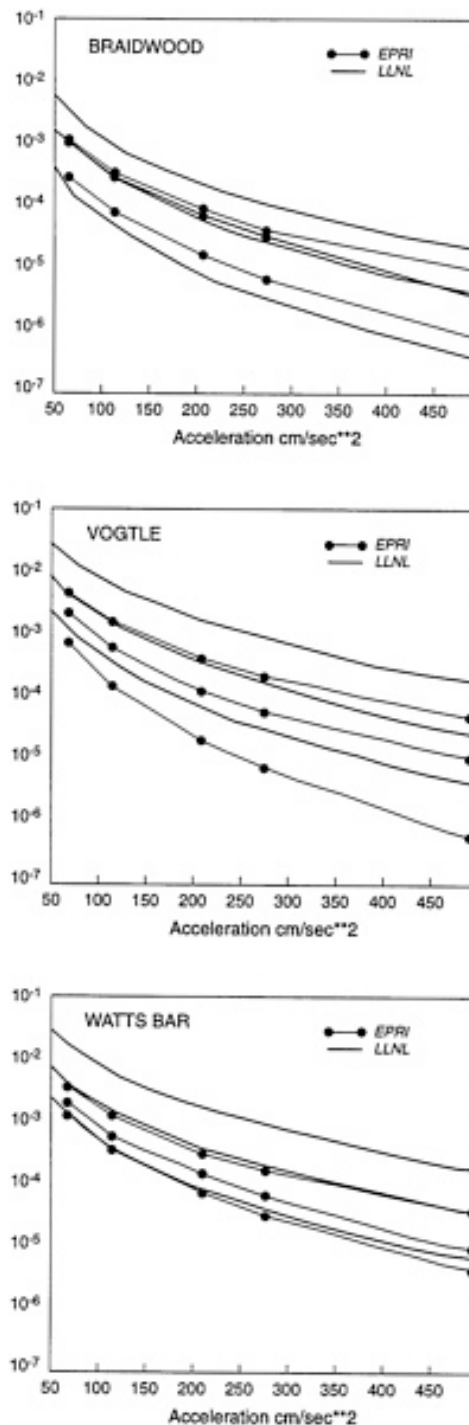


Fig. 5.51 - Median, 15th, and 85th percentile hazard curves for three representative separated sites in the eastern United States, illustrating the differences in results of the LLNL and EPRI studies. The ordinate is the estimated annual frequency of exceedance of the PGA shown as the abscissae (from Panel on Seismic Hazard Evaluation, 1997).

It should be recognized that SSHAC did not call for the defence or promotion of PSHA as a method for evaluating earthquake hazards. SSHAC has produced a document that sets forth its conclusions and recommendations on the proper way to do a PSHA if that is the approach chosen by project developers and their analysts.

SSHAC recognized that a PSHA can be carried out at different levels of effort and emphasized that the effort expended should match the importance of the facility, the degree of controversy,

uncertainty, and complexity associated with the relevant scientific issues, and external decision factors, such as regulatory concerns and the resources available (Table 5.9). Consequently, four levels of study are defined, the first three of which rely on a single entity called the technical integrator (TI), who is responsible for all aspects of the PSHA, including specifying the input. Although experts may be involved on a consulting basis, there is no formal elicitation of their views. The highest level of study (level 4) makes use of formally elicited expert judgment. As such, the new entity of TFI is needed. It would be inappropriate to infer that all PSHAs require the considerable resources needed to carry out the level 4 PSHA described by SSHAC.

SSHAC points out that most site-specific studies make use of some type of TI approach. The TI performs analyses, accumulates information relevant to each issue, and develops a representation of the technical community's views on the relevant input models, parameters, and their uncertainties. At the lowest level of effort (level 1) the technical community's views are determined primarily by a literature search. At higher levels the TI makes use of outside technical researchers and proponents to gain insight into different data sets and models.

The TFI process views experts as acting in different roles: proponents, evaluators, and integrators. The proponent role is one in which the expert explains, and argues for, the choice of a particular model or set of parameters. The aim is to make sure that the different views in the technical community are presented and discussed by the expert panel. If necessary, individuals outside the expert panel may be brought in to argue points of view with which panel members may not be comfortable. The next role the experts are asked to assume is that of independent evaluators representing their own views of the information presented. Mean estimates of model, component, or parameter values are elicited, along with their uncertainties as appropriate. The result should be the group's composite views of the issues at hand. The experts are encouraged to evaluate their own and other models according to their own technical judgment, without regard to who originally proposed the models.

To more truly represent the technical community's view, the SSHAC approach recommends that the experts be specifically asked to assume the role of integrators and to characterize their perception of how the technical community as a whole would view the issues at hand.

Table 5.9 - Degrees of PSHA issues and levels of study.

Issue Degree	Decision Factors	Study Level
A Non-controversial; and/or insignificant to hazard		1 TI evaluates/weights models based on literature review and experience; estimates community distribution
B Significant uncertainty and diversity; controversial; and complex	Regulatory concern Resources available Public perception	2 TI interacts with proponents & resource experts to identify issues and interpretations; estimates community distribution
C Highly contentious; significant to hazard; and highly complex		3 TI brings together proponents & resource experts for debate and interaction; TI focuses debate and evaluates alternative interpretations; estimates community distribution
		4 TFI organizes panel of experts to interpret and evaluate; focuses discussions; avoids inappropriate behavior on part of evaluators; draws picture of evaluators' estimate of the community's composite distribution; has ultimate responsibility for project

At present, the SSHAC methodology at the highest level (level 4) was applied only in two studies: that for the Jucca Mountains waste depository (Stepp et al., 2001) and that for the Swiss nuclear power plans (Musson et al., 2005).

In the case of strategic and special facilities, such as, for example, nuclear power plants, the greatest attention must be paid in considering all reasonable possibilities, including the very remote ones, because the hazard calculations refer to very low levels of annual exceedance probability [i.e., to very long return periods, see Eq. (5.77)]. Fig. 5.52 illustrates the logic tree suggested by an expert group of the project Pegasos (Abrahamson et al., 2002) to calculate the seismic hazard at the sites of the existing Swiss nuclear power plants. The level of annual exceedance probability requested in the study was  $10^{-7}$  and, therefore, both extreme seismogenic situations (Fig. 5.52a) and possible variability of seismicity (Fig. 5.52b) were taken into account. In such a way, the logic tree consisted of 21 branches referring to different possible geometries of the seismic sources for the characterization of their seismicity, for a total of 378 branches (Schmid and Slejko, 2009).

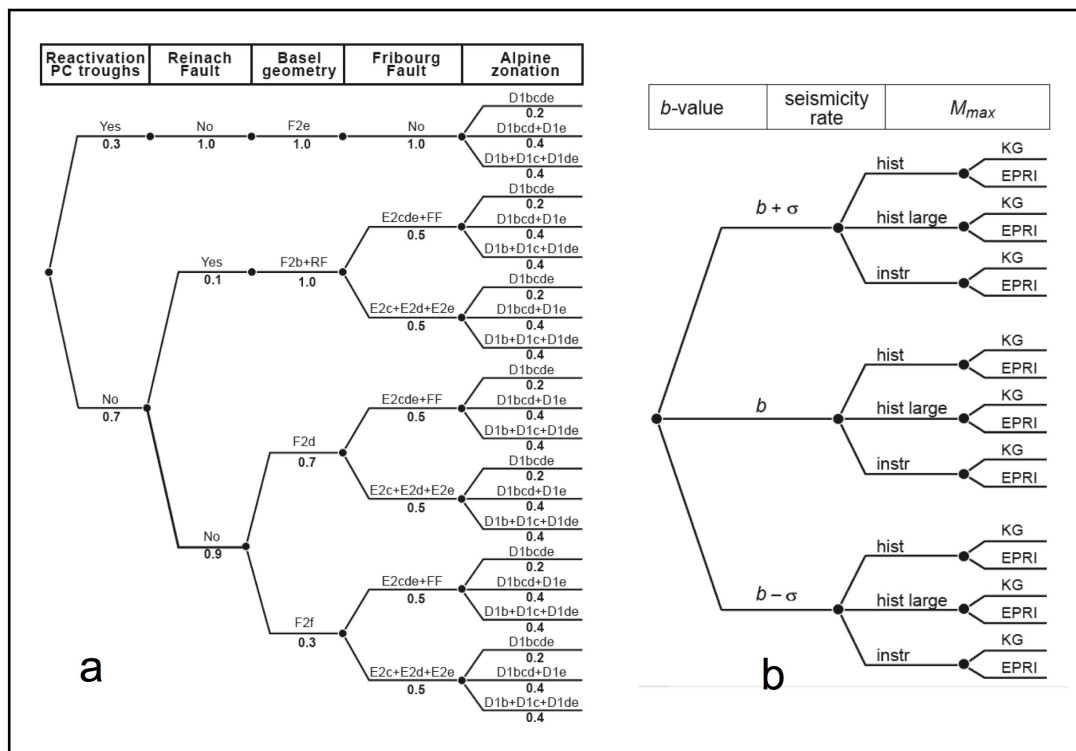


Fig. 5.52 – Logic trees used by Schmid and Slejko (2009) in the frame of the Pegasos project: a) for the space definition of the seismic sources; b) for the characterization of their seismicity.

## 6. SEISMIC RISK

**“Earthquakes don't kill people ..... buildings do”.** With the exception of tsunamis (earthquake tidal waves) and earthquake-triggered landslides, most earthquake related fatalities are caused by the collapse of people's homes upon them, or from fires that develop after earthquakes. A doubling in world population (6 billion to 12 billion) is expected in the next 100 years. Half of the world's supercities and many newly developing megacities are located in seismically hazardous locations where new housing starts are at an all-time high. A simple calculation (Bilham, 1998) shows that 1 billion new housing starts are expected in the first few decades of the 21<sup>st</sup> century. These are the houses that will pose a future threat to the next generation of urban dwellers. Now is the time to prepare for future urban earthquakes. Earthquake resistant construction costs only 10% more than non-resistant construction.

Although the human losses due to earthquakes can be terrible and protecting human lives must be the number one priority of earthquake engineering, the economic impact cannot be ignored. The losses due to the 1994 Northridge (California) earthquake represented the largest insured loss in history and the 1995 Kobe (Japan) earthquake was the largest single loss due to a disaster in history. It is clear, however, that in poorer countries the problem is still one of massive death tolls rather than massive economic losses (Fig. 6.1).

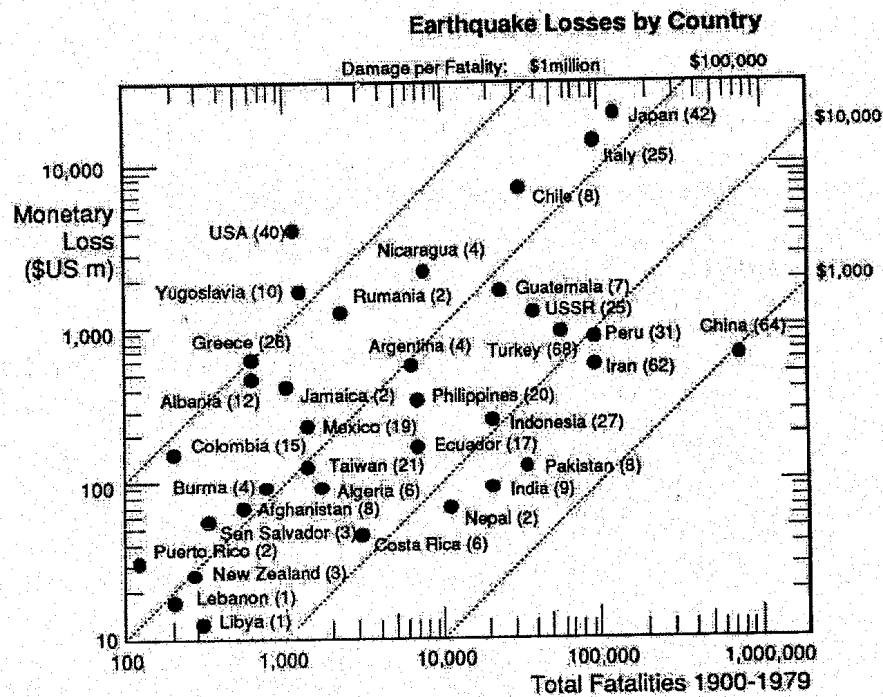


Fig. 6.1 - Fatalities and economic losses in earthquakes by country; the numbers in parentheses are the numbers of earthquakes per country (from Bommer, 2004).

Ambraseys and Bilham (2011) have pointed out that the number of deaths have continued to increase despite advances in earthquake-resistant design (Fig. 6.2). Averaged over the past decade, the fatality rate is 60,000 a year, including fatalities from building collapse and from secondary causes such as tsunamis, landslides and fire, despite of the positive contribution of earthquake-resistant design. This average is dominated by the earthquakes in Indonesia in 2004, Kashmir in 2005, Iran in 2005, China in 2008 and Haiti in 2010. The recent increase in earthquake fatality rates is not linked with average global populations (Fig. 6.2). Considering that the construction industry is recognized as being the most corrupt segment of the global economy, the authors show that decades of poor construction caused catastrophic consequences during earthquakes. By comparing earthquake fatalities from 1980 to 2010 with measures of corruption and wealth, the authors have found a direct relationship between poverty and deaths and also found that corrupt societies have the largest death tolls from earthquakes. In fact, 83% of all deaths from building collapse in earthquakes over the past

30 years occurred in countries that are anomalously corrupt (Fig. 6.3).

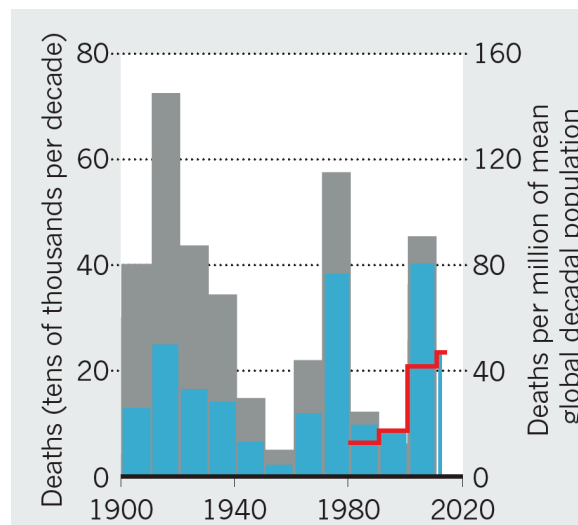


Fig. 6.2 - Earthquake deaths (from Ambraseys and Bilham, 2011). Despite advances in earthquake engineering, the number of people killed by earthquakes each decade has surged (blue), and the number of deaths as a proportion of global population has not dropped much (dark grey). Many of these deaths can be attributed to building collapse (red).

It is interesting that, within the earthquakes that caused a large number of victims, secondary effects (tsunami, fire, landslides, liquefaction, fault rupture, etc.) have played a major role, causing around 40% of economic losses and fatalities as compared to shaking effects (Tables 6.1 to 6.4).

Table 6.1 - The effect of the larger landslide events since 1900.

Date and location	Magnitude of event	Fatalities due to landslides
1920 Haiyuan	Mw 8.3/8.6	136,700 deaths (50%)
1970 Ancash	Mw 7.9	26,700 deaths (40%)
2005 Kashmir	Mw 7.6	26,500 deaths (31%)
2008 Sichuan	Mw 7.9	26,500 deaths (30%)
1949 Khait	Mw 7.6	11,760 deaths (98%)
1976 Irian Jaya	Mw 7.1	5,520 deaths (92%)
1907 Karatag	Mw 7.2	4,900 deaths (35%)
1917 Daguang	Mw 7.3	1,800 deaths (96%)
1950 Assam, Chayu	Mw 8.6	1,450 deaths (30%)
1998 Badakhshan and Takhar Provinces	Mw 6.5	1,350 deaths (30%)

## 6.1. Risk and hazard

In the Webster's (1977) dictionary hazard is defined as "a source of danger" and risk as the "possibility of loss or injury" and the "degree of probability of such loss". Hazard, therefore, simply exists as a source, while risk includes the likelihood of conversion of that source into actual delivery of loss, injury, or some form of damage. The concept can, therefore, be expressed symbolically as (Kaplan and Garrick, 1981):

$$\text{risk} = \text{uncertainty} + \text{damage} \quad (6-1)$$

$$\text{risk} = \text{hazard over safeguards} \quad (6-2)$$

where Eq. (6-2) shows that risk can be reduced by increasing the safeguards, if hazard remains constant. In other words, the risk associated to the occurrence of an event is determined by two

factors: the probability of occurrence of such event, and the entity of its consequences. For the scientific community, irrespectively of the common use, hazard is synonymous of rare event not directly involving any special connotation of danger. It derives semantically from the Arab "azzahr", the dice, because dice players in Florence during the 13th century used to shout "zara" when the lowest probability result occurred (Siccardi, 1991).

Table 6.2 - The effect of the larger liquefaction events since 1900.

Date and location	Magnitude of event	Fatalities and/or economic losses
2010/2011 Christchurch Sequence	Mw 7.1, Mw 6.3, and subsequent aftershocks	No known fatalities, but 6,000+ buildings red zoned, and many other clean-up costs. Likely around \$10bn+ associated with liquefaction losses
1964 Niigata	Mw 7.6	2 deaths, many collapses of multi-storey apartments
1995 Kobe	Mw 6.9	3 deaths, widespread damage
1999 Izmit	Mw 7.7	Extensive damage
1935 Taiwan; 2016 Taiwan	Multiple	16 deaths were believed to be associated in 1935; with liquefaction also believed to be a factor in the 2016 quake
1920 Haiyuan, 1989 Tajikistan, 2013 Dixi	Multiple	Loess liquefaction caused many fatalities (included above in landslide)

Table 6.3 - The effect of the larger tsunami events since 1900.

Date and location	Magnitude of event	Fatalities and/or economic losses <sup>a</sup>
2004 Indian Ocean	Mw 9.1	168,000 (Indonesia), 35,300 (Sri Lanka), 15,800 (India), 8,200 (Thailand) (ca. 99%) deaths, and \$10bn+ (event year)
2011 Tohoku	Mw 9.0	17,931 deaths (96% not including indirect) / \$120bn + (event year)
1941 Andaman Islands	Mw 7.7	7,960 deaths (99.5%)
1976 Moro Gulf	Mw 8	6,229 deaths (88.0%)
1945 Makran	Mw 8	3,700 deaths (92.5%)
1933 Sanriku-oki	Mw 8.4	3,002 deaths (98.0%)
1998 Papua New Guinea	Mw 7	2,683 deaths (100.0%)
1908 Messina	Mw 7.24	2,578 deaths (3.0%)
1992 Flores	Mw 7.7	2,519 deaths (100.0%)
1952 Kamchatka	Mw 9.0	2,336 deaths (100.0%)

Coming to engineering seismology, seismic hazard, or shakeability, represents the probability that a fixed value of shaking (macroseismic intensity, PGA, etc.) could be exceeded in a certain time interval because of an earthquake, while risk describes quantitatively the probable damage that a site will experience. A formal definition of seismic risk  $R$  is not available; seismic risk takes into account the influence of three parameters: the seismic hazard, the vulnerability, and the exposed value (or urban exposition), and even a simple rough quantification of risk is not possible by mean of one physical quantity only (Fournier d'Albe, 1985). Precise definitions refer to the seismic hazard  $H$ , as said before, to the vulnerability  $V$  (measure of the attitude of a general object to suffer damage because of an earthquake), and the "exposed" value  $E$  (economic measure of the object or of its use). A notable difference between seismic hazard and risk does exist and, consequently, the use of the information is different: a seismic hazard map can be the basis for designing seismically resistant buildings (although during the realization of the project choices of acceptable risk, on the basis of cost/benefit analysis, are



made), and a seismic risk map could indicate the zones where priority of retrofitting to old buildings is needed.

Table 6.4 - The effect of the larger fire events since 1900.

Date and location	Magnitude of event	Fatalities and/or economic losses <sup>a</sup>
1923 Great Kanto	Mw 7.9	92,190 deaths (87%); 2/3 of the damage (\$40bn+ CPI adjusted); ca. \$220bn HNDECI
1906 San Francisco	Mw 7.9	1,800 deaths (60%); ca. 5/6 of damage (ca. \$10bn CPI adjusted); \$50.6bn HNDECI
1995 Great Hanshin, Aawji, Kobe	Mw 6.9	570 deaths (9%)
1948 Fukui	Mw 7	513 deaths (10%)
1925 Dali	Ms 7	400 deaths (7%)
1906 Valparaiso	Mw 8.5	388 deaths (10%)

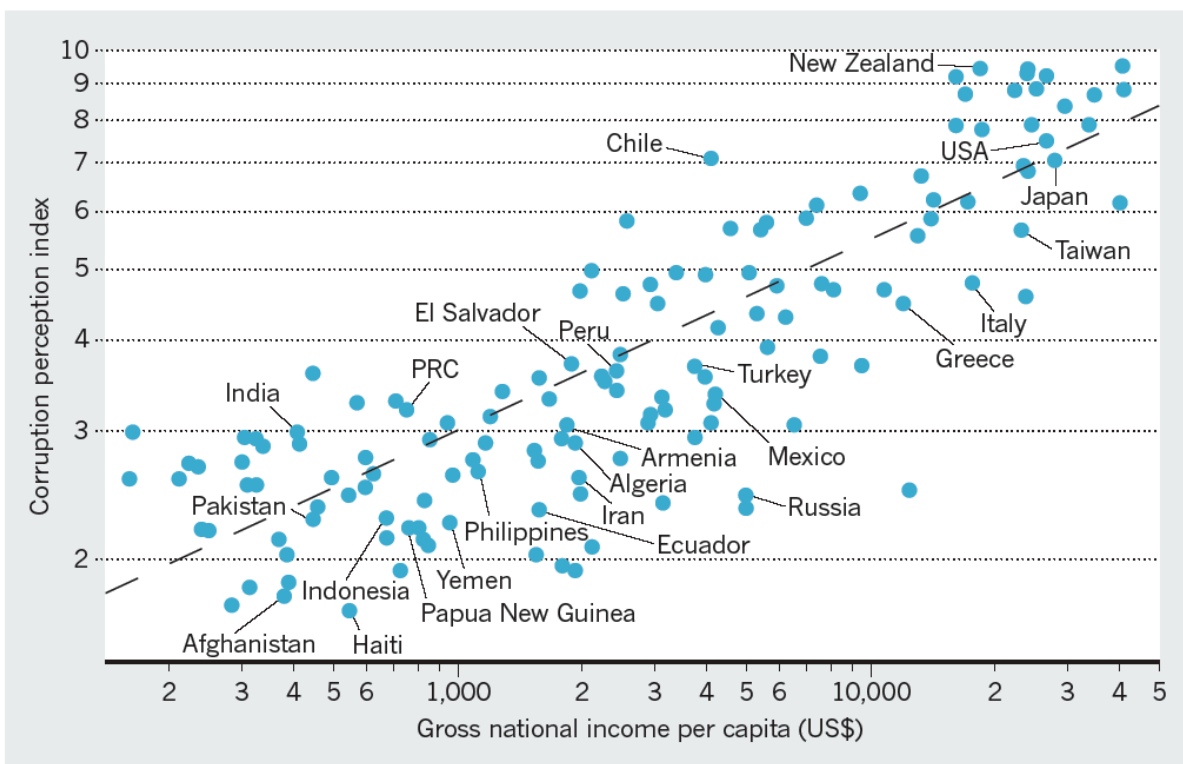


Fig. 6.3 - Cash and corruption (from Ambraseys and Bilham, 2011). The poorest countries are the most corrupt, but some are more corrupt than others. A weighted regression line (dashed) divides nations that are perceived as more corrupt (below the line) than might be expected from the average income per capita from those that are less corrupt (above the line). Named countries have lost citizens in building collapse caused by earthquakes since 1980.

$R$  has been expressed analytically as the convolution of  $H$  and  $V$  (the result represents the probability of not exceeding a certain damage level) times  $E$  and expresses the probability of not exceeding a certain damage cost (Ambraseys, 1983):

$$R = H * V \cdot E \tag{6-3}$$

where  $V$  qualifies the preservation status of the buildings as well as the situation of the social structures, lifelines, etc., which can go out of service because of the earthquake, and  $E$  is an economic measure of all the structures (human lives, buildings, factories, artistic works, etc.) hit. More precisely,  $H$  can be represented by  $HR+HL$ , where  $HR$  is the regional seismic hazard and  $HL$  is the local one.  $H$  is represented by the hazard curve of the study site and  $V$  is generally quantified by the fragility curve of

the studied object. The fragility curve describes the damage probability corresponding to a specific damage state, for various ground shakings.

People safety depends, then, on what they build. In fact, it is possible to live in a region of high seismic hazard with no (or limited) danger if the house was built to sound engineering principles. On the other hand, it is possible to live in a low seismicity area, in an ancient, poorly maintained brick building, suffering settlement problems on a filled swamp. Although the seismic hazard is low, the risk in this case might be as high, or higher than, in a well-built building in a high seismicity zone.

Seismic risk calculations are the foundation for risk mitigation decision-making, a key step in risk management. Large corporations analyse their portfolio of properties, to determine how to best allocate limited funds for structural strengthening of buildings, or other risk reduction measures such as emergency planning. In calculating the risk of each facility in the portfolio, potential life safety and economic losses due not only to structural damage, but also to equipment, contents and business interruption are considered. Public agencies (local, state governments and federal agencies) similarly analyze their portfolios. For lifelines such as water, road and highway, electric power, etc. systems, the interconnectedness of the network is considered. Lastly, insurance companies routinely employ estimates of seismic risk in their operations, to determine appropriate insurance rates, to monitor over-accumulation of policies in a small area, and to purchase reinsurance.

To estimate seismic risk, computer programs take all the seismic hazard inputs, and combine them with the known susceptibilities of structures and facilities, such as buildings, bridges, electrical power switching stations, etc. The result gives probabilities for economic damage or casualties. While the results can be used as a general measure of seismic risk for types of buildings, the actual seismic risk for any individual building may vary considerably and will depend upon its exact configuration and condition. Acquiring and analyzing the specific data for an individual building or facility is one of the most expensive and daunting aspects of seismic risk estimation

Seismic risk can be reduced by active programs that improve emergency response, and improve basic infrastructure. Building codes are intended to help to manage seismic risk and are constantly being updated as more is learned about the effects of seismic ground motion on buildings. However, the changes generally do not immediately improve seismic risk in a community since existing buildings are rarely required to be upgraded to meet the revisions.

## 6.2. Examples of studies on seismic risk assessment

Usually, risk analyses are based on probabilistic studies or approaches by scenarios depending on the goal of the analyses themselves: probabilistic approaches are suitable to identify priorities of prevention intervention, while approaches by scenarios are suitable to civil protection planning.

Some methodological examples for the quantitative assessment of the seismic risk have been performed in the last years. The seismological approach to seismic risk assessment leads to an evaluation of the global effects, while the engineering approach leads to a evaluation of the most probable damage levels to some building classes. Generally both kinds of studies do not consider all the components of risk ( $HR$ ,  $HL$ ,  $V$ ,  $E$ ), because of the complexity of the problem but focus the attention only on a few, analysing the consequent influence on the risk assessment. Ambraseys and Jackson (1981) have found strict correlation between total damage, normalized per demographic density unity, and magnitude of the earthquakes which occurred during the last century in Greece and Turkey, and this correlation is even better considering different building types, although information on population and building types is not satisfactory. In this case  $HR$ ,  $V$ , and  $E$  are taken into account and, therefore, the study gives a general idea of risk. The concepts of damage state (level) and damage probability matrix were introduced by Whitman and Cornell (1976) and can be considered the basis for the engineering approach. The vulnerability of the different building types is given by the distribution function of the damage probability which is associated to the damage state (which is given, for example, by the ratio between the cost for repairing the damage at a building and the cost for rebuilding it). As application of these concepts, a social decision analysis of the earthquake safety problem has been performed by considering the unreinforced masonry buildings that were built in Los Angeles before 1933, that is prior to code requirements designed to withstand earthquakes (Sarin, 1983). By considering four risk classes for the buildings on the basis of their importance or their

occupant load, by postulating four scenarios of an earthquake in the Los Angeles Basin and their probabilities, by taking into account the consequences on four building types to which the existing buildings can be upgraded by restoration, it resulted that the upgrading to the best quality standards for essential buildings (schools, hospitals, fire stations, etc.) and to medium quality standards for residential buildings represents the best cost/benefit balance. The occupants of the remaining buildings should be aware of the hazard. In this case,  $V$ , and  $E$  are taken into account while  $H$  is not probabilistically computed but postulated by scenarios. A similar result was found in Italy, where it was pointed out that differences in seismic hazard determine large differences of the expected damage only in the high vulnerability buildings (Petrini, 1991). Also in Italy the seismic risk assessment from the engineering point of view has been performed, as well as studies of variation of risk after reinforcement interventions to existing buildings. A risk assessment based on the damage probability matrix definition has been performed for the buildings of the historical centre of Gubbio in central Italy (Benzoni and Parisi, 1986) by using the information of the damage caused by a 5.5 magnitude earthquake which occurred in spring 1984. The damage annual probability distribution for five damage classes and its variation because of three different reinforcement interventions are the results of the study. It is worth noting that the economic amount of the preserved damage within 51-82 years will overcome the cost of the reinforcement intervention according to the different strategies taken, and, in any case, the softest reinforcement intervention reduces drastically the annual probability of severe damage, when even human lives are lost. This study was continued during the following years with more analysis on the damage and considering the Friuli region in north-eastern Italy too (Benedetti et al., 1988). In the case of the two previous studies only  $V$  is adequately considered as risk descriptor.

Some quantitative risk assessment have been performed for the Friuli - Venezia Giulia region (NE Italy) solving Eq. (6-3). Only some factors of risk have been considered because it is hard to quantify some parameters, as the vulnerability of the social and productive structures; therefore, the modelled and assessed risk is only a specific risk. A first example, more devoted to the methodology than to the actual calculation, refers to the Pordenone province in Friuli, NE Italy (Slejko et al., 1988). In that study only statistical data published by the Regional Administration (demographic census and requests for financial support for restoration or rebuilding of buildings hit by the 1976 Gemona earthquake) have been considered and the risk model has been defined by solving Eq. (6-3) with  $R$  taking the meaning of number of requests for financial support. The present risk for the Pordenone province has been subsequently calculated by considering the expected ground shaking not exceeded at 63% probability in 200 years and the present values of  $V$  and  $A$ , defined according to the proposed model (Fig. 6.4).

A more rigorous application again for the Friuli - Venezia Giulia region (NE Italy) has been performed by mean of the definition of the damage probability matrix for the rooms in the study region (Yang et al., 1989). Rooms instead of houses were used because of their greater size homogeneity. The data for the definition of the damage probability matrix were taken from the damage reports after the 1976 Gemona earthquake. The so defined model has been applied as to forecast the maximum expected damage at 37% probability in 100 years for the whole Friuli - Venezia Giulia region (Fig. 6.5). Also in this case, as in the previous one, the vulnerability of the buildings has been defined according to their age and their behaviour during the 1976 earthquake, without, therefore, an actual analysis of their structural characteristics. In both cases, then, the results indicate only a possible way for assessing quantitatively the seismic risk and  $H$ ,  $V$ , and  $R$  are considered with only a slight consideration of  $E$ .

The most interesting study on this subject remains the evaluation of the seismic risk of the town of Ancona (Stucchi, 1988). Its very peculiar characteristic is the goal of the study: it is directly devoted to support the drawing up and up-dating of the town plan, taking into account the seismological information and some geotechnical tests for a kind of microzoning, and the vulnerability and the exposition of the buildings for evaluating the expected damage. At the end, suggestions to reduce the seismic risk to buildings and lifelines are given.

A study by Codermatz et al. (2003) illustrates the seismic risk preliminary estimates of two different groups of structures located on the territory of the Friuli - Venezia Giulia region (NE Italy): the first group includes some special industrial plants, and the second, bridges and tunnels belonging to the regional highway network. The part of the study on special industrial plants tries to evaluate the

degree of expected damage, taking into account their structural typology and ground shaking expressed in terms of macroseismic intensity. The second part of the study is an application of the HAZUS methodology to the tunnels and bridges of a highway network: the combination of expected ground shaking and the construction characteristics (Fig. 6.6) lead to very different risk levels, especially when considering the bridges (Fig. 6.7). The resulting damage levels to bridges and tunnels are still only indicative, because of the fragility curves used in the evaluations: they were developed for existing bridge and tunnel structural typologies in the U.S.A. Moreover, both examples show the power of GIS technology in storing, elaborating, and mapping spatial data.

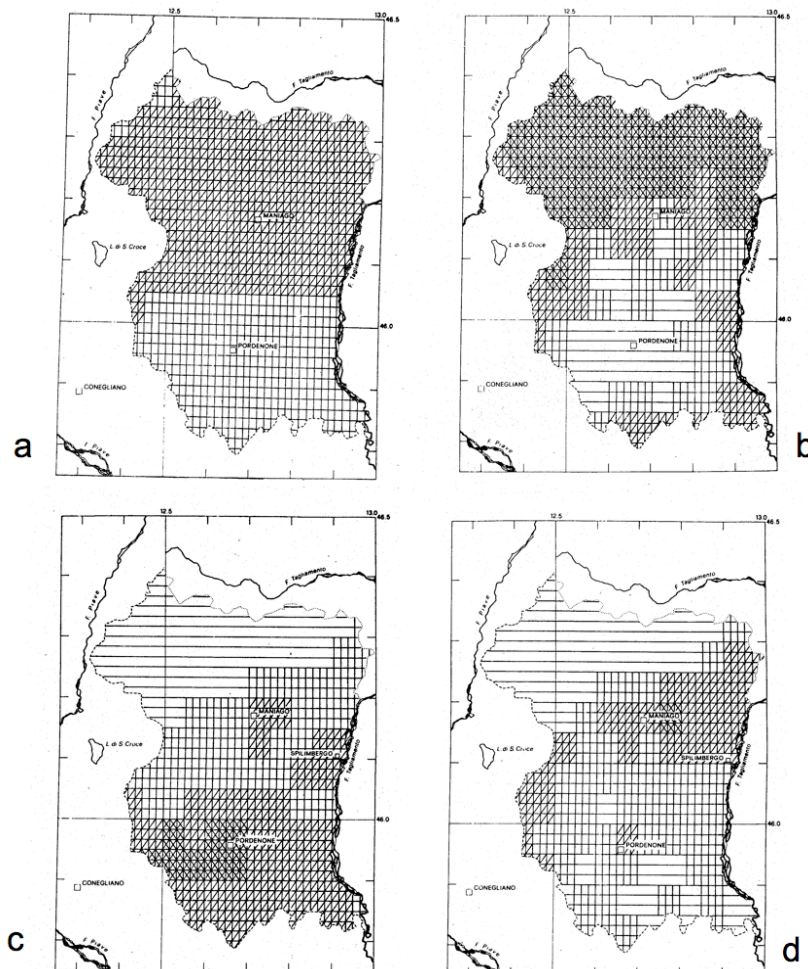


Fig. 6.4 – Seismic risk of the Pordenone province (Friuli – Venezia Giulia region in NE Italy): a) macroseismic intensity with 63% non-exceedance probability in 200 years (light dashing = VII <math>< I \leq VIII</math> MCS, dark dashing = VIII <math>< I \leq IX</math> MCS); b) vulnerability represented by the ratio between the demographic density in 1961 and 1981; c) exposed value, represented by the inhabitant number in 1981; d) seismic risk, represented by the number of requests for financial support for reconstruction after earthquakes expected with a 63% non-exceedance probability in 200 years (from Slejko et al., 1988).

A study by Di Pasquale et al. (2005) illustrates some improvements in the seismic risk assessments in Italy and describes the differences deriving from the use of different approaches to calculate the losses and the influence exerted by different hazard results. The first method of risk evaluation, termed as ‘direct’, evaluates the losses by using only the mean values of the main variables involved (rate of events and frequency of the damage levels), thus providing an approximation of the expected losses. The second method, named ‘probabilistic’, takes into account the uncertainties related to the number of events (hazard) and the damage levels (vulnerability), thus determines the probability associated to each level of loss (Fig. 6.8). Both methods express the risk as the economic losses to dwellings within a reference period of time. Two alternative hazard results are also used to show the influence on the calculated risk: the first one considering the seismicity uniformly distributed within seismic source zones; the second one clustering the strong seismicity in

geographically narrowed source zones and scattering the low seismicity over large source zones. The results obtained show that the losses estimated by the direct method are, at national level, a little bit lower than those obtained with the probabilistic method (about 6%). The differences are more pronounced at local level, generally within  $\pm 20\%$  with larger values in the zones of lower risk. Nevertheless, also the two hazard results show more pronounced differences at local rather than at national scale. The risk estimates in the high seismicity areas are greater if using the seismic hazard results based on the clustered seismicity, but the reverse is true, in the low seismicity areas, if using the hazard results based on the uniformly distributed seismicity. As a concluding remark, the direct method for calculating losses and the implementation of any seismic hazard result, may be acceptable for a general picture of the risk; whereas, when a detailed description of the territorial distribution of risk is needed, the probabilistic method for computing losses and a well-focused seismic hazard method should be used, as they are more pertinent to describe and highlight local differences.

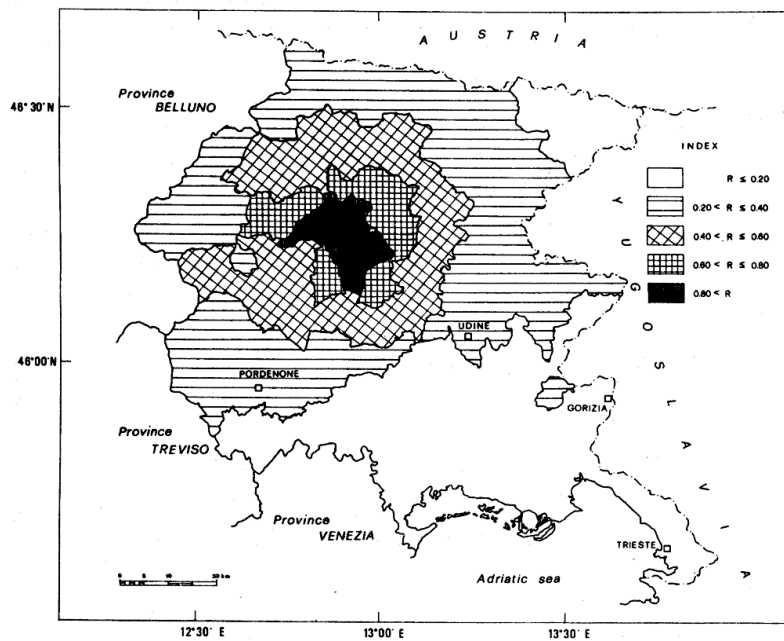


Fig. 6.5 - Map of the seismic risk in 100 years. The concentric distribution of  $R$  is easily observed in the central area of the region (from Yang et al., 1989).

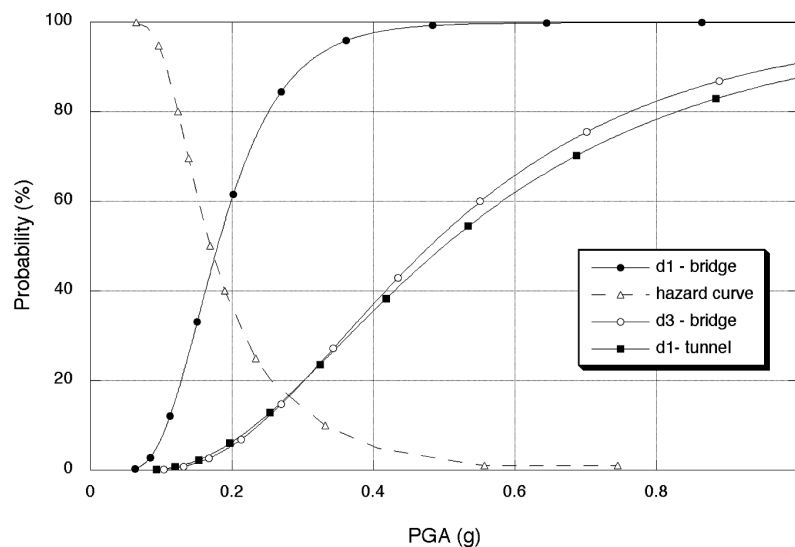


Fig. 6.6 - Fragility curves (non-exceedance probability) for a bridge of a specific vulnerability class according to two damage states; fragility curve for a tunnel according to one damage state; hazard curve, in terms of a 50-year exceedance probability, for one of the bridges considered in the study (from Codermatz et al., 2003).

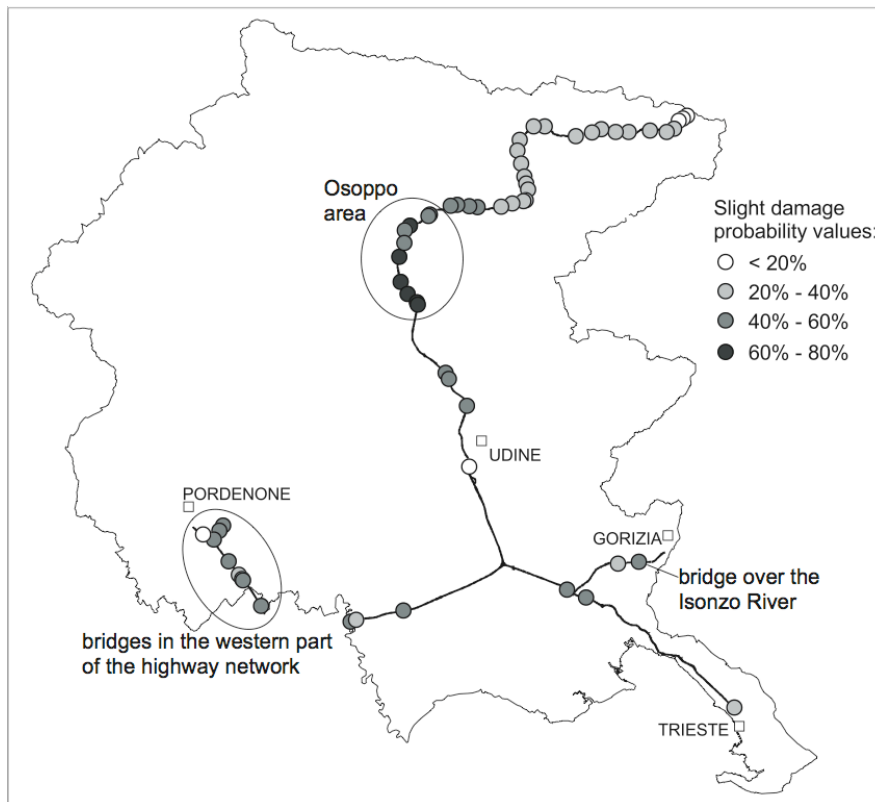


Fig. 6.7 - A 50-year probability of observing a slight damage for the bridges of the regional highway network (from Codermatz et al., 2003).

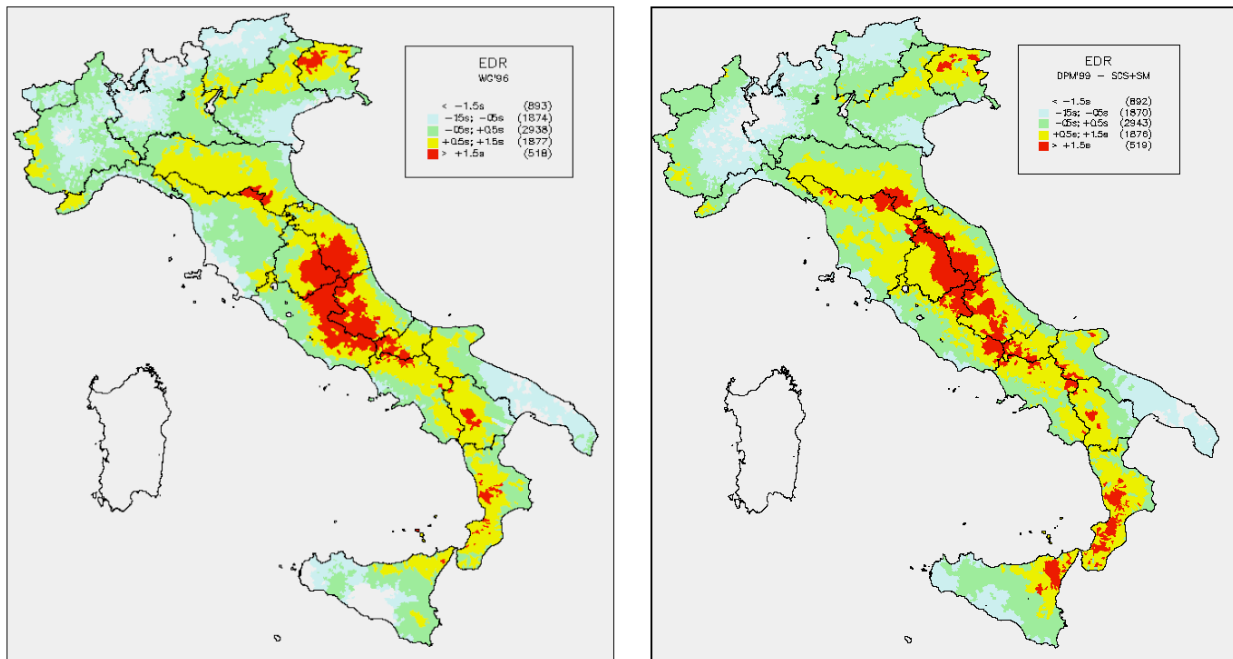


Fig. 6.8 - Economic normalized losses having a 10% chance of being exceeded within 50 years, computed with the full probabilistic approach. The map shows the effect exerted by the two seismic hazard results considered in the study (from Di Pasquale et al., 2005).

A few examples of a study of seismic risk sponsored by a public administration are available, at least in Italy. They refer to the Toscana, Emilia -Romagna and Friuli - Venezia Giulia regions. Furthermore, a detailed description of the analyses concerning the risk assessment and the methodologies suitable to develop such a study are summarized in C.N.R. - Gruppo Nazionale per la Difesa dai Terremoti (1993).

The study developed for the Emilia - Romagna region (C.N.R. - Gruppo Nazionale per la Difesa



dai Terremoti and Regione Emilia – Romagna, 1993) considers only the public buildings and is based on a detailed inventory of the vulnerability of the analysed buildings. The study developed for the Toscana region (C.N.R. – Istituto di Ricerca sul Rischio Sismico and Regione Toscana, 1995) considers all kinds of buildings and is based on the census information. In both studies an evaluation of the expected damage is given together with an estimate of the related costs.

In the study performed for the Friuli – Venezia Giulia region (NE Italy), a soil hazard assessment has been coupled with the information taken from the census data. More precisely, the vulnerability and exposed value of the civil buildings have been estimated (Fig. 6.9). The detailed scale of the operation (all parameters have been linked to the census sections, a detailed administrative subdivision of the territory) has produced results which are suitable for an application at the municipality level (Fig. 6.10)

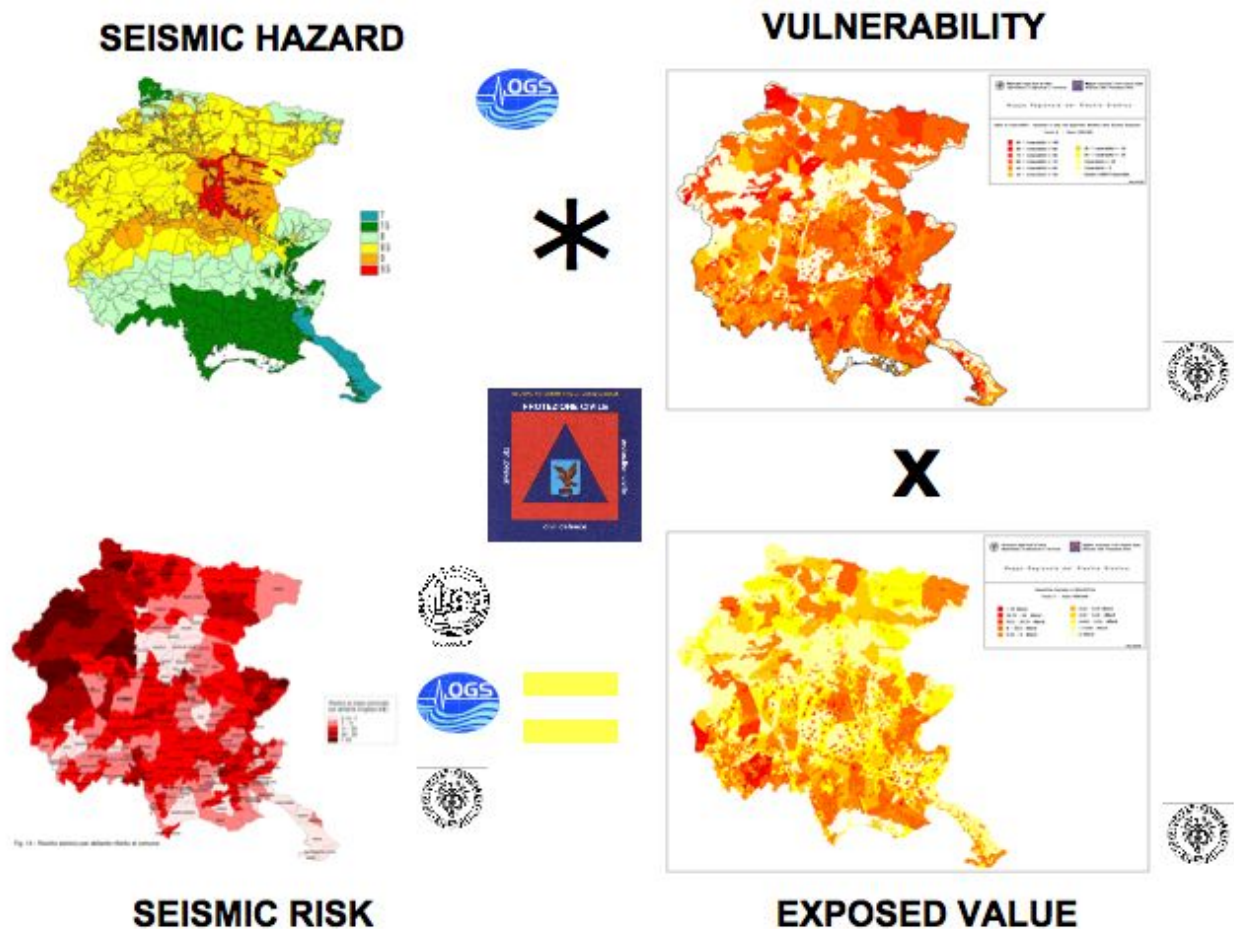


Fig. 6.9 – Scheme of the seismic risk map of the Friuli – Venezia Giulia region.

The main objective of the RISMUR Project (Benito et al., 2006) was to provide a general seismic risk assessment of the Murcia region, in Spain, associated with expected ground motions for a return period of 475 years. In the first phase of the project, seismic hazard at generic rock site was calculated for a grid covering the entire region. Results are represented in maps of PGA and spectral acceleration (SA) of periods 0.1, 0.2, 0.5, 1 and 2 s, for the prescribed return period of 475 years. A geotechnical characterization of the region, mainly inferred from geological maps and refined with on-site observations at specific locations, is the basis for a soil classification that represents ground response to seismic shaking. Subsequently, amplification factors for each soil class were derived. These amplification factors are integrated with rock acceleration estimates in order to compose hazard maps that incorporate local soil effects. The highest hazard for a return period of 475 years results in the lower Segura River basin, where some of the most populated cities of the region are located (including Murcia city). Other areas with high hazard include the zone of La Manga del Mar Menor. In parallel, a vulnerability assessment of the Murcian building stock that distinguishes between rural and urban environments was carried out, based fundamentally on the age of construction. In the definition of the

vulnerability classes and damage degrees, the EMS-98 criteria were followed. The towns presenting large overall vulnerability are mainly located in rural areas. It is remarkable that the Murcian building stock predominately presents medium-to-high overall vulnerability. Taking into account the expected ground motions and building vulnerabilities, the distribution of expected damage was estimated by application of probability damage matrixes derived from the 1980 Irpinia earthquake. Several damage indexes are defined, and relative and total damage estimates at each location were derived. With these data, a suite of maps representing seismic risk in terms of damage parameters for the entire Murcia region were traced. These maps allow the identification of sites with large potential risk, where specific studies of damage scenarios, associated to earthquakes presenting large hazard contribution, should be carried out.

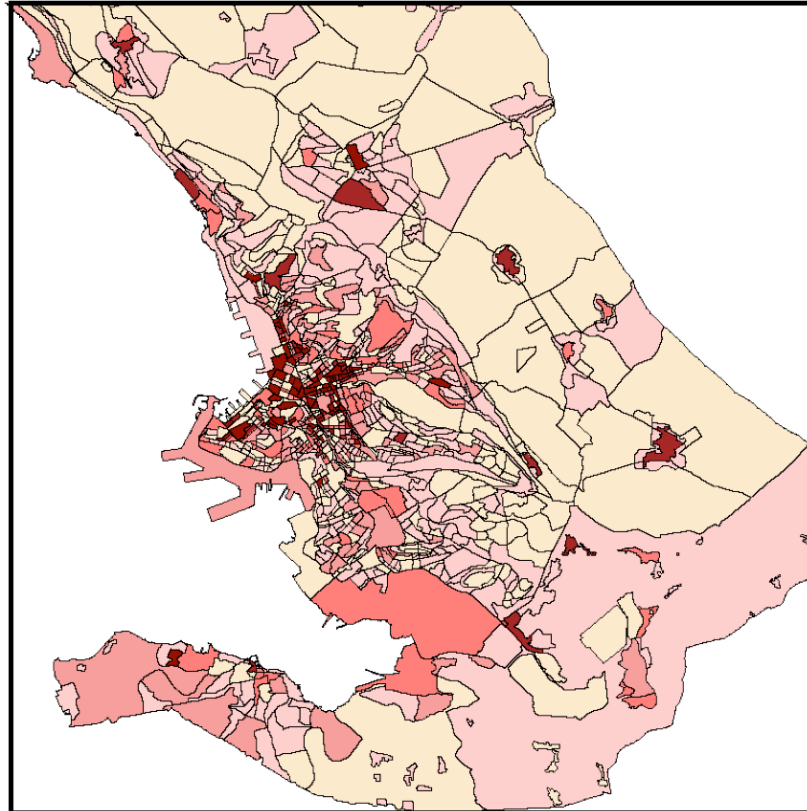


Fig. 6.10 – Blow-up of the seismic risk map of the Friuli – Venezia Giulia region for Trieste.

More frequently, risk, or better the expected damage because of earthquakes, has been evaluated by means of risk scenarios, where generally only the most hazardous event is considered. Among the many studies which have been developed, it is worth citing the project “RISK-UE” (Mouroux and Le Brun; 2011), financed by the EU. This project developed a general and modular methodology for creating earthquake-risk scenarios that concentrates on the distinctive features of European towns, including both current and historical buildings. It was based on seismic-hazard assessment, a systematic inventory and typology of the elements at risk and an analysis of their relative value and vulnerability, in order to identify the weak points of urban systems. The resulting scenarios give concrete figures of direct and indirect damage of possible earthquakes. With the participation of urban council representatives, the methodology was applied to seven selected cities map from the EU and eastern Europe (Fig. 6.11) for its adaptation and validation.

Such kind of studies are performed also by the insurance companies, that must forecast the possible economic impact of future earthquakes. Socio-economic analyses of the expected losses during the next future have pointed out that the highest risk is concentrated in the fastest growing cities, especially in the developing countries.





Fig. 6.11 – Selected cities of the “Risk EU” project.

The seismic risk reduction of strategic and relevant facilities is one of the most delicate problems that administrators are being asked to deal with. In fact, in a seismic area, a major concern of the public administrators is to ensure the safety of people in the case of earthquake, especially in public buildings and, in particular, in school buildings. This problem was addressed in the ASSESS project (AnalySis of SEismic Scenarios of School buildings for a definition of intervention priorities for the seismic risk reduction), aimed at knowing, as a preventive measure, the level of seismic risk of school buildings in the Friuli Venezia Giulia region. The ASSESS project was a prototypal study, developed on sound technical and scientific bases, useful to define decisional tools for preventive purposes. In particular, the ASSESS methodology identified the possible actions for improving the seismic safety, it made an economic evaluation of these actions and, moreover, defined, through specific indicators, the intervention priorities to reduce seismic risk of school buildings throughout the studied area. The project led to the development of specific and innovative decision supports aimed at facilitating public administrators in the development and management of strategies for seismic risk mitigation of schools. The estimation of seismic risk of the regional school heritage (Grimaz et al., 2016) was performed in the 2008-2011 period and was funded by the Civil Protection of Friuli - Venezia Giulia. The study followed an interdisciplinary and holistic approach organized on three levels of analysis (Fig. 6.12): the basic level (desk approach), where the seismic hazard of the site and the building were studied using data from the literature (census); the first level (screening approach), where the seismic hazard was calculated on the basis of all the latest regional information, also supported by in situ measurements, while the building vulnerability was rated by visual surveys; and the second level (advanced approach), in which material testing and detailed modelling described the building behaviour under the seismic action. The basic level was applied to all 1022 regional school buildings, the first level to 10% of the buildings and the second level of 1% of the same. The comparison among the results obtained by the three levels of analysis showed that the results obtained in the first level, summarized by 3 risk indicators can be considered satisfactory to characterize the actions necessary to secure school buildings on the basis of to current national seismic standards. Moreover, to facilitate the communication with administrators, it was decided to use simple and known symbols making the recognition of the situations and the identification of intervention priorities simple and similar to other sectors (Fig. 6.13).

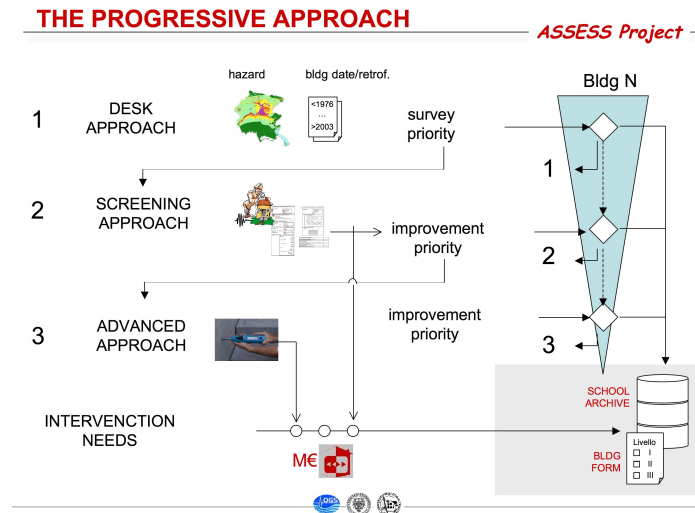


Fig. 6.12 – The structure of the ASSESS project.

SCHOOL ID	SCHOOL TYPOLOGY	STRUCTURAL PERFORMANCE CLASS	INTERVENTION REQUIREMENT ROSE	ASSESS SAFETY STARS	Costs (K€)
GO 000 XXX	Preschool	A	Low	★★★★★	0
GO 000 XXX	Preschool	A	Low	★★★☆☆	Technical verification
GO 000 XXX	Primary school	B	Low-Medium	★★☆☆☆	47÷63
GO 000 XXX	Secondary school	D	Medium-High	★★☆☆☆	1.380÷1.870
GO 000 XXX	High school	E	High	★☆☆☆☆	2.300÷3.150
PN 000 XXX	Primary school	D	Medium-High	★★☆☆☆	920÷1.250

Fig. 6.13 –ASSESS indicators of performance and requested interventions.

### 6.3. Global urbanization and increased seismic risk

According to Bilham (1998), by the year 2025 more than 5500 million people will live in cities, more than the entire 1990 combined rural and urban population. The growth of these giant urban agglomerations is a new experiment for life on Earth. Tragically, a significant fraction of the largest of these agglomerations (supercities and megacities) are located close to regions of known seismic hazard. With few exceptions (Tokyo 1923, Tangshan 1976), recent large earthquakes ( $M > 7.5$ ) have

spared the world's major urban centres, but this will not persist indefinitely. In the next millennium several megacities will be damaged by significant earthquakes. We are most certain of the fate of those cities near plate boundaries, however, mid-continent earthquakes also occur, albeit infrequently (e.g.,  $M > 8$  events in the eastern United States and India in the early 18<sup>th</sup> century), and these events will wreak great havoc in mid-continent cities where earthquake resistant construction is not mandated.

For the above reasons it is certain that the annual fatality rate from earthquakes will rise in the next 30 years, attributable partly to moderate earthquakes near large cities, but principally from a few catastrophic earthquakes near supercities (populations 2-28 million). Fig. 6.14 illustrates the predictable fatality rates from low mortality earthquakes, and the erratically growing death toll from high fatality earthquakes in the past 125 years.

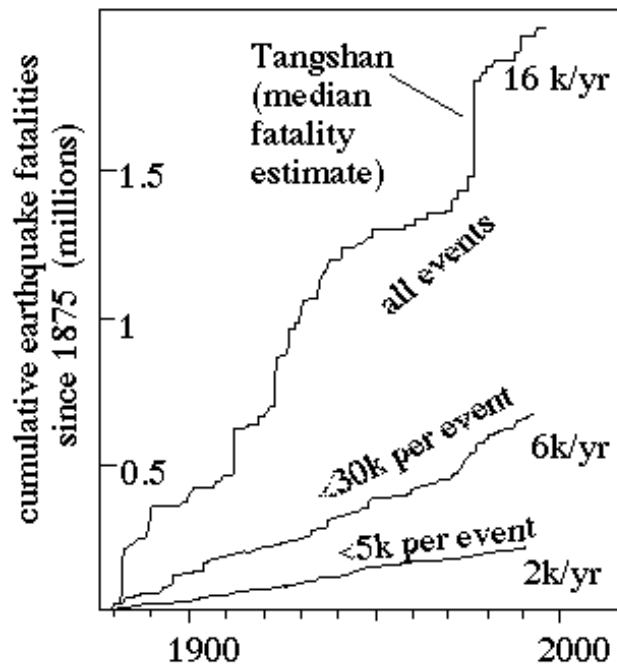


Fig. 6.14 – Comparison of the number of fatalities in high and low mortality earthquakes (from Bilham, 1998).

#### 6.4. Earthquake preparedness

Earthquake preparedness refers to a variety of measures designed to help individuals, businesses, and local and state governments in earthquake prone areas to prepare for significant earthquakes. Preparedness measures are part of the emergency management cycle.

Earthquake preparedness measures can be divided into:

- retrofitting and earthquake resistant designs of new buildings and lifeline structures (e.g., bridges, hospitals, power plants);
- response doctrines for state and local government emergency services;
- preparedness plans for individuals and businesses.

In the United States, buildings codes in earthquake prone states currently often have specific requirements designed to increase new buildings' resistance to earthquakes. Older buildings and homes that are not up to code may be retrofitted to increase their resistance. Such retrofitting is often required for older commercial and governmental buildings under state laws. Retrofitting and earthquake resistant design are also employed in elevated highways and bridges. Current building codes are not designed to make buildings earthquake proof in the sense of them suffering zero damage. The goal of most building designs is to reduce earthquake damage to a building such that it protects the lives of occupants and thus tolerance of some limited damage is accepted and considered a necessary tradeoff. Earthquake retrofitting techniques and modern building codes are designed to

prevent total destruction of buildings for earthquakes of magnitude not greater than 8.5.

Homeowners, renters, and businesses in earthquake territory are encouraged by governments to have an earthquake kit available with enough supplies for three days. From experience, this is considered the amount of time it takes for emergency services to reach full strength. Such emergency kits are also useful in other natural hazards. State and federal governments publish earthquake preparedness booklets.

Furthermore concerning risk, and associated preparedness, it must be mentioned the HAZUS software program for estimating potential losses from disasters, which was developed by the Federal Emergency Management Agency (FEMA) under contract with the National Institute of Building Sciences (NIBS). HAZUS is a powerful risk assessment software program for analyzing potential losses from floods, hurricane winds, and earthquakes. In HAZUS, current scientific and engineering knowledge is coupled with the latest GIS technology to produce estimates of hazard related damage before, or after, a disaster occurs. HAZUS estimates include:

- physical damage to residential and commercial buildings, schools, critical facilities, and infrastructure;
- economic loss, including lost jobs, business interruptions, repair and reconstruction costs; and
- social impacts, including estimates of shelter requirements, displaced households, and population exposed to scenario floods, earthquakes and hurricanes.

HAZUS uses state-of-the-art geographic information system software to map and display hazard data and the results of damage and economic loss estimates for buildings and infrastructure. It also allows users to estimate the impacts of earthquakes, floods, and hurricane winds on populations.

Estimating losses is essential to decision-making at all levels of government, providing a basis for developing mitigation plans and policies, emergency preparedness, and response and recovery planning.





## 7. BUILDING CODES

Most earthquake-related deaths are caused by the collapse of structures and the construction practices play a tremendous role in the death toll of an earthquake. In southern Italy in 1909 more than 100,000 people perished in an earthquake that struck the region. Almost half of the people living in the region of Messina were killed due to the easily collapsible structures that dominated the villages of the region. A larger earthquake that struck San Francisco three years earlier had killed fewer people (about 700) because of the different building construction practices (predominantly wood). Survival rates in the San Francisco earthquake was about 98%, that in the Messina earthquake was between 33% and 45%. Building practices can make all the difference in earthquakes, even a moderate earthquake close to a city with structures unprepared for shaking can produce tens of thousands of casualties.

Although probably the most important, direct shaking effects are not the only hazard associated with earthquakes, other effects such as landslides, liquefaction, fires, and tsunamis have also played important part in destruction produced by earthquakes.

The level of damage done to a structure depends on the amplitude and the duration of shaking. Both amplitudes and duration of the shaking generally increase with the magnitude of the earthquake (larger quakes shake longer because they rupture larger areas). Regional geology can affect the level and duration of shaking but more important are local site conditions. Although the process can be complicated for strong shaking: generally, shaking in soft sediments is larger and longer than that at a "hard rock" site.

The first step in preparing structures for shaking is to understand how buildings respond to ground motions: this is the field of study for earthquake and structural engineers. When the ground shakes, buildings respond to the accelerations transmitted from the ground through the structure's foundation. The inertia of the building (it wants to stay at rest) can cause shearing of the structure which can concentrate stresses on the weak walls or joints in the structure resulting in failure or perhaps total collapse. The type of shaking and the frequency of shaking depends on the structure. Tall buildings tend to amplify the longer period motions when compared with small buildings. Each structure has a resonance frequency that is characteristic of the building. Predicting the precise behaviour of buildings is complicated, a rule of thumb is that the period of resonance is about equal to 0.1 times the number of stories in the structure.

Taller buildings also tend to shake longer than short buildings, which can make them relatively more susceptible to damage. Fortunately many tall buildings are constructed to withstand strong winds and some precautions have been taken to reduce their tendency to shake. And they can be made resistant to earthquake vibrations.

In many regions of limited resources and/or old structures, the structures are not very well suited to earthquake induced strains and collapse of adobe-style construction has caused thousands of deaths in the last decade. The worst possible structure for earthquake regions is the unreinforced masonry although bad surprises have been registered sometimes also for reinforced concrete buildings.

Preparing structures (either new or old) for earthquakes is expensive and the level of investment is a social and political decision. The choice of building design is a compromise between appearance, function, structure, strength, and of course, cost. Standards are instituted through the establishment of building codes, which regulate the design and construction of buildings. Most of our building codes are designed to protect first the building occupants, and second the building integrity. Building codes are usually drafted to meet the demands of the expected shaking in a given region that are summarized by seismologists and earthquake engineers in hazards maps.

We have two approaches for preparing buildings for earthquakes: you either secure the building components (walls, floors, foundation, etc.) together and have the entire structure behave as a single stiff unit that moves with the ground, or you construct a strong and flexible structure that distorts but does not break and absorbs some of the shaking energy. Either approach can be expensive so we cannot build all our structures to withstand the largest possible earthquake. We must make compromises and accept some risk.

We need different levels of resistance for different classes of structures. Critical structures such as hospitals, power, water-treatment, and chemical plants, dams, etc. must not only survive the

shaking, but must remain in operation. These structures require the largest investment of resources to insure that they can provide services following an earthquake.

More general requirements for ordinary buildings are:

- . sustain little damage in small-to-moderate quakes ( $M < 5.5$ );
- . sustain some repairable damage for moderate quakes ( $5.5 < M < 7.0$ );
- . not collapse in large earthquakes ( $M > 7.0$ ).

To insure that we meet these goals we can take a number of steps, beginning with thoughtful and responsible planning and zoning laws. Since we know that sites with soft, water-saturated foundations are prone to damage, we should resist the temptation to build on those sites and we should certainly not put critical structures on such sites, and avoid building on these sites at all if possible. If that is not possible, try to compact the soft sediments before the constructing or anchor the structure in the basement.

We can take a number of steps to strengthen buildings including using steel frame construction, adequately securing the structure to the ground through a solid foundation, incorporating shear walls and/or cross-bracing into the structure, or more sophisticated approaches such as using rubber or steel pads to isolate the structure from the shaking.

A building code is a set of rules that specify the minimum acceptable level of safety for constructed objects such as buildings and non-building structures except major lifelines and safety-critical installations such as nuclear power plants, both of which are usually governed by specific codes. The main purpose of the building codes is to protect public health, safety and general welfare as they relate to the construction and occupancy of buildings and structures. The building code becomes law of a particular jurisdiction when formally enacted by the appropriate authority.

In building codes, the shaking-hazard maps are converted into seismic zone maps, which are used for seismic analysis of structural components of buildings. The seismic zone maps depict seismic hazards as zones of different risk levels. Such zones are typically designated as Seismic Zone 0, Seismic Zone 1, Seismic Zone 2 and so on. The seismic zone maps usually show the severity of expected earthquake shaking for a particular level of probability, such as the levels of shaking that have a 10% chance of being exceeded in a 50-year period. Buildings and other structures must be designed with adequate strength to withstand the effects of probable seismic ground motions within the seismic zone where the building or structure is being constructed.

According to Bommer (2004), the information presented in the code must be relatively simple since the majority of applications of the code will be performed by engineers without special training in earthquake engineering. The basic information that the code needs to provide is:

- the earthquake actions to be considered in design;
- the method of structural analysis to be applied and the way in which the seismic actions are to be applied to the structure;
- the performance criteria, in terms of stresses and displacements, which the structure must meet when subjected to the earthquake actions.

The method of structural analysis employed in all seismic design codes is the equivalent lateral force method, in which the earthquake action is modelled as a horizontal force acting at the base of the structure. This is a simplified case of a more general approach, which is spectral modal analysis, considering only the fundamental mode of the structure's response. For both of these methods, the earthquake actions are represented in the form of a response spectrum.

Some codes do require dynamic analysis to be performed for certain structures, such as those above a certain height or having a large degree of irregularity in their architectural configuration. The designer is usually given the option of using either spectral modal analysis or time-history analysis, although a few codes do make full dynamic analysis compulsory in certain cases, including the codes of China, Costa Rica, France, Iran, FYR Macedonia, New Zealand and Portugal (Bommer, 2004). However, the guidance provided in codes on the input to time-history analysis, in terms of sources of data, selection or generation of records, scaling and the number of records to be used, is generally very poor and in many cases practically non-existent.

The practice of developing, approving, and enforcing building codes may vary widely from country to country.

In some countries building codes are developed by the government agencies or quasi-governmental standards organizations and then enforced across the country by the central government. Such codes are known as the national building codes (in a sense they enjoy a mandatory nation-wide application).

In other countries, where the power of regulating construction and fire safety is vested in local authorities, a system of model building codes is used. A model building code is a building code that is developed and maintained by a standards organization independent of the jurisdiction responsible for enacting the building code. Model building codes have no legal status unless adopted or adapted by an authority having jurisdiction. The developers of model codes urge public authorities to reference model codes in their laws, ordinances, regulations, and administrative orders. When referenced in any of these legal instruments, a particular model code becomes law. This practice is known as “adoption by reference”. When an adopting authority decides to delete, add, or revise any portions of the model code being adopted, it is usually required by the model code developer to follow a formal adoption procedure in which those modifications can be documented for legal purposes.

The concept of the model building codes has successfully been applied since the early 1900s in the countries where regulation of building construction is a responsibility of the local authorities. The popularity of model building codes can be attributed to two factors: a) the developing of proprietary building codes is prohibitively expensive and b) the ability of the model codes to accommodate local conditions. Since modern building regulations are very complex, their development and effective maintenance are far beyond the technical and financial capabilities of most jurisdictions. Rather than drafting its own building codes, a local authority might choose to use the model building codes instead. The model building codes are either adopted (accepted without modifications) or adapted (modified) to a particular jurisdiction and then enforced by the adopting authority.

There are instances when some local jurisdictions choose to develop their own building codes. For example, at some point in time all major cities in the United States had their own building codes as part of their municipal codes. Since having its own building code can be very expensive for a municipality, many have decided to adopt model codes instead. Only the cities of New York and Chicago continue to use the building codes they developed on their own; yet these codes also include multiple references to model codes, such as the National Electrical Code.

Model building codes are developed by standards organizations through a network of development committees comprised of representatives from the various affected entities, both government and private. This method allows the pooling of financial and intellectual resources to produce codes that remain current and technically sound. The model code developers are constantly working to update their codes to incorporate latest research results and building technologies.

Normally, model building codes have a 3-5 year update cycle. That is, a new edition of the building code comes out every 3 to 5 years. However, due to the length of time that it takes for a jurisdiction to review and approve a new code, the currently enforced version of the local code is often not the most recent edition of the model building code on which the adopted code is based.

Also, when any given jurisdiction adopts a model building code, it adopts a specific edition of the model code (for example, the 1997 Uniform Building Code or the 2000 International Building Code), which then becomes the law of that jurisdiction. As a result of this practice, the adopted codes are not automatically updated. When a new edition of the model code is released by the model code developer, the adopting authority may choose to ignore it and continue using the older version of the model code it adopted. Otherwise, the jurisdiction must vote to update its code and bring its inspectors up to date on the changes being made to the code. Most jurisdictions update their codes regularly to avoid backlash from architects and building contractors, who respond to outdated codes by seeking variances to permit the use of more efficient design solutions and technologies accepted in areas using more modern codes.

All current seismic codes present the earthquake actions to be considered in design in terms of a response spectrum of absolute acceleration. Reduction factors are usually applied to the ordinates of the elastic spectrum to account for the dissipation of energy through inelastic deformations in the structure. These factors, such as the q-factors in Eurocode 8 and the R-factors in the Uniform Building Code, are defined as a function of the lateral load bearing system, the construction materials and the ductility characteristics of the structure (Bommer, 2004). These behaviour, ductility or reduction factors are defined independently of the nature of the expected ground shaking.

The application of the behaviour factor is the final stage before application of the earthquake actions to the structural model. The first stage in the process is to build up an elastic acceleration response spectrum, which is the basic representation of the seismic hazard. Most current seismic codes define the elastic spectrum in two parts.

Firstly, a seismic zonation maps is provided from which a zonation factor,  $Z$ , is read;  $Z$  is directly related to PGA. Then a spectral shape is defined according to the classification of the site in terms of the soil profile. The elastic spectrum is then obtained by anchoring the spectral shape to the zonation factor  $Z$ . This approach to constructing the elastic spectrum, adopted in most codes, has the drawback that the shape of the response spectrum does not change with the hazard level. In the latest version of Eurocode 8 there is an attempt to overcome this problem by using two spectral shapes, one for regions affected only by relatively low magnitude earthquakes, the other for areas with larger earthquakes. Other codes overcome the problem by mapping two ground-motion parameters, one related to PGA and the other to PGV, such as in the Canadian seismic code. A similar approach is adopted in the 1984 Colombian seismic code, which presents two seismic zonation maps, one for an acceleration-related parameter and another for a velocity-related parameter (Bommer, 2004).

## 7.1. The Eurocode 8

Eurocode is a set of pan-European model building codes developed by the European Committee for Standardization.

The Eurocode is organised in 57 parts, each part published as a separate European Standard. By 2002, ten Eurocodes have been developed and published:

- . EN 1990: (Eurocode 0) Basis of structural design
- . EN 1991: (Eurocode 1) Actions on structures
- . EN 1992: (Eurocode 2) Design of concrete structures
- . EN 1993: (Eurocode 3) Design of steel structures
- . EN 1994: (Eurocode 4) Design of composite steel and concrete structures
- . EN 1995: (Eurocode 5) Design of timber structures
- . EN 1996: (Eurocode 6) Design of masonry structures
- . EN 1997: (Eurocode 7) Geotechnical design
- . EN 1998: (Eurocode 8) Design of structures for earthquake resistance
- . EN 1999: (Eurocode 9) Design of aluminium structures

The Eurocodes form a common European set of structural design codes for civil engineering work. They will eventually replace the national codes published by national standard bodies after a period of co-existence. At the moment some Eurocodes are still in a trial phase. Additionally, each country may have a National Annex to the Eurocodes which will need referencing for a particular country.

The main features of the Eurocode 8 (CEN, 2002) are described in the following.

### 7.1.1. Fundamental requirements

Structures in seismic regions shall be designed and constructed in such a way, that the following requirements are met, each with an adequate degree of reliability:

- **No-collapse requirement.** The structure shall be designed and constructed to withstand the design seismic action defined in the next chapters without local or global collapse, thus retaining its structural integrity and a residual load bearing capacity after the seismic events. The design seismic action is expressed in terms of: a) the reference seismic action associated with a reference probability of exceedance,  $P_{NCR}$ , in 50 years or a reference return period,  $T_{NCR}$ , and b) the importance factor  $\gamma$  to take into account reliability differentiation.

Note 1: The values to be ascribed to  $P_{NCR}$  or to  $T_{NCR}$  for use in a country may be found in its National Annex. The recommended values are  $P_{NCR} = 10\%$  and  $T_{NCR} = 475$  years.

Note 2: The value of the probability of exceedance,  $P_R$ , in  $T_L$  years of a specific level of the seismic action is related to the mean return period,  $T_R$ , of this level of the seismic action as:  $T_R = T_L / \ln(1 - P_R)$ . So for given  $T_L$ , the seismic action may equivalently be specified either via its mean return period,  $T_R$ , or its probability of exceedance,  $P_R$ , in  $T_L$  years.

- **Damage limitation requirement.** The structure shall be designed and constructed to withstand a seismic action having a larger probability of occurrence than the design seismic action, without the occurrence of damage and the associated limitations of use, the costs of which would be disproportionately high in comparison with the costs of the structure itself. The seismic action to be taken into account for the "damage limitation requirement" has a probability of exceedance,  $P_{DLR}$  in 10 years and a return period,  $T_{DLR}$ . In the absence of more precise information, the reduction factor applied on the design seismic action may be used to obtain the seismic action for the verification of the "damage limitation requirement".

Note 3: The values to be ascribed to  $P_{DLR}$  or to  $T_{DLR}$  for use in a country may be found in its National Annex. The recommended values are  $P_{DLR} = 10\%$  and  $T_{DLR} = 95$  years,

Target reliabilities for the "no-collapse requirement" and for the "damage limitation requirement" are established by the National Authorities for different types of buildings or civil engineering works on the basis of the consequences of failure.

Reliability differentiation is implemented by classifying structures into different importance classes (Table 7.1). To each importance class an importance factor  $\gamma$ , is assigned. Wherever feasible this factor should be derived so as to correspond to a higher or lower value of the return period of the seismic event (with regard to the reference return period), as appropriate for the design of the specific category of structures. The values to be ascribed to  $\gamma_I$  for use in a country may be found in its National Annex. The values of  $\gamma_I$  may be different for the various seismic zones of the country, depending on the seismic hazard conditions and on public safety considerations. The recommended values of  $\gamma_I$  for importance classes I, III and IV are equal to 0,8, 1,2 and 1,4, respectively.

Table 7.1 – Importance classes.

Importance class	Buildings
I	Buildings of minor importance for public safety, e.g. agricultural buildings, etc.
II	Ordinary buildings, not belonging in the other categories.
III	Buildings whose seismic resistance is of importance in view of the consequences associated with a collapse, e.g. schools, assembly halls, cultural institutions etc.
IV	Buildings whose integrity during earthquakes is of vital importance for civil protection, e.g. hospitals, fire stations, power plants, etc.

The different levels of reliability are obtained by multiplying the reference seismic action or, when using linear analysis, the corresponding action effects by this importance factor.

Note: At most sites the annual rate of exceedance,  $H(a_{gR})$ , of the reference peak ground acceleration  $a_{gR}$  may be considered to vary with  $a_{gR}$  as:  $H(a_{gR}) \approx k_0 \cdot a_{gR}^{-k}$ , with the value of the exponent  $k$  depending on seismicity, but being generally in the order of 3. Then, if the seismic action is defined in terms of the reference peak ground acceleration  $a_{gR}$ , the value of the importance factor  $\gamma$ , multiplying the reference seismic action to achieve the same probability of exceedance in  $T_L$  years as in the  $T_{LR}$  years for which the reference seismic action is defined, may be computed as:  $\gamma \approx (T_{LR}/T_L)^{-1/k}$ . Alternatively, the value of the importance factor  $\gamma$ , that needs to



multiply the reference seismic action to achieve a probability of exceedance of the seismic action  $P_L$  in  $T_L$  years other than the reference probability of exceedance  $P_{LR}$  over the same  $T_L$  years, may be estimated as:  $\gamma \approx (P_L/P_{LR})^{-1/k}$ .

In order to satisfy the fundamental requirements described before the following limit states shall be checked:

Ultimate limit states: are those associated with collapse or with other forms of structural failure which may endanger the safety of people.

Damage limitation states: are those associated with damage occurrence, corresponding to states beyond which specified service requirements are no longer met.

In order to limit the uncertainties and to promote a good behaviour of structures under seismic actions more severe than the design one, a number of pertinent specific measures shall also be taken.

For well defined categories of structures in cases of low seismicity, the fundamental requirements may be satisfied through the application of rules simpler than those given in the relevant Parts of EN 1998.

In cases of very low seismicity, the provisions of EN 1998 need not be observed.

Specific rules are given for "simple masonry buildings". By complying with those rules, the fundamental requirements for such "simple masonry buildings" are deemed to be satisfied without analytical safety verifications.

### 7.1.2. Ground conditions

Appropriate investigations shall be carried out in order to identify the ground conditions according to the types given in the following.

The construction site and the nature of the supporting ground should normally be free from risks of ground rupture, slope instability and permanent settlements caused by liquefaction or densification in the event of an earthquake.

For buildings of low importance, ground investigations additional to those necessary for the design for non-seismic actions may be omitted. In this case and in the absence of more accurate information on soil conditions, the seismic action may be determined assuming ground conditions according to ground type B.

The influence of local ground conditions on the seismic action shall generally be accounted for by considering the five ground types A, B, C, D and E, described by the stratigraphic profiles and parameters given in Table 7.2.

The average shear wave velocity in the surficial 30 m,  $V_{S30}$ , is computed according to the following expression:

$$V_{S30} = \frac{30}{\sum_{i=1}^N \frac{h_i}{V_i}} \quad (7-1)$$

where  $h_i$  and  $V_i$  denote the thickness (in m) and shear-wave velocity (at shear strain level of  $10^{-6}$  or less) of the  $i$ -th formation or layer, in a total of  $N$ , existing in the top 30 m. The site will be classified according to the value of  $V_{S30}$  if this is available, otherwise the value of  $N_{SPT}$  will be used.

For sites with ground conditions matching the two special ground types  $S_1$  and  $S_2$ , special studies for the definition of the seismic action are required. For these types, and particularly for  $S_2$ , the possibility of soil failure under the seismic action shall be considered.

Further sub-division of this classification is permitted to better conform with special ground conditions. The seismic actions defined for any sub-type should not be less than those corresponding to the main type as specified in Table 7.2, unless this is supported by special site-classification studies.

Table 7.2 - Ground types.

Ground type	Description of stratigraphic profile	Parameters		
		$V_{30}$ (m/s)	$N_{SPT}$ (blows/30 cm)	$c_u$ (kPa)
A	Rock or other rock-like geological formation, including at most 5 m of weaker material at the surface	> 800		
B	Deposits of very dense sand, gravel, or very stiff clay, at least several tens of m in thickness, characterised by a gradual increase of mechanical properties with depth	360 - 800	>50	> 250
C	Deep deposits of dense or medium dense sand, gravel or stiff clay with thickness from several tens to many hundreds of m	180 - 360	15-50	70-250
D	Deposits of loose-to-medium cohesionless soil (with or without some soft cohesive layers), or of predominantly soft-to-firm cohesive soil	< 180	<15	< 70
E	A soil profile consisting of a surface alluvium layer with $V_{30}$ values of type C or D and thickness varying between about 5 m and 20 m, underlain by stiffer material with $V_{30} > 800$ m/s			
S1	Deposits consisting - or containing a layer at least 10 m thick - of soft clays/silts with high plasticity index ( $PI > 40$ ) and high water content	< 100 indicative		10-20
S2	Deposits of liquefiable soils, of sensitive clays, or any other soil profile not included in types A -E or S,			

### 7.1.3. Seismic zones

National territories shall be subdivided by the national authorities into seismic zones, depending on the local hazard. By definition, the hazard within each zone is assumed to be constant.

The hazard is described in terms of a single parameter, i.e., the value of the reference ground acceleration on type A ground,  $k \cdot a_{gR}$ , where  $a_{gR}$  is the reference peak ground acceleration on type A ground and  $k$  a modification factor to account for special regional situations. The value to be ascribed to  $k$  for use in a country may be found in its National Annex. The recommended value is  $k=1$ . The reference peak ground acceleration on type A ground,  $a_{gR}$ , or the reference ground acceleration on type A ground,  $k \cdot a_{gR}$ , may be derived from zonation maps in the National Annex.

The reference peak ground acceleration, chosen by the National Authorities for each seismic zone, corresponds to the reference return period  $T_{NCR}$  of the seismic action for the no-collapse requirement (or equivalently the reference probability of exceedance in 50 years,  $P_{NCR}$ ) chosen by National Authorities. To this reference return period an importance factor  $\gamma$  equal to 1.0 is assigned. For return periods other than the reference, the design ground acceleration on type A ground  $a_g$  is equal to  $a_{gR}$  times the importance factor  $\gamma$  and the modification factor  $k$  ( $a_g = \gamma \cdot k \cdot a_{gR}$ ).

In cases of low seismicity, reduced or simplified seismic design procedures for certain types or categories of structures may be used. The selection of the categories of structures, ground types and seismic zones in a country for which the provisions of low seismicity apply may be found in its National Annex. It is recommended to consider as low seismicity cases those in which the product  $a_g \cdot S$  is not greater than 0.1 g.

In cases of very low seismicity, the provisions need not be observed. The selection of the categories of structures, ground types and seismic zones in a country for which the present provisions need not be observed (cases of very low seismicity) may be found in its National Annex. It is recommended to consider as very low seismicity cases those in which the product  $a_g \cdot S$  is not greater than 0.05 g.

#### 7.1.4. Seismic action

The earthquake motion at a given point of the surface is represented by an elastic ground acceleration response spectrum, henceforth called "elastic response spectrum". The shape of the elastic response spectrum is taken the same for the two levels of seismic action introduced in the previous chapters for the no-collapse requirement (ultimate limit state - design seismic action) and for the damage limitation requirement.

The horizontal seismic action is described by two orthogonal components considered as independent and represented by the same response spectrum.

For the three components of the seismic action one or more alternative shapes of response spectra may be adopted, depending on the seismic sources and the earthquake magnitudes generated from them. The selection of the shape of the elastic response spectrum to be used in a country or part thereof may be found in its National Annex. In selecting the appropriate shape of the spectrum, consideration should be given to the magnitude of earthquakes that contribute most to the seismic hazard defined for the purpose of probabilistic hazard assessment, rather than on conservative upper limits (e.g., Maximum Credible Earthquake) defined for that purpose.

When the earthquakes affecting a site are generated by widely differing sources, the possibility of using more than one shape of spectra should be contemplated to adequately represent the design seismic action. In such circumstances, different values of  $a_g$  will normally be required for each type of spectrum and earthquake.

For important structures ( $\gamma > 1.0$ ) topographic amplification effects should be taken into account.

Time-history representations of the earthquake motion may be used.

For the horizontal components of the seismic action, the elastic response spectrum  $S_e(T)$  is defined by the following expressions (see Fig. 7.1):

$$0 \leq T \leq T_B : S_e(T) = a_g \cdot S \cdot \left[ 1 + \frac{T}{T_B} (\eta \cdot 2.5 - 1) \right] \quad (7-2)$$

$$T_B \leq T \leq T_C : S_e(T) = a_g \cdot S \cdot \eta \cdot 2.5 \quad (7-3)$$

$$T_C \leq T \leq T_D : S_e(T) = a_g \cdot S \cdot \eta \cdot 2.5 \left( \frac{T_C}{T} \right) \quad (7-4)$$

$$T_D \leq T \leq 4s : S_e(T) = a_g \cdot S \cdot \eta \cdot 2.5 \left( \frac{T_C T_D}{T^2} \right) \quad (7-5)$$

where

$S_e(T)$  = elastic response spectrum,

$T$  = vibration period of a linear SDOF system,

$a_g$  = design ground acceleration on type A ground ( $a_g = \gamma \cdot k \cdot a_{gR}$ ),

$T_B, T_C$  limits of the constant spectral acceleration branch,

$T_D$  = value defining the beginning of the constant displacement response range of the spectrum,

$S$  = soil factor,

$\eta$  = damping correction factor with reference value  $\eta = 1$  for 5% viscous damping.

The values of the periods  $T_B, T_C$  and  $T_D$  and of the soil factor  $S$  describing the shape of the elastic response spectrum depend on ground type.

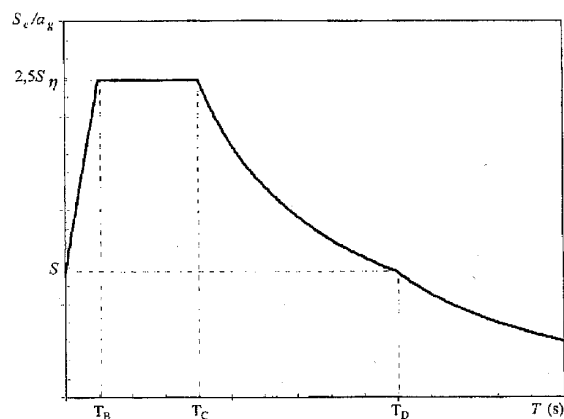


Fig. 7.1 - Shape of elastic response spectrum.

The values to be ascribed to  $T_B$ ,  $T_C$  and  $T_D$  and  $S$  for each ground type and type (shape) of spectrum to be used in a country may be found in its National Annex. The recommended choice is the use of two types of spectra: Type 1 and Type 2. If the earthquakes that contribute most to the seismic hazard defined for the site for the purpose of probabilistic hazard assessment has an  $M_S$  not greater than 5.5, it is recommended that the Type 2 spectrum is adopted. For the five ground types A, B, C, D and E the recommended values of the parameters  $S$ ,  $T_B$ ,  $T_C$  and  $T_D$  and are given in Table 7.3 for the Type 1 Spectrum and in Table 7.4 for the Type 2 Spectrum. Figs. 7.2 and 7.3 show the shapes of the recommended Type 1 and Type 2 spectra, respectively, for 5% damping and normalised by  $a_g$ .

Table 7.3 - Values of the parameters describing the recommended Type 1 elastic response spectrum.

Ground type	$S$	$T_B(s)$	$T_C(s)$	$T_D(s)$
A	1.0	0.15	0.4	2.0
B	1.2	0.15	0.5	2.0
C	1.15	0.20	0.6	2.0
D	1.35	0.20	0.8	2.0
E	1.4	0.15	0.5	2.0

A review of the provisions of the national building codes with respect to seismic hazard and zonation can be found in Solomos et al. (2008).

Table 7.4 - Values of the parameters describing the recommended Type 2 elastic response spectrum.

Ground type	$S$	$T_B(s)$	$T_C(s)$	$T_D(s)$
A	1.0	0.05	0.25	1.2
B	1.35	0.05	0.25	1.2
C	1.5	0.10	0.25	1.2
D	1.8	0.10	0.30	1.2
E	1.6	0.05	0.25	1.2

## 7.2. The U.S. building provisions

The primary purpose of seismic building codes is to provide a uniform method to determine the seismic forces for any location with enough accuracy to ensure a safe and economical design. Different regions of the United States have adopted different codes to deal with the differing levels of seismic risk. Some codes seek to protect life; others seek to protect life and property, by minimizing damage sustained during an earthquake. Seismic design provisions are based on the "Recommended Provisions for Seismic Regulations for New Buildings and Other Structures" (BSSC, 2004) prepared by the National Earthquake Hazards Reduction Program (NEHRP). Although not a code, the NEHRP Provisions are designed to assist in code development.

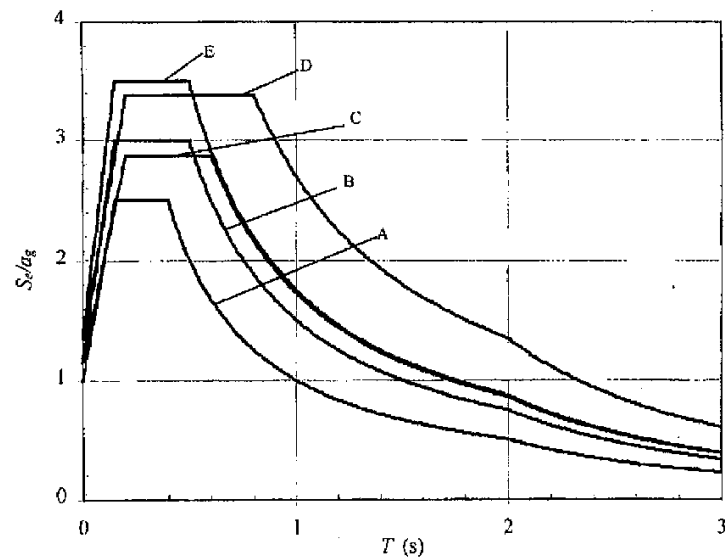


Fig. 7.2 - Recommended Type 1 elastic response spectrum for ground types A to E (5% damping).

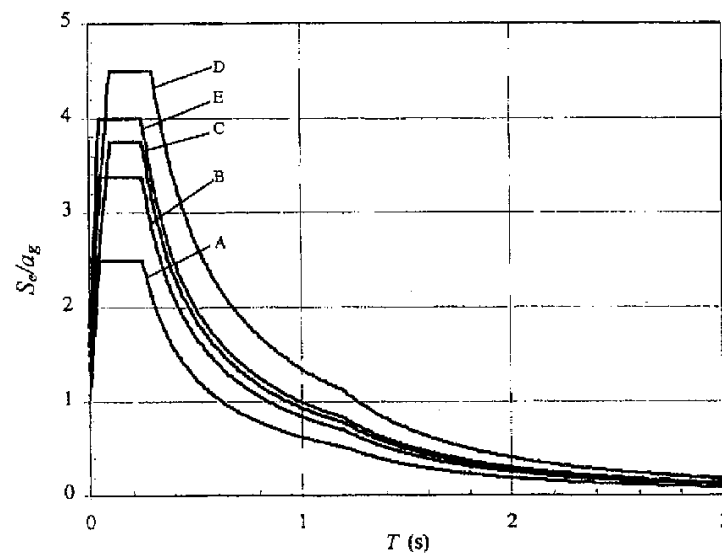


Fig. 7.3 - Recommended Type 2 elastic response spectrum for ground types A to E (5% damping).

The International Code Council (ICC) was established in 1994 as a non-profit organization dedicated to developing a single set of comprehensive and coordinated national model construction codes. The founders of the ICC are Building Officials and Code Administrators International Inc. (BOCA), International Conference of Building Officials (ICBO), and Southern Building Code Congress International Inc. (SBCCI). Since the early part of the last century, these non-profit organizations developed the three separate sets of model codes used throughout the United States. Although regional code development has been effective and responsive to our country's needs, the time came for a single set of codes. The nation's three model code groups responded by creating the International Code Council and by developing codes without regional limitations: the International Building Code.

The main U.S. codes and provisions are described in the following.

- NEHRP Recommended Provisions for Seismic Regulations for New Buildings and Other Structures. Prepared for FEMA (<http://www.fema.gov>) by the Building Seismic Safety Council ([www.bssconline.org](http://www.bssconline.org)), this multi-edition two-volume publication begun in 1985 has been updated through the years to reflect the changing needs of the architectural, engineering and construction communities.
- International Building Code (<http://www.iccsafe.org>). The scope of version 2006 of this code covers all buildings except 3-story one- and two-family dwellings and town homes. This comprehensive code features time-tested safety concepts, structural, and fire and life safety provisions covering means of egress, interior finish requirements, comprehensive roof provisions, seismic

engineering provisions, innovative construction technology, occupancy classifications, and the latest industry standards in material design. It is founded on broad-based principles that make possible the use of new materials and new building designs. The 2003 edition establishes the minimum regulations for building systems using prescriptive and performance-related provisions. The version of 2000 addresses design and installation of building systems with requirements that emphasize performance. The IBC is coordinated with all the international codes: Uniform Building Code (UBC), BOCA National Building Code (NBBC), and the Standard Building Code (SBC). The code provides design specifications for: earthquake loads; architectural, mechanical and electrical components; non-building structures; and seismically isolated structures.

- Seismic Design for Buildings; Technical Manual, October 1992 (<http://www.ntis.gov>). The manual provides criteria and guidance for the design of structures to resist the effects of earthquakes. It includes the seismic design of buildings, as well as architectural components, mechanical and electrical equipment supports, some structures other than buildings, and utility systems. A Seismic Zone Tabulation for the United States and a seismic zone map for the United States are provided.
- Uniform Building Code: Structural Engineering Design Provisions (UBC) (<http://www.iccsafe.org>). The UBC covers standards for earthquake recording instrumentation, seismic zones for specific cities throughout the United States, and a seismic zoning map of the United States.

### *7.2.1. The NEHRP provisions*

The National Earthquake Hazards Reduction Program (NEHRP) is the Federal Government's program to reduce the risks to life and property from earthquakes. The NEHRP agencies are the Federal Emergency Management Agency (FEMA), the National Institute of Standards and Technology (NIST); the National Science Foundation (NSF); and the USGS. The four goals of the NEHRP are as follows:

- . develop effective practices and policies for earthquake loss-reduction and accelerate their implementation;
- . improve techniques to reduce seismic vulnerability of facilities and systems;
- . improve seismic hazards identification and risk-assessment methods and their use;
- . improve the understanding of earthquakes and their effects.

The four NEHRP agencies work in close coordination to improve the nation's understanding of earthquake hazards and to mitigate their effects. The missions of the four agencies are complementary, and the agencies work together to improve our understanding, characterization, and assessment of hazards and vulnerabilities; improve model building codes and land use practices; reduce risks through post-earthquake investigations and education; improve design and construction techniques; improve the capacity of government at all levels and the private sector to reduce and manage earthquake risk; and accelerate the application of research results

The main features of the NEHRP provisions follow.

Ground motion accelerations, represented by response spectra and coefficients derived from these spectra, shall be determined in accordance with the general procedure or the site-specific procedure. The general procedure in which spectral response acceleration parameters for the maximum considered earthquake ground motions are derived using the maps enclosed to the Provisions, modified by site coefficients to include local site effects and scaled to design values, are permitted to be used for any structure except as specifically indicated in the Provisions. The site-specific procedure also is permitted to be used for any structure and shall be used where specifically required by the Provisions.

The maximum considered earthquake ground motions shall be as represented by the mapped spectral response acceleration at short periods,  $S_s$ , and at 1 s,  $S_1$ , obtained from the maps of the Provisions, respectively, and adjusted for site class effects using the site coefficients. When a site-specific procedure is used, maximum considered earthquake ground motion shall be determined in accordance with the proper rules.



For structures located within those regions of the maps having values of  $S_5$  less than or equal to 0.15 and values of  $S_1$  less than or equal to 0.04, accelerations need not be determined. Such structures are permitted to be directly categorized as Seismic Design Category A.

For all other structures, the site class shall be determined together with the maximum considered earthquake spectral response accelerations adjusted for site class effects,  $S_{MS}$ , and  $S_{M1}$ , and the design spectral response accelerations,  $S_{DS}$ , and  $S_{D1}$ . The general response spectrum, when required by the Provisions, shall be determined as well.

For all structures located within those regions of the maps having values of  $S_5$  greater than 0.15 or values of  $S_1$  greater than 0.04, the site shall be classified as in Table 7.5.

Table 7.5 - Ground types.

Ground type	Description of stratigraphic profile	$V_{S30}$ (m/s)	$N$ or $N_{ch}$	$s_u$
A	Hard rock	> 1500		
B	Rock	760 - 1500		
C	Very dense soil and soft rock	360 - 760	> 50	> 2,000 (> 100 kPa)
D	Stiff soil	180 - 360	15 - 50	1,000 to 2,000 psf (50 to 100 kPa)
E	A soil profile with $V_{30} < 180$ m/s	< 180	< 15	< 1,000 psf (< 50 kPa)
F	Soils requiring site-specific evaluations: <ol style="list-style-type: none"> <li>1. Soils vulnerable to potential failure or collapse under seismic loading such as liquefiable soils, quick and highly sensitive clays, and collapsible weakly cemented soils. Exception: for structures having fundamental periods of vibration equal to or less than 0,5 second, site-specific evaluations are not required to determine spectral accelerations for liquefiable soils.</li> <li>2. Peats and/or highly organic clays (<math>H &gt; 3</math> m of peat and/or highly organic clay where <math>H</math> = thickness of soil);</li> <li>3. Very high plasticity clays (<math>H &gt; 8</math> m with <math>PI &gt; 75</math>)</li> <li>4. Very thick soft/medium stiff clays (<math>H &gt; 36</math> m).</li> </ol>			

NOTE: If the  $s_u$  method is used and the  $N$  and  $s_u$  criteria differ, select the category with the softer soils (e.g., use site class E instead of D).

When the soil properties are not known in sufficient detail to determine the site class, site class D shall be used. Site classes E or F need not be assumed unless the authority having jurisdiction determines that site classes E or F could be present at the site or in the event that site classes E or F are established by geotechnical data.

The steps for classifying a site are as follows.

Step 1: Check for the four categories of site class F requiring site-specific evaluation. If the site corresponds to any of these categories, classify the site as site class F and conduct a site-specific evaluation.

Step 2: Check for the existence of a total thickness of soft clay > 3 m where a soft clay layer is defined by:  $s_u < 500$  psf (25 kPa),  $w > 40\%$ , and  $PI > 20$ . If these criteria are satisfied, classify the site as site class E.

Step 3: Categorize the site using one of the following three methods with  $V_{S30}$ ,  $N$ , and  $S_u$  computed in all cases as specified by the definitions:

- $V_{S30}$  for the top 30 m (v method);
- $N$  for the top 30 m (N method);
- $N_{ch}$  for cohesionless soil layers ( $PI < 20$ ) in the top 30 m and average  $s_u$  for cohesive soil layers ( $PI > 20$ ) in the top 30 m ( $s_u$  method).

The shear wave velocity for rock, site class B, shall be either measured on site or estimated for competent rock with moderate fracturing and weathering. Softer and more highly fractured and weathered rock shall either be measured on site for shear wave velocity or classified as site class C.

The hard rock category, site class A, shall be supported by shear wave velocity measurements either on site or on profiles of the same rock type in the same formation with an equal or greater degree of weathering and fracturing. Where hard rock conditions are known to be continuous to a depth of 30 m, surficial shear wave velocity measurements may be extrapolated to assess  $V_{S30}$ .

The rock categories, site classes A and B, shall not be used if there is more than 3 m of soil between the rock surface and the bottom of the spread footing or mat foundation.

The definitions presented below apply to the upper 30 m of the site profile. Profiles containing distinctly different soil layers shall be subdivided into those layers designated by a number that ranges from 1 to  $n$  at the bottom where there are a total of  $n$  distinct layers in the upper 30 m. The symbol  $i$  then refers to any one of the layers between 1 and  $n$ .

$V$  is the shear wave velocity in m/s;  $d_i$  is the thickness of any layer between 0 and 30 m;  $V_{S30}$  is:

$$V_{S30} = \frac{\sum_{i=1}^n d_i}{\sum_{i=1}^n \frac{d_i}{V_i}} \quad (7-6)$$

where  $\sum_{i=1}^n d_i$  is equal to 30 m.

$N_j$  is the Standard Penetration Resistance not to exceed 100 blows/ft as directly measured in the field without corrections.

$N$  is:

$$N = \frac{\sum_{i=1}^n d_i}{\sum_{i=1}^n \frac{d_i}{N_i}} \quad (7-7)$$

$N_{ch}$  is

$$N_{ch} = \frac{d_s}{\sum_{i=1}^m \frac{d_i}{N_i}} \quad (7-8)$$

where  $\sum_{i=1}^m d_i = d_s$ .

$d_s$  is the total thickness of cohesionless soil layers in the top 30 m.

$S_{MS}$  and  $S_{M1}$  shall be determined as follows:

$$S_{MS} = F_a S_S \quad (7-9)$$

and

$$S_{M1} = F_v S_1 \quad (7-10)$$

where site coefficients  $F_a$  and  $F_v$  are defined in Tables 7.6 and 7.7, respectively.

$S_{DS}$  and  $S_{D1}$  shall be determined as follows:

$$S_{DS} = 2/3 S_{MS} \quad (7-11)$$

and

$$S_{D1} = 2/3 S_{M1} \quad (7-12)$$

Table 7.6 - Values of  $F_a$  as a function of site class and mapped short-period maximum considered earthquake spectral acceleration.

Site Class	Mapped response	maximum acceleration	considered at	earthquake short	spectral periods
	$S_S \leq 0.25$	$S_S \leq 0.50$	$S_S \leq 0.75$	$S_S \leq 1.00$	$S_S \leq 1.25$
A	0.8	0.8	0.8	0.8	0.8
B	1.0	1.0	1.0	1.0	1.0
C	1.2	1.2	1.1	1.0	1.0
D	1.6	1.4	1.2	1.1	1.0
E	2.5	1.7	1.2	0.9	0.9
F	a	a	a	a	a

NOTE: Use straight line interpolation for intermediate values of  $S_S$ .

a = Site-specific geotechnical investigation and dynamic site response analyses shall be performed. Exception: for structures with periods of vibration equal to or less than 0.5 s, values of  $F_a$  for liquefiable soils may be assumed equal to the values for the site class determined without regard to liquefaction in Step 3.

Table 7.7 - Values of  $F_v$  as a function of site class and mapped 1 s period maximum considered earthquake spectral acceleration.

Site Class	Mapped response	maximum acceleration	considered at	earthquake 1 second	spectral periods
	$S_1 \leq 0.1$	$S_1 \leq 0.2$	$S_1 \leq 0.3$	$S_1 \leq 0.4$	$S_1 \leq 0.5$
A	0.8	0.8	0.8	0.8	0.8
B	1.0	1.0	1.0	1.0	1.0
C	1.7	1.6	1.5	1.4	1.3
D	2.4	2.0	1.8	1.6	1.5
E	3.5	3.2	2.8	2.4	2.4
F	a	a	a	a	a

NOTE: Use straight line interpolation for intermediate values of  $S_1$ .

a = Site-specific geotechnical investigation and dynamic site response analyses shall be performed. Exception: for structures with periods of vibration equal to or less than 0.5 s, values of  $F_v$  for liquefiable soils may be assumed equal to the values for the site class determined without regard to liquefaction.

Where a design response spectrum is required by the Provisions and site-specific procedures are not used, the design response spectrum curve shall be developed as indicated in Fig. 7.4a and as follows.

For periods less than or equal to  $T_0$ , the design spectral response acceleration,  $S_a$ , is:

$$S_a = 0.6 \frac{S_{DS}}{T_0} T + 0.4 S_{DS} \quad (7-13)$$

For periods greater than or equal to  $T_0$  and less than or equal to  $T_S$ , the design spectral response acceleration,  $S_a$ , shall be taken as equal to  $S_{DS}$ .

For periods greater than  $T_S$ , the design spectral response acceleration,  $S_a$ , is:

$$S_a = \frac{S_{D1}}{T} \quad (7-14)$$

where:

$T$  = the fundamental period of the structure,

$T_0 = 0.2 S_{D1}/S_{DS}$ , and

$T_S = S_{D1}/S_D$ .

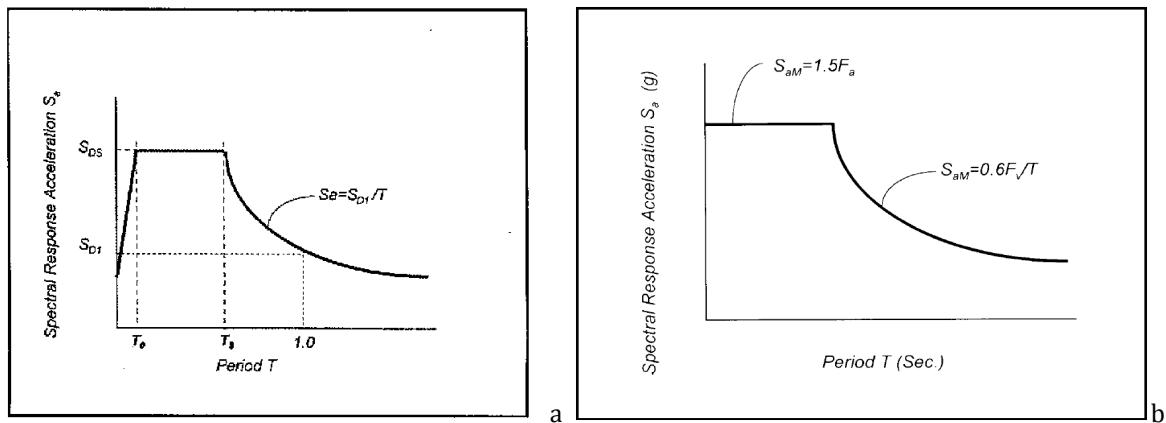


Fig. 7.4 – Design response spectrum (a) and deterministic limit on maximum considered earthquake response spectrum (b).

A site-specific study shall account for the regional seismicity and geology, the expected recurrence rates and maximum magnitudes of events on known faults and source zones, the location of the site with respect to these, near source effects if any, and the characteristics of subsurface site conditions.

When site-specific procedures are utilized, the maximum considered earthquake ground motion shall be taken as that motion represented by a 5% damped acceleration response spectrum having a 2% probability of exceedance within a 50 year period. The maximum considered earthquake spectral response acceleration,  $S_{aM}$ , at any period,  $T$ , shall be taken from that spectrum.

Exception: where the spectral response ordinates for a 5% damped spectrum having a 2% probability of exceedance within a 50 year period at periods of 0.2 or 1 s exceed the corresponding ordinate of the deterministic limit on maximum considered earthquake ground motion, the maximum considered earthquake ground motion shall be taken as the lesser of the probabilistic maximum considered earthquake ground motion or the deterministic maximum considered earthquake ground motion but shall not be taken less than the deterministic limit ground motion.

The deterministic limit on maximum considered earthquake ground motion shall be taken as the response spectrum determined in accordance with Fig. 7.5, where  $F_a$  and  $F_v$  are determined in accordance with Tables 7.5 and 7.6 with the value of  $S_S$  taken as 1.5 and the value of  $S_I$  taken as 0.6.

The deterministic maximum considered earthquake ground motion response spectrum shall be calculated as 150% of the median 5% damped spectral response accelerations,  $S_{aM}$ , at all periods resulting from a characteristic earthquake on any known active fault within the region.

Where site-specific procedures are used to determine the maximum considered earthquake ground motion response spectrum, the design spectral response acceleration at any period shall be

determined as:

$$S_a = S_{aM} \quad (7-15)$$

and shall be greater than or equal to 80% of the  $S_a$  determined by the general response spectrum (Fig. 7.4b).

.

## References

- Abrahamson N.A. and Shedlock K.M.; 1997: Overview. *Seism. Res. Lett.*, 68, 9-23.
- Abrahamson N. A., Birkhauser P., Koller M., Mayer-Rosa D., Smit P., Sprecher C., Tinic S. and Graf R.; 2002: PEGASOS - a comprehensive probabilistic seismic hazard assessment for nuclear power plants in Switzerland. In: *Proceedings of the Twelfth European Conference on Earthquake Engineering*, London, paper no. 633.
- Adams J. and Halchuk S.; 2003: Forth generation seismic hazard maps of Canada: values for over 650 Canadian localities intended for the 2005 National Building Code of Canada. Open File 4459, Geological Survey of Canada, Ottawa, 155 pp.
- Adams J., Weichert D.H and Halchuk S.; 1999: Trial seismic hazard maps of Canada - 1999: 2%/50 year values for selected Canadian cities. Open File 3724, Geological Survey of Canada, Ottawa, 114 pp.
- Aguilar-Meléndez A., Ordaz Schroeder M.G., De la Puente J., González-Rocha S.N., Rodríguez-Lozoya H.E., Córdova-Ceballos A., García-Elías A., Calderón-Ramón C., Escalante-Martínez J.E., Laguna-Camacho J.R., Campos-Rios A.; 2017: Development and Validation of Software CRISIS to Perform Probabilistic Seismic Hazard Assessment with Emphasis on the Recent CRISIS2015. *Computacion y Sistemas*, DOI: 10.13053/CyS-21-1-2578.
- Aki K.; 1965: Maximum likelihood estimate of  $b$  in the formula  $\log N = a - bM$  and its confidence limits. *Bull. Earthquake Res. Inst.*, 43, 237-239.
- Albarelo D., Bosi V., Brammerini F., Lucantoni A., Naso G., Peruzza L., Rebez A., Sabetta F. e Slejko D; 2000: Carte di pericolosità sismica del territorio nazionale. *Quaderni di Geofisica*, n. 12, Editrice Compositori, Bologna, 7 pp.
- Albini P., Garcia Acosta V., Musson M.W. and Stucchi M. (eds); 2004: Investigating the records of past earthquakes. *Annals of Geophysics*, 47(2-3).
- Algermissen S.T. and Perkins D.M.; 1976: A probabilistic estimate of maximum acceleration in rock in the contiguous United States. U.S. Geological Survey, Open File Report 76-416.
- Algermissen S.T., Perkins D.M., Isherwood W., Gordon D., Reagor G. and Howard C.; 1976: Seismic risk evaluation of the Balkan region. In: Karnik V. and Radu C. (eds), *Proceedings of the Seminar on Seismic Zoning Maps*, Vol. 2, Unesco, Skopje, pp. 172 - 240.
- Algermissen S.T., Perkins D.M., Thenhaus P.C., Hanson S.L., and Bender B.L.; 1982: Probabilistic estimates of maximum acceleration and velocity in rock in the contiguous United States.. U.S. Geological Survey Open-File Report 82-1033, 99 pp. (plus appendix).
- Allen C.R.; 1976: Responsibilities in earthquake prediction. *Bull. Seism. Soc. Am.*, 66, 2069-2074.
- Ambraseys N.N.; 1983: Evaluation of seismic risk. In: Ritsema A.R. and Gurpinar A. (eds), *Seismicity and seismic risk in the offshore North Sea area*, Reidel Publishing Company, Dordrecht, pp. 317-345.
- Ambraseys N.N.; 2002: Value of historical seismicity. In: *Environmental Catastrophes and Recoveries in the Holocene August 29 - September 2 2002*, Department of Geography & Earth Sciences, Brunel University, Uxbridge, UK, Atlas Conferences Inc., Document # caji-35.
- Ambraseys N.N.; 2003: Reappraisal of magnitude of 20<sup>th</sup> century earthquakes in Switzerland. *J. Earthquake Engin.*, 7, 149-191.
- Ambraseys N. and Bilham R.; 2011: Corruption kills. *Nature*, 469, 153-155.
- Ambraseys N.N. and Jackson J.A.; 1981: Earthquake hazard and vulnerability in the northern Mediterranean: the Corinth earthquake sequence of February - March 1981. *Disasters*, 5, 355 - 368.
- Ambraseys N.N., Simpson K.A. and Bommer J.J.; 1996: Prediction of horizontal response spectra in Europe. *Earthquake Eng. Struct. Dyn.*, 25, 371-400.
- Anderson J.G.; 1978: Program EQRISK: a computer program for finding uniform risk spectra of strong earthquake ground motion. Report CE 78-11, Dpt. Civil Engineering University of Southern California, Los Angeles, 54 pp.
- Applied Technology Council; 1978: Tentative provisions for the development of seismic regulations for buildings. Publication ATC 3-06, NBS Special Publication 78-8, U.S. Government Printing Office, Washington, DC.
- Arias A.; 1970: A measure of earthquake intensity. In: Hansen R.J. (ed), *Seismic design of nuclear power plants*, M. I. T. Press, Cambridge, pp. 438-483.
- Ashford S.A., Sitar N., Lysmer J. and Deng N.; 1997: Topographic effects on the seismic response of steep slopes. *Bull. Seism. Soc. Am.*, 87, 701-709.
- ATC; 78: Tentative provisions for the development of seismic regulations for buildings. ATC3-06, Applied Technology Council, Palo Alto, Ca.
- Bakun W.H. and Lindh A.G.; 1985: The Parkfield, California, earthquake prediction experiment. *Science*, 229, 619-624.



- Bakun W. H. Wentworth C. M.; 1997: Estimating earthquake location and magnitude from seismic intensity data. *Bull. Seism. Soc. Am.*, 87, 1502-1521.
- Barani S., Spallarossa D., Eva C. and Bazzurro P.; 2007: Sensitivity analysis of parameters for probabilistic seismic hazard assessment of western Liguria (north-western Italy). *Boll. Geof. Teor. Appl.*, 48, 127-150.
- Bath M.; 1965: Lateral inhomogeneities of the upper mantle. *Tectonophysics*, 2, 483-514.
- Bazzurro P. and Cornell C.A.; 2004: Nonlinear soil-site effects in probabilistic seismic-hazard analysis. *Bull. Seismol. Soc. Am.*, 94, 2110-2123.
- Bender, B., and D.M. Perkins, 1982, SEISRISK II: A computer program for seismic hazard estimation, U.S. Geological Survey Open-File Report 82-293, 103 pp.
- Bender B. and Perkins D.M.; 1987: Seisrisk III: a computer program for seismic hazard estimation. *Bulletin 1772*, U.S. Geological Survey, Denver, 48 pp.
- Benedetti D., Benzoni G. and Parisi M.A.; 1988: Seismic vulnerability and risk evaluation for old urban nuclei. *Earth. Eng. Struct. Dyn.*, 16, 183 - 201.
- Benito M.B., Murphy P., Tsige M., Jiménez Peña M.E., García-Rodríguez M.J., Gaspar-Escribano J.M. and García-Mayordomo J.; 2006: Seismic risk in the Region of Murcia. RISMUR Project. *Geophysical Research Abstracts*, 8.
- Benjamin J.R. and Associates; 1988: A criterion for determining exceedance of the Operating Basis Earthquake. EPRI Report NP-5930, Electric Power Research Institute, Palo Alto, Ca.
- Benzoni G. e Parisi M.A.; 1986: Adeguamento antisismico e variazioni del rischio nei centri storici. *Ingegneria Sismica*, 3, 3 - 11.
- Bilham R.; 1998: Death toll from earthquakes. *Geotimes*, 7(4).
- Blake A.; 1941: On the estimation of focal depth from macroseismic data. *Bull. Seism. Soc. Am.*, 31, 225-231.
- Bolt B.A.; 1969: Duration of strong motion. In: *Proceedings of the 4th World Conference on Earthquake Engineering*, Santiago Chile, pp. 1304-1315.
- Bommer J.J.; 2004: Basics of seismology and seismic hazard assessment. Rose School, Pavia, 237 pp.
- Bommer J.J. and Abrahamson N.A.; 2006: Why do modern probabilistic seismic-hazard analyses often lead to increased hazard estimates? *Boll. Seism. Soc. Am.*, 96, 1967-1977.
- Bonilla M.G., Mark M.K. and Lienkaemper J.J.; 1984: Statistical relations among earthquake magnitude, surface rupture length, and surface fault displacement. *Boll. Seism. Soc. Am.*, 74, 2379 - 2411.
- Boore D.M.; 1983: Stochastic simulation of high-frequency ground motion based on seismological models of the radiated spectra. *Bull. Seism. Soc. Am.*, 73, 1865-1884.
- Boore D.M., Joyner W.B. and Fumal T.E.; 1993: Estimation of response spectra and peak acceleration from western north American earthquakes: an interim report. Open-File Report 93-509, U.S.G.S., Denver, 72 pp.
- Bortugno E. and Eisner R.; 1990: The scenario for the next big earthquake in northern California. In: *Irpinia dieci anni dopo - Riassunti degli interventi*, Tipolito La Sorrentina, Sorrento, pp. 181 - 185.
- BSSC (Building Seismic Safety Council); 2004: NEHRP recommended provisions for seismic regulations for new buildings and other structures (FEMA 450). Part 1: Provisions, 2003 edition. BSSC, Washington D.C., 356 pp.
- Bune V., Radu C. and Polyakova T.; 1986: Analysis of isoseismal maps of Vrancea earthquakes November 10, 1940 and March 4, 1977. Detailed engineering and seismological research. *Questions of earthquake engineering*. Nauka, 27, 126-135.
- Burton P.W.; 1979: Seismic risk in southern Europe through to India examined using Gumbel's third distribution of extreme values. *Geophys. J. R. Astr. Soc.*, 59, 249-280.
- Burton P.W., Main I.G. and Long R.E.; 1983: Perceptible earthquakes in the central and eastern United States (examined using Gumbel's third distribution of extreme values). *Bull. Seism. Soc. Am.*, 73, 497-518.
- Camassi R. and Stucchi M.; 1997: NT4.1, un catalogo parametrico di terremoti di area italiana al di sopra della soglia del danno (versione NT4.1.1). C.N.R. GNDT, Milano, 96 pp.
- Campbell K.W.; 1981: Near source attenuation of peak horizontal acceleration. *Bull. Seism. Soc. Am.*, 71, 2039-2070.
- Campbell K.W. and Bozorgnia Y.; 1994: Near-source attenuation of peak horizontal acceleration from worldwide accelerograms recorded from 1957 to 1993. In: *Proceedings 5th U.S. National Conference on Earthquake Engineering*, Earthquake Engineering Research Institute, Berkeley Ca., vol. 1, pp. 283-292.
- Cauzzi C. and Faccioli E.; 2008: Broadband (0.05 to 20 s) prediction of displacement response spectra based on worldwide digital records. *J. Seismol.*, 12, 453-475, doi 10.1007/s10950-008-9098-y.
- CEN (Comité Européen de Normalisation); 2002: Eurocode 8: design of structures for earthquake resistance. Part 1: general rules, seismic actions and rules for buildings. Draft No 5, Doc CEN/T250/SC8/N317, CEN, Brussels, 100 pp.
- Chang F.K. and Krinitzsky E.L.; 1977: Duration, spectral content, and predominant period of strong motion earthquake records from western United States. *Miscellaneous Paper 5-73-1*, U.S. Army Corps of Engineers Waterways Experiment Station, Vicksburg Mississippi.

- Chiang W.-L., Guidi G.A., Mortgat C.P., Schoof C.C. and Shah H.C.; 1984: Computer Program for Seismic Hazard Analysis - A User Manual - (Stanford Seismic Hazard Analysis - STASHA). The John Blume Earthquake Engineering Center, Stanford University, T.R. 62.
- Chuhan Zhang and Chongbin Zhao; 1986: Effects of canyon topography and geological conditions on strong ground motion. *Earthq. Engin. Struct. Dyn.*, 16, 81-97.
- CNR Gruppo Nazionale Difesa Terremoti; 1993: Rischio sismico di edifici pubblici Parte I Aspetti metodologici. CNR Gruppo Nazionale Difesa Terremoti, Roma, 126 pp.
- CNR Gruppo Nazionale Difesa Terremoti; 1993: Rischio sismico di edifici pubblici Parte II Risultati per la regione Emilia-Romagna. CNR Gruppo Nazionale Difesa Terremoti, Roma, 163 pp.
- Codermatz R., Nicolich R. and Slejko D.; 2003: Seismic risk assessment and GIS technology: applications to infrastructures in the Friuli - Venezia Giulia region (NE Italy). *Earth. Eng. Struct. Dyn.*, 32, 1677-1690.
- Coppersmith K.J. and Youngs R.R.; 1986: Capturing uncertainty in probabilistic seismic hazard assessments within intraplate environments. In: *Proceedings of the Third U.S. National Conference on Earthquake Engineering*, August 24-28, 1986, Charleston, SC, Earthquake Engineering Research Institute, El Cerrito CA U.S.A., vol. 1, pp 301-312.
- Cornell C.A.; 1968: Engineering seismic risk analysis. *Bull. Seism. Soc. Am.*, 58, 1583-1606.
- Cornell C.A. and Merz H.A.; 1975: Seismic risk analysis of Boston. *J. Struct. Division ASCE*, 101 (ST10), 2027-2043.
- Cornell C.A. and Van Marke E.H.; 1969: The major influences on seismic risk. In: *Proceedings of the Third World Conference on Earthquake Engineering*, Santiago, Chile, Vol. A-1, pp. 69-93.
- Der Kiureghian A. and Ang H.S.; 1977: A fault rupture model for seismic risk analysis. *Bull. Seism. Soc. Am.*, 67, 1173-1194.
- Di Pasquale G., Orsini G. and Romeo R.W.; 2005: New developments in seismic risk assessment in Italy. *Bulletin of Earthquake Engineering*, 3, 101-128.
- Douglas J.; 2003: Earthquake ground motion estimation using strong-motion records: a review of equations for the estimation of peak ground acceleration and response spectral ordinates. *Earth-Science Reviews*, 61, 43-104.
- Douglas J.; 2011: Ground-motion prediction equations 1964-2010. Report BRGM/RP-59356-FR, BRGM, Orlean, France
- Eaton J.P.; 1969: HYPOLAYR, a computer program for determining hypocenters of local earthquakes in an earth consisting of uniform flat layers over a half space. Open File Report, U.S. Geological Survey, 155 pp.
- EERI Committee on Seismic Risk; 1984: Glossary of terms for probabilistic seismic-risk and hazard analysis. *Earthq Spectra*, 1, 33-40.
- Ekström G. and Dziewonski A.; 1988: Evidence of bias in estimations of earthquake size. *Nature*, 332, 319-323.
- Ellsworth W.L.; 2003: Appendix D - Magnitude and Area Data for Strike Slip Earthquakes. In: *Working Group On California Earthquake Probabilities, Earthquake Probabilities in the San Francisco Bay Region: 2002-2031*, Open-File Report 03-214, U.S. Geological Survey.
- Ellsworth W.L., Matthews M.V., Nadeau R.M., Nishenko S.P., Reasenberg P.A., and Simpson R.W.; 1999: A physically-based earthquake recurrence model for estimation of long-term earthquake probabilities. *United States Geological Survey Open-File Report 99-552*, 22 pp.
- EPRI; 1986: Seismic hazard methodology for the central and eastern United States. Report NP-4726, Electric Power Research Institute, Palo Alto Ca.
- Epstein B. and Lomnitz C.; 1966: A model for the occurrence of large earthquakes. *Nature*, 211, 954-956.
- Esteva L.; 1967: Criteria for the construction of spectra for seismic design. In: *Third Panamerican Symposium on Structures*, Caracas, Venezuela.
- Esteva L.; 1968: Bases para la formulacion de decisiones de diseno sismico. Ph.D. Thesis, Universidad Nacional Autonoma de Mexico, Mexico City.
- Esteva L.; 1969: Seismicity prediction: a Bayesian approach. In: *Proceedings of the Fourth World Conference on Earthquake Engineering*, Santiago de Chile, Vol. 1, A-1, pp. 172-185.
- Esteva L.; 1970: Seismic risk and seismic design decisions. In: Hansen R.J. (ed), *Seismic Design for Nuclear Power Plants*, MIT Press, Cambridge, Massachusetts, pp. 142-182.
- Faccioli E.; 1979: Engineering seismic risk analysis of the Friuli region. *Boll. Geof. Teor. Appl.*, 21, 173 - 190.
- Finetti I. and Morelli C.; 1972: Deep seismic refraction exploration on eastern Alps. *Boll. Geof. Teor. Appl.*, 14, 59 - 66.
- Field E.H., Jordan T.H. and Cornell C.A.; 2003: OpenSHA: A developing community-modeling environment for seismic hazard analysis. *Seismol. Res. Letters*, 74, 406-419.
- Fisher R.A. and Tippett L.H.C.; 1928: Limiting forms of the frequency distribution of the largest and smallest member of a sample. *Proc. Cambridge Phil. Soc.*, 24, 180-190.
- Fournier d'Albe E.M.; 1985: Risk assessment based on observed vulnerability. In: *Abstracts 3rd Int. Symp. Analysis of Seismicity and Seismic Risk*, Liblice, June 17 - 22, 1985, pp. 13.
- Frankel A.; 1995: Mapping seismic hazard in the Central and Eastern United States. *Seismological Research Lett.*

- 66(4), 8-21.
- Frankel A., Mueller C., Barnhard T., Perkins D., Leyendecker E., Dickman N., Hanson S. and Hopper M.; 1996: National seismic hazard maps: documentation June 1996. Open-File Report 96-532, U.S. Geological Survey, Denver Co.
- Frankel A., Mueller C., Harmsen S., Wesson R., Leyendecker E., Klein F., Barnhard T., Perkins D., Dickman N., Hanson S. and Hopper M.; 2000: USGS National Seismic Hazard Maps. Earthquake Spectra, 16, 1-20.
- Frankel A.D., Petersen M.D., Mueller C.S., Haller K.M., Wheeler R.L., Leyendecker E.V., Wesson R.L., Harmsen S.C., Cramer C.H., Perkins D.M. and Rukstales K.S.; 2002: Documentation for the 2002 update of the national seismic hazard maps. Open-File Report 02-420, U.S. Geological Survey, Denver Co.
- Galli P.; 2000: New empirical relationships between magnitude and distance for liquefaction. Tectonophysics 324, 169-187.
- Gardner J.K. and Knopoff L.; 1974: Is the sequence of earthquakes in southern California, with aftershocks removed, Poissonian? *Bull. Seism. Soc. Am.*, 64, 1363-1367.
- Gasperini P., Bernardini F., Valensise G. and Boschi E.; 1999: Defining seismogenic sources from historical earthquake felt reports. *Bull. Seism. Soc. Am.*, 89, 94-110.
- Geiger L.; 1912: Probability method for the determination of earthquake epicenters from the arrival time only. *Bull. St. Louis University*, 8(1), 56-71.
- Geli L., Bard P-Y. and Jullien B.; 1988: The effect of topography on earthquake ground motion: a review and new results. *Bull. Seism. Soc. Am.*, 78, 42-63.
- Geller R.J.; 1997: Earthquake prediction: a critical review. *Geophys. J. Int.*, 131, 425-450.
- Giardini D. and Basham P.(eds); 1993: Global Seismic Hazard Assessment Program. *Annali di Geofisica*, 33, n. 3 - 4.
- Giardini D., Gruenthal G., Shedlock K.M. and Zhang P; 1999: The GSHP global seismic hazard map. *Annali di Geofisica*, 42, 1225-1230.
- Giner-Robles J.L., Rodríguez-Pascua M.A., Pérez-López R., Silva P.G., Bardají T., Grützner C. and Reicherter K. (eds); 2009: Structural analysis of Earthquake Archaeological Effects (EAE): Baelo Claudia Examples (Cádiz, South Spain). *Notebook of Baelo 2009*, vol. 2.
- Giorgetti F., Nieto D. and Slejko D.; 1980: Seismic risk of the Friuli - Venezia Giulia region. *Publ. Inst. Geoph. Pol. Acad. Sc.*, A-9 (135), 149-169.
- Grigorten I.L.; 1963: A plotting rule for extreme probability paper. *J. Geophys. Res.*, 68, 813-814.
- Grimaz S., Slejko D., Cucchi F. and Working Group ASSESS (Barazza F., Biolchi S., Delpin E., Franceschinis R., Garcia J., Gattesco N., Malisan P., Moretti A., Pipan M., Prizzon S., Rebez A., Santulin M., Zini L., Zorzini F.); 2016: The ASSESS project: assessment for seismic risk reduction of school buildings in the Friuli Venezia Giulia region (NE Italy). *Boll. Geof. Teor. Appl.*, 57, 111-128.
- Gruenthal G.; 1998: European Macroseismic Scale 1998. *Cahiers du Centre Europeen de Geodynamique et de Seismologie*, vol. 15. Centre Europeen de Geodynamique et de Seismologie, Luxembourg, 99 pp.
- Gruppo di Lavoro; 2004: Redazione della mappa di pericolosità sismica prevista dall'Ordinanza PCM 3274 del 20 marzo 2003. Rapporto conclusivo per il Dipartimento della Protezione Civile, INGV, Milano - Roma, 65 pp. + 5 App.
- Gruppo di Lavoro Scuoibilità; 1979: Carte preliminari di scuotibilità del territorio nazionale. C.N.R. P.F. Geodinamica pubbl. 227, ESA, Roma, 25 pp.
- Guidi G.A.; 1979: Computer Programs for Seismic Hazard Analysis - A User Manual (Stanford Seismic Hazard Analysis - STASHA). The John Blume Earthquake Engineering Center, Stanford University, T.R. 36.
- Gumbel E.J.; 1945: Floods estimated by probability methods. *Engng. News Rec.*, 134, 97-101.
- Gumbel E. J.; 1958: Statistics of extremes. Columbia Univ. Press, New York, 375 pp.
- Gutenberg B.; 1945: Amplitudes of surface waves and magnitude of shallow earthquakes. *Bull. Seism. Soc. Am.*, 35, 3-12.
- Gutenberg B. and Richter C.F.; 1942; Earthquake Magnitude, Intensity, Energy and Acceleration, *Bull. Seism. Soc. Am.*, 32, 163-191.
- Gutenberg B. and Richter C.F.; 1944: Frequency of earthquakes in California. *Bull. Seism. Soc. Am.*, 34, 1985-1988.
- Gutenberg B. and Richter C.F.; 1949: Seismicity of the Earth and associated phenomena. Princeton University Press, Princeton, New Jersey, 273 pp.
- Gutenberg B. and Richter C.F.; 1956: Earthquake magnitude, intensity, energy and acceleration (second paper). *Bull. Seism. Soc. Am.*, 46, 104-145.
- Hanks T.C. and Kanamori H.; 1979: A moment magnitude scale. *J. Geophys. Res.*, 84, 2348-2350.
- Hanks T.C. and Thatcher M.; 1972: A graphical representation of seismic source parameters. *J. Geoph. Res.*, 77, 4393-4405.
- Hays W.W. and Hamilton R.M.; 1990: Earthquake risk assessment in California. In: *Irpinia dieci anni dopo - Riassunti degli interventi*, Tipolito La Sorrentina, Sorrento, pp. 159 - 175.

- Hershberger J.; 1956: A comparison of earthquake accelerations with intensity ratings. *Bull. Seism. Soc. Am.*, 46, 317-320.
- Housner G.W.; 1941: Calculation of the response of an oscillator to arbitrary ground motion. *Bull. Seism. Soc. Am.* 31, 143-149.
- Housner G.W.; 1959: Behavior of structures during earthquakes. *J. Engineering Mechanics division, ASCE*, 85(EM14), 109-129.
- Imoto M.; 1991: Changes in the magnitude-frequency b value prior to large ( $M \geq 6$ ) earthquakes in Japan. *Tectonophysics*, 193, 311-325.
- Isacks B. and Oliver J.; 1964: Seismic waves with frequencies from 1 to 100 cycles per second recorded in a deep mine in northern New Jersey. *Bull. Seism. Soc. Am.*, 54, 1941-1979.
- Jànosi J. V.; 1907: Makroszeizmikus rengések feldolgozása a çancani-féle egyenlet alapján. *Az 1906 èvi Magyarorszàgi földrengések*, 77-88.
- Jenkinson A.F.; 1955: The frequency distribution of the annual maximum (or minimum) values of meteorological elements. *Q. J. R. Met. Soc.*, 87, 158-171.
- Jimenez M-J, Giardini D., Gruenthal G. and the SESAME Working Group (Erdik M., Garcia-Fernandez J., Lapajne J., Makropoulos K., Musson R., Papaioannou Ch., Rebez A., Riad S., Sellami S., Shapira A., Slejko D. van Eck T., El Sayed A.); 2001: Unified seismic hazard modelling throughout the Mediterranean region. *Boll. Geof. Teor. Appl.*, 42, 3-18.
- Jimenez M-J, Giardini D., Gruenthal G.; 2003: The ESC-SESAME unified hazard model for the European-Mediterranean region. *EMSC/CSEM Newsletter*, 19, 2-4.
- Johnston A.C., Coppersmith K.J., Kanter L.R. and Cornell C.A.; 1994: The earthquakes of stable continental regions. Volume 1: assessment of large earthquake potential. EPRI, Palo Alto CA. U.S.A., 62 pp.
- Joyner, W.B. and Boore, D.M.: 1981, Peak horizontal acceleration and velocity from strong-motion records including records from the 1979 Imperial Valley, California, earthquake, *Bull. Seism. Soc. Am.* 71, 2011-2038.
- Kagan Y.Y. and Knopoff L.; 1987: Random stress and earthquake statistics: time dependence. *Geophys. J. R. Astron. Soc.*, 88, 723-731.
- Kanamori H; 1977: The energy release in great earthquakes. *J. Geophys. Res.*, 82, 2981-2987.
- Kanamori H.; 2003: Earthquake prediction: an overview. In: Lee W.H.K., Kanamori H., Jennings P. and Kisslinger C. (eds), *International Handbook of Earthquake and Engineering Seismology, Part B*, Academic Press, San Diego, pp. 1205-1216.
- Kaplan S. and Garrik J.; 1981: On the quantitative definition of risk. *Risk Analysis*, 1, 11-27.
- Karnik V. and Klima K.; 1993: Magnitude-frequency distribution in the European - Mediterranean earthquake regions. *Tectonophysics*, 220, 309-323.
- Karnik V., Kondorsaya N.V., Riznichenko Y.V., Savarensky Y.F., Solovev S.L., Shebalin N.V., Vanek J. and Zatopek A.; 1962: Standardization of the earthquake magnitude scales. *Studia Geophys. et Geodet.*, 6, 41-48.
- Karnik V., Prochazkova, Schenkova Z., Ruprechtova L., Dudek A., Drimmel J., Schmedes E., Leydecker G., Rothè J.P., Guterch B., Lewandowska H., Mayer-Rosa D., Cvijanovic D., Kuk V., Giorgetti F., Grunthal G. and Hurtig E.; 1978: Map of isoseismals of the main Friuli earthquake of 6 May 1976. *Pageoph*, 116, 1307-1313.
- Keefer D.K. and Wilson R.C.; 1989: Predicting earthquake-induced landslides, with emphasis on arid and semiarid environments. In: Sadler P.M. and Morton D.M (eds), *Landslides in a Semiarid Environment*, Inland Geological Society of Southern California Publications, Riverside, California, 2, part 1, pp. 118-149.
- Keilis-Borok V.I., Knopoff L., Rotwain I.M. and Allen C.R.; 1988: Intermediate-term prediction of occurrence times of strong earthquakes. *Nature*, 335, 690-694.
- Kijko A. and Graham G.; 1998: Parametric-historic procedure for probabilistic seismic hazard analysis. Part I: estimation of maximum regional magnitude  $m_{max}$ . *Pure Appl. Geophys.*, 152, 413-442.
- King G., Stein R. and Lin J.; 1994: Static stress changes and triggering of earthquakes. *Bulletin of the Seismological Society of America*, 84, 935-953.
- Klein F.W.; 1978: Hypocenter location program HYPOINVERSE: Part I. Users guide to Versions 1, 2, 3, and 4. Part II. Source listings and notes. OFR 78-694, U. S. Geological Survey.
- Klein F.W.; 2002: User's guide to HYPOINVERSE-2000, a Fortran program to solve for earthquake locations and magnitudes. OFR 2002-171, U. S. Geological Survey.
- Kossobokov V.G.; 1990: Identification of time of increased probability for strong earthquakes occurrence in Apennines and Sicily. In: *Irpinia dieci anni dopo - Riassunti degli interventi*, Tipolito La Sorrentina, Sorrento, pp. 153 - 158.
- Kovesligethy (de) R.; 1906: *Seismonomia*. *Boll. Soc. Sism. It.*, 11, 113-250.
- Knopoff L.; 2000: The magnitude distribution of declustered earthquakes in Southern California. *Proc. Nat. Acad. Sci. USA*, 97, 11880-11884.
- Knopoff L. and Kagan Y.; 1977: Analysis of the theory of extremes as applied to earthquake problems. *Journ. Geoph. Res.*, 82, 5647-5657.

- Kramer S.L.; 1996: Geotechnical earthquake engineering. Prentice Hall, Upper Saddle River N.J., 653 pp.
- Kulkarni R.B., Youngs R.R. and Coppersmith K.J.; 1984: Assessment of confidence intervals for results of seismic hazard analysis. In: Proceedings of the Eighth World Conference on Earthquake Engineering, July 21-28, 1984, San Francisco CA U.S.A., Prentice-Hall Inc., Englewood Cliffs NJ U.S.A., Vol 1, pp 263-270.
- Lahr J.C.; 1979: HYPOELLIPSE: a computer program for determining local earthquake hypocentral parameters, magnitude, and first motion pattern. OFR 79-431, U. S. Geological Survey.
- Lahr J.C.; 1999: HYPOELLIPSE; a computer program for determining local earthquake hypocentral parameters, magnitude, and first-motion pattern (Y2K compliant version), 1999 version 1.0. OFR 99-23, U. S. Geological Survey.
- Lay T. and Wallace T.C.; 1995: Modern global seismology. Academic Press, San Diego Ca., 521 pp.
- Lee W.H.K. and Lahr J.C.; 1972: HYP071: A computer program for determining hypocenter, magnitude, and first motion pattern of local earthquakes. Open File Report, U. S. Geological Survey, 100 pp.
- Lee W.H.K. and Lahr J.C.; 1975: HYP071 (Revised): A computer program for determining hypocenter, magnitude, and first motion pattern of local earthquakes. U. S. Geological Survey Open File Report 75-311, 113 pp.
- Lee W.H.K. and Valdes C.M.; 1985: HYP071PC: A personal computer version of the HYP071 earthquake location program. U. S. Geological Survey Open File Report 85-749, 43 pp.
- Linkimer L.; 2008: Relationship between peak round acceleration and Modified Mercalli intensity in Costa Rica. *Revista Geológica de América Central*, 38, 81-94.
- Lomnitz C.; 1966: Statistical prediction of earthquakes. *Rev. Geophys.*, 4, 377-393.
- Lomnitz C.; 1974: Global tectonics and earthquake risk. Elsevier Sc. Publ. Co., Amsterdam-London-New York, 320 pp.
- Luongo G. e Marturano A.; 1990: L'Appennino centro-meridionale: analisi della sismicità, ipotesi sismogenetiche e pericolosità. In: *Irpinia dieci anni dopo - Riassunti degli interventi*, Tipolito La Sorrentina, Sorrento, pp. 135 - 140.
- Main I.; 1996: Statistical physics, seismogenesis, and seismic hazard. *Reviews of Geophysics*, 34, 433-462.
- Makropoulos, K.C. and Burton, P.W., 1986. HAZAN: a Fortran program to evaluate seismic hazard parameters using Gumbel's theory of extreme value statistics. *Computer & Geosciences*, 12, 29-49.
- Mallet R. and Mallet J.W.; 1858: The earthquake catalogue of the British Association, with the discussion, curves, and maps, etc. Report of the British Association for the Advancement of Science, Leeds 1858, Part 1, pp 1-136.
- Matthews M.V., Ellsworth W.L., and Reasenber P.A.; 2002: A Brownian model for recurrent earthquakes. *Bull. Seismol. Soc. Am.*, 92, 2233-2250.
- Mayer-Rosa D., Slejko D. and Zonno G.; 1990: Assessment of seismic hazard for the Sannio-Matese area, southern Italy. In: *Irpinia dieci anni dopo - Riassunti degli interventi*, pp. 149 - 152.
- McGuire R.K.; 1976: Fortran computer program for seismic risk analysis. U.S.G.S. Open File Report 76-67, 92 pp.
- McGuire R.K.; 1977: Seismic design spectra and mapping procedures using hazard analysis based directly on oscillator response. *Earthq. Engin. Struct. Dyn.*, 5, 211-234.
- McGuire R.K.; 1978: FRISK: computer program for seismic risk analysis using faults as earthquake sources. U.S.G.S. Open File Report 78-1007, 54 pp.
- McGuire R.K. (ed); 1993: The practice of earthquake hazard assessment. IASPEI ESC, Denver, 284 pp.
- McGuire R.K.; 1995: Probabilistic seismic hazard analysis and design earthquakes: closing the loop. *Bull. Seism. Soc. Am.*, 85, 1275-1284.
- McGuire R.K.; 2001: Deterministic vs. probabilistic earthquake hazards and risks. *Soil Dynamics and Earthquake Engineering*, 21, 377-384.
- McGuire R.K.; 2004: Seismic hazard and risk analysis. EERI MNO-10, Earthquake Engineering Research Institute, Oakland Ca, 221 pp.
- McGuire R.K. and Arabasz W.J.; 1990: An introduction to probabilistic seismic hazard analysis. In: Ward S.H. (ed), *Geotechnical and environmental geophysics*, Soc. Exploration Geophysicists, vol. 1, pp. 333-353.
- McGuire R.K. and Shedlock K.M.; 1981: Statistical uncertainties in seismic hazard evaluations in the United States. *Bull. Seism. Soc. Am.*, 71, 1287-1308.
- Meletti C., Galadini F., Valensise G., Stucchi M., Basili R., Barba S., Vannucci G., Boschi E.; 2008: A seismic source zone model for the seismic hazard assessment of the Italian territory. *Tectonophysics*, 450, 85-108.
- Meletti C., Patacca E. and Scandone P.; 2000: Construction of a seismotectonic model: the case of Italy. *Pure Appl. Geophys.*, 157, 11-35.
- Merz H.A. and Cornell C.A.; 1973: Seismic risk based on a quadratic magnitude-frequency law. *Bull. Seism. Soc. Am.*, 73, 1949-2006.
- Merz H.A. and Cornell C.A.; 1973: Aftershocks in engineering seismic risk analysis. Report R73-25, Dpt. Civil Engineering, Massachusetts Institute of Technology, Cambridge Ma.
- Milne J; 1900: Fifth report of the Committee on Seismological Investigation. Plate II. British Association for the Advancement of Science, London.

- Milne W.G. and Davenport A.G.; 1969: Distribution of earthquake risk in Canada. *Bull. Seism. Soc. Am.*, 59, 729-754.
- Ministro delle Infrastrutture; 2008: Decreto 14/01/2008 - Norme Tecniche per le Costruzioni. Ministero delle Infrastrutture, Roma, 438 pp.
- Mogi K; 1969: Some features of recent seismic activity in and near Japan (2) Activity before and after great earthquakes. *Bull. Earthq. Res. Inst.*, 47, 395-417.
- Mouroux P. and Le Brun B.; 2006: Presentation of RISK-UE Project. *Bull. Earthquake Engineering*, 4, 323-339, doi: 10.1007/s10518-006-9020-3.
- Moroni A. and Stucchi M.; 1993: Materials for the investigation of the 1564, Maritime Alps earthquake. In: Stucchi M. (ed), *Historical investigation of European earthquakes 1*, CNR, Milano, pp. 101-125.
- Muir-Wood R.; 1993: From global seismotectonics to global seismic hazard. *Annali di Geofisica*, 36, 153-168.
- Murphy A.J. and O'Brien L.J.; 1977: The correlation of peak ground acceleration amplitude with seismic intensity and other physical parameters. *Bull. Seism. Soc. Am.*, 67, 877-915.
- Musson R.M.W.; 2006: A short history of intensity and intensity scales. [http://www.earthquakes.bgs.ac.uk/hazard/History\\_intensity.htm](http://www.earthquakes.bgs.ac.uk/hazard/History_intensity.htm).
- Musson R.M.W., Toro G.R., Coppersmith K.J., Bommer J.J., Deichmann N., Bungum H., Cotton F., Scherbaum F., Slejko D. and Abrahamson N.A.; 2005: Evaluating hazard results for Switzerland and how not to do it: A discussion of "Problems in the application of the SSHAC probability method for assessing earthquake hazards at Swiss nuclear power plants" by J-U Klugel. *Engineering Geology*, 82, 43-55.
- Nasir A., Lenhardt W., Hintersberger E. and Decker K.; 2013: Assessing the completeness of historical and instrumental earthquake data in Austria and the surrounding areas. *Austrian Journal of Earth Sciences*, 106/1, 90-102.
- Newmark N.M. and Hall W.J.; 1982: *Earthquake spectra and design*. EERI Monograph, Earthquake Engineering Research Institute, Berkeley Ca., 103 pp.
- Nordquist J.M.; 1945: Theory of largest values applied to earthquake magnitudes. *Trans. Am. Geophys. Un.*, 26, 29-31.
- Nuttli O.W.; 1979: The relation of sustained maximum ground acceleration and velocity to earthquake intensity and magnitude. *Miscellaneous Paper S-73-1*, Report 16, U.S. Army Corps of Engineers Waterways Experiment Station, Vicksburg Mississippi, 74 pp.
- Omori F.; 1894: On the aftershocks of earthquakes. *Journal of the College of Science, Imperial University of Tokyo*, 7, 111-200.
- Ordaz M., Aguilar A. and Arboleda J.; 1999: CRISIS99 Program for computing seismic hazard, UNAM, Mexico.
- Panel on Seismic Hazard Evaluation; 1997: *Review of Recommendations for Probabilistic Seismic Hazard Analysis: Guidance on Uncertainty and Use of Experts*. National Academy Press, Washington DC, 73 pp.
- Paolucci R.; 2002: Amplification of earthquake ground motion by steep topographic irregularities. *Earthquake Engineering & Struct. Dyn.*, 31, 1831-1853.
- Petersen M.D., Bryant W.A., Cramer C.H., Cao T., Reichle M.S., Frankel A.D., Lienkaemper J.J., McCrory P.A. and Schwartz D.P.; 1996: Probabilistic seismic hazard assessment for the state of California. California Division of Mines and Geology Open-File Report 96-08, U.S. Geological Survey Open-File Report 96-706.
- Petersen M.D., Frankel A.D., Harmsen S.C., Mueller C.S., Haller K.M., Wheeler R.L., Wesson R.L., Zeng Y., Boyd O.S., Perkins D.M., Luco N., Field E.H., Wills C.J., and Rukstales K.S.; 2008: Documentation for the 2008 update of the United States national seismic hazard maps. U.S.G.S., Open-File Report 2008-1128, 61 pp.
- Petersen M.D., Moschetti M.P., Powers P.M., Mueller C.S., Haller K.M., Frankel A.D., Zeng Y., Rezaeian S., Harmsen S.C., Boyd O.S., Field N., Chen R., Rukstales K.S., Luco N., Wheeler R.L., Williams R.A. and Olsen A.H.; 2014: Documentation for the 2014 update of the United States national seismic hazard maps. Open-File Report 2014-1091, U.S. Geological Survey 243 pp.,
- Petrini V. (ed.); 1980: *Proposta di riclassificazione sismica del territorio nazionale*. C.N.R. P.F.Geodinamica pubbl. 361, ESA, Roma, 83 pp.
- Petrini V.; 1991: Il rischio sismico in Italia. In: Boschi E. (a cura di), *Il rischio sismico*, Le Scienze quaderni 59, Le Scienze S.p.A., Milano, pp. 3 - 5.
- Petrini V. (a cura di); 1995: *Pericolosità sismica e prime valutazioni di rischio in Toscana*. C.N.R. Ist. Ric. Rischio Sismico e Regione Toscana Dip. Ambiente, Firenze, 120 pp. + 28 tav.
- Petrini V., Bosi C., Bigi G., Eva C., Grandori G., Iaccarino E., Luongo G., Postpischl D., Praturlon A., Riuscetti M., Scandone P., Scarpa R., Stucchi M., Vezzani L.; 1981: *Carta della pericolosità sismica d'Italia*. C.N.R. P.F.Geodinamica, Pubbl. 442.
- Petrini V., Stucchi M. and Tento A.; 1987: *Classificazione sismica e revisione del catalogo sismico: analisi dell'influenza del catalogo sulla carta di pericolosità sismica ed alcune ipotesi per la revisione di quest'ultimo*. In: Boschi E. and Dragoni M. (a cura di), *Aree sismogenetiche e rischio sismico in Italia*. I. Galilei Ed., Lausanne, pp. 147 - 165.
- Reid H.F.; 1910: *The mechanics of the California earthquake of April 18, 1906: Report of the State Earthquake*



- Investigative Committee. Carnegie Institute, Washington DC.
- Reiter L.; 1990: Earthquake Hazard Analysis: issues and insights. Columbia University Press, New York, 252 pp.
- Richter C.F.; 1935: An instrumental earthquake magnitude scale. *Bull. Seism. Soc. Am.*, 25, 1-32.
- Richter C.F.; 1958: Elementary seismology. Freeman and Co., San Francisco, 768 pp.
- Rikitake T.; 1986: Earthquake premonitory phenomena: database for earthquake prediction. Tokyo Univ. Press, Tokyo, 232 pp.
- Rivera Z.C., Slejko D., Garcia J., Peruzza L., Rebez A. and Santulin M.; 2004: Seismic hazard of the Bayamo region (eastern Cuba) considering local soil typologies. *Boll. Geof. Teor. Appl.*, 45, 15-33.
- Riznichenko Y. V.; 1959: On quantitative determination and mapping of seismic activity. *Ann. Geof.*, 12, 227 - 237.
- Riznichenko Y.V., Zakharova A.I. and Seiduzova S.S.; 1969: Seismic activity and shakeability of the Apenninian region. *Boll. Geof. Teor. Appl.*, 11, 227-238.
- Rosenblueth E.; 1964: Probabilistic design to resist earthquakes. *J. Eng. Mech. ASCE*, 90, no. EM5, 189-220.
- Roth F.; 1988: Modelling of stress patterns along the western part of the North Anatolian fault zone. *Tectonophysics*, 152, 215-226.
- Sanchez-Sesma F.J. and Rosenblueth E.; 1979: Ground motion at canyons of arbitrary shape under incident SH waves. *Earthq. Engin. Struct. Dyn.*, 7, 441-450.
- Sarin R.K.; 1983: A social decision analysis of the earthquake safety problem: the case of existing Los Angeles buildings. *Risk Analysis*, 3, 35 - 50.
- Sauter F. and Shah H.C.; 1978: Estudio de seguro contra terremoto. Franz Sauter y Asociados Ltda, San José, Costa Rica, 250 pp.
- Schmid S.M. and Slejko D.; 2009: Seismic source characterization of the Alpine foreland in the context of a probabilistic seismic hazard analysis by PEGASOS Expert Group 1 (EG1a). *Swiss J. Geosci.*, 102, 121-148, DOI 10.1007/s00015-008-1300-2.
- Scholz C.H., Sykes L.R. and Aggarwal Y.P.; 1973: Earthquake prediction: a physical basis. *Science*, 181, 803-810.
- Schwartz D.P. and Coppersmith K.J.; 1984: Fault behavior and characteristic earthquakes: examples from the Wasatch and San Andreas fault zones. *J. Geophys. Res.*, 89, 5681-5698.
- Seed H.B., Mori K. and Chan C.K.; 1975: Influence of seismic history on the liquefaction characteristics of sands. Report EERC 75-25, Earthquake Engineering Research Center, University of California, Berkeley, 21 pp.
- Senior Seismic Hazard Analysis Committee; 1997: Recommendation for probabilistic seismic hazard analysis: guidance on uncertainty and use of experts. Lawrence Livermore National Laboratory, Livermore, 256 pp.
- Servizio Sismico del Consiglio Superiore dei Lavori Pubblici; 1986: Atlante della classificazione sismica nazionale. Ist.Poligrafico e Zecca dello Stato, Roma, 209 pp.
- Shimazaki K. and Nakata T.; 1980: Time-predictable recurrence model for large earthquakes. *Geophysical Research Letters*, 7, 279-282.
- Siccardi F.; 1991: Coping with floods: the Italian research policy. *Hazards '91 preprint*, 16 pp.
- Siro L. and Del Grosso A.; 1990: Local site control of ground motion parameters: state-of-the-art, advances in Italy from 1980 to present. In: *Irpinia dieci anni dopo - Riassunti degli interventi*, Tipolito La Sorrentina, Sorrento, pp. 102 - 112.
- Slejko D.; 1988: Rischio sismico = pericolosità sismica \* vulnerabilità \* valore. *Geologia Tecnica*, 3(2), 32 - 37.
- Slejko D., Carulli G.B., Ruscetti M., Cucchi F., Grimaz S., Rebez A., Accaino F., Affatato A., Biolchi S., Nieto D., Puntel E., Sanò T., Santulin M., Tinivella U. and Zini L.; 2011: Soil characterization and seismic hazard maps for the Friuli Venezia Giulia region (NE Italy). *Boll. Geof. Teor. Appl.*, 52, 59-104.
- Slejko D., Vezzoli D. and Gasparo F.; 1988: A methodological example for the assessment of the seismic risk. In: *Recent seismological investigations in Europe*, Nauka, Moscow, pp. 180 - 187.
- Slejko D., Peruzza L. and Rebez A.; 1998: Seismic hazard maps of Italy. *Annali di Geofisica*, 41, 183 - 214.
- Slemmons D.B.; 1977: Faults and earthquake magnitude. *Miscellaneous Paper S-73-1, Report 6, U.S. Army Corps of Engineers Waterways Experiment Station, Vicksburg Mississippi*, 129 pp.
- Solomos G., Pinto A. and Dimora S.; 2008: A review of the seismic hazard zonation in national building codes in the context of Eurocode 8. *JRC Scientific and Technical Reports, EUR23563EN-2008*, Ispra, 72 pp.
- Somerville P., Irikura K., Graves R., Sawada S., Wald D., Abrahamson N., Iwasaki Y., Kagawa T., Smith N., Kowada A.; 1999: Characterizing crustal earthquake slip models for the prediction of strong ground motion. *Seismological Research Letters*, 70, 59-80, DOI: 10.1785/gssrl.70.1.59.
- Sponheuer W.; 1960: Berechnungsverfahren mit Schrittwiseiger Nahorung. In: *Sponheuer W. (ed), Methoden zur Herdtiefen Bestimmung in der Makroseismic*, Freiburger Forshungshefte C88, Akademie Verlag, Berlin, pp. 16-32.
- Stepp J.C.; 1972: Analysis of completeness of the earthquake sample in the Puget Sound area and its effect on statistical estimates of earthquake hazard. In: *Proceedings of First Int. Conference on Microzonation*, Seattle Washington, vol. 2, pp. 897-910.

- Stegg J.C., Wong I., Whitney J., Quittmeyer R., Abrahamson N., Toro G., Youngs R., Coppersmith K., Savy J., Sullivan T. and Yucca Mountain PSHA Project Members; 2001: Probabilistic seismic hazard analyses for ground motion and fault displacement at Yucca Mountain, Nevada. *Earthquake Spectra*, 17, 113-151.
- Stewart J.P., Chiou S.-J., Bray J.D., Graves R.W., Somerville P.G. and Abrahamson N.A.; 2001: Ground motion evaluation procedures for performance-based design. Pacific Earthquake Engineering Research Center (PEER), Report 2001/9.
- Stucchi M. (coord.); 1988: Comune di Ancona. Indagine per la valutazione e la riduzione del rischio sismico. Consiglio Nazionale delle Ricerche, Roma, 77 pp.
- Stucchi M.; 1990: Informazioni macrosismiche e pericolosità sismica. In: *Irpinia dieci anni dopo - Riassunti degli interventi*, Tipolito La Sorrentina, Sorrento, pp. 141 - 145.
- Stucchi M.; 1994: Recommendations for the compilation of a European parametric earthquake catalogue, with special reference to historical records. In: Albini P. and Moroni A. (eds), *Historical investigation of European earthquakes 2*, CNR, Milano, pp. 181-190.
- Sykes L.R., Shaw B.E. and Scholz C.H.; 1999: Rethinking earthquake prediction. *Pure Appl. Geophys.*, 155, 207-232.
- Thier H.D.; 1990: Public perception of seismic risk: the education implications. In: *Irpinia dieci anni dopo - Riassunti degli interventi*, Tipolito La Sorrentina, Sorrento, pp. 186 - 188.
- Toro G.R., Abrahamson N.A. and Schneider J.F.; 1997: Model of strong motions from earthquakes in central and eastern North America: best estimates and uncertainties. *Seism. Res. Lett.*, 68, 41-57.
- Trifunac M.D. and Brady A.G.; 1975: A study of the duration of strong earthquake ground motion. *Bull. Seismol. Soc. Am.*, 65, 581-626.
- Utsu T.; 1961: A statistical study on the occurrence of aftershocks. *Geophys. Mag.*, 30, 521-605.
- Utsu T.; 1965: A method for determining the value of b in the formula  $\log N = a - bM$  showing the magnitude-frequency relation for earthquakes. *Geophys. Bull. Hokkaido Univ.*, 13, 99-103.
- Utsu T.; 1966: A statistical significance test of the difference in b-value between two earthquake groups. *J. Phys. Earth*, 14, 37-40.
- Vanini M., Corigliano M., Faccioli E., Figini R., L. Luzi L., F. Pacor F. and Paolucci R.; 2017: Improving seismic hazard approaches for critical infrastructures: a pilot study in the Po Plain. *Bull. Earthquake Eng.*, doi 10.1007/s10518-017-0102-1.
- Varotsos P. and Alexopoulos K.; 1984: Physical properties of the variations of the electric field of the earth preceding earthquakes, I. *Tectonophysics*, 110, 73-98.
- Veneziano D.C., Cornell A. and O'Hara T.; 1984: Historical method of seismic hazard analysis. Rep. NP-3428, Palo Alto, California.
- Von Thun J.L., Rochim, L.H., Scott G.A. and Wilson J.A.; 1988: Earthquake Ground Motions for Design and Analysis of Dams. In: *Earthquake Engineering and Soil Dynamics II - Recent Advance in Ground Motion Evaluation*, ASCE, New York, NY.
- Wadati K.; 1932: On the frequency distribution of earthquakes. *J. Meteorol. Soc. Japan*, 10, 559-568 (in Japanese).
- Wald D.J., Quitoriano V., Heaton T.H. and Kanamori H.; 1999: Relationships between peak ground acceleration, peak ground velocity, and Modified Mercalli intensity in California. *Earthquake Spectra*, 15, 557-564.
- Webster's; 1977: *New Collegiate Dictionary*. G. & C. Merriam Co., Springfield.
- Weichert D.H.; 1980: Estimation of the earthquake recurrence parameters for unequal observation periods for different magnitudes. *Bull. Seism. Soc. Am.*, 70, 1337-1346.
- Wells D.L. and Coppersmith K.J.; 1994: New empirical relationship among magnitude, rupture length, rupture width, rupture area, and surface displacement. *Bull. Seism. Soc. Am.*, 84, 974-1002.
- Wesnously S.G.; 1994: The Gutenberg - Richter or characteristic earthquake distribution, which is it? *Bull. Seism. Soc. Am.*, 84, 1940-1959.
- Wesnously S.G., Scholz C.H., Shimazaki K. and Matsude T.; 1984: Integration of geological and seismological data for the analysis of seismic hazard: a case study of Japan. *Bull. Seism. Soc. Am.*, 74, 687-708.
- Whitman R.V. and Cornell C.A.; 1976: Design. In: Lomnitz C. and Rosenblueth E. (eds), *Seismic risk and engineering decisions*, Elsevier, Amsterdam, pp. 339-380.
- Woo G.; 1996: Kernel estimation methods for seismic hazard area source modeling. *Bull. Seism. Soc. Am.*, 86, 353-362.
- Working Group on California Earthquake Probabilities; 1990: Probabilities of large earthquakes in the San Francisco bay region, California. U.S.G.S. circular 1053, U.S.G.S., Denver, 51 pp.
- Working Group on California Earthquake Probabilities; 2003: Earthquake Probabilities in the San Francisco Bay Region: 2002-2031. United States Geological Survey Open-File Report 03-214, 234 pp.
- Wu S. C., Cornell C. A. and Winterstein S. R.; 1995: A hybrid recurrence model and its implication on seismic hazard results. *Bull. Seism. Soc. Am.*, 85, 1 - 16.
- Wyss M.; 1979: Estimating maximum expected magnitude of earthquakes from fault dimensions. *Geology*, 7(7), 336-340.

- Wyss M.; 1991: Evaluation of earthquake precursors. In: IUGG, Vienna, August 1991.
- Yang W.S., Slejko D. e Viezzoli D.; 1986: Matrice di vulnerabilità per il calcolo del rischio sismico. Atti 5 Convegno GNGTS, 301 - 307.
- Yang W.S., Slejko D., Viezzoli D. and Gasparo F.; 1989: Seismic risk in Friuli-Venezia Giulia: an approach. Soil Dynamics and Earthquake Engineering, 8, 96 - 105.
- Youngs R.R. and Coppersmith K.J.; 1985: Implications of fault slip rates and earthquake recurrence models to probabilistic seismic hazard assessments. Bull. Seism. Soc. Am., 75, 939-964.
- Youngs R.R., Day S.M. and Stevens J.L.; 1988: Near field ground motions on rock for large subduction earthquakes. In: Proceedings Earthquake Engineering and Soil Dynamics 2: Recent advances in ground motion evaluation, Geotechnical Special Publ. 20, ASCE, New York, pp. 445-462.

## **Appendix A**

### **Glossary of Interest to Earthquake and Engineering Seismologists**

K. Aki and W. H. K. Lee (2003)

In: W. H. K. Lee, H. Kanamori, P. C. Jennings and C. Kisslinger (eds.), International Handbook of Earthquake and Engineering Seismology, part B, published by Academic Press, Appendix 1

#### **Key glossary:**

- Ground motion** - The vibration of the ground primarily due to earthquakes. It is measured by seismograph that records acceleration, velocity, or displacement. In engineering seismology, it is usually given in terms of a time series (an accelerogram), a response spectrum, or a Fourier spectrum.
- Ground motion parameter** - A parameter characterizing ground motion, such as peak acceleration, peak velocity, and peak displacement (peak parameters), or ordinates of response spectra and Fourier spectra (spectral parameters).
- Seismic hazard** - Any physical phenomenon associated with an earthquake (e.g., ground motion, ground failure, liquefaction, and tsunami) and its effects on land use, man-made structures, and socioeconomic systems that have the potential to produce a loss. It is also used without regard to a loss to indicate the probable level of ground shaking occurring at a given point within a certain period of time.
- Seismic hazard analysis (SHA)** - The calculation of the seismic hazard, expressed in probabilistic terms, as contrasted with deterministic seismic hazard analysis, for a site or group of sites. The result is usually displayed as a seismic hazard curve or seismic hazard map.
- Seismic hazard curve** - A plot of probabilistic seismic hazard (usually specified in terms of annual probability of exceedance) or return period versus a specified ground-motion parameter for a given site.
- Seismic hazard map** - A map showing contours of a specified ground-motion parameter or response-spectrum ordinate for a given probabilistic seismic hazard or return period.
- Seismic risk** - The risk to life and property from earthquakes. In probabilistic risk analysis, it is the probability that a specified loss will exceed some quantifiable level during a given exposure time.
- Seismic risk analysis (SRA)** - The calculation of seismic risk for a given property, or portfolio of properties, usually performed in a probabilistic framework and displayed as a seismic risk curve or seismic risk map.

**Seismic risk curve** - A plot of seismic risk (usually specified in terms of annual probability of exceedance or return period) versus a specified loss for a given property or portfolio of properties.

**Strong ground motion** - A ground motion having the potential to cause significant risk to structure's architectural or structural components, or to its contents. One common practical designation of strong ground motion is a peak ground acceleration of 0.05g or large. Here g is a commonly used unit for the acceleration due to the gravity of the Earth; and gal, being 1 cm/s<sup>2</sup>, is approximately one-thousandth of 1g.

**Strong motion parameter** - A parameter characterizing the amplitude of strong ground motion in the time domain (time domain parameter) or frequency domain (frequency domain parameter).

### **Technique terms:**

**Accelerograph** - A seismograph designed to record acceleration, especially for strong ground shaking caused by large earthquakes nearby. Incorporating analog or digital recoding, a traditional strong-motion accelerograph begins recording when the motion exceeds a certain specified trigger level. At present, some seismic networks record high-dynamic-range acceleration continuously at free-field sites or in building structures.

**Accelerometer** - An acceleration sensor, or transducer, that converts ground acceleration to an electrical signal, typically voltage, proportional to the acceleration. In early analog accelerographs, the accelerometer converted acceleration to movements of a light beam. Accelerometers may be within an accelerograph, but for studies of structural systems, they are typically located remotely and their signals transmitted (usually by cables) to a central recorder.

**Active fault** - A fault that has moved in historic (e.g., past 10,000 years) or recent geological time (e.g., past 500,000 years). Although faults that move in earthquakes today are active, not all active faults generate earthquakes - some are capable of moving aseismically.

**Active tectonic regime** - A term that refers to regions where tectonic deformation is relatively large and earthquakes are relatively frequent, usually near plate boundaries.

**Active tectonics** - The tectonic movements that are expected to occur or that have occurred within a time span of concern to society.

**Aleatory uncertainty** - The uncertainty in seismic hazard analysis due to inherent random variability of the quantity being measured. Aleatory uncertainties cannot be reduced by refining modeling of analytical techniques.

**Alluvium** - The loose gravel, sand, silt, or clay deposited by streams after the last ice age.

- Amplification** - The term used for describing the increase of amplitudes of seismic waves due to the recording site's condition.
- Annual probability of exceedance** - The probability that a given level of seismic hazard (typically some measure of ground motions, e.g., seismic magnitude or intensity) or seismic risk (typically economic loss or casualties) can be equaled or surpassed within an exposure time of one year.
- Attenuation relationship** - A mathematical expression that relates a ground-motion parameter, such as the peak ground acceleration, to the source and propagation path parameters of an earthquake such as the magnitude, source-to-site distance, or fault type. Its coefficients are usually derived from statistical analysis of earthquake records. It is a common engineering term for a ground motion relation.
- Base isolation** - A technique to reduce earthquake forces in a structure by the installation of horizontally flexible devices at the foundation level. Such devices greatly increase the lowest natural periods of the structure for horizontal motions and thereby lower the accelerations experienced by the structure. The most common applications of base isolation are to old historic buildings, hospitals, and bridges.
- Bedrock** - A relatively hard, solid rock that commonly underlies soil or other unconsolidated materials.
- Blind fault** - A fault that does not extend upward to the Earth's surface. It usually terminates upward in the axial region of an anticline. If its dip is less than 45 degrees, it is a blind thrust.
- b-value** - A coefficient in the frequency-magnitude relation,  $\log N(M) = a - bM$ , obtained by Gutenberg and Richter, where  $M$  is the earthquake magnitude and  $N(M)$  is the number of earthquakes with magnitude greater than or equal to  $M$ .
- Capable fault** - A mapped fault that is deemed a possible site for a future earthquake with magnitude greater than some specified threshold. - In nuclear reactor siting, a fault capable of surface rupture but which may or may not generate earthquakes.
- Catalogue of earthquakes** - A chronological listing of earthquakes. Early catalogues were purely descriptive, giving the date of earthquakes and some descriptions of its effects. Modern catalogues are usually quantitative, listing a set of parameters describing the origin time, hypocenter location, magnitude, moment tensor, etc.
- Corner frequency** - In earthquake source studies, a parameter characterizing the far-field body-wave displacement spectrum.
- Corrected acceleration** - An acceleration time history that has been 'corrected' from the raw data recorded by an accelerograph. The correction typically involves removing drift, spikes, and any distorting effects created by the instrument or digitizing process.



- Critical facility** - A man-made structure whose ongoing performance during an emergency is required or whose failure could threaten many lives. This may include: 1) structures such as nuclear-power reactors or large dams whose failure might be catastrophic; 2) major communication, utility, and transportation systems; 3) high-occupancy buildings such as schools or offices; and 4) emergency facilities such as hospitals, police and fire stations, and disaster-response centers.
- Damage scenario** - A representation of the possible damage caused by an earthquake to the built environment in an area, in terms of parameters useful for economical and engineering assessment or post-earthquake emergency management.
- Design ground motion** - A level of ground motion used in structural design. It is usually specified by one or more specific strong-motion parameters or by one or more time series. The structure is designed to resist this motion at a specified level of response, for example, within a given ductility level.
- Design spectrum** - The specification of the required strength or capacity of the structure plotted as a function of the natural period or frequency of the structure and of the damping appropriate to earthquake response at the required level. Design spectra are often composed of straight-line segments and/or simple curves (e.g., as in most building codes), but they can also be constructed from statistics of response spectra of a suite of ground motions appropriate to the design earthquake/s. To be implemented, the requirements of a design spectrum are associated with allowable levels of stresses, ductilities, displacements, or other measures of response.
- Deterministic earthquake scenario** - A representation, in terms of useful descriptive parameters, of an earthquake of specified size postulated to occur at a specified location (typically an active fault), and of its effects.
- Ductility** - The property of a structure or a structural component that allows it to continue to have significant strength after it has yielded or begun to fail. Typically, a well-designed ductile structure or component will show, up to a point, increasing strength as its deflection increases beyond yielding, or cracking in the case of reinforced concrete or masonry.
- Dynamic range** - The amplitude ratio between the smallest and the largest signal that can be faithfully recorded by a system, usually expressed in decibels.
- Empirical Green's function method** - A method for calculating strong ground motion for a large earthquake using actual records of small earthquakes originating on or near the fault plane of the large one, with Green's function representing the propagation-path effect.
- Epistemic uncertainty** - The uncertainty in seismic hazard analysis due to imperfect knowledge in model parametrization and other limitations of the methods employed. Epistemic uncertainty can be reduced by improvements in the modeling and analysis.

- f<sub>max</sub>** - Above a limiting frequency,  $f_{max}$ , the observed spectrum of a typical local earthquake decays more steeply with increasing frequency than is expected from the standard omega-squared model.
- Focusing effect** - The special amplification of ground motion found just above the corner of the basin bottom or layer interfaces. In a 2D or 3D basin with strong lateral variation, rays of an incident body wave are warped at these interfaces, and constructive (or destructive) interference takes place at some point on the surface.
- Free-field motion** - A strong ground motion that is not modified by the earthquake-caused motions of nearby buildings or other structures or geologic features. In analyses, it is often defined as the motion that would occur at the interface of the structure and the foundation if the structure were not present. A fully instrumented building site typically includes one or more accelerographs located some distance from the structure to obtain a better approximation of the free-field motion.
- Great earthquake** - An earthquake with magnitude greater than about 7 3/4 or 8.
- Ground failure** - A permanent deformation of the ground, e.g., liquefaction, fault displacement, and landslides, typically resulting from an earthquake capable of causing damage to engineered structures.
- Ground-shaking scenario** - A representation for a site or region depicting the possible ground-shaking level or levels due to earthquake in terms of useful descriptive parameters.
- H/V spectral ratio** - The ratio of the Fourier amplitude spectra of horizontal and vertical components of ambient noise, or of earthquake ground motions, recorded at a site, typically used to identify the presence of site-specific dominant frequencies in such motions. If this technique is applied to microtremor data, it is sometimes called Nakamura's method.
- Intensity** - Non-instrumental measure of the strength of earthquake motion. The values in an intensity scale are pegged to observed physical damage or perceived motions.
- Isoseismal** - A closed curve bounding the area within which the intensity from a particular earthquake was predominantly equal to or higher than a given value.
- Liquefaction** - The transformation of a granular material from a solid state into a liquefied state as a consequence of increased pore water pressures and reduced effective stress. In engineering seismology, it refers to the loss of soil strength as a result of an increase in pore pressure due to ground motion.
- Local site conditions** - A qualitative or quantitative description of the topography, geology, and soil profile at a site that affect ground motions during an earthquake.

- Macroseismology** - The study of any effects of earthquakes that are observable without instruments, such as felt by people, landslides, fissures, and knocked-down chimneys.
- Maximum probable earthquake (MPE)** - The maximum earthquake that could strike a given area with a significant probability of occurrence.
- Microzonation** - The identification and mapping at local or site scales of areas having different potentials for hazardous earthquake effects, such as ground-shaking intensity, liquefaction, or landslide potential.
- Moderate earthquake** - An earthquake with magnitude ranges from 5 to 7.
- Omega-squared model** - A widely used model of earthquake source associated with the far-field body wave characterized by the displacement amplitude spectrum having the flat low-frequency part and the high-frequency power-law decay (with the power of -2) part separated by the corner frequency. The height of the flat part is proportional to the seismic moment, and the corner frequency is inversely proportional to the linear dimension of the source.
- Peak ground acceleration (PGA)** - The maximum acceleration amplitude measured or expected in a strong-motion accelerogram of an earthquake.
- Probabilistic earthquake scenario** - A representation, in terms of useful descriptive parameters, of earthquake effects with a specified probability of exceedance during a prescribed period in an area.
- Probabilistic seismic hazard analysis (PSHA)** - Available information on earthquake sources in a given region is combined with theoretical and empirical relations among earthquake magnitude, distance from the source, and local site conditions to evaluate the exceedance probability of a certain ground-motion parameter, such as the peak acceleration, at a given site during a prescribed period.
- Probability of exceedance** - The probability that, in a given area or site, an earthquake ground motion will be greater than a given value during some time period.
- Probable maximum loss** - A probable upper limit of the losses that are expected to occur as a result of a damaging earthquake, normally defined as the largest monetary loss associated with one or more earthquakes proposed to occur on specific faults or within specific source zones.
- Response spectrum** - The maximum response to a specified acceleration time series of a set of single-degree-of-freedom oscillators with chosen levels of viscous damping, plotted as a function of the undamped natural period or undamped natural frequency of the system. The response spectrum is used for the prediction of the earthquake response of buildings or other structures.

- Return period** - The average time between exceedance of a specified level of ground motion at a specified location, equal to the inverse of the annual probability of exceedance.
- Seismicity** - A term introduced by Gutenberg and Richter to describe quantitatively the space, time, and magnitude distribution of earthquake occurrences. Seismicity within a specific source zone or region is usually quantified in terms of a Gutenberg-Richter relationship.
- Seismic zonation** - The geographic delineation of areas having different potentials for hazardous effects from future earthquakes. Seismic zonation can be done at any scale, national, regional, local, or site, the latter two often referred to as micrization.
- Seismic zoning map** - A map used to portray seismic hazard or seismic design variables, for example, maps used in building codes to identify areas of uniform seismic design requirements.
- Site category** - The category of site geologic conditions affecting earthquake ground motions based on descriptions of the geology, measurements of the S-wave velocity standard penetration test, shear strength, or other properties of the subsurface. For example, the site geologic condition is classified into categories from A (hard rock) to F (very soft soil), and different amplification factors are assigned for them.
- Site classification** - The process of assigning a site category to a site by means of geologic properties (e.g., crystalline rock or Quaternary deposits) or by means of a geotechnical characterization of the soil profile (e.g., standard penetration test and S-wave velocity).
- Site effect** - The effect of local geologic and topographic conditions at a recording site on ground motions. It is implicitly assumed that the source, path, and site effects on ground motions are separable.
- Site response** - The modification of earthquake ground motion in the time or frequency domain caused by local site conditions.
- Small earthquake** - An earthquake with magnitude ranges from 3 to 5.
- Synthetic ground motion** - The time history of a strong ground motion, calculated for engineering purposes by a deterministic or stochastic simulation.
- Time history** - An engineering term for a seismogram or a time-dependent response. Examples include an accelerogram and the displacement of point in a structure.
- Topographic site effect** - A site effect caused by surface irregularities such as canyons or mountains. In practice, it is difficult to separate topographic effects from effects caused by subsurface layering.
- Two-D site amplification** - A site effect calculated for a geologic structure varying in a vertical direction and in only one horizontal direction. In a purely 2D case, incident waves are assumed to be homogeneous along the same

horizontal direction. The case in which the incident wave field is allowed to be 3D, such as spherical waves, is sometimes called 2.5D.

## Appendix B

### U.S. Nuclear Regulatory Commission Regulatory Guide 1.165 - Appendix A - Definitions

**Controlling Earthquakes** -- Controlling earthquakes are the earthquakes used to determine spectral shapes or to estimate ground motions at the site. There may be several controlling earthquakes for a site. As a result of the probabilistic seismic hazard analysis (PSHA), controlling earthquakes are characterized as mean magnitudes and distances derived from a deaggregation analysis of the median estimate of the PSHA.

**Earthquake Recurrence** -- Earthquake recurrence is the frequency of occurrence of earthquakes having various magnitudes. Recurrence relationships or curves are developed for each seismic source, and they reflect the frequency of occurrence (usually expressed on an annual basis) of magnitudes up to the maximum, including measures of uncertainty.

**Intensity** -- The intensity of an earthquake is a measure of vibratory ground motion effects on humans, on human-built structures, and on the earth's surface at a particular location. Intensity is described by a numerical value on the Modified Mercalli scale.

**Magnitude** -- An earthquake's magnitude is a measure of the strength of the earthquake as determined from seismographic observations.

**Maximum Magnitude** -- The maximum magnitude is the upper bound to recurrence curves.

**Nontectonic Deformation** -- Nontectonic deformation is distortion of surface or near-surface soils or rocks that is not directly attributable to tectonic activity. Such deformation includes features associated with subsidence, karst terrane, glaciation or deglaciation, and growth faulting.

**Safe Shutdown Earthquake Ground Motion (SSE)** -- The SSE is the vibratory ground motion for which certain structures, systems, and components are designed, pursuant to Appendix S to 10 CFR Part 50, to remain functional.

The SSE for the site is characterized by both horizontal and vertical free-field ground motion response spectra at the free ground surface.

**Seismic Potential** -- A model giving a complete description of the future earthquake activity in a seismic source zone. The model includes a relation giving the frequency (rate) of earthquakes of any magnitude, an estimate of the largest earthquake that could occur under the current tectonic regime, and a complete description of the uncertainty. A typical model used for PSHA is the use of a truncated exponential model for the magnitude distribution and a stationary Poisson process for the temporal and spatial occurrence of earthquakes.

**Seismic Source** -- Seismic source is a general term referring to both seismogenic sources and capable tectonic sources.



**Capable Tectonic Source** -- A capable tectonic source is a tectonic structure that can generate both vibratory ground motion and tectonic surface deformation such as faulting or folding at or near the earth's surface in the present seismotectonic regime. It is described by at least one of the following characteristics:

- a. Presence of surface or near-surface deformation of landforms or geologic deposits of a recurring nature within the last approximately 500,000 years or at least once in the last approximately 50,000 years.
- b. A reasonable association with one or more moderate to large earthquakes or sustained earthquake activity that are usually accompanied by significant surface deformation.
- c. A structural association with a capable tectonic source having characteristics of either section a or b in this paragraph such that movement on one could be reasonably expected to be accompanied by movement on the other.

In some cases, the geological evidence of past activity at or near the ground surface along a potential capable tectonic source may be obscured at a particular site. This might occur, for example, at a site having a deep overburden. For these cases, evidence may exist elsewhere along the structure from which an evaluation of its characteristics in the vicinity of the site can be reasonably based. Such evidence is to be used in determining whether the structure is a capable tectonic source within this definition.

Notwithstanding the foregoing paragraphs, the association of a structure with geological structures that are at least pre-Quaternary, such as many of those found in the Central and Eastern regions of the United States, in the absence of conflicting evidence will demonstrate that the structure is not a capable tectonic source within this definition.

**Seismogenic Source** -- A seismogenic source is a portion of the earth that we assume has uniform earthquake potential (same expected maximum earthquake and recurrence frequency), distinct from the seismicity of the surrounding regions. A seismogenic source will generate vibratory ground motion but is assumed not to cause surface displacement. Seismogenic sources cover a wide range of possibilities from a well-defined tectonic structure to simply a large region of diffuse seismicity (seismotectonic province) thought to be characterized by the same earthquake recurrence model. A seismogenic source is also characterized by its involvement in the current tectonic regime (the Quaternary, or approximately the last 2 million years).

**Stable Continental Region** -- A stable continental region (SCR) is composed of continental crust, including continental shelves, slopes, and attenuated continental crust, and excludes active plate boundaries and zones of currently active tectonics directly influenced by plate margin processes. It exhibits no significant deformation associated with the major Mesozoic-to-Cenozoic (last 240 million years) orogenic belts. It excludes major zones of Neogene (last 25 million years) rifting, volcanism, or suturing.

**Stationary Poisson Process** -- A probabilistic model of the occurrence of an event over time (space) that is characterized by (1) the occurrence of the event in small intervals is constant over time (space), (2) the occurrence of two (or more) events in a small interval is negligible, and (3) the occurrence of the event in non-overlapping intervals is independent.

**Tectonic Structure** -- A tectonic structure is a large-scale dislocation or distortion, usually within the earth's crust. Its extent may be on the order of tens of meters (yards) to hundreds of kilometers (miles).



## C. BASICS OF STATISTICS AND PROBABILITY CONCEPTS

Earthquake engineering problems are fraught with uncertainty. At a particular site, earthquake-induced loading depends on the size and location of the earthquake, none of which can be predicted with certainty. Because of the inherent variability of soils and the inevitable limits on exploration of subsurface conditions, the resistance of the soil to that loading is not known with certainty. When both loading and resistance are uncertain, the resulting effects are uncertain as well. A number of earthquake engineering analyses attempt to quantify the uncertainty in the various input parameters for a particular problem, and compute the resulting uncertainty in the output.

If the degree of uncertainty of a parameter is small or its consequence is not significant, uncertainty is generally neglected and the "best estimate" is taken as value of the parameter. If the uncertainty is significant, a "cautious estimate" is generally taken (e.g.: its minimum or maximum value). Sometimes it is not easy to guess the influence of the uncertainties and we are not ed to consider simply "best" or "cautious" estimates. The definition and quantification of uncertainties are, then, necessary by the use of statistics and probability theory.

In this appendix, a brief introduction to some basic concepts of probability is provided and several probability distributions used in engineering seismology are described.

### C.1. Ways of representing a data set

The first step for the identification of the uncertainties related to our problem consists in the detailed analysis of the data set. As a non-ranked list of measurements is not easily readable, a first step consists in producing frequency histograms. The relative frequency histogram of a set of  $n$  data points  $x_1, \dots, x_n$  is obtained by dividing the variability range of the data in classes and computing the ratio between the number  $n_i$  of the data in each class and the total number of data:

$$f_i = n_i/n \quad (C-1)$$

The relative cumulative frequencies are the frequencies of all data lower than the upper border of each class

$$F_i = \sum_{k=1}^i f_k. \quad (C-2)$$

The choice of the number of classes is very important: an empiric rule suggests  $(1+3.3 \log n)$  classes of equal amplitude, where  $n$  is the number of data.

Some particular values can represent the whole data set. They are:

- the arithmetic mean value

$$\bar{x} = \frac{\sum_{i=1}^n x_i}{n} \quad (C-3)$$

or, if the data are grouped

$$\bar{x} = \sum_{i=1}^n x_i f_i; \quad (\text{C-4})$$

- the modal value, that is the most frequent value in the data set;
- the median value, that is the central value of the data or the mean value of the two central data.

The behaviour of the data around the mean value is called dispersion and can be measured by the following parameters:

- the variance  $\sigma^2 = \frac{\sum_{i=1}^n (x_i - \bar{x})^2}{n}$  (C-5)

or, if the data are grouped  $\sigma^2 = \sum_{i=1}^n (x_i - \bar{x})^2 f_i;$  (C-6)

- the standard deviation  $\sigma = \sqrt{\sigma^2};$  (C-7)

- the variation coefficient  $v = \frac{\sigma}{\bar{x}};$  (C-8)

that is independent from the measure unit

- the order k moment  $\sigma^k = \frac{\sum_{i=1}^n (x_i - \bar{x})^k}{n};$  (C-9)

- the skewness  $\frac{s^3}{\sigma^3}$  (C-9bis)

that measures the asymmetry of data around the mean value (if positive the queue is longer to the right and viceversa);

- the kurtosis  $\frac{s^4}{\sigma^4}$  (C-9ter)

that measures the steepness of the data around the mean value (the bell shaped normal curve has a kurtosis equal to 3, flatter curves have lower kurtosis).

If our data are function of two variables,  $x$  and  $y$ , their tendency to group in sectors of the  $xy$  plane is measured by the covariance

$$S_{xy} = \frac{1}{n} \sum_{i=1}^n (x_i - \bar{x})(y_i - \bar{y}). \quad (\text{C-10})$$

The correlation coefficient

$$r_{xy} = \frac{S_{xy}}{\sigma_x \sigma_y} = \frac{1}{n} \sum_{i=1}^n \left( \frac{x_i - \bar{x}}{\sigma_x} \right) \left( \frac{y_i - \bar{y}}{\sigma_y} \right) \quad (\text{C-11})$$

varies between -1 and +1 and assumes the extreme values when the data are aligned. Values around 0 indicate that the data are not linearly correlated but they can be grouped around a higher order curve.

## C.2. Sample spaces and events

Experiments are a basic approach in science and a fundamental principle states that experiments done in the same conditions lead to the same results. There are experiments, viceversa, that although done in the same conditions lead to different results: they are called random experiments. Probability theory deals with the results, or outcomes, of those kinds of experiments. The set of all possible outcomes of an experiment is called the sample space, and each outcome of an experiment is called a sample point. The sample space therefore consists of all possible sample points. The sample space may be continuous, in which case the number of sample points is infinite, or it may be discrete, as when the number of sample points are finite and countable.

An event is a subset of a sample space, and therefore represents a set of sample points. A single (or elementary) event consists of a single sample point, and a compound event consists of more than one sample point. If  $\Omega$  represents a sample space and  $A$  represents an event, the complementary event,  $\bar{A}$ , is the set of all sample points in  $\Omega$  that are not in  $A$ . The interrelationships among sets can be conveniently illustrated by means of a Venn diagram (Fig. C.1). In Fig. C.1 the sample space is represented by the rectangle  $\Omega$  and the event  $A$  by the circle. Thus  $A$  is a subset of  $\Omega$ . The complementary event corresponds to the part of the rectangle that lies outside the circle. Because no sample points are in both  $A$  and  $\bar{A}$ , the intersection of  $A$  and  $\bar{A}$  is the null set, (i.e.,  $A \cap \bar{A} = \emptyset$ ). Similarly, all sample points are in either  $A$  or  $\bar{A}$ , so the union of  $A$  and  $\bar{A}$  is  $\Omega$  (i.e.,  $A \cup \bar{A} = \Omega$ ). Two events,  $A$  and  $B$ , are said to be mutually exclusive if they share no common sample points (i.e.,  $A \cap B = \emptyset$ ).

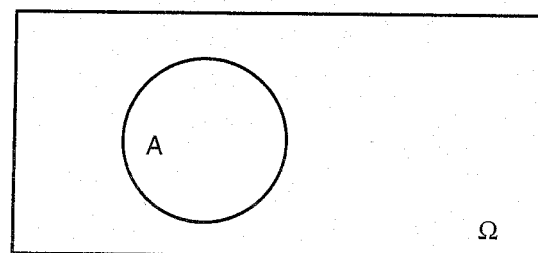


Fig. C.1 - Venn diagram illustrating event  $A$  in sample space  $\Omega$ .

## C.3. Axioms of probability

A probability measure,  $P$ , can be assigned to each sample point or set of sample points in a sample space. The probability of an event  $A$  is denoted by the symbol  $P[A]$ . There are three important approaches to estimate the probability of an event.



1) The classic or "a priori" approach states that if an event can happen in  $h$  different ways over  $n$  that are equally possible, then the probability of that event is  $h/n$ .

2) The "frequency" or "a posteriori" approach states that if the experiment is repeated  $n$  times, with  $n$  very large, and an event occurs  $h$  times, then the probability of that event is  $h/n$ .

3) The "axiomatic" approach uses the set theory and is based on the following three fundamental axioms.

**Axiom 1.** The probability of an event is represented by a number greater than or equal to zero but less than or equal to 1:

$$\forall A, 0 \leq P[A] \leq 1 \quad (\text{C-12a})$$

**Axiom 2.** The probability of an event equal to the entire sample space  $\Omega$  is 1:

$$P[\Omega] = 1 \quad (\text{C-12b})$$

**Axiom 3.** The probability of an event representing the union of  $n$  mutually exclusive events is equal to the sum of the probabilities of the events:

$$P[A_1 \cup A_2 \cup A_3 \cup \dots \cup A_n] = P[A_1] + P[A_2] + P[A_3] + \dots + P[A_n].$$

In the case of two mutually exclusive events:

$$P[A \cup B] = P[A] + P[B] \quad (\text{C-12c})$$

These axioms can be used to develop the rules and theorems that comprise the mathematical theory of probability.

Moreover, some theorems are fundamental in the probability theory:

- if  $A_1 \subset A_2$ , then  $P[A_1] \leq P[A_2]$  and  $P[A_2 - A_1] = P[A_2] - P[A_1]$ ;
- $P[\bar{A}] = 1 - P[A]$  and, consequently,  $P[\emptyset] = 1 - P[\Omega] = 1 - 1 = 0$ ; that is the impossible event has probability null;
- if  $A = A_1 \cup A_2 \cup \dots \cup A_n$ , where  $A_1, A_2, \dots, A_n$  are mutually exclusive and  $A = \Omega$ , the sample space, then
 
$$P[\Omega] = P[A] = P[A_1] + P[A_2] + \dots + P[A_n] = 1;$$
- if  $A$  and  $B$  are two general events
 
$$P[A \cup B] = P[A] + P[B] - P[A \cap B]$$
 and if  $A_1, A_2, A_3$  are three general events
 
$$P[A_1 \cup A_2 \cup A_3] = P[A_1] + P[A_2] + P[A_3] - P[A_1 \cap A_2] - P[A_2 \cap A_3] - P[A_3 \cap A_1] + P[A_1 \cap A_2 \cap A_3];$$
- if  $A$  and  $B$  are two general events
 
$$P[A] = P[A \cap B] + P[A \cap \bar{B}];$$
- if the event  $A$  follows from one of the mutually exclusive events  $A_1, A_2, \dots, A_n$  then
 
$$P[A] = P[A \cap A_1] + P[A \cap A_2] + \dots + P[A \cap A_n].$$

### C.4. Probabilities of events

Probabilities are often thought of in terms of relative frequencies of occurrence. If the existence of a water content greater than the optimum water content in a compacted fill is considered to be an event, the probability of that event can be estimated by determining the relative frequency of water content measurements that exceed the water content. If the total number of water content measurements is small, the relative frequency may only approximate the actual probability, but as the number of measurements becomes large, the relative frequency will approach the actual probability. This frequentist point of view is not very helpful, however, for situations in which an experiment cannot be repeated. In such cases, probabilities can be viewed as relative likelihoods (or degrees of belief), as in the probability that a newly discovered fault is capable of producing maximum earthquake magnitudes of 7.0 or 7.5. The latter interpretation lends itself to the subjective evaluation of probability.

Regardless of how probabilities are interpreted, the axioms of probability allow statements to be made about the probabilities of occurrence of single or multiple events. These can be visualized with the help of *Venn diagrams* drawn such that the area of the rectangle representing the sample space  $\Omega$  is 1 and the areas of all events within the sample space are equal to their probabilities. Consider the nonexclusive events  $A$  and  $B$  in Fig. C.2. The event  $A \cap B$  (which means that *both A and B* occur) is represented by the shaded region in Fig. C.2a;  $P[A \cap B]$  is given by the area of the shaded region. The event  $A \cup B$  (which means that either  $A$  or  $B$  occurs) is represented by the shaded region in Fig. C.2b;  $P[A \cup B]$  is given by the area of that shaded region, or

$$P[A \cup B] = P[A] + P[B] - P[A \cap B] \quad (\text{C-13})$$

In many instances, the probability of one event depends on the occurrence of another event. The conditional probability of event  $A$  given the occurrence of event  $B$  is denoted  $P[A|B]$  and is defined (for  $P[B > 0]$ ) by

$$P[A|B] = P[A \cap B] / P[B] \quad (\text{C-14})$$

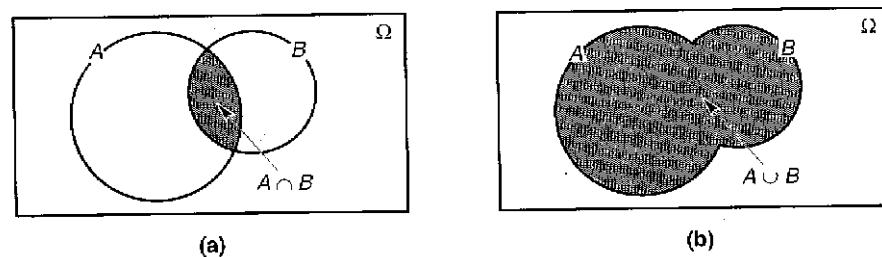


Fig. C.2 - Venn diagrams for events  $A$  and  $B$  in sample space  $\Omega$ : a) the set  $A \cap B$  is given by the shaded area; if the area of  $\Omega$  is 1,  $P[A \cap B]$  is equal to the area that is shaded; b) the set  $A \cup B$  is given by the shaded area;  $P[A \cup B]$  is equal to the shaded area.

The conditional probability is easily visualized with the Venn diagram (Fig. C.2a) as the ratio of the area of  $A \cap B$  to the area of  $B$ . Event  $A$  is statistically independent of event  $B$  if the occurrence of  $B$  does not affect the probability of occurrence of  $A$ ; that is,

$$P[A|B] = P[A] \quad (\text{C-15})$$

Rearranging Eq. (C-13), the probability that both  $A$  and  $B$  occur, is given by

$$P[A \cap B] = P[A|B]P[B] \quad (\text{C-16})$$

which if  $A$  and  $B$  are statistically independent becomes

$$P[A \cap B] = P[A] \cdot P[B] \quad (\text{C-17})$$

This is known as the multiplication rule and can be extended to the multiple, mutually independent events  $A, B, C, \dots, N$  by

$$P[A \cap B \cap C \cap \dots \cap N] = P[A] \cdot P[B] \cdot P[C] \cdot \dots \cdot P[N] \quad (\text{C-18})$$

The multiplication rule states that the probability of joint occurrence of statistically independent events is equal to the product of their individual probabilities.

For a set of events,  $B_1, B_2, \dots, B_N$ , which are mutually exclusive ( $B_i \cap B_j = \emptyset$ ) for all  $i \neq j$  but collectively exhaustive ( $B_1 \cup B_2 \cup \dots \cup B_N = \Omega$ ), like that shown in the Venn diagram of Fig. C.3, the probability of another event  $A$  can be expressed as

$$P[A] = P[A \cap B_1] + P[A \cap B_2] + \dots + P[A \cap B_N] \quad (\text{C-19})$$

Using Eq. (C-16) for each term on the right side of Eq. (C-19) yields

$$\begin{aligned} P[A] &= P[A|B_1]P[B_1] + P[A|B_2]P[B_2] + \dots + P[A|B_N]P[B_N] = \\ &= \sum_{i=1}^N P[A|B_i]P[B_i] \end{aligned} \quad (\text{C-20})$$

which is known as the total probability theorem. The total probability theorem forms the backbone of the probability calculations required for probabilistic seismic hazard analyses.

Considering that

$$P[A \cap B] = P[A|B] \cdot P[B] = P[B|A] \cdot P[A]$$

we obtain

$$P[A|B] = \frac{P[A]P[B|A]}{P[B]}$$

which is known as the Bayes theorem. In its general form it can be written as

$$P[A_k|A] = \frac{P[A_k]P[A|A_k]}{\sum_{k=1}^n P[A_k]P[A|A_k]} \quad (\text{C-21})$$

This theorem allows us to compute the probabilities of the events  $A_1, A_2, \dots, A_n$  that produce the event  $A$ . It allows us also to introduce new information to the prior probabilities: these new conditioned probabilities are called posterior probabilities.

Two events are called independent if

$$P[A|B] = P[A] \text{ and } P[B|A] = P[B]$$

and consequently

$$P[A \cap B] = P[A] \cdot P[B]. \quad (\text{C-22})$$

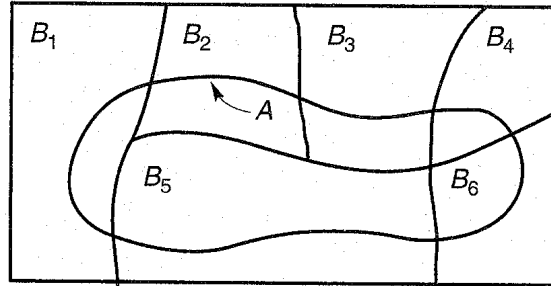


Fig. C.3 - Intersection of event A with mutually exclusive but collectively exhaustive events  $B_i$ .

### C.5. Random variables

All fields of science and engineering attempt to describe various quantities or phenomena with numerical values. In most cases, the precise numerical value cannot be predicted in advance of some process, or experiment, of interest. In such cases, a particular quantity or phenomenon is described by a random variable. The random variable is used to describe an event in a sample space in quantitative terms. An experiment is defined by its results  $s$ , belonging to the result space  $S$ , by the events, which are subsets of  $S$ , and by the probabilities associated to those events. We can associate a number  $X(s)$  to each result  $s$ : the random variable is a function defined in  $S$  (the dominion is  $S$ ) and the co-dominion is a certain numerical set.

Let  $X$  a discrete random variable with values  $x_1, x_2, \dots, x_n$ , these values are ranked in an increasing order and have associated the probabilities

$$P[X=x_k] = p(x_k) \quad k=1, 2, \dots, n. \quad (\text{C-23})$$

We can introduce the probability function, called also probability mass function (PMF)

$$P[X=x_k] = p_X(x).$$

For  $X = x_k$  it is equivalent to (C-23) and for the other values of  $x$ ,  $p_X(x)=0$ .

In general  $p_X(x)$  is a probability function if:

1.  $0 \leq p_X(x) \leq 1$ ;

2.  $\sum_{i=1}^n p_X(x_i) = 1$

3.  $P[a < x < b] = \sum_{\substack{x_i \leq b \\ x_i \geq a}} p_X(x_i)$

The related cumulative distribution function (CDF) is  $P[X \leq x] = F_X(x)$ , where  $x$  is a real number, i.e.:  $-\infty < x < +\infty$ . The CDF can be obtained from the PMF

$$F_X(x) = P[X \leq x] = \sum_{x_i \leq x} p_X(x_i) \quad (\text{C-24})$$

If  $X$  can have only a finite number of values  $x_1, x_2, \dots, x_n$  then the CDF is

$$F_X(x) = \begin{cases} 0 \\ p_X(x_1) \\ p_X(x_1) + p_X(x_2) \\ \dots \\ p_X(x_1) + \dots + p_X(x_n). \end{cases}$$

A continuous random variable can take on any value within one or more intervals. Because a continuous random variable can take on any of an infinite number of values, the probability of it taking on any specific value is  $1/\infty = 0$ . The probability distribution of a continuous random variable can also be described by its probability density function or PDF,  $f_X(x)$ , which must satisfy the conditions

$$f_X(x) \geq 0 \quad \text{for all } x$$

$$\int_{-\infty}^{\infty} f_X(x) dx = 1$$

$$P[a \leq X \leq b] = \int_a^b f_X(x) dx. \quad (\text{C-25})$$

According to these conditions, the area under the PDF between two values  $a$  and  $b$  represents the probability that the random variable will have a value in the interval bounded by  $a$  and  $b$ .  $f_X(x)$  is not, then, a probability but it is the measure of the density, or intensity, of the probability in  $x$ .

The probability distribution of a random variable can also be described by its cumulative distribution function (CDF), which is given by

$$F_X(x) = P[X \leq x] = P[-\infty < X \leq x] = \int_{-\infty}^x f_U(u) du \quad (\text{C-26})$$

Therefore, the CDF satisfies the following properties

1.  $0 \leq F_X(x) \leq 1$ ;
2.  $F_X(-\infty) = 0$ ;
3.  $F_X(+\infty) = 1$ ;
4.  $F_X(x+\varepsilon) \geq F_X(x) \quad \forall \varepsilon > 0$ ;
5.  $P[a \leq X \leq b] = F_X(b) - F_X(a)$  (C-27)

Obviously, the PDF and CDF are closely related, one can be obtained from the other by integration or differentiation. The PDF and CDF of a typical probability distribution are shown in Fig. C.4.

From the total probability theorem and the definition of the PDF, the probability of the random variable  $Y$  having some value  $y$  given that the random variable  $X$  is between two values,  $a$  and  $b$ , can be expressed as

$$P[Y=y] = P[Y=y|a \leq X \leq b] \cdot P[a \leq X \leq b]$$

$$= \tag{C-28}$$

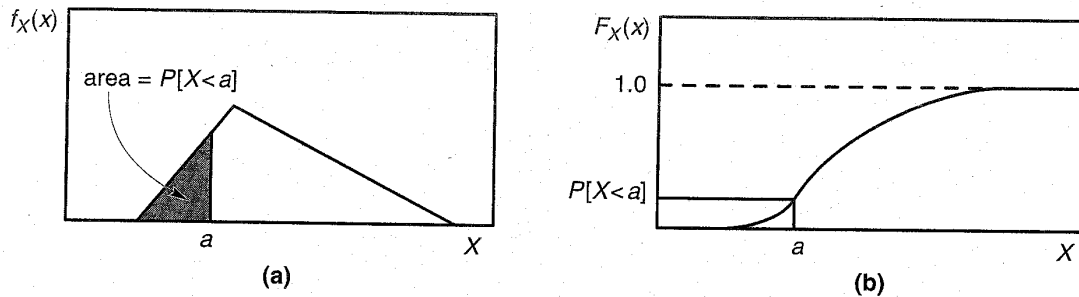


Fig. C.4 – Distributions for a random variable  $X$ : a) PDF, the probability that  $X < a$  is given by the area under the PDF to the left of  $a$ ; b) CDF, the probability that  $X < a$  is given by the value of the CDF at  $X = a$ .

*C.5.1. Double distributions*

Let  $X$  and  $Y$  two discrete random variables, the joint PMF is

$$P[(X=x) \cap (Y=y)] = p_{X,Y}(x,y)$$

where

1.  $p_{X,Y}(x,y) \geq 0$ ;
2.  $\sum_x \sum_y p_{X,Y}(x,y) = 1$ .

The probability that  $X = x_j$  is given by

$$P(X = x_j) = p_1(x_j) = \sum_{k=1}^n p(x_j, y_k).$$

Similarly, the probability that  $Y = y_k$  is given by

$$P(Y = y_k) = p_2(y_k) = \sum_{j=1}^m p(x_j, y_k).$$

$p_1(x)$  and  $p_2(y)$  are called marginal probability functions.

It can be seen that

$$\sum_{j=1}^m p_1(x_j) = 1$$



$$\sum_{k=1}^n p_2(y_k) = 1$$

$$\sum_{j=1}^m \sum_{k=1}^n p(x_j, y_k) = 1.$$

The double CDF is given by

$$F_{X,Y}(x,y) = P[X \leq x, Y \leq y] = \sum_{u < x} \sum_{v < y} p_{U,V}(u,v). \quad (\text{C-29})$$

In the case of two continuous random variables we obtain the joint PDF as

$$f_{X,Y}(x,y) \geq 0$$

$$\int_{-\infty}^{+\infty} \int_{-\infty}^{+\infty} f_{X,Y}(x,y) dx dy = 1. \quad (\text{C-30})$$

Graphically,  $z=f(x,y)$  represents a surface, called probability surface, the volume between this surface and the  $xy$  plane is equal to 1. The probability that  $X$  be between  $a$  and  $b$ , and that  $Y$  be between  $c$  and  $d$  is given graphically by the volume expressed by

$$P[a < X < b, c < Y < d] = \int_{x=a}^b \int_{y=c}^d f_{X,Y}(x,y) dx dy. \quad (\text{C-31})$$

More generally, the event  $A$  is represented by a region  $R_A$  of the  $xy$  plane and the probability of  $A$  is given by

$$P[A] = \int \int_{R_A} f_{X,Y}(x,y) dx dy. \quad (\text{C-32})$$

The double distribution function is given by

$$F_{X,Y}(x,y) = P[X \leq x, Y \leq y] = \int_{u=-\infty}^x \int_{v=-\infty}^y f_{U,V}(u,v) du dv. \quad (\text{C-33})$$

Similarly to the case of discrete random variables we have

$$P[X \leq x] = F_1(x) = \int_{u=-\infty}^x \int_{v=-\infty}^{+\infty} f_{U,V}(u,v) du dv \quad (\text{C-34})$$

$$P[Y \leq y] = F_2(y) = \int_{u=-\infty}^{+\infty} \int_{v=-\infty}^y f_{U,V}(u,v) du dv \quad (\text{C-35})$$

$F_1(x)$  and  $F_2(y)$  are called marginal CDFs; their derivatives are called marginal PDFs

$$f_1(x) = \int_{v=-\infty}^{+\infty} f(x,v) dv \quad (\text{C-36})$$

$$f_2(y) = \int_{u=-\infty}^{+\infty} f(u,y)du. \quad (C-37)$$

### C.5.2. Conditional distributions

We know that, if  $P[A]>0$

$$P[B|A] = \frac{P[A \cap B]}{P[A]}.$$

If  $X$  and  $Y$  are discrete random variables and we have the events  $A:X=x$ ,  $B:Y=y$ , we can write

$$P[Y = y | X = x] = \frac{p(x,y)}{p_1(x)}$$

where  $p(x,y) = P[X=x, Y=y]$  is the double PMF and  $p_1(x)$  is the marginal probability of  $X$ .

Let's define

$$p(y|x) = \frac{p(x,y)}{p_1(x)} \quad (C-38)$$

as the conditional PMF of  $Y$  given  $X$ . Similarly

$$p(x|y) = \frac{p(x,y)}{p_2(y)}. \quad (C-39)$$

These ideas can easily translated to continuous random variables and we obtain the conditional PDF

$$f(y|x) = \frac{f(x,y)}{f_1(x)} \quad (C-40)$$

where  $f(x,y)$  is the double PDF of  $X$  and  $Y$  and  $f_1(x)$  is the marginal PDF of  $X$ . Consequently, we are able to compute the probability that  $Y$  be between  $c$  and  $d$  given  $x < X < x+dx$

$$P[c < Y < d | x < X < x + dx] = \int_c^d f(y|x)dx. \quad (C-41)$$

### C.5.3. Independent random variables

Let  $X$  and  $Y$  two discrete random variables. If the events  $X=x$  and  $Y=y$  are independent for every  $x$  and  $y$ , we say that  $X$  and  $Y$  are independent random variables. In this case

$$P[X=x, Y=y] = P[X=x] \cdot P[Y=y]$$

and

$$p(x,y) = p_1(x) \cdot p_2(y). \quad (C-42)$$

On the other side, if for every  $x$  and  $y$  the double PMF  $p(x,y)$  can be expressed as the product of the marginal PMFs of  $X$  and  $Y$ ,  $X$  and  $Y$  are independent.

If  $X$  and  $Y$  are continuous random variables, we say they are independent random variables if the events  $X \leq x$  and  $Y \leq y$  are independent for all  $x$  and  $y$

$$P[X \leq x, Y \leq y] = P[X \leq x] \cdot P[Y \leq y]$$

and

$$F(x,y) = F_1(x) F_2(y) \quad (C-43)$$

where  $F_1(x)$  and  $F_2(y)$  are the marginal CDFs of  $X$  and  $Y$ . On the other side, if for every  $x$  and  $y$  the double CDF  $F(x,y)$  can be expressed as the product of the marginal CDFs of  $X$  and  $Y$ ,  $X$  and  $Y$  are independent.

Moreover, we have

$$\begin{aligned} f(x,y) &= f_1(x) f_2(y); \\ f_{x|y}(x,y) &= f_1(x); \\ f_{y|x}(x,y) &= f_2(y); \\ F_{x|y}(x,y) &= F_1(x). \end{aligned}$$

#### C.5.4. Function of a random variable

Given the random variable  $X$ , let  $x$  one of its values; given a real function  $y=g(x)$  for every  $x$ . Let's consider the variable  $Y=g(X)$ : it is defined for every result  $s$  in the following way

$$s \rightarrow X(s) \rightarrow Y(s) = g[X(s)].$$

Under not very restrictive conditions also  $Y$  is a random variable and its CDF is

$$F_Y(y) = P[Y \leq y] = P[g(X) \leq y].$$

#### C.5.5. Convolution

It can be demonstrated that the PDF of the sum of two continuous random variables  $U=X+Y$ , having double PDF  $f(x,y)$  is

$$g_U(u) = \int_{-\infty}^{+\infty} f(x, u-x) dx.$$

If  $X$  and  $Y$  are independent,  $f(x,y) = f_1(x) f_2(y)$ , we have

$$g_U(u) = \int_{-\infty}^{+\infty} f_1(x) f_2(u-x) dx \quad (C-44)$$

and it is called the convolution of  $f_1$  and  $f_2$  and is abbreviated as  $f_1 * f_2$ . The convolution has the following properties:

1.  $f_1 * f_2 = f_2 * f_1$ ,
2.  $f_1 * (f_2 * f_3) = (f_1 * f_2) * f_3$ ,
3.  $f_1 * (f_2 + f_3) = (f_1 * f_2) + (f_1 * f_3)$ .

### C.6. Expected values and standard deviations

The uncertainty of a random variable can often be characterized with reasonable accuracy by a few statistical parameters. The mean, or expected value, of a discrete random variable,  $X$ , taking the values  $x_1, \dots, x_n$  is given by

$$E(X) = x_1 P[X = x_1] + \dots + x_n P[X = x_n] = \sum_{j=1}^n x_j P[X = x_j].$$

If  $P[X=x_j] = p(x_j)$ , we have

$$E(X) = x_1 p(x_1) + \dots + x_n p(x_n) = \sum_{j=1}^n x_j p(x_j) = \sum xp(x)$$

where the last sum takes all the values of  $x$ .

There are some analogies with the arithmetic mean when it is written as  $\bar{x} = \sum_{i=1}^r x_i f_i$ , where  $f_i$  is the frequency ( $n_i/n$ ) of the value  $x_i$  in the sample.  $r$  is the total number of observations that can be multiple for every  $r < n$ . We handle, anyway, two different quantities:  $\bar{x}$  is calculated from the observations while  $E(X)$  from the probability function (PMF or CDF).

Similarly, the mean, or expected value, of a continuous random variable,  $X$ , is given by

$$E(X) = \int_{-\infty}^{\infty} x f_X(x) dx. \quad (C-45)$$

The mean, generally represented as  $\mu$ , is a very useful measure of the central tendency of the random variable. By itself, however, it does not adequately describe the shape of the PDF. The dispersion of the random variable about the mean is also very important. This dispersion is usually characterized by the variance

$$\sigma_x^2 = \int_{-\infty}^{\infty} (x - \mu)^2 f_X(x) dx \quad (C-46)$$

or the standard deviation

$$\sigma_x = \sqrt{\sigma_x^2}. \quad (C-47)$$

Both of these parameters reflect how widely the random variable is dispersed about the mean. Because its units are the same as those of the random variable, the standard deviation is more commonly used than the variance. This characteristic also allows the dispersion to be expressed in dimensionless form by the coefficient of variation

$$COV_x = \sigma_x / \mu \quad (C-48)$$

The mean and standard deviation (or mean and coefficient of variation) go far toward describing the uncertainty in a random variable. Many simple probability distributions, including those most commonly used in earthquake engineering, are completely described by these two parameters. Other distributions may require additional parameters to characterize their symmetry, limits, and/or other characteristics.

### C.7. Common probability distributions

The results of statistical experiments often exhibit the same general type of behaviour. As a result, the random variables associated with those experiments can be described by essentially the same PDF. Many PDFs exist, but only a few are required for the earthquake engineering analyses.

#### C.7.1 Uniform distribution

The simplest probability distribution is one in which all possible values of the random variable are equally likely. Such a random variable is described by a uniform distribution. The PDF for a continuous random variable,  $X$ , that is uniformly distributed between two values  $a$  and  $b$  is

$$\begin{aligned} f_X(x) &= 0 & \text{for } x \leq a \\ f_X(x) &= 1/(b-a) & \text{for } a < x \leq b \\ f_X(x) &= 0 & \text{for } x > b \end{aligned} \tag{C-49}$$

The PDF and CDF for a uniform distribution are illustrated in Fig. C.5.

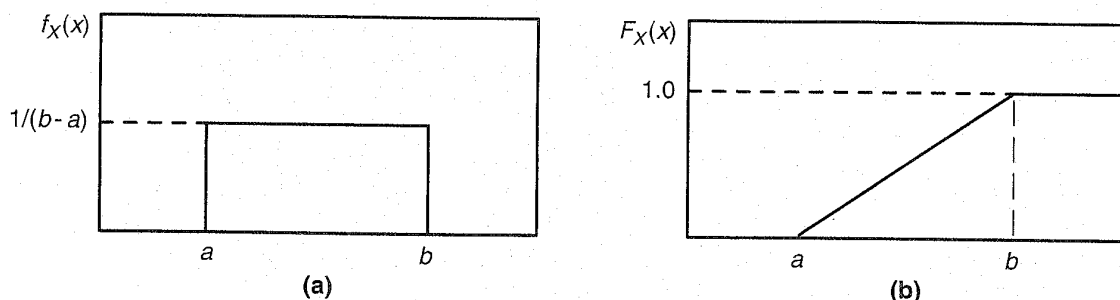


Fig. C.5 - Uniform distribution: (a) PDF; (b) CDF.

#### C.7.2 Normal distribution

The most commonly used probability distribution in statistics is the normal (or Gaussian) distribution: it is the distribution of the sum of random variables uniformly distributed. Its PDF, which plots as the familiar bell-shaped curve of Fig. C.6a, describes sets of data produced by a wide variety of physical processes. The normal distribution is completely defined by two parameters: the mean and standard deviation. Mathematically, the PDF of a normally distributed random variable  $X$  with mean  $\mu$  and standard deviation  $\sigma_x$  is given by

$$f_X(x) = \frac{1}{\sigma_x \sqrt{2\pi}} \exp\left[-\frac{1}{2} \left(\frac{x - \mu}{\sigma_x}\right)^2\right] \tag{C-50}$$

The PDF and CDF for a normal distribution are illustrated in Fig. C.6. Examples of normal pdf's for random variables with different means and standard deviations are shown in Fig. C.7.

Integration of the PDF of the normal distribution does not produce a simple expression for the CDF, so values of the normal CDF are usually expressed in tabular form.

$$F(x) = P[X \leq x] = \frac{1}{\sigma \sqrt{2\pi}} \int_{-\infty}^x \exp\left[-\frac{(v - u)^2}{2\sigma^2}\right] dv.$$

The normal CDF is most efficiently expressed in terms of the standard normal variable,  $Z$ , which can be computed for any random variable,  $X$ , using the transformation

$$Z = \frac{X - \mu}{\sigma_x} \tag{C-51}$$

Whenever  $X$  has a value,  $x$ , the corresponding value of  $Z$  is  $z = \frac{x - \mu}{\sigma_x}$ . Thus, the mean value of  $Z$  is 0 and the standard deviation is 1. Tabulated values of the standard normal CDF can be found in all books of statistics.

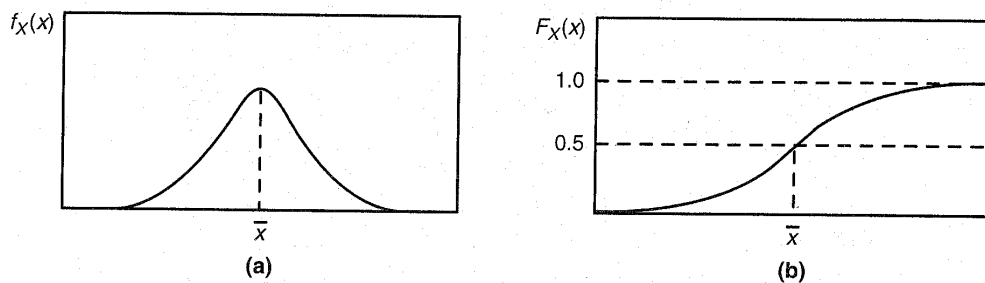


Fig. C.6 - Normal distribution: (a) PDF; (b) CDF.

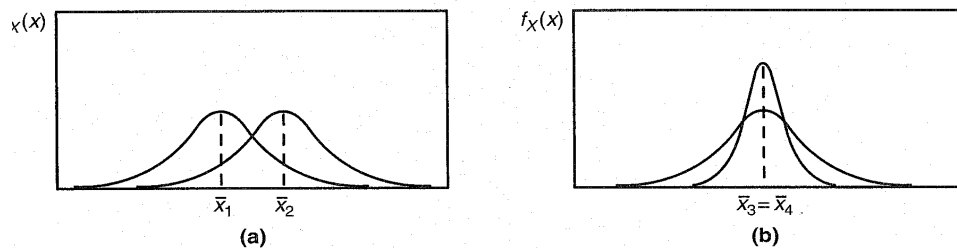


Fig. C.7 - Normal distributions for (a) two random variables,  $X_1$  and  $X_2$ , with different means but the same standard deviation, and (b) two random variables,  $X_3$  and  $X_4$ , with the same mean but different standard deviations.



### C.7.3 Lognormal distribution

Some problems, particularly those involving ground motion parameters, are formulated in terms of the logarithm of a parameter rather than the parameter itself. If  $X$  is a random variable, then  $Y = \ln X$  is also a random variable. If  $Y$  is normally distributed, then  $X$  is *lognormally distributed*. In other words, a random variable is lognormally distributed if its logarithm is normally distributed. The lognormal distribution is the distribution of the product of random variables. The PDF of a lognormally distributed random variable  $X$  is given by

$$f_X(x) = \frac{1}{x\sqrt{2\pi}\sigma_{\ln x}} \exp\left[-\frac{1}{2}\left(\frac{\ln x - \overline{\ln x}}{\sigma_{\ln x}}\right)^2\right]$$

$$f_i = n_i/n$$

$$F_i = \sum_{k=1}^i f_k$$

$$\bar{x} = \frac{\sum_{i=1}^n x_i}{n}$$

$$\bar{x} = \sum_{i=1}^n x_i f_i; \tag{C-52}$$

where  $\overline{\ln x}$  indicates the mean value of  $\ln x$ .

The shape of the lognormal distribution is shown in Fig. C.8. Note that the PDF is not symmetric, and that it assigns zero probability to negative values of the random variable. These characteristics can be very useful for some random variables (the normal distribution, for example, assigns nonzero probabilities for values ranging from  $-\infty$  to  $+\infty$ ; when applied to a random variable such as soil density, it can assign some, hopefully small, probability that the soil will have a negative density).

Values of the CDF of the lognormal distribution are usually obtained from those of the normal distribution, using the modified transformation

$$\tag{C-53}$$

### C.7.4. Bernoulli or binomial distribution

Some experiments consist in repeating an operation, e.g.: flip a coin or a dice, or to choose a ballot from a box. Every flip or choice is called proof. At any proof, to every event, e.g.: the head for the coin, number 4 for the dice, the red ballot for the choice from the box, a probability remains associated. Sometimes the probability does not change from one proof to the other (as in the case of the coin or the dice). Such a kind of proofs are called independent or Bernoulli proofs.

Let  $p$  the probability of an event in a Bernoulli trial (it is called success probability). Then,  $q=1-p$  is the probability that the event will not occur. Then

$$f_X(x) = p \quad \text{if } x=1$$

$$f_X(x) = 1-p \quad \text{if } x=0$$

$$\begin{aligned}\mu &= p \\ \sigma^2 &= (1-p)p\end{aligned}$$

The probability that an event occurs exactly  $x$  times in  $n$  Bernoulli proofs [i.e.:  $x$  successes and  $(n-x)$  negative outcomes] is given by

$$f_X(x) = P[X = x] = \binom{n}{x} p^x q^{n-x} = \frac{n!}{x!(n-x)!} p^x q^{n-x} \quad (\text{C-54})$$

where  $X$  indicates the number of successes in  $n$  proofs and  $x = 0, 1, \dots, n$ . The above discrete PMF is called Bernoulli or binomial distribution and a random variable with a Bernoulli distribution is called a Bernoulli random variable.

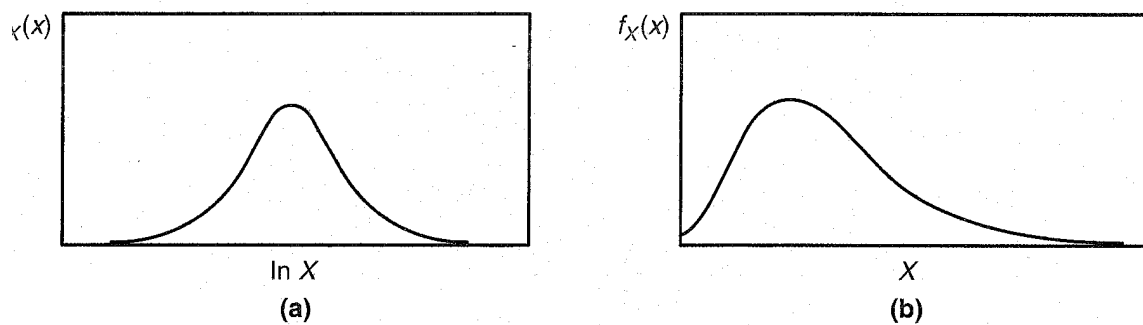


Fig. C.8 Two views of the lognormal distribution: a) because the logarithm of a lognormally distributed random variable,  $X$ , is normally distributed, the PDF of  $\ln X$  is a bell-shaped curve; b) The PDF of  $X$  itself has no negative values and is not symmetric.

#### C.7.5. The geometric distribution

Let  $X$  the number of Bernoulli trials that are necessary to obtain the first success and  $p$  the probability of success in a single trial:

$$\begin{aligned}f_X(x) &= P[X = x] = pq^{x-1} \\ \mu &= \frac{1}{p} \\ \sigma^2 &= \frac{q}{p^2}.\end{aligned} \quad (\text{C-55})$$

#### C.7.6. The Pascal distribution or negative binomial distribution

Let  $X$  the number of Bernoulli trials that are necessary to obtain  $r$  successes (if  $r=1$  we obtain the geometric distribution):

$$f_X(x) = P[X = x] = \binom{x-1}{r-1} p^r p^{x-r}$$

$$\mu = \frac{r}{p} \tag{C-56}$$

$$\sigma^2 = \frac{rq}{p^2}.$$

### C.7.7. Poisson distribution

In many situations it is not possible to identify the individual discrete experiments following which the events occur, but it is known that the number of these experiments is very large or, in other words, the events can occur at any moment of a time interval or in any place (on a line or on a surface).

The Poisson distribution is a discrete probability distribution. It expresses the probability of a number of events occurring in a fixed period of time if these events occur with a known average rate, and are independent of the time since the last event. The distribution was discovered by Siméon-Denis Poisson (1781-1840) belonging to certain random variables  $N$  that count, among other things, a number of discrete occurrences (sometimes called "arrivals") that take place during a time-interval of given length. The probability that there are exactly  $x$  occurrences ( $x$  being a non-negative integer,  $k = 0, 1, 2, \dots$ ) in  $n$  Bernoulli proofs is

$$f_X(x) = \binom{n}{x} p^x (1-p)^{n-x}$$

where  $x = 0, 1, \dots, n$ . Let's suppose that  $n$  is very large and  $p$  very small (it is the case of proofs referring to little time intervals where the individual probability of occurrence is small). The total number of expected events remains the same and it is  $pn = \lambda$ . Putting  $p = \lambda/n$ , the PMF of  $X$  for  $n \rightarrow \infty$  and  $p \rightarrow 0$  is

$$f_X(x) = \frac{n!}{x!(n-x)!} \left(\frac{\lambda}{n}\right)^x \left(1 - \frac{\lambda}{n}\right)^{n-x}.$$

Substituting and passing to the limit we obtain

$$P[X = x] = f_X(x; \lambda) = \frac{e^{-\lambda} \lambda^x}{x!} \quad x = 0, 1, \dots, \infty \tag{C-57}$$

where  $\lambda$  is a positive real number, equal to the expected number of occurrences that occur during the given interval.

The Poisson distribution is the discrete counterpart of the more famous continuous normal distribution.

The parameter  $\lambda$  is not only the mean number of occurrences, but also its variance. Thus, the number of observed occurrences fluctuates about its mean  $\lambda$  with a standard deviation  $\sqrt{\lambda}$ . These fluctuations are denoted as Poisson noise or (particularly in electronics as shot noise).

## C.8. Random process

A random process is a random function of time. Given an experiment  $S$  defined by its results  $s_i$ , which form the sample space  $S$ , by the events, which are the sub-sets of  $S$ , and by the probabilities of these events, we can associate the time function  $X(t,s)$ , generally indicated as  $X(t)$ , to each result  $s$ . We have in such a way a family of functions, one for each  $s$ : this family is a random process if for every  $t$ ,  $X(t)$  is a random variable. In this case,  $\{X(t) \leq x\}$  is an event. The probability of this event

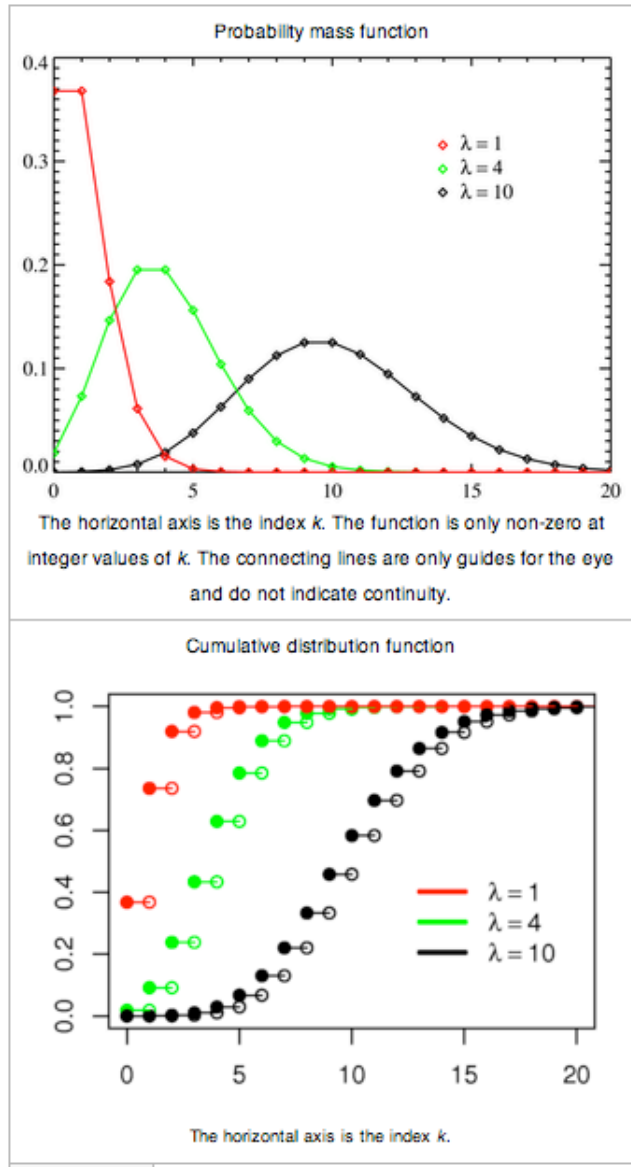


Fig. C.9 – PMF and CDF of the Poisson distribution.

$$P[X(t) \leq x] = F_{X(t)}(x, t)$$

is a function generally depending on  $t$ : we call it again “distribution” and it defines completely the process  $X(t)$ .

*C.8.1. Poisson process*

Let's consider events that can occur in any moment of a certain time interval (or in any point of a segment or of a plane), and define the random process  $N(t)$ , whose value in every  $t$  is the random number of events occurring in the interval  $(0, t)$ .

Let's suppose that the following proprieties are satisfied:

1. stationarity: the probability of occurrence of an event in a "small" interval  $(t, t+\Delta t)$  is proportional to  $\Delta t$ , i.e., equals to  $\nu\Delta t$ , if  $\nu$  is the proportionality constant;
2. non-multiplicity: the probability of more than one event in a "small"  $\Delta t$  is marginal with respect to  $\nu\Delta t$ ;
3. independence: the number of events in  $(t, t+\Delta t)$  is independent from the number of events that occurred before  $t$ .

Such a process is called a Poisson process.

Sometimes  $\nu$  is taken to be the rate, i.e., the average number of occurrences per unit time (we have put  $\lambda$  of Eq. (C-57) equal to  $\nu t$ ). In that case, if  $Nt$  is the number of occurrences before time  $t$  then we have

$$P[N_t = k] = f_{N_t}(k; \nu t) = \frac{e^{-\nu t} \nu t^k}{k!}$$

and the waiting time  $T$  until the first occurrence is a continuous random variable with an exponential distribution (with parameter  $\nu$ ). This probability distribution may be deduced from the fact that

$$P[T > t] = P[N_t = 0] = e^{-\nu t}.$$

The expected value of  $N(t)$  is then

$$\begin{aligned} E[N(t)] &= \mu = 1\nu t e^{-\nu t} + 2 \frac{(\nu t)^2}{2!} e^{-\nu t} + 3 \frac{(\nu t)^3}{3!} e^{-\nu t} + \dots = \\ &= \nu t e^{-\nu t} \left[ 1 + \nu t + \frac{(\nu t)^2}{2!} \right] = \nu t e^{-\nu t} e^{\nu t} = \nu t \end{aligned} \tag{C-58}$$

When time becomes involved, then we have a 1-dimensional Poisson process, which involves both the discrete Poisson-distributed random variables that count the number of arrivals in each time interval, and the continuous Erlang-distributed waiting times. There are also Poisson processes of dimension higher than 1.

In several of the above examples the events being counted are actually the outcomes of discrete trials, and would more precisely be modelled using the binomial distribution. However, the binomial distribution with parameters  $n$  and  $\nu/n$ , i.e., the probability distribution of the number of successes in  $n$  trials, with probability  $\nu/n$  of success on each trial, approaches the Poisson distribution with expected value  $\nu$  as  $n$  approaches infinity. This limit is sometimes known as the law of rare events. It provides a means by which to approximate random variables using the Poisson distribution rather than the more-cumbersome binomial distribution.

For sufficiently large values of  $\nu$  (say  $\nu > 1000$ ), the normal distribution with mean  $\nu$  and variance  $\nu$  is an excellent approximation to the Poisson distribution. If  $\nu$  is greater than about 10, then the normal distribution is a good approximation if an appropriate continuity correction is performed, i.e.,  $P(X \leq x)$ , where (lower-case)  $x$  is a non-negative integer, is replaced by  $P(X \leq x + 0.5)$ .

The word law is sometimes used as a synonym of probability distribution, and convergence in law means convergence in distribution. Accordingly, the Poisson distribution is sometimes called the law of small numbers because it is the probability

distribution of the number of occurrences of an event that happens rarely but has very many opportunities to happen. "The Law of Small Numbers" is a book by Ladislaus Bortkiewicz about the Poisson distribution, published in 1898.

### C.8.2. Exponential distribution

In probability theory and statistics, the exponential distributions are a class of continuous probability distribution. They are often used to model the time between events that happen at a constant average rate.

Let  $N(t)$  a Poisson process and  $t$  the random variable representing the interoccurrence time between 2 subsequent events:  $N(t)$  and  $t$  are correlated. If we indicate the events on the time axis with stars,  $t$  is the random variable time between 2 stars and  $x$  are its possible values. Then:

$$P[\tau \leq x] = F_{\tau}(x) = 1 - e^{-\nu x}$$

and

$$P[x \leq \tau < x + dx] = f_{\tau}(x)dx = \nu e^{-\nu x} dx.$$

Consequently:

$$f_{\tau}(x) = \nu e^{-\nu x}. \quad (\text{C-59})$$

The CDF defines the random variable waiting time of the first event, but, for the conditions of stationarity and independence of the Poisson process, it defines the random variable  $t$ , interoccurrence time between 2 successive events. We can conclude that the interoccurrence times in a Poisson process are independent and exponentially distributed. We have also that:

$$E(\tau) = \bar{\tau} = \int_0^{\infty} x \nu e^{-\nu x} dx = \frac{1}{\nu} \quad (\text{C-60})$$

$$E[(\tau - \bar{\tau})^2] = \sigma^2 = \frac{1}{\nu^2}.$$

The hazard rate is the function defined as:

$$\Phi_{\tau}(x) = f_{\tau}(x | \tau \geq x) = \frac{P[x \leq \tau \leq x + dx, \tau \geq x]}{P[\tau \geq x]} =$$

$$= \frac{P[x \leq \tau < x + dx]}{P[\tau \geq x]} = \frac{f_{\tau}(x)}{1 - F_{\tau}(x)}$$

and it defines the probability that the event occurs at the time  $x$ , given that it has not yet occurred (i.e.: between 0 and  $x$ ).

In a Poisson process, the hazard rate is constant and viceversa a random process with constant hazard rate is a Poisson process:

$$\Phi_{\tau}(x) = \nu.$$



Furthermore, the Poisson process is memoryless because the future is independent from the past and present.

Summarizing, the PDF of an exponential distribution has the form

$$f(x; \nu) = \begin{cases} \nu e^{-\nu x}, & x \geq 0, \\ 0, & x < 0. \end{cases}$$

where  $\nu > 0$  is a parameter of the distribution, often called the *rate parameter*. The distribution is supported on the interval  $[0, \infty)$ . If a random variable  $X$  has this distribution, we write  $X \sim \text{Exponential}(\nu)$ .

The exponential distributions can alternatively be parameterized by a scale parameter  $\mu = 1/\nu$ .

The CDF is given by

$$F(x; \nu) = \begin{cases} 1 - e^{-\nu x}, & x \geq 0, \\ 0, & x < 0. \end{cases} \quad (\text{C-61})$$

A commonly used alternate specification is to define the PDF of an exponential distribution as

$$f(x; \nu) = \begin{cases} \frac{1}{\nu} e^{-x/\nu}, & x \geq 0, \\ 0, & x < 0. \end{cases} \quad (\text{C-62})$$

where  $\nu > 0$  is a parameter of the distribution and can be thought of as the multiplicative inverse of the rate parameter defined above. In this specification,  $\nu$  is a *survival parameter* in the sense that if a random variable  $X$  is the duration of time that a given biological or mechanical system  $M$  manages to survive and  $X \sim \text{Exponential}(\nu)$  then  $E[X] = \nu$ . That is to say, the expected duration of survival of  $M$  is  $\nu$  units of time.

This alternate specification is sometimes more convenient than the one given above, and some authors will use it as a standard definition. We shall not assume this alternate specification. Unfortunately this gives rise to a notational ambiguity. In general, the reader must check which of these two specifications is being used if an author writes " $X \sim \text{Exponential}(\nu)$ ."

The exponential distribution is used to model Poisson processes, which are situations in which an object initially in state A can change to state B with constant probability per unit time  $\nu$ . The time at which the state actually changes is described by an exponential random variable with parameter  $\nu$ . Therefore, the integral from 0 to  $T$  over  $f$  is the probability that the object is in state B at time  $T$ .

The exponential distribution may be viewed as a continuous counterpart of the geometric distribution, which describes the number of Bernoulli trials necessary for a *discrete* process to change state. In contrast, the exponential distribution describes the time for a continuous process to change state.

In real-world scenarios, the assumption of a constant rate (or probability per unit time) is rarely satisfied. The length of a process that can be thought of as a sequence of several independent tasks is better modeled by a variable following the gamma distribution (which is a sum of several independent exponentially distributed variables).

The mean or expected value of an exponentially distributed random variable  $X$  with rate parameter  $\nu$  is given by  $E[X] = 1/\nu$ .

The variance of  $X$  is given by  $V[X] = 1/\nu^2$ .

An important property of the exponential distribution is that it is memoryless.

This means that if a random variable  $T$  is exponentially distributed its conditional probability obeys

$$P[T > s + t | T > t] = P[T > s] \quad \text{for all } s, t \geq 0.$$

This says that the conditional probability that we need to wait, for example, more than another 10 seconds before the first arrival, given that the first arrival has not yet happened after 30 seconds, is no different from the initial probability that we need to wait more than 10 seconds for the first arrival. The fact that  $P(T > 40 | T > 30) = P(T > 10)$  does *not* mean that the events  $T > 40$  and  $T > 30$  are independent. To summarize: "memorylessness" of the probability distribution of the waiting time  $T$  until the first arrival means

$$P[T > 40 | T > 30] = P[T > 10]$$

It does *not* mean

$$P[T > 40 | T > 30] = P[T > 40]$$

that would be independence, while these two events are **not** independent.

The exponential distributions and the geometric distributions are the only memoryless probability distributions.

The exponential distribution also has a constant hazard function.

### C.8.3. Gamma distribution

Similarly to the negative binomial distribution for the Bernoulli trials, we can study the distribution of time  $X_k$  of the  $k$ -th success in a Poisson process: it is called Gamma distribution. It can be demonstrated that:

$$f_{X_k}(x) = \frac{\nu(\nu x)^{k-1} e^{-\nu x}}{(k-1)!} \quad (\text{C-63})$$

with  $x \geq 0$  and

$$\mu = \frac{k}{\nu}$$

$$\sigma^2 = \frac{k}{\nu^2}.$$

The Gamma distribution can be defined more generally by the distribution of the sum of  $k$  exponential random variables independently and identically distributed. In fact,  $k$  can be a real (non integer) number by substituting the denominator with the Gamma function.

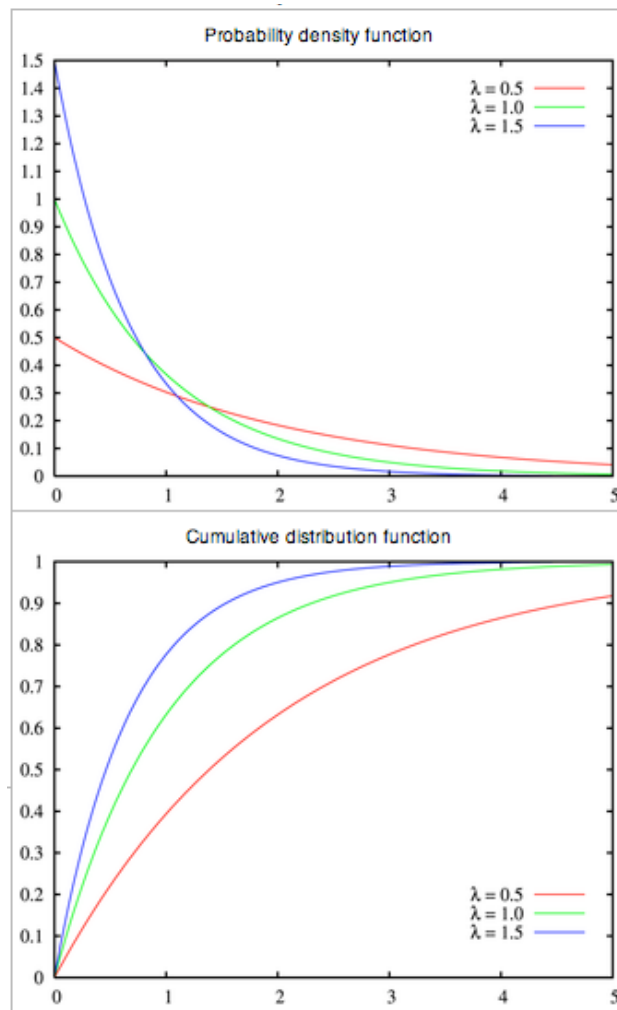


Fig. C.10 – PDF and CDF of the exponential distribution. Note: the parameter  $\lambda$  of the figure corresponds to  $\nu$  of the text for analogy of the formulae of PSHA.

### C.9. Generalized extreme value distribution

In probability theory and statistics, the generalized extreme value distribution (GEV) is a family of continuous probability distributions developed within extreme value theory to combine the Gumbel, Fréchet and Weibull families also known as Type I, II and III extreme value distributions. Its importance arises from the fact that it is the limit distribution of the maxima of a sequence of independent and identically distributed random variables. Because of this, the GEV is used as an approximation to model the maxima of long (finite) sequences of random variables.

Let  $X_1, \dots, X_n$  be a sequence of independent identically distributed random variables with distribution function,  $F$ . Then let  $M_n = \max\{X_1, \dots, X_n\}$ . For known  $F$ , the distribution of  $M_n$  can be derived exactly for all values of  $n$  because  $P[M_n \leq u] = P[X_i \leq u; \text{ for all } i=1, \dots, n]$ , which by the fact that the  $X_i$  are independent is equivalent to  $P[X_1 \leq u] \cdot P[X_2 \leq u] \cdot \dots \cdot P[X_n \leq u]$  and because the  $X_i$  are identically distributed this is equivalent to  $(P[X_1 \leq u])^n$ . Thus,  $P[M_n \leq u] = (F(u))^n$ . Note, however, that the independence assumption, which virtually never occurs for weather and climate variables, can be relaxed.

### C.10. Gumbel distributions

In probability theory and statistics the Gumbel distribution (named after Emil Julius Gumbel (1891-1966)) is used to find the minimum (or the maximum) of a number of samples of various distributions. For example we would use it to find the maximum level of a river in a particular year if we had the list of maximum values for the past ten years. It is therefore useful in predicting the chance that an extreme earthquake, flood or other natural disaster will occur.

The distribution of the samples could be of the normal or exponential type. The Gumbel distribution, and similar distributions, are used in extreme value theory.

### C.10.1. Gumbel Type 1 distribution

It is the distribution of the maximum values of many independent and identically distributed random variables. Let the distribution of  $X_i$  non limited for positive values and decays exponentially, i.e.: the CDF common for all  $X_i$ , at least for the coda of the largest values, has the form

$$F_X(x) = 1 - e^{-g(x)}.$$

This is the case of the exponential, normal, and Gamma distributions. It can be demonstrated that  $Y$ , the maximum of many independent random variables, has the following distributions

$$\begin{aligned} F_Y(y) &= \exp\left[-e^{-\alpha(y-u)}\right] \\ f_Y(y) &= \alpha \exp\left[-\alpha(y-u) - e^{-\alpha(y-u)}\right] \end{aligned} \tag{C-64}$$

with  $-\infty \leq y \leq +\infty$  and  $\alpha$  and  $u$  parameters computed from the data.

We have

$$\begin{aligned} \mu &\approx u + \frac{0.577}{\alpha} \\ \sigma^2 &\approx \frac{1.645}{\alpha^2} \\ \sigma &\approx \frac{1.282}{\alpha}. \end{aligned}$$

Introducing the reduced variable  $w = \alpha(y-u)$ , we obtain

$$F_W(w) = e^{-e^{-w}}.$$

### C.10.2. Gumbel Type 2 distribution

It is the distribution of the maximum values of many independent and identically distributed random variables, with  $\lim(X_i) = 0$  for  $X_i \rightarrow -\infty$  and  $\lim(X_i) = \infty$  for  $X_i \rightarrow +\infty$  (in the coda of interest). Let the CDF of the  $X_i$  codas

$$F_X(x) = 1 - \beta \left(\frac{1}{x}\right)^k$$

with  $x \geq 0$ .

The distribution of the maximum values is:

$$F_Y(y) = e^{-\left(\frac{u}{y}\right)^k} \quad (C-65)$$

$$f_Y(y) = \frac{k}{u} \left(\frac{u}{y}\right)^{k+1} e^{-\left(\frac{u}{y}\right)^k}$$

with  $y \geq 0$ .

### C.10.3. Gumbel Type 3 distribution

It is the distribution of the maximum values of many independent and identically distributed random variables, with a finite limit in the coda of interest:

$$F_X(x) = 1 - c(w - x)^k$$

with  $x \leq w$  and  $k > 0$ .

The distribution of the maximum values is:

$$F_Y(y) = \exp\left[-\left(\frac{w - y}{w - u}\right)^k\right] \quad (C-66)$$

$$f_Y(y) = \frac{k}{w - u} \left(\frac{w - y}{w - u}\right)^{k-1} \exp\left[-\left(\frac{w - y}{w - u}\right)^k\right]$$

with  $y > w$ .